**Universidad de Valladolid**

Escuela Técnica Superior de Ingenieros de Telecomunicación

Dpto. de Teoría de la Señal y Comunicaciones e Ing. Telemática

Programa de Doctorado en Tecnologías de la Información y las Telecomunicaciones

# TESIS DOCTORAL

# A multimodal analysis of Magnetic Resonance Imaging for the study of brain abnormalities in migraine: gray matter morphometry, white matter integrity and structural connectivity

Presentada por **Álvaro Planchuelo Gómez** para optar al grado de doctor por la Universidad de Valladolid

Dirigida por los doctores

**Santiago Aja Fernández** y **Rodrigo de Luis García**

Fecha

Valladolid, España

| | |
|---|---|
| TÍTULO: *Title*: | A multimodal analysis of Magnetic Resonance Imaging for the study of brain abnormalities in migraine: gray matter morphometry, white matter integrity and structural connectivity |
| AUTOR: *Author*: | Álvaro Planchuelo Gómez |
| DIRECTORES: *Advisors*: | Santiago Aja Fernández & Rodrigo de Luis García |
| DEPARTAMENTO: *Department*: | Teoría de la Señal y Comunicaciones e Ing. Telemática |

TRIBUNAL/*Committee*

| | |
|---|---|
| PRESIDENTE: *Chairwoman*: | Dr. |
| VOCAL: *Member*: | Dr. |
| SECRETARIO: *Secretary*: | Dr. |

acuerda otorgarle la calificación de

En Valladolid, a

# *Agradecimientos*

En primer lugar, me gustaría comenzar los agradecimientos con mis directores de tesis, los doctores Santiago Aja Fernández y Rodrigo de Luis García. Les agradezco que me aceptaran desde el primer momento que entré en el LPI apareciendo de imprevisto, con un gran trato personal, así como la libertad que me han dado para trabajar y su guía para mejorar mucho en diversos y aumentar la calidad de la investigación, desde los aspectos más formales hasta la aportación de interesantes ideas. No me podía imaginar el buen sitio en el que fui a parar para realizar la tesis. Gracias.

También tengo mucho que agradecer a mis 'supervisores'neurólogos, los doctores Ángel Luis Guerrero y David García Azorín, del Grupo de Investigación de Cefaleas en Valladolid (INCEVAL) del Hospital Clínico Universitario de Valladolid. Gracias a ellos, he podido apreciar lo apasionante que es la ciencia de las cefaleas, particularmente la migraña, sobre las que aún hay mucho que descubrir a pesar de lo comunes que son. Además, quiero agradecer su inmejorable trato, incluyendo ayuda para asistir a congresos, y la confianza que han depositado en mí para participar en proyectos de diversa índole.

Entre mis agradecimientos también está la doctora Margarita Rodríguez, que se ha encargado de coordinar las adquisiciones de los pacientes con migraña desde antes de mi llegada a Valladolid y que además ha realizado los informes radiológicos de las imágenes de los sujetos.

Así mismo, incluyo en mis agradecimientos al doctor Vicente Molina, coordinador del Grupo de Sustratos Cerebrales de la Psicosis (SUCEDE) de Valladolid y a las investigadoras del grupo con las que he tenido más contacto, la doctora Alba Lubeiro al principio, e Inés Fernández Linsenbarth posteriormente. Considero que mi colaboración con el grupo ha sido especialmente fructífera y fruto de la misma se han publicado y realizado artículos impactantes desde las perspectivas técnica y clínica.

No podían faltar en mis agradecimientos mis compañeros del LPI, especialmente con los que he pasado la mayor parte del periodo de la tesis doctoral, Carlos, Rosa, Alejandro, Susana, Elena y Elisa, y Emilio de manera más reciente. Deben estar presentes antiguos miembros del LPI, en concreto Óscar, Santiago, Daniel e Iñaki. Les agradezco la compañía y compartir su tiempo durante estos años.

En relación con el último año, me gustaría incluir entre mis agradecimientos a la doctora Alicia González Martínez, del servicio de Neurología del Hospital Universitario de La Princesa. Agradezco que me haya involucrado en diversos proyectos de gran interés y haber tratado algunos puntos de esta tesis doctoral, en especial alguna de las líneas futuras. Adicionalmente, agradezco la buena relación y lo gratificante que es trabajar con una persona de tanta valía personal y profesional, con un perfil distinto pero complementario respecto al mío.

Desde la perspectiva personal, me gustaría expresar mi gratitud a mis mejores amigos de la carrera por los excelentes momentos compartidos durante estos años, Ángel, Andrei y César por un lado, y en especial a mis amigos que están inmersos en la realización de la tesis doctoral, Virginia, Pablo y Martín. Desde luego incluyo a mis mejores amigos previos a la carrera, Gabriel, Moisés y Martín.

Por supuesto, mi último agradecimiento personal va dedicado a mi hermana Irene, con la que he pasado momentos maravillosos a lo largo de mi vida, y a mis padres Joaquín y María Teresa, que me han apoyado siempre y se han encargado de que no me faltara nada en ningún momento.

Finalmente, agradezco a la Consejería de Educación de la Junta de Castilla y León y el Fondo Social Europeo la financiación proprocionada para llevar a cabo el proyecto de tesis doctoral.

I would also like to thank the International Headache Society and the International Society for Magnetic Resonance in Medicine for the funding provided for the grants related to the International Headache Congress 2019 and the 2020 ISMRM Annual Meeting.

# *Abstract*

Migraine is one of the most common causes of disability, especially among young women. Despite the high migraine prevalence and its consequences, currently there are no migraine biomarkers and the diagnosis is exclusively based on the description of the symptoms by the patient. Furthermore, the migraine pathophysiology is not completely understood yet. In order to find a migraine biomarker and better understand the migraine pathophysiology, Magnetic Resonance Imaging (MRI) has been employed thanks to its excellent tissue contrast and spatial resolution using non-ionizing radiation. Multiple studies that have assessed gray matter and white matter structure in patients with migraine have shown conflicting results, although some patterns such as loss of gray matter volume have been widely described. From the clinical point of view, other important assessments like the comparison between the two current main migraine types, Chronic Migraine (CM) and Episodic Migraine (EM), have been barely carried out. Considering the technical perspective, specific evaluations of the structural connections between gray matter regions and the relationships between the MRI findings from different modalities have not been performed.

In the present doctoral thesis, the main objective was the characterization of gray matter and white matter structural properties of patients with CM and EM. With regard to both migraine groups, the comparison between the two migraine types through the employment of diverse MRI processing techniques is also included in the main objective. The use of advanced and novel diffusion measures not employed previously in the migraine literature was also considered to provide an additional strategy for the assessment of white matter. An evaluation of the diffusion MRI (dMRI) acquisition parameters in association with the sample size was carried out to identify possible sources of the variability. Moreover, the structural connections between gray matter regions through the white matter tracts were assessed, bearing in mind their possible relationship with gray matter morphometry.

On the one hand, the analysis of the migraine patients was performed using methods previously employed in the literature. These methods include morphometry measures for gray matter and diffusion tensor imaging (DTI) parameters in combination with tract-based spatial statistics (TBSS) for white matter. On the other hand, more advanced techniques were implemented to assess migraine patients. These techniques cover methods employed in previous studies, such as tractography and connectomics. Moreover, novel methods recently developed such as Apparent Measures Using Reduced Acquisitions (AMURA) to evaluate diffusion properties were applied. To analyze the relationship between the changes identified in the diverse MRI modalities, the fusion method multimodal Canonical Correlation Analysis followed by joint Independent Component Analysis (mCCA-jICA) was used. This method including was adapted from previous proposals for the assessment of morphometry and connectomics variables.

The sample of the diverse assessments with dMRI data included 56 patients with CM, 54 patients with EM and 50 healthy controls, and 57 and 52 subjects in both migraine groups and the control group, respectively, in the analysis of gray matter morphometry. In the morphometry comparisons, higher cortical curvature values (seven regions) and lower cortical thickness (nine regions), gray matter volume (15 regions) and surface area (25 regions) values were found in migraine patients (one or both groups) compared to controls. These gray matter results are statistically significant with $p < 0.05$ after False Discovery Rate correction for multiple comparisons and post-hoc tests. Regarding the white matter analysis with the DTI descriptors, different trends were obtained in CM with respect to controls. Higher (10 regions, including duration of migraine, aura and medication overuse headache as covariates) and lower fractional anisotropy (other 12 regions, including time from onset of CM as covariate), and lower radial diffusivity (14 regions, adjusted by three covariates) were found in CM compared to controls. Higher axial diffusivity in EM compared to controls was identified in eight regions (adjusted by three covariates). With AMURA, additional differences between EM and controls that could not be identified with conventional DTI parameters were found. Lower return-to-origin probability values were observed in 24 regions in EM compared to controls (no covariates). Additionally, it was observed that lower sample size may be counterbalanced with higher number of diffusion orientations in TBSS studies. The TBSS results are statistically significant with $p < 0.05$ after Family Wise Error or False Discovery Rate correction for multiple comparisons. With regard to connectomics, two different trends were found. The first trend was composed of debilitated structural connections between regions within the diverse lobes (seven connections with lower number of streamlines in patients), and the second trend included strengthened connections with pain processing regions (10 connections with higher number of streamlines in patients). These results were recognized using the connectomics analysis and the mCCA-jICA approach, with specific results provided by each method. The changes of structural connectivity were associated with cortical curvature alterations. These structural connectivity results are statistically significant with $p < 0.05$ after False Discovery Rate correction for multiple comparisons and post-hoc tests.

Diverse statistically significant differences were detected between CM and EM. With respect to gray matter morphometry, surface area differences between both migraine groups in 28 regions were identified, with lower values in CM. In the white matter analysis, lower axial diffusivity values in CM compared to EM were found in 38 regions, obtaining similar results with AMURA and other DTI parameters. Weakened structural connectivity (lower number of streamlines) in CM was detected connections between the caudate nucleus and regions from the orbitofrontal cortex, while strengthened specific altered connectivity (higher number of streamlines) was found in connections with the hippocampus in CM patients. The statistical significance is the same with respect to the comparisons between migraine groups and controls.

Migraine (CM and EM) is characterized by a series of structural gray and white matter changes, including connections between specific gray matter regions. Considering the comparison between both migraine groups, CM follows a set of alterations different from the changes between EM

and controls. The results suggest that CM is an entity with unique properties and substantially different from EM. The surface area could work as a CM biomarker. The findings of this doctoral thesis demonstrated that the DTI model may be insufficient to provide a complete description of the white matter state. AMURA can be employed to complement the results of the classical DTI approach, even in suboptimal conditions for the extraction of advanced diffusion measures. The use of sophisticated fusion approaches such as mCCA-jICA allows the identification of the relationship between the changes observed in diverse MRI modalities and also the identification of additional alterations. Future research should be focused on the analysis of possible migraine subgroups bearing in mind the migraine heterogeneity, longitudinal studies to assess the evolution of CM and EM, and the analysis of the relationships between structural, functional and non-MRI modalities.

---

**Keywords**: Migraine, Gray Matter Morphometry, Diffusion Magnetic Resonance Imaging, Tract-Based Spatial Statistics, Connectomics, Multimodal fusion

# *Acronyms*

**2D** Two-dimensional.

**3D** Three-dimensional.

**4D** Four-dimensional.

**5TT** Five-tissue-type.

**ACT** Anatomically-Constrained Tractography.

**AD** Axial Diffusivity.

**ADC** Apparent Diffusion Coefficient.

**AMURA** Apparent Measures Using Reduced Acquisitions.

**ANCOVA** Analysis of Covariance.

**ANOVA** Analysis of Variance.

**BOLD** Blood Oxygen Level Dependent.

**CCA** Canonical Correlation Analysis.

**CGRP** Calcitonin gene-related peptide.

**CM** Chronic Migraine.

**CSD** Cortical Spreading Depression.

**CSF** Cerebrospinal fluid.

**DKI** Diffusion Kurtosis Imaging.

**dMRI** Diffusion Magnetic Resonance Imaging.

**DSI** Diffusion Spectrum Imaging.

**DTI** Diffusion Tensor Imaging.

**EAP** Ensemble Average diffusion Propagator.

**EEG** Electroencephalography.

**EM** Episodic Migraine.

**EPI** Echo-Planar Imaging.

**FA** Fractional Anisotropy.

**FACT** Fiber Assignment by Continuous Tracking.

**FID** Free-Induction Decay.

**fMRI** Functional Magnetic Resonance Imaging.

**FOD** Fiber Orientation Distribution.

**FSL** FMRIB Software Library.

**HARDI** High Angular Resolution Diffusion Imaging.

**HC** Healthy Controls.

**ICA** Independent Component Analysis.

**ICHD-3** Third edition of the International Classification of Headache Disorders.

**jICA** Joint Independent Component Analysis.

**mCCA** Multimodal Canonical Correlation Analysis.

**MD** Mean Diffusivity.

**miRNA** Micro Ribonucleic Acid.

**MNI** Montreal Neurological Institute.

**MOH** Medication Overuse Headache.

**MRI** Magnetic Resonance Imaging.

**MRS** Magnetic Resonance Spectroscopy.

**MWA** Migraine with Aura.

**MWoA** Migraine without Aura.

**NMR** Nuclear Magnetic Resonance.

**PCA** Principal Component Analysis.

**RD** Radial Diffusivity.

**RF** Radiofrequency.

**ROI** Region of Interest.

**RTAP** Return-to-axis Probability.

**RTOP** Return-to-origin Probability.

**RTPP** Return-to-plane Probability.

**SBM** Surface-Based Morphometry.

**SE** Spin Echo.

**SNR** Signal-to-Noise Ratio.

**TBSS** Tract-Based Spatial Statistics.

**TE** Echo Time.

**TR** Repetition Time.

**VBM** Voxel-Based Morphometry.

**WMH** White Matter Hyperintensities.

# *Contents*

# Part I

# Overview of the doctoral thesis

# *Chapter 1*

# *Introduction*

## 1.1. Context and motivation

In our society, the collaboration between Engineering and Medicine has become crucial to solve clinical problems and provide better healthcare thanks to new diagnosis tools, monitoring devices or surgical instruments. Among the Engineering applications to Health Sciences, a relevant branch is biomedical signal or image processing. In this way, the analysis of the signals or images allows the assessment of the physiological mechanisms or the biological systems and the detection of pathological conditions. However, in some pathologies, the direct visualization of the signals or images by an expert clinician does not give enough information to understand the pathophysiological process. A clear example of this situation takes place with migraine. In patients with migraine, there are no clear alterations of Electroencephalography (EEG) or Magnetic Resonance Imaging (MRI) data, in contrast to other neurological disorders such as epilepsy (specific EEG patterns), stroke or brain tumors (observable lesions in the images). Therefore, in migraine, additional advanced processing steps are necessary in order to quantify the in vivo brain changes and understand the pathological mechanisms using the information contained in MRI or EEG data to provide adequate treatments.

The present doctoral thesis is a clear example of interdisciplinary research that involves the technical and the clinical fields to overcome the limitations of the radiological exploration in patients with migraine. Particularly, this thesis is focused on the study of the in vivo structural properties of gray and white matter of patients with migraine using MRI, a technique that has high spatial resolution and soft tissue contrast using non-ionizing radiation. Thus, the Engineering field gives the support to identify the structural patterns of the migraine brain. In this thesis, advanced methods are developed to extract gray matter and white matter parameters, the properties of structural connections between gray matter regions through white matter and the relationship between the gray matter and connectivity alterations. From the clinical perspective, the analysis of the parameters extracted with the implemented methods allowed the identification of structural alterations and its types. The findings of this thesis can be interpreted to better understand the migraine pathology and define biomarkers for the disease.

With respect to the relevance of the clinical perspective of this thesis, headache is among the most prevalent disorders, and is a cause of large burden. Migraine is the most common type of

primary headache after tension-type headache and it is more widespread among young and middle-aged women. Despite the high prevalence of migraine, the pathophysiological mechanisms of this disorder are not well known and there is no current biomarker for migraine.

Previous migraine MRI studies have been carried out to characterize white matter and gray matter alterations. Regarding the radiological findings, only White Matter Hyperintensities (WMH) have been found, but they have also been found in other pathologies. T1-weighted and Diffusion Magnetic Resonance Imaging (dMRI) data processing techniques have been used to analyze gray and white matter, respectively. The results reported in the migraine studies are conflicting, especially in the case of dMRI studies. The most reported result is the loss of gray matter volume in patients with migraine compared to controls, although the opposite result has also been identified.

In this doctoral thesis, advanced MRI processing techniques applied to T1-weighted and diffusion data are employed to assess the gray and white matter of the brain in migraine patients. On the one hand, methods used previously in the state of art are employed to analyze the structural properties of the migraine brain. In this thesis, there is special focus on the two main migraine types distinguished currently: Episodic Migraine (EM) and Chronic Migraine (CM). These two types have barely been assessed in the literature concerning MRI studies. On the other hand, novel MRI processing methods that have not been applied to the study of migraine or other neurological diseases are implemented.

Therefore, this thesis presents relevant multidisciplinary results. From the technical perspective, a complete framework to study the cross-sectional structural alterations of neurological or psychiatric disorders is provided, including the application of novel methods. Furthermore, the clinical findings contribute to the understanding of migraine, especially regarding the differences between the two types, EM and CM.

## 1.2. Hypotheses and Objectives

MRI is a non-invasive technique that has been demonstrated to serve as an adequate tool to evaluate the brain properties in vivo. Nevertheless, the conventional radiological examination is insufficient to provide information that allows the understanding of the physiological and pathological mechanisms taking place in the migraine brain. This doctoral thesis is focused on the advanced processing of diverse MRI modalities to characterize the brain structural alterations that may be developed in migraine. The research proposal of this doctoral thesis is conducted following the hypotheses and objectives described in this section. Some of the hypotheses stated on this section are based on a detailed analysis of the state of art, which can be found in Chapter 2. Sections 2.2.2 and 2.4 are especially recommended in association with this section.

The **main hypothesis of this study is that the brain of patients with migraine is characterized by specific structural patterns related to the gray and white matter properties**. In patients with CM, the hypothesis is that different patterns are present with respect to the characteristic of EM. The first specific hypotheses of this doctoral thesis are described below:

1. Gray matter cortical and subcortical regions present different properties in patients with migraine compared to Healthy Controls (HC), and in patients with CM compared to EM.

2. White matter properties are distinct between EM and HC, and between CM and EM.

Taking into account that the migraine studies that employ dMRI data have obtained conflicting or non-significant results in the analysis of specific regions, a new hypothesis is stated:

3. The diverse dMRI acquisition parameters influence the results obtained in the statistical comparisons of DTI-based parameters.

In relation to the previous hypothesis and the oversimplification of the DTI model, another hypothesis arises:

4. The use of advanced diffusion models with alternative measures will provide additional information with respect to DTI.

Considering the structural gray matter and white matter properties in migraine patients, the last two hypotheses arise:

5. The gray and white matter specific properties of patients with migraine are associated with unique patterns of structural connectivity.

6. Particular characteristics of gray matter regions are linked to special structural connectivity features of patients with migraine.

Bearing in mind the multidisciplinary nature of this research, some objectives of this thesis are related to the clinical perspective, while others are focused on the technical point of view. The technical objectives can be generally are related to the general study of neurological and psychiatric disorders.

The **main clinical objective of this doctoral thesis is the characterization of the structural gray and white matter alterations that take place in migraine**. The distinction of possible specific features of CM and EM and the extraction of neuroimaging potential biomarkers is also included as main clinical objective. In addition, **another central objective is the identification of possible different structural properties in CM compared to EM**.

The **main technical objective is the evaluation of alternative diffusion models with respect to the diffusion tensor**. These models can overcome the limitations and complement the results from the tensor model. Moreover, **the development of a technique able to assess simultaneously diverse types of MRI data** is a central technical objective of this thesis. This technique includes the analysis of parameters such as morphometry or connectivity in addition to original images or maps.

The specific objectives related to the hypotheses previously described in this section are:

1. To characterize gray matter alterations in CM and EM using morphometric parameters: cortical curvature, cortical thickness, surface area and gray matter volume.

2. To define white matter changes in CM and EM using DTI-based parameters previously employed in the literature: Fractional Anisotropy (FA), Axial Diffusivity (AD), Mean Diffusivity (MD) and Radial Diffusivity (RD).

3. To assess whether advanced measures beyond the diffusion tensor, based on q-space, calculated with a novel approach so-called Apparent Measures Using Reduced Acquisitions (AMURA) (Aja-Fernández et al., 2020) are able to provide additional diffusion information in white matter regions using a dMRI standard acquisition protocol. The advanced measures are the Return-to-axis Probability (RTAP), Return-to-origin Probability (RTOP) and Return-to-plane Probability (RTPP).

4. To evaluate the effect of dMRI acquisition parameters on the statistical comparisons of DTI-based descriptors, together with the effect of the modification of the sample size.

5. To determine the specific alterations of structural connectivity between gray matter regions in CM and EM using a connectomics approach.

6. To find the particular relationships between the gray matter morphometric changes and the structural connectivity alterations in patients with CM and EM.

In the objectives that compare groups of patients (1, 2, 3, 5 and 6), a secondary objective is to analyze the relationship between the MRI parameters and the clinical features. The clinical variables were the duration and frequency of migraine, the presence of aura and suffering from Medication Overuse Headache (MOH). In patients with CM, the time from onset of CM was also assessed.

## 1.3. Methods

This thesis is focused on the study of the migraine brain from different perspectives. To assess the white matter and gray matter changes in migraine, the following approaches were considered:

1. Extraction of morphometry parameters to assess gray matter.
2. Use of the DTI model to analyze white matter regions.
3. Application of a novel alternative diffusion approach to overcome limitations of DTI.
4. Assessment of the dMRI acquisition parameters on the effect of the statistical comparisons. Diverse specific comparisons of the diffusion descriptors between groups of interest were evaluated considering different diffusion acquisition schemes.
5. Study of the white matter connections between gray matter regions with tractography and connectomics.
6. Implementation of a novel fusion procedure to characterize the relationship between gray matter and white matter changes.

In the first stage of this doctoral thesis, gray matter and white matter were assessed independently with methods previously employed in the migraine literature. The gray matter analysis was performed with the statistical analysis of morphometry parameters, extracted from the segmentation of the brain regions using T1-weighted images. The white matter analysis was carried out with the comparison of descriptors based on the diffusion tensor, a model widely employed in the assessment of dMRI.

With regard to dMRI, the diffusion tensor model could be excessively simple to obtain white matter features. Hence, recent alternatives with measures different to those employed in previous migraine studies are applied in order to determine results that could not be found with the model based on the diffusion tensor. Furthermore, an analysis of the influence of the dMRI acquisition parameters on specific differences between the assessed groups was carried out.

In a posterior stage, the gray matter and white matter information from the T1-weighted and dMRI modalities was integrated with a connectomics approach. This technique allows to characterize changes in the structural connectivity between gray matter regions through the white matter tracts. This method is based on tractography and allows to compare adjacency matrices between the groups of interest.

Finally, the relationship between the gray matter morphometry and the structural connectivity was analyzed using a novel fusion analysis approach. The fusion methodology allows to associate the changes in one modality of interest with the alterations in other modality.

## 1.4. Scientific production

In this section, the publications of the author of this doctoral thesis that have been published or accepted for publication during the execution of this thesis are shown. First, the contributions that are included in the compendium of the thesis are detailed, including five journal papers and one international conference, all of them already published. Next, the journal papers with no direct relationship with this thesis are mentioned, together with the international and the national conferences in which the author of this doctoral thesis participated. In the last subsection, the awards and honors associated with the publications of the doctoral thesis are briefly described.

### *1.4.1.* ***Contributions that compose the compendium of publications***

1. **Planchuelo-Gómez, Á.**, García-Azorín, D., Guerrero, Á. L., Rodríguez, M., Aja-Fernández, S., & de Luis-García, R. (2020). Gray matter structural alterations in chronic and episodic migraine: A morphometric magnetic resonance imaging study. *Pain Medicine*, 21 (11), 2997-3011. DOI: 10.1093/pm/pnaa271. (Impact factor: 2.513) (Planchuelo-Gómez, García-Azorín, Guerrero, Rodríguez, et al., 2020)
2. **Planchuelo-Gómez, Á.**, García-Azorín, D., Guerrero, Á. L., Aja-Fernández, S., Rodríguez, M., & de Luis-García, R. (2020). White matter changes in chronic and episodic migraine:

a diffusion tensor imaging study. *The Journal of Headache and Pain*, 21 (1), 1. DOI: 10.1186/s10194-019-1071-3. (Impact factor: 4.797) (Planchuelo-Gómez, García-Azorín, Guerrero, Aja-Fernández, Rodríguez, & de Luis-García, 2020b)

3. **Planchuelo-Gómez, Á.**, García-Azorín, D., Guerrero, Á. L., de Luis-García, R., Rodríguez, M., & Aja-Fernández, S. (2020). Alternative Microstructural Measures to Complement Diffusion Tensor Imaging in Migraine Studies with Standard MRI Acquisition. *Brain Sciences*, 10 (10),711. DOI: 10.3390/brainsci10100711. (Impact factor: 3.332) (Planchuelo-Gómez, García-Azorín, Guerrero, de Luis-García, et al., 2020)
4. **Planchuelo-Gómez, Á.**, Aja-Fernández, S., García-Azorín, D., Guerrero, Á. L., & de Luis-García, R. (2020). Fewer number of gradient directions in diffusion MRI can be counterbalanced with higher sample size: a migraine clinical study. In *Proceedings of the 28th Annual Meeting of the International Society for Magnetic Resonance in Medicine* (Vol. 4550). (Planchuelo-Gómez, Aja-Fernández, García-Azorín, Guerrero, & de Luis-García, 2020)
5. **Planchuelo-Gómez, Á.**, García-Azorín, D., Guerrero, Á. L., Aja-Fernández, S., Rodríguez, M., & de Luis-García, R. (2020). Structural connectivity alterations in chronic and episodic migraine: A diffusion magnetic resonance imaging connectomics study. *Cephalalgia*, 40 (4), 367-383. DOI: 10.1177/0333102419885392. (Impact factor: 4.868) (Planchuelo-Gómez, García-Azorín, Guerrero, Aja-Fernández, Rodríguez, & de Luis-García, 2020a)
6. **Planchuelo-Gómez, Á.**, García-Azorín, D., Guerrero, Á. L., Aja-Fernández, S., Rodríguez, M., & de Luis-García, R. (2021). Multimodal fusion analysis of structural connectivity and gray matter morphology in migraine. *Human Brain Mapping*, 42 (4): 908-921. DOI: 10.1002/hbm.25267. (Impact factor: 4.421) (Planchuelo-Gómez et al., 2021)

### *1.4.2. Papers not included in the Doctoral Thesis*

1. **Planchuelo-Gómez, Á.**, Lubeiro, A., Núñez-Novo, P., Gomez-Pilar, J., de Luis-García, R., del Valle, P.,... Molina, V. (2020). Identification of MRI-based psychosis subtypes: Replication and refinement. *Progress in Neuro-Psychopharmacology and Biological Psychiatry*, 100, 109907. DOI: 10.1016/j.pnpbp.2020.109907
2. Odriozola-González, P., **Planchuelo-Gómez, Á.**, Irurtia, M.J., & de Luis-García, R. (2020). Psychological effects of the COVID-19 outbreak and lockdown among students and workers of a Spanish university. *Psychiatry Research*, 290, 113108. DOI: 10.1016/j.psychres.2020.113108
3. Trigo, J., García-Azorín, D., **Planchuelo-Gómez, Á.**, Martínez-Pías, E., Talavera, B., Hernández-Pérez, I.,... Guerrero, Á.L. (2020). Factors associated with the presence of headache in hospitalized COVID-19 patients and impact on prognosis: a retrospective cohort study. *The Journal of Headache and Pain*, 21(1), 1-10. DOI: 10.1186/s10194-020-01165-8
4. **Planchuelo-Gómez, Á.**, Odriozola-González, P., Irurtia, M.J. & de Luis-García, R. (2020). Longitudinal evaluation of the psychological impact of the COVID-19 crisis in Spain. *Journal of Affective Disorders*, 277, 842-849. DOI: 10.1016/j.jad.2020.09.018

5. Odriozola-González, P., **Planchuelo-Gómez, Á.**, Irurtia, M.J. and de Luis-García, R. (2020). Psychological symptoms of the outbreak of the COVID-19 confinement in Spain. *Journal of Health Psychology* [Epub ahead of print]. DOI: 10.1177/1359105320967086

6. Trigo López, J., García-Azorín, D., **Planchuelo-Gómez, Á.**, García-Iglesias, C., Dueñas-Gutiérrez & Guerrero, Á.L. (2020). Phenotypic characterization of acute headache attributed to SARS-CoV-2: An ICHD-3 validation study on 106 hospitalized patients. *Cephalalgia*, 40(13):1432-1442. DOI: 10.1177/0333102420965146

7. Fernández-Linsenbarth, I., **Planchuelo-Gómez, Á.**, Díez, Á., Arjona-Valladares, A., de Luis, R., Martín-Santiago, Ó.,... Molina, V. (2020). Neurobiological underpinnings of cognitive subtypes in psychoses: A cross-diagnostic cluster analysis. *Schizophrenia Research* [Epub ahead of print]. DOI: 10.1016/j.schres.2020.11.013

8. **Planchuelo-Gómez, Á.**, García-Azorín, D., Guerrero, Á.L., Aja-Fernández, S., Antón-Juarros, S. & de Luis-García, R. (2020). Response prediction for chronic migraine preventive treatment by gray matter morphometry in magnetic resonance imaging: a pilot study. *Revista de Neurologia*, 71(11):399-406. DOI: 10.33588/rn.7111.2020488

9. **Planchuelo-Gómez, Á.**, Trigo J, de Luis-García, R., Guerrero, Á.L., Porta-Etessam, J. & García-Azorín, D. Deep Phenotyping of headache in hospitalized COVID-19 patients via Principal Component Analysis. *Frontiers in Neurology*, 11:583870. DOI: 10.3389/fneur.2020.583870

10. Gonzalez-Martinez, A., **Planchuelo-Gómez, Á.**, Guerrero, Á.L., García-Azorín, D., Santos-Lasaosa, S., Navarro-Pérez, M.P.,... Gago-Veiga, A.B. (2021). Evaluation of the impact of the Covid-19 lockdown in the clinical course of migraine. *Pain Medicine* [Epub ahead of print]. DOI: 10.1093/pm/pnaa449. Note: the first two authors contributed equally to this work.

11. Sánchez-Rodríguez, C, Sierra, Á, **Planchuelo-Gómez, Á.**, Martínez-Pías, E., Guerrero, Á.L. & García-Azorín, D. (2021). Real world effectiveness and tolerability of Candesartan in the treatment of migraine: a retrospective cohort study. *Scientific Reports*, 11:3846. DOI: 10.1038/s41598-021-83508-2

12. García-Azorín, D, Abelaira-Freire, J, Rodriguez-Adrada, E, González-García, N, **Planchuelo-Gómez, Á.**, Guerrero, Á.L.,... Martín-Sánchez, F.J. (2021). Temporal distribution of emergency room visits in patients with migraine and other headaches. *Expert Review of Neurotherapeutics* [Epub ahead of print]. DOI: 10.1080/14737175.2021.1906222

13. Gonzalez-Martinez, A., **Planchuelo-Gómez, Á.**, Guerrero, Á.L., García-Azorín, D., Santos-Lasaosa, S., Navarro-Pérez, M.P.,... Gago-Veiga, A.B. (2021). Effects of the onabotulinumtoxinA follow-up delay in migraine course during the COVID-19 lockdown. *Neurological Sciences* [Epub ahead of print]. DOI: 10.1007/s10072-021-05180-8. Note: the first two authors contributed equally to this work.

### 1.4.3. Conference contributions not included in the Doctoral Thesis

International conferences:

1. **Planchuelo-Gómez, Á.**, García-Azorín, D., Guerrero, Á.L., Aja-Fernández, S., Rodríguez, M. & de Luis-García, R. (2019). White Matter Alterations in Chronic Migraine: A Diffusion Tensor Imaging and Structural Connectivity Study. In *Abstracts of the 19th International Headache Congress of the International Headache Society*, 2019 Sep 5-8; Dublin, Ireland. *Cephalalgia*, 39(1_suppl):171.
2. **Planchuelo-Gómez, Á.**, de Luis-García, R., Tristán-Vega, A., García-Azorín, D., Guerrero, Á.L. & Aja-Fernández, S. (2020). AMURA with standard single-shell acquisition can detect changes beyond the Diffusion Tensor: a migraine clinical study. In *Proceedings of the 28th Annual Meeting of the International Society for Magnetic Resonance in Medicine*, 2020 Aug 8-14; Virtual Conference; vol. 4549.

National conferences:

1. **Planchuelo Gómez, Á.**, García Azorín, D., Guerrero Peral, Á.L., Aja Fernández, S., Antón-Juarros, S. & de Luis García, R. (2019). Desarrollo de un modelo de predicción de respuesta al tratamiento preventivo en migraña crónica mediante medición de sustancia gris en resonancia magnética. In *Abstracts de la LXXI Reunión Anual de la Sociedad Española de Neurología*, 2019 Nov 19-23; Seville, Spain.
2. **Planchuelo Gómez, Á.**, García Azorín, D., Guerrero Peral, Á.L., Aja Fernández, S., Rodríguez Velasco, M. & de Luis García, R. (2020). Análisis multimodal conjunto de conectividad estructural y morfología de sustancia gris para detección de nuevos patrones de cambio en migraña crónica y episódica. In *Abstracts de la LXXII Reunión Anual de la Sociedad Española de Neurología*, p. 15, 2020 Nov 23-Dec 3; Virtual Conference.
3. González Martínez, A., Martínez Dubarbie, F., Vieira Campos, A., **Planchuelo Gómez, Á.**, Vivancos, J. & de Toledo Heras, M. (2020). Utilidad de las escalas de ansiedad GAD-7, depresión NDDI-E, somnolencia Epworth y calidad de vida QOLIE-31-P en pacientes con epilepsia en práctica clínica real. In *Abstracts de la LXXII Reunión Anual de la Sociedad Española de Neurología*, p. 93, 2020 Nov 23-Dec 3; Virtual Conference.

### 1.4.4. Awards and Honors

Financially supported awards:

- Grant to fund the hiring of predoctoral research staff. Four-year contract to develop the doctoral thesis project. Project: *Resonancia magnética para el estudio de la migraña episódica y crónica: análisis multimodal de la estructura y conectividad cerebral* (Magnetic Resonance for the study of episodic and chronic migraine: multimodal brain structure and connectivity analysis). Funders: Junta de Castilla y León and European Social Fund. Date: June 2018.

- International Headache Congress 2019 Travel Grant. Grant to fund the costs associated with the registration to the congress, flights and stay (hotel costs). Funder: International Headache Society. Date: September 2019.
- International Society for Magnetic Resonance in Medicine (ISMRM) Educational Stipend. Grant to fund the costs associated with the registration to the congress (originally, it also included costs related to the flight and stay, but the congress was held virtually due to the COVID-19 pandemic). Funder: International Society for Magnetic Resonance in Medicine. Date: August 2020.

Reports and interviews related to the doctoral thesis research:

- Interview related to the article *Structural connectivity alterations in chronic and episodic migraine: A diffusion magnetic resonance imaging connectomics study*. The interview was conducted by the International Headache Society. Original link (available January 7, 2020): `https://www.youtube.com/watch?v=39lPKXEh7mY`. Link 2: `https://drive.google.com/file/d/1pLikJybONG_dF-jUbyMSUdOXywItOvgZ/view?usp=sharing`. Date: December 2019.
- Report in Spanish entitled *Imágenes cerebrales permiten diferenciar migraña episódica y crónica* (Brain images allow to differentiate episodic and chronic migraine). The report was conducted by the Agencia Iberoamericana para la difusión de la ciencia y la tecnología (DiCYT). Link (available November 28, 2020): `https://www.dicyt.com/noticias/imagenes-cerebrales-permiten-diferenciar-migrana-episodica-y-cronica`. Date: April 2020.
- Report entitled *Research Points to a Potential Imaging Biomarker for Migraine*. The report was conducted by the Radiology Society of North America. Link: (available November 28, 2020): `https://www.rsna.org/en/news/2020/July/Migraine-Imaging-Biomarkers`. Date: July 2020.

Main cover of scientific journals in relation to the articles that compose the compendium:

- Main cover illustration for Volume 40, Issue 4 of *Cephalalgia*. Date: April 2020.
- Main cover illustration for Volume 42, Issue 4 of *Human Brain Mapping*. Date: March 2021.

## 1.5. Structure of the document

This thesis is composed of two main parts. The first part is an extended overview of the thesis, considering the thesis as a whole, i.e., the results of the articles that compose the compendium of publications are grouped and a joint discussion is carried out. In the first part, there is no independent and exhaustive description of the results of each paper. In the second part, the consistency between the articles of the compendium is described in detail and the papers that compose the compendium are adapted and reproduced. The detailed description of each set of results is included in the second part.

Regarding part I, in Chapter 2, the background and state of art related to MRI and migraine are detailed. In Chapter 3, the database and the methods employed in the analysis of the patients

with migraine are outlined. In Chapter 4, the results of the thesis are exposed. In Chapters 5 and 6, the discussion and conclusions of the doctoral thesis are depicted.

The state of art detailed in Chapter 2 includes firstly the explanation of the most important features of migraine, concepts of MRI and the modalities employed in the structural analysis (T1-, T2- and diffusion-weighted imaging). Next, the description of methods associated with the analysis of structural connectivity and the combination of MRI modalities are described. A detailed exposition of the previous neuroimaging studies with migraine patients is covered in the final sections of Chapter 2.

The total number of subjects and the characteristics of the patients with migraine and the controls included in the sample are described on the first part of Chapter 3. In the second part of the chapter, the methods implemented and the associated concepts for the analysis of migraine patients are explained. These methods include the gray matter morphometry and the dMRI preprocessing and processing steps. DMRI processing covers the diffusion tensor model and the alternative presented in this thesis, Apparent Measures Using Reduced Acquisitions (AMURA), connectomics, the fusion of MRI modalities and the statistical analysis.

In Chapter 4, the results of the thesis are presented, regarding the comparisons between migraine patients and controls on the one hand, and between patients with CM and EM on the other hand. All the comparisons were carried out after the methods mentioned in the previous paragraph. Two additional assessments are included in this chapter. The first evaluation is the relationship between the clinical and MRI measures. The other analysis is focused on the effects of the diffusion acquisition parameters and the sample size on specific comparisons of diffusion parameters.

The discussion of the clinical and technical findings and the limitations of the thesis is carried out in Chapter 5. With regard to the clinical findings, the most important aspects of the discussion are related to the structure of the migraine brain and the specific characteristics of CM. In the case of the technical findings, the importance of sophisticated MRI processing and multimodal MRI is discussed. The conclusions reported in Chapter 6 are referred to the outcomes and contributions of this thesis, particularly the publications that compose the compendium, and future research lines.

With regard to Part II, the relationship between the different publications is explained, bearing in mind the objectives of the doctoral thesis. In this relationship, the assessment of the individual white matter and gray matter features and the advanced processing methods integrating diverse modalities for the extraction sophisticated information are considered. The remaining chapters of Part II (Chapters 1-6) contain each publication that composes the compendium. These chapters start with a brief introduction at the beginning followed by the proper adapted publication.

# *Chapter 2*

# *Background and state of the art*

In this chapter, the most important concepts about migraine and magnetic resonance are outlined and the state of the art of neuroimaging migraine studies is depicted.

## 2.1. Migraine

This thesis is focused in the analysis of migraine and its types, CM and EM. Migraine is a disabling primary disorder characterized by recurrent episodes of headache. According to the Third edition of the International Classification of Headache Disorders (ICHD-3), headache attacks usually last 4-72 hours (Headache Classification Committee of the International Headache Society, 2018). Headache in migraine presents at least two of the following four characteristics:

1. Unilateral location.
2. Pulsating quality.
3. Moderate to severe pain intensity.
4. Aggravated by routine physical activity.

During headache, at least one of the following symptoms is present in migraine:

1. Nausea and/or vomiting.
2. Photophobia and phonophobia.

In addition to the previous symptoms, osmophobia is present frequently, although it is not considered among the migraine clinical criteria. Moreover, migraine attacks are sometimes preceded or accompanied by the aura, a set of visual, sensitive and language neurological symptoms. The first distinction of migraine types was precisely related to the aura, classified as Migraine with Aura (MWA) and Migraine without Aura (MWoA). However, it is unclear whether these two types are manifestations of the same pathophysiological substrate manifested on two different phenotypes (Granziera, DaSilva, Snyder, Tuch, & Hadjikhani, 2006; Pietrobon & Moskowitz, 2013), or whether aura is just a migraine phase (Dodick, 2018).

Currently, two types of migraine are considered: Episodic Migraine (EM) and Chronic Migraine (CM). Despite this classification, the differences between both types have been barely assessed in

the neuroimaging literature. The analysis of the differences between CM and EM is one of the main goals of this thesis. According to the ICHD-3, CM is defined by recurrent headache episodes during 15 or more days per month for more than three months, with at least eight of these days of headache with the migrainous characteristics (Headache Classification Committee of the International Headache Society, 2018). Patients with EM suffer from headache less than 15 days per month. Nevertheless, other cutoffs such as 8 and 10 days per month have been proposed to distinguish both types (Chalmer et al., 2020; Torres-Ferrús, Quintana, Fernandez-Morales, Alvarez-Sabin, & Pozo-Rosich, 2017).

### 2.1.1. Epidemiology of migraine

The prevalence of migraine depends on the geographic area, gender and age. The prevalence in Africa and Asia (6-8% in women and 2-2.5% in men) is lower compared to the prevalence in Europe and America (14-22% in women and 5-8% in men). Women are about twice as likely to suffer from migraine than men, and prevalence is higher in ages 25-55 (Lipton & Bigal, 2005). According to data from the United States of America, the prevalence of migraine is inversely related to socioeconomic status, but this result has not been replicated in European studies (Lipton & Bigal, 2005). In relation to CM, approximately 2.5% of the patients with EM develop CM each year and 7-10% of the total patients with migraine present CM (Adams et al., 2015; Manack, Buse, & Lipton, 2011).

Migraine is an important public health problem not only because of its relative high prevalence, but also due to the associated costs. Direct costs include migraine medication and health care expenses, and indirect costs are related to worse work performance and reduced productivity associated with absenteeism (Lipton & Bigal, 2005). Migraine has been reported as the neurological disorder with the highest disability-adjusted life years, standarized by age, in a study conducted in the United States (Bazargan-Hejazi et al., 2020). In Europe, the annual cost of migraine was €1222 on average per person, including 93% of indirect costs, according to a study conducted in 2012 (Linde et al., 2012).

Considering the prevalence of migraine and its impact on the public health, the study of the migraine pathophysiological mechanisms is highly relevant in order to apply appropriate preventive and therapeutic measures.

### 2.1.2. The migraine cycle

Migraine is a cyclic disorder that can be divided in four symptomatic stages and one intermediate stage between attacks. The four symptomatic stages are briefly described next:

1. **Premonitory phase** (also known as prodromal phase). This stage can begin three days before an attack, and some patients can predict migraine headache up to 12 hours before its onset (Dodick, 2018). Among the symptoms experienced in this phase, the most common

are fatigue, mood changes, food cravings, yawning, muscle tenderness, photophobia, phonophobia and nausea (A. Charles, 2013; Dodick, 2018). Functional MRI studies have shown the involvement of the hypothalamus during this phase (Dodick, 2018).

2. **Aura**. This phase is present approximately in one third of migraine attacks (Noseda & Burstein, 2013). Characteristics of aura have been described previously (section 2.1). The visual disturbances are the most common symptoms of aura (Dodick, 2018). The aura is accompanied, or followed within one hour, by headache and the symptoms last 5-20 minutes (Headache Classification Committee of the International Headache Society, 2018).
3. **Headache** (also known as ictal phase). This phase presents the features described previously (section 2.1). Blood flow changes together with functional alterations in the brainstem, thalamus, hypothalamus and the cortex are associated with this stage. Among the chemical mediators of migraine, the Calcitonin gene-related peptide (CGRP) has been highlighted as a key element in the migraine pathogenesis (Dodick, 2018). The development of neuronal sensitization and pain generation in migraine has been associated with the somatosensory function of CGRP (Iyengar, Ossipov, & Johnson, 2017).
4. **Postdromal phase**. In this stage, some symptoms occur for hours or days after the headache phase. Among these symptoms, the most frequent include tiredness, weakness, cognitive difficulties and mood change (A. Charles, 2013).

The interictal phase is the period between attacks. The patients that compose the database employed in this thesis were in interictal state during the MRI acquisition.

### *2.1.3.* ***Pathophysiology of migraine***

The pathophysiology of migraine is complex and, according to the previous research, there are differences between the interictal phase and the four symptomatic stages of migraine.

A characteristic of the migrainous brain in all the phases is that it is hyperexcitable, i.e., very sensitive to visual, auditive and somatosensory stimuli. This hyperexcitability could be related to an imbalance between excitatory and inhibitory neurotransmitters, with a possible genetic codification (Morollón Sánchez-Mateos, 2020).

Regarding the prodromal phase, it has been hypothesized that the migraine pathogenesis is associated with the imbalance of the brainstem nuclei regulating antinociception and vascular control (Weiller et al., 1995). Furthermore, the activation of the hypothalamus has been suggested to explain the prodromal symptoms (Maniyar, Sprenger, Monteith, Schankin, & Goadsby, 2014). In contrast to the suggested role of the brainstem nuclei, it has been reported that the real driver of migraine attacks would be the alterations of the functional connectivity between the brainstem and the hypothalamus (Schulte & May, 2016).

With respect to aura, it has been associated with Cortical Spreading Depression (CSD). CSD is a slowly propagating wave of sustained depolarization (cortical excitation followed by inhibition) associated with functional neuronal, glial and vascular changes (A. C. Charles & Baca, 2013). CSD

involves molecular changes in cortical upregulation of genes linked to the inflammatory process (Borsook, Maleki, & Burstein, 2015). Migraine with aura would start by waves of CSD and this mechanism would lead to delayed activation of the trigeminovascular pathway (Borsook et al., 2015). The relationship between CSD and migraine without aura is not clear yet.

The main pathophysiological theory of the migraine ictal state comes from the central and peripheral (trigeminovascular) theories. Following these theories, exogenous (e.g. stress or weather) or endogenous (e.g. hormonal imbalances or sleep deprivation) factors would cause a cortical depolarization of the hyperexcitable migrainous brain (Morollón Sánchez-Mateos, 2020). These factors or triggers are highly variable between patients. The origin of the ictal phase in migraine would be related to the peripheral innervation of the trigeminovascular system. The activation of nociceptors innervating meningeal blood vessels, cerebral arteries and sinuses would generate the pain with migraine characteristics (pulsating and throbbing) and the migrainous symptoms such as nausea, photophobia and phonophobia (Noseda & Burstein, 2013). The unmyelinated and slightly myelinated axons are involved in the nociceptive innervation of intracranial and meningeal vasculature. When the meningeal nociceptive fibers are activated, possibly in association with CSD, vasoactive neuropeptides such as substance P and CGRP are released, which would cause hyperemia and vasodilation related to the activation of the nociceptors (Morollón Sánchez-Mateos, 2020; Noseda & Burstein, 2013).

An important previous migraine theory is the vasogenic theory. Briefly, vasoconstriction would be associated with aura and followed by vasodilation, which would be the origin of pain through the activation of peripheral nociceptive fibers (Morollón Sánchez-Mateos, 2020). However, this theory is not widely accepted because there is no evidence for extracranial vasodilation in patients undergoing spontaneous attacks (Amin et al., 2013).

The mechanisms that activate the trigeminovascular pathway and CSD, especially in migraine without aura, are not well understood yet. Among the concepts related to this activation and CSD, the role of serotonin, excitatory neurotransmitters (glutamate) or magnesium among some molecules should be elucidated. Another important question that should be answered is whether migraine structural alterations are cause or consequence of migraine.

### *2.1.4.* ***Diagnosis and Neuroimaging***

To date, the diagnosis of migraine is exclusively based on the symptoms described previously according to the ICHD-3. This implies that currently there is no biomarker for migraine. Moreover, the phenotype of chronic headaches is frequently unclear (Weatherall, 2015). Sometimes, not all criteria for migraine from the ICHD-3 are fulfilled in migraine-like or other headaches, including classifications such as Probable migraine or Headache unspecified in the ICHD-3. These types of headache are associated with the variability of migraine and lack of information about the headaches. Consequently, in some patients, it is especially difficult to provide an adequate treat-

ment. Hence, biomarkers would contribute to determine an accurate diagnosis and prescribe an appropriate treatment.

With respect to neuroimaging, the main employed modalities for the examination of patients with migraine are MRI and computed tomography. In the clinical routine, there is no need to acquire neuroimaging data in patients with migraine who have a normal neurological examination (Evans et al., 2020). Neuroimaging is recommended with grade A[1] in specific situations such as increasing frequency or severity, first or worst migraine, and unusual, prolonged or persistent aura (Evans et al., 2020).

Regarding radiological findings, increased risk of WMH detected on MRI has been reported in patients with migraine (Porter, Gladstone, & Dodick, 2005). WMH have been also associated with pain in patients with EM and an adverse prognosis (Xie et al., 2018; Yalcin, Ceylan, Bayraktutan, & Akkurt, 2018). However, WMH are not specific to migraine and are frequently found in patients with cerebrovascular diseases and severe cognitive decline (Carole et al., 2009).

The lack of migraine-specific radiological findings makes necessary the advanced processing of MRI data in order to identify migraine image-based biomarkers. Taking into account the absence of knowledge about some aspects of the migraine pathophysiology, as described in section 2.1.3, this thesis can provide important information to the state of art. This information is related to the extraction of migraine biomarkers using advanced MRI processing techniques, a central objective of this thesis, as stated in the section 1.2.

### *2.1.5.* ***Treatment***

Currently, there is no treatment to suppress migraine. Treatments for migraine are organized in three main groups: non-pharmacological treatment, acute treatment and preventive treatment.

The non-pharmacological treatment is mainly related to lifestyle habits and following a routine. Some recommendations for the patients include a balanced diet, especially to avoid overweight, maintain an adequate hydration, and regular exercise (Burch, 2019). Stress related to work and sleep quality and duration also has a great impact on migraine. There are no non-pharmacological interventions for migraine with level A evidence[2], but some level B[3] treatments include magnesium and relaxation training or cognitive-behavioral therapy for prevention (Burch, 2019).

The acute or symptomatic treatment is employed to relieve the pain of a migraine episode, although an excessive use may lead to a headache known as Medication Overuse Headache (MOH). The main types of acute treatments are the analgesics, non-steroidal anti-inflammatory drugs,

[1]Recommendation Grade A is the highest level of evidence for diagnostic tests. Other levels are B (fair evidence), C (conflicting or poor-quality evidence) and I (insufficient evidence)

[2]Level A represents the highest level of evidence for the results of a treatment. It requires support by at least two class I studies, i.e., randomized control clinical trials with concealed allocation, clearly defined primary outcomes and inclusion-exclusion criteria, and adequate accounting for dropouts

[3]Level B is the second level of evidence after level A. It requires support by one class I study or two class II studies, which include randomized clinical trials fulfilling the same criteria except one of the class I studies and prospective cohort studies with the same criteria as class I studies except concealed allocation

triptans and ergot derivatives and opioids (Burch, 2019). The previous classes present at least one option with level A evidence except the opioids, with level B (Burch, 2019). Moreover, without applicable level of evidence, the antiemetics can be used as symptomatic treatment for migraine (Burch, 2019).

The preventive treatment is used to gradually reduce frequency and/or intensity of headache, especially when the exclusive employment of acute treatment is unsatisfactory to manage migraine. The main classes of preventive treatment are the antidepressants, antihypertensives, antiepileptic drugs and other treatments (Burch, 2019). Among other treatments, two groups should be highlighted. The first group is referred to the Onabotulinumtoxin A, which is used in patients with high frequency of headache. The most recent group of preventive treatments refers to the monoclonal antibodies to CGRP, developed specifically for migraine, in contrast to the other treatments (Burch, 2019).

The characterization of structural and functional properties using neuroimaging can contribute to the *personalized medicine* with the definition of the targets of treatment for each patients. A clear example of this definition has been proposed for psychiatric disorders and the use of transcranial magnetic stimulation (Etkin, 2014). In this case, neuroimaging would be used to identify the altered brain circuit and the involved areas would be stimulated. In the case of migraine, transcranial magnetic stimulation has not been widely studied, although promising results have been reported stimulating motor cortex areas, with minimal side effects (Hulla & Liegey-Dougall, 2019).

## 2.2. Magnetic Resonance Imaging

This thesis is focused on the advanced processing of MRI data for the study of migraine. To fully understand the methods and the associated results, it is important to introduce the most basic concepts of MRI.

Thanks to its advantages, MRI is one of the main biomedical imaging modalities with clinical applications. It is used to study tissues in vivo in diverse medical disciplines, including multiple regions such as the brain, heart, vertebral column, liver, prostate and knee. The main advantage of MRI is the use of non-ionizing radiation, which is less dangerous for the health in comparison with the ionizing radiation of X-rays and gamma-rays employed by other medical imaging modalities. Other advantages are the acquisition of Two-dimensional (2D) or Three-dimensional (3D) images, excellent contrast of soft tissue and good spatial resolution (around 1 $mm^3$ in T1-weighted images). Some disadvantages are the long acquisition time with respect to other medical imaging modalities like computed tomography and medical ultrasound, the high cost of the scanners and the limited use in some people due to reasons such as some metallic implants or claustrophobia.

With respect to the origin of MRI, in 1938 it was proposed that the nuclear spins of the molecules are reoriented if a small oscillating magnetic field is applied at right angles to a much larger constant field when the frequency of the oscillating field is close to the Larmor frequency of precession of the specific angular momentum vector (Rabi, Zacharias, Millman, & Kusch, 1938). In

1946, Bloch and Purcell independently demonstrated Nuclear Magnetic Resonance (NMR) (Bloch, 1946; Purcell, Torrey, & Pound, 1946). In 1971, the first medical application of NMR for tumor detection was reported (Damadian, 1971). Two years later, Lauterbur proposed a technique called Zeugmatrography, using linear magnetic field gradients for the spatial localization of the NMR signal to generate images, and Mansfield refined the image acquisition and processing techniques (Garroway, Grannell, & Mansfield, 1974; Lauterbur, 1973; Mansfield & Grannell, 1973). Due to the discoveries concerning MRI, Sir Peter Mansfield and Paul C. Lauterbur won the Nobel Prize in Physiology or Medicine 2003.

To understand the basic principles of the contrast of the main MRI modalities, some concepts of MRI physics are briefly described.

The NMR principle of medical MRI is based on the magnetic properties of the atomic nuclei of the biological tissues. Water constitutes 60-80% of human tissues and two thirds of water are composed of hydrogen atoms (a unique proton), whose properties are usually employed for the extraction of MRI. When an external strong external magnetic field is applied, most hydrogen unpaired nuclei align themselves with the direction of the magnetic field. This uniform external magnetic field is known as $B_0$.

After the application of $B_0$, a second Radiofrequency (RF) field known as perpendicular to $B_0$ is applied. The RF field is known as $B_1$. The RF pulse causes the net magnetic moment to tilt away from $B_0$. Once the RF pulse has ceased, the atomic nuclei emit the electromagnetic energy back, the magnetic resonance signal, at the resonance frequency. This signal is termed Free-Induction Decay (FID) response signal and is measured by a conductive field coil place around the Region of Interest (ROI). The reconstruction of this measurement allows the 3D MRI extraction.

The production of a 3D image requires the spatial encoding of the FID signal for each dimension. To this end, multiple gradients are applied in each direction. These gradients are the slice selection gradient, the phase codification gradient and the frequency codification gradient. Briefly, these gradients are generally used to select a slice ($z$-direction) and the positions in the $y$- and $x$-directions, respectively. Alternatively, the phase and frequency gradients can be employed to codify the 3D position and not just 2D slices.

The signal and contrast of each type of tissue mostly depend on three additional properties. These properties are the proton density, the longitudinal relaxation or spin-lattice relaxation time (T1), and the transverse relaxation or spin-spin relaxation time (T2). Briefly, proton density is the number of protons per volume unit and is linked to stronger FID. T1 is related to the time needed for the magnetic moment of the displaced nuclei to realign with $B_0$. T2 is associated with the time needed for the FID signal to decay and for the spins to dephase. Considering $B_0$ inhomogeneities, the term $T2^*$ is used instead of T2. For a specific tissue, $T2^*$ is always shorter than T2.

To carry out measures based on T1, T2 or proton density and highlight specific tissues, two parameters selected by the operator with no relationship with any biological property are used:

- **Repetition Time (TR)**. This is the time between one RF pulse and the next one.

- **Echo Time (TE)**. This is the time between the application of a RF pulse and the measurement of the FID signal.

To acquire images with diverse contrasts, pulse sequences are employed. These pulse sequences are composed of diverse combinations of RF pulses and the gradients described in this section. Currently, there are many types of pulse sequences that can be used in the clinical routine. These sequences are used to reduce the acquisition time, increase contrast, reduce possible artifacts or suppress the signal from certain types of tissues, among other reasons. A detailed analysis of pulse sequences and the previous concepts of this section, as well as a discussion of fast or parallel acquisitions, is beyond the scope of this thesis.

In the following sections, the main MRI modalities employed to evaluate brain structure are described.

### *2.2.1.* ***T1- and T2-weighted imaging***

The adjustment of TR and TE allows the contrast of diverse tissues in MRI. T1-weighted images are characterized by high quality compared to other biomedical imaging techniques, good resolution (the best among MRI modalities) and good contrast between gray matter and white matter. These properties allow an adequate segmentation of diverse gray matter and white matter regions. Processing of T1-weighted images is a central method of this thesis to segment gray matter regions and determine their corresponding morphometry characteristics.

Basically, the contrast of T1-weighted images is based on the longitudinal magnetization, which is related to the values of TR. In the simplest case, this relation is as shown in the following equation:

$$M_z(\mathrm{TR}) = M_0(1 - e^{-\frac{\mathrm{TR}}{\mathrm{T1}}}), \tag{2.1}$$

where $M_z$ is the longitudinal magnetization and $M_0$ is the value of the magnetic moment in the state of equilibrium. T1 is characteristic for each tissue and is defined as the time when $M_z$ reaches the value equal to the 63% of $M_0$.

The contrast of T2-weighted images is essentially based on the transverse magnetization, which is based on the values of TE. In the most elementary case, this relation is as shown in the following equation:

$$M_{xy}(\mathrm{TE}) = M_0 \cdot e^{-\frac{\mathrm{TE}}{\mathrm{T2}}}, \tag{2.2}$$

where $M_{xy}$ is the transverse magnetization. T2 is characteristic for each tissue and is defined as the time when $M_{xy}$ reaches the value equal to the 37% of $M_0$. It is worth noting that the contrast of T1- and T2-weighted images varies depending on the employed pulse sequence, and thus the previous statements are a simplification of the factors that contribute to the contrast.

Liquids have long T1 and T2 because of the dispersed structure of water, which is composed of small molecules with high movement frequency and minimum spin-spin interaction. Solids present

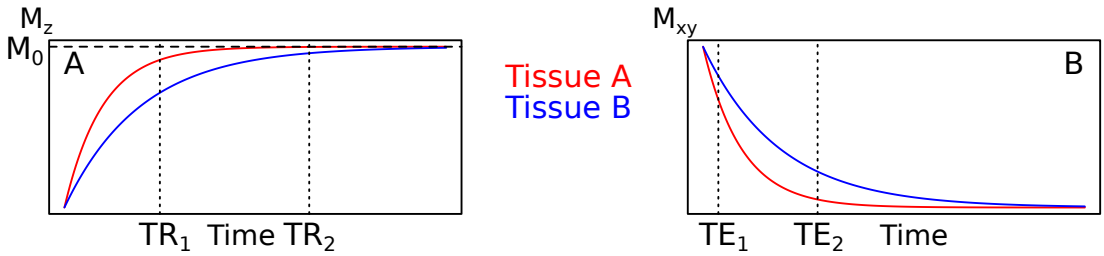


**Figure 2.1:** Constrast of T1- and T2-weighted images. In Subfigure A, the difference of $M_z$ values between both tissues is higher for a short TR ($TR_1$) than for a long TR ($TR_2$). In Subfigure B, the difference of $M_{xy}$ values between both tissues is higher for a long TE ($TE_2$) than for a short TE ($TE_1$).

intermediate T1 and short T2 values (great interaction spin-spin), while fats present short T1 and intermediate T2 values.

To illustrate the contrast of the different tissues in T1- and T2-weighted images, an example with two tissues A and B is shown in Figure 2.1.

Considering that short TR values are related to higher T1-based contrast, T1-weighted images are obtained using short TR and TE values. In contrast, T2-weighted images are extracted using long TR and TE values.

The human brain tissue is composed of three main elements (excluding pathological tissues):

- **Gray matter**. Its properties are similar to solids. In T1-weighted images it looks gray, while in T2-weighted images it looks light gray.
- **White matter**. Its properties are similar to fat due to the myelin sheath surrounding the nerve cell axons. In T1-weighted images it looks white, while in T2-weighted images it looks dark gray.
- **Cerebrospinal fluid (CSF)**. Its properties are similar to water. In T1-weighted images it looks black, while in T2-weighted images it looks white.

An example of a T1- and a T2-weighted image is shown in Figure 2.2.

In this thesis, T1-weighted images are used to analyze gray matter morphometric features. In migraine studies, T2-weighted images are sometimes employed to assess the presence of WMH.

### *2.2.2. Diffusion MRI*

One of the most relevant MRI modalities is diffusion MRI. The objective of dMRI is to capture and quantify the microscopic movement of the water molecules caused by diffusion. This modality has been widely employed to assess brain structure and connectivity, and it has been particularly useful in the management of stroke (Le Bihan, 2014). Furthermore, dMRI allows to study the white matter integrity. In this thesis, dMRI processing is used to evaluate the microstructural properties in diverse white matter regions and the structural connectivity between gray matter regions.

The diffusion phenomenon is based on the microscopic stochastic thermal motion of molecules. This movement is known as Brownian motion. If there are no restrictions, the water molecules

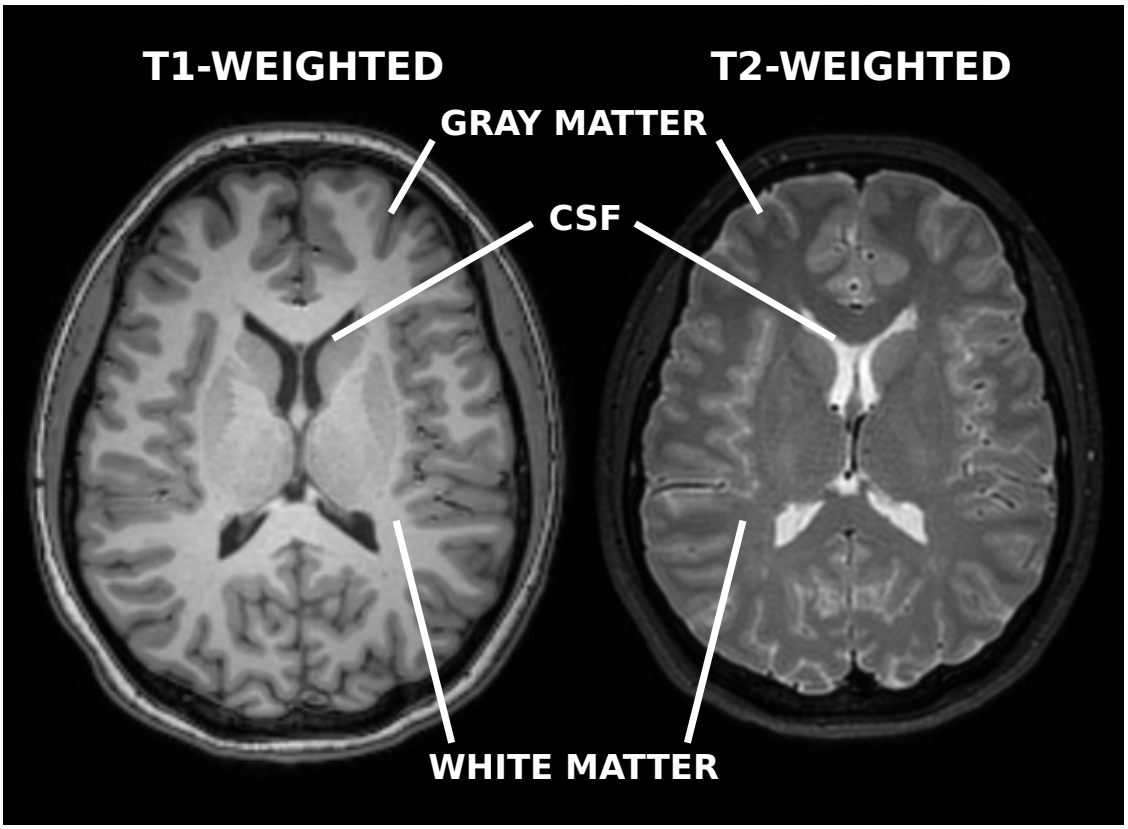


**Figure 2.2:** Example of a T1- (left) and a T2-weighted (right) image (axial slice). Locations of gray matter, white matter and cerebrospinal fluid (CSF) are shown.

diffuse freely in all directions and describe a chaotic route due to continuous collisions with the particles of the environment. The mean squared displacement of the particles in a specific period of time depends on the diffusivity of the medium. This diffusivity or diffusion coefficient describes how fast the molecules can diffuse through a medium and its value depends on the temperature. In unrestricted Brownian motion, the free diffusion of molecules causes that the location of the particles over time follows a Gaussian distribution whose width expands with time (Jones, 2010). In this case, the diffusion coefficient is constant. This free motion is also isotropic, because the diffusion does not depend on the direction considered.

The measurement of the diffusion signal is based on the Spin Echo (SE) sequence. Basically, the SE sequence firstly employs a RF pulse with flip angle equal to 90 degrees and the slice selection gradient is turned on followed by the phase selection gradient. The flip angle is the amount of rotation of the net magnetization selected by the operator. Next, an inversion RF pulse (180 degrees) applied at a time equal to the half of TE and the frequency selection gradient during the readout are used.

From the SE sequence, the diffusion is measured using a Pulse Gradient Spin Echo sequence (Stejskal & Tanner, 1965), described in Figure 2.3. Briefly, the Stejskal-Tanner sequence is a SE that incorporates the application of additional diffusion-sensitizing gradients to measure the diffusion-weighted signal. These gradients can be applied to the three directions of space ($x$, $y$

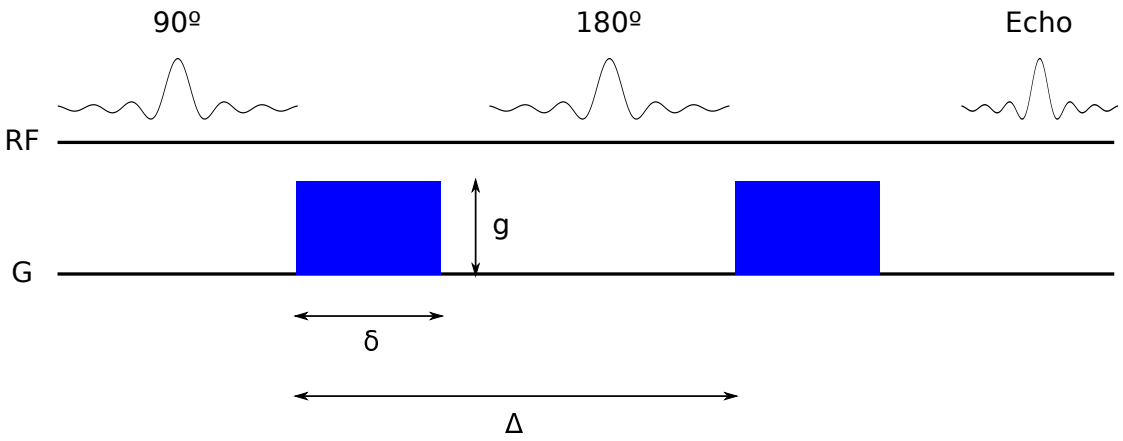


**Figure 2.3:** Scheme of the Pulsed Gradient Spin-Echo sequence. First, the RF pulse is applied and the first pulsed diffusion gradient (G) is activated, inducing a phase-shift (90°) in the precession motion. A RF pulse is used to invert the phase of the precession motion (180°) and then a second pulsed diffusion gradient is applied.

and $z$ considering Cartesian coordinates). The vector in which each diffusion-sensitizing gradient is applied is the diffusion direction or orientation. The diffusion direction is an unit vector.

From (Stejskal & Tanner, 1965), the diffusion-weighted signal intensity can be extracted in relation to an image with no diffusion-weighting, as shown in equation (2.3):

$$\frac{S}{S_0} = e^{-bD}, \tag{2.3}$$

where $S$ is the diffusion-weighted signal, $S_0$ the original T2 signal with no diffusion gradients, $b$ is the b-value and $D$ the diffusion coefficient. In human tissues, the molecular motion is not only caused by the diffusion coefficient, but also by the blood flow, breathing or CSF pulsation (Drake-Pérez, Boto, Fitsiori, Lovblad, & Vargas, 2018). Considering this point, the diffusion coefficient $D$ is replaced by the term Apparent Diffusion Coefficient (ADC), and the equation (2.4) is rewritten:

$$\frac{S}{S_0} = e^{-b\,\mathrm{ADC}}. \tag{2.4}$$

The ADC is specific to each tissue and is widely employed in the clinical practice. For example, low ADC values are related to stroke and neurodegeneration (Drake-Pérez et al., 2018) and generally higher tumor grade in gliomas (Surov, Meyer, & Wienke, 2017). From equation (2.4), it could be considered that diffusion-weighted images are attenuated T2-weighted images by a exponential law that depends on the b-value and the ADC. The b-value is expressed as follows:

$$b = \gamma^2 g^2 \delta^2 \frac{\Delta - \delta}{3}, \tag{2.5}$$

where $g$ represents the strength of the diffusion gradient, $\delta$ its duration and $\Delta$ the time between the two pulsed diffusion gradients. These values are represented in Figure 2.3.

The b-value determines the contribution of diffusion to the obtained image. A baseline image (b = 0 s/mm$^2$) is used as the image that represents the T2 signal with no diffusion gradients ($S_0$ in equation (2.4)). As the b-value is increased, the effect of diffusion becomes apparent, and

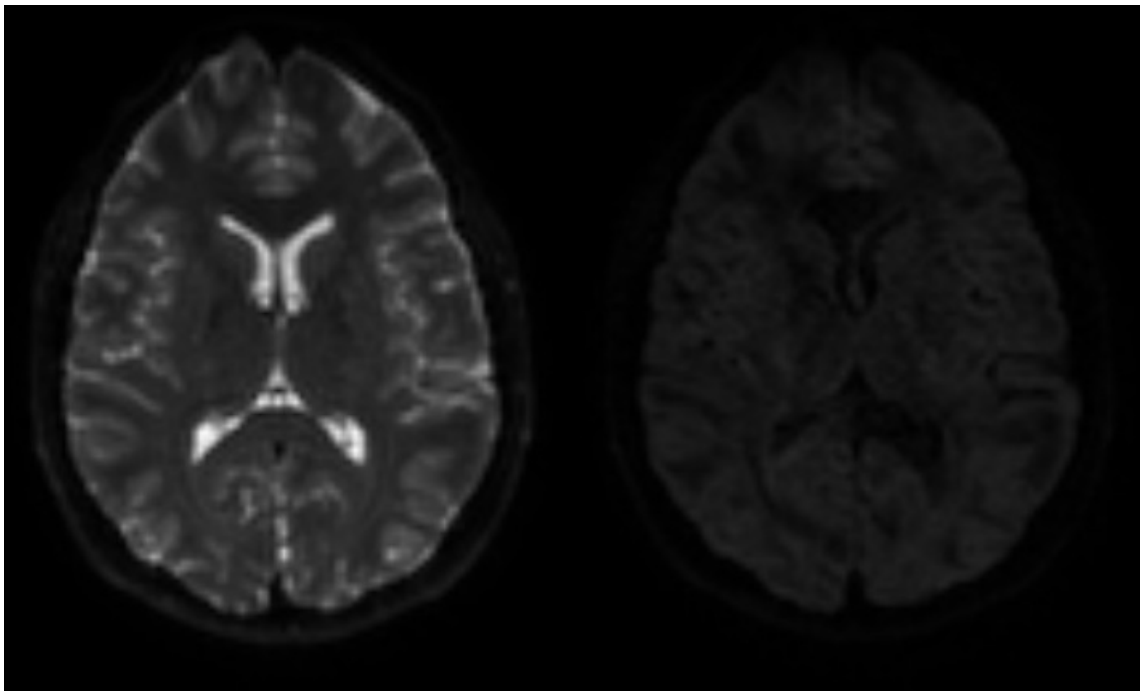

**Figure 2.4:** Example of a Diffusion-Weighted Image with b = 0 (left) and b = 1000 s/mm$^2$ (right).

voxels with a higher diffusion coefficient exhibit an increased with respect to regions with a lower diffusivity. Images with a high b-value thus present a lower signal intensity, which translates in a degradation of the Signal-to-Noise Ratio (SNR). An example of this effect is shown in Figure 2.4.

For each slice, there is at least one T2-weighted image (b = 0 s/mm$^2$) and a set of diffusion-weighted images, each of them weighted in one diffusion direction. To obtain isotropic images, three diffusion-weighted images (one image per each $x$, $y$ and $z$ direction) and the b = 0 image are commonly acquired.

However, biological tissues are highly structured and generally the diffusion varies with direction. For example, in the human brain, the water diffusion is restricted along white matter. In directions perpendicular to the axons, the diffusion is more restricted compared to the main axonal direction. This phenomenon is called anisotropy. The axonal membranes and myelination are the reasons for anisotropy in white matter (Beaulieu, 2002). The membranes have been suggested to play the main role for anisotropy, while myelination would modulate the degree of anisotropy (Beaulieu, 2002).

In anisotropic tissues, multiple diffusion directions can be used to characterize the properties of this diffusion along each of those directions. However, this information is difficult to visualize or analyze in this manner. Because of this, several models of anisotropic diffusion that provide more convenient representations have been developed. Among them, Diffusion Tensor Imaging (DTI) is the most simple and widely employed approach. The DTI model is described in the following subsection.

### *A. Diffusion Tensor Imaging*

The DTI model assumes that the directional profile of the anisotropic diffusion can be accurately described by an ellipsoid in space. Six parameters are needed to describe such an ellipsoid, and thus (at least) six gradient directions must be acquired on top of the baseline (b-value = 0) acquisition in order to estimate the diffusion tensor, which encodes the ellipsoid characteristics. In this thesis, parameters based on the DTI model are used to characterize diverse microstructural properties.

The set of diffusion volumes allows the identification of the predominant diffusion direction in DTI. As disclosed in section 2.2.2, the minimum number of directions, i.e. diffusion volumes, to capture non-isotropic diffusion is six. Taking into account the use of three unit vectors and the length of the three axes, each length would be an eigenvalue, and each vector would be an eigenvector.

The diffusion tensor is a symmetric second order tensor, and each element can be interpreted as the ADC in each of the encoded directions:

$$\mathbf{D} = \begin{bmatrix} D_{xx} & D_{xy} & D_{xz} \\ D_{xy} & D_{yy} & D_{yz} \\ D_{xz} & D_{yz} & D_{zz} \end{bmatrix}. \tag{2.6}$$

In equation (2.6), the diffusion tensor is defined by six independent parameters. The equation (2.4) models the diffusion signal intensity only when diffusion is isotropic or when diffusion is measured along one axis (Mori, 2007). The diffusion signal intensity equation is updated:

$$\frac{S_k}{S_0} = e^{-b\mathbf{g_k}^T \mathbf{D}\, \mathbf{g_k}},\ k = \{1, \ldots, n\}, \tag{2.7}$$

where $k$ corresponds to each acquired diffusion-weighted volume, $n$ is the number of acquired volumes (minimum of six) and $\mathbf{g_k}$ is a vector representing the diffusion gradient orientation. In equation (2.7), $b$ and $\mathbf{g_k}$ are known, $S_k$ and $S_0$ are determined by the experiment, and the elements of $\mathbf{D}$ are estimated. As stated before, at least six diffusion gradient directions must be employed to obtain a tensor by solving a system of six equations with six variables. However, a higher number of directions is commonly employed, and the diffusion tensor is determined using methods such as least squares or weighted least squares in order to obtain a more robust estimation.

The diagonalization of the diffusion tensor defines the six parameters that characterize the diffusion ellipsoid. The relationship between the diffusion tensor, the eigenvalues and the eigenvectors is shown in equation (2.8):

$$\mathbf{D}\mathbf{v} = \lambda \mathbf{v}, \tag{2.8}$$

where $\lambda$ is the set of the three eigenvalues ($\lambda = \{\lambda_1, \lambda_2, \lambda_3\}$, ordered from the highest to lowest eigenvalue), and $\mathbf{v}$ the set of the three eigenvectors ($\mathbf{v} = \{\mathbf{v_1}, \mathbf{v_2}, \mathbf{v_3}\}$).

Despite the advances of DTI to model anisotropy, there are also some important disadvantages related to information loss, which can be classified in three levels (Mori, 2007):

- Level 1. The use of water diffusion information is used to describe axonal structure when water diffusion is associated with many biological structures. Thus, water diffusion is not specific to any particular tissue or cellular structure. Moreover, the voxel resolution employed in diffusion-weighted images (typically 2-3 mm per each of the three dimensions) is excessively large to characterize the diffusion properties within a voxel.
- Level 2. The diffusion is measured using a restricted number of directions (in the clinical routine, generally more than 20 but less than 70), which limits the amount of information that can be employed.
- Level 3. The diffusion tensor contains only six parameters, and regardless of the number of acquired diffusion volumes (number of orientations), all the information is summarized in six values.

Level 1 information loss is associated with measurement itself, and it would be corrected using better image resolution.

DTI uses a simple Gaussian regressor, i.e., it is a first-order model of the water diffusion mechanism that oversimplifies the reality. For example, DTI presents problems in populations of crossing fibers in a voxel, because the associated model assumes that there is one dominant population of fibers. To solve the oversimplification issues, some non-tensor approaches have been proposed. Some of these approaches are briefly explained in the next subsection, with special focus on the Ensemble Average diffusion Propagator (EAP) because of its relation to methods employed in this thesis.

### *B. Non-tensor approaches*

The use of non-tensor approaches usually requires higher b-values with respect to those employed in DTI (approximately 1000 s/mm$^2$). Higher b-values allow to appreciate better the diffusion effects and there is more contrast between regions with different grades of anisotropic diffusion, at the cost of lower SNR (Burdette, Durden, Elster, & Yen, 2001).

For these approaches, a frequently employed acquisition method is High Angular Resolution Diffusion Imaging (HARDI). This method employs a single or multiple b-values with multiple diffusion orientations and it is able to distinguish multiple intravoxel populations (Tuch et al., 2002). Multiple non-tensor approaches have been implemented to model the brain structure from HARDI data (Özarslan, Shepherd, Vemuri, Blackband, & Mareci, 2006; Tristán-Vega, Westin, & Aja-Fernández, 2009; Tuch, 2004).

One technique similar to DTI but based on a second-order equation is Diffusion Kurtosis Imaging (DKI), which quantifies the amount of water diffusion that is non-Gaussian (Jensen, Helpern, Ramani, Lu, & Kaczynski, 2005). With respect to the equation (2.4), DKI adds a quadratic term and an apparent kurtosis term (Steven, Zhuo, & Melhem, 2014) (written in logarithmic form):

$$\log\left(\frac{S}{S_0}\right) = -b\mathrm{ADC} + \frac{1}{6}b^2\mathrm{ADC}^2 K_{\mathrm{app}}, \tag{2.9}$$

where $K_{app}$ is the apparent kurtosis. When $K_{app}$ is equal to 0, the kurtosis model is equal to the Gaussian model. The kurtosis is a value employed in Statistics to describe the peakedness of a probability distribution in comparison with the Gaussian curve. Higher kurtosis is related to more impediments to Gaussian diffusion and greater complexity (Steven et al., 2014). With respect to DTI, the DKI model uses three additional parameters, the three kurtosis values, associated with the eigenvalues and eigenvectors employed in DTI. It has also been observed that DKI fits better than DTI to the monoexponential decay model for high b-values ($1500 < b < 2500$ s/mm$^2$) (Steven et al., 2014).

An example of application of HARDI takes place in multi-compartment models. These models represent the diffusion signal as a combination of models of diverse tissues. One of the simplest examples is the ball and stick model (Behrens et al., 2003), which considers the axons as sticks (anisotropic diffusion) and anything else as balls (isotropic diffusion). In multi-compartment diffusion models, it has been observed that $K_{app}$ is always positive, except for the Gaussian diffusion situation (Tabesh, Jensen, Ardekani, & Helpern, 2011).

For the understanding of some non-tensor approaches, two concepts should be introduced: q-space (Callaghan, 1994) and multi-shell methods. The q-space can be compared to the k-space of MRI. Briefly, the k-space is the representation of the spatial frequencies of the MR image given by the Fourier transform. The k-space encoding is given by the frequency codification gradient while the q-space encoding is defined by the diffusion-sensitizing gradient. The Fourier transform is used to represent the spatial distribution and the EAP in the k-space and the q-space, respectively. The EAP is also known as the spin displacement probability density function and diffusion spectrum (Tian et al., 2019)- The EAP is the 3D probability density function of the diffusion displacement. More details about the EAP are shown later in this section. Multi-shell methods are those that employ multiple b-values different from 0.

In recent years, the use of non-tensor techniques has been performed with the acquisition of a large amount of diffusion-weighted images and diverse shells composed of moderate-to-high b-values (multi-shell acquisition). This type of dMRI acquisition has been employed to obtain more advanced diffusion descriptors, for example, the EAP. Diffusion Spectrum Imaging (DSI) has been used to reconstruct the EAP. DSI is a model-free approach that requires a large number of diffusion samples of the q-space and the EAP is reconstructed by the discrete Fourier transform of the measured signal (Wedeen, Hagmann, Tseng, Reese, & Weisskoff, 2005). An important issue of DSI is the high number of images needed for the reconstruction, which makes its use almost unfeasible in the clinical routine due to an excessively long acquisition time. Alternative model-based multi-shell methods have been proposed to reconstruct the EAP. Among these methods, the mean average propagator-MRI (Özarslan et al., 2013) and especially its developed version, the Laplacian-regularized mean average propagator-MRI (Fick, Wassermann, Caruyer, & Deriche, 2016), should be highlighted after their positive results in clinical studies to characterize brain microstructure (Avram et al., 2016).

A recent approach related to the EAP is Apparent Measures Using Reduced Acquisitions (AMURA). Briefly, the main idea of this method is that a constrained model for radial diffusion is able to reflect relevant information with simpler dMRI acquisitions compared to the computation of the whole EAP (Aja-Fernández et al., 2020). From this model, a group of extracted *apparent* scalar measures at a single-shell can provide a comparable sensitivity to microstructural changes in comparison with the *non-apparent* measures from the full EAP obtained with the whole average for diverse b-values (Aja-Fernández et al., 2020). The scalar measures employed in AMURA are Return-to-origin Probability (RTOP), Return-to-plane Probability (RTPP) and Return-to-axis Probability (RTAP). Further details about the extraction of these scalar measures with AMURA can be found in the next subsection and subsection C of section 3.2.2.

To understand the three scalar measures, it is important to describe the EAP. The EAP is the 3D probability density function of the water molecules inside a voxel moving an effective distance $\mathbf{R}$ (in a sphere) in an effective diffusion time $\tau$ (equal to $\frac{\Delta-\delta}{3}$ in equation (2.5), $\Delta$ and $\delta$ can be observed in Figure 2.3). The EAP is given by the Fourier transform of the normalized magnitude image provided by the MRI scanner (Callaghan, Eccles, & Xia, 1988):

$$P(\mathbf{R}) = \int_{\mathbb{R}^3} E(\mathbf{q}) e^{-2\pi j \mathbf{q}\cdot\mathbf{R}} d\mathbf{q} = \mathcal{F}\{|E(\mathbf{q})|\}(\mathbf{R}), \tag{2.10}$$

where $P(\mathbf{R})$ is the EAP, $E(\mathbf{q})$ is the normalized magnitude image, and the exact information from the $\mathbf{R}$-space would require the sampling of the whole $\mathbf{q}$-space. $E(\mathbf{q})$ is the adaptation of equation (2.4) to the $\mathbf{q}$-space (Özarslan et al., 2006):

$$E(\mathbf{q}) = e^{-b\,D(\mathbf{q})} = e^{-4\pi^2\tau q_0^2\,D(\mathbf{q})}, \tag{2.11}$$

where $D(\mathbf{q})$ is the ADC, $b$ is the b-value, $\mathbf{q}$ is the spherical system that describes the $\mathbf{q}$-space (defined by a radius and two angles), and $q_0$ is the parameter that defines the radius of the spherical system $\mathbf{q}$.

### *C. Parameters to describe white matter integrity*

To describe white matter integrity, quantitative descriptors are used to assess diverse properties of white matter. These parameters are usually derived from diverse diffusion models, such as DTI or DKI. These parameters allow the statistical comparison between groups of interest to study microstructural differences, as it is performed in this thesis with CM, EM and controls.

Regarding DTI, the eigenvalues of the diffusion tensor are used to obtain diffusion descriptors. The four most employed DTI-based measures in the literature are the Fractional Anisotropy (FA), Axial Diffusivity (AD), Mean Diffusivity (MD) and Radial Diffusivity (RD). These four parameters have been employed to compare groups of patients with migraine and controls in Chapters 2, 3 and 5 of Part II. The FA is expressed as follows:

$$\mathrm{FA} = \sqrt{\frac{(\lambda_1-\lambda_2)^2+(\lambda_2-\lambda_3)^2+(\lambda_1-\lambda_3)^2}{2(\lambda_1^2+\lambda_2^2+\lambda_3^2)}}. \tag{2.12}$$

The minimum value of the FA is 0 and the maximum value is 1. The FA measures the degree of anisotropy of water molecules, with higher values associated with higher anisotropy. Lower FA values have been related to lower packing density, change of membrane permeability and demyelination, depending on the axonal diameter or the fiber organization (lower values with decreased organization) (Beaulieu, 2002; Kochunov et al., 2007).

The AD is expressed as follows:

$$\mathrm{AD} = \lambda_1. \tag{2.13}$$

It is easy to check that the AD is simply equal to the first eigenvalue of the diffusion tensor. The first eigenvalue is associated with the main direction, which is the axonal direction in white matter. Different interpretations have been given to the AD values. On the one hand, lower values have been associated with short-term demyelination (Winklewski et al., 2018). On the other hand, reduced AD has been linked to axonal damage instead of demyelination and secondary white matter degeneration (Alexander, Lee, Lazar, & Field, 2007; Pierpaoli et al., 2001; Sun, Liang, Cross, & Song, 2008).

The MD is expressed as follows:

$$\mathrm{MD} = \frac{\lambda_1 + \lambda_2 + \lambda_3}{3}. \tag{2.14}$$

The MD is the mean of the three eigenvalues or the trace of the diffusion tensor divided by three. The MD describes the rotationally invariant magnitude of water diffusion within the brain tissue (Clark et al., 2011). Increased MD values have been related to atrophy and axonal density reduction (Clark et al., 2011; J. Zhang et al., 2018).

The RD is expressed as follows:

$$\mathrm{RD} = \frac{\lambda_2 + \lambda_3}{2}. \tag{2.15}$$

The RD reflects the perpendicular diffusivity with respect to the main direction, the axonal direction in white matter as commented with the AD. Lower RD values have been associated with myelin damage (Sun et al., 2008).

The previous description of the connections between the diverse DTI-based descriptors and white matter should be interpreted cautiously because there is no definite confirmation of their relationship with physiology or pathophysiology. An important factor contributing to the difficult biophysical interpretation of DTI-based descriptors is that the voxel size is considerably higher than the axonal size or the water diffusion distance considering typical diffusion times in DTI studies (O'Donnell & Westin, 2011). In relation to this issue, a voxel represents the average of the diffusion characteristics from different fiber populations within that voxel, which becomes a problem when two or more populations are present in a single voxel (Basser & Jones, 2002). Furthermore, multiple pathological factors can cause similar changes for a particular DTI-based measure (O'Donnell &

Westin, 2011). The analysis of the values of DTI-based parameters may be insufficient to identify clearly the particular reason of the studied alterations.

With respect to non-tensor approaches, RTOP, RTPP and RTAP are derived from the EAP. The RTOP is the value of the EAP at the origin in relation to the volume of the diffusion signal. It is associated with the probability density of water molecules with minimal diffusion during the diffusion effective time. According to the definition of the RTOP, its equation is the following:

$$\text{RTOP} = P(0) = \int_{\mathbb{R}^3} E(\mathbf{q}) d\mathbf{q}. \tag{2.16}$$

RTPP and RTAP are the decomposition of the RTOP into a parallel and a perpendicular component to the maximum diffusion, respectively (Özarslan et al., 2013). The RTPP and RTAP are defined as follows:

$$\text{RTPP} = \int_{\mathbb{R}^2} P(\mathbf{R}_\perp) d\mathbf{R}_\perp = \int_{\mathbb{R}} E(q_{||}) dq_{||}. \tag{2.17}$$

$$\text{RTAP} = \int_{\mathbb{R}} P(\mathbf{R}_{||}) d\mathbf{R}_{||} = \int_{\mathbb{R}^2} E(q_\perp) dq_\perp. \tag{2.18}$$

### *D. Tractography*

Due to its relevance in the analysis of the connections between the brain regions, tractography methods are explained. In this thesis, tractography is the central method to evaluate structural connectivity. DMRI-based tractography has become a tool that presents exclusive properties to map whole-brain structural connections (Sinke et al., 2018). Tractography is the technique employed to represent nerve tracts using dMRI data (Basser, Pajevic, Pierpaoli, Duda, & Aldroubi, 2000) and it is the method employed to assess structural connectivity. In relation to connectomics and structural connectivity, tractography allows to determine the connections between specified anatomical ROIs and reconstruct the diverse white matter tracts or the trajectories that follow the white matter fibers throughout the brain. Moreover, as connectivity parameters, descriptors based on DTI (e.g. FA) or other diffusion models can be employed to evaluate connections between ROIs or analyze the white matter integrity in specific connections.

The most simple form of fiber tracking is voxel-linking. In this method, the orientations of adjacent voxels with respect to a seed are compared and if one of the surrounding voxels meets certain conditions, the two voxels are joined in the same tract. This process would be repeated until a stop criterion is met. This method is similar to the region growing technique used in ROI neuroimaging segmentation.

A more sophisticated fiber tracking approach is global tractography. The idea of this method is to estimate simultaneously the set of all pathways considering non-local effects. This type of tractography allows more biologically plausible reconstructions. Two types of algorithms are distinguished:

- **Deterministic algorithms**. A unique streamline is associated with one seed point and the streamline is fully determined by the seed.
- **Probabilistic algorithms**. In contrast to deterministic algorithms, there is a possible range of estimated connections for a seed point, with diverse sources of uncertainty. Some examples of these algorithms are bootstrap methods, models based in Bayesian inference and heuristic functions.

DTI or DKI, among other models, can be employed for fiber tracking. In this case, the first eigenvalue would be used to determine the direction of the fiber tract. However, this method would be problematic in some situations, such as crossing fibers and possible lesions (e.g. edema).

A widely employed algorithm for tractography is Fiber Assignment by Continuous Tracking (FACT) (Mori, Crain, Chacko, & Van Zijl, 1999). In FACT, the 3D space is considered continuous and the reconstruction algorithm follows local fiber orientations in small incremental steps. The seed is selected by the user and, from this point, a streamline is drawn. A streamline can be defined as each 3D curve of the computed trajectories of a white matter fiber tract. The advantage of FACT compared to voxel-linking is that it is not mandatory to use the voxel centers. However, this type of tractography generates undirected reconstructions, i.e., there is no identification of afferent or efferent fibers. Among the particular FACT methods, some examples are nearest neighbor, trilinear interpolation or the use of the raw diffusion-weighted signal.

A recent type of tractography algorithms are the brute-force methods. Basically, these methods perform whole-brain tracking using a huge number of streamlines seeded from all brain voxels. In this case, fiber tracking is independent of the exact seed region place. Brute-force methods can be combined with tract-editing techniques that use logical operations (de Luis-García, Westin, & Alberola-López, 2013). These methods can be used to obtain high-resolution white matter images, as it is performed with Track-Density Imaging (Calamante, Tournier, Jackson, & Connelly, 2010). Another example of a brute-force method is Anatomical Connectivity Mapping, which computes the number of streamlines for each voxel and is independent of original diffusion data (Bozzali et al., 2011).

It is highly important to define appropriately the stopping criteria of the fiber tracking algorithms. Three main aspects may be considered:

1. **Mask**. A mask should be employed to delimit the area where the streamlines are reconstructed. The most simple mask would be a brain mask. More complex masks would be extracted from segmentation of different regions such as CSF, white matter and gray matter.
2. **Scalar measures**. A DTI-based parameter, for example, can be used to end the reconstruction of a streamline for a range of values. The use of low DTI eigenvalues may be problematic due to the influence of noise.
3. **Curvature based criterion**. A maximum angle is used to delimit the fiber tracking. If the angle between two steps is excessively large, the algorithm stops.

The three previous criteria can be used simultaneously.

The main problem of tractography or fiber tracking algorithms is that there is no gold standard method. The most appropriate method to analyze the tractography results is also conflicting, including among the possible options the analysis of the number of streamlines or graph theory approaches. Both methods present important issues, although the use of streamlines to assess structural connectivity is considered as an acceptable measure under certain conditions (Yeh, Jones, Liang, Descoteaux, & Connelly, 2020).

Other limitation would be the estimation of crossing fibers for DTI-based approaches and the partial volume averaging. Due to this last limitation, the reconstruction of the streamlines would be incomplete because gray matter, CSF and lesions may reduce the real value of the anisotropy in areas with high diffusivity and high T2 (b = 0 s/mm$^2$) signal.

There are some sources of uncertainty that can produce important alterations in the result of the tractography algorithm. These sources include the effects of noise, the shape of the tracts and the angular and spatial resolution. Noise can be the main source of uncertainty and cause important deviations from the real trajectory of the reconstructed streamlines. With respect to the shape of the white matter tracts, some of them can present a high curvature within a voxel, which would produce a false negative (no identification of a real fiber). This type of false negatives are related to one of the stopping criteria that discards tracts with excessive curvature angle, which would be true for most but not all cases. Regarding the angular and the spatial resolution, some single discrete orientations may not be identified because of possible blurring effects. Acquisition protocols employed in the clinical routine present important angular resolution limitations to resolve relative high crossing angles, especially considering that the voxel size may be a bit large to assess some tracts in detail. An example of a result of a tractography is shown in Figure 2.5.

### *E. Noise and artifacts*

Despite the advantages of the use of dMRI, this modality presents diverse specific sources of variability that can have a great impact on the measured signal. In this section, some of these sources, especially those treated in the preprocessing (subsection A of section 3.2.2), are outlined. In relation to the noise and artifacts, it is important to treat them to reduce the bias and the variance that they cause on the measured signal. The corresponding treatment of noise and artifacts allows better discrimination in clinical studies using robust measures thanks to the reduction of variance or corrections to low SNR.

The mentioned sources of variability are caused by thermal noise, which is the primary origin of fluctuation in MRI signals (Aja-Fernández & Vegas-Sánchez-Ferrero, 2016), and artifacts. An appropriate noise filtering method is important in order to remove information that can disturb the image processing and interpretation without erasing important data or adding spurious signal. The artifacts are generated by the scanner hardware, the employed fast sequences, motion or physiological processes.

Some artifacts are related to the strong diffusion gradient pulses used in dMRI. When these gradient pulses are switched on and off quickly, the so-called eddy currents are generated (Le Bihan,

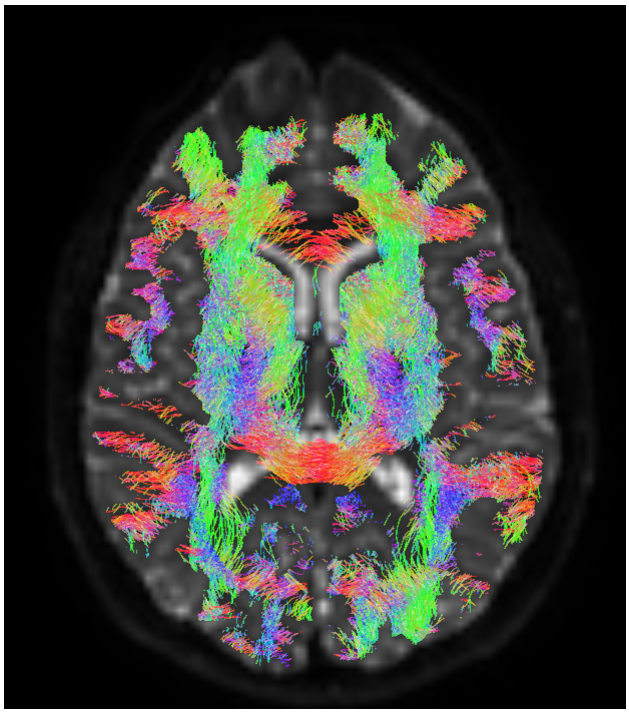

**Figure 2.5:** Example of the result of tractography over an axial slice of a diffusion-weighted image. Red means left-right direction, green anterior-posterior direction and blue inferior-superior direction.

Poupon, Amadon, & Lethimonnier, 2006). The eddy currents are electrical currents that produce unwanted magnetic field gradients that interact with the imaging gradient pulses and cause geometric distortions in the captured images (Le Bihan et al., 2006). The correction of eddy currents allows the extraction of diffusion descriptor maps of higher quality, including the measures considered in this thesis. For example, regarding the diffusion descriptors, the correction of eddy currents has produced sharper contours and reduced blurring in anisotropy maps (Bodammer, Kaufmann, Kanowski, & Tempelmann, 2004).

Another major artifact in dMRI is the subject motion. All MRI modalities are affected by motion artifacts, but in dMRI this artifact is more relevant compared to most modalities, especially for long acquisition times. The macroscopic motion (e.g. head motion) may cause a phase shift producing the so-called ghosting artifact along the phase-encoding direction (Le Bihan et al., 2006). This ghosting artifact causes that the signal is not restricted to the original voxels and a signal loss that is directly proportional to the gradient strength (Le Bihan et al., 2006). It is important to correct the motion artifact to rectify misalignments between the volumes with different diffusion gradient orientations. The motion and the eddy currents corrections are crucial for a right estimation of diffusion parameters and fiber orientation (Jones & Cercignani, 2010). Both corrections have been applied in this thesis.

To reduce the effect of motion artifacts, the fast Echo-Planar Imaging (EPI) sequence is employed. This sequence allows to acquire an image with a unique or multiple shot scheme. However, the EPI sequence is associated with other artifacts. Due to the relative low spatial resolution associated with EPI (approximately $2 \times 2 \times 2$ mm$^3$), related to hardware limitations, blurring effects

are produced (Le Bihan et al., 2006). Other artifacts are related to the differences in the resonance frequencies between adjacent voxels (bandwidth) that cause phase shifts in the phase encoding direction (Le Bihan et al., 2006). In EPI, the inhomogeneities of the $B_0$ magnetic field cause shape distortions in the phase-encoding direction due to small frequency differences (magnetic susceptibility artifact) (Le Bihan et al., 2006).

Other important dMRI artifacts are related to inhomogeneities in the RF or $B_1$ pulse or deficient spatial sampling. An inappropriate spatial sampling frequency can lead to the Gibbs ringing artifact, which causes significant alterations on the extraction of diffusion descriptors (Veraart, Fieremans, Jelescu, Knoll, & Novikov, 2016). The $B_1$ inhomogeneities can produce geometric distortions (S. M. Smith et al., 2004). Non-uniform $B_1$ fields cause a reduction of the effective flip angle (Ramos Delgado et al., 2020). The variation of the effective flip angle is related to a change of the effective b-value. Thus, the correction of $B_1$ inhomogeneities is important to reduce the variance caused in diffusion measures, a crucial point in this doctoral thesis.

## 2.3. Methods to compare groups of interest in MRI studies

The main methods related to the MRI modalities employed in the literature to compare groups of interest are described in this section. Some of these methods have been applied in this thesis.

### *2.3.1.* ***Analysis of gray matter***

The most employed technique to assess gray matter changes from T1-weighted images is Voxel-Based Morphometry (VBM). VBM is an automatic and independent tool that allows to detect voxel-level gray matter volume in the brain (Ashburner & Friston, 2000). The objective of VBM is the voxelwise comparison of the local gray matter concentration between groups of interest. Surface-Based Morphometry (SBM), a refined version of VBM, has also been employed, but there are less studies using this technique. Compared to VBM, SBM additionally measures cortical thickness, surface area and gyrification index (Fischl & Dale, 2000). Some limitations of VBM are worth noting. The VBM warping method is relatively simple and there could be misalignment for some regions, it assumes that data are normally distributed and it does not provide information about the specific source of the identified alterations (Mechelli, Price, Friston, & Ashburner, 2005).

In the last years, many studies have employed a different approach, most of them using a software tool called FreeSurfer. Briefly, a cortical reconstruction and a volume segmentation are carried out using this software. Among the parameters provided by this method, gray matter volume, surface area, cortical thickness and cortical curvature (similar to the gyrification index from SBM) are included. As a result of the reconstruction, the mentioned parameters are obtained for each segmented gray matter region. Compared to VBM, the FreeSurfer pipeline provides better registration quality and robust results, and the extraction of area and thickness provides more

information about the volumetric changes, together with additional parameters such as curvature. Limitations of the FreeSurfer pipeline include overestimation of volume values (Klasson, Olsson, Eckerström, Malmgren, & Wallin, 2018; McCarthy et al., 2015) and no estimation of the volume of small regions such as the hypothalamus. More details about this approach are provided in section 3.2.1.

The different morphometry parameters characterizing the gray matter that can be extracted using this approach are described hereunder.

The cortical curvature is the inverse value of the radius of the circles that compose the diverse gyri or sulci of each point of the surface on the gray-white matter junction, reflecting the folding of the cortex. The value used for a single region is the mean value of the radii. A schematic representation of the cortical curvature is shown in Figure 2.6. The role of the cortical curvature is unclear, but it has been suggested as a biomarker of white matter atrophy (Deppe et al., 2014) and related to the integrity of structural connections between cortical regions (Lubeiro et al., 2017).

Regarding the other three morphometry parameters, thickness and area are related to volume. The cortical thickness is the distance between the inner (gray-white matter boundary) and the outer (gray matter-CSF boundary) surface of a gray matter region. As in the measure of the cortical curvature, the final value was the average of the diverse values of the distance. The surface area measures the space of a gray matter region in the white matter surface (gray-white matter boundary). A schematic representation of the thickness and the area is shown in Figure 2.7. The gray matter volume is obtained from the contribution of the cortical thickness and the surface area. In a simplified VBM representation, the gray matter volume would be approximately the sum of the cubic voxels that a gray matter region occupies, where the base of each cube would be the surface area and the height would be the cortical thickness.

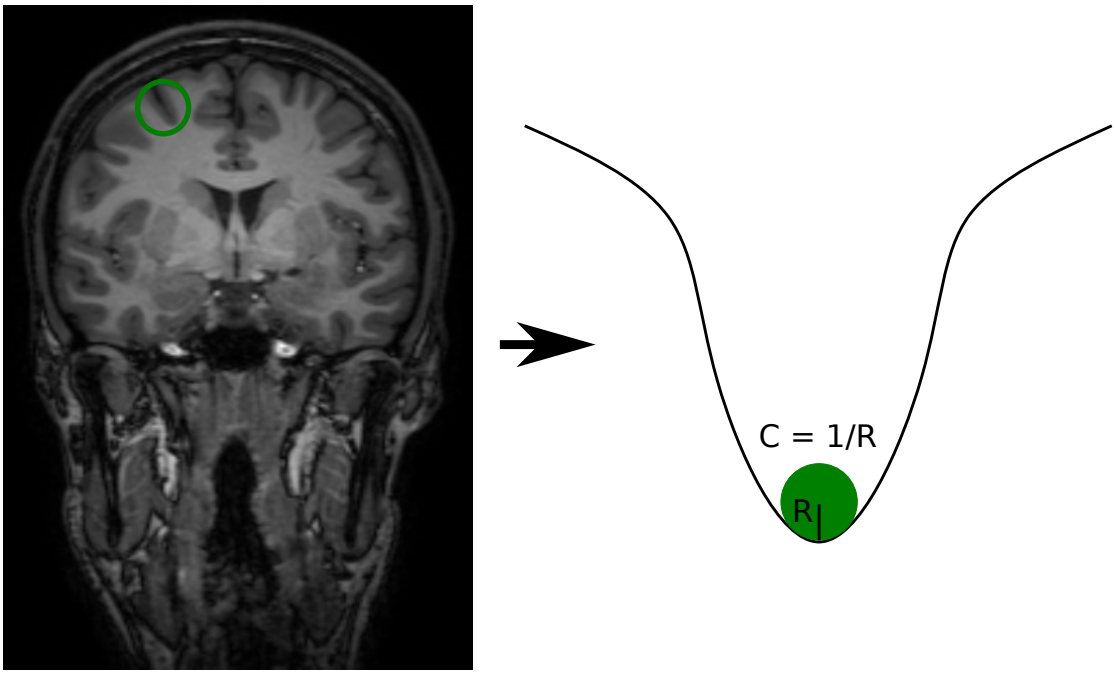


**Figure 2.6:** Example of a coronal slice of a T1-weighted image (left) and the schematic representation of the cortical curvature (right). C = curvature; R = radius.

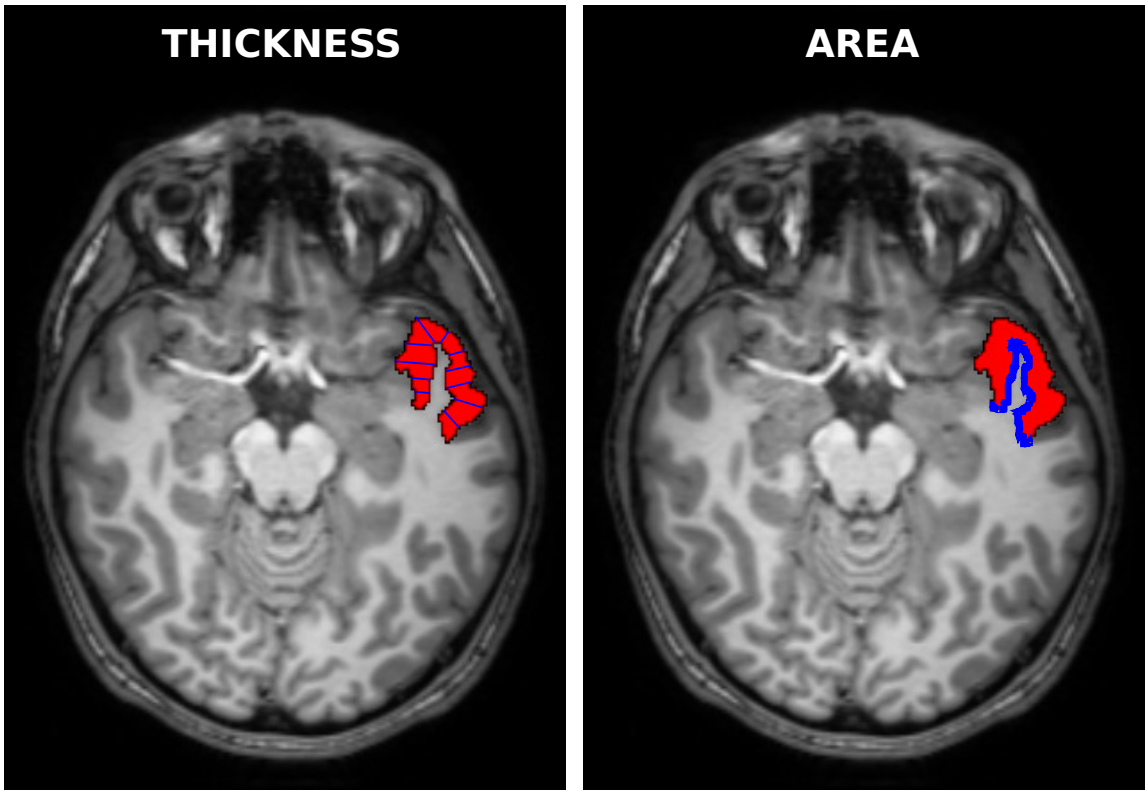


**Figure 2.7:** Schematic representation of cortical thickness (left) and surface area (right) in a cortical region (in red). The blue lines indicate the thickness (multiple values) and area. The area should be projected in two dimensions. The region used as example is the superior temporal gyrus.

### 2.3.2. Analysis of white matter

To analyze the white matter using dMRI data, the first set of steps is related to the preprocessing of the diffusion-weighted images. There are multiple diffusion preprocessing options. Thus, in this section no description of preprocessing methods is provided, but the details concerning the particular steps of this thesis are described in section A of section 3.2.2.

Many dMRI studies have used DTI-based parameters to evaluate changes of white matter structure. The main DTI-based parameters are the FA, AD, MD and RD, all of them described in subsection C of section 2.2.2.

Considering studies that assessed patients with migraine, before 2012, the methods employed to assess dMRI data were heterogeneous. Among these methods, some examples are the comparison of diffusion indexes histogram peaks (Rocca, Ceccarelli, Falini, Tortorella, et al., 2006; Rocca et al., 2003), point-by-point FA comparison (Granziera et al., 2006), comparison of manually segmented ROI (A. F. M. DaSilva et al., 2007; X. L. Li et al., 2011) and ADC map comparison in segmented ROI (Degirmenci, Yaman, Haktanir, Albayrak, & Acar, 2007).

Since 2012, more complex techniques have been used to compare diffusion descriptors between patients with migraine and controls. The most employed method is Tract-Based Spatial Statistics (TBSS) (S. M. Smith et al., 2006). Briefly, the TBSS pipeline projects the diffusion descriptors onto a skeleton that represents the center of the white matter tracts. The main steps are the non-linear registration of the diffusion descriptors map and the projection to the skeleton.

The advantage of the skeleton obtained with TBSS is that the edge issue of other approaches (e.g. ROI-based methods) is avoided. Moreover, for a specific white matter region or tract, the diffusion properties can vary from the central to the external area of a region, which can bias the values of the diffusion descriptor. Therefore, TBSS allows to identify white matter differences between groups of interest in specific regions reducing considerably the possible bias of possible misalignments with the segmented regions or diverse properties of different areas of the ROI.

However, TBSS also presents important limitations. It has to be assumed that the effects of interest take place in the center of the tract, it does not consider orientation information and the statistical results and the shape of the skeleton are rotationally variant (Bach et al., 2014). TBSS also presents problems differentiating individual tracts in areas with high levels of noise, complex fiber architecture or where different fiber bundles merge (Bach et al., 2014).

### 2.3.3. Connectomics

Connectomics is a technique used to describe the brain connectivity by mapping the brain elements and the interconnections between them (Fornito & Bullmore, 2015). Three main types of connectivity have been described (Friston, 1994):

- **Structural connectivity**. This type of connectivity analyzes the connections between gray matter cortical and subcortical areas of the brain interconnected by white matter tracts. A

detailed analysis provides information about the connections between each pair of regions. The assessment of this type of connectivity is performed using dMRI. The structural connectivity is assessed in this thesis, particularly in Chapter 5 of part II.

- **Functional connectivity**. This modality analyzes the temporal correlation between the neurophysiological activity of distant regions. The assessment of this type of connectivity is carried out acquiring Functional Magnetic Resonance Imaging (fMRI) data (better spatial resolution) or Electroencephalography (EEG) and magnetoencephalography (better temporal resolution) data.
- **Effective connectivity**. This type of connectivity is related to the union of structural and functional connectivity. The aim of this connectivity modality is to characterize the directional effects of one neural element over another (causality). The methods related to effective connectivity can be model-based or model-free (e.g. Granger causality or transfer entropy). With regard to MRI modalities, fMRI has been the modality mostly employed to assess this type of connectivity, but in a recent approach it has been combined with dMRI (Hahn et al., 2019).

The results of connectomics methods are usually expressed with a connectivity or adjacency matrix. Each row and its respective column represent a brain region, and each cell of the matrix represents a connection between a pair of regions.

According to the values of the matrix, this can be binary or weighted. Binary matrices represent the presence (value 1) or absence (value 0) of a connection between a pair of regions. In weighted matrices, the value of each cell shows the strength of the connection.

Regarding the symmetry of the matrix, it can be undirected or directed. The undirected matrices are symmetric, which is the usual case of functional connectivity, i.e., the connectivity from a region A to a region B is equal to the connectivity from B to A. Directed matrices are non-symmetric and the connection from one region A to another region B one can be different that the connection from B to A, which is the case of effective connectivity matrices. Structural connectivity matrices are usually undirected, although they can be directed depending on the method used to obtain them. Examples of these types of adjacency matrices are shown in Figure 2.8.

Graph theory is another approach employed to analyze connectivity. Graph theory models the brain as a network composed of a set of nodes (brain regions) and edges (fiber tracts) that connect the nodes, providing an abstract representation of brain regions and their interactions (Bullmore & Sporns, 2009). There is a great variety of local and global graph theory measures, which can be checked in detail in (Rubinov & Sporns, 2010).

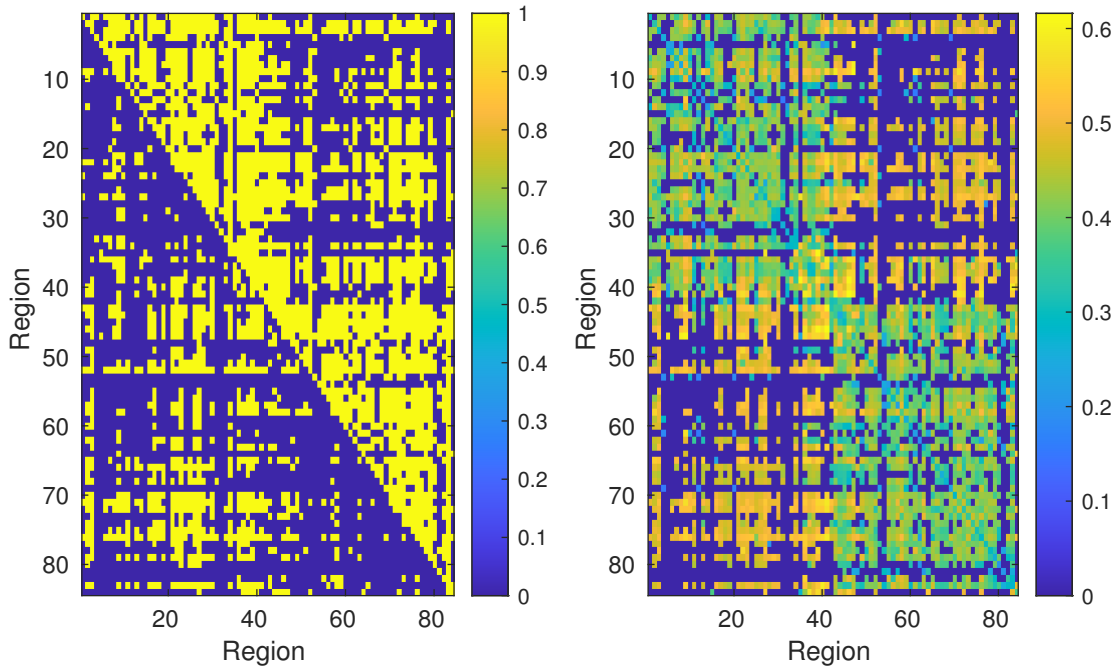


**Figure 2.8:** Examples of adjacency matrices with 84 regions. Left: binary directed matrix. Right: weighted undirected matrix.

### *2.3.4.* ***Techniques to combine MRI modalities***

The simultaneous analysis of different MRI modalities may reflect specific brain alterations patterns that could not be totally described with single-modality studies. The simplest method to assess data from multiple modalities is the correlation analysis, but this technique is unable to detect covariance patterns between the modalities.

More complex fusion methods have been implemented to analyze neurological diseases. Frequently, methods based on Canonical Correlation Analysis (CCA) and Independent Component Analysis (ICA) have been employed. Among these techniques, Multimodal Canonical Correlation Analysis (mCCA) followed by Joint Independent Component Analysis (jICA) has been used to analyze simultaneously images from different modalities focused on gray and white matter (Sui et al., 2011). Other methods have focused on the analysis of healthy subjects, including hybrid connICA (Amico & Goñi, 2018) and linked ICA (Llera, Wolfers, Mulders, & Beckmann, 2019).

To assess simultaneously structural connectivity and gray matter morphometry in Chapter 6 of part II, a method based on mCCA followed by jICA (Sui et al., 2011) with some modifications was employed. An adaptation of CCA for datasets of different dimensionality is used to measure the associations between them maximizing their correlation. ICA is employed to summarize the information from the datasets into a low number of statistically independent subcomponents with the objective of obtaining independent sources of information. The CCA step makes that each independent component from a modality is correlated with the same component of the other modality simultaneously analyzed. More details about this fusion methodology in relation to this thesis are explained in section 3.2.5.

## 2.4. Neuroimaging studies in migraine

Three main MRI modalities have been employed in combination with advanced processing in the analysis of brain structure and function in migraine: T1-weighted, dMRI and fMRI. T2-weighted images are employed to assess WMH, but no further processing has been performed. Other neuroimaging modalities have been also used to assess migraine, such as Magnetic Resonance Spectroscopy (MRS) and Positron Emission Tomography.

In the following subsections, the findings of MRI studies with migraine patients are exposed. First, the previous results studies based on T1-weighted processing are described, with special focus on the gray matter morphometry parameters that are employed in this thesis. The results of studies that used T2-weighted, fMRI and MRS are summarized. Furthermore, the results of studies using dMRI and simultaneous analysis of diverse MRI modalities are detailed.

### *2.4.1.* ***T1-weighted MRI studies***

Due to the good contrast between gray matter and white matter in T1-weighted MRI, this modality is used frequently to quantify gray matter.

One migraine study should be highlighted (Schwedt, Chong, et al., 2015). In this study, the authors classified patients with CM and EM and controls using Principal Component Analysis (PCA) to summarize information of volume, area and thickness from gray matter. Diagonal quadratic discriminant analysis and decision trees were employed as classification methods in this study, with no direct comparison of the parameters with statistical tests between the three groups. The average accuracy of the classification of CM with respect to EM and controls was 84.2% and 86.3%, respectively. Thickness, area and volume values of diverse regions were used in the previous classifications. Worse classification results were obtained in the classification between all the patients with migraine and controls (average accuracy = 68.0%) and EM and controls (average accuracy = 67.2%).

In the following subsections, the results of the analysis of gray matter morphometry parameters in previous migraine studies are described, together with the results of the classification study commented in the previous paragraph.

#### *A. Gray Matter Volume results*

The most frequent result of these studies was significantly reduced gray matter volume in patients with migraine compared to controls (Coppola et al., 2015; Jin et al., 2013; J. H. Kim et al., 2008; Maleki et al., 2012a; Messina, Rocca, et al., 2018; Messina et al., 2017; Morollón Sánchez-Mateos, 2020; Rocca, Ceccarelli, Falini, Colombo, et al., 2006; Schmidt-Wilcke, Gänßbauer, Neuner, Bogdahn, & May, 2008; Schmitz, Arkink, et al., 2008; Yuan et al., 2013), result that has also been reported in a meta-analysis (Jia & Yu, 2017). In this meta-analysis, reduced volume was identified in frontal regions and the cingulate gyrus.

However, the opposite result, i.e., higher gray matter volume values in patients with migraine, has also been reported in visual processing regions (Messina et al., 2017; Morollón Sánchez-Mateos, 2020; J. Zhang et al., 2017) and particularly CM in subcortical regions (Neeb et al., 2017). Other studies have reported no significant differences between patients with migraine and controls after corrections for multiple comparisons (Husøy et al., 2019; Schmitz, Admiraal-Behloul, et al., 2008; Tedeschi et al., 2016; Valfrè, Rainero, Bergui, & Pinessi, 2008).

With respect to the comparison between patients with CM and EM, two studies compared both groups, although none of them obtained significant results after corrections for multiple comparisons (Neeb et al., 2017; Valfrè et al., 2008), both with low sample size (less than 25 subjects per group). Considering uncorrected results, lower gray matter volume values in CM were identified in diverse regions (Neeb et al., 2017; Valfrè et al., 2008), while increased values in CM were detected in the middle and inferior temporal gyri (Neeb et al., 2017). In high-frequency EM patients, lower volume values were identified in comparison with the low-frequency EM in the insula (Maleki et al., 2012a).

### *B. Cortical Thickness results*

Cortical thickness has been less studied than gray matter volume in migraine studies. In the comparison between patients with migraine and controls, lower thickness values have been found in migraine (Chong, Dodick, Schlaggar, & Schwedt, 2014; Hougaard et al., 2016; Magon et al., 2019; Maleki et al., 2012a; Messina et al., 2013; J. Zhang et al., 2017). In contrast, increased thickness values have also been reported in migraine against controls (A. F. DaSilva, Granziera, Snyder, & Hadjikhani, 2007; Gaist et al., 2018; Granziera et al., 2006; J. H. Kim et al., 2014; J. Zhang et al., 2017) and in high-frequency EM compared to controls (Maleki et al., 2012a). In one whole-brain study, no significant differences were found between patients with migraine and controls (Datta, Detre, Aguirre, & Cucchiara, 2011). Increased cortical thickness has been identified in the hemisphere contralateral to pain (Hougaard et al., 2015) and in the postcentral gyrus (Morollón Sánchez-Mateos, 2020) in patients with migraine .

This parameter has not been compared directly between patients with CM and EM. However, higher thickness values have been identified in several regions of patients with high-frequency EM with respect to low-frequency EM (Maleki et al., 2012a). In CM, the patients with a positive response to onabotulinumtoxinA treatment showed higher thickness than non-responders (Hubbard et al., 2016).

### *C. Surface Area results*

Only one study compared directly whole-brain surface area values between patients with migraine and controls, finding widely statistically significant lower values in the patients (Messina et al., 2013). Another study with participants aged 50 to 66 years assessing the anterior cingulate and the prefrontal cortex and the insula found no significant differences between patients with migraine and controls (Husøy et al., 2019). No studies assessed directly differences between CM and EM.

### *D. Gyrification Index and Cortical Curvature results*

Only one study assessed differences of the gyrification index between patients with migraine (migraine without aura specifically) and controls, finding increased and decreased values in the patients group (J. Zhang et al., 2017).

There was no previous study comparing cortical curvature values between migraine patients and controls as main objective. This comparison has been performed in regions where differences between patients with migraine and persistent post-traumatic headache were identified, but no differences were detected between patients with migraine and controls (Schwedt, Chong, Peplinski, Ross, & Berisha, 2017).

## *2.4.2.* ***T2-weighted MRI findings***

As stated in section 2.4, T2-weighted images have been employed in the assessment of WMH in migraine. A meta-analysis reported that migraine is associated with an increased risk of WMH (Swartz & Kern, 2004). WMH have been found in more recent studies in patients with migraine (Degirmenci et al., 2007; Messina et al., 2015, 2017, 2013; Rocca, Ceccarelli, Falini, Colombo, et al., 2006), although they are not always present in patients with migraine (Schmitz, Admiraal-Behloul, et al., 2008; Tedeschi et al., 2016). The percentage of patients with no WMH is moderate-to-high in some studies reporting them (42% in (Messina et al., 2017), and 87% in (Messina et al., 2015)).

Regarding the relationship between WMH and migraine, they have been associated with pain in patients with EM and an unfavorable prognosis (Xie et al., 2018; Yalcin et al., 2018).

## *2.4.3.* ***Diffusion MRI studies***

DTI-based descriptors are the main parameters employed to analyze white matter integrity in patients with migraine. The most popular method to assess dMRI data from migraine patients is TBSS, although an important variety of methods has been applied in the literature.

In the following three subsections (A, B and C), the results of the comparisons between the main groups are described. In the next subsection (D), the results of the correlation analysis between DTI-based parameters and clinical features are shown. In the last additional two subsections (E and F), results employing graph theory and non-DTI measures, respectively, are stated.

### *A. Migraine versus Healthy Controls*

The most reported result in the comparison of patients with migraine and controls is reduced FA in the patients with respect to controls in multiple regions (A. F. M. DaSilva et al., 2007; Gomez-Beldarrain et al., 2015; Granziera et al., 2006; Kattem Husøy, Eikenes, Håberg, Hagen, & Stovner, 2019; X. L. Li et al., 2011; Morollón Sánchez-Mateos, 2020; Rocca et al., 2008; Schmitz, Admiraal-Behloul, et al., 2008; Shibata, Ishiyama, & Matsushita, 2018; Szabó et al., 2018, 2012; Yu, Yuan, Qin, et al., 2013; Yu, Yuan, Zhao, et al., 2013; Yuan et al., 2012). In contrast, higher

FA values in patients have been identified in the thalamus (Coppola et al., 2014), a gray matter subcortical region, and in pediatric patients in the optic radiations (Messina et al., 2015).

For the other DTI measures, i.e., AD, MD and RD, there is no clear pattern and the results are conflicting, finding contradictory trends in specific regions. Regarding AD, lower values in migraine have been identified in three studies (Messina et al., 2015; Yu, Yuan, Qin, et al., 2013; Yu, Yuan, Zhao, et al., 2013), while higher values in migraine have been detected in other three studies (Kattem Husøy et al., 2019; Marciszewski et al., 2019; Qin et al., 2019). Some regions included in these studies are the corticospinal tract, the inferior and superior longitudinal fasciculus, the corpus callosum or the brainstem.

With respect to MD, lower values in the patients were identified in the same three studies that detected lower AD values (Messina et al., 2015; Yu, Yuan, Qin, et al., 2013; Yu, Yuan, Zhao, et al., 2013). The opposite result, increased MD values in the patients with migraine, has been found with higher frequency (nine studies) (Chong & Schwedt, 2015; Ito et al., 2016; Kattem Husøy et al., 2019; Marciszewski et al., 2018, 2019; Qin et al., 2019; Rocca et al., 2008; Shibata et al., 2018; Szabó et al., 2012). In another study, the reported result was higher ADC in patients with MWoA compared to controls (Kara et al., 2013). In this context, the ADC is equivalent to the MD.

In the case of RD, lower values in patients with migraine were reported in three studies, two of them different with respect to the studies that found reduced AD and MD values (Chong, Peplinski, Berisha, Ross, & Schwedt, 2019; Messina et al., 2015; Szabó et al., 2018). Higher RD values in patients were identified in six studies (Chong et al., 2019; Chong & Schwedt, 2015; Marciszewski et al., 2019; Qin et al., 2019; Shibata et al., 2018; Szabó et al., 2012). It is worth noting that in one study the two trends with statistically significant differences between migraine patients and controls were detected (Chong et al., 2019). Interestingly, these opposite trends were found in the cingulum, but in different sections.

In all the previous studies from this subsection, statistically significant differences were described. In five studies, no significant differences for any of the four DTI-based parameters were found between migraine patients and controls (Neeb et al., 2015; Petrušić, Daković, Kačar, Mićić, & Zidverc-Trajković, 2018; Tedeschi et al., 2016; Tessitore et al., 2015; J. Zhang et al., 2017).

### *B. Migraine with aura versus Migraine without aura*

An important part of the studies included simultaneously patients with Migraine with Aura (MWA) and Migraine without Aura (MWoA), and the DTI-based parameters of these patients were compared to controls. However, differences between both groups of migraine patients were directly compared exclusively in seven studies.

In five of these studies, no significant differences between MWA and MWoA were identified (Granziera et al., 2006; Morollón Sánchez-Mateos, 2020; Shibata et al., 2018; Tedeschi et al., 2016; Tessitore et al., 2015). With respect to the other two studies, opposite results were obtained. On the one hand, lower FA values were found in patients with MWA compared to MWoA in the optic

radiation (Rocca et al., 2008). On the other hand, higher FA values were identified in patients with MWA in comparison with MWoA in the left parieto-occipital white matter (Szabó et al., 2018).

The two regions with significant differences are involved in visual perception. The tracts of the optic radiation transmit information from the retina to the visual cortex, while the parieto-occipital cortex contains visual areas. Considering that aura is mainly related to visual symptoms, the reported differences may be associated with these symptoms and not with distinct types of migraine, as stated at the beginning of section 2.1.

### *C. Chronic Migraine vs Episodic Migraine*

Patients with CM were included only in four studies analyzing migraine with dMRI data, but in three of these studies these patients were not directly compared to EM patients. In one of these studies, EM patients were finally excluded because after a six-month follow-up the EM group was composed of patients with both EM and CM at baseline (Gomez-Beldarrain et al., 2015). In another study, there were only four patients with CM, an insufficient sample size to perform comparisons with EM (Chong & Schwedt, 2015). In the third study, there was no comparison between CM and EM because the sample size of the EM group was relatively small to carry out a direct statistical comparison (Chong et al., 2019).

In the study that compared the CM and EM groups, no statistically significant differences were found after the correction for multiple comparison (Neeb et al., 2015). In this study, the sample size was relatively small (21 subjects per group).

A very recent study should be noted. In this study, patients with CM showed decreased FA and increased MD values compared to the patients with EM (Coppola et al., 2020). This study was published after the the second contribution of this thesis (Chapter 2 of Part II) (Planchuelo-Gómez, García-Azorín, Guerrero, Aja-Fernández, Rodríguez, & de Luis-García, 2020b), which presents a similar analysis compared to (Coppola et al., 2020). A comparison of both studies is included in section 5.2 of Chapter 5 of Part I.

### *D. Correlation between diffusion and clinical features*

Significant correlations between DTI-based measures and clinical features were found in diverse studies. The clinical features were the duration of migraine and the headache or migraine frequency in most studies.

For the FA,MD and AD, statistically significant negative correlation was found between duration of migraine in patients with EM and MWA (X. L. Li et al., 2011; Szabó et al., 2018; Yu, Yuan, Qin, et al., 2013). In contrast, a significant positive correlation has also been reported between duration of migraine and MD, although in different regions compared to the negative correlations with MD (Chong & Schwedt, 2015).

The analysis of headache or migraine frequency was assessed using the number of monthly days or the number of days since the last attack. A negative correlation with the number of monthly days, referred as headache/migraine frequency for the rest of this section, is equivalent

to a positive correlation with the number of days since the last attack. A significant negative correlation has been found between FA and headache or migraine frequency (Coppola et al., 2014; Gomez-Beldarrain et al., 2015; X. L. Li et al., 2011). A significant positive correlation has been identified between MD and headache frequency (Chong et al., 2019).

Statistically significant correlations with other features such as scores from the Hamilton test (levels of anxiety and depression) (X. L. Li et al., 2011), aura frequency (Petrušić et al., 2018) and lifetime attack (Szabó et al., 2018) with FA, MD and AD have also been found.

No significant correlations were found in diverse studies (A. F. M. DaSilva et al., 2007; Kara et al., 2013; Kattem Husøy et al., 2019; Marciszewski et al., 2018, 2019; Messina et al., 2015; Neeb et al., 2015; Qin et al., 2019; Shibata et al., 2018).

### *E. Studies with Graph Theory measures*

Three studies have employed Graph Theory to assess structural connectivity in patients with MWoA using DTI-based measures and compare these patients with controls.

In the first study, higher connection global distance and altered topology in structural networks were reported in MWoA (J. Liu et al., 2013). The second study used two datasets (one of them for replication) and, in patients with MWoA, higher feeder connection density, abnormal small-world organization, higher global efficiency and lower strength of structural-functional connectivity coupling were found (K. Li et al., 2017). In the last study, in patients with MWoA, higher network integration and nodal efficiency were identified (J. Liu et al., 2017).

### *F. Studies with advanced diffusion measures*

In this section, results from two studies are described. Interestingly, in both studies gray matter was assessed instead of white matter, in contrast to most dMRI studies.

In the first study, DKI was employed to assess periaqueductal gray matter differences between patients with EM and controls (Ito et al., 2016). In the evaluated region, mean kurtosis and MD values were higher in the patients with migraine, while no statistically significant FA differences were found.

In the second study, the mean average propagator-MRI model was used to evaluate gray matter differences between patients with migraine without aura and controls (Xiaoyun et al., 2020). Increased and decreased RTAP, RTOP and RTPP values were higher in patients compared to controls in diverse gray matter regions. These three parameters are described in section C of section 2.2.2.

## *2.4.4.* ***Functional MRI studies***

The target of fMRI is to estimate hemodynamic changes using the Blood Oxygen Level Dependent (BOLD) signal. To understand the basic principle of fMRI, it is important to define the role of hemoglobin. Hemoglobin is a protein in the red blood cells that transports the oxygen to the

tissues. Oxyhemoglobin is the oxygenated form of hemoglobin and it is present in the arteries for the delivery of oxygen to the cells, while deoxyhemoglobin is the deoxygenated form present in the veins after the delivery of oxygen. Considering that deoxyhemoglobin is paramagnetic and that oxyhemoglobin is diamagnetic, the BOLD signal aims to measure signal changes from the tissues surrounding the blood vessels (Ogawa, Lee, Kay, & Tank, 1990).

Two main fMRI modalities are distinguished. The first one is the so-called *resting state* fMRI. In this modality, the subject executes no special activity and must be relaxed, with closed or opened eyes depending on the experiment. The other modality is *task-based* fMRI. The subject must accomplish specific activities while the images are acquired or the response to specific stimuli, e.g. painful stimuli, is measured during the acquisition.

In migraine fMRI studies, especially in those acquired using the *resting state* modality, the functional connectivity is estimated, regarding a possible link to the microstructure or the structural connectivity (Coppola, Di Renzo, Tinelli, Di Lorenzo, et al., 2016; Coppola, Di Renzo, Tinelli, Lepre, et al., 2016; K. Li et al., 2017). The diverse techniques employed in these studies include connectivity between different ROIs (ROI-to-ROI analysis), between one specific region and other regions (seed-to-ROI analysis), between all voxels (voxel-to-voxel analysis) and in specific networks obtained with Independent Component Analysis (ICA).

Previous review studies have reported functional alterations of the so-called pain matrix (May, 2007, 2009). The pain matrix is a group of regions which have been related to pain and headache processing. The pain matrix involves subcortical regions, mainly the thalamus and the amygdala, and cortical regions from every lobe such as the insula, the prefrontal cortex, the cingulate cortex, the primary sensory cortex and the posterior parietal cortex (May, 2009).

A review has shown that migraine is associated with atypical brain activation in response to sensory stimuli and functional connectivity leading to enhanced sensory facilitation and reduced inhibition and habituation between migraine attacks (Schwedt, Chiang, Chong, & Dodick, 2015). In another review study, it has been suggested that the pain threshold is lower in patients with migraine during the ictal phase with respect to the interictal phase in response to pressure, cold and heat stimuli (Russo et al., 2018).

Regarding the comparison between patients with CM and EM, increased *resting state* functional connectivity has been identified in CM in regions of the pain matrix (Lee et al., 2019).

Despite the advantages of fMRI, the migraine studies present a poor level of reproducibility and no specific migraine pattern has been found (Skorobogatykh et al., 2019).

### *2.4.5.* ***Magnetic Resonance Spectroscopy studies***

The objective of MRS is to detect biochemical changes in the brain by the identification of certain metabolites involved in physiological or pathological processes (Lai et al., 2015).

Based on $^{31}$P-MRS studies, reduced availability of neuronal energy and mitochondrial dysfunction in the migraine brain has been suggested, together with abnormalities in glutamate and

$\gamma$-aminobutyric acid, and reduced N-Acetylaspartate levels (Younis, Hougaard, Vestergaard, Larsson, & Ashina, 2017). In another review study, a slight increase in lactate peak in migraine with aura compared to migraine without aura patients and controls has been reported (Lakhan, Avramut, & Tepper, 2013).

### *2.4.6.* ***Combination of MRI modalities***

Two studies have employed information from diverse MRI modalities to evaluate simultaneous structural and functional changes in patients with migraine.

In one study, correlations between functional activity and DTI-based parameters in white matter were assessed in patients with migraine with aura and controls (Faragó et al., 2019). The authors found positive correlation between FA and frontal activity, and negative correlation between RD and frontal activity.

In the other study, the functional connectivity was analyzed in regions where gray matter volume loss was reported in patients with imgraine according to the meta-analysis of (Jia & Yu, 2017). The authors identified positive functional connections with the insula and negative connections with the hypothalamus and the visual cortex in migraine patients with respect to controls (Burke et al., 2020).

None of these studies actually employed a simultaneous analysis with data from more than one MRI modality. The correlation analysis is unable to detect covariance patterns, while the other study used the results from a meta-analysis to investigate functional connectivity alterations.

# *Chapter 3*

# *Materials and Methods*

In this chapter, the most important aspects of the dataset employed in all the contributions of this thesis and the methods used to process the MRI data are explained. The groups of interest compared in the diverse studies that compose the compendium are described together with the details of the MRI acquisition. The different methods used to obtain quantitative parameters for the comparisons between the groups of interest in each contribution of the compendium and the statistical analysis carried out for the corresponding comparisons are reported. The full details are available in each contribution included in the chapters of Part II.

## 3.1. Database

The complete dataset used in this doctoral thesis was composed of:

- 52 Healthy Controls (HC), including 41 women (79%), aged 36.4 ± 13.1 years (mean ± standard deviation).
- 57 patients with Episodic Migraine (EM), including 48 women (84%), aged 37.3 ± 8.4 years. The duration of migraine history was 14.3 ± 11.2 years. No patients suffered from Medication Overuse Headache (MOH) and 10 patients suffered from Migraine with Aura (MWA) (17.5%).
- 57 patients with Chronic Migraine (CM), including 51 women (89%), aged 38.1 ± 9.3 years. The duration of migraine history was 19.8 ± 10.8 years. The time from onset of CM was 26.3 ± 34.9 months. Forty-three patients suffered from MOH (75.4%) and two patients suffered from MWA (3.5%).

All the subjects included in this study, patients and controls, were aged between 18 and 60 years, both limits included, and had an available T1-weighted image. All the subjects except one HC and one patient with EM presented a complete set of diffusion-weighted MRI volumes. In one subject from each group, there were errors in the dMRI processing pipeline described in section 3.2.2. Therefore, the database was composed of 50 HC, 54 EM and 56 CM in the studies that employed dMRI data.

In sections 3.1.1 and 3.1.2, specific conditions of the HC and patients with migraine are described. In section 3.1.3, the acquisition details of the MRI protocol, typically used in the clinical routine, are described.

### *3.1.1.* ***Healthy Controls***

It is worth noting that, in migraine studies, it is difficult to find controls who do not harbor a headache or migraine pathology (Messina, Filippi, & Goadsby, 2018). Considering this point, all the controls who were scanned fulfilled a questionnaire. The questionnaire was composed of three groups of questions:

- **Group 0**. This group included two questions. This part of the questionnaire included questions related to a previous diagnosis of migraine, made by a neurologist or a primary care physician (first question), and previous history of headache (suffering from any headache), with no need of a previous diagnosis (second question). If the subject confirmed a previous diagnosis of migraine in the first question, s/he was not included in the dataset for this thesis. If the subject reported no previous headaches, the corresponding subject was included in the dataset, with no need to answer the questions from groups 1 and 2.
- **Group 1**. This group included five questions. The first question was related to the frequency of headache in more than 15 days per month. The remaining questions were associated with the criterion C of Migraine without Aura (MWoA) from the Third edition of the International Classification of Headache Disorders (ICHD-3) (Headache Classification Committee of the International Headache Society, 2018). These questions were referred to a pulsating quality, unilateral location, need to stop an activity or rest for at least two hours, and pain aggravated by physical movement. If three or more questions of this group were positively answered, the subject was discarded and not included in the dataset.
- **Group 2**. This group included three questions, all of them associated with the criterion D of MWoA from the ICHD-3 (Headache Classification Committee of the International Headache Society, 2018). The questions asked about situations during the headache attack. These situations were photophobia, phonophobia and nausea and/or vomiting. If two or more questions were positively answered, the subject was discarded and not included in the dataset.

The complete questionnaire is provided in Appendix A. In any of the combinations to the questions of the three groups not explicitly mentioned in the previous paragraphs of this section, the subject was included in the dataset, except if other exclusion criteria were met. In case of doubtful cases, a neurologist specialized in headaches was asked and decided whether to include finally the corresponding subject in the study.

The HC were recruited by snowball and convenience sampling and were discarded for the study if they presented a history (current or past) of psychiatric or neurological diseases, except infrequent tension-type headache.

### 3.1.2. Patients with Migraine

The patients with migraine were screened and recruited by neurologists specialized in headaches from the Headache Unit at the Hospital Clínico Universitario de Valladolid (Valladolid, Spain). When these patients were recruited, they were visiting the Headache Unit for first time and their diagnosis was based on the criteria for EM and CM from the available version of the ICHD-3 (the current or the beta version). The inclusion criteria for the patients were the following:

- Stable clinical situation for at least three months before the visit to the Headache Unit.
- No intake of any preventive treatment at the moment of the visit.
- Migraine onset before the age of 50 years.
- Suffering from migraine for at least one year.

If a preventive treatment was prescribed at the visit, the patient started the treatment after the MRI acquisition. The patients were required to fulfill a headache diary the three months before the final inclusion in the dataset. From this diary, the information about the frequency of headache and migraine was gathered. The exclusion criteria were the following:

- Suffering from headache between 10 and 14 days per month, both limits included. The reason was that these patients are the so-called high-frequency EM, and to avoid any misclassification between CM and EM, they were not included.
- Painful disorders or conditions different to migraine or headache for at least 10 days per month.
- Primary or secondary headaches except infrequent tension-type headache and MOH.
- Psychiatric or neurological disorders different from migraine.
- Pregnancy.
- Previous diagnosis of anxiety or depression or with a positive diagnosis according to the Hospital Anxiety and Depression Scale thresholds (Zigmond & Snaith, 1983).

MOH was considered as the consumption of analgesics and/or triptans for at least 10 days per month, following the ICHD-3 (Headache Classification Committee of the International Headache Society, 2018).

### 3.1.3. MRI acquisition

Regarding the patients with migraine, the MRI acquisition was performed during an interictal period, one or two weeks after the visit at the Headache Unit.

In the same session, a set of T1- and diffusion-weighted images were acquired with a Philips Achieva 3T MRI unit (Philips Healthcare, Best, The Netherlands). The T1-weighted images were acquired in first place, being followed by the diffusion-weighted images. A 32-channel head coil was employed in the acquisition. The MRI unit was located in the MRI facility at the Universidad

de Valladolid (Valladolid, Spain). The total acquisition time for each subject was approximately 18 minutes.

The acquisition parameters for the high-resolution 3D T1-weighted were the following:

- Turbo Field Echo sequence.
- TR = 8.1 ms, TE = 3.7 ms.
- Flip angle = 8°.
- Matrix size = 256 × 256 (each slice), with 160 sagittal slices to cover the whole brain.
- Spatial resolution = 1 × 1 × 1 $mm^3$.

The acquisition parameters for the diffusion-weighted images were:

- TR = 9000 ms, TE = 86 ms.
- Flip angle = 90°.
- Matrix size = 128 × 128 (each slice), with 66 axial slices to cover the whole brain.
- Spatial resolution = 2 × 2 × 2 $mm^3$.
- One baseline volume (b = 0 $s/mm^2$) and single-shell acquisition with 61 different gradient orientations and b-value = 1000 $s/mm^2$.

The 61 gradient directions were obtained following a sampling strategy in a way that the directions could be subsampled into one 40 gradient directions scheme and another 21 gradient directions scheme.

The acquisitions were performed between May 2014 and July 2018.

## 3.2. Methodology

The main objective of the methods implemented in this thesis is to extract quantitative parameters in diverse voxels, ROIs or connections for the comparison of these values between patients with CM and EM and HC.

In this section, the diverse processing steps for the different contributions are described in detail. The main neuroimaging software employed for the image processing were FreeSurfer (`https://surfer.nmr.mgh.harvard.edu/`), MRtrix (Tournier et al., 2019) and FMRIB Software Library (FSL) (Jenkinson, Beckmann, Behrens, Woolrich, & Smith, 2012). MATLAB and R statistical software were employed to complement and perform the analyses and processing carried out with the neuroimaging software. Furthermore, some steps of the neuroimaging software ran under MATLAB environment or use MATLAB scripts.

The three neuroimaging software platforms previously mentioned were used because of their versatility and wide use in the literature. FreeSurfer was employed to analyze in detail gray matter morphometry parameters from different regions and a segmentation of multiple brain structures. FSL was the software used for the TBSS analysis, and allowed the computation of DTI-based

parameters and dMRI preprocessing among multiple functions. MRtrix was used because of its similar functions with respect to FSL, but it allowed to perform additional dMRI preprocessing steps and to carry out tractography and connectomics analysis.

### *3.2.1.* ***Gray Matter Morphometry***

The FreeSurfer pipeline was applied to the T1-weighted images in order to obtain the gray matter morphometry parameters. Briefly, this pipeline segmented diverse regions and tissues of the brain and also other parameters, including those associated with gray matter morphometry, were extracted. The objective of the implementation of the FreeSurfer pipeline was to obtain diverse descriptors of the structure in multiple regions to characterize the pattern of gray matter alterations in migraine compared to controls and between CM and EM. The extraction of the gray matter morphometry parameters through the FreeSurfer pipeline is the key element of the analysis in Chapter 1 of Part II and the extracted parameters are also employed in Chapter 6 of Part II.

A summary of all the steps carried out in the FreeSurfer pipeline is shown below:

1. **Motion correction**. This step was carried out to correct small motions between source volumes, including an average of the volumes (Reuter, Rosas, & Fischl, 2010). If there is only one volume, as in the case of a unique T1-weighted image, the original volume is used in subsequent steps.
2. **Intensity normalization**. A non-parametric approach was used for the automatic correction of intensity non-uniformity (Sled, Zijdenbos, & Evans, 1998).
3. **Talairach transformation**. This transformation was an automated affine registration from the original volume to the MNI305 atlas in the Montreal Neurological Institute (MNI) space.
4. **Normalization**. Another normalization was carried out to scale the intensity of all voxels so that the mean intensity of the white matter voxels was equal to 110.
5. **Skull strip**. The watershed algorithm was applied in order to remove the skull (Segonne et al., 2004).
6. **Automatic Subcortical Segmentation**. This step included six stages. These stages were initial registration to a template (the CGA atlas), canonical normalization, canonical registration (nonlinear transformation) to the template, neck removal from the image of the global second step, registration with the skull and subcortical labeling (Fischl et al., 2002; Fischl, Salat, et al., 2004).
7. **Computation of subcortical values**. In this step, the values of the volume, among other variables, were obtained for subcortical gray matter regions and other regions such as the CSF or divisions of the corpus callosum.
8. **Second normalization**. An intensity correction was performed, but without the skull, in contrast to the previous major normalization.
9. **White matter segmentation**. A mask of the white matter was created using the intensity, neighborhood and smoothness constraints.

10. **Cut and fill**. From the white matter image, the subcortical mass was created. The brain hemispheres were separated and binarized to 255 (left) and 127 (right). The mid brain was cut from the cerebrum.
11. **Tessellation**. The surface model of the subject was created from the result of the previous step. The generation of the surface was based on covering the filled hemisphere with triangles, creating vertices in the points where the triangles met (Fischl, Liu, & Dale, 2001; Segonne, Pacheco, & Fischl, 2007).
12. **Surface smoothing**. The vertices were adjusted to reduce the angle between triangles.
13. **Surface inflation**. The objective of this step was to minimize metric distortion, but preserving distances and areas (Fischl, Sereno, & Dale, 1999).
14. **QSphere**. A quasi-homeomorphic spherical transformation was applied to the inflated surface. This was the initial stage of the automatic topology fixing and the objective was to detect topological defects, i.e., holes in a filled hemisphere.
15. **Automatic Topology Fixer**. The defects identified in the previous step were corrected and the number of vertices was changed.
16. **Surface deformation**. The intensity gradients were employed to determine the placement of the borders between gray and white matter, and between gray matter and CSF (Dale, Fischl, & Sereno, 1999; Fischl & Dale, 2000). The white matter and pial surfaces were generated and the information from thickness and curvature was gathered. The pial surface was created from the expansion of the white matter surface following the gray matter-CSF intensity gradient.
17. **Cortical Ribbon Mask**. Binary volume masks of the cortical ribbon were created.
18. **Spherical Inflation**. The original surface was inflated again for the registration of the the surface to the spherical atlas.
19. **Ipsilateral Surface Registration**. Registration of the spherically inflated surface to the spherical atlas (Fischl, Sereno, Tootell, & Dale, 1999). This step was important to match cortical geometry across subjects.
20. **Contralateral Surface Registration**. Same technique compared to the previous step, but the registration was carried out to the contralateral atlas.
21. **Average Curvature**. The average curvature was resampled from the atlas to the subject curvature.
22. **Cortical Parcellation**. A neuronanatomical label was assigned to each region of the cortical surface considering the geometric information from the cortical model (Fischl, van der Kouwe, et al., 2004).
23. **Parcellation values**. Different values were assigned to each neuroanatomical cortical label. Among these values, the surface area, the gray matter volume, the cortical thickness and the mean curvature were included.

**Figure 3.1:** Example of a T1-weighted image (left) and the corresponding cortical parcellation from the FreeSurfer pipeline (right).

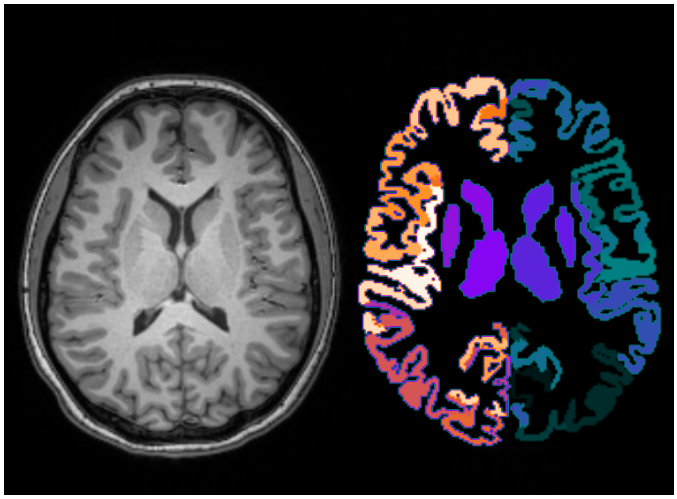

**Figure 3.2:** Example of a T1-weighted image (left) and the corresponding cortical parcellation from the FreeSurfer pipeline including only regions from the Desikan-Killiany atlas (right).

The result of the cortical parcellation was an image with 2034 labeled regions, including the background (value 0). An example of the final image created by the FreeSurfer pipeline is shown in Figure 3.1.

In the analysis carried out in this thesis, the Desikan-Killiany atlas was used (Desikan et al., 2006). This atlas is composed of 68 cortical regions (34 bilateral regions), the cerebellum (bilateral) and 14 subcortical regions (seven bilateral regions). The gray matter volume is computed for the 84 regions, while the cortical curvature, cortical thickness and surface area only for the 68 cortical regions. The regions of the Desikan-Killiany atlas are detailed in Appendix B. An example of the cortical parcellation including only some regions of the Desikan-Killiany atlas is shown in Figure 3.2.

## *3.2.2.* ***Diffusion MRI processing***

DMRI processing is the key element of the comparisons to extract quantitative parameters to assess the white matter integrity in patients with CM and EM and HC in Chapters 2 and 3 of Part II. The objective of the evaluation of diffusion descriptors was the identification of white matter structural differences between patients with migraine and controls and between CM and EM.

In the next subsections, the most important aspects of the preprocessing of diffusion-weighted images (subsection A), the TBSS analysis (subsection B) and the advanced diffusion measures obtained with AMURA (subsection C) are described. These methods have been directly applied in Chapters 2 and 3 of Part II.

### *A. Preprocessing*

All the preprocessing steps were carried out using the MRtrix and the FSL software. The dMRI preprocessing pipeline was composed of three steps.

The first step was image noise reduction. Based on the redundancy of dMRI data, a PCA denoising algorithm was applied. This algorithm assumes that the eigenvalues of the principal components associated exclusively with noise follow the Marchenko-Pastur distribution, parametrized by non-Gaussian noise variance (Veraart, Fieremans, & Novikov, 2016; Veraart, Novikov, et al., 2016). The objective of this step was to preserve the components that carry diffusion signal information, removing the components that only contained noise. The algorithm was computed in diverse sliding windows or kernels that include a 3D neighborhood of the diffusion-weighted image. The *dwidenoise* command from MRtrix was employed for this step.

The second step consisted of correction for motion and eddy currents-induced distortions. The eddy currents-induced field and the subject movement were estimated using a Gaussian Process and a theoretical prediction was compared to the observed diffusion-weighted volume to correct the distortion and movement effects (Andersson & Sotiropoulos, 2016). This step was implemented using the *dwipreproc* command from MRtrix, which employs the *eddy* tool from FSL. It is worth noting that, in this step, susceptibility-induced distortion correction could be also carried out, but at least two baseline volumes with opposite diffusion encoding directions, unavailable in our sample, are needed. This last distortion is related to $B_0$ field inhomogeneities.

The last step was a $B_1$ field inhomogeneity correction. Briefly, the bias field was estimated using a stochastic process, a hidden Markov random field model, and incorporating an expectation-maximization algorithm (Y. Zhang, Brady, & Smith, 2001). For this step, the *dwibiascorrect* command from MRtrix was employed.

After these preprocessing steps, a dMRI mask was created using the *dwi2mask* command from MRtrix and the diffusion tensor was fitted at each voxel with the *dtifit* tool from FSL. The *dtifit* tool uses the values from the diffusion tensor to extract the values of the DTI-based parameters (FA, AD, RD and MD in this thesis) at each voxel and create a map with the values of the descriptors. An example of these maps for the four parameters is shown in Figure 3.3. These maps were used

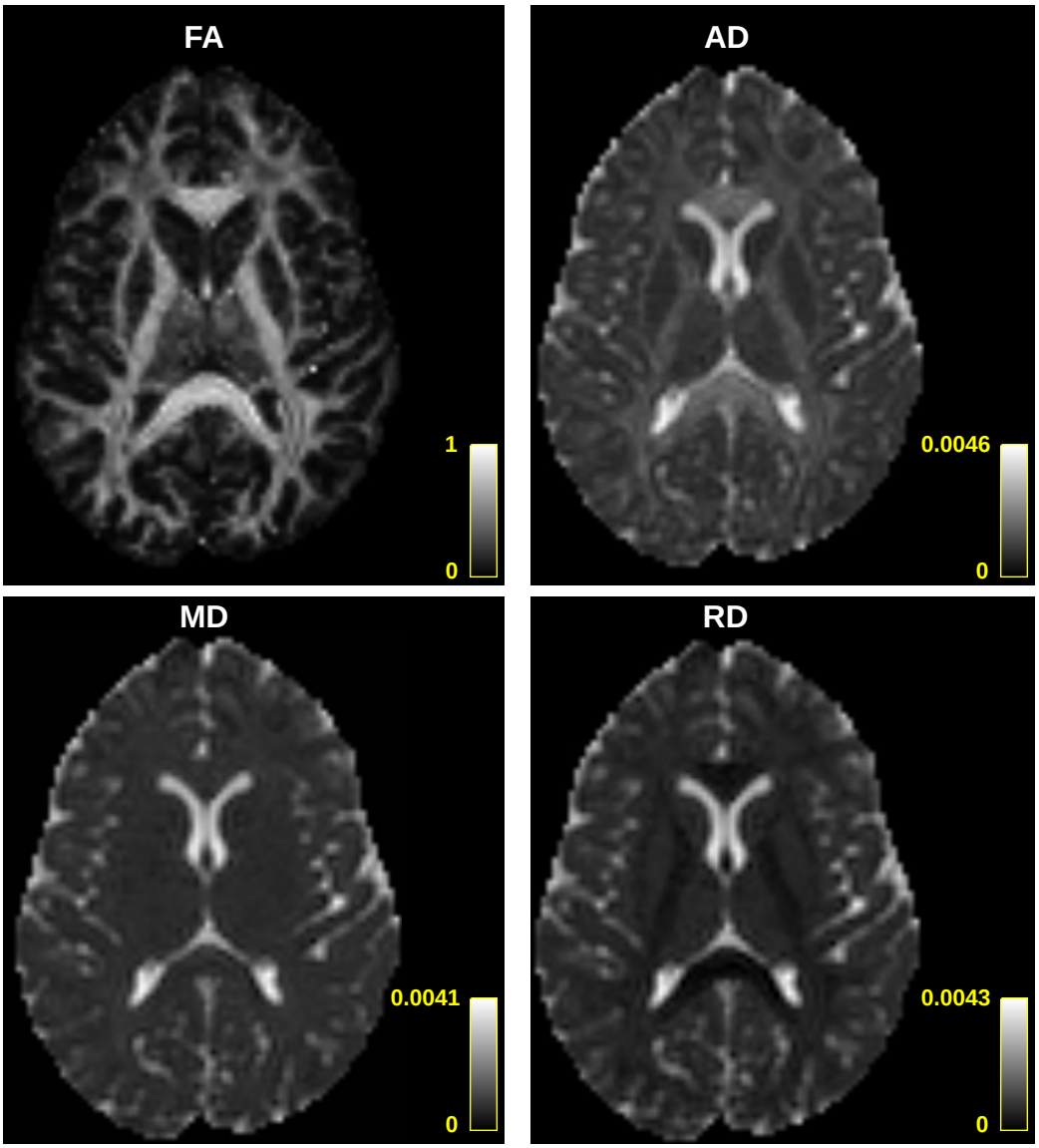


**Figure 3.3:** Example of an axial slice for each of the four main DTI-based parameters. Top-left: FA, top-right: AD, bottom-left: MD, bottom-right: RD.

in Chapters 2 and 3 of Part II to characterize white matter properties of patients with CM and EM and HC.

### *B. TBSS*

Tract-Based Spatial Statistics (TBSS) is used to overcome the limitations of other methods by measuring the values of the diffusion descriptors in the center of the white matter tracts. The TBSS pipeline creates a skeleton where the statistical comparisons of the diffusion measures between the groups of interest are carried out, while the remaining parts of the brain are ignored in the comparisons. This pipeline was carried out to determine the white matter integrity differences between patients with CM and EM and HC in Chapters 2 and 3 of Part II. Moreover, it was also used to evaluate the impact of sample size and the number of diffusion orientations in comparisons between groups in dMRI in Chapter 4 of Part II. The TBSS pipeline is carried out in four steps

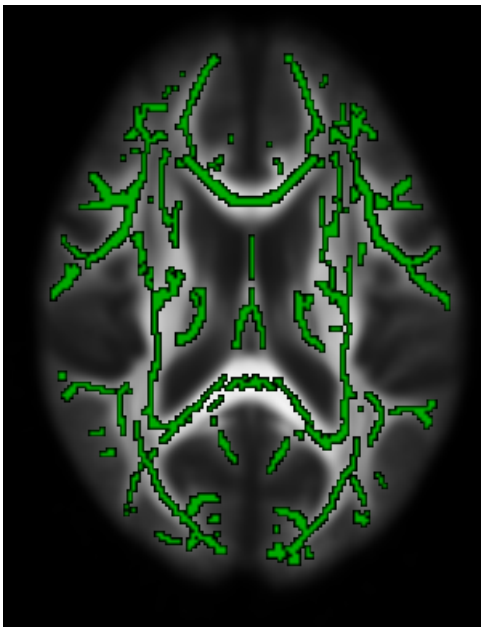

**Figure 3.4:** Example of an axial slice of the mean FA image with its corresponding mask of the skeleton in green.

to carry out voxelwise statistical comparisons between the groups in the obtained skeleton. These four steps are firstly applied to the FA images. Next, the TBSS pipeline was applied to the remaining diffusion descriptors based on DTI or from Apparent Measures Using Reduced Acquisitions (AMURA), all of them described in section C of section 2.2.2.

The first step was simply an organization of the FA images in a common directory. The FA images of all the subjects, including every group of interest, CM, EM and HC in this thesis, were stored in the directory.

The second step was the non-linear registration of the FA images to the $1 \times 1 \times 1$ mm$^3$ MNI standard space. This step was initialized with a linear transformation, implemented with the *FLIRT* tool from FSL, and the non-linear transformation was obtained with the *FNIRT* tool from FSL.

The third step was the application of the non-linear transformation to each FA image. Each image was registered to the MNI space. In this space, all the registered FA images were merged into a single Four-dimensional (4D) file, with the fourth dimension representing each subject. The mean of all FA images was created and the resulting mean image was skeletonized, i.e., an image composed of the central area of the white matter tracts was obtained.

The fourth step was the projection of the FA images onto the mean FA image, considering that FA values lower than 0.2 were considered as non-white matter voxels. This 0.2 threshold was used to create a binary mask. The result of this step was a 4D image with the skeletonized FA for each subject. The voxelwise statistical analysis was performed on the skeleton voxels. An example of the skeleton is shown in Figure 3.4.

For any non-FA diffusion measure, an organization of the images equivalent to the one mentioned in the first TBSS step was carried out. The transformations of the FA images were used to skeletonize each diffusion measure of interest.

Bearing in mind that the TBSS analysis of the groups of interest presents special characteristics, its most important aspects are outlined. The statistical comparison was carried out with the *randomise* tool from FSL, based on the nonparametric permutations test, with 5000 permutations (Nichols & Holmes, 2002). In this analysis, the values between the groups for the original sample (first permutation) and for additional 4999 permutations, i.e. random sampling of the subjects, were compared. Basically, if the statistic of the original sample is among the 5% highest values (considering a threshold of 0.05 for statistical significance), there are significant differences between the assessed groups. To correct for multiple comparisons (voxels) in each assessment, the threshold-free cluster enhancement option was employed (S. M. Smith & Nichols, 2009), which is a family-wise error correction. Further corrections considering the number of comparisons are detailed in Chapter 2 of Part II and (Planchuelo-Gómez, García-Azorín, Guerrero, Aja-Fernández, Rodríguez, & de Luis-García, 2020b).

To localize the white matter regions with statistically significant differences, two atlases were employed. The main atlas was the Johns Hopkins University ICBM-DTI-81-White Matter Atlas (Oishi et al., 2008), whose regions are detailed in Appendix C. To cover areas that are not included in the ICBM-DTI-81 White Matter Atlas, the White-Matter Tractography Atlas was employed (Hua et al., 2008), whose regions are detailed in Appendix D. The minimum volume to consider statistically significant results was 30 $mm^3$.

## *C. AMURA*

AMURA is a method used to obtain diffusion descriptors alternative to the DTI-based measures and overcome the limitations of the diffusion tensor. AMURA is used to find differences not identified with DTI due to the oversimplification of the diffusion tensor model. The details of its implementation to compare diffusion descriptors using TBSS between patients with CM and EM and HC are included in Chapter 3 of Part II.

AMURA (`https://www.lpi.tel.uva.es/AMURA`) is based on the use of a reduced number of acquisitions of the estimated EAP. An important problem linked to the Ensemble Average diffusion Propagator (EAP) is the long acquisition time needed to obtain large datasets with many samples in different shells and even large b-values related to low SNR and diffusion artifacts. This acquisition time is longer compared to the protocol employed for DTI studies due to the use of multiple b-values with a high number of diffusion orientations. The long time required for the estimation of the EAP makes the associated dMRI acquisitions almost unfeasible for the clinical practice. Moreover, some b-values (the highest) are unavailable in diverse commercial MRI scanners.

The main idea of AMURA is that a constrained model with simpler acquisition protocols, including a single-shell acquisition, can exhibit microstructural changes with apparent measures in comparison with the non-apparent measures from the whole EAP (Aja-Fernández et al., 2020; Aja-Fernández, Tristán-Vega, & Jones, 2021). This hypothesis is based on the EAP methods that average the radial behavior of the diffusion signal with a radial integral, causing that a part of

the information from the multi-shell acquisitions is not actually used. Briefly, AMURA uses an apparent value at a single b-value instead of an average for a set of b-values.

The scalar measures used to characterize microstructural properties are the Return-to-axis Probability (RTAP), Return-to-origin Probability (RTOP) and Return-to-plane Probability (RTPP). The computation of these measures is simpler with AMURA compared to the whole EAP. Details of the equations and implementation for each measure are provided in (Aja-Fernández et al., 2020). In Chapter 3 of Part II, the implementation details applied to the dataset of this thesis are described. Briefly, using single-shell acquisitions, the integrals employed to characterize the diffusion signal in a sphere are simplified. For example, in the case of RTOP, the 3D integration of the whole space (q-space) is reduced to the integral on the surface of a sphere. For the extraction of the scalar measures, the numerical implementation of their respective integrals is based on spherical harmonics series, which basically is the spherical equivalent to the Cartesian Fourier series. Some assumptions are used for the numerical implementations considering single-shell acquisitions in AMURA. The ADC is independent from the radial direction, the RTOP is reduced to the integration on the surface of a single shell (no sampling of the whole q-space), the RTPP is integrated with respect to the radial component and the RTAP is reduced to a line integral independent from the radial component.

To define the numerical implementation of the RTOP, firstly it is important to define the 0-th order coefficient of the spherical harmonics expansion:

$$C_{0,0}\{H(\theta,\phi)\} = \frac{1}{\sqrt{4\pi}} \int_S H(\theta,\phi) dS, \tag{3.1}$$

where $C_{0,0}$ is the 0-th order coefficient of the spherical harmonics expansion and is related to the integral of a signal $H(\theta,\phi)$ over the surface of the unit sphere $S$, and $\theta$ and $\phi$ are the angular coordinates used to define a spherical system. The RTOP is defined implemented as follows:

$$\text{RTOP} = \frac{1}{(4\pi)^2 \tau^{3/2}} C_{0,0}\{(D(\theta,\phi))^{-3/2}\}, \tag{3.2}$$

where $\tau$ is an effective diffusion time to compute the motion of water molecules in a voxel, described in subsection B of section 2.2.2 in association with the b-value, and $D(\theta,\phi)$ is the ADC, independent from the radial direction. The RTPP is defined as follows:

$$\text{RTPP} = \frac{1}{\sqrt{4\pi\tau}} \cdot \frac{1}{\sqrt{D_{SH}(r_0)}}, \tag{3.3}$$

where $D_{SH}$ is a version of the original diffusion signal regularized using spherical harmonics and $r_0$ is the direction of maximum diffusion. The RTAP is defined as follows:

$$\text{RTAP} = \frac{1}{2 \cdot 4\pi^2 \tau} \mathscr{G} \left\{ \frac{1}{D(\theta')} \right\} (r_0) = 2\Psi(r_0), \tag{3.4}$$

where $\mathscr{G}$ is the Funk-Radon transform and $\Psi(r)$ is the pQ-Balls, detailed in (Tristán-Vega, Westin, & Aja-Fernández, 2010). Further details can be found in (Aja-Fernández et al., 2020).

Although AMURA does not employ the eigenvalues from the diffusion tensor, they can be used to obtain the RTAP, RTOP and RTPP. To better understand the interpretation of these three scalar measures, their value as a function of the eigenvalues from the diffusion tensor assuming a Gaussian probability density function for the diffusion signal are shown below, starting with the RTOP:

$$\mathrm{RTOP} = \frac{1}{\sqrt{(4\pi\tau)^3}} \cdot \frac{1}{\sqrt{\lambda_1 \cdot \lambda_2 \cdot \lambda_3}}. \tag{3.5}$$

The RTOP has been described as a better marker for cellularity and diffusion restrictions compared to the MD (Avram et al., 2016).

The RTPP is inversely related to the AD, as shown below:

$$\mathrm{RTPP} = \frac{1}{\sqrt{4\pi\tau}} \cdot \frac{1}{\sqrt{\lambda_1}}. \tag{3.6}$$

The RTPP has been remarked as a biomarker of restrictive barriers to the diffusion in the axial or main direction, being related to the mean pore length (Özarslan et al., 2013).

The RTAP is inversely associated in the Gaussian diffusion model, as shown below:

$$\mathrm{RTAP} = \frac{1}{\sqrt{(4\pi\tau)^2}} \cdot \frac{1}{\sqrt{\lambda_2 \cdot \lambda_3}}. \tag{3.7}$$

In contrast to the RTPP, the RTAP is an indicator of restrictive diffusion in the radial direction. The inverse relationships between the DTI- and EAP-based measures can also be seen in Figure 3.5.

The previous mathematical expressions are, however, extremely sensitive to very low values of the diffusion tensor, which can appear due to noise and outliers, leading to numerical instabilities. This problem can make it impossible to carry out the comparisons that are intended. Therefore, specific numerical implementations such as those shown in equations (3.2), (3.3) and (3.4) are necessary for advanced dMRI approaches.

### *3.2.3.* ***Effects of diffusion acquisition parameters and sample size on diffusion MRI***

The effect of changes in diffusion acquisition parameters in DTI-based parameters has been previously assessed (Aja-Fernández et al., 2018; Barrio-Arranz, de Luis-García, Tristán-Vega, Martín-Fernández, & Aja-Fernández, 2015; Jones, 2004). With regard to the number of gradients, a higher value has been associated with lower mean FA and AD and lower variance for the AD (Barrio-Arranz et al., 2015). In contrast, higher mean RD, particularly at low resolution, has been observed (Barrio-Arranz et al., 2015). Moreover, in a study with schizophrenia patients, the FA has been shown to be particularly sensitive to changes in the number of diffusion gradients and the SNR, while the MD showed greater robustness (Aja-Fernández et al., 2018).

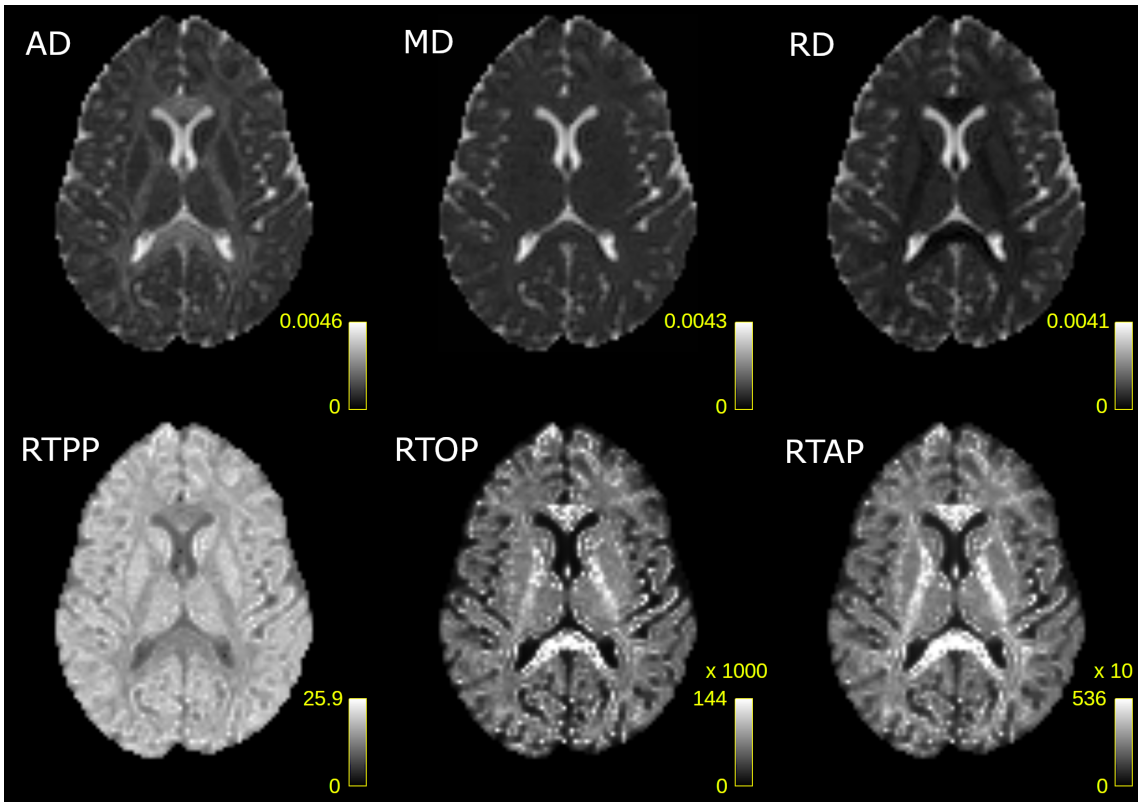


**Figure 3.5:** Example of an axial slice for each of the three EAP-based parameters obtained with AMURA and the corresponding inversely related DTI-based parameters.

These previous studies did not assess simultaneously the effects of the variation of the number of diffusion gradients and the effect of changing the sample size, important sources of variance. Considering the results from (Planchuelo-Gómez, García-Azorín, Guerrero, Aja-Fernández, Rodríguez, & de Luis-García, 2020b), reported also in section 4.2.2 and Chapter 2 of Part II, the AD differences were compared between the two migraine groups using the TBSS procedure, but with 1000 permutations instead of 5000. The 61 gradient directions scheme of the dMRI acquisition was designed to be subsampled it into a 40 gradient and a 21 gradient directions scheme. The details of this analysis are included in Chapter 4 of Part II.

To analyze the effect of the sample size, subsamples of the original sample of patients with CM and EM were generated. After the comparison with the original sample, 25 random subsamples with 50 subjects per group were simulated from the whole sample. In each subsample, the TBSS inference procedure was carried out and the number of regions with significant differences was collected. The median value of the number of regions with significant differences across the 25 comparisons in each subsample was considered as the figure of merit. The same procedure was repeated with five less subjects per group (e.g. 45 subjects in the next iteration) until no significant differences for any gradient scheme was found. This process is represented in Figure 3.6.

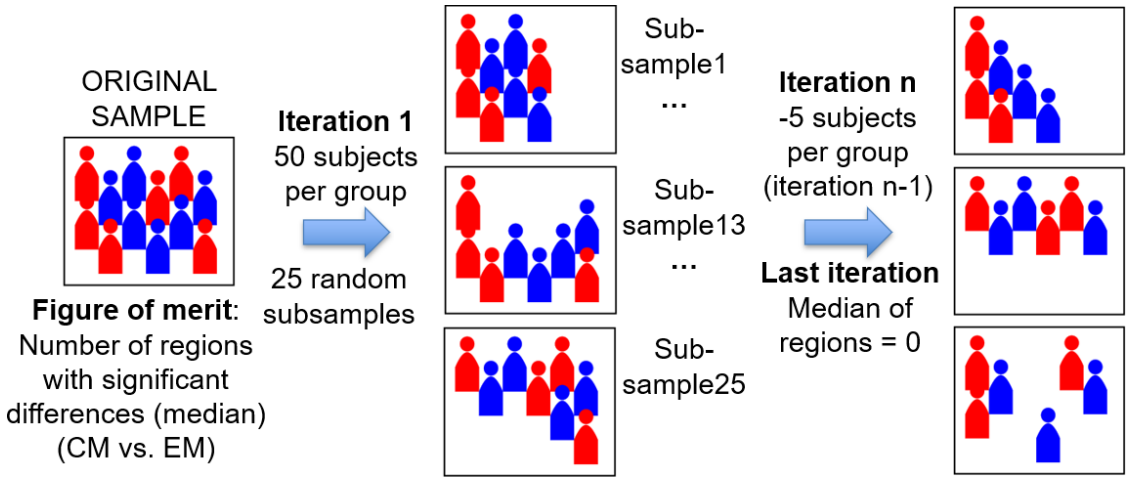


**Figure 3.6:** Schematic diagram showing the strategy to obtain the subsamples used to compare the AD between patients with CM and EM.

### *3.2.4. Connectomics processing*

The connectomics processing allows the specific analysis of the connections between gray matter regions through white matter. With respect to the TBSS analysis, connections between ROIs are evaluated instead of white matter regions. For the evaluation of the structural connections, two main components are necessary, a tractography to define the trajectories of the reconstructed white matter tracts, and a segmentation of the cortical and subcortical regions that include the ROIs to be considered. The segmentation was extracted with the FreeSurfer pipeline. The objective of connectomics was to assess the different structural connectivity patterns between patients with CM and EM and HC. The details of the connectomics analysis are described in Chapter 5 of Part II.

The connectomics processing was based on Anatomically-Constrained Tractography (ACT) as tractography method (R. E. Smith, Tournier, Calamante, & Connelly, 2012). Before the ACT, some processing steps of the results from T1- and diffusion-weighted images were necessary.

With regard to the procedure related to the T1-weighted images, a Five-tissue-type (5TT) image was obtained. This image is a 4D binary image with masks of five types of brain tissues, which are cortical gray matter, subcortical gray matter, white matter, CSF and pathological tissue. The pathological tissue mask could have only 0 values, i.e., no pathological tissue. Moreover, the parcellation from FreeSurfer was linearly registered to the FA image for each subject using the FLIRT tool from FSL.

The objective of the dMRI processing was to estimate the Fiber Orientation Distribution (FOD), which was necessary to perform the ACT. For this step, it was assumed that all white matter fiber bundles present the same diffusion features. From this assumption, the diffusion-weighted signal attenuation over the surface of a sphere would be expressed as the convolution over a sphere of a response function with the FOD (Tournier, Calamante, Gadian, & Connelly, 2004). Then, the response function, which is the diffusion-weighted attenuation profile for a typi-

cal fiber bundle, was estimated with the *dwi2response* function from MRtrix before the extraction of the FOD (Tournier, Calamante, & Connelly, 2013). Constrained spherical deconvolution was employed to estimate the FOD with the *dwi2fod* function from MRtrix (Tournier, Calamante, & Connelly, 2007). This spherical convolution-deconvolution procedure was based on the spherical harmonic series.

ACT was performed using a probabilistic algorithm based on a second-order integration over the FOD represented with spherical harmonics with the *tckgen* function from MRtrix (Tournier, Calamante, & Connelly, 2010). The streamlines followed with higher probability the paths where the FOD amplitude was large. The number of streamlines per tractography was 10 million for each subject. The tractography results were filtered with the second version of the Spherical-deconvolution Informed Filtering of Tractograms algorithm (R. E. Smith, Tournier, Calamante, & Connelly, 2015). The filtering step was carried out considering the information from the spherical deconvolution model to adjust properly the streamline count of each from the tractography. This adjustment allows to obtain an adequate quantification of the number of streamlines using the information from the dMRI data and reducing possible errors or bias from the tractography algorithm. The basic idea of the filtering algorithm is the application of a cross-sectional multiplier to the reconstructed streamline to optimize the whole-brain tractogram.

From the tractography, a structural connectivity matrix composed of the 84 regions from the Desikan-Killiany atlas was created for each subject. This matrix was undirected, i.e. symmetric, and represented the number of streamlines in each connection. The mean value of the DTI-based measures was also computed in each connection. Thus, there was one matrix with the number of streamlines and one matrix per each DTI parameter (e.g. FA). The diagonal elements were considered as *self-connections*. This was made because a streamline can start and end in different areas from the same region.

For the statistical analysis, if the mean of the number of streamlines in the three groups (CM, EM and HC) was lower than 1000 in a connection (cell of the structural connectivity matrix), this connection was not included in the analysis. The reason of the exclusion of these *weak* connections was that the results related to these connections may be unreliable, i.e., associated with false positives.

A summary of the whole connectomics processing is shown in Figure 3.7.

### *3.2.5.* ***Fusion of MRI modalities***

The aim of the fusion analysis of diverse MRI modalities is to characterize the relationship between the alterations of diverse structural properties with no dependence relationship (independent modalities). The most simple approach to determine the relationship between two modalities is the correlation analysis, but the covariance patterns between the modalities are not captured. Thus, more sophisticated approaches are employed to assess if the changes in a modality are associated with the alterations in another modality. In this thesis, the objective was the characterization of

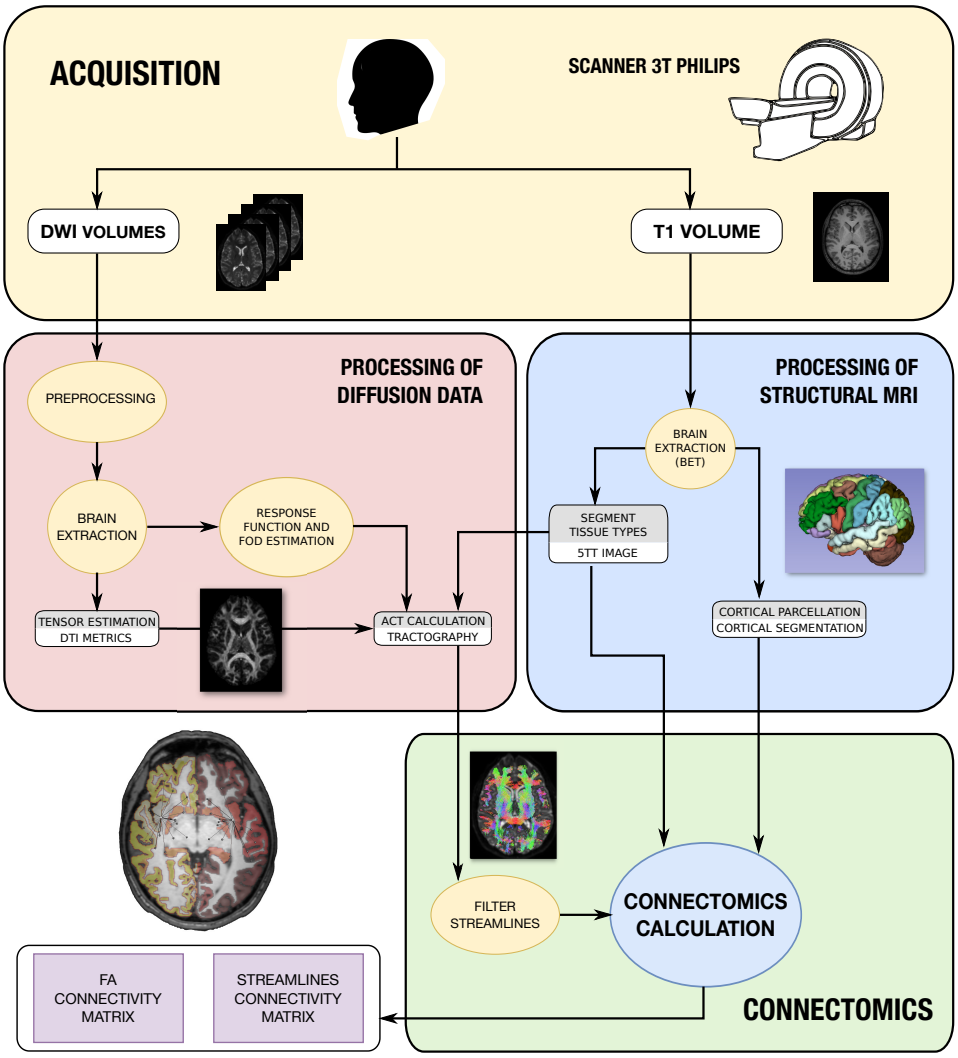


**Figure 3.7:** Connectomics processing pipeline. Schematic diagram showing the steps followed to obtain the structural connectivity matrix in each subject. Figure from (Planchuelo-Gómez, García-Azorín, Guerrero, Aja-Fernández, Rodríguez, & de Luis-García, 2020a).

the relationship between the alterations of gray matter structure and structural connectivity in patients with CM and EM compared to HC, assessing possible differences between both migraine types. The complete details of the fusion analysis of structural MRI data are reported in Chapter 6 of Part II.

In this analysis, the four gray matter morphometry parameters and the number of streamlines from the connectomics assessment were the employed features and they were analyzed in pairs. The gray matter volume was not assessed with thickness and area because of their direct relationship, considering that the objective was the assessment of independent types of data, i.e., with no clear straightforward association. The analysis of the relationship between the features from both modalities was carried out using the mCCA and jICA methods. In this case, it was assumed that the multimodal dataset was a linear mixture of mixing profiles and independent sources. The approach employed in this analysis was based on the worked firstly developed in (Sui et al., 2011) using the Fusion ICA Toolbox (`http://trendscenter.org/software/fit/`), version 2.0d.

With respect to the original implementation of the Fusion ICA Toolbox, two main modifications have been included in this thesis.

The first modification is related to the adaptation of the data to the use of the toolbox. Considering MRI data, the toolbox was designed to use original images (e.g. fMRI data) or processed images (e.g. FA maps). A consequence is that no gray matter morphometry (no possible voxelwise map currently) or structural connectural connectivity data (cells from adjancency matrices) could be included in the fusion analysis. The target of this modification is to extend the method for the application of any type of numerical data, removing the restriction of the exclusive use of volumetric maps or original images. Therefore, the code of the toolbox was adapted to accept data of any type based on a set of numerical values. Furthermore, data from modalities such as gray matter morphometry and structural modality could be assessed following the same mathematical procedure as in the original implementation.

The second modification is related to the number of components selected to carry out the fusion analysis. The aim of this modification is to develop a new method to determine the number of components, completely independent with respect to the approach employed originally. As mentioned in the previous paragraph, the toolbox was designed to process MRI original data or images with the same dimensions of MRI data. Considering this dimensionality, the procedure followed to determine the number of components to summarize the data was designed to manage datasets with a large amount of values (the number of voxels), but it is not optimal for relatively small datasets. Therefore, an alternative approach to estimate the number of components was implemented. Further details about this approach are described throughout this section and in Chapter 6 of Part II.

Two important concepts should be explained before describing the fusion method itself: the principal components and the canonical variants.

From PCA, the principal components are obtained. The PCA is used to summarize the information from a large set of variables into a group of uncorrelated variables that are ordered from highest to lowest explained variance of the original variables. Therefore, the principal components are variables that explain the variability of a dataset, and a few of them are employed to summarize a dataset of interest. In the case of ICA, the independent components (equivalent to the principal components) are equally important and there is no order dependence.

CCA is used to characterize the relationships between two groups of variables, and the canonical variants are extracted from this analysis. The canonical variants explain not only, the variability of one group of variables, but also between the two groups of variables. The pairs of canonical variants are independent and ordered from highest to lowest correlation.

The previous steps to the mCCA-jICA procedure were the determination of the optimal number of components and of canonical variants, and the dimension reduction via singular value decomposition. The determination of the number of components was based on the Horn's test (Horn, 1965). Briefly, the eigenvalues of each original dataset were obtained and compared to the eigenvalues of 500 random datasets of the same dimensionality. The number of components to be retained was

equal to the number of eigenvalues from the original dataset greather than the 95th percentile of the corresponding eigenvalues from the random datasets. Further details about these steps are included in Chapter 6 of Part II and (Planchuelo-Gómez et al., 2021).

Regarding the fusion methodology, mCCA was carried out before jICA. The objective of the combination of both methods was to link the independent components for each modality, gray matter morphometry and structural connectivity. This objective was possible thanks to the initialization by mCCA, related to the maximum correlation across the modalities provided by the canonical variants (Correa, Li, Adali, & Calhoun, 2008).

The advantage of mCCA over CCA is that variables of different size or dimension, as it could be expected from data of multiple MRI modalities, can be assessed simultaneously. The objective of mCCA was to maximize the correlation between the assessed modalities. The canonical variants from each modality represented the mixing profile, i.e., the contribution of each component (the source from each modality) to the individual features (S.-G. Kim, Jung, Kim, Jang, & Kwon, 2015).

The objective of jICA was the maximization of the independence of the associated components from mCCA in order to extract independent sources for each modality. The obtained joint independent components represented the independent sources.

To sum up, the sources for each group and a mixing profile per modality for every subject were obtained. The mixing coefficients were compared between the groups following standard statistical procedures, as described in section 3.2.6. The sources were expressed as Z-scores and represented the weight of the regions or connections to a joint independent component. To determine the regions or connections altered in a component, the positive and negative outliers of the Z-scores were identified. More detailed description of the method is included in Part II and (Planchuelo-Gómez et al., 2021).

With regard to the differences between groups, two main options were possible. The first option was based on differences of the regions or connections detected by the Z-score outliers, for example, negative Z-scores in controls and positive Z-scores in the migraine groups. The second option was based on the comparison of the mixing coefficients, also considering the values of the Z-scores. The diverse possible situations are summarized below:

- **Positive Z-scores and mixing coefficients**. In this case, the group with significantly higher values of mixing coefficients would present higher expression of the assessed parameter (e.g. number of streamlines).
- **Negative Z-scores and positive mixing coefficients**. The group with significantly higher values of mixing coefficients would present lower expression of the assessed parameter.
- **Positive Z-scores and negative mixing coefficients**. The group with significantly higher values of mixing coefficients would present lower expression of the assessed parameter.
- **Negative Z-scores and mixing coefficients**. The group with significantly higher values of mixing coefficients would present higher expression of the assessed parameter.

The summary of the mCCA-jICA fusion methodology, including the data which were employed, is shown in Figure 3.8.

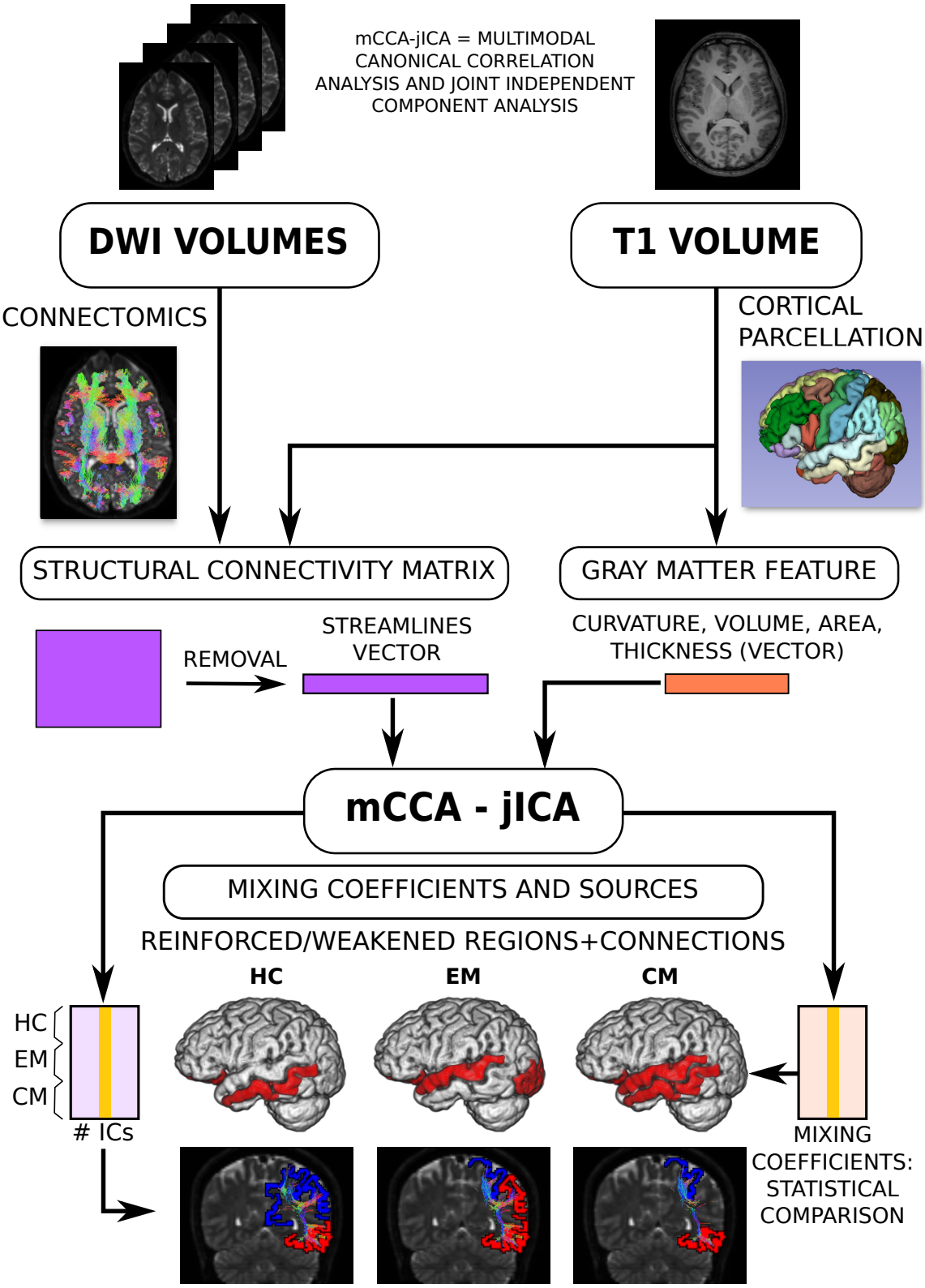


**Figure 3.8:** mCCA-jICA processing pipeline. Schematic diagram showing the steps followed to obtain the mixing coefficients and spatial sources. The regions and connections included in this figure have only illustrative purpose and should not be confused with the results. Figure from (Planchuelo-Gómez et al., 2021).

### *3.2.6.* ***Statistical analysis***

The statistical analysis was similar for all the studies included in the doctoral thesis, with the exception of the TBSS analysis, which has been described in section B. Other particular aspects related to the fusion MRI analysis are described in section 3.2.5.

For the assessment of continuous variables, which included the variables from the MRI processing, Kolmogorov-Smirnov and Levene's test were conducted to determine the normality and homogeneity of variance of the data. If the normality and homogeneity assumptions were met for all the variables from the three groups (HC, EM and CM) a one-way Analysis of Variance (ANOVA) was used, while the Kruskal-Wallis test was employed otherwise. For comparisons between the two migraine groups, the two-tailed unpaired t-test or the Mann-Whitney U test were employed. To assess two-by-two post-hoc comparisons, the Tukey-Kramer test was employed after the ANOVA and the Conover-Iman test was used after the Kruskal-Wallis test. If a covariate was added to the analysis of the three groups, an Analysis of Covariance (ANCOVA) test was employed, using the Tukey-Kramer test for post-hoc comparisons.

The comparison of categorical variables was carried out with a chi-square test for analysis between the three groups, and with a Fisher's exact test in case of analysis between two groups.

To correct for multiple comparisons, the Benjamini-Hochberg false discovery rate method was used (Benjamini & Hochberg, 1995). The threshold for statistical significance was set at $p < 0.05$. For the correlation analysis, the Spearman's rank correlation test (most analyses conducted in this doctoral thesis) or the Pearson correlation coefficient was employed.

# *Chapter 4*

# ***Results***

The objective of this chapter is to give an overview of the results obtained in the thesis instead of providing separately detailed results from each contribution. The detailed description of these results can be found in the each chapter of Part II.

The results of this thesis are mainly based on the comparisons of numerical descriptors of diverse structural properties of the brain between patients with Chronic Migraine (CM) and with Episodic Migraine (EM) and Healthy Controls (HC) (three groups). The structural parameters that were compared between the three groups were gray matter morphometry (Chapter 1 of Part II), DTI-based and Ensemble Average diffusion Propagator (EAP)-based measures from Apparent Measures Using Reduced Acquisitions (AMURA) in white matter regions (Chapters 2 and 3 of Part II, respectively). DTI-based descriptors and number of streamlines were assessed in connections between gray matter regions (Chapter 5 of Part II). Moreover, the number of streamlines and the gray matter morphometry parameters were simultaneously assessed to determine the relationships between these parameters and identify additional patterns in both migraine groups (Chapter 6 of Part II).

Taking into account the comparisons between both migraine groups and controls, this chapter is organized in two main blocks. In the first block, the comparisons between the patients with migraine (both CM and EM) and HC are described (section 4.1), considering that the identified differences in EM and CM with respect to controls were similar. In the second block, the comparisons between both groups of migraine, CM and EM, are defined (section 4.2). In the following section, the correlation results between the diverse clinical parameters and the MRI measures (section 4.3) is outlined. Finally, the results of the effects of changing sample size and dMRI acquisition parameters in statistical comparisons (section 4.4 and Chapter 4 of Part II) are detailed.

**Table 4.1:** Minimum (first row of each group) and maximum (second row of each group) values of the gray matter morphometry parameters for each group in regions where statistically significant differences were found. Values are expressed as mean ± standard deviation. CC = cortical curvature; CT = cortical thickness; GMV = gray matter volume; SA = surface area. More details can be found in Chapter 1 of Part II.

| Group | CC ($mm^{-1}$) | CT (mm) | SA ($mm^2$) | GMV ($mm^3$) |
|---|---|---|---|---|
| HC | 0.105 ± 0.009 | 2.377 ± 0.151 | 291 ± 37 | 590 ± 129 |
| | 0.181 ± 0.026 | 2.858 ± 0.163 | 6685 ± 1003 | 50121 ± 5689 |
| EM | 0.111 ± 0.009 | 2.308 ± 0.121 | 269 ± 42 | 661 ± 109 |
| | 0.196 ± 0.024 | 2.771 ± 0.154 | 6639 ± 648 | 47858 ± 5331 |
| CM | 0.111 ± 0.009 | 2.305 ± 0.147 | 272 ± 40 | 659 ± 112 |
| | 0.191 ± 0.027 | 2.765 ± 0.188 | 6453 ± 701 | 46482 ± 4142 |

# 4.1. Comparison between migraine patients and controls

## *4.1.1.* ***Gray matter morphometry***

Statistically significant differences were found between both groups of migraine and HC for the four gray matter morphometry parameters. For gray matter volume, cortical curvature and cortical thickness, differences in both migraine groups, only in EM and only in CM compared to the HC were identified. For surface area, no exclusive differences in EM compared to HC were identified.

For all the regions with significant differences, cortical curvature values were higher in patients with migraine (seven regions), while cortical thickness (nine regions) and surface area (15 regions) values were lower in the patient groups. In the case of gray matter volume, lower values in the migraine groups were found in 23 cortical regions with significant differences, the cerebellum and the pallidum, while higher values in the patients were identified in the putamen and the nucleus accumbens, two subcortical regions. In Table 4.1, minimum and maximum values for each parameter and group are shown. The purpose of Table 4.1 is to show the range of values for each parameter and support the comparative results between groups. The number of regions with statistically significant differences for each comparison is depicted in Table 4.2. A graphical summary of the results of Table 4.2 with general trends is shown in Figure 4.1. The main regions with statistically significant differences are shown in Figure 4.2.

More details about these comparisons can be found in Chapter 1 of Part II or (Planchuelo-Gómez, García-Azorín, Guerrero, Rodríguez, et al., 2020).

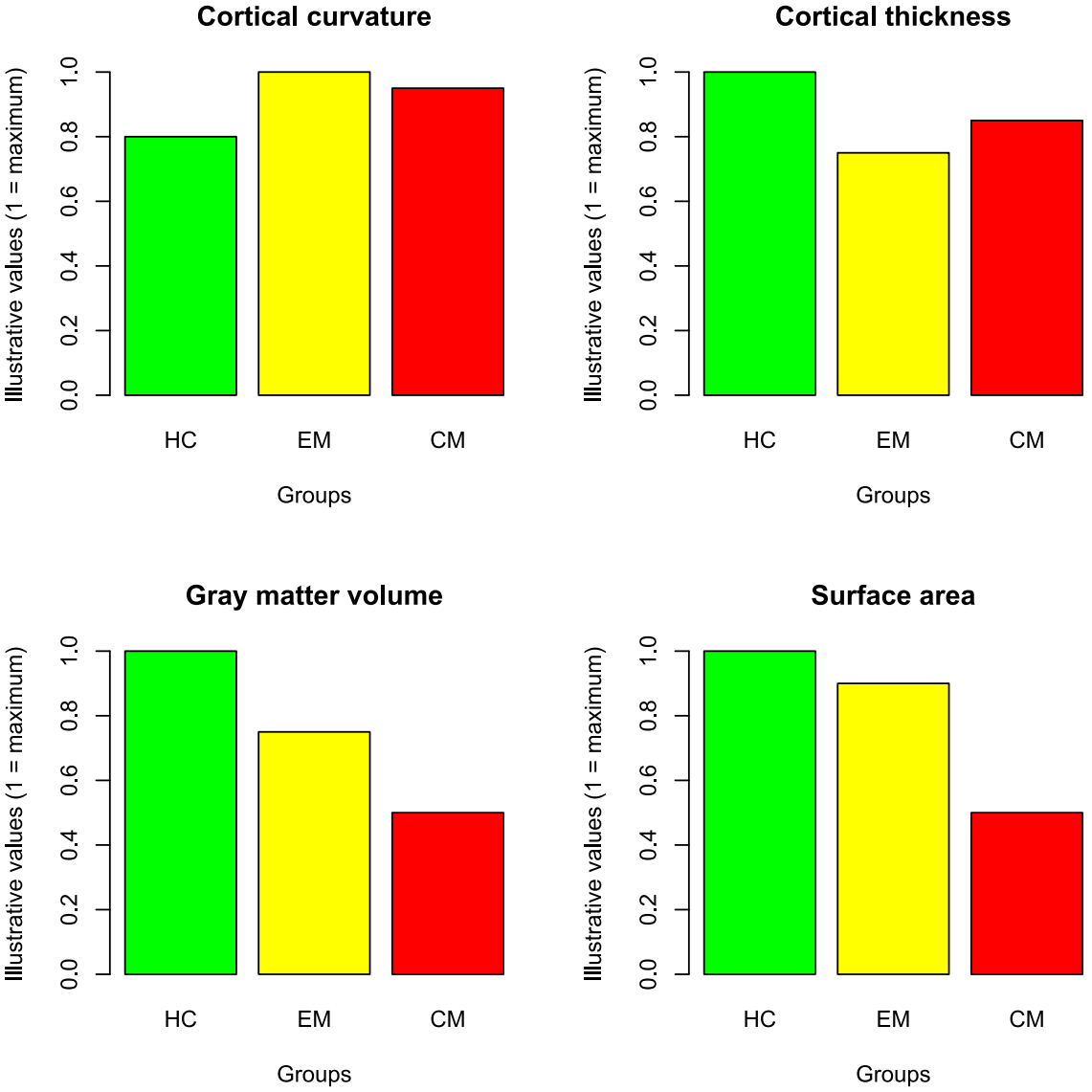


**Figure 4.1:** Summary of the trends of the differences of the gray matter morphometry parameters between HC and patients with CM and EM. These values are shown for illustrative purpose and orientation and must not be interpreted as real values.

### *4.1.2. Diffusion measures*

This section includes the TBSS results using DTI-based descriptors and the parameters obtained with AMURA.

Regarding the direct comparison between the two migraine groups and the controls with TBSS, statistically significant RTOP differences were found between patients with EM and HC. Lower RTOP values were found in patients with EM. In this analysis, the results were not adjusted by any covariate different to the assessed diffusion descriptor. No statistically significant differences were found with DTI-based parameters in this analysis. The results from this analysis are shown in Figure 4.3.

Considering any analysis with or without additional covariates, for all the parameters obtained from either DTI or AMURA, there were no simultaneous statistically significant differences between the two migraine groups and HC. For each parameter, only differences between one of the migraine groups and HC were identified. Significant differences between EM and HC were found with AD (higher values in EM), RTPP and RTOP (lower values in EM in both cases). Significant differences between CM and HC were detected with FA, RD (lower values in CM) and RTAP (higher values in CM). With respect to FA differences, both higher (adjusting by the time from the onset of CM) and lower (adjusting by the presence of aura and Medication Overuse Headache (MOH) and duration of migraine history) values were found in CM. The number of regions from the ICBM-DTI-81 White Matter Atlas with significant differences between migraine groups and HC is shown in Table 4.3, following the same organization as in Table 4.2. The regions with significant FA differences between CM and HC were found in separate locations. A graphical summary of the results of Table 4.3 with general trends is shown in Figure 4.4. In Tables 4.4 and 4.5, minimum and maximum values for each parameter and group are shown. The purpose of these tables is to show the range of values for each parameter and support the comparative results between groups. It is worth noting that the average values from the skeleton are shown in these two tables. This implies that there could be some discrepancies with respect to the TBSS results due to the differences between specific areas and the whole ROI.

More details about these comparisons can be found in Chapters 2 and 3 of Part II or (Planchuelo-Gómez, García-Azorín, Guerrero, Aja-Fernández, Rodríguez, & de Luis-García, 2020b; Planchuelo-Gómez, García-Azorín, Guerrero, de Luis-García, et al., 2020).

### *4.1.3.* ***Connectomics***

Statistically significant differences were found between both migraine groups and HC for the number of streamlines and all the DTI-based parameters except the MD. For the RD, higher values were found for both migraine groups or EM patients compared to HC in two connections. For the streamline count, the AD and the FA lower and higher values were identified for one or both migraine groups with respect to HC. Lower values in patients were observed in nine, three and two connections for the streamline count, AD and FA, respectively. Higher values in patients were identified in 12 connections for the streamline count, and in one connection for the AD and FA. In Table 4.6, minimum and maximum values for each parameter and group are shown. The purpose of Table 4.6 is to show the range of values for each parameter and support the comparative results between groups. The number of regions with statistically significant differences for each comparison is depicted in Table 4.7. The specific connections with significant differences between the migraine groups and controls can be observed in Figures 4.5 and 4.6.

More details about these comparisons can be found in Chapter 5 of Part II or (Planchuelo-Gómez, García-Azorín, Guerrero, Aja-Fernández, Rodríguez, & de Luis-García, 2020a).

### *4.1.4.* ***Multimodal MRI analysis***

In this analysis, the results were divided in two groups. The first group was referred to the mixing coefficients, which were compared between the migraine groups and the controls. In the comparisons of the mixing coefficients with statistically significant differences, the two-by-two connections with higher absolute values of the Z-scores (outliers) were assessed. In some cases, the same connections between the three groups could be directly compared because the Z-scores were outliers for the groups, and the differences would be determined by the comparison of the mixing coefficients. In the second group of results, a specific group of connections may present outlier Z-scores in one of the groups. In this last case, a debilitated or strengthened connection for a negative and a positive Z-score, respectively, was considered. Regarding debilitated and strengthened connections, it is assumed that weakened connections are associated with a significant lower number of streamlines, while enhanced connections are associated with a higher number of streamlines.

Regarding the mixing coefficients of gray matter morphometry parameters, only higher cortical curvature values in the bilateral frontal pole were detected in patients with EM compared to HC. Taking into account the Z-scores, higher curvature in CM with respect to HC was observed in the rostral anterior cingulate cortex.

With regard to the structural connectivity (number of streamlines), higher and lower values were obtained in both migraine groups compared to controls. The most frequent result was lower connectivity in both migraine groups. A network was created by joining diverse groups of two-by-two connections with one common region. The ratio of the number of connections and networks per comparison to the total number of comparisons with significant differences is shown below:

- CM, EM > HC → 8/44 (18.2%) from two networks.
- Enhanced in CM → 8/44 (18.2%) from two networks.
- Enhanced in EM → 6/44 (13.6%) from two networks.
- **CM, EM < HC** → 13/44 (29.5%) from five networks.
- Worsened in CM → 5/44 (11.4%) from two networks.
- Worsened in EM → 2/44 (4.5%) from one network.

The specific regions and connections with significant changes are summarized in Figure 4.7.

Further details of the results from the fusion multimodal MRI analysis can be found in Chapter 6 of Part II and (Planchuelo-Gómez et al., 2021). The summary of the comparisons between the groups of patients and controls is shown in Table 4.8.

**Table 4.2:** Number of regions with gray matter morphometry statistically significant differences between groups of migraine patients and healthy controls. The ratio of the number of regions with significant differences to the total number of comparisons with significant differences per parameter is shown. For each parameter, the cell in yellow remarks the comparison with higher ratio. CC = cortical curvature; CT = cortical thickness; GMV = gray matter volume; SA = surface area.

| Comparison | CC | CT | GMV | SA |
|---|---|---|---|---|
| CM,EM > HC | **7/12 (58.3%)** | 0 | 1/30 (3.3%) | 0 |
| CM > HC | 1/12 (8.3%) | 0 | 0 | 0 |
| EM > HC | 4/12 (33.3%) | 0 | 1/30 (3.3%) | 0 |
| CM,EM < HC | 0 | **8/13 (61.5%)** | 10/30 (33.3%) | 4/34 (11.8%) |
| CM < HC | 0 | 1/13 (7.7%) | **15/30 (50.0%)** | **21/34 (61.8%)** |
| EM < HC | 0 | 4/13 (30.8%) | 2/30 (6.7%) | 0 |

**Table 4.3:** Number of regions with diffusion descriptors statistically significant differences between groups of migraine patients and healthy controls. The ratio of the number of regions with significant difference to the total number of regions from the ICBM-DTI-81 White Matter Atlas is shown. In case of some analyses with significant differences on a specific comparison, the comparison with higher number of regions with significant differences is shown. For each parameter, the cell in yellow remarks the comparison with higher ratio. No differences were found for the MD.

| Comparison | FA | AD | RD | RTAP | RTOP | RTPP |
|---|---|---|---|---|---|---|
| CM,EM > HC | 0 | 0 | 0 | 0 | 0 | 0 |
| CM > HC | 10/48 (20.8%) | 0 | 0 | 0 | 0 | 0 |
| EM > HC | 0 | **8/48 (16.7%)** | 0 | 0 | 0 | 0 |
| CM,EM < HC | 0 | 0 | 0 | 0 | 0 | 0 |
| CM < HC | **15/48 (31.3%)** | 0 | **14/48 (29.2%)** | **4/48 (8.3%)** | 0 | 0 |
| EM < HC | 0 | 0 | 0 | 0 | **24/48 (50.0%)** | **8/48 (16.7%)** |

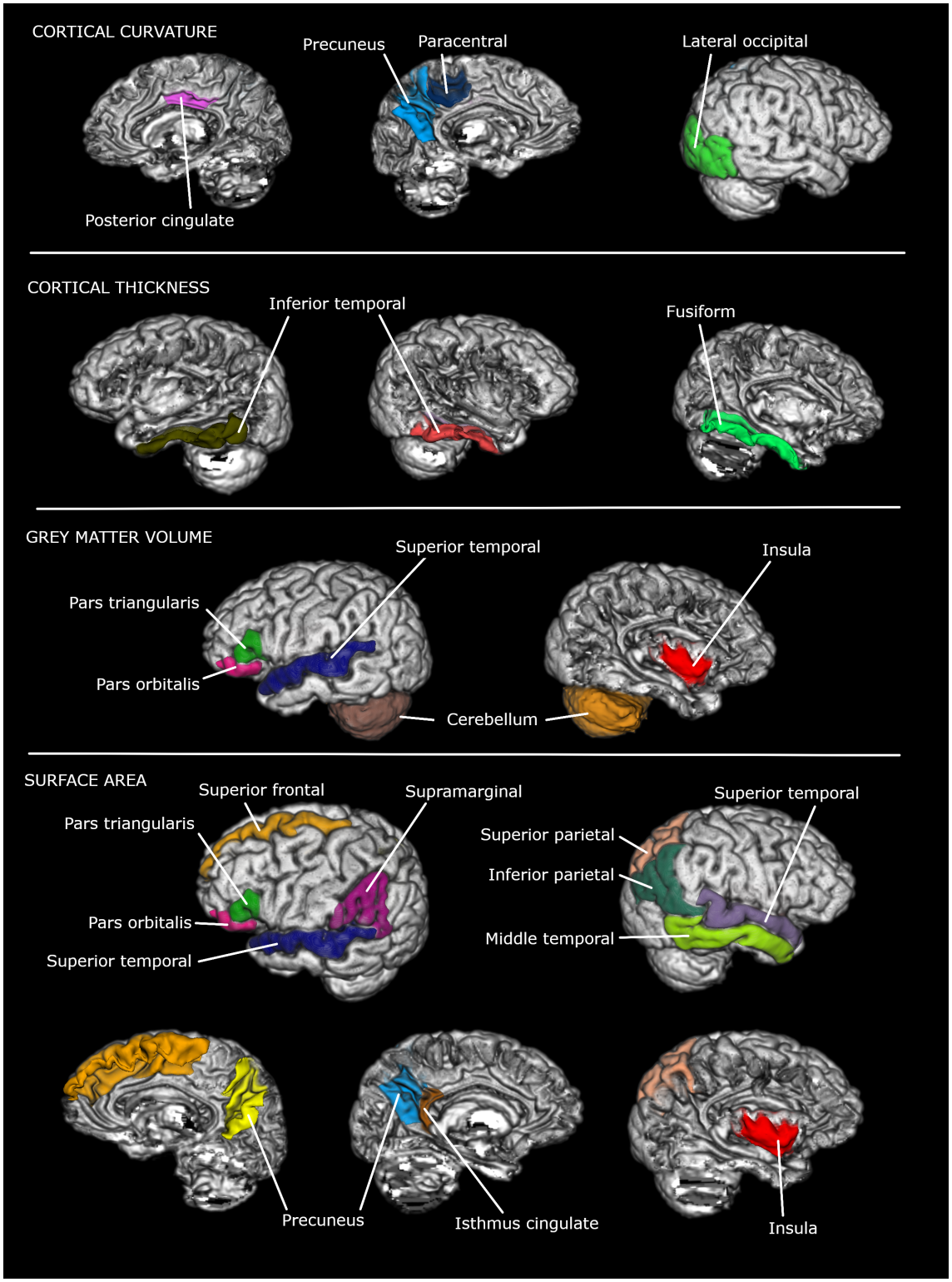


**Figure 4.2:** Main gray matter cortical regions with statistically significant differences between one or both groups of patients with migraine and healthy controls. In these regions, the comparison between the three groups presented $p < 0.001$, significant after correction for multiple comparisons. Figure from (Planchuelo-Gómez, García-Azorín, Guerrero, Rodríguez, et al., 2020).

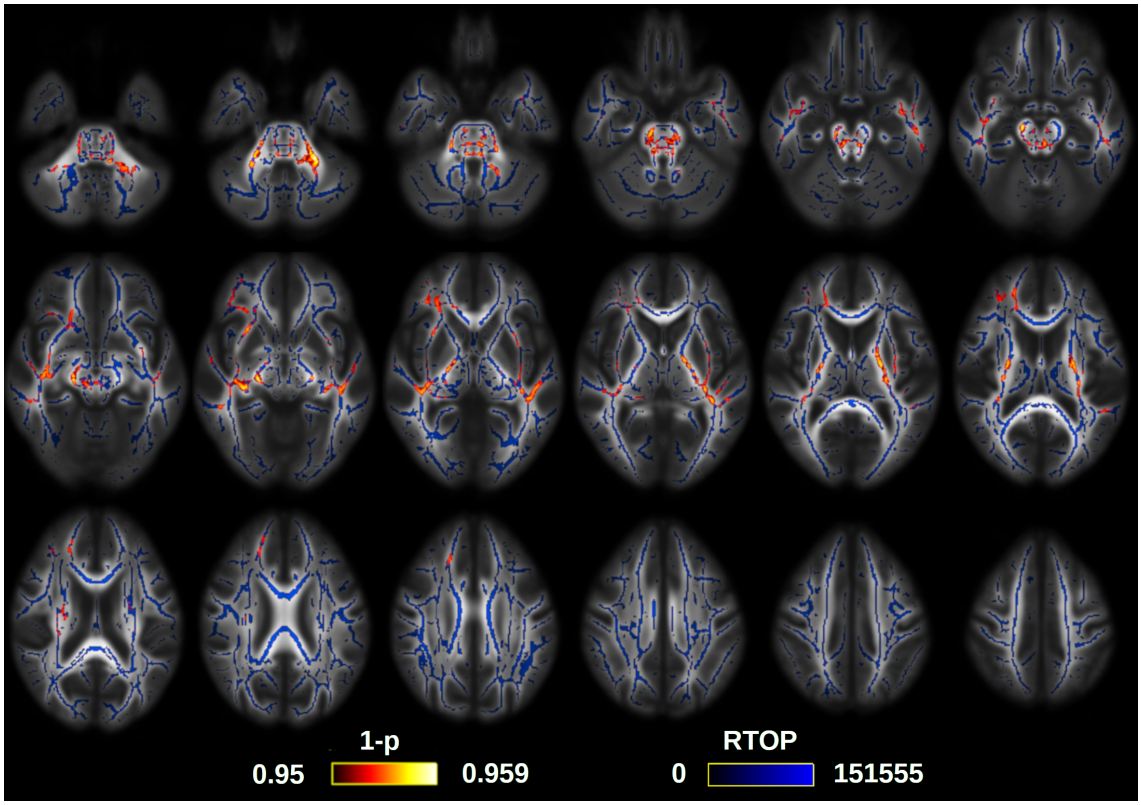


**Figure 4.3:** Regions with statistically significant lower RTOP values in EM patients compared to controls. Figure adapted from (Planchuelo-Gómez, García-Azorín, Guerrero, de Luis-García, et al., 2020).

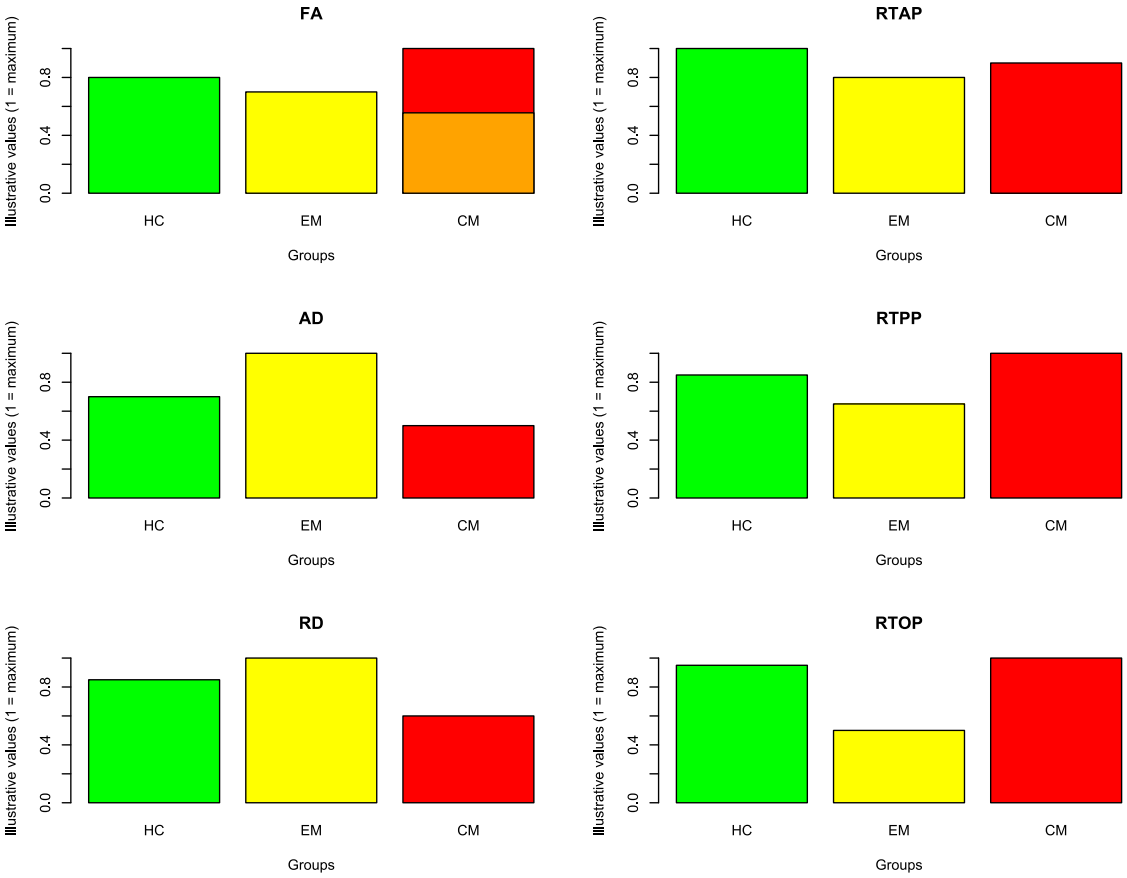


**Figure 4.4:** Summary of the trends of the differences of the white matter descriptors based on DTI and extracted with AMURA between HC and patients with CM and EM. These values are shown for illustrative purpose and orientation and must not be interpreted as real values. The orange bar shows one of the opposite trends that was appreciated in the assessment of FA values.

**Table 4.4:** Minimum (first row of each group) and maximum (second row of each group) values of the DTI-based parameters for each group in regions where statistically significant differences were found. Average values from the TBSS skeleton are shown. Values are expressed as mean ± standard deviation. FA is dimensionless. The detailed results from the statistical comparisons can be found in Chapters 2 and 3 of Part II.

| Group | FA | AD ($mm^2s^{-1}\times10^{-5}$) | RD ($mm^2s^{-1}\times10^{-6}$) | MD ($mm^2s^{-1}\times10^{-6}$) |
|---|---|---|---|---|
| HC | 0.492 ± 0.091 | 111 ± 13 | 307 ± 73 | 678 ± 57 |
| | 0.776 ± 0.128 | 158 ± 22 | 539 ± 96 | 873 ± 96 |
| EM | 0.481 ± 0.089 | 113 ± 13 | 316 ± 77 | 678 ± 57 |
| | 0.769 ± 0.130 | 157 ± 22 | 538 ± 93 | 869 ± 93 |
| CM | 0.485 ± 0.089 | 113 ± 13 | 307 ± 73 | 668 ± 58 |
| | 0.773 ± 0.128 | 157 ± 25 | 530 ± 56 | 863 ± 97 |

**Table 4.5:** Minimum (first row of each group) and maximum (second row of each group) values of the EAP-based parameters extracted with AMURA for each group in regions where statistically significant differences were found. Average values from the TBSS skeleton are shown. Values are expressed as mean ± standard deviation. The detailed results from the statistical comparisons can be found in Chapter 3 of Part II.

| Group | RTOP ($mm^{-3} \times 10^2$) | RTAP ($mm^{-2} \times 10$) | RTPP ($mm^{-1} \times 10^{-1}$) |
|---|---|---|---|
| HC | 688 ± 54 | 219 ± 47 | 140 ± 4 |
| | 1059 ± 72 | 437 ± 23 | 165 ± 2 |
| EM | 686 ± 56 | 223 ± 48 | 141 ± 3 |
| | 1030 ± 79 | 428 ± 24 | 164 ± 3 |
| CM | 686 ± 45 | 238 ± 43 | 142 ± 3 |
| | 1049 ± 64 | 433 ± 21 | 165 ± 3 |

**Table 4.6:** Minimum (first row of each group) and maximum (second row of each group) values of the structural connectivity parameters for each group in connections where statistically significant differences were found. Values are expressed as mean ± standard deviation. FA is dimensionless. More details can be found in Chapter 5 of Part II.

| Group | Streamline count | FA | AD ($mm^2\ s^{-1} \times 10^{-5}$) | RD ($mm^2\ s^{-1} \times 10^{-6}$) |
|---|---|---|---|---|
| HC | 334 ± 445 | 0.244 ± 0.028 | 116 ± 3 | 506 ± 25 |
| | 27047 ± 6478 | 0.421 ± 0.020 | 126 ± 6 | 634 ± 56 |
| EM | 767 ± 788 | 0.265 ± 0.035 | 119 ± 4 | 525 ± 27 |
| | 34109 ± 6863 | 0.407 ± 0.023 | 124 ± 5 | 672 ± 59 |
| CM | 981 ± 434 | 0.273 ± 0.033 | 117 ± 3 | 520 ± 24 |
| | 31342 ± 5420 | 0.404 ± 0.016 | 121 ± 6 | 629 ± 55 |

**Table 4.7:** Number of regions with connectomics statistically significant differences between groups of migraine patients and healthy controls. The ratio of the number of connections with significant differences in any comparison (adjusted or unadjusted) to the total number of comparisons with significant differences per parameter is shown. For each parameter, the cell in yellow remarks the comparison with higher ratio. SC = streamline count.

| Comparison | SC | FA | AD | RD |
|---|---|---|---|---|
| CM,EM > HC | 8/21 (38.1%) | 1/3 (33.3%) | 0 | **1/2 (50%)** |
| CM > HC | 4/21 (19.0%) | 0 | 0 | 0 |
| EM > HC | 0 | 0 | 1/4 (25%) | **1/2 (50%)** |
| CM,EM < HC | **9/21 (42.9%)** | **2/3 (66.7%)** | 1/4 (25%) | 0 |
| CM < HC | 0 | 0 | **2/4 (50.0%)** | 0 |
| EM < HC | 0 | 0 | 0 | 0 |

**Table 4.8:** Summary of the comparisons with significant differences between patients with CM and EM and healthy controls. CC = cortical curvature; CT = cortical thickness; GMV = gray matter volume; SA = surface area; SC = streamline count; X = no significant differences.

| **Comparison** | **Morphometry** | **Diffusion MRI** | **Connectomics** | **Fusion MRI** |
|---|---|---|---|---|
| CM,EM > HC | CC+GMV | X | SC+FA+RD | SC |
| CM > HC | CC | FA | SC | SC+CC |
| EM > HC | CC+GMV | AD | AD+RD | SC+CC |
| CM,EM < HC | CT+GMV+SA | X | SC+FA+AD | SC |
| CM < HC | CT+GMV+SA | FA+RD+RTAP | AD | SC |
| EM < HC | CT+GMV | RTOP+RTPP | X | SC |

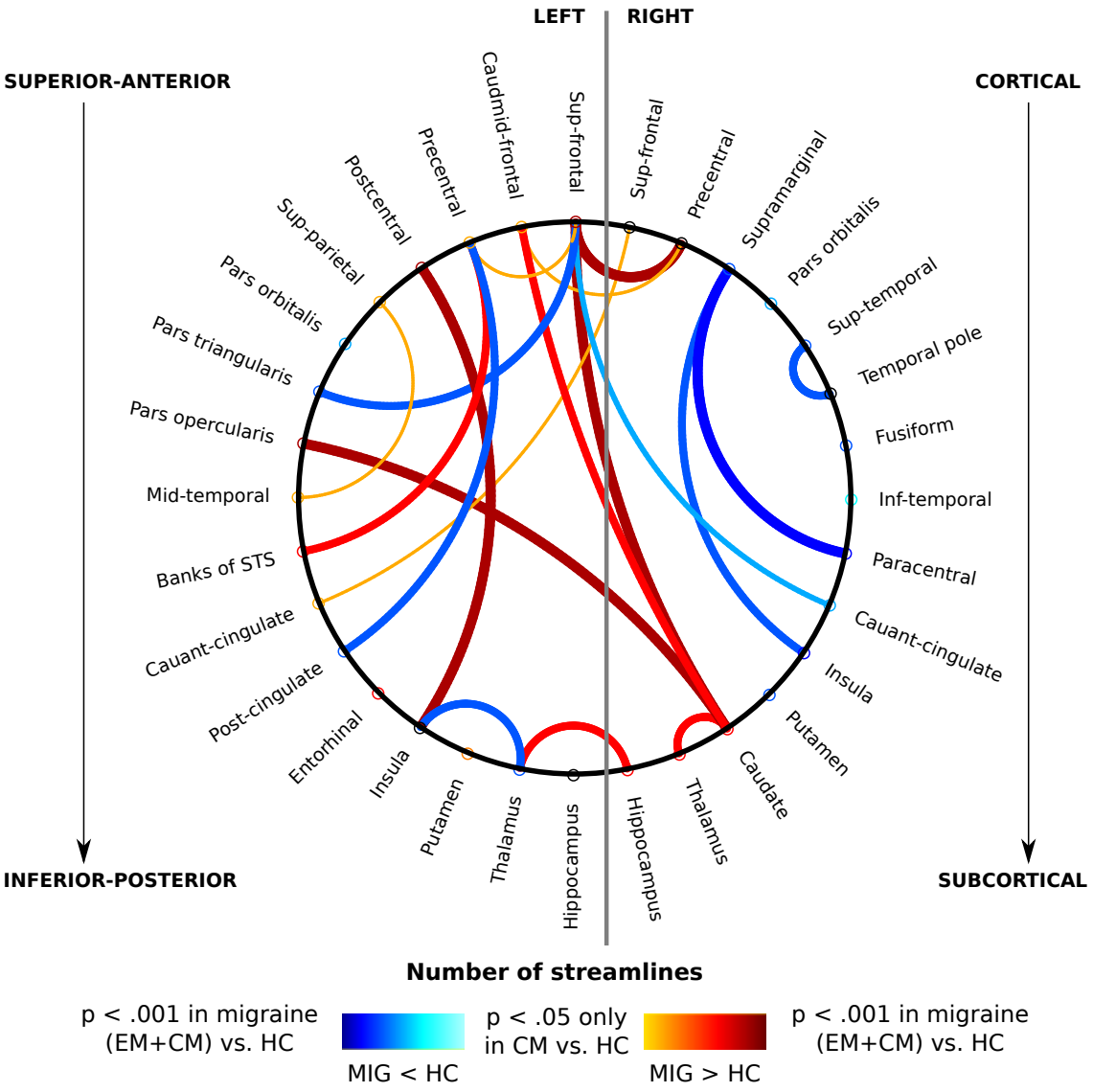


**Figure 4.5:** Circular graph of structural connections with significant differences in number of streamlines. Blue lines represent lower streamline count in the patient groups, while warm colors represent higher count. Cauant = caudal anterior; Caudmid = caudal middle; MIG = migraine; Post = posterior; STS = superior temporal sulcus; Sup = superior. Figure adapted from (Planchuelo-Gómez, García-Azorín, Guerrero, Aja-Fernández, Rodríguez, & de Luis-García, 2020a).

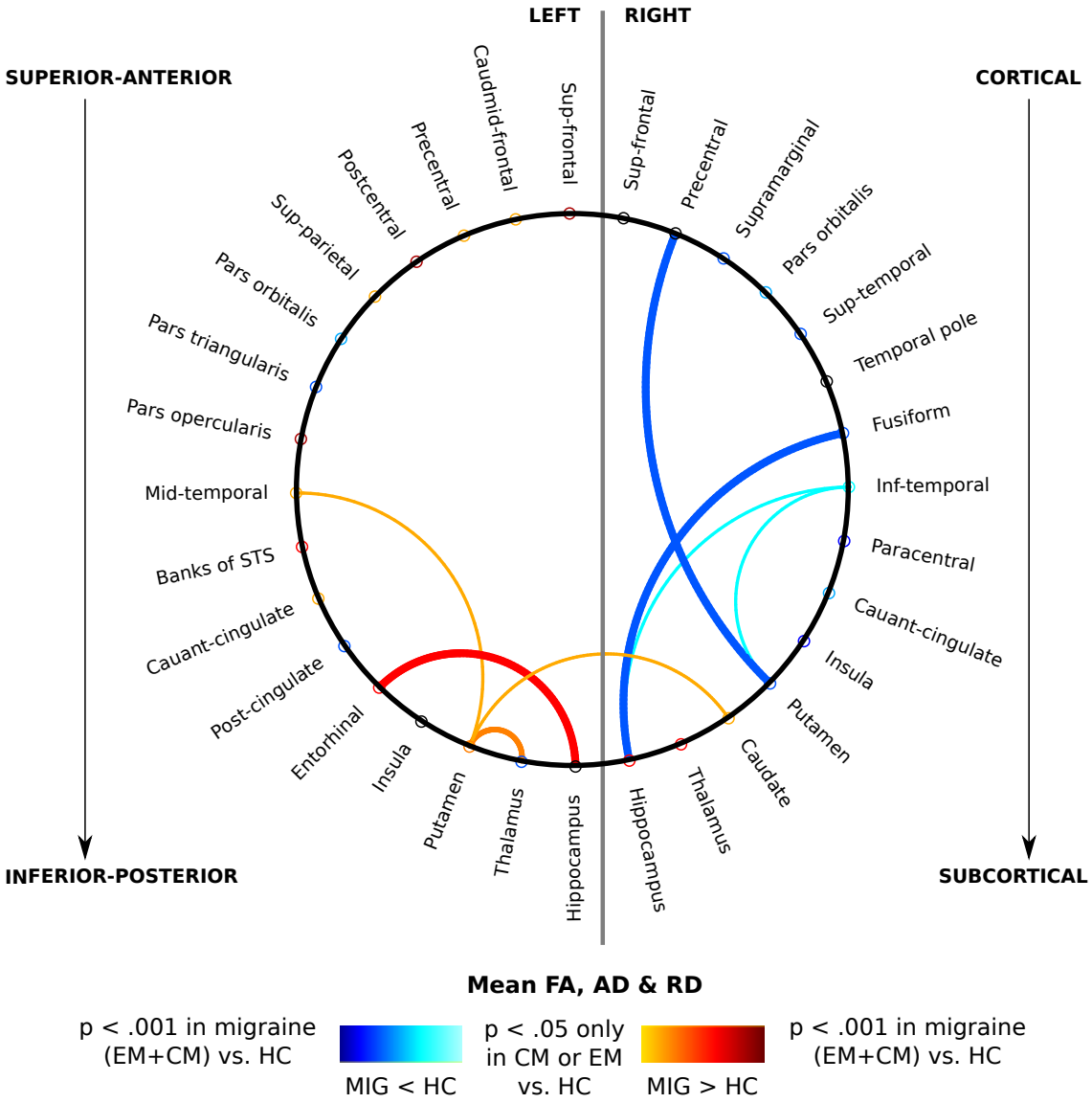


**Figure 4.6:** Circular graph of structural connections with significant differences in DTI-based parameters. Blue lines represent lower values in the patient groups, while warm colors represent higher values. Cauant = caudal anterior; Caudmid = caudal middle; Inf = inferior; MIG = migraine; Post = posterior; STS = superior temporal sulcus; Sup = superior. Figure from (Planchuelo-Gómez, García-Azorín, Guerrero, Aja-Fernández, Rodríguez, & de Luis-García, 2020a).

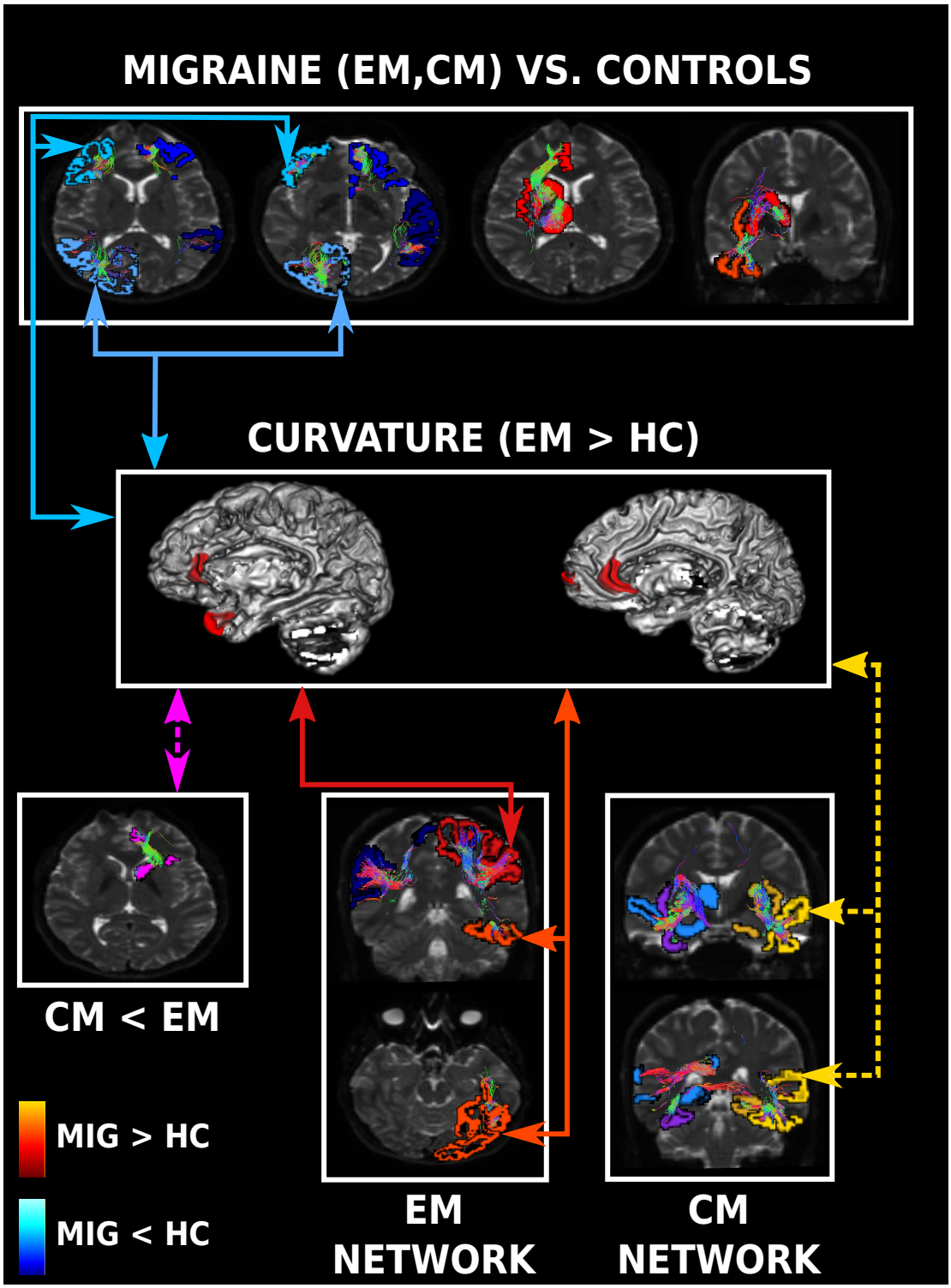


**Figure 4.7:** Summary of the identified structural networks and morphometry differences with multimodal fusion MRI analysis. Blue colors represent lower structural connectivity (streamline count) and warm colors represent higher connectivity and curvature. The arrows show simultaneous changes in curvature and connectivity. The dashed arrows indicate differences not directly associated with comparisons between EM and HC. Magenta is used to discern specific differences between the migraine groups. MIG = migraine (EM and CM simultaneously). Figure from (Planchuelo-Gómez et al., 2021).

# 4.2. Comparison between chronic and episodic migraine

## 4.2.1. Gray matter morphometry

Statistically significant differences were found for the gray matter volume, cortical thickness and surface area in the comparison between both migraine groups. No differences were observed for the cortical curvature.

Significant higher thickness in CM compared to EM was found in the right inferior temporal gyrus. In contrast, lower gray matter volume and surface area values were found in CM with respect to EM.

The number of regions with statistically significant differences for the comparisons between both groups of migraine is shown in Table 4.9.

More details about these comparisons can be found in Chapter 1 of Part II and (Planchuelo-Gómez, García-Azorín, Guerrero, Rodríguez, et al., 2020).

## 4.2.2. Diffusion measures

In the TBSS analysis with no additional covariates, higher RTPP values in the middle cerebellar peduncle and lower AD values in 38 regions from the ICBM-DTI-81 White Matter Atlas were identified in CM compared to EM. The regions with significant differences from the AD analysis showing the uncorrected and the adjusted results by the effect of time from onset of CM are shown in Figure 4.8. More details about the AD results, including further corrections, can be found in Chapter 2 of Part II and (Planchuelo-Gómez, García-Azorín, Guerrero, Aja-Fernández, Rodríguez, & de Luis-García, 2020b).

Considering any analysis with or without covariates, for all the parameters obtained from either DTI or AMURA, there were significant differences between both migraine groups. For the DTI-based parameters, lower values in CM were identified for the AD, MD and RD. In contrast, all the AMURA parameters (RTAP, RTOP and RTPP) and the FA presented higher values in CM compared to EM.

The number of regions from the ICBM-DTI-81 White Matter Atlas with significant differences between both migraine groups is shown in Table 4.10.

More details about these comparisons can be found in Chapters 2 and 3 of Part II and (Planchuelo-Gómez, García-Azorín, Guerrero, Aja-Fernández, Rodríguez, & de Luis-García, 2020b; Planchuelo-Gómez, García-Azorín, Guerrero, de Luis-García, et al., 2020).

**Table 4.9:** Number of regions with gray matter morphometry statistically significant differences between CM and EM. The ratio of the number of regions with significant differences to the total number of comparisons with significant differences per parameter is shown. CC = cortical curvature; CT = cortical thickness; GMV = gray matter volume; SA = surface area.

| Comparison | CC | CT | GMV | SA |
|---|---|---|---|---|
| CM > EM | 0 | 1/13 (7.7%) | 0 | 0 |
| CM < EM | 0 | 0 | 4/30 (13.3%) | 27/34 (79.4%) |

**Table 4.10:** Number of regions with diffusion descriptors statistically significant differences between CM and EM. The ratio of the number of regions with significant difference to the total number of regions from the ICBM-DTI-81 White Matter Atlas is shown. In case of some analyses with significant differences on a specific comparison, the comparison with higher number of regions with significant differences is shown.

| Comparison | FA | AD | RD | MD | RTAP | RTOP | RTPP |
|---|---|---|---|---|---|---|---|
| CM > EM | 4/48 (8.3%) | 0 | 0 | 0 | 39/48 (81.3%) | 42/48 (87.5%) | 15/48 (31.3%) |
| CM < EM | 0 | 38/48 (79.2%) | 39/48 (81.3%) | 34/48 (70.8%) | 0 | 0 | 0 |

**Table 4.11:** Number of regions with connectomics statistically significant differences between CM and EM. The ratio of the number of connections with significant differences in any comparison (adjusted or unadjusted) to the total number of comparisons with significant differences per parameter is shown. For each parameter, the cell in yellow remarks the comparison with higher ratio. SC = streamline count.

| Comparison | SC | AD | RD |
|---|---|---|---|
| CM > EM | 4/21 (19.0%) | 0 | 0 |
| CM < EM | 0 | 2/4 (50%) | 1/2 (50%) |

### *4.2.3.* ***Connectomics***

Statistically significant differences were found between both groups of migraine for the number of streamlines, the AD and the RD, while no differences were identified for the FA and the MD. A higher number of streamlines was found in CM compared to EM, while lower AD and RD values were identified in CM.

The number of regions with statistically significant differences for each comparison is depicted in Table 4.11.

The detailed connections with significant differences between CM and EM can be found in Chapter 5 of Part II and (Planchuelo-Gómez, García-Azorín, Guerrero, Aja-Fernández, Rodríguez, & de Luis-García, 2020a).

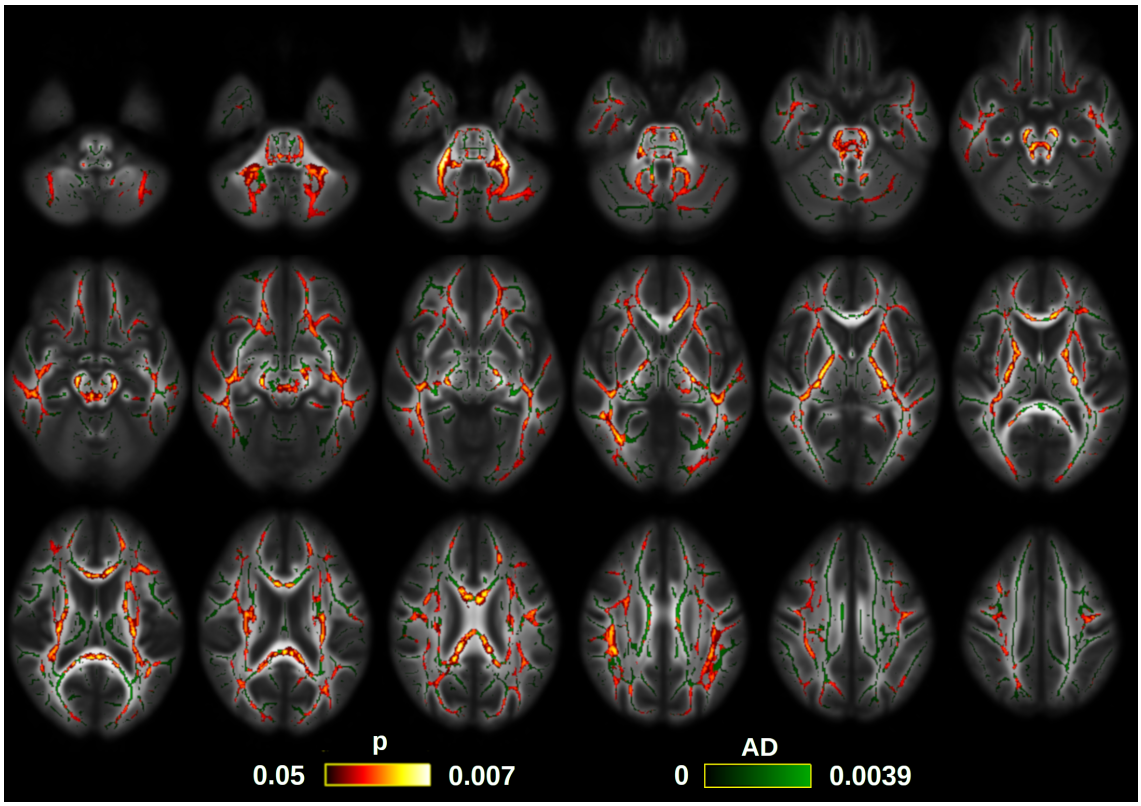


**Figure 4.8:** Regions with statistically significant lower AD values in CM patients with respect to EM. The family-wise error corrected p-value is shown in red-yellow.

**Table 4.12:** Summary of the comparisons with significant differences between patients with CM and EM and controls. CT = cortical thickness; GMV = gray matter volume; SA = surface area; SC = streamline count.

| Comparison | Morphometry | Diffusion MRI | Connectomics | Fusion MRI |
|---|---|---|---|---|
| CM > EM | CT | FA+RTAP+ RTOP+RTPP | SC | SC |
| CM < EM | GMV+SA | AD+RD+MD | SC+AD+RD | SC |

### *4.2.4. Multimodal MRI analysis*

There were no significant differences of any gray matter morphometry parameter between CM and EM patients. With respect to the comparison of the number of streamlines, one network composed of the lateral and medial orbitofrontal cortex and the caudate nucleus presented lower values in CM. Bearing in mind the enhanced and weakened networks in CM and EM reported in section 4.1.4, the ratio of the number of connections and networks per comparison to the total number of comparisons with significant differences is shown below:

- Enhanced in CM → 8/44 (18.2%) from two networks.
- Enhanced in EM → 6/44 (13.6%) from two networks.
- CM < EM → 2/44 (4.5%) from one network.

- Weakened in CM → 5/44 (11.4%) from two networks.
- Weakened in EM → 2/44 (4.5%) from one network.

The specific network with significant differences between both migraine groups can be observed in Figure 4.7. Further details are available in Chapter 6 of Part II and (Planchuelo-Gómez et al., 2021).

The summary of the comparisons between CM and EM is shown in Table 4.12.

## 4.3. Correlation between clinical and MRI measures in migraine

Statistically significant correlations were obtained between MRI measures and both the duration of migraine in years and the time from the onset of CM in months. These correlations were obtained with gray matter morphometry parameters and DTI-based parameters in white matter regions or structural connections.

Significant negative correlations were obtained between the surface area of the insula and the duration of migraine, and the gray matter volume of three regions, including the insula, and the duration of migraine. No significant correlations were identified with the time from the onset of CM. The scatter plots of these correlations are shown in Figure 4.9. Considering the known relationship between age and gray matter volume, we have included the age as color dimension in the scatter plots of Figure 4.9. It can be observed that the scatter plots for the duration of migraine are similar to the age patterns.

In contrast, considering the DTI-based parameters in white matter, statistically significant correlations were identified with the time from onset of CM, but not with the duration of migraine. Significant positive correlations with the mean FA and negative correlations with the mean RD were found in the bilateral external capsule. The scatter plots of these correlations can be found in Figure 4.10.

In the case of connectomics, a significant positive correlation was detected between the mean FA and the time from onset of CM in the right insula *self-connection*. An additional positive correlation was found between the mean AD and the duration of migraine history (only in CM patients) in the connection between the right hippocampus and the right inferior temporal gyrus. The scatter plots of these correlations can be found in Figure 4.11. Following the example of Figure 4.9, we have included the age values in the scatter plot related to duration of migraine in Figure 4.11. It can be observed that the relationship between the relationship between the mean AD and duration of migraine is very similar to that with the age.

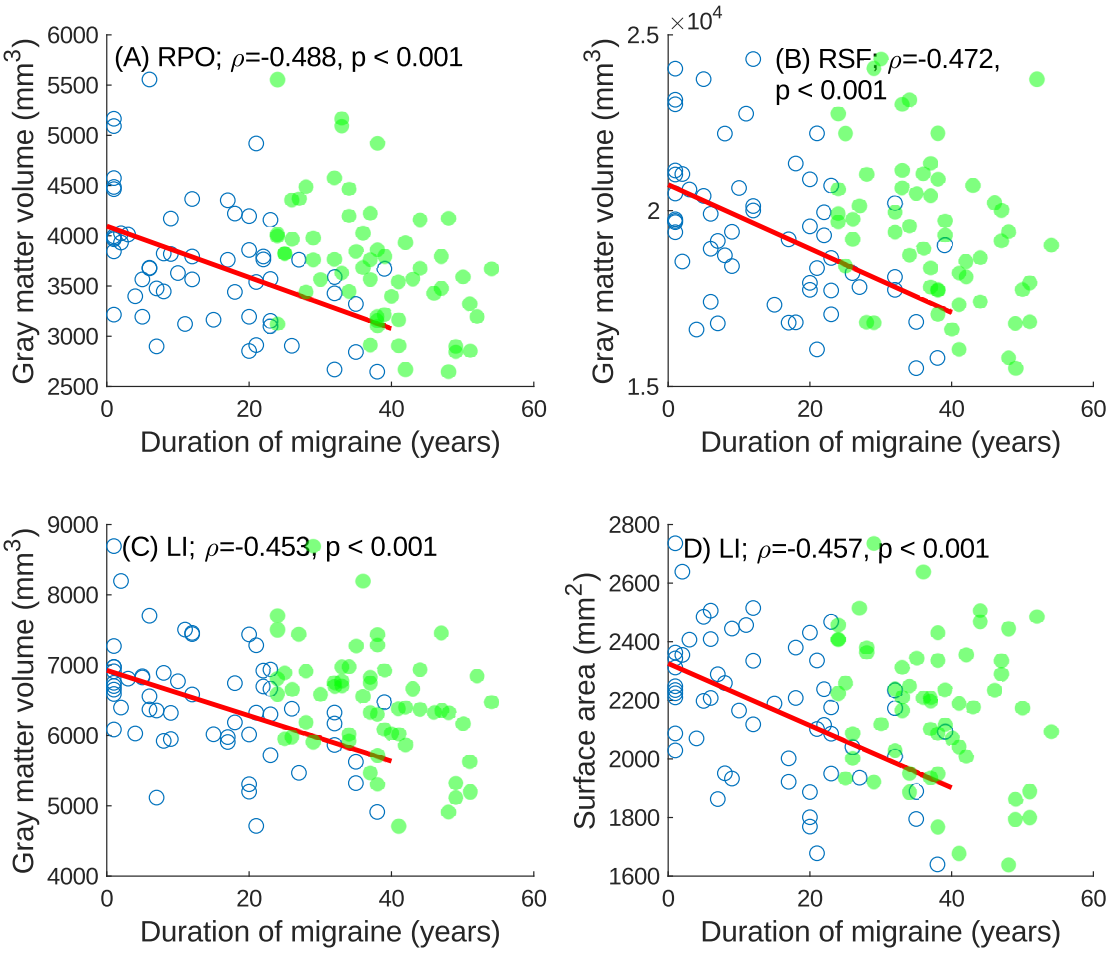


**Figure 4.9:** Scatter plots between duration of migraine history and gray matter morphometry parameters. The values of duration are shown in blue while the age in years is shown in green. LI = left insula; RPO = right pars opercularis; RSF = right superior frontal gyrus. Figure adapted from (Planchuelo-Gómez, García-Azorín, Guerrero, Rodríguez, et al., 2020).

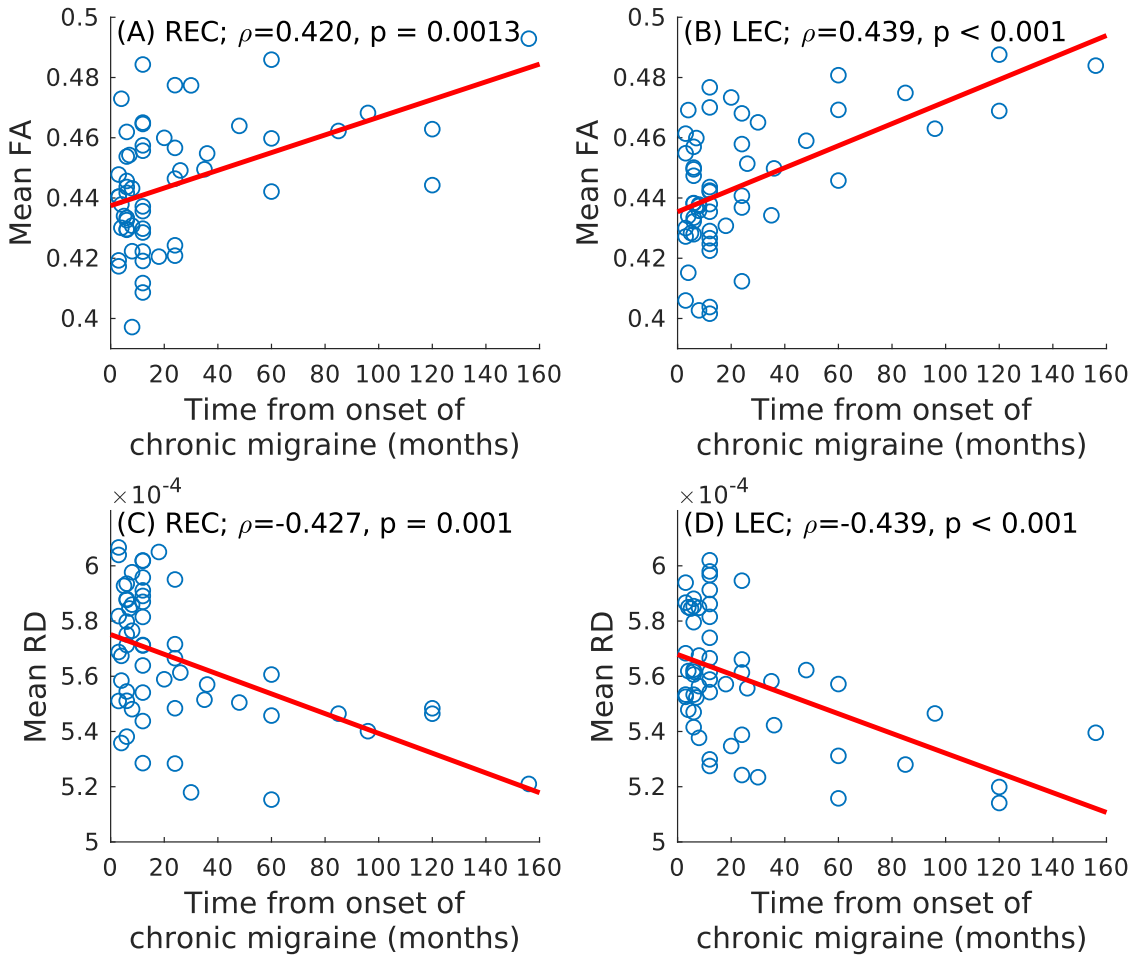


**Figure 4.10:** Scatter plots between time from onset of CM and gray matter DTI parameters in white matter regions. LEC = left external capsule; REC = right external capsule. Figure from (Planchuelo-Gómez, García-Azorín, Guerrero, Aja-Fernández, Rodríguez, & de Luis-García, 2020b).

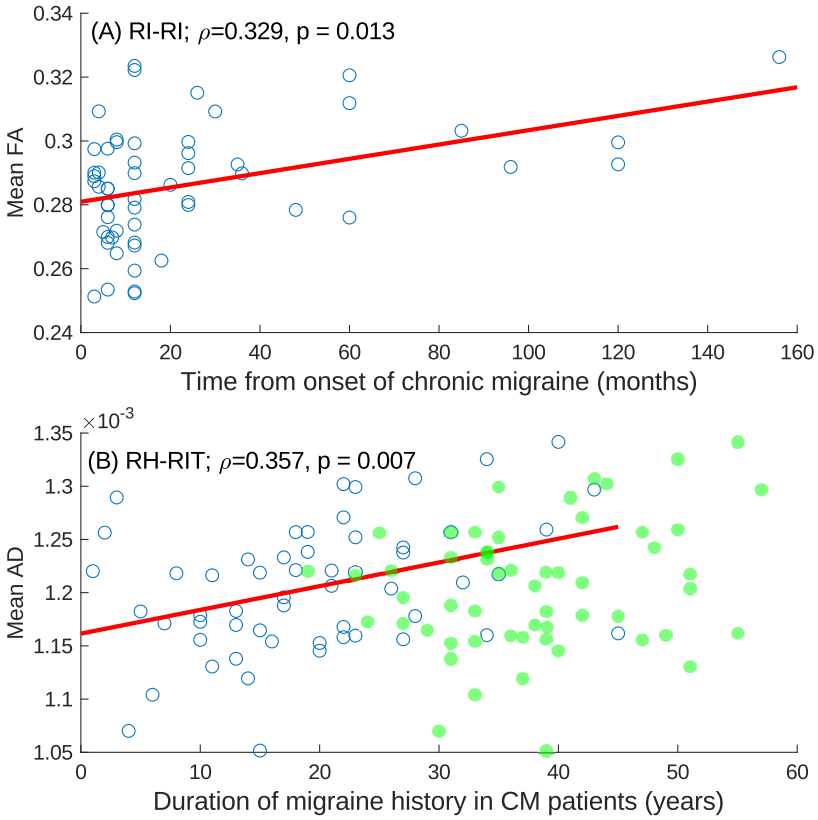


**Figure 4.11:** Scatter plots between clinical features in CM patients and DTI-based connectomics parameters. The values of duration are shown in blue while the age in years is shown in green. RH = right hippocampus; RI = right insula; RIT = right inferior temporal gyrus. Figure adapted from (Planchuelo-Gómez, García-Azorín, Guerrero, Aja-Fernández, Rodríguez, & de Luis-García, 2020a).

## 4.4. Effects of changing sample size and diffusion acquisition parameters

Using the original sample, 61 gradient directions and 1000 permutations, significant lower AD values were obtained in 37 white matter regions in CM compared to EM. With respect to the results reported in section 4.2.2 with 5000 permutations, there is one less region with statistically significant differences.

Regarding the analysis of the sample size, in the first reduction (50 subjects per migraine group) no significant differences were identified using the 21-directions scheme. For the 40- and 61- directions scheme, the number of regions with statistically significant differences was lower for each reduction of the sample size until both groups were composed of 35 subjects, when no regions with significant differences between CM and EM were found. In Figure 4.12, detailed values of the number of regions with significant differences per gradient-orientations scheme and sample size are shown.

In the analysis with the original sample but reducing the number of diffusion gradients, lower number of regions with significant differences were detected for 40 (27 regions) and 21 directions (20 regions). The regions identified with 40 and 21 orientations were a subset of the regions with significant differences from the original analysis with 1000 permutations, as shown in Figure 4.13. Some regions with significant differences identified with 21 directions were not found in the analysis with 40 directions, which can be seen in Figure 4.13.

These results are included in Chapter 4 of Part II.

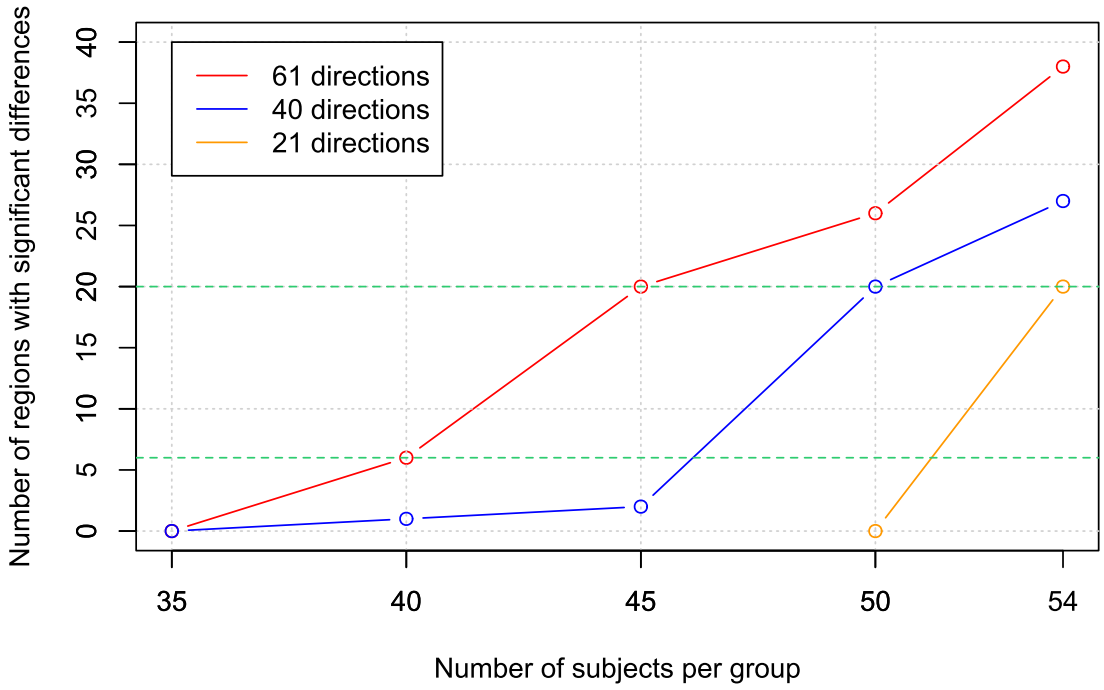


**Figure 4.12:** Comparison of the number of regions with significant differences between patients with CM and EM using 61, 40 and 21 diffusion orientations depending on the sample size. The 54 value of the number of subjects represents the original sample, with 56 subjects in the CM group and 54 in the EM group. Figure from (Planchuelo-Gómez, Aja-Fernández, et al., 2020).

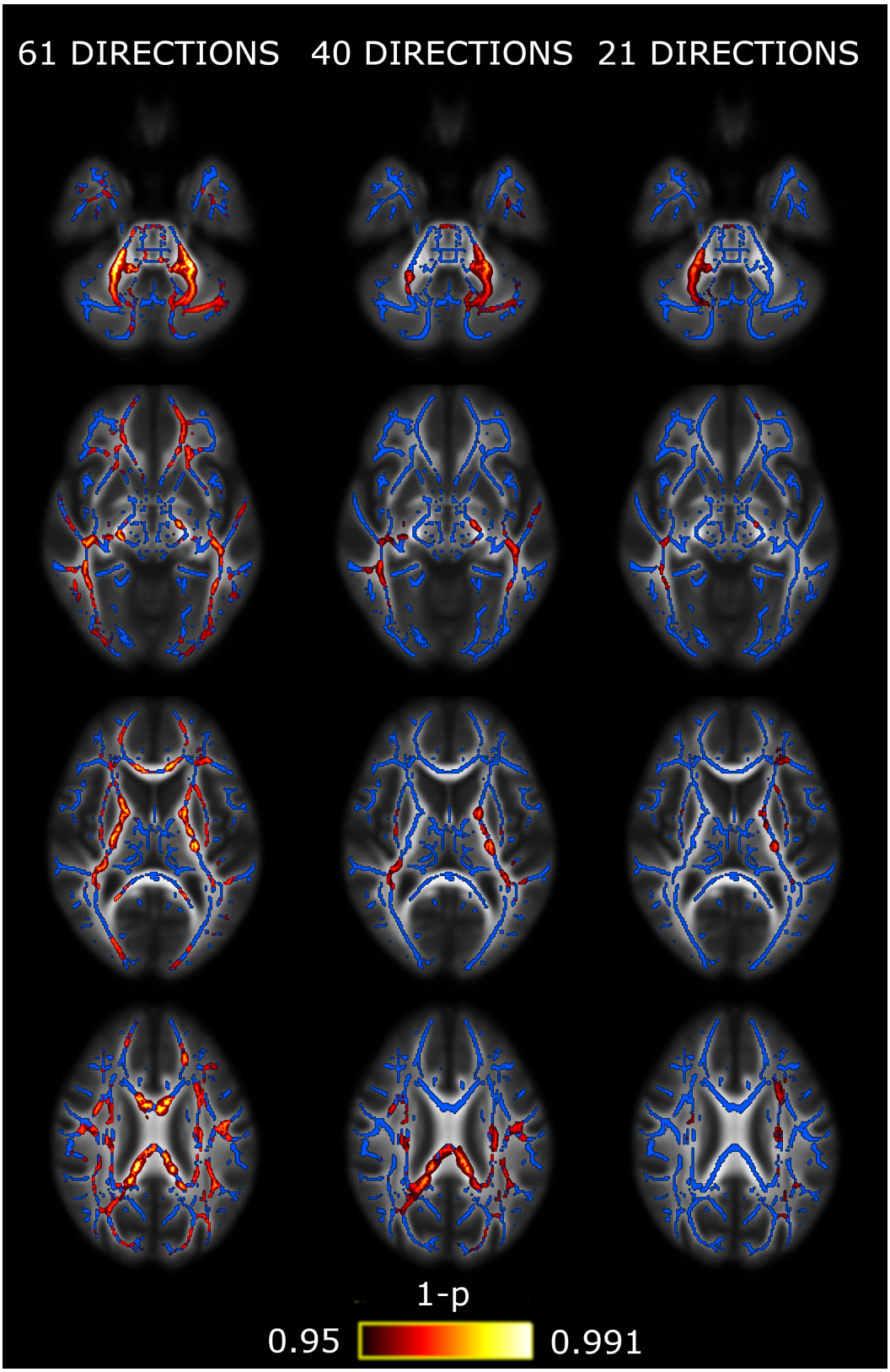


**Figure 4.13:** Comparison of the TBSS analysis between patients with CM and EM using 61 (left), 40 (center) and 21 diffusion orientations (right). White matter skeleton is shown in blue and voxels with significant differences in red-yellow. The color bar shows the 1-p values (family-wise error corrected). Figure from (Planchuelo-Gómez, Aja-Fernández, et al., 2020).

# *Chapter 5*

# *Discussion*

Advanced MRI processing methods have led to the extraction of novel results in relation to the characterization of gray matter and white matter alterations in Chronic Migraine (CM) and Episodic Migraine (EM). Regarding the first objective of the study, consistent gray matter abnormalities have been detected in both groups of migraine patients with respect to controls (Chapter 1 of Part II). With respect to white matter properties, different trends were identified in both groups of patients compared to controls and, depending on the covariates of the analysis, opposite FA results were reported in the same comparison but different regions (Chapter 2 of Part II). In the white matter analysis, advanced diffusion measures obtained with Apparent Measures Using Reduced Acquisitions (AMURA) were useful to detect statistically significant differences between patients with EM and controls that were not identified using traditional DTI-based measures (Chapter 3 of Part II). Following the comparisons of white matter parameters with TBSS analysis, the number of diffusion gradients and the sample size were described as key factors in the comparison between groups of interest (Chapter 4 of Part II). Furthermore, in the connectomics analysis, reinforced and weakened structural connectivity was found in both groups of migraine patients compared to controls (Chapter 5 of Part II). In addition, the multimodal fusion analysis showed a relationship between the cortical curvature and the structural connectivity differences in patients with EM, and additional patterns with respect to the analysis with a unique modality (Chapter 6 of Part II).

In the sections of this chapter, considering the clinical perspective of this thesis, the aforementioned findings are discussed based on the specific characteristics of migraine and the differences between both types of migraine. From the technical perspective, the relevance of advanced MRI processing in the analysis of migraine and the importance of the fusion analysis to understand the association between multiple alterations found with diverse modalities are discussed. A detailed discussion of the diverse structural findings can be found in each chapter of the Part II, while this chapter is employed to summarize the most important points of the thesis and provide a global perspective.

## 5.1. Characterization of the brain structure in migraine

With all the modalities, either assessed separately or in a multimodal analysis, statistically significant differences were detected between patients with migraine and controls.

Gray matter alterations were consistent in both groups of migraine patients with respect to controls. On the one hand, cortical curvature could be the parameter which better describes differences between migraine, without the consideration of a specific group, and controls, presenting higher values on the patients. On the other hand, lower gray matter volume values in migraine patients compared to controls was the most reported result in the analysis of these two previous groups, although higher values were identified in subcortical regions in our results and also in (Neeb et al., 2017). The loss of gray matter volume is the most reported result in gray matter migraine studies (Jia & Yu, 2017). A detailed discussion regarding gray matter changes in migraine is found in Chapter 1 of Part II.

The results of the analysis of the white matter structure in the comparison between both migraine groups and controls were not as consistent as those from the gray matter analysis in this thesis. Similar results were obtained in the assessment of structural connectivity. The hypothesis stated in the articles that compose this thesis about the different white matter and structural connectivity trends is that different patterns affecting distinct subnetworks in the brain may coexist in migraine. It appeared to be debilitated networks composed of regions within each lobe and strengthened connections with subcortical and pain processing regions. The simultaneous changes produced in diverse regions and the structural connectivity alterations, together with the functional alterations previously identified in the literature, may suggest that migraine is a *network disorder*. This term has been previously suggested and means that groups of interconnected regions present changes associated with migraine (Messina, Filippi, & Goadsby, 2018). Among the implicated regions according to our results, the insula seems to be a key area affected in migraine. The insula has been described as a hub of activity in migraine with altered structure and function in migraine, being a potential target for migraine treatments (Borsook et al., 2016). In any case, it is not clear whether the identified patterns in migraine patients are cause or consequence of the disease. A detailed discussion regarding white matter and structural connectivity changes is found in Chapters 2, 3, 5 and 6 of Part II.

Another possible explanation for these results and the conflicting results of literature may be related to the heterogeneity of migraine. This might imply that there could be subgroups of migraine that have not yet been identified. These migraine subgroups could explain the conflicting results of the literature and other issues related to migraine such as the occasional presence of White Matter Hyperintensities (WMH) or the great differences of migraine triggers between the patients. Regarding the migraine triggers, a recent study focused on the prediction of attacks, with poor prediction results (lower than 60%) in patients with EM (Holsteen, Hittle, Barad, & Nelson,

2020). This poor predictability and the conflicting neuroimaging results of the literature, together with the variability of symptoms, may reflect different subtypes of migraine.

Interestingly, no gray matter differences have been identified between controls and migraine patients with older age (mean age equal to 49 years or older) compared to the migraine peak (35-40 years), except in CM with respect to controls (Husøy et al., 2019; Neeb et al., 2017). These results may reflect that the effects of migraine in the gray matter structure would be similar to aging effects in younger patients.

## 5.2. Chronic Migraine portrait

Diverse statistically significant differences were obtained between patients with CM and EM using gray matter morphometry, white matter diffusion descriptors and structural connectivity parameters.

Regarding the gray matter differences between both migraine groups, lower surface area values in CM patients were identified in multiple regions, with a considerable higher number of differences with respect to the other parameters. This result may reflect that the surface area could be a biomarker of CM for the differentiation between the current types of migraine. In a previous study that classified HC and patients with CM and EM, the surface area was an important parameter in the classification of CM patients with respect to the other two groups, with worse classification results between EM and HC (Schwedt, Chong, et al., 2015). This is a similar result compared to the one identified in this thesis. In contrast to the surface area, higher cortical thickness values were found in the inferior temporal gyrus in CM patients according to our results. The same result was reported in high frequency EM compared to low frequency EM (Maleki et al., 2012b). These different trends in cortical thickness and surface area may be related to the opposite genetic effects of both parameters (Grasby et al., 2020). It is worth noting that the area is determined largely prenatally and the thickness postnatally (Frye et al., 2010; Kapellou et al., 2006; Messina et al., 2013). This fact may imply that there could be genetic differences between both migraine types, being the area a possible predictor of transition into CM. The thickness changes may be more affected by environmental factors. Further discussion of gray matter differences between CM and EM is included in Chapter 1 of Part II.

With respect to white matter, the values of DTI-based parameters and the AMURA results suggested that the patients with CM presented higher white matter integrity compared to EM. The correlation results and the adjusted results by factors such as presence of Medication Overuse Headache (MOH) and particularly time from onset of CM or duration of migraine history may reflect very different temporal patterns in both types of migraine. In CM, it is possible that white matter structure and connectivity are progressively reinforced, perhaps because the CM could be equivalent to a continuous ictal-like state, as suggested in (Neeb et al., 2015, 2017), in association with continuous headache attacks. However, another study reported increased MD and decreased FA values in CM patients without MOH compared to EM, suggesting debilitated

white matter integrity in CM (Coppola et al., 2020). High frequency EM could be an intermediate state between CM and EM that should be assessed, with possible initial axonal damage in the transition from EM to CM according to the AD results. An extended discussion about white matter microstructural differences between CM and EM is developed in Chapters 2 and 3 of Part II.

The connectomics results were in line with the white matter results, with lower AD and RD and higher number of streamlines in patients with CM compared to EM. In the connectomics single and multimodal analyses, structural connectivity differences between both migraine groups were observed in connections with subcortical regions, particularly the hippocampus and the caudate nucleus. The structural connectivity with these two regions could also be a possible CM biomarker. The hippocampus, which is implicated in strengthened and weakened networks in CM according to our results, has been remarked as an important region in association with migraine prognosis (H.-Y. Liu, Chou, & Chen, 2018). The caudate nucleus has been suggested to influence in the management of the pain experience (Wunderlich et al., 2011). Further details with regard to structural connectivity and differences between CM and EM are discussed in Chapters 5 and 6 of Part II.

With regard to the objectives of this study, it was mentioned that it should be elucidated whether CM could be a kind of more frequent EM, or rather a distinct entity. Our results demonstrated that the differences between both migraine groups were different with respect to the differences between the migraine patients and controls. Therefore, it seems that CM is an entity with different characteristics with respect to simply an EM with higher frequency.

## 5.3. Importance of advanced MRI processing and acquisitions

As described in section 2.1.4, the radiological examinations are insufficient to characterize brain changes related to migraine, with the possible exception of WMH. In this thesis and the literature, diverse types of differences between patients with migraine and controls have been detected, and also between patients with CM and EM. To examine in detail the diverse brain structural properties, it is important to acquire non-conventional MRI data (dMRI in this thesis). Thanks to the advanced processing of MRI data from diverse modalities, structural patterns could be identified in migraine. These patterns are related to gray and white matter properties, and the structural connections between gray matter regions through white matter tracts. The results of MRI studies give novel insights about the migraine pathophysiology, which currently is not completely understood, and allow to better understand the pathological mechanisms associated with the migraine experience.

The use of sophisticated processing methods also provides advantages with respect to other classical methods that have been employed in the migraine literature. In the case of the gray

matter analysis, the morphometry analysis including diverse parameters, as it is the case of the FreeSurfer pipeline (method employed in Chapter 1 of Part II) or SBM, gives additional information that cannot be obtained with VBM. For example, the use of surface area provided a potential biomarker of CM that could not be extracted with VBM. The advanced gray matter morphometry processing allows a complete characterization of diverse properties of gray matter which cannot be identified with the single use of gray matter volume.

Regarding the analysis with dMRI, the TBSS analysis has been useful to assess microstructural alterations of white matter tracts in the whole brain. The DTI model has also been widely employed in the assessment of white matter, although more sophisticated models are needed due to the oversimplification of DTI. Advanced dMRI methods, such as DKI or the Ensemble Average diffusion Propagator (EAP)-based measures obtained with AMURA in this thesis (Chapter 3 of Part II), are able to extract additional diffusion properties. In this thesis, despite the suboptimal conditions for the extraction of advanced diffusion descriptors (a unique and relatively low b-value), additional differences between EM patients and controls were detected only with AMURA. Thus, new diffusion methods extracted from appropriate dMRI acquisition protocols are crucial in the assessment of microstructural changes between groups of interest, as shown in Chapter 4 of Part II. With regard to the dMRI acquisition, the use of advanced microstructural models and multi-shell schemes would allow to identify more specific white matter changes.

Migraine has been suggested to be a *network disorder* due to the simultaneous changes in diverse regions. To better define the network properties, connectomics rises as an essential technique, as it is able to describe the connections between the specific gray matter processing regions. In this way, a network is not only be a set of regions with specific structural properties, but also a group of regions with particular structural connectivity patterns. For this analysis, the combination of information from T1- and diffusion-weighted MRI modalities is necessary, as described in Chapter 6 of Part II. Therefore, for the characterization of the structural properties of migraine and other neurological or psychiatric diseases, the use of individual and combined information from gray and white matter based on diverse MRI modalities should be performed.

## 5.4. Significance of the study of multimodal MRI fusion analysis

The use of a multimodal fusion analysis allows to find specific relationships between the properties obtained from diverse MRI modalities, taking into account possible covariance patterns. Additionally, in Chapter 6 of Part II, it was useful to find some alterations that were not detected in single-modality analyses.

In the simultaneous analysis of gray matter morphometry and structural connectivity, it was observed that curvature changes were linked to structural connectivity alterations in patients with EM. This identified association would confirm the hypothesis stated in previous studies suggesting

that cortical curvature could be a marker of white matter damage (Deppe et al., 2014; Lubeiro et al., 2017).

Regarding the gray matter morphometry parameters, their changes might be related to functional connectivity alterations, although no data were available in this thesis to confirm this hypothesis. The fusion analysis could allow to integrate functional and structural alterations, in individual regions and diverse connections, to better understand the interactions between function and structure in migraine or other disorders. Moreover, the fusion analysis could also allow the assessment of data from other sources such as genetics, which could be especially relevant as described in section 5.2.

The advantages of the multimodal fusion analysis do not implicate that the single-modality analysis should not be carried out. The fusion analysis can detect alterations based on the relationships between specific features, but not all the possible sources of variance. With a single-modality analysis, the differences found between groups of interest reflect the influence of all the possible sources of variance that affect the modality of interest. Hence, the complete analysis of diverse modalities should be performed using both single and multiple fusion modality analysis.

## 5.5. Limitations of the thesis

In this thesis, some important limitations related to the sample and technical issues need to be pointed out.

Despite not suffering from headache attacks in the 24 hours before the MRI acquisition, there was no control of the next 24 (or more) hours to the acquisition. This lack of control may imply that some patients could be in the prodromal instead of the interictal state, which may have biased some results. The bias would come from physiological and functional connectivity changes that have been detected in the prodromal stage (Karsan & Goadsby, 2018; May, 2017). Nevertheless, considering that in this thesis only structural changes have been assessed, this impact would be probably lower compared to the effect found in functional connectivity studies. In the controls, there was no headache diary to assess in detail the diagnosis of infrequent tension-type headache, although a questionnaire was provided in order to discard migraine-type headache. With regard to the patients with CM, an important percentage of the patients suffered from MOH, which could have some impact on all the results, as suggested by the white matter results.

With respect to the analysis of diverse aspects related to migraine, some assessments could not be performed. For example, the lack of patients with anxiety and/or depression to use a homogeneous sample did not allow to assess the effect of both comorbidities. Furthermore, the number of patients with aura was excessively small to carry out a proper comparison between migraine with and without aura, an analysis that has been performed frequently in the literature. The lack of an appropriate MRI sequence to assess WMH, such as T2-weighted imaging, implied the lack of a variable which could have been important in the differences between the migraine groups. With regard to the MRI acquisition protocol, neither functional MRI acquisition from

the patients to study the functional alterations, nor sophisticated diffusion acquisition measures compatible with advanced models were obtained. This previous issue avoided an excessively long acquisition time, but a full analysis of brain structural and functional alterations could not be performed. In association with the dMRI preprocessing, some important steps such as the Gibbs ringing correction or susceptibility correction were not conducted because of software limitations or lack of necessary images, i.e., non-diffusion weighted image with opposite phase encoding direction. The lack of some preprocessing steps may have caused some alterations on the extracted values, although in this thesis more steps were applied compared to the dMRI migraine studies from the literature. In addition, the lack of high frequency EM patients in the sample was important to characterize differences between CM and EM, but there was no analysis of a group of patients who might be particularly relevant to understand the transition from CM to EM.

With respect to connectomics, the number of streamlines is a controversial measure in the literature. It is worth noting that the total number of streamlines per tractography is an arbitrary value chosen by the user and there is no golden standard for the structural connectivity analysis. However, the ACT methodology reduces the impact of some negative aspects of the number of streamlines as connectivity measure, making it an acceptable metric (Yeh et al., 2020). Moreover, in the analysis of the number of streamlines, some connections with non-zero values of streamlines were removed to avoid false positives, at the cost of losing information that could have been relevant in the comparisons between migraine groups and controls. In the multimodal fusion analysis, the use of Z-score outliers to identify the independent sources with alterations in the three groups of interest was not based on an actual statistical comparison.

# *Chapter 6*

# *Conclusions*

This doctoral thesis is focused on the use of advanced MRI processing methods for the characterization of brain structure in migraine. This thesis is based on two perspectives: the clinical and the technical. From the clinical point of view, this thesis provided novel results with respect to the patterns that define the migrainous brain, and particularly in the comparison between patients with CM and EM. Moreover, in this thesis new results focused on the structural connectivity between specific gray matter regions were obtained. From the technical point of view, this thesis presented innovative results considering the analysis of dMRI data and the analysis of multimodal data with a fusion approach, using features instead of raw images.

Bearing in mind the gray matter morphometry results, common patterns in the regions with significant differences were found in both migraine groups compared to controls, with the exception of gray matter volume in subcortical regions. The detailed gray matter morphometry results are included in Chapter 1 of Part II. In contrast, the analysis of the white matter structure showed different trends in each of the migraine groups compared to controls (Chapters 2 and 3 of Part II). Furthermore, the structural connectivity assessment exhibited distinct patterns in migraine patients depending on the interconnected regions (Chapters 5 and 6 of Part II).

With respect to the dMRI analysis, it has been demonstrated that AMURA is able to supply additional results compared to the common DTI-based descriptors, even in suboptimal conditions for the extraction of advanced diffusion measures (Chapter 3 of Part II). Furthermore, the number of diffusion gradient orientations and the sample size were identified as key factors in the results from the TBSS analysis (further details in Chapter 4 of Part II). The mCCA-jICA multimodal analysis gave additional results compared to the single-modality analysis of the employed features and determined specific relationships between specific parameters (Chapter 6 of Part II).

Therefore, the studies from this doctoral thesis support a processing strategy for the characterization of structural properties of the brain not only in migraine, but also in other neurological or psychiatric disorders. In the case of migraine, the framework presented in this thesis provided possible biomarkers for migraine and CM and allowed to improve the understanding of migraine mechanisms. In this chapter, the contributions and main conclusions related to the diverse publications of this thesis are exposed. Finally, future research lines that emerge from the results of this thesis are described.

# 6.1. Contributions

The main contributions of this thesis are the following:

1. Direct comparison of four gray matter morphometric features in 68 cortical regions and 16 subcortical regions between HC and patients, CM and EM: cortical curvature, cortical thickness, gray matter volume and surface area. To our knowledge, this thesis presents the first study that compares curvature values between the three groups (Chapter 1 of Part II) (Planchuelo-Gómez, García-Azorín, Guerrero, Rodríguez, et al., 2020). The main results were higher curvature in both migraine groups compared to HC, and also lower thickness, volume and area values. As a result of the comparisons, the surface area has been remarked as a potential CM biomarker, finding lower values with respect to EM, in contrast to the cortical thickness, which showed higher values in patients with CM.

2. Assessment of four DTI parameters in 48 and 20 white matter tracts from two atlases in HC and patients with CM and EM using a TBSS approach: FA, AD, MD and RD. This thesis presents the first study that has found statistically significant white matter differences between patients with CM and EM (Chapter 2 of Part II) (Planchuelo-Gómez, García-Azorín, Guerrero, Aja-Fernández, Rodríguez, & de Luis-García, 2020b). Moreover, considering the TBSS and correlation results, a new hypothesis about the temporal changes of the white matter state between different stages of migraine has been proposed. In this hypothesis, opposite variations in the onset of EM are present with respect to the worsening to CM.

3. Extraction of alternative diffusion descriptors (EAP-based measures) using a new approach called AMURA: RTAP, RTOP and RTPP. This thesis presents the first application of AMURA in a migraine study using a dMRI acquisition protocol frequently employed in the clinical routine (Chapter 3 of Part II) (Planchuelo-Gómez, García-Azorín, Guerrero, de Luis-García, et al., 2020), which is however suboptimal for the complete exploitation of the method. The use of EAP-based measures allowed to identify additional statistically significant differences between patients with EM and HC that were not identified using DTI scalar measures. The use of the AMURA approach contributes to the characterization of the white matter properties in groups of patients with the provision of additional information with respect to conventional DTI measures.

4. Evaluation of the effect of the variation of sample size and number of diffusion orientations in the comparison of diffusion scalar measures between groups of patients. This thesis provides an analysis of variation of the statistically significant differences between groups of migraine patients in order to explain the conflicting results reported in dMRI migraine studies (Chapter 4 of Part II) (Planchuelo-Gómez, Aja-Fernández, et al., 2020). The use of 40 and 21 diffusion gradient orientations showed smaller subsets of regions with significant differences compared to the 61 gradient original scheme, with different regions identified in the two

schemes with less directions. The conducted study demonstrated that the use of a lower number of diffusion orientations can be partially counterbalanced with an increased sample size, but an appropriate characterization of the white matter structure requires a high number of orientations.

5. Application of a connectomics approach in order to characterize the connections between individual gray matter cortical and subcortical regions. The number of streamlines and the DTI measures to study differences in the structural connectivity between HC and patients with EM and CM were employed for the characterization. This thesis implements the first connectomics analysis in a migraine study, especially with regard to connections between specific gray matter regions (Chapter 5 of Part II) (Planchuelo-Gómez, García-Azorín, Guerrero, Aja-Fernández, Rodríguez, & de Luis-García, 2020a). In this analysis, two groups of results were identified. The first set was related to a potential weakening of the structural connectivity in migraine, and the second to a possible strengthening associated mostly with pain processing regions. The connectomics results provided new insights to understand the migraine pathophysiology, suggesting a plastic maladaptation of white matter to frequent painful stimuli and axonal disturbance in the transition from EM to CM.

6. Development of a fusion method to assess the simultaneous changes of gray matter morphometric parameters and structural connectivity in patients with CM and EM. The mCCA-jICA fusion technique was employed for the analysis. This thesis contains the first study to employ this type of methodology to assess at the same time morphometric and connectomics parameters, instead of the images from different MRI modalities. From the clinical perspective, this thesis presents the first application of a multimodal approach to a group of patients with CM and EM (Chapter 6 of Part II) (Planchuelo-Gómez et al., 2021). This research reflected the direct relationship between the variations of the cortical curvature and structural connectivity, represented by the number of streamlines, in migraine. Furthermore, specific networks were altered particularly in CM according to the fusion results, providing potential novel network biomarkers of CM.

## 6.2. Main conclusions

The main conclusions of this doctoral thesis are shown below:

- Migraine is characterized by a series of structural gray and white matter patterns, including connections between specific gray matter regions. These patterns are more consistent in gray matter compared to white matter parameters, i.e., CM and EM showed similar gray matter changes compared to HC, but different white matter modifications.

- Different types of changes in structural networks appear to coexist in migraine. The first group of alterations consist of debilitated networks composed of gray matter regions within

each lobe. The other set of changes are associated with strengthened networks which include pain processing regions.

- CM is an entity that presents different specific alterations with respect to low-frequency EM, being substantially distinct from an EM with higher frequency. Changes in surface area, axonal properties and structural connections with the hippocampus and the caudate nucleus are presented as possible CM biomarkers.

- The temporal evolution of the white matter state in CM seems to follow a different path compared to than in EM. The diffusion measures suggest an adaptation to the continuous headache attacks in CM and lower white matter integrity in EM.

- The employment of advanced MRI processing techniques is necessary to determine in detail structural properties of the brain in neurological and psychiatric disorders. These methods overcome the limitations of the radiological examinations and provide quantitative measures that contain important information about pathophysiological mechanisms.

- To characterize white matter microstructural properties, advanced diffusion models or methods that surmount DTI limitations are necessary. If diffusion-weighted imaging typical protocols from the clinical routine are employed, AMURA can complement DTI-based results.

- In white matter diffusion MRI studies, the number of diffusion gradient orientations should be as high as possible. The use of low sample size deeply limits the potential differences that could be found in a TBSS analysis.

- The use of sophisticated multimodal fusion analysis such as mCCA-jICA allows to determine specific relationships between multiple data modalities and their associated features, including MRI and non-MRI parameters. These fusion methods are also useful to characterize changes in the assessed individual modalities.

## 6.3. Future research lines

The results of this thesis helped to elucidate some questions that were present in the state of the art. However, these results raise new hypotheses and research lines. Possible future research lines are shown below:

- First, the obtained results should be replicated in other samples with similar characteristics, especially regarding the comparisons between CM and EM. Previous studies have assessed CM, EM and HC simultaneously using gray matter morphometry and DTI-based descriptors, but the mean age of the subjects was considerably higher (Husøy et al., 2019; Kattem Husøy et al., 2019; Neeb et al., 2015, 2017). In addition, high frequency EM patients should be included in future studies.

- Determination of possible migraine subgroups. MRI parameters from diverse modalities can be used to uncover unknown migraine types, further than the current classification between CM and EM. Unsupervised machine learning techniques could be employed for this purpose. This kind of methods would also be helpful to compare high frequency EM with CM and low frequency EM. The author of this doctoral thesis has participated as first author in a study with patients with psychotic disorder (schizophrenia and bipolar disorder) that obtained subgroups of patients based on gray matter morphometry parameters (Planchuelo-Gómez, Lubeiro, et al., 2020). This study could be useful to provide a framework for this suggested subgroup analysis.

- The employed MRI parameters could be useful to analyze the effect of treatments, including those that are frequently used such as topiramate or OnabotulinumtoxinA and the new treatments based on monoclonal antibodies to CGRP. The author of this study has participated as first author in a pilot study to predict the effects of topiramate using gray matter morphometry parameters as predictors (Planchuelo-Gómez, García-Azorín, Guerrero, Aja-Fernández, Antón-Juarros, & de Luis-García, 2020). Regarding the new preventive treatments for migraine, decreased activation in regions such as the thalamus and reduction of hypothalamic activation in responders were identified in another study with a low sample size (Ziegeler, Mehnert, Asmussen, & May, 2020).

- MRI and genetics data could be assessed simultaneously to determine possible relationships between them, especially in the comparison between CM and EM patients. In this simultaneous analysis, the surface area and cortical thickness results of both groups should be considered. With regard to genetics, diverse expressions of micro ribonucleic acid (known as miRNA) in peripheral blood mononuclear cells has shown statistically significant differences between patients with CM and EM (Greco et al., 2020). Using the proposed multimodal fusion analysis (mCCA-jICA) in this thesis, specific patterns associating neuroimaging and genetics could be identified.

- The structural properties of the migraine brain should be complemented with functional information from fMRI or even EEG. In relation to the white matter properties, advanced diffusion measures using the AMURA tool or other approaches should be employed for a complete characterization. The advanced diffusion methods could also be employed to assess gray matter, as it has been performed (Xiaoyun et al., 2020). An important reason related to a lack of a complete structural and functional profile in a unique migraine sample is the high acquisition time of the diffusion-weighted and the functional sequences, which require an approximated minimum time of 10 minutes per modality. A similar issue is associated with diffusion-weighted acquisition protocols with high and diverse b-values and large number of diffusion gradient orientations that cause longer acquisition times than the acquisitions used for the DTI model. The optimization of these sequences should be considered in future studies.

- Longitudinal studies are necessary not only to assess the migraine course, but also to analyze the suggested different longitudinal courses of CM and EM. Taking into account the correlation results, these results would be especially important in the assessment of white matter. Longitudinal studies would provide more accurate results with respect to correlation results. These studies would also be strongly related to the effect of the preventive treatment in patients with CM and high frequency EM. Moreover, the longitudinal studies would contribute to understand the lack of statistically significant differences between patients with EM older than the migraine peak age and controls in the literature.

- The changes in migraine should be compared with other headache and painful disorders, such as chronic tension-type headache and fibromyalgia. Previous studies have been conducted comparing migraine and tension-type headache, finding no statistically significant differences between them (Husøy et al., 2019; Kattem Husøy et al., 2019). In contrast, significant differences of the four assessed gray matter morphometry parameters have been found between persistent post-traumatic headache and migraine (Schwedt et al., 2017).

- Studies in pediatric patients would be important to elucidate whether the reported patterns in migraine are cause or consequence of the disease. Only one study has assessed white matter abnormalities in pediatric patients (Messina et al., 2015) and the statistically significant differences between the migraine patients and controls followed opposite trends compared to most studies included in the literature. To determine the nature of the structural changes, other possible subjects who could be longitudinally assessed are healthy young people with family history of migraine.

To sum up, the use of advanced processing methods of T1- and diffusion-weighted MRI data was employed to characterize the structural properties of the brain in migraine, with special focus on the differences between CM and EM. Gray matter morphometry parameters obtained from more sophisticated approaches than VBM, DTI- and EAP-based (extracted via AMURA) parameters and connectomics provide a framework for the analysis of the brain structure, bearing in mind the relevance of a high sample size and number of diffusion gradient orientations in the assessment of white matter. A sophisticated fusion method, mCCA-jICA, gives an approach to assess the relationships between the employed features and obtain additional results. With these methods, gray matter, white matter and structural connectivity patterns in migraine were detected together with differences between CM and EM. The employment of multiple modalities, including both MRI and non-MRI data, must be addressed in the future for the understanding of migraine pathophysiology, including the relationship between brain structure and function.

# *Chapter 7*

# *Resumen en castellano*

## 7.1. Introducción

La migraña es una enfermedad primaria discapacitante que se caracteriza por episodios recurrentes de cefalea. Las características de la cefalea en la migraña incluyen localización unilateral, dolor de tipo pulsátil (acompasado con los latidos del corazón) y de intensidad al menos moderada que se agrava con la actividad física, y náuseas y/o vómitos además de fotofobia y/o sonofobia durante los ataques de cefalea. Los tipos que se distinguen actualmente son migraña crónica y migraña episódica, que se diferencian por el número de días de cefalea al mes. La migraña crónica se define por episodios de cefalea en 15 o más días al mes durante un mínimo de tres meses, con al menos ocho días al mes presentando la cefalea características de migraña.

Actualmente, el diagnóstico de la migraña se realiza exclusivamente a partir de los síntomas previamente descritos, sin existir ningún biomarcador que permita identificar la migraña. Respecto a los hallazgos radiológicos realizados con neuroimagen, solamente se han detectado hiperintensidades de sustancia blanca en secuencias de imagen por resonancia magnética ponderadas en T2, aunque dichos hallazgos no son exclusivos de migraña ni están presentes en todos los pacientes, y su interpretación no está clara.

Para estudiar el cerebro de la migraña in vivo, la imagen por resonancia magnética se ha convertido en una modalidad ampliamente empleada debido a su buena resolución espacial y excelente contraste entre diferentes tipos de tejido mediante el uso de radiación no ionizante.

En la literatura previa, se han llevado a cabo múltiples estudios para analizar la estructura de la sustancia gris y la sustancia blanca en migraña haciendo uso de procesado de imagen por resonancia magnética ponderada en T1 y difusión, respectivamente. Además, se ha analizado la función cerebral mediante resonancia magnética funcional. Respecto a los estudios de sustancia gris, el resultado reportado con mayor frecuencia es pérdida de volumen en diversas regiones en los pacientes con migraña, aunque el resultado opuesto también se ha identificado. Además, resultados similares han sido obtenidos en el estudio del grosor cortical. En relación con el análisis de la sustancia blanca, no se han encontrado patrones claros empleando parámetros obtenidos a partir del tensor de difusión, siendo el resultado reportado con mayor frecuencia menor anisotropía fraccional en los pacientes con migraña respecto a los controles. Apenas se han realizado estudios

comparando pacientes con migraña crónica y episódica entre sí, sin haberse obtenido diferencias estadísticamente significativas.

## 7.2. Hipótesis y objetivos

La hipótesis principal de esta tesis doctoral es que el cerebro de los pacientes con migraña sufre una serie de alteraciones estructurales relacionada con cambios en sustancia gris y blanca. Además, también se plantea que el uso de modelos basados en el tensor de difusión puede ser insuficiente para la caracterización de las propiedades estructurales de la sustancia blanca y que los cambios de sustancia gris y blanca están asociados entre sí, incluyendo las conexiones entre regiones de sustancia gris a través de las regiones de sustancia blanca.

El principal objetivo de esta tesis doctoral es la caracterización de las alteraciones estructurales que tienen lugar en los pacientes con migraña, incluyendo las diferencias entre los pacientes con migraña crónica y migraña episódica. Respecto a la comparación entre ambos tipos de migraña, también se pretende analizar si la migraña crónica es una especie de migraña episódica intensificada o con mayor frecuencia o si es una entidad distinta con alteraciones específicas. Los objetivos de esta tesis doctoral se detallan a continuación:

- Caracterizar las alteraciones de sustancia gris en migraña crónica y episódica usando parámetros de morfometría.
- Definir los cambios de sustancia blanca en migraña crónica y episódica usando parámetros obtenidos a partir del tensor de difusión que han sido previamente empleados en la literatura.
- Analizar una nueva aproximación, *Apparent Measures Using Reduced Acquisitions* (AMURA), y comprobar si es capaz de aportar nueva información acerca de la difusión en regiones de sustancia blanca en comparación con el tensor de difusión.
- Evaluar conjuntamente el efecto del tamaño muestral y de los parámetros de adquisición en la resonancia de difusión en las comparaciones estadísticas de parámetros obtenidos a partir del tensor de difusión.
- Determinar alteraciones específicas de conectividad estructural entre regiones de sustancia gris en migraña crónica y episódica a partir de conectómica.
- Encontrar relaciones particulares entre los cambios de morfometría de sustancia gris y las alteraciones de conectividad estructural en pacientes con migraña crónica y episódica.

## 7.3. Materiales y métodos

La base de datos empleada en esta tesis doctoral estuvo compuesta por 52 controles sanos, 57 pacientes con migraña episódica y 57 pacientes con migraña crónica. Debido a errores surgidos

durante el procesamiento de las imágenes de resonancia de difusión o a la ausencia de dichas imágenes, en los estudios que emplearon dichos datos se incluyeron finalmente 50 controles sanos, 54 pacientes con migraña episódica y 56 pacientes con migraña crónica. Respecto a los controles, se comprobó que fueran adecuados para estudios de cefaleas. Los pacientes con migraña incluidos en los estudios fueron reclutados cuando visitaron la unidad de cefaleas del Hospital Clínico Universitario de Valladolid por primera vez.

En el análisis global de la sustancia gris, se realizó un procesado de las imágenes de resonancia magnética ponderadas en T1 para estudiar diversos parámetros morfométricos. Dichos parámetros fueron la curvatura cortical, el grosor cortical, la superficie y el volumen de sustancia gris. Para obtener dichas medidas en 68 regiones corticales (incluyendo el cerebelo) y 16 subcorticales, se empleó el software FreeSurfer, que realiza una segmentación de las diferentes estructuras. Los cuatro parámetros mencionados se obtienen para las 68 regiones corticales, mientras que en las regiones subcorticales solamente se extraen los valores de volumen de sustancia gris.

Respecto al procesado de la sustancia blanca a partir de las imágenes de resonancia de difusión, en primer lugar se llevó a cabo un preprocesado de estas imágenes con el objetivo de reducir el ruido asociado a esta modalidad y corregir las inhomogeneidades producidas por los campos magnéticos $B_0$ y $B_1$, el movimiento y las *eddy currents*. Tras este preprocesado, por un lado se obtuvieron medidas basadas en el modelo del tensor de difusión, que fueron la anisotropía fraccional (FA), la difusividad radial (RD), la difusividad media (MD) y la difusividad axial (AD). Por otro lado, se hizo uso de la metodología AMURA para calcular los mapas de medidas avanzadas de difusión, que fueron la *return-to-axis probability* (RTAP), *return-to-origin probability* (RTOP) y *return-to-plane probability* (RTPP). Para el análisis de la sustancia blanca mediante las medidas descritas en este párrafo, se utilizó el método *tract-based spatial statistics* (TBSS), que obtiene un esqueleto de la sustancia blanca a partir de las imágenes de todos los sujetos que componen el estudio.

Para determinar los efectos de la variación del tamaño muestral en relación con el número de orientaciones de los gradientes de difusión, se analizaron diferentes submuestras de la comparación de la AD mediante TBSS entre los dos grupos de migraña, con 25 submuestras por cada cantidad fijada de sujetos. Por un lado, se simularon diferentes subconjuntos de la muestra original y, aprovechando la técnica de adquisición utilizada en la resonancia de difusión, también se analizaron tres conjuntos de gradientes de difusión, el original (61 direcciones) y dos subconjuntos de 40 y 21 direcciones. El valor de la mediana del número de regiones con diferencias estadísticamente significativas en las diferentes comparaciones se empleó como medida de comparación entre los diferentes esquemas planteados.

El análisis de la conectividad estructural se basó en la técnica de la tractografía, que reconstruye las fibras que conectan las diversas regiones de sustancia gris en todo el cerebro. A partir de la tractografía, se determinó el número de *streamlines* en las conexiones entre las regiones corticales y subcorticales de interés. La cuenta de streamlines, junto con las medidas obtenidas a partir del tensor de difusión, se utilizó como medida de conectividad estructural en las comparaciones entre los grupos de interés.

La fusión de la información de diversas modalidades, la morfometría de la sustancia gris y la conectividad estructural en el caso de esta tesis doctoral, se realizó mediante la integración de las técnicas de análisis de la correlación canónica multimodal (mCCA) seguida por la de análisis conjunto de componentes independientes (jICA). Esta combinación de métodos permitió identificar las alteraciones de los parámetros asociados a una modalidad con los cambios de conectividad estructural, además de captar alteraciones individuales en cada una de las modalidades que no fueron detectadas en las comparaciones previamente mencionadas.

En todos los casos, se realizó la comparación estadística de los grupos de interés, esto es, el grupo de controles sanos y los grupos de migraña crónica y episódica.

## 7.4. Resultados

En relación con el análisis de morfometría de sustancia gris, se detectaron de manera significativa mayores valores de curvatura cortical en los dos grupos de migraña en comparación con los controles, así como menores valores de grosor cortical, volumen de sustancia gris (excepto en regiones subcorticales) y la superficie en múltiples regiones. Además, se identificaron mayores valores de grosor cortical y menores de volumen de sustancia gris y, en numerosas regiones, de área de la superficie en pacientes con migraña crónica respecto a migraña episódica.

Respecto a los resultados estadísticamente significativos del análisis con los descriptores de difusión en sustancia blanca, considerando comparaciones ajustadas por diversas covariables, se hallaron mayores valores de AD en migraña episódica respecto a controles, menores valores de RTOP y RTPP en migraña episódica respecto a controles y menores valores de RD y RTAP en migraña crónica en comparación con los controles. Con la FA, en diferentes zonas, se detectaron tanto mayores como menores valores en migraña crónica respecto a los controles. Adicionalmente, con las medidas obtenidas mediante la herramienta AMURA, se hallaron diferencias significativas entre migraña episódica y controles que no se pudieron detectar con las medidas del tensor de difusión. En la comparación entre ambos tipos de migraña, se encontraron mayores valores de FA, RTAP, RTOP y RTPP en migraña crónica respecto a episódica, y al contrario con la AD, MD y RD.

En el análisis de los efectos de la reducción del tamaño muestral y del número de direcciones de los gradientes de difusión se halló que un bajo tamaño muestral podía compensarse con un mayor número de gradientes de difusión y viceversa. Para una cantidad fijada de sujetos, se observó mayor cantidad de diferencias significativas con el empleo de más orientaciones, excepto para tamaños muestrales muy bajos en los que no se identifican diferencias estadísticamente significativas.

Los resultados del análisis de conectómica mostraron dos tendencias distintas en la comparación entre los pacientes con migraña y los controles, obteniéndose tanto conexiones reforzadas en conexiones con regiones de procesamiento del dolor como conexiones debilitadas en conexiones entre regiones dentro de cada lóbulo en los pacientes respecto a los controles. Estos resultados se identificaron tanto con la comparación estadística directa del número de *streamlines* como con el

análisis multimodal con mCCA-jICA, en el que se determinó que los cambios de curvatura cortical están asociados a los de conectividad estructural en migraña episódica. En cuanto a la comparación entre ambos tipos de migraña, se identificaron alteraciones en conexiones con el hipocampo en migraña crónica, así como conexiones debilitadas entre la corteza orbitofrontal y el núcleo caudado en migraña crónica respecto a migraña episódica.

## 7.5. Discusión

De acuerdo con los resultados obtenidos, la migraña está relacionada con una serie de cambios en la sustancia gris, especialmente pérdida de volumen excepto en regiones subcorticales. Además, la migraña se vincula con alteraciones de redes estructurales cerebrales„ esto es, que varias regiones y las conexiones estructurales que las unen se ven afectadas, en lugar de simplemente haber cambios en regiones aisladas de sustancia gris. Quedaría por determinar si los cambios detectados son causa o consecuencia de la migraña.

Teniendo en cuenta que los dos grupos de migraña presentaron cambios comunes respecto a los controles sanos, también se apreciaron diferencias estadísticamente significativas entre migraña crónica y episódica. En el conjunto de cambios, destacan los menores valores de superficie en numerosas regiones de sustancia gris en migraña crónica, lo que puede indicar que dicho parámetro podría ser un biomarcador de migraña crónica. Respecto a las alteraciones de sustancia blanca, los resultados obtenidos sugieren, sorprendentemente, mayor integridad de la sustancia blanca en migraña crónica que en migraña episódica, especialmente teniendo en cuenta el efecto temporal. Por lo tanto, la migraña crónica parece una entidad distinta respecto a una especie de migraña episódica intensificada, esto es, la migraña crónica tiene características específicas.

Los resultados de esta tesis doctoral muestran la importancia del procesado avanzado de imagen por resonancia magnética para el análisis del cerebro en diversas patologías. Las técnicas que analizan las diversas modalidades de resonancia magnética permiten estudiar diferentes tipos de tejidos y propiedades del cerebro. De esta manera, se pueden obtener hallazgos que permiten comprender mejor los mecanismos fisiopatológicos de la migraña u otras enfermedades neurológicas y psiquiátricas, además de posibles asociaciones entre dichos mecanismos.

## 7.6. Conclusiones

Las principales conclusiones de esta tesis doctoral son:

- La migraña se caracteriza por una serie de cambios estructurales en sustancia gris y sustancia blanca. Además, dos tipos de redes estructurales con comportamientos opuestos parecen coexistir en la migraña.

- La migraña crónica tiene características distintas respecto a la migraña episódica. La superficie de sustancia gris se presenta como un biomarcador entre ambos tipos de migraña. Ambos tipos de migraña podrían presentar una evolución temporal distinta.

- El empleo de modelos alternativos al tensor de difusión es necesario para caracterizar las propiedades de la sustancia blanca, incluso con posible aplicación al análisis de la sustancia gris. En estos estudios, se debe procurar que el tamaño muestral y el número de direcciones en los gradientes de difusión sea lo más alto posible.

- El uso de métodos sofisticados de fusión de datos provenientes de diferentes modalidades permite caracterizar las asociaciones entre cambios de diferente naturaleza e identificar alteraciones específicas en cada modalidad.

Algunas líneas futuras de investigación incluyen el análisis longitudinal, el estudio de las alteraciones estructurales en conjunto con propiedades funcionales o datos que incluso no provengan de resonancia magnética (por ejemplo, la genética), la comparación con otras cefaleas y patologías caracterizadas por el dolor (por ejemplo, la fibromialgia) y la realización de estudios en pacientes pediátricos para comprender mejor si los cambios observados son causa o consecuencia de la migraña.

# *References*

Adams, A. M., Serrano, D., Buse, D. C., Reed, M. L., Marske, V., Fanning, K. M., & Lipton, R. B. (2015). The impact of chronic migraine: The Chronic Migraine epidemiology and Outcomes (CaMEO) Study methods and baseline results. *Cephalalgia*, *35*(7), 563-578. doi: 10.1177/0333102414552532

Aja-Fernández, S., de Luis-García, R., Afzali, M., Molendowska, M., Pieciak, T., & Tristán-Vega, A. (2020). Micro-structure diffusion scalar measures from reduced MRI acquisitions. *PLOS ONE*, *15*(3), e0229526. doi: 10.1371/journal.pone.0229526

Aja-Fernández, S., Pieciak, T., Tristán-Vega, A., Vegas-Sánchez-Ferrero, G., Molina, V., & de Luis-García, R. (2018). Scalar diffusion-MRI measures invariant to acquisition parameters: A first step towards imaging biomarkers. *Magnetic Resonance Imaging*, *54*, 194-213. doi: 10.1016/j.mri.2018.03.001

Aja-Fernández, S., Tristán-Vega, A., & Jones, D. K. (2021). Apparent propagator anisotropy from single-shell diffusion MRI acquisitions. *Magnetic Resonance in Medicine*, *85*(5), 2869-2881. doi: 10.1002/mrm.28620

Aja-Fernández, S., & Vegas-Sánchez-Ferrero, G. (2016). *Statistical Analysis of Noise in MRI: Modeling, Filtering and Estimation* (1st ed.). Springer, Cham.

Alexander, A. L., Lee, J. E., Lazar, M., & Field, A. S. (2007). Diffusion tensor imaging of the brain. *Neurotherapeutics : the journal of the American Society for Experimental NeuroTherapeutics*, *4*(3), 316-329. doi: 10.1016/j.nurt.2007.05.011

Amico, E., & Goñi, J. (2018). Mapping hybrid functional-structural connectivity traits in the human connectome. *Network Neuroscience*, *2*(3), 306-322. doi: 10.1162/netn_a_00049

Amin, F. M., Asghar, M. S., Hougaard, A., Hansen, A. E., Larsen, V. A., de Koning, P. J., ... Ashina, M. (2013). Magnetic resonance angiography of intracranial and extracranial arteries in patients with spontaneous migraine without aura: a cross-sectional study. *The Lancet Neurology*, *12*(5), 454-461. doi: 10.1016/S1474-4422(13)70067-X

Andersson, J. L., & Sotiropoulos, S. N. (2016). An integrated approach to correction for off-resonance effects and subject movement in diffusion MR imaging. *NeuroImage*, *125*, 1063-1078. doi: 10.1016/j.neuroimage.2015.10.019

Ashburner, J., & Friston, K. J. (2000). Voxel-Based Morphometry—The Methods. *NeuroImage*, *11*(6), 805-821. doi: 10.1006/nimg.2000.0582

Avram, A. V., Sarlls, J. E., Barnett, A. S., Özarslan, E., Thomas, C., Irfanoglu, M. O., ...

Basser, P. J. (2016). Clinical feasibility of using mean apparent propagator (MAP) MRI to characterize brain tissue microstructure. *NeuroImage*, *127*, 422-434. doi: 10.1016/j.neuroimage.2015.11.027

Bach, M., Laun, F. B., Leemans, A., Tax, C. M., Biessels, G. J., Stieltjes, B., & Maier-Hein, K. H. (2014). Methodological considerations on tract-based spatial statistics (tbss). *NeuroImage*, *100*, 358-369. doi: 10.1016/j.neuroimage.2014.06.021

Barrio-Arranz, G., de Luis-García, R., Tristán-Vega, A., Martín-Fernández, M., & Aja-Fernández, S. (2015). Impact of MR Acquisition Parameters on DTI Scalar Indexes: A Tractography Based Approach. *PLOS ONE*, *10*(10), e0137905. doi: 10.1371/journal.pone.0137905

Basser, P. J., & Jones, D. K. (2002). Diffusion-tensor MRI: theory, experimental design and data analysis - a technical review. *NMR in Biomedicine*, *15*, 456-467. doi: 10.1002/nbm.783

Basser, P. J., Pajevic, S., Pierpaoli, C., Duda, J., & Aldroubi, A. (2000). In vivo fiber tractography using DT-MRI data. *Magnetic Resonance in Medicine*, *44*(4), 625-632. doi: 10.1002/1522-2594(200010)44:4<625::AID-MRM17>3.0.CO;2-O

Bazargan-Hejazi, S., Dehghan, K., Edwards, C., Mohammadi, N., Attar, S., Sahraian, M. A., & Eskandarieh, S. (2020). The health burden of non-communicable neurological disorders in the USA between 1990 and 2017. *Brain Communications*, *2*(2). (fcaa097) doi: 10.1093/braincomms/fcaa097

Beaulieu, C. (2002). The basis of anisotropic water diffusion in the nervous system – a technical review. *NMR in Biomedicine*, *15*, 435-455. doi: 10.1002/nbm.782

Behrens, T., Woolrich, M., Jenkinson, M., Johansen-Berg, H., Nunes, R., Clare, S., ... Smith, S. (2003). Characterization and propagation of uncertainty in diffusion-weighted MR imaging. *Magnetic Resonance in Medicine*, *50*(5), 1077-1088. doi: 10.1002/mrm.10609

Benjamini, Y., & Hochberg, Y. (1995). Controlling the False Discovery Rate: A Practical and Powerful Approach to Multiple Testing. *Journal of the Royal Statistical Society: Series B (Methodological)*, *57*(1), 289-300. doi: 10.1111/j.2517-6161.1995.tb02031.x

Bloch, F. (1946). Nuclear Induction. *Phys. Rev.*, *70*, 460-474. doi: 10.1103/PhysRev.70.460

Bodammer, N., Kaufmann, J., Kanowski, M., & Tempelmann, C. (2004). Eddy current correction in diffusion-weighted imaging using pairs of images acquired with opposite diffusion gradient polarity. *Magnetic Resonance in Medicine*, *51*(1), 188-193. doi: 10.1002/mrm.10690

Borsook, D., Maleki, N., & Burstein, R. (2015). Chapter 42 - Migraine. In *Neurobiology of Brain Disorders* (p. 693-708). San Diego: Academic Press.

Borsook, D., Veggeberg, R., Erpelding, N., Borra, R., Linnman, C., Burstein, R., & Becerra, L. (2016). The Insula: A "Hub of Activity" in Migraine. *The Neuroscientist : a review journal bringing neurobiology, neurology and psychiatry*, *22*(6), 632-652. doi: 10.1177/1073858415601369

Bozzali, M., Parker, G. J., Serra, L., Embleton, K., Gili, T., Perri, R., ... Cercignani, M. (2011). Anatomical connectivity mapping: A new tool to assess brain disconnection in Alzheimer's disease. *NeuroImage*, *54*(3), 2045-2051. doi: 10.1016/j.neuroimage.2010.08.069

Bullmore, E., & Sporns, O. (2009). Complex brain networks: graph theoretical analysis of structural and functional systems. *Nature Reviews Neuroscience*, *10*(3), 186-198. doi: 10.1038/nrn2575

Burch, R. (2019). Migraine and Tension-Type Headache: Diagnosis and Treatment. *Medical Clinics of North America*, *103*(2), 215-233. doi: 10.1016/j.mcna.2018.10.003

Burdette, J. H., Durden, D. D., Elster, A. D., & Yen, Y.-F. (2001). High b-value Diffusion-Weighted MRI of Normal Brain. *Journal of Computer Assisted Tomography*, *25*(4). doi: 10.1097/00004728-200107000-00002

Burke, M. J., Joutsa, J., Cohen, A. L., Soussand, L., Cooke, D., Burstein, R., & Fox, M. D. (2020). Mapping migraine to a common brain network. *Brain*, *143*(2), 541-553. doi: 10.1093/brain/awz405

Calamante, F., Tournier, J.-D., Jackson, G. D., & Connelly, A. (2010). Track-density imaging (TDI): Super-resolution white matter imaging using whole-brain track-density mapping. *NeuroImage*, *53*(4), 1233-1243. doi: 10.1016/j.neuroimage.2010.07.024

Callaghan, P. T. (1994). *Principles of Nuclear Magnetic Resonance Microscopy* (1st ed.). Oxford University Press.

Callaghan, P. T., Eccles, C. D., & Xia, Y. (1988, Aug). NMR microscopy of dynamic displacements: k-space and q-space imaging. *Journal of Physics E: Scientific Instruments*, *21*(8), 820-822. doi: 10.1088/0022-3735/21/8/017

Carole, D., Ophélia, G., John, C., Oghuzan, C., Stephen, M., Nathalie, T.-M., ... Christophe, T. (2009). Severe Cerebral White Matter Hyperintensities Predict Severe Cognitive Decline in Patients With Cerebrovascular Disease History. *Stroke*, *40*(6), 2219-2221. doi: 10.1161/STROKEAHA.108.540633

Chalmer, M. A., Hansen, T. F., Lebedeva, E. R., Dodick, D. W., Lipton, R. B., & Olesen, J. (2020). Proposed new diagnostic criteria for chronic migraine. *Cephalalgia*, *40*(4), 399-406. doi: 10.1177/0333102419877171

Charles, A. (2013). The evolution of a migraine attack - a review of recent evidence. *Headache*, *53*(2), 413-419. doi: 10.1111/head.12026

Charles, A. C., & Baca, S. M. (2013). Cortical spreading depression and migraine. *Nature Reviews Neurology*, *9*(11), 637-644. doi: 10.1038/nrneurol.2013.192

Chong, C. D., Dodick, D. W., Schlaggar, B. L., & Schwedt, T. J. (2014). Atypical age-related cortical thinning in episodic migraine. *Cephalalgia*, *34*(14), 1115-1124. doi: 10.1177/0333102414531157

Chong, C. D., Peplinski, J., Berisha, V., Ross, K., & Schwedt, T. J. (2019). Differences in fibertract profiles between patients with migraine and those with persistent post-traumatic headache. *Cephalalgia*, *39*(9), 1121-1133. doi: 10.1177/0333102418815650

Chong, C. D., & Schwedt, T. J. (2015). Migraine affects white-matter tract integrity: A diffusion-tensor imaging study. *Cephalalgia*, *35*(13), 1162-1171. doi: 10.1177/0333102415573513

Clark, K. A., Nuechterlein, K. H., Asarnow, R. F., Hamilton, L. S., Phillips, O. R., Hageman,

N. S., ... Narr, K. L. (2011). Mean diffusivity and fractional anisotropy as indicators of disease and genetic liability to schizophrenia. *Journal of psychiatric research*, *45*(7), 980-988. doi: 10.1016/j.jpsychires.2011.01.006

Coppola, G., Di Renzo, A., Tinelli, E., Di Lorenzo, C., Di Lorenzo, G., Parisi, V., ... Pierelli, F. (2016). Thalamo-cortical network activity during spontaneous migraine attacks. *Neurology*, *87*(20), 2154. doi: 10.1212/WNL.0000000000003327

Coppola, G., Di Renzo, A., Tinelli, E., Iacovelli, E., Lepre, C., Di Lorenzo, C., ... Pierelli, F. (2015). Evidence for brain morphometric changes during the migraine cycle: A magnetic resonance-based morphometry study. *Cephalalgia*, *35*(9), 783-791. doi: 10.1177/0333102414559732

Coppola, G., Di Renzo, A., Tinelli, E., Lepre, C., Di Lorenzo, C., Di Lorenzo, G., ... Pierelli, F. (2016). Thalamo-cortical network activity between migraine attacks: Insights from MRI-based microstructural and functional resting-state network correlation analysis. *The Journal of Headache and Pain*, *17*(1), 100. doi: 10.1186/s10194-016-0693-y

Coppola, G., Di Renzo, A., Tinelli, E., Petolicchio, B., Di Lorenzo, C., Parisi, V., ... Pierelli, F. (2020). Patients with chronic migraine without history of medication overuse are characterized by a peculiar white matter fiber bundle profile. *The Journal of Headache and Pain*, *21*(1), 92. doi: 10.1186/s10194-020-01159-6

Coppola, G., Tinelli, E., Lepre, C., Iacovelli, E., Di Lorenzo, C., Di Lorenzo, G., ... Pierelli, F. (2014). Dynamic changes in thalamic microstructure of migraine without aura patients: a diffusion tensor magnetic resonance imaging study. *European Journal of Neurology*, *21*(2), 287-e13. doi: 10.1111/ene.12296

Correa, N. M., Li, Y.-O., Adali, T., & Calhoun, V. D. (2008). Canonical Correlation Analysis for Feature-Based Fusion of Biomedical Imaging Modalities and Its Application to Detection of Associative Networks in Schizophrenia. *IEEE Journal of Selected Topics in Signal Processing*, *2*(6), 998-1007. doi: 10.1109/JSTSP.2008.2008265

Dale, A., Fischl, B., & Sereno, M. I. (1999). Cortical Surface-Based Analysis: I. Segmentation and Surface Reconstruction. *NeuroImage*, *9*(2), 179 - 194. doi: 10.1006/nimg.1998.0395

Damadian, R. (1971). Tumor Detection by Nuclear Magnetic Resonance. *Science*, *171*(3976), 1151-1153. doi: 10.1126/science.171.3976.1151

DaSilva, A. F., Granziera, C., Snyder, J., & Hadjikhani, N. (2007). Thickening in the somatosensory cortex of patients with migraine. *Neurology*, *69*(21), 1990. doi: 10.1212/01.wnl.0000291618.32247.2d

DaSilva, A. F. M., Granziera, C., Tuch, D. S., Snyder, J., Vincent, M., & Hadjikhani, N. (2007). Interictal alterations of the trigeminal somatosensory pathway and periaqueductal gray matter in migraine. *Neuroreport*, *18*(4), 301-305. doi: 10.1097/WNR.0b013e32801776bb

Datta, R., Detre, J. A., Aguirre, G. K., & Cucchiara, B. (2011). Absence of changes in cortical thickness in patients with migraine. *Cephalalgia*, *31*(14), 1452-1458. doi: 10.1177/0333102411421025

Degirmenci, B., Yaman, M., Haktanir, A., Albayrak, R., & Acar, M. (2007). Cerebral and cerebellar ADC values during a migraine attack. *Neuroradiology*, *49*(5), 419-426. doi: 10.1007/s00234 -006-0201-1

de Luis-García, R., Westin, C.-F., & Alberola-López, C. (2013). Geometrical constraints for robust tractography selection. *NeuroImage*, *81*, 26-48. doi: 10.1016/j.neuroimage.2013.04.096

Deppe, M., Marinell, J., Krämer, J., Duning, T., Ruck, T., Simon, O. J., ... Meuth, S. G. (2014). Increased cortical curvature reflects white matter atrophy in individual patients with early multiple sclerosis. *NeuroImage: Clinical*, *6*, 475-487. doi: 10.1016/j.nicl.2014.02.012

Desikan, R. S., Ségonne, F., Fischl, B., Quinn, B. T., Dickerson, B. C., Blacker, D., ... Killiany, R. J. (2006). An automated labeling system for subdividing the human cerebral cortex on MRI scans into gyral based regions of interest. *NeuroImage*, *31*(3), 968-980. doi: 10.1016/ j.neuroimage.2006.01.021

Dodick, D. W. (2018). A Phase-by-Phase Review of Migraine Pathophysiology. *Headache*, *58*(S1), 4-16. doi: 10.1111/head.13300

Drake-Pérez, M., Boto, J., Fitsiori, A., Lovblad, K., & Vargas, M. I. (2018). Clinical applications of diffusion weighted imaging in neuroradiology. *Insights into imaging*, *9*(4), 535-547. doi: 10.1007/s13244-018-0624-3

Etkin, A. (2014). Neuroimaging and the future of personalized treatment in psychiatry. *Depression and Anxiety*, *31*, 899-901. doi: 10.1002/da.22325

Evans, R. W., Burch, R. C., Frishberg, B. M., Marmura, M. J., Mechtler, L. L., Silberstein, S. D., & Turner, D. P. (2020). Neuroimaging for Migraine: The American Headache Society Systematic Review and Evidence-Based Guideline. *Headache*, *60*(2), 318-336. doi: 10.1111/ head.13720

Faragó, P., Tóth, E., Kocsis, K., Kincses, B., Veréb, D., Király, A., ... Kincses, Z. T. (2019). Altered Resting State Functional Activity and Microstructure of the White Matter in Migraine With Aura. *Frontiers in Neurology*, *10*, 1039. doi: 10.3389/fneur.2019.01039

Fick, R. H., Wassermann, D., Caruyer, E., & Deriche, R. (2016). MAPL: Tissue microstructure estimation using Laplacian-regularized MAP-MRI and its application to HCP data. *NeuroImage*, *134*, 365-385. doi: 10.1016/j.neuroimage.2016.03.046

Fischl, B., & Dale, A. M. (2000). Measuring the thickness of the human cerebral cortex from magnetic resonance images. *Proceedings of the National Academy of Sciences*, *97*(20), 11050. doi: 10.1073/pnas.200033797

Fischl, B., Liu, A., & Dale, A. M. (2001). Automated manifold surgery: constructing geometrically accurate and topologically correct models of the human cerebral cortex. *IEEE Transactions on Medical Imaging*, *20*(1), 70-80. doi: 10.1109/42.906426

Fischl, B., Salat, D. H., Busa, E., Albert, M., Dieterich, M., Haselgrove, C., ... Dale, A. M. (2002). Whole brain segmentation: automated labeling of neuroanatomical structures in the human brain. *Neuron*, *33*, 341-355. doi: 10.1016/s0896-6273(02)00569-x

Fischl, B., Salat, D. H., van der Kouwe, A. J., Makris, N., Ségonne, F., Quinn, B. T., & Dale, A. M.

(2004). Sequence-independent segmentation of magnetic resonance images. *NeuroImage*, *23*, S69-S84. doi: 10.1016/j.neuroimage.2004.07.016

Fischl, B., Sereno, M. I., & Dale, A. M. (1999). Cortical Surface-Based Analysis: II: Inflation, Flattening, and a Surface-Based Coordinate System. *NeuroImage*, *9*(2), 195-207. doi: 10 .1006/nimg.1998.0396

Fischl, B., Sereno, M. I., Tootell, R. B., & Dale, A. M. (1999). High-resolution intersubject averaging and a coordinate system for the cortical surface. *Human Brain Mapping*, *8*(4), 272–284. doi: 10.1002/(SICI)1097-0193(1999)8:4<272::AID-HBM10>3.0.CO;2-4

Fischl, B., van der Kouwe, A., Destrieux, C., Halgren, E., Ségonne, F., Salat, D. H., ... Dale, A. M. (2004). Automatically Parcellating the Human Cerebral Cortex. *Cerebral Cortex*, *14*(1), 11-22. doi: 10.1093/cercor/bhg087

Fornito, A., & Bullmore, E. T. (2015). Connectomics: A new paradigm for understanding brain disease. *European Neuropsychopharmacology*, *25*(5), 733-748. doi: 10.1016/j.euroneuro.2014 .02.011

Friston, K. J. (1994). Functional and effective connectivity in neuroimaging: A synthesis. *Human Brain Mapping*, *2*, 56-78. doi: 10.1002/hbm.460020107

Frye, R. E., Liederman, J., Malmberg, B., McLean, J., Strickland, D., & Beauchamp, M. S. (2010). Surface Area Accounts for the Relation of Gray Matter Volume to Reading-Related Skills and History of Dyslexia. *Cerebral Cortex*, *20*(11), 2625-2635. doi: 10.1093/cercor/bhq010

Gaist, D., Hougaard, A., Garde, E., Reislev, N. L., Wiwie, R., Iversen, P., ... Ashina, M. (2018). Migraine with visual aura associated with thicker visual cortex. *Brain*, *141*(3), 776-785. doi: 10.1093/brain/awx382

Garroway, A. N., Grannell, P. K., & Mansfield, P. (1974). Image formation in NMR by a selective irradiative process. *Journal of Physics C: Solid State Physics*, *7*(24), L457-L462. doi: 10 .1088/0022-3719/7/24/006

Gomez-Beldarrain, M., Oroz, I., Zapirain, B. G., Ruanova, B. F., Fernandez, Y. G., Cabrera, A., ... Garcıa-Monco, J. C. (2015). Right fronto-insular white matter tracts link cognitive reserve and pain in migraine patients. *The journal of headache and pain*, *17*, 4-4. doi: 10.1186/s10194-016-0593-1

Granziera, C., DaSilva, A. F. M., Snyder, J., Tuch, D. S., & Hadjikhani, N. (2006). Anatomical Alterations of the Visual Motion Processing Network in Migraine with and without Aura. *PLOS Medicine*, *3*(10), e402. doi: 10.1371/journal.pmed.0030402

Grasby, K. L., Jahanshad, N., Painter, J. N., Colodro-Conde, L., Bralten, J., Hibar, D. P., ... Medland, S. E. (2020). The genetic architecture of the human cerebral cortex. *Science*, *367*(6484), eaay6690. doi: 10.1126/science.aay6690

Greco, R., De Icco, R., Demartini, C., Zanaboni, A. M., Tumelero, E., Sances, G., ... Tassorelli, C. (2020). Plasma levels of CGRP and expression of specific microRNAs in blood cells of episodic and chronic migraine subjects: towards the identification of a panel of peripheral biomarkers of migraine? *The Journal of Headache and Pain*, *21*(1), 122. doi: 10.1186/

s10194-020-01189-0

Hahn, G., Skeide, M. A., Mantini, D., Ganzetti, M., Destexhe, A., Friederici, A. D., & Deco, G. (2019). A new computational approach to estimate whole-brain effective connectivity from functional and structural MRI, applied to language development. *Scientific Reports*, *9*(1), 8479. doi: 10.1038/s41598-019-44909-6

Headache Classification Committee of the International Headache Society. (2018). The International Classification of Headache Disorders, 3rd edition. *Cephalalgia*, *38*(1), 1-211. doi: 10.1177/0333102417738202

Holsteen, K. K., Hittle, M., Barad, M., & Nelson, L. M. (2020). Development and Internal Validation of a Multivariable Prediction Model for Individual Episodic Migraine Attacks Based on Daily Trigger Exposures. *Headache*, *60*, 2364-2379. doi: 10.1111/head.13960

Horn, J. L. (1965). A rationale and test for the number of factors in factor analysis. *Psychometrika*, *30*(2), 179-185. doi: 10.1007/BF02289447

Hougaard, A., Amin, F. M., Arngrim, N., Vlachou, M., Larsen, V. A., Larsson, H. B. W., & Ashina, M. (2016). Sensory migraine aura is not associated with structural grey matter abnormalities. *NeuroImage: Clinical*, *11*, 322-327. doi: 10.1016/j.nicl.2016.02.007

Hougaard, A., Amin, F. M., Hoffmann, M. B., Larsson, H. B., Magon, S., Sprenger, T., & Ashina, M. (2015). Structural gray matter abnormalities in migraine relate to headache lateralization, but not aura. *Cephalalgia*, *35*(1), 3-9. doi: 10.1177/0333102414532378

Hua, K., Zhang, J., Wakana, S., Jiang, H., Li, X., Reich, D. S., ... Mori, S. (2008). Tract probability maps in stereotaxic spaces: analyses of white matter anatomy and tract-specific quantification. *NeuroImage*, *39*(1), 336-347. doi: 10.1016/j.neuroimage.2007.07.053

Hubbard, C. S., Becerra, L., Smith, J. H., DeLange, J. M., Smith, R. M., Black, D. F., ... Borsook, D. (2016). Brain Changes in Responders vs. Non-Responders in Chronic Migraine: Markers of Disease Reversal. *Frontiers in Human Neuroscience*, *10*, 497. doi: 10.3389/fnhum.2016.00497

Hulla, R., & Liegey-Dougall, A. (2019, Jan 01). A systematic review of high-frequency transcranial magnetic stimulation on motor cortex areas as a migraine preventive treatment. *Cephalalgia Reports*, *2*, 2515816319889971. doi: 10.1177/2515816319889971

Husøy, A. K., Håberg, A. K., Rimol, L. M., Hagen, K., Vangberg, T. R., & Stovner, L. J. (2019). Cerebral cortical dimensions in headache sufferers aged 50 to 66 years: a population-based imaging study in the Nord-Trøndelag Health Study (HUNT-MRI). *PAIN*, *160*(7). doi: 10.1097/j.pain.0000000000001550

Ito, K., Kudo, M., Sasaki, M., Saito, A., Yamashita, F., Harada, T., ... Terayama, Y. (2016). Detection of changes in the periaqueductal gray matter of patients with episodic migraine using quantitative diffusion kurtosis imaging: preliminary findings. *Neuroradiology*, *58*(2), 115-120. doi: 10.1007/s00234-015-1603-8

Iyengar, S., Ossipov, M. H., & Johnson, K. W. (2017). The role of calcitonin gene–related peptide in peripheral and central pain mechanisms including migraine. *PAIN*, *158*(4). doi:

10.1097/j.pain.0000000000000831

Jenkinson, M., Beckmann, C. F., Behrens, T. E., Woolrich, M. W., & Smith, S. M. (2012). FSL. *NeuroImage*, *62*(2), 782-790. doi: 10.1016/j.neuroimage.2011.09.015

Jensen, J. H., Helpern, J. A., Ramani, A., Lu, H., & Kaczynski, K. (2005). Diffusional kurtosis imaging: The quantification of non-gaussian water diffusion by means of magnetic resonance imaging. *Magnetic Resonance in Medicine*, *53*(6), 1432-1440. doi: 10.1002/mrm.20508

Jia, Z., & Yu, S. (2017). Grey matter alterations in migraine: A systematic review and meta-analysis. *NeuroImage: Clinical*, *14*, 130-140. doi: 10.1016/j.nicl.2017.01.019

Jin, C., Yuan, K., Zhao, L., Zhao, L., Yu, D., von Deneen, K. M., ... Tian, J. (2013). Structural and functional abnormalities in migraine patients without aura. *NMR in Biomedicine*, *26*(1), 58-64. doi: 10.1002/nbm.2819

Jones, D. K. (2004). The effect of gradient sampling schemes on measures derived from diffusion tensor MRI: A Monte Carlo study†. *Magnetic Resonance in Medicine*, *51*(4), 807-815. doi: 10.1002/mrm.20033

Jones, D. K. (2010). *Diffusion MRI: theory, methods, and applications*. Oxford University Press. doi: 10.1093/med/9780195369779.001.0001

Jones, D. K., & Cercignani, M. (2010). Twenty-five pitfalls in the analysis of diffusion MRI data. *NMR in Biomedicine*, *23*(7), 803-820. doi: 10.1002/nbm.1543

Kapellou, O., Counsell, S. J., Kennea, N., Dyet, L., Saeed, N., Stark, J., ... Edwards, A. D. (2006). Abnormal Cortical Development after Premature Birth Shown by Altered Allometric Scaling of Brain Growth. *PLOS Medicine*, *3*(8), e265. doi: 10.1371/journal.pmed.0030265

Kara, B., Kiyat Atamer, A., Onat, L., Ulusoy, L., Mutlu, A., & Sirvanci, M. (2013). DTI Findings During Spontaneous Migraine Attacks. *Clinical Neuroradiology*, *23*(1), 31-36. doi: 10.1007/s00062-012-0165-y

Karsan, N., & Goadsby, P. J. (2018). Biological insights from the premonitory symptoms of migraine. *Nature Reviews Neurology*, *14*(12), 699-710. doi: 10.1038/s41582-018-0098-4

Kattem Husøy, A., Eikenes, L., Håberg, A. K., Hagen, K., & Stovner, L. J. (2019). Diffusion tensor imaging in middle-aged headache sufferers in the general population: a cross-sectional population-based imaging study in the Nord-Trøndelag health study (HUNT-MRI). *The Journal of Headache and Pain*, *20*(1), 78. doi: 10.1186/s10194-019-1028-6

Kim, J. H., Kim, J. B., Suh, S.-i., Seo, W.-K., Oh, K., & Koh, S.-B. (2014). Thickening of the somatosensory cortex in migraine without aura. *Cephalalgia*, *34*(14), 1125-1133. doi: 10.1177/0333102414531155

Kim, J. H., Suh, S.-I., Seol, H. Y., Oh, K., Seo, W.-K., Yu, S.-W., ... Koh, S.-B. (2008). Regional Grey Matter Changes in Patients With Migraine: A Voxel-Based Morphometry Study. *Cephalalgia*, *28*(6), 598-604. doi: 10.1111/j.1468-2982.2008.01550.x

Kim, S.-G., Jung, W. H., Kim, S. N., Jang, J. H., & Kwon, J. S. (2015). Alterations of Gray and White Matter Networks in Patients with Obsessive-Compulsive Disorder: A Multimodal Fusion Analysis of Structural MRI and DTI Using mCCA+jICA. *PLOS ONE*, *10*(6), e0127118.

doi: 10.1371/journal.pone.0127118

Klasson, N., Olsson, E., Eckerström, C., Malmgren, H., & Wallin, A. (2018). Estimated intracranial volume from freesurfer is biased by total brain volume. *European Radiology Experimental*, *2*, 24. doi: 10.1186/s41747-018-0055-4

Kochunov, P., Thompson, P. M., Lancaster, J. L., Bartzokis, G., Smith, S., Coyle, T., ... Fox, P. T. (2007). Relationship between white matter fractional anisotropy and other indices of cerebral health in normal aging: Tract-based spatial statistics study of aging. *NeuroImage*, *35*(2), 478-487. doi: 10.1016/j.neuroimage.2006.12.021

Lai, T.-H., Protsenko, E., Cheng, Y.-C., Loggia, M. L., Coppola, G., & Chen, W.-T. (2015). Neural Plasticity in Common Forms of Chronic Headaches. *Neural Plasticity*, *2015*, 205985. doi: 10.1155/2015/205985

Lakhan, S. E., Avramut, M., & Tepper, S. J. (2013). Structural and Functional Neuroimaging in Migraine: Insights From 3 Decades of Research. *Headache*, *53*(1), 46-66. doi: 10.1111/j.1526-4610.2012.02274.x

Lauterbur, P. C. (1973). Image Formation by Induced Local Interactions: Examples Employing Nuclear Magnetic Resonance. *Nature*, *242*(5394), 190-191. doi: 10.1038/242190a0

Le Bihan, D. (2014). Diffusion MRI: what water tells us about the brain. *EMBO molecular medicine*, *6*(5), 569-573. doi: 10.1002/emmm.201404055

Le Bihan, D., Poupon, C., Amadon, A., & Lethimonnier, F. (2006). Artifacts and pitfalls in diffusion MRI. *Journal of Magnetic Resonance Imaging*, *24*(3), 478-488. doi: 10.1002/jmri.20683

Lee, M. J., Park, B.-y., Cho, S., Kim, S. T., Park, H., & Chung, C.-S. (2019). Increased connectivity of pain matrix in chronic migraine: a resting-state functional MRI study. *The Journal of Headache and Pain*, *20*(1), 29. doi: 10.1186/s10194-019-0986-z

Li, K., Liu, L., Yin, Q., Dun, W., Xu, X., Liu, J., & Zhang, M. (2017). Abnormal rich club organization and impaired correlation between structural and functional connectivity in migraine sufferers. *Brain Imaging and Behavior*, *11*(2), 526-540. doi: 10.1007/s11682-016-9533-6

Li, X. L., Fang, Y. N., Gao, Q. C., Lin, E. J., Hu, S. H., Ren, L., ... Luo, B. N. (2011). A Diffusion Tensor Magnetic Resonance Imaging Study of Corpus Callosum From Adult Patients With Migraine Complicated With Depressive/Anxious Disorder. *Headache*, *51*(2), 237-245. doi: 10.1111/j.1526-4610.2010.01774.x

Linde, M., Gustavsson, A., Stovner, L. J., Steiner, T. J., Barré, J., Katsarava, Z., ... Andrée, C. (2012). The cost of headache disorders in Europe: the Eurolight project. *European Journal of Neurology*, *19*(5), 703-711. doi: 10.1111/j.1468-1331.2011.03612.x

Lipton, R. B., & Bigal, M. E. (2005). Migraine: Epidemiology, Impact, and Risk Factors for Progression. *Headache*, *45*(s1), S3-S13. doi: 10.1111/j.1526-4610.2005.4501001.x

Liu, H.-Y., Chou, K.-H., & Chen, W.-T. (2018). Migraine and the Hippocampus. *Current Pain and Headache Reports*, *22*(2), 13. doi: 10.1007/s11916-018-0668-6

Liu, J., Ma, S., Mu, J., Chen, T., Xu, Q., Dun, W., ... Zhang, M. (2017). Integration of white

matter network is associated with interindividual differences in psychologically mediated placebo response in migraine patients. *Human Brain Mapping*, *38*(10), 5250-5259. doi: 10.1002/hbm.23729

Liu, J., Zhao, L., Nan, J., Li, G., Xiong, S., von Deneen, K. M., ... Tian, J. (2013). The trade-off between wiring cost and network topology in white matter structural networks in health and migraine. *Experimental Neurology*, *248*, 196-204. doi: 10.1016/j.expneurol.2013.04.012

Llera, A., Wolfers, T., Mulders, P., & Beckmann, C. F. (2019). Inter-individual differences in human brain structure and morphology link to variation in demographics and behavior. *eLife*, *8*, e44443. doi: 10.7554/eLife.44443

Lubeiro, A., de Luis-García, R., Rodríguez, M., Álvarez, A., de la Red, H., & Molina, V. (2017). Biological and cognitive correlates of cortical curvature in schizophrenia. *Psychiatry Research: Neuroimaging*, *270*, 68-75. doi: 10.1016/j.pscychresns.2017.10.011

Magon, S., May, A., Stankewitz, A., Goadsby, P. J., Schankin, C., Ashina, M., ... Sprenger, T. (2019). Cortical abnormalities in episodic migraine: A multi-center 3T MRI study. *Cephalalgia*, *39*(5), 665-673. doi: 10.1177/0333102418795163

Maleki, N., Becerra, L., Brawn, J., Bigal, M., Burstein, R., & Borsook, D. (2012a). Concurrent functional and structural cortical alterations in migraine. *Cephalalgia : an international journal of headache*, *32*(8), 607-620. doi: 10.1177/0333102412445622

Maleki, N., Becerra, L., Brawn, J., Bigal, M., Burstein, R., & Borsook, D. (2012b). Concurrent functional and structural cortical alterations in migraine. *Cephalalgia*, *32*(8), 607-620. doi: 10.1177/0333102412445622

Manack, A. N., Buse, D. C., & Lipton, R. B. (2011). Chronic Migraine: Epidemiology and Disease Burden. *Current Pain and Headache Reports*, *15*(1), 70-78. doi: 10.1007/s11916-010-0157-z

Maniyar, F. H., Sprenger, T., Monteith, T., Schankin, C., & Goadsby, P. J. (2014). Brain activations in the premonitory phase of nitroglycerin-triggered migraine attacks. *Brain*, *137*(1), 232-241. doi: 10.1093/brain/awt320

Mansfield, P., & Grannell, P. K. (1973). NMR 'diffraction' in solids? *Journal of Physics C: Solid State Physics*, *6*(22), L422-L426. doi: 10.1088/0022-3719/6/22/007

Marciszewski, K. K., Meylakh, N., Di Pietro, F., Macefield, V. G., Macey, P. M., & Henderson, L. A. (2018). Altered brainstem anatomy in migraine. *Cephalalgia*, *38*(3), 476-486. doi: 10.1177/0333102417694884

Marciszewski, K. K., Meylakh, N., Di Pietro, F., Macefield, V. G., Macey, P. M., & Henderson, L. A. (2019). Fluctuating Regional Brainstem Diffusion Imaging Measures of Microstructure across the Migraine Cycle. *eneuro*, *6*(4), ENEURO.0005-19.2019. doi: 10.1523/ENEURO.0005-19.2019

May, A. (2007). Neuroimaging: visualising the brain in pain. *Neurological sciences*, *28 Suppl 2*, S101-7. doi: 10.1007/s10072-007-0760-x

May, A. (2009). New insights into headache: an update on functional and structural imaging findings. *Nature Reviews Neurology*, *5*(4), 199-209. doi: 10.1038/nrneurol.2009.28

May, A. (2017). Understanding migraine as a cycling brain syndrome: reviewing the evidence from functional imaging. *Neurological Sciences*, *38*(1), 125-130. doi: 10.1007/s10072-017-2866-0

McCarthy, C. S., Ramprashad, A., Thompson, C., Botti, J.-A., Coman, I. L., & Kates, W. R. (2015). A comparison of FreeSurfer-generated data with and without manual intervention. *Frontiers in Neuroscience*, *9*, 379. doi: 10.3389/fnins.2015.00379

Mechelli, A., Price, C. J., Friston, K. J., & Ashburner, J. (2005). Voxel-Based Morphometry of the Human Brain: Methods and Applications. *Current Medical Imaging*, *1*, 105. doi: 10.2174/1573405054038726

Messina, R., Filippi, M., & Goadsby, P. J. (2018). Recent advances in headache neuroimaging. *Current Opinion in Neurology*, *31*(4). doi: 10.1097/WCO.0000000000000573

Messina, R., Rocca, M. A., Colombo, B., Pagani, E., Falini, A., Comi, G., & Filippi, M. (2015). White matter microstructure abnormalities in pediatric migraine patients. *Cephalalgia*, *35*(14), 1278-1286. doi: 10.1177/0333102415578428

Messina, R., Rocca, M. A., Colombo, B., Pagani, E., Falini, A., Goadsby, P. J., & Filippi, M. (2018). Gray matter volume modifications in migraine. *Neurology*, *91*(3), e280. doi: 10.1212/WNL.0000000000005819

Messina, R., Rocca, M. A., Colombo, B., Teggi, R., Falini, A., Comi, G., & Filippi, M. (2017). Structural brain abnormalities in patients with vestibular migraine. *Journal of Neurology*, *264*(2), 295-303. doi: 10.1007/s00415-016-8349-z

Messina, R., Rocca, M. A., Colombo, B., Valsasina, P., Horsfield, M. A., Copetti, M., ... Filippi, M. (2013). Cortical Abnormalities in Patients with Migraine: A Surface-based Analysis. *Radiology*, *268*(1), 170-180. doi: 10.1148/radiol.13122004

Mori, S. (2007). *Introduction to Diffusion Tensor Imaging* (1st ed.). Elsevier Science.

Mori, S., Crain, B. J., Chacko, V. P., & Van Zijl, P. C. M. (1999). Three-dimensional tracking of axonal projections in the brain by magnetic resonance imaging. *Annals of Neurology*, *45*(2), 265-269. doi: 10.1002/1531-8249(199902)45:2<265::AID-ANA21>3.0.CO;2-3

Morollón Sánchez-Mateos, N. (2020). *Biomarcadores de migraña en resonancia magnética cerebral avanzada* (Doctoral dissertation). Universitat Autònoma de Barcelona.

Neeb, L., Bastian, K., Villringer, K., Gits, H. C., Israel, H., Reuter, U., & Fiebach, J. B. (2015). No microstructural white matter alterations in chronic and episodic migraineurs: a case-control diffusion tensor magnetic resonance imaging study. *Headache*, *55*(2), 241-251. doi: 10.1111/head.12496

Neeb, L., Bastian, K., Villringer, K., Israel, H., Reuter, U., & Fiebach, J. B. (2017). Structural Gray Matter Alterations in Chronic Migraine: Implications for a Progressive Disease? *Headache*, *57*(3), 400-416. doi: 10.1111/head.13012

Nichols, T. E., & Holmes, A. P. (2002). Nonparametric permutation tests for functional neuroimaging: A primer with examples. *Human Brain Mapping*, *15*(1), 1-25. doi: 10.1002/hbm.1058

Noseda, R., & Burstein, R. (2013). Migraine pathophysiology: anatomy of the trigeminovascular pathway and associated neurological symptoms, CSD, sensitization and modulation of pain.

*Pain*, *154 Suppl 1*, 10.1016/j.pain.2013.07.021. doi: 10.1016/j.pain.2013.07.021

O'Donnell, L. J., & Westin, C.-F. (2011). An introduction to diffusion tensor image analysis. *Neurosurgery clinics of North America*, *22*(2), 185-196. doi: 10.1016/j.nec.2010.12.004

Ogawa, S., Lee, T. M., Kay, A. R., & Tank, D. W. (1990). Brain magnetic resonance imaging with contrast dependent on blood oxygenation. *Proceedings of the National Academy of Sciences of the United States of America*, *87*(24), 9868-9872. doi: 10.1073/pnas.87.24.9868

Oishi, K., Zilles, K., Amunts, K., Faria, A., Jiang, H., Li, X., ... Mori, S. (2008). Human brain white matter atlas: Identification and assignment of common anatomical structures in superficial white matter. *NeuroImage*, *43*(3), 447-457. doi: 10.1016/j.neuroimage.2008.07.009

Özarslan, E., Koay, C. G., Shepherd, T. M., Komlosh, M. E., İrfanoğlu, M. O., Pierpaoli, C., & Basser, P. J. (2013). Mean apparent propagator (MAP) MRI: a novel diffusion imaging method for mapping tissue microstructure. *NeuroImage*, *78*, 16-32. doi: 10.1016/j.neuroimage.2013.04.016

Özarslan, E., Shepherd, T. M., Vemuri, B. C., Blackband, S. J., & Mareci, T. H. (2006). Resolution of complex tissue microarchitecture using the diffusion orientation transform (DOT). *NeuroImage*, *31*(3), 1086-1103. doi: 10.1016/j.neuroimage.2006.01.024

Petrušić, I., Daković, M., Kačar, K., Mićić, O., & Zidverc-Trajković, J. (2018). Migraine with aura and white matter tract changes. *Acta Neurologica Belgica*, *118*(3), 485-491. doi: 10.1007/s13760-018-0984-y

Pierpaoli, C., Barnett, A., Pajevic, S., Chen, R., Penix, L., Virta, A., & Basser, P. (2001). Water Diffusion Changes in Wallerian Degeneration and Their Dependence on White Matter Architecture. *NeuroImage*, *13*(6), 1174-1185. doi: 10.1006/nimg.2001.0765

Pietrobon, D., & Moskowitz, M. A. (2013). Pathophysiology of Migraine. *Annual Review of Physiology*, *75*(1), 365-391. doi: 10.1146/annurev-physiol-030212-183717

Planchuelo-Gómez, Á., Aja-Fernández, S., García-Azorín, D., Guerrero, Á. L., & de Luis-García, R. (2020). Fewer number of gradient directions in diffusion MRI can be counterbalanced with higher sample size: a migraine clinical study. In *Proceedings of the 28th annual meeting of the international society for magnetic resonance in medicine* (Vol. 4550).

Planchuelo-Gómez, Á., García-Azorín, D., Guerrero, Á. L., Aja-Fernández, S., Antón-Juarros, S., & de Luis-García, R. (2020). Response prediction for chronic migraine preventive treatment by gray matter morphometry in magnetic resonance imaging: a pilot study. *Revista de Neurologia*, *71*(11), 399-406. doi: 10.33588/rn.7111.2020488

Planchuelo-Gómez, Á., García-Azorín, D., Guerrero, Á. L., Aja-Fernández, S., Rodríguez, M., & de Luis-García, R. (2020a). Structural connectivity alterations in chronic and episodic migraine: A diffusion magnetic resonance imaging connectomics study. *Cephalalgia*, *40*(4), 367-383. doi: 10.1177/0333102419885392

Planchuelo-Gómez, Á., García-Azorín, D., Guerrero, Á. L., Aja-Fernández, S., Rodríguez, M., & de Luis-García, R. (2020b). White matter changes in chronic and episodic migraine: a

diffusion tensor imaging study. *The Journal of Headache and Pain*, *21*(1), 1. doi: 10.1186/s10194-019-1071-3

Planchuelo-Gómez, Á., García-Azorín, D., Guerrero, Á. L., Aja-Fernández, S., Rodríguez, M., & de Luis-García, R. (2021). Multimodal fusion analysis of structural connectivity and gray matter morphology in migraine. *Human Brain Mapping*, *42*(4), 908-921. doi: 10.1002/hbm.25267

Planchuelo-Gómez, Á., García-Azorín, D., Guerrero, Á. L., de Luis-García, R., Rodríguez, M., & Aja-Fernández, S. (2020). Alternative Microstructural Measures to Complement Diffusion Tensor Imaging in Migraine Studies with Standard MRI Acquisition. *Brain Sciences*, *10*(10). doi: 10.3390/brainsci10100711

Planchuelo-Gómez, Á., García-Azorín, D., Guerrero, Á. L., Rodríguez, M., Aja-Fernández, S., & de Luis-García, R. (2020). Gray Matter Structural Alterations in Chronic and Episodic Migraine: A Morphometric Magnetic Resonance Imaging Study. *Pain Medicine*, *21*(11), 2997-3011. doi: 10.1093/pm/pnaa271

Planchuelo-Gómez, Á., Lubeiro, A., Núñez-Novo, P., Gomez-Pilar, J., de Luis-García, R., del Valle, P., ... Molina, V. (2020). Identificacion of MRI-based psychosis subtypes: Replication and refinement. *Progress in Neuro-Psychopharmacology and Biological Psychiatry*, *100*, 109907. doi: 10.1016/j.pnpbp.2020.109907

Porter, A., Gladstone, J. P., & Dodick, D. W. (2005). Migraine and white matter hyperintensities. *Current Pain and Headache Reports*, *9*(4), 289. doi: 10.1007/s11916-005-0039-y

Purcell, E. M., Torrey, H. C., & Pound, R. V. (1946, Jan). Resonance Absorption by Nuclear Magnetic Moments in a Solid. *Phys. Rev.*, *69*, 37-38. doi: 10.1103/PhysRev.69.37

Qin, Z., He, X.-W., Zhang, J., Xu, S., Li, G.-F., Su, J., ... Du, X. (2019). Structural changes of cerebellum and brainstem in migraine without aura. *The Journal of Headache and Pain*, *20*(1), 93. doi: 10.1186/s10194-019-1045-5

Rabi, I. I., Zacharias, J. R., Millman, S., & Kusch, P. (1938, Feb). A New Method of Measuring Nuclear Magnetic Moment. *Phys. Rev.*, *53*, 318–318. doi: 10.1103/PhysRev.53.318

Ramos Delgado, P., Kuehne, A., Periquito, J. S., Millward, J. M., Pohlmann, A., Waiczies, S., & Niendorf, T. (2020). B1 inhomogeneity correction of RARE MRI with transceive surface radiofrequency probes. *Magnetic Resonance in Medicine*, *84*(5), 2684-2701. doi: 10.1002/mrm.28307

Reuter, M., Rosas, H. D., & Fischl, B. (2010). Highly accurate inverse consistent registration: A robust approach. *NeuroImage*, *53*(4), 1181-1196. doi: 10.1016/j.neuroimage.2010.07.020

Rocca, M. A., Ceccarelli, A., Falini, A., Colombo, B., Tortorella, P., Bernasconi, L., ... Filippi, M. (2006). Brain Gray Matter Changes in Migraine Patients with T2-Visible Lesions. *Stroke*, *37*(7), 1765-1770. doi: 10.1161/01.STR.0000226589.00599.4d

Rocca, M. A., Ceccarelli, A., Falini, A., Tortorella, P., Colombo, B., Pagani, E., ... Filippi, M. (2006). Diffusion tensor magnetic resonance imaging at 3.0 tesla shows subtle cerebral grey matter abnormalities in patients with migraine. *Journal of Neurology, Neurosurgery & Psychiatry*, *77*(5), 686. doi: 10.1136/jnnp.2005.080002

Rocca, M. A., Colombo, B., Inglese, M., Codella, M., Comi, G., & Filippi, M. (2003). A diffusion tensor magnetic resonance imaging study of brain tissue from patients with migraine. *Journal of Neurology, Neurosurgery & Psychiatry*, *74*(4), 501. doi: 10.1136/jnnp.74.4.501

Rocca, M. A., Pagani, E., Colombo, B., Tortorella, P., Falini, A., Comi, G., & Filippi, M. (2008). Selective Diffusion Changes of The Visual Pathways in Patients with Migraine: A 3-T Tractography Study. *Cephalalgia*, *28*(10), 1061-1068. doi: 10.1111/j.1468-2982.2008.01655.x

Rubinov, M., & Sporns, O. (2010). Complex network measures of brain connectivity: Uses and interpretations. *NeuroImage*, *52*(3), 1059-1069. doi: 10.1016/j.neuroimage.2009.10.003

Russo, A., Coppola, G., Pierelli, F., Parisi, V., Silvestro, M., Tessitore, A., & Tedeschi, G. (2018). Pain Perception and Migraine. *Frontiers in Neurology*, *9*, 576. doi: 10.3389/fneur.2018.00576

Schmidt-Wilcke, T., Gänßbauer, S., Neuner, T., Bogdahn, U., & May, A. (2008). Subtle Grey Matter Changes Between Migraine Patients and Healthy Controls. *Cephalalgia*, *28*(1), 1-4. doi: 10.1111/j.1468-2982.2007.01428.x

Schmitz, N., Admiraal-Behloul, F., Arkink, E. B., Kruit, M. C., Schoonman, G. G., Ferrari, M. D., & Van Buchem, M. A. (2008). Attack Frequency and Disease Duration as Indicators for Brain Damage in Migraine. *Headache*, *48*(7), 1044-1055. doi: 10.1111/j.1526-4610.2008.01133.x

Schmitz, N., Arkink, E. B., Mulder, M., Rubia, K., Admiraal-Behloul, F., Schoonmann, G. G., ... van Buchem, M. A. (2008). Frontal lobe structure and executive function in migraine patients. *Neuroscience Letters*, *440*(2), 92-96. doi: 10.1016/j.neulet.2008.05.033

Schulte, L. H., & May, A. (2016). The migraine generator revisited: continuous scanning of the migraine cycle over 30 days and three spontaneous attacks. *Brain*, *139*(7), 1987-1993. doi: 10.1093/brain/aww097

Schwedt, T. J., Chiang, C.-C., Chong, C. D., & Dodick, D. W. (2015). Functional MRI of migraine. *The Lancet Neurology*, *14*(1), 81-91. doi: 10.1016/S1474-4422(14)70193-0

Schwedt, T. J., Chong, C. D., Peplinski, J., Ross, K., & Berisha, V. (2017). Persistent post-traumatic headache vs. migraine: an MRI study demonstrating differences in brain structure. *The Journal of Headache and Pain*, *18*(1), 87. doi: 10.1186/s10194-017-0796-0

Schwedt, T. J., Chong, C. D., Wu, T., Gaw, N., Fu, Y., & Li, J. (2015). Accurate Classification of Chronic Migraine via Brain Magnetic Resonance Imaging. *Headache*, *55*(6), 762-777. doi: 10.1111/head.12584

Segonne, F., Dale, A. M., Busa, E., Glessner, M., Salat, D., Hahn, H. K., & Fischl, B. (2004). A hybrid approach to the skull stripping problem in MRI. *NeuroImage*, *22*(3), 1060 - 1075. doi: DOI:10.1016/j.neuroimage.2004.03.032

Segonne, F., Pacheco, J., & Fischl, B. (2007). Geometrically accurate topology-correction of cortical surfaces using nonseparating loops. *IEEE Trans Med Imaging*, *26*, 518-529. doi: 10.1109/TMI.2006.887364

Shibata, Y., Ishiyama, S., & Matsushita, A. (2018). White matter diffusion abnormalities in migraine and medication overuse headache: A 1.5-T tract-based spatial statistics study.

*Clinical Neurology and Neurosurgery*, *174*, 167-173. doi: 10.1016/j.clineuro.2018.09.022

Sinke, M. R. T., Otte, W. M., Christiaens, D., Schmitt, O., Leemans, A., van der Toorn, A., ... Dijkhuizen, R. M. (2018). Diffusion MRI-based cortical connectome reconstruction: dependency on tractography procedures and neuroanatomical characteristics. *Brain Structure and Function*, *223*(5), 2269-2285. doi: 10.1007/s00429-018-1628-y

Skorobogatykh, K., van Hoogstraten, W. S., Degan, D., Prischepa, A., Savitskaya, A., Ileen, B. M., ... of Advanced Studies (EHF-SAS), E. H. F. S. (2019). Functional connectivity studies in migraine: what have we learned? *The Journal of Headache and Pain*, *20*(1), 108. doi: 10.1186/s10194-019-1047-3

Sled, J., Zijdenbos, A., & Evans, A. (1998). A nonparametric method for automatic correction of intensity nonuniformity in MRI data. *IEEE Trans Med Imaging*, *17*, 87-97. doi: 10.1109/42.668698

Smith, R. E., Tournier, J.-D., Calamante, F., & Connelly, A. (2012). Anatomically-constrained tractography: Improved diffusion MRI streamlines tractography through effective use of anatomical information. *NeuroImage*, *62*(3), 1924-1938. doi: 10.1016/j.neuroimage.2012.06.005

Smith, R. E., Tournier, J.-D., Calamante, F., & Connelly, A. (2015). SIFT2: Enabling dense quantitative assessment of brain white matter connectivity using streamlines tractography. *NeuroImage*, *119*, 338-351. doi: 10.1016/j.neuroimage.2015.06.092

Smith, S. M., Jenkinson, M., Johansen-Berg, H., Rueckert, D., Nichols, T. E., Mackay, C. E., ... Behrens, T. E. (2006). Tract-based spatial statistics: Voxelwise analysis of multi-subject diffusion data. *NeuroImage*, *31*(4), 1487-1505. doi: 10.1016/j.neuroimage.2006.02.024

Smith, S. M., Jenkinson, M., Woolrich, M. W., Beckmann, C. F., Behrens, T. E., Johansen-Berg, H., ... Matthews, P. M. (2004). Advances in functional and structural MR image analysis and implementation as FSL. *NeuroImage*, *23*, S208-S219. doi: 10.1016/j.neuroimage.2004.07.051

Smith, S. M., & Nichols, T. E. (2009). Threshold-free cluster enhancement: Addressing problems of smoothing, threshold dependence and localisation in cluster inference. *NeuroImage*, *44*(1), 83-98. doi: 10.1016/j.neuroimage.2008.03.061

Stejskal, E. O., & Tanner, J. E. (1965). Spin Diffusion Measurements: Spin Echoes in the Presence of a Time-Dependent Field Gradient. *Journal of Chemical Physics*, *42*, 288-292. doi: 10.1063/1.1695690

Steven, A. J., Zhuo, J., & Melhem, E. R. (2014). Diffusion Kurtosis Imaging: An Emerging Technique for Evaluating the Microstructural Environment of the Brain. *American Journal of Roentgenology*, *202*(1), W26-W33. doi: 10.2214/AJR.13.11365

Sui, J., Pearlson, G., Caprihan, A., Adali, T., Kiehl, K. A., Liu, J., ... Calhoun, V. D. (2011). Discriminating schizophrenia and bipolar disorder by fusing fMRI and DTI in a multimodal CCA+ joint ICA model. *NeuroImage*, *57*(3), 839-855. doi: 10.1016/j.neuroimage.2011.05.055

Sun, S.-W., Liang, H.-F., Cross, A. H., & Song, S.-K. (2008). Evolving Wallerian degeneration after

transient retinal ischemia in mice characterized by diffusion tensor imaging. *NeuroImage*, *40*(1), 1-10. doi: 10.1016/j.neuroimage.2007.11.049

Surov, A., Meyer, H. J., & Wienke, A. (2017). Correlation between apparent diffusion coefficient (ADC) and cellularity is different in several tumors: a meta-analysis. *Oncotarget*, *8*, 59492-59499. doi: 10.18632/oncotarget.17752

Swartz, R. H., & Kern, R. Z. (2004). Migraine is Associated With Magnetic Resonance Imaging White Matter Abnormalities: A Meta-analysis. *Archives of Neurology*, *61*(9), 1366-1368. doi: 10.1001/archneur.61.9.1366

Szabó, N., Faragó, P., Király, A., Veréb, D., Csete, G., Tóth, E., ... Kincses, Z. T. (2018). Evidence for Plastic Processes in Migraine with Aura: A Diffusion Weighted MRI Study. *Frontiers in neuroanatomy*, *11*, 138-138. doi: 10.3389/fnana.2017.00138

Szabó, N., Kincses, Z. T., Párdutz, Á., Tajti, J., Szok, D., Tuka, B., ... Vécsei, L. (2012). White matter microstructural alterations in migraine: A diffusion-weighted MRI study. *PAIN*, *153*(3). doi: 10.1016/j.pain.2011.11.029

Tabesh, A., Jensen, J. H., Ardekani, B. A., & Helpern, J. A. (2011). Estimation of tensors and tensor-derived measures in diffusional kurtosis imaging. *Magnetic Resonance in Medicine*, *65*(3), 823-836. doi: 10.1002/mrm.22655

Tedeschi, G., Russo, A., Conte, F., Corbo, D., Caiazzo, G., Giordano, A., ... Tessitore, A. (2016). Increased interictal visual network connectivity in patients with migraine with aura. *Cephalalgia*, *36*(2), 139-147. doi: 10.1177/0333102415584360

Tessitore, A., Russo, A., Conte, F., Giordano, A., De Stefano, M., Lavorgna, L., ... Tedeschi, G. (2015). Abnormal Connectivity Within Executive Resting-State Network in Migraine With Aura. *Headache*, *55*(6), 794-805. doi: 10.1111/head.12587

Tian, Q., Yang, G., Leuze, C., Rokem, A., Edlow, B. L., & McNab, J. A. (2019). Generalized diffusion spectrum magnetic resonance imaging (GDSI) for model-free reconstruction of the ensemble average propagator. *NeuroImage*, *189*, 497-515. doi: 10.1016/j.neuroimage.2019.01.038

Torres-Ferrús, M., Quintana, M., Fernandez-Morales, J., Alvarez-Sabin, J., & Pozo-Rosich, P. (2017). When does chronic migraine strike? a clinical comparison of migraine according to the headache days suffered per month. *Cephalalgia*, *37*(2), 104-113. doi: 10.1177/0333102416636055

Tournier, J.-D., Calamante, F., & Connelly, A. (2007). Robust determination of the fibre orientation distribution in diffusion MRI: Non-negativity constrained super-resolved spherical deconvolution. *NeuroImage*, *35*(4), 1459-1472. doi: 10.1016/j.neuroimage.2007.02.016

Tournier, J.-D., Calamante, F., & Connelly, A. (2010). Improved probabilistic streamlines tractography by 2nd order integration over fibre orientation distributions. In *Proceedings of the 18th annual meeting of the international society for magnetic resonance in medicine* (Vol. 1670).

Tournier, J.-D., Calamante, F., & Connelly, A. (2013). Determination of the appropriate b value

and number of gradient directions for high-angular-resolution diffusion-weighted imaging. *NMR in Biomedicine*, *26*(12), 1775-1786. doi: 10.1002/nbm.3017

Tournier, J.-D., Calamante, F., Gadian, D. G., & Connelly, A. (2004). Direct estimation of the fiber orientation density function from diffusion-weighted MRI data using spherical deconvolution. *NeuroImage*, *23*(3), 1176-1185. doi: 10.1016/j.neuroimage.2004.07.037

Tournier, J.-D., Smith, R., Raffelt, D., Tabbara, R., Dhollander, T., Pietsch, M., ... Connelly, A. (2019). MRtrix3: A fast, flexible and open software framework for medical image processing and visualisation. *NeuroImage*, *202*, 116137. doi: 10.1016/j.neuroimage.2019.116137

Tristán-Vega, A., Westin, C.-F., & Aja-Fernández, S. (2009). Estimation of fiber Orientation Probability Density Functions in High Angular Resolution Diffusion Imaging. *NeuroImage*, *47*(2), 638-650. doi: 10.1016/j.neuroimage.2009.04.049

Tristán-Vega, A., Westin, C.-F., & Aja-Fernández, S. (2010). A new methodology for the estimation of fiber populations in the white matter of the brain with the Funk–Radon transform. *NeuroImage*, *49*(2), 1301-1315. doi: 10.1016/j.neuroimage.2009.09.070

Tuch, D. S. (2004). Q-ball imaging. *Magnetic Resonance in Medicine*, *52*(6), 1358-1372. doi: 10.1002/mrm.20279

Tuch, D. S., Reese, T. G., Wiegell, M. R., Makris, N., Belliveau, J. W., & Wedeen, V. J. (2002). High angular resolution diffusion imaging reveals intravoxel white matter fiber heterogeneity. *Magnetic Resonance in Medicine*, *48*(4), 577-582. doi: 10.1002/mrm.10268

Valfrè, W., Rainero, I., Bergui, M., & Pinessi, L. (2008). Voxel-Based Morphometry Reveals Gray Matter Abnormalities in Migraine. *Headache*, *48*(1), 109-117. doi: 10.1111/j.1526-4610.2007.00723.x

Veraart, J., Fieremans, E., Jelescu, I. O., Knoll, F., & Novikov, D. S. (2016). Gibbs ringing in diffusion MRI. *Magnetic resonance in medicine*, *76*(1), 301-314. doi: 10.1002/mrm.25866

Veraart, J., Fieremans, E., & Novikov, D. S. (2016). Diffusion MRI noise mapping using random matrix theory. *Magnetic Resonance in Medicine*, *76*(5), 1582-1593. doi: 10.1002/mrm.26059

Veraart, J., Novikov, D. S., Christiaens, D., Ades-aron, B., Sijbers, J., & Fieremans, E. (2016). Denoising of diffusion MRI using random matrix theory. *NeuroImage*, *142*, 394-406. doi: 10.1016/j.neuroimage.2016.08.016

Weatherall, M. W. (2015). The diagnosis and treatment of chronic migraine. *Therapeutic advances in chronic disease*, *6*(3), 115-123. doi: 10.1177/2040622315579627

Wedeen, V. J., Hagmann, P., Tseng, W.-Y. I., Reese, T. G., & Weisskoff, R. M. (2005). Mapping complex tissue architecture with diffusion spectrum magnetic resonance imaging. *Magnetic Resonance in Medicine*, *54*(6), 1377-1386. doi: 10.1002/mrm.20642

Weiller, C., May, A., Limmroth, V., Jüptner, M., Kaube, H., Schayck, R. V., ... Dlener, H. C. (1995). Brain stem activation in spontaneous human migraine attacks. *Nature Medicine*, *1*(7), 658-660. doi: 10.1038/nm0795-658

Winklewski, P. J., Sabisz, A., Naumczyk, P., Jodzio, K., Szurowska, E., & Szarmach, A. (2018). Understanding the Physiopathology Behind Axial and Radial Diffusivity Changes-What Do

We Know? *Frontiers in neurology*, *9*, 92-92. doi: 10.3389/fneur.2018.00092

Wunderlich, A. P., Klug, R., Stuber, G., Landwehrmeyer, B., Weber, F., & Freund, W. (2011). Caudate nucleus and insular activation during a pain suppression paradigm comparing thermal and electrical stimulation. *The open neuroimaging journal*, *5*, 1-8. doi: 10.2174/1874440001105010001

Xiaoyun, S., Jing, W., Bin, C., Qing, Z., Huiting, Z., Xiaoyong, Z., & Chuansheng, Z. (2020, 2020). Detection of microstructural abnormalities of gray matter in migraineurs without aura using Mean Apparent Propagator (MAP) MRI model. In *Proceedings of the 28th annual meeting of the international society for magnetic resonance in medicine* (Vol. 1823).

Xie, H., Zhang, Q., Huo, K., Liu, R., Jian, Z.-J., Bian, Y.-T., ... Luo, G.-G. (2018). Association of white matter hyperintensities with migraine features and prognosis. *BMC neurology*, *18*(1), 93-93. doi: 10.1186/s12883-018-1096-2

Yalcin, A., Ceylan, M., Bayraktutan, O. F., & Akkurt, A. (2018). Episodic Migraine and White Matter Hyperintensities: Association of Pain Lateralization. *Pain Medicine*, *19*(10), 2051-2057. doi: 10.1093/pm/pnx312

Yeh, C.-H., Jones, D. K., Liang, X., Descoteaux, M., & Connelly, A. (2020). Mapping Structural Connectivity Using Diffusion MRI: Challenges and Opportunities. *Journal of Magnetic Resonance Imaging*. doi: 10.1002/jmri.27188

Younis, S., Hougaard, A., Vestergaard, M. B., Larsson, H. B., & Ashina, M. (2017). Migraine and magnetic resonance spectroscopy: a systematic review. *Current Opinion in Neurology*, *30*(3).

Yu, D., Yuan, K., Qin, W., Zhao, L., Dong, M., Liu, P., ... Tian, J. (2013). Axonal loss of white matter in migraine without aura: A tract-based spatial statistics study. *Cephalalgia*, *33*(1), 34-42. doi: 10.1177/0333102412466964

Yu, D., Yuan, K., Zhao, L., Dong, M., Liu, P., Yang, X., ... Tian, J. (2013). White matter integrity affected by depressive symptoms in migraine without aura: a tract-based spatial statistics study. *NMR in Biomedicine*, *26*(9), 1103-1112. doi: 10.1002/nbm.2924

Yuan, K., Qin, W., Liu, P., Zhao, L., Yu, D., Zhao, L., ... Tian, J. (2012). Reduced Fractional Anisotropy of Corpus Callosum Modulates Inter-Hemispheric Resting State Functional Connectivity in Migraine Patients without Aura. *PLOS ONE*, *7*(9), e45476. doi: 10.1371/journal.pone.0045476

Yuan, K., Zhao, L., Cheng, P., Yu, D., Zhao, L., Dong, T., ... Tian, J. (2013). Altered Structure and Resting-State Functional Connectivity of the Basal Ganglia in Migraine Patients Without Aura. *The Journal of Pain*, *14*(8), 836-844. doi: 10.1016/j.jpain.2013.02.010

Zhang, J., Gregory, S., Scahill, R. I., Durr, A., Thomas, D. L., Lehericy, S., ... investigators, t. T.-H. (2018). In vivo characterization of white matter pathology in premanifest Huntington's disease. *Annals of Neurology*, *84*(4), 497-504. doi: 10.1002/ana.25309

Zhang, J., Wu, Y.-L., Su, J., Yao, Q., Wang, M., Li, G.-F., ... Du, X. (2017). Assessment of gray and white matter structural alterations in migraineurs without aura. *The journal of*

*headache and pain*, *18*(1), 74-74. doi: 10.1186/s10194-017-0783-5

Zhang, Y., Brady, M., & Smith, S. (2001). Segmentation of brain MR images through a hidden Markov random field model and the expectation-maximization algorithm. *IEEE Transactions on Medical Imaging*, *20*(1), 45-57. doi: 10.1109/42.906424

Ziegeler, C., Mehnert, J., Asmussen, K., & May, A. (2020). Central effects of erenumab in migraine patients. *Neurology*, *95*(20), e2794. doi: 10.1212/WNL.0000000000010740

Zigmond, A. S., & Snaith, R. P. (1983). The Hospital Anxiety and Depression Scale. *Acta Psychiatrica Scandinavica*, *67*(6), 361-370. doi: 10.1111/j.1600-0447.1983.tb09716.x

# Part II

# Compendium of publications

# *Thematic consistency between the publications*

As mentioned in the Introduction of Part I, this thesis presents contributions in the technical and the clinical fields using MRI data from patients with migraine. Conventional qualitative radiological exploration of MRI data from these patients cannot detect the specific features of the migrainous brain. Regarding pathological findings in the radiological examinations, only white matter hyperintensities have been described in migraine, but these are not specific to migraine and their relationship with pathological mechanisms is unclear. Thus, the lack of radiological abnormalities requires advanced MRI processing to characterize the migraine brain in-vivo. The characterization of the structural properties of the brain, the main objective of this doctoral thesis, is described in detail in the publications that compose the compendium. In this thesis, diverse processing methods have been applied to T1-weighted and dMRI data to study the gray and white matter, also considering the connections between gray matter regions through the white matter tracts.

With respect to one of the main MRI modalities not treated in this thesis, fMRI, previous studies with migraine patients have generally shown that a group of regions is activated in relation to pain and headache (May, 2009). These regions compose the called pain matrix. The pain matrix involves subcortical regions, mainly the thalamus and the amygdala, and cortical regions from every lobe such as the insula, the prefrontal cortex, the cingulate cortex, the primary sensory cortex and the posterior parietal cortex (May, 2009).

Currently, there are two main migraine types based on clinical characteristics: Episodic Migraine (EM) and Chronic Migraine (CM). According to the Third edition of the International Classification of Headache Disorders (ICHD-3), CM and EM are differentiated only by the number of days with headache per month. Patients with CM suffer from a headache 15 or more days per month, showing eight or more of these days headache with migraine characteristics, during at least three months (Headache Classification Committee of the International Headache Society, 2018). In contrast, patients with EM suffer from a headache less than 15 days per month. However, there is no biomarker to distinguish either migraine or CM. Therefore, the main objective of this thesis is the extraction of MRI biomarkers of migraine compared to HC, and of CM with respect to EM, using diverse MRI modalities.

From the main objective, some questions arise:

1. Are there brain structural differences between patients with migraine and Healthy Controls (HC)?

2. Are there brain structural differences between patients with CM and EM?

3. If there are differences between CM and EM, does this imply that they are different entities, or just diverse grades of the same pathology?

Regarding the first question, loss of gray matter volume has been reported in a meta-analysis in patients with migraine compared to HC (Jia & Yu, 2017) and lower FA values in white matter regions have been found in migraine (Gomez-Beldarrain et al., 2015; Shibata et al., 2018; Szabó et al., 2012; Yu, Yuan, Zhao, et al., 2013), although the opposite result has also been identified (Messina et al., 2015).

With respect to the second question, no white matter differences have been identified previously between CM and EM (Neeb et al., 2015). The same lack of statistically significant results was found for gray matter assessment following the originally planned statistical analysis (Neeb et al., 2017; Valfrè et al., 2008). In these previous studies, low sample sizes were employed, with around 20 subjects per group.

Therefore, the first step is the acquisition of a database including the proper MRI data for the analysis of gray matter and white matter. The MRI modalities used for that purpose are T1- and diffusion-weighted imaging, both acquired during the same session. The subjects who compose the dataset should be patients with CM and EM, and HC, all of them balanced for age and sex.

Bearing in mind the implication of multiple regions in pain processing, an analysis of the diverse gray matter subcortical and cortical regions and the white matter tracts connecting the gray matters areas should be carried out in order to understand the migraine pathophysiology.

To date, the main finding in migraine morphometric studies is the loss of gray matter volume in pain-transmitting areas (Jia & Yu, 2017; May, 2009). Another frequently assessed morphometric parameter is the cortical thickness, but the results associated with this parameter are conflicting, showing opposite trends in diverse studies. Additional morphometric parameters include surface area, which has been barely assessed in migraine studies, and cortical curvature, not analyzed previously. The analysis of the four morphometric parameters can provide a rather complete perspective of the migraine pathophysiology, especially considering the difference between the changes of the surface area, largely determined prenatally, and the cortical thickness, with major variations driven postnatally (Frye et al., 2010; Kapellou et al., 2006).

Regarding the analysis of the morphometric parameters (Planchuelo-Gómez, García-Azorín, Guerrero, Rodríguez, et al., 2020), two main results were obtained:

- Lower values of gray matter volume, cortical thickness and surface area in both groups of migraine compared to HC were identified, and increased curvature in the migraine groups with respect to HC was found.

- In the comparison between patients with CM and EM, lower values of gray matter volume and especially surface area in multiple regions were obtained in CM, while cortical thickness values were higher in CM.

Following an analysis of the relationship between genetics and MRI morphometric parameters, the surface area and the cortical thickness present opposite genetic influence leading to different effects of both parameters (Grasby et al., 2020). Therefore, the main findings of this analysis are the extraction of a potential gray matter CM biomarker, lower widespread surface area values, and the identification of CM as a different entity with respect to a more intense or more frequent EM.

From the previous analysis, it seems that there are structural differences between both types of migraine. But do these significant differences persist in the analysis of white matter?

The results from previous migraine white matter studies using DTI parameters are conflicting. The DTI parameters assessed in previous studies are the FA, the AD, the RD and the MD, being TBSS the most commonly employed analysis method.

Our TBSS analysis showed widespread lower AD values in CM compared to EM, while these values were higher in EM with respect to HC (Planchuelo-Gómez, García-Azorín, Guerrero, Aja-Fernández, Rodríguez, & de Luis-García, 2020b). FA and RD presented a positive and negative correlation, respectively, with the time from onset of CM (Planchuelo-Gómez, García-Azorín, Guerrero, Aja-Fernández, Rodríguez, & de Luis-García, 2020b).

The main findings of the white matter assessment are the extraction of a possible white matter CM biomarker, lower widespread AD, and the different temporal evolution of DTI parameters from HC to EM and throughout CM. These findings likely reflect different pathophysiological mechanisms in the course of EM and CM. This result is in line with the gray matter results, suggesting that the clinical course of CM is substantially different from EM.

In our TBSS analysis, the most reported result in the literature, i.e., lower FA values in patients with EM with respect to HC, was not found. Furthermore, differences between both types of migraine had not been found previously, possibly due to the fact that these differences are very subtle. Then, two questions arise:

- Do white matter differences between patients with migraine and HC actually exist?
- Why are these white matter differences so difficult to find in migraine, especially between CM and EM?

To answer the first question, an approach focused on the calculation of additional diffusion measures using a new approach called Apparent Measures Using Reduced Acquisitions (AMURA) (Aja-Fernández et al., 2020) was carried out. In this approach, the following scalar measures based on the Ensemble Average diffusion Propagator (EAP) were obtained: Return-to-axis Probability (RTAP), Return-to-origin Probability (RTOP) and Return-to-plane Probability (RTPP). The answer to the second question was examined with the evaluation of the effects of the variation of diffusion-specific acquisition parameters on the TBSS statistical comparisons of DTI parameters taking into account the diversity of MRI acquisition protocols between studies.

The additional EAP-based measures obtained from AMURA showed white matter structural differences between patients with EM and HC, with lower RTOP values in patients with EM (Planchuelo-Gómez, García-Azorín, Guerrero, de Luis-García, et al., 2020), a result in line with the previous literature. Higher RTPP values were also found in patients with CM compared to EM, in line with the AD results.

The new RTOP results identified with AMURA but not with DTI measures present a new approach to complement the classical diffusion descriptors using a dMRI acquisition protocol employed in the clinical routine, despite the suboptimal conditions to exploit AMURA. Additional diffusion measures would be necessary to further analyze the white matter microstructure.

With respect to the evaluation of the diffusion acquisition parameters, a lower number of regions with statistically significant differences with respect to the original TBSS analysis was obtained when reducing the number of diffusion orientations for a fixed sample size (Planchuelo-Gómez, Aja-Fernández, et al., 2020). For a fixed number of diffusion orientations, the number of regions with statistically significant differences between the assessed groups was lower when reducing the sample size, as could be expected (Planchuelo-Gómez, Aja-Fernández, et al., 2020). For a fixed sample size, a lower number of regions with significant differences was obtained when employing a lower number of gradient orientations (Planchuelo-Gómez, Aja-Fernández, et al., 2020). The regions extracted with lower number of orientations were a subset with respect to the original scheme with the highest number of directions.

These results showed that an acquisition scheme with a low number of diffusion directions and the comparisons using a low number of subjects could explain the lack of significant differences between these groups of interest in the literature, particularly between CM and EM. These results highlight the importance of using a high number of diffusion orientations and a relative large sample size to assess diffusion measures in migraine.

Regarding the differences identified in the gray and white matter analysis, a question emerges: How are the white matter connections between specific affected gray matter regions?

The independent analysis of the gray matter morphometric parameters and the white matter tracts provided insufficient information about the state of the connections between specific pain processing regions, with no previous results in migraine studies. A connectomics approach was employed to allow the assessment of specific changes in the white matter that connects specific gray matter regions. To analyze the structural connectivity between the gray matter regions, tractography was performed. The number of streamlines and the DTI parameters were employed as metrics. The gray matter regions included in the structural connectivity matrix were the same regions where the morphometric parameters were assessed.

The connectomics analysis showed both higher and lower number of streamlines and diffusion descriptor values in different connections in patients with migraine with respect to HC (Planchuelo-Gómez, García-Azorín, Guerrero, Aja-Fernández, Rodríguez, & de Luis-García, 2020a). Most connections with higher number of streamlines included pain processing regions.

These results suggest two different pathophysiological mechanisms in migraine related to structural connectivity. These mechanisms are the possible coexistence of strengthening associated with pain processing and weakening of other connections.

The connectomics analysis exhibited two opposite trends in structural connections. This result drives to the following question: How do the alterations of gray and white matter intertwine?

To evaluate the relationship between the gray matter changes and the diverse structural connectivity results in migraine, a fusion method analysis was carried out in order to integrate simultaneously the information from both sources. The fusion method was Multimodal Canonical Correlation Analysis (mCCA) combined with Joint Independent Component Analysis (jICA). The fusion method allows to characterize the specific variations of one modality linked to the variations of another modality.

The mCCA-jICA fusion method revealed a relationship between cortical curvature and the streamline count, with higher curvature values related to a higher streamline count in patients with EM compared to HC (Planchuelo-Gómez et al., 2021). A higher number of streamlines was found in both groups of migraine patients with respect to HC in connections between subcortical regions and pain processing regions, while a lower number was found in connections within each lobe. Specific connections with the hippocampus were altered in CM compared to EM, together with the network composed of the caudate nucleus and the orbitofrontal cortex. These results indicate that migraine can be explained, at least partially, as a *network disease*, with groups of regions simultaneously altered following different pathophysiological mechanisms.

The results from this thesis suggest that groups of regions in migraine would be affected in different ways with respect to HC. On the one hand, migraine could be defined as a *network disease*, i.e., groups of regions would be connected and involved in the diverse pathophysiological mechanisms related to the maldapaptation of white matter. The mechanisms would be hypothetical strengthening of the structural connectivity in pain processing areas and the possible weakening of other connections. On the other hand, CM would be a different entity with respect to EM with a higher number of attacks, presenting a distinct temporal course and particularly altered structural networks in comparison with EM.

A scheme of the relationship between the contributions of this doctoral thesis is shown in Figure 1.

In the following chapters of this part of the doctoral thesis, the published papers that are part of the compendium are included. Before each article, the corresponding context is described and a summary of its relevance is shown. The figures from the papers that were already included in part I are referenced with the name used in part I, while the remaining figures are referenced and displayed following the order of the original article.

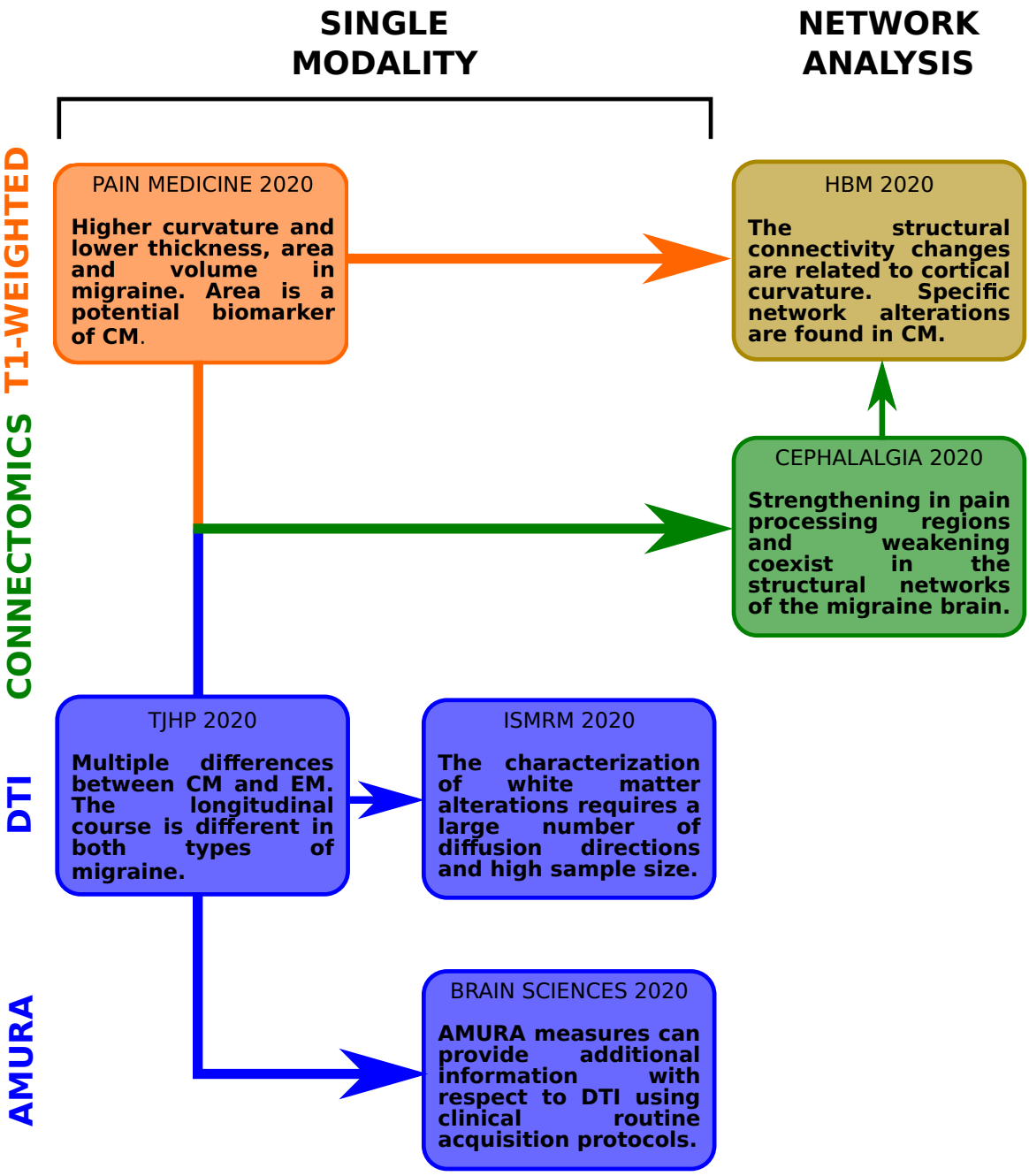


**Figure 1:** Relationship between the publications included in the compendium. HBM = human brain mapping; ISMRM = Proceedings of the 28th Annual Meeting of the International Society for Magnetic Resonance in Medicine; TJHP = The Journal of Headache and Pain.

*Chapter 1*

# *Contribution 1: Gray Matter Structural Alterations in Chronic and Episodic Migraine: A Morphometric Magnetic Resonance Imaging Study*

**Published as**:

*Planchuelo-Gómez, Á.[1], García-Azorín, D.[2], Guerrero, Á.L.[2,3], Rodríguez, M.[4], Aja-Fernández, S.[1] and de Luis-García, R[1] (2020). Gray Matter Structural Alterations in Chronic and Episodic Migraine: A Morphometric Magnetic Resonance Imaging Study. Pain Medicine, 21(11):2997-3011. doi: 10.1093/pm/pnaa271.*

1. Laboratorio de Procesado de Imagen (LPI), Universidad de Valladolid, Valladolid, Spain
2. Headache Unit, Department of Neurology, Hospital Clínico Universitario de Valladolid, Valladolid, Spain
3. Institute for Biomedical Research of Salamanca (IBSAL), Salamanca, Spain
4. Department of Radiology, Hospital Clínico Universitario de Valladolid, Valladolid, Spain

The purpose of this study was the assessment of diverse morphometry parameters to characterize whole-brain gray matter properties in patients with CM and EM. In this research, a whole-brain comparison of the cortical curvature between migraine patients and controls, and the surface area between patients with CM and EM were carried out for the first time in a migraine context. The most frequent statistically significant differences were lower gray matter volume values in migraine patients compared to controls (except subcortical regions) and lower surface area values in CM compared to EM patients.

## Abstract

**Objective**. This study evaluates different parameters describing the gray matter structure to analyze differences between healthy controls, patients with episodic migraine, and patients with chronic migraine.

**Design**. Cohort study.

**Setting**. Spanish community.

**Subjects**. Fifty-two healthy controls, 57 episodic migraine patients, and 57 chronic migraine patients were included in the study and underwent T1-weighted magnetic resonance imaging acquisition.

**Methods**. Eighty-four cortical and subcortical gray matter regions were extracted, and gray matter volume, cortical curvature, thickness, and surface area values were computed (where applicable). Correlation analysis between clinical features and structural parameters was performed.

**Results**. Statistically significant differences were found between all three groups, generally consisting of increases in cortical curvature and decreases in gray matter volume, cortical thickness, and surface area in migraineurs with respect to healthy controls. Furthermore, differences were also found between chronic and episodic migraine. Significant correlations were found between duration of migraine history and several structural parameters.

**Conclusions**. Migraine is associated with structural alterations in widespread gray matter regions of the brain. Moreover, the results suggest that the pattern of differences between healthy controls and episodic migraine patients is qualitatively different from that occurring between episodic and chronic migraine patients.


**Key Words**: Chronic Migraine; Migraine; Magnetic Resonance Imaging; Cortical Curvature; Cortical Thickness; Gray Matter Volume; Surface Area

# 1.1. Introduction

Patients with chronic migraine (CMs) suffer from headache during 15 or more days per month for more than three months, with at least eight of these days of headache with migrainous characteristics, according to the third edition of the International Classification of Headache Disorders (ICHD-3) [1]. In contrast, patients with episodic migraine (EMs) suffer <15 headache days per month. Between 2% and 3% of migraine patients evolve annually from EM to CM [2]. Although some risk factors have been associated with progression from EM to CM, the pathophysiological mechanisms of this conversion remain to be elucidated. Furthermore, it is not clear whether EM and CM could represent two ranges of the same entity or, alternatively, if they are two subgroups with distinctive characteristics.

Neuroimaging, particularly magnetic resonance imaging (MRI), has revealed itself as a powerful tool for the study of migraine. Using conventional MRI, some early studies reported an increased risk of subclinical brain damage in migraine patients compared with healthy controls (HCs), including white matter hyperintensities [3, 4]. Later, more focus was devoted to the analysis of possible structural alterations in migraine patients. A recent meta-analysis found a gray matter volume decrease in migraine patients with respect to healthy controls in several regions [5]. Most of the studies included in the meta-analysis employed voxel-based morphometry (VBM) as the analysis tool. This technique automatically performs voxel-wise comparisons of the local concentration of gray matter [6].

Some studies have tried to determine whether structural differences in gray matter between EM and CM patients exist using T1-weighted magnetic resonance (MR) scans. Using VBM, one of these studies

found a gray matter volume reduction in chronic vs episodic migraine patients in some regions [7]. Also employing VBM, another study reported increased and decreased gray matter volume in different regions in CM compared with EM patients [8]. Moreover, features based not only on gray matter volume, but also on cortical thickness and surface area were employed by Schwedt et al. to develop classifiers between CMs, EMs, and HCs using principal component analysis (PCA) [9]. Higher cortical thickness in high-frequency (eight to 14 attacks per month) vs low-frequency (less than two attacks per month) migraine patients was found by Maleki et al. in the inferior temporal gyrus of the right hemisphere and in the postcentral gyrus of the left hemisphere [10].

The present study compares the structural properties of the gray matter in patients with EM, CM, and healthy controls. The aims are to:

1. Replicate previous findings about differences in the gray matter between EMs and CMs [7, 8] using a different analysis method that provides more information about the structure of the gray matter regions and employing a larger data set;
2. Investigate structural brain differences between both subtypes of migraine patients and healthy controls;
3. Examine how gray matter structural features relate to demographics and clinical characteristics of patients.

# 1.2. Methods

## *1.2.1.* ***Participants***

We conducted an observational analytic study with a cohort design. The target population included patients with migraine. Patients were recruited from the outpatient headache unit at the Hospital Clínico Universitario de Valladolid (Spain), a tertiary center that receives patients both from specialized care and directly from primary care. Inclusion criteria were a) diagnosis of migraine according to the ICHD-3 beta and ICHD-3 criteria [1, 11]; b) stable clinical situation in the previous six months; c) agreeing to participate and signing the informed consent. We excluded patients with a) high-frequency episodic migraine, suffering between 10 and 14 headache days per month; b) other painful conditions; c) known major psychiatric diseases (described as anamnesis or presence of depression or anxiety according to the Hospital Anxiety and Depression Scale [12]); d) other neurological diseases; e) drug or substance abuse; f) pregnancy. Patients received no preventive therapy at inclusion. Participants were asked to keep a headache diary and were classified as having episodic migraine when they had <10 headache days per month or chronic migraine (CM) according to ICHD-3 criteria. No healthy controls were included if they showed a present or past history of migraine, or if any other neurological or psychiatric condition was present. We used a nonprobabilistic sampling method by convenience sampling. Age- and sex-matched healthy controls were recruited through hospital and university colleagues and advertisements in these facilities by convenience sampling and snowball sampling.

In all patients, we collected sociodemographic and clinical data, including the duration of migraine disease (years), headache and migraine frequency (days per month), and time from onset of chronic migraine (months) when applicable.

The local Ethics Committee of Hospital Clínico Universitario de Valladolid approved the study (PI: 14–197). All participants read and signed a written consent form before their participation.

### 1.2.2. MRI Acquisition

Image acquisitions were performed for migraine patients during interictal periods (defined as at least 24 hours from last migraine attack). High-resolution 3D T1-weighted MRI data were acquired using a Philips Achieva 3T MRI unit (Philips Healthcare, Best, the Netherlands) with a 32-channel head coil in the MRI facility at the Laboratorio de Técnicas Instrumentales from the Universidad de Valladolid (Spain) between May 2014 and July 2018.

For the anatomical T1-weighted images, the following acquisition parameters were employed: Turbo Field Echo (TFE) sequence, repetition time (TR) = 8.1 ms, echo time (TE) = 3.7 ms, flip angle = 8°, 256 x 256 matrix size, 1 x 1 x 1 $mm^3$ of spatial resolution, and 160 slices covering the whole brain.

### 1.2.3. Image Processing

MRI images were processed to obtain cortical curvature, cortical thickness, gray matter volume, and surface area of the different gray matter regions.

From the T1 images, automatic cortical parcellation was performed using FreeSurfer. FreeSurfer parcellation includes skull stripping, automated Talairach transformation, segmentation of subcortical gray and white matter, intensity normalization, gray-white matter boundary tessellation, and surface deformation [13–16]. The automated parcellations were manually inspected to check the quality. Afterwards, mean curvature, average thickness, gray matter volume, and surface area of all subjects were extracted from FreeSurfer and exported to MATLAB (2017b, MathWorks) for further analysis. Gray matter volume was obtained for all the 84 gray matter regions from the Desikan-Killiany atlas [17]. Also, cortical curvature, cortical thickness, and area were calculated for the 68 regions from the atlas that are cortical regions. Considering the four morphometric parameters, a total of 288 comparisons were analyzed, which correspond to 84 comparisons for the gray matter volume of cortical and subcortical regions, and 68 for each of the other three parameters: curvature, area, and thickness of cortical regions.

### 1.2.4. Statistical Analysis

We estimated sample size according Schwedt et al. [18]. We calculated in a worst possible scenario model with an estimated effect size of difference between groups of 0.04 and a variance of 0.01, a type 1 error rate of 1% and 80% power, anticipating a loss of 10% of patients; the expected sample size was 139 participants. We include a sensitivity analysis in the Supplementary Data.

The Kolmogorov-Smirnov test and Levene's test for equality of variances were used to assess normality and homogeneity of variance in age and duration of migraine in years. To test for significant differences in the ages of the three groups, a one-way analysis of variance (ANOVA) was used if the null hypothesis in the Kolmogorov-Smirnov and Levene tests was not rejected; otherwise, the Kruskal-Wallis test was employed. To test for sex-related significant differences, a chi-square test was used. To compare clinical features between migraine patients (i.e., duration of migraine history in years for both groups of patients and duration of chronic migraine in months for chronic migraine patients), a two-tailed unpaired t test

was used if the null hypothesis in the Kolmogorov-Smirnov and Levene tests was not rejected; otherwise, the Mann-Whitney U test was employed.

Cortical curvature and cortical thickness data were tested for normal distribution with the Kolmogorov-Smirnov test, and homogeneity of variance was tested by the Levene test. If data met these assumptions, one-way ANOVA was performed, and if not, the Kruskal-Wallis test was performed. To control for differences in overall brain size, an analysis of covariance (ANCOVA) was performed on gray matter volume and surface area, with total intracranial volume and total surface area, respectively, as covariates. To correct for multiple comparisons, the Benjamini-Hochberg false discovery rate (FDR) procedure was used [19]. To assess differences between the two groups, the Tukey-Kramer post hoc test was applied.

After correction for multiple comparisons using FDR, the critical P value for the results was 0.0154; that is, only the tests with P values equal or lower than this critical P value survived the correction and were therefore considered to be statistically significant. In comparison to the Bonferroni correction, the cutoff P value is relatively large because the Benjamini-Hochberg method adjusts this cutoff using not only the total number of comparisons, but also the number of significant comparisons with relatively small or very small P values. In our case, there were many very small P values ($P<0.001$) and a large amount of comparisons with small P values ($P<0.01$), which justify the final cutoff.

Spearman correlation analysis was employed to perform correlation analysis for clinical features from the migraine patients and the structural parameters (i.e., cortical curvature, cortical thickness, gray matter volume, and surface area). To correct for multiple comparisons, the Benjamini-Hochberg procedure was also applied.

In all comparisons, the level of statistical significance was set at $P<0.05$.

# 1.3. Results

During the study period, 52 healthy controls, 57 episodic migraine patients, and 57 chronic migraine patients were recruited for the study after matching the inclusion and exclusion criteria. Five patients with episodic migraine and 11 with chronic migraine were screened but excluded due to the presence of anxiety or depression according to the Hospital Anxiety and Depression Scale (HADS). Demographic and clinical data for the three groups are summarized in Table 1. Significant differences were found in duration of migraine history in years between the two migraine groups. Significant differences were also found in headache and migraine frequency between the migraine groups, as expected. No poor-quality automated parcellations were detected.

After correction for multiple comparisons, ANOVA/ Kruskal-Wallis/ANCOVA results revealed significant differences between groups in cortical curvature, cortical thickness, gray matter volume, and surface area. Eightyfour cortical comparisons and five subcortical comparisons, considering all structural parameters, had significant differences. In this section, we report only 26 results with $P<0.001$ (ANOVA, Kruskal-Wallis, or ANCOVA). The 63 remaining significant differences ($0.001<P<0.0154$) are reported in the Supplementary Data.

Taking into account the large number of significant results in this study, we also computed the effect size of significant results with Cohen's d in order to identify the results with the largest effect size that were least likely to be due to chance. For every comparison, the mean value of the most pathological group was subtracted from the mean value of the least pathological group.

Considering the significant differences in duration of migraine history between episodic and chronic migraine patients (Table 1), ANCOVA analysis was repeated for all the structural parameters including the duration of migraine history as a covariate. ANCOVA results showed that the regions with significant P values were the same regions obtained in the original analysis, except the left supramarginal gyrus, which was nonsignificant when considering the duration of migraine history as a covariate. The critical P value in this analysis was 0.0149. The P values from the ANCOVA with the duration of migraine history as a covariate were almost equal to the P values from the original analysis, with the difference in P values between both analyses close to 0.001 or 0.002 in regions where significant differences were reported in the original analysis. In the case of pairwise post hoc comparisons between EM and CM patients, every region that showed significant differences in the original analysis still had significant differences after adding duration of migraine as a covariate.

### *1.3.1.* ***Cortical Curvature***

Differences in cortical curvature with P<0.001 were identified in the left posterior division of the cingulate cortex, right lateral occipital cortex, right paracentral lobule, and right precuneus cortex. For all these comparisons, both groups of migraine patients had increased curvature compared with HCs. Tukey-Kramer post hoc results for these comparisons are shown in Table 2, Figure 4.2, and the Supplementary Data. The results with P values $\geq$ 0.001 are shown and discussed in the Supplementary Data.

When comparing between EM and HC patients, all Cohen's d values (except for left cuneus cortex) were higher than 0.5, indicating a medium effect size according to the threshold established by Cohen [20]. The left posterior division of the cingulate cortex achieved a large effect (i.e., a Cohen's d value >0.8 [20]).

The same trend was found for the comparison between CM patients with respect to HCs, but the effect size was lower compared with EMs vs HCs. In the comparison between CM and EM patients, no value reached the medium effect size threshold, but cortical curvature values tended to be higher in EM patients. These results can be seen in the Supplementary Data.

### *1.3.2.* ***Cortical Thickness***

Differences in cortical thickness with P<0.001 were identified in three regions. In the left inferior temporal gyrus and in the right fusiform gyrus, both EMs and CMs showed decreased cortical thickness compared with HCs. In the right inferior temporal gyrus, HCs and CM patients showed increased cortical thickness compared with EM patients. Tukey-Kramer post hoc results for these comparisons are shown in Table 3, Figure 4.2, and the Supplementary Data. The results with P values $\geq$ 0.001 are shown and discussed in the Supplementary Data.

All Cohen's d absolute values, except for left banks of the superior temporal sulcus, indicated a medium effect size (in this case, more negative) in the comparison between EM patients and HCs, reaching, for the right inferior temporal gyrus, a large effect size. The same trend, but with lower effect sizes (less negative), was found when comparing CM patients and HCs. Finally, no medium effect sizes were found in the comparison between CM and EM patients, although cortical thickness values were consistently higher in CM patients. These results are depicted in the Supplementary Data.

### 1.3.3. Gray Matter Volume

Differences in gray matter volume with P<0.001 were found in four cortical regions and the bilateral cerebellum. In the left pars orbitalis, left pars triangularis, right insula, and bilateral cerebellum, both groups of migraine patients showed decreased gray matter volume compared with HCs. In the left superior temporal gyrus, CMs showed decreased gray matter volume compared with both HCs and EMs. Tukey-Kramer post hoc results for these comparisons are shown in Table 4, Figure 4.2, and the Supplementary Data. The results with P values $\geq$ 0.001 are shown and discussed in the Supplementary Data. Notably, decreased volume in CMs compared with EMs was observed in five regions (Supplementary Data).

Cohen's d absolute values in the comparison between CM patients and HCs indicated medium effect sizes (more negative) in most regions, reaching the large effect size threshold in the right insula and having a contrary trend in subcortical regions, particularly the nucleus accumbens. The same trend, but with generally smaller effect sizes, was observed in the comparison between EM patients and HCs. In the comparison between CMs and EMs, medium effect sizes were found in the left banks of the superior temporal sulcus (d = –0.65), the left superior temporal gyrus (d = –0.51), the left transverse temporal cortex (d $\approx$ –0.50), and the right isthmus cingulate gyrus. These results are illustrated in the Supplementary Data.

### 1.3.4. Surface Area

Differences in cortical surface area with P<0.001 were identified in 13 regions. In the bilateral precuneus cortex, bilateral superior temporal gyrus, left superior frontal gyrus, left supramarginal gyrus, right inferior parietal cortex, and right middle temporal gyrus, CMs showed decreased surface area compared with both HCs and EMs. In the right isthmus division of the cingulate cortex and right superior parietal cortex, CMs showed decreased surface area compared only with EMs. In the left pars triangularis, CMs showed decreased surface area compared only with HCs. In the left pars orbitalis and right insula, both EMs and CMs showed decreased surface area compared with HCs. Tukey-Kramer post hoc results for these comparisons are shown in Tables 5 and 6 (showing the results for left and right hemisphere, respectively), Figure 4.2, and the Supplementary Data. The results with P values $\geq$0.001 are shown and discussed in the Supplementary Data. These include decreased area in CMs compared with both EMs and HCs in nine regions (Supplementary Data) and decreased area in CMs compared with EMs in eight more regions (Supplementary Data).

In the comparison between EM patients and HCs, and in the comparison between CM patients and HCs, the left pars orbitalis, the right frontal pole, and the right insula showed medium effect sizes. For the comparison between CM patients and HCs, a medium effect size was also found in the left pars triangularis. No clear trend in EM patients with respect to HCs was observed. With regard to the comparison between CM and EM patients, medium effect sizes were observed in the left banks of the superior temporal sulcus (d = –0.66), left transverse temporal cortex (d = –0.58), right banks of the superior temporal sulcus (d = –0.51), right inferior parietal cortex (d = –0.64), right isthmus cingulate gyrus (d = –0.65), and right

superior parietal cortex (d = –0.53). CM cortical surface values were lower than EM values in all regions except the right frontal pole (d = 0.06). These results can be seen in the Supplementary Data.

**Table 1.** Clinical and demographic characteristics of healthy controls (HC), episodic migraine (EM) and chronic migraine (CM) patients.

| | HC (n=52) | EM (n=57) | CM (n=57) | Statistical test |
|---|---|---|---|---|
| Women (n) | 41 (79% ) | 48 (84% ) | 51 (89% ) | $\chi^2_{(2,\ N\ =\ 166)} = 2.3$, p = 0.31† |
| Age (years) | 36.4 ± 13.1 | 37.3 ± 8.4 | 38.1 ± 9.3 | $\chi^2(2) = 2.19$, p = 0.33‡ |
| Duration of migraine history (years) | | 14.3 ± 11.2 | 19.8 ± 10.8 | $t_{(112)}$ = -2.7, p = 0.008§ |
| Duration of chronic migraine (months) | | | 26.3 ± 34.9 | |
| Headache frequency (days/month) | | 3.8 ± 2.4 | 23.6 ± 6.3 | U = 48.5, p < 0.001 |
| Migraine frequency (days/month) | | 3.8 ± 2.4 | 14.1 ± 7.1 | U = 145.5, p < 0.001 |

Data are expressed as means ± SD. †Chi-square test. ‡ Kruskal-Wallis test. §Two-tailed, unpaired Student's t-test. Mann-Whitney U test.

**Table 2**. Cortical curvature comparison between different brain regions in healthy controls (HC), episodic migraine (EM) and chronic migraine (CM) patients.

| Region | HC mean curvature | EM mean curvature | CM mean curvature | EM vs. HC p-value | CM vs. HC p-value | CM vs. EM p-value |
|---|---|---|---|---|---|---|
| Left posterior division of the cingulate cortex | 141 ± 12 | 151 ± 11 | 148 ± 10 | < **0.001** | **0.004** | 0.47 |
| Right lateral occipital cortex | 141 ± 8 | 146 ± 8 | 147 ± 7 | **0.003** | **0.002** | 0.98 |
| Right paracentral lobule | 105 ± 9 | 111 ± 9 | 111 ± 9 | **0.002** | **0.003** | 0.99 |
| Right precuneus cortex | 130 ± 8 | 135 ± 7 | 136 ± 7 | < **0.001** | < **0.001** | 0.94 |

Tukey-Kramer post hoc test was used, where p-values from ANOVA or Kruskal-Wallis test were lower than 0.001. Data are expressed as means ± SD ($m^{-1}$).

**Table 3**. Cortical thickness comparison between different brain regions in healthy controls (HC), episodic migraine (EM) and chronic migraine (CM) patients.

| Region | HC average thickness | EM average thickness | CM average thickness | EM vs. HC p-value | CM vs. HC p-value | CM vs. EM p-value |
|---|---|---|---|---|---|---|
| Left inferior temporal gyrus | 2.726 ± 0.151 | 2.611 ± 0.161 | 2.652 ± 0.153 | $<$ **0.001** | **0.035** | 0.33 |
| Right fusiform gyrus | 2.756 ± 0.114 | 2.661 ± 0.126 | 2.686 ± 0.141 | $<$ **0.001** | **0.011** | 0.56 |
| Right inferior temporal gyrus | 2.747 ± 0.152 | 2.613 ± 0.150 | 2.687 ± 0.183 | $<$ **0.001** | 0.13 | **0.043** |

Tukey-Kramer post hoc test was used, where p-values from ANOVA or Kruskal-Wallis test were lower than 0.001. Data are expressed as means ± SD (mm).

**Table 4**. Gray matter volume comparison between different cortical and subcortical regions in healthy controls (HC), episodic migraine (EM) and chronic migraine (CM) patients.

| Region | HC grey matter volume | EM grey matter volume | CM grey matter volume | EM vs. HC p-value | CM vs. HC p-value | CM vs. EM p-value |
|---|---|---|---|---|---|---|
| Left pars orbitalis | 2215 ± 356 | 1977 ± 258 | 2034 ± 330 | $<$ **0.001** | **0.001** | 0.46 |
| Left pars triangularis | 3588 ± 606 | 3293 ± 537 | 3161 ± 532 | **0.011** | $<$ **0.001** | 0.37 |
| Left superior temporal gyrus | 11616 ± 1673 | 11232 ± 1462 | 10560 ± 1171 | 0.26 | $<$ **0.001** | **0.015** |
| Left cerebellum | 49756 ± 5594 | 47080 ± 5770 | 45903 ± 4440 | **0.004** | $<$ **0.001** | 0.31 |
| Right insula | 6728 ± 899 | 6279 ± 735 | 6085 ± 564 | **0.001** | $<$ **0.001** | 0.25 |
| Right cerebellum | 50121 ± 5689 | 47858 ± 5331 | 46482 ± 4142 | **0.015** | $<$ **0.001** | 0.19 |

Tukey-Kramer post hoc test was used, where p-values from ANCOVA tests were lower than 0.001. Data are expressed as means ± SD ($mm^3$) and p-values are adjusted by the effect of total intracranial volume.

**Table 5**. Cortical surface area comparison between different left hemisphere brain regions in healthy controls (HC), episodic migraine (EM) and chronic migraine (CM) patients.

| Region | HC surface area | EM surface area | CM surface area | EM vs. HC p-value | CM vs. HC p-value | CM vs. EM p-value |
|---|---|---|---|---|---|---|
| Pars orbitalis | 657 ± 96 | 611 ± 73 | 609 ± 89 | **0.002** | **0.001** | 0.99 |
| Pars triangularis | 1296 ± 215 | 1230 ± 169 | 1166 ± 168 | 0.068 | < **0.001** | 0.069 |
| Precuneus cortex | 3616 ± 491 | 3598 ± 434 | 3417 ± 416 | 0.93 | < **0.001** | < **0.001** |
| Superior frontal gyrus | 6975 ± 1084 | 6857 ± 657 | 6665 ± 666 | 0.27 | < **0.001** | **0.029** |
| Superior temporal gyrus | 3677 ± 495 | 3679 ± 429 | 3466 ± 385 | 1 | < **0.001** | < **0.001** |
| Supramarginal gyrus | 3718 ± 620 | 3675 ± 525 | 3447 ± 470 | 0.82 | < **0.001** | **0.004** |

Tukey-Kramer post hoc test was used, where p-values from ANCOVA tests were lower than 0.001. Data are expressed as means ± SD ($mm^2$) and p-values are adjusted by the effect of total surface area.

**Table 6**. Cortical surface area comparison between different right hemisphere brain regions in healthy controls (HC), episodic migraine (EM) and chronic migraine (CM) patients.

| Region | HC surface area | EM surface area | CM surface area | EM vs. HC p-value | CM vs. HC p-value | CM vs. EM p-value |
|---|---|---|---|---|---|---|
| Inferior parietal gyrus | 5101 ± 783 | 5201 ± 693 | 4812 ± 510 | 0.50 | **0.004** | < **0.001** |
| Isthmus-cingulate cortex | 855 ± 134 | 899 ± 133 | 817 ± 116 | 0.064 | 0.12 | < **0.001** |
| Middle temporal gyrus | 3254 ± 450 | 3281 ± 375 | 3110 ± 347 | 0.83 | **0.005** | < **0.001** |
| Precuneus cortex | 3753 ± 475 | 3732 ± 446 | 3564 ± 470 | 0.92 | **0.002** | **0.006** |
| Superior parietal cortex | 5037 ± 609 | 5107 ± 496 | 4850 ± 479 | 0.55 | 0.15 | < **0.001** |
| Superior temporal gyrus | 3443 ± 428 | 3449 ± 352 | 3290 ± 316 | 0.99 | **0.003** | **0.001** |
| Insula | 2214 ± 297 | 2082 ± 228 | 2054 ± 212 | < **0.001** | < **0.001** | 0.68 |

Tukey-Kramer post hoc test was used, where p-values from ANCOVA tests were lower than 0.001. Data are expressed as means ± SD ($mm^2$) and p-values are adjusted by the effect of total surface area.

### 1.3.5. Correlation Analysis

After correction for multiple comparisons, correlation analysis showed a significant negative correlation between duration of migraine history in years in EMs and gray matter volume in the right pars opercularis ($\rho$ = –0.488, P<0.001), in the right superior frontal gyrus ($\rho$ = –0.472, P<0.001), and in the left insula ($\rho$ =–0.453, P<0.001). Also, a significant negative correlation between duration of migraine history in EMs and surface area was found in the left insula ($\rho$ = –0.457, P<0.001). All these significant results are shown in Figure 4.9. No significant correlations were found in CMs for duration of migraine history or duration of chronic migraine. Also, no significant correlations were found for headache and migraine frequency in either CMs or EMs.

## 1.4. Discussion

Gray matter volume, cortical curvature, thickness, gray matter volume, and surface area were analyzed (where applicable) for a total of 68 cortical and 16 subcortical gray matter regions. Comparisons were made between HCs, patients with low-frequency EM (<10 headache days per month), and patients with CM. A total of 89 differences out of 288 comparisons were found to be statistically significant after correction for multiple comparisons (FDR). Pairwise differences were also found to be significant in several comparisons, including not only HCs vs EMs or CMs but also, notably, comparisons between EMs and CMs. These significant findings suggest structural brain differences between subtypes of migraine and HCs, as we stated in the objectives of the study.

There are two main reasons why these results can be considered highly relevant. First, there is a high number of statistically significant differences between migraine patients and healthy controls. Many of these differences were found in parameters infrequently analyzed in the previous literature, such as the cortical curvature and cortical surface area [9, 18, 21, 22]. The second reason is related to the statistically significant differences between EMs and CMs. Differences between these two groups have only been previously found in a few studies [7–9], and they are important pieces of information to elucidate the neural underpinnings of the progression from EM to CM.

Compared with previous studies, a remarkably higher number of significant results was found in this work. Several factors may have contributed to this difference. First, compared with other similar studies comparing EM and CM patients in their sample, our sample size was much bigger. Neeb et al. included 21 patients from each group and 21 HCs, that is, 63 participants [8], and Valfrè et al. included 27 HCs, 16 EM patients, and 11 CM patients [7]. Neeb et al. included no high-frequency EM patients [8], as in our study, and Valfrè et al. did not provide enough information to elucidate whether they included high-frequency EM patients in their study [7]. In our study, exclusion of high-frequency EM patients may have influenced the number of significant results, as it would likely have accentuated differences between EM and CM, if the change in the brain from one state to the other is a fluid continuation. Also, in both studies, voxelwise methods were employed for the analysis. This type of analysis is very restrictive due to the employed multiple comparison correction; that is, differences must be very profound in order to be detected as significant results. Additionally, in the case of the study by Neeb et al., the mean age of the participants was almost 50 years [8], while the mean age of the participants from our sample was <40 years. In older people, it could be more difficult to detect differences between groups due to normal

cortical changes associated with age. Some other studies employed a priori selected region of interest (ROI) approaches [18, 23–25], which limits the number of possible significant results with respect to whole-brain analysis. Furthermore, we analyzed four morphometric parameters, while most studies analyzed only one parameter, commonly gray matter volume or cortical thickness. Other possible reasons for the difference in significant results in each structural parameter are explained later.

In regions where significant results were found, there were usually one or two structural parameters with differences. In nine other regions, however, there were significant differences in three or more parameters. Table 7 summarizes the findings in those regions. One of them, the left superior temporal gyrus, involved in auditory processing, was also considered to be especially relevant as a classifier between CM and EM patients in a study by Schwedt et al. [9]. In this study, and in order to distinguish migraine patients from healthy controls and EMs from CMs, the authors obtained principal components for each group of features (cortical thickness, volume, and surface area from 68 regions) and built classification models using algorithms such as diagonal quadratic discriminant analysis and decision trees. Classification accuracies of 84.2% and 86.3% were achieved at classifying between CMs and EMs and between CMs and HCs, respectively. Some of the most relevant features in the classification between CMs and HCs were cortical surface area in the insula (as in our study) and the temporal pole, cortical thickness in the cingulate cortex, and gray matter volume in the entorhinal cortex, cuneus cortex, and pericalcarine cortex. In the classification between CMs and EMs, the most relevant features were cortical surface area in the superior temporal gyrus (as in our study), cortical thickness in the medial orbital frontal cortex and anterior cingulate cortex, and gray matter volume in the pars triangularis, transverse temporal cortex, and caudal anterior cingulate cortex.

Changes in the gray matter volume in migraine have been reported in several studies in the literature. We found decreased gray matter volume in migraine patients (one or both groups) compared with HCs in several regions, a result that agrees for the most part with the studies comparing migraine patients and HCs, including a meta-analysis by Jia et al. [5]. The decreased volume in gray matter could be caused by the effect of migraine attacks. In CM, with a higher number of migraine attacks compared with EM (especially if we consider lowfrequency EM patients), this reduction in cortical volume would be more pronounced. However, taking into account the correlation results, a relationship between decreased values in gray matter volume and headache frequency was not detected. The correlation analysis assessed frequencies within EMs and CMs and did not compare the effect of headache frequency from EMs to CMs, as this comparison was made in the main analysis. Moreover, the lack of significant results in the correlation analysis could also be partially due to the correction for multiple comparisons.

Future studies should consider a third patient cohort with high-frequency EM and even the use of generalized linear models considering number of headache days per month as the main independent variable of interest. The use a continuous variable (headache frequency) instead of a qualitative variable (low-frequency EM, highfrequency EM and CM) in the analysis would give us a better understanding of the effect of headache attacks on gray matter volume. In a high-frequency EM cohort, studies should consider whether high-frequency EM patients are actually closer to low-frequency EM or to CM.

In our study, gray matter volume was larger both in EMs and CMs compared with HCs in the right nucleus accumbens. Similar findings were reported by Neeb et al. [8], where increased gray matter volume in CMs compared with EMs and HCs was obtained, particularly in subcortical regions comparing CMs and HCs. The increased gray matter volume from subcortical regions may reflect structural brain

plasticity as a result of permanent activation of pain-related pathways, as suggested by Neeb et al. [8]. The nucleus accumbens is located in the basal forebrain, rostral to hypothalamus, and has a role in addiction, impulsivity, fear, and sleep processing, consisting of the regulation of cognitive and behavioral processes in cortico-striatal circuits [26]. Kim et al. found an association between migraine and primary sleep disorders, particularly with insomnia [27]. Moreover, Yang and Wang reported that CM patients experience more frequent and severe insomnia symptoms that EM patients [28]. Sardi et al. showed that increased adenosinergic A2A activity and decreased D2 activity in the nucleus accumbens mediate the pronociceptive effect of REM sleep deprivation [29]. The more frequent sleep disorders in CM and the role of the nucleus accumbens in the pronociceptive effect of sleep deprivation could explain the increased gray matter volume found in CM patients.

In the comparison of the right insula between CMs and HCs, a large effect size was observed. In a previous review, Borsook et al. defined the insula as a hub of activity in migraine, involved in afferent pathways in migraine such as the trigeminovascular or the vestibular, and in efferent pathways such as the autonomic, and in connections with regions such as the cingulate cortex [30]. Borsook et al. suggested that the insula is a convergence point for nociceptive inputs and that it may be involved in migraine processes like altered attention, pain during headache, dizziness, nausea, and social-emotional changes [30].

Regarding changes between both groups of migraine patients, we observed decreased gray matter volume in CMs compared with EMs in several regions. Such decreases were also observed by Valfrè et al. [7] and by Neeb et al. [8], and in high-frequency compared with low-frequency migraine patients by Maleki et al. [10]. In Valfrè et al. [7] and Neeb et al. [8], no significant differences were found using a conservative (family-wise error corrected) $P<0.05$ threshold. In the same studies, the authors used a less conservative criterion of an uncorrected $P<0.001$, finding significant differences with this criterion. A possible reason for the lack of significant differences using conservative criteria in the previous studies could be small sample sizes. Another reason, suggested by our effect size values (values $<0.8$, which correspond to a large effect size as established by Cohen), is that differences between EMs and CMs are subtle and not easily detectable. Notably, two of the significant morphometric differences between EMs and CMs observed in this study, the left transverse temporal cortex and the right superior temporal gyrus gray matter volumes, were used in Schwedt et al. [9] as parameters to accurately classify EMs vs CMs using MRI morphometry.

The other three structural parameters (cortical curvature, thickness, and surface area) have been much less studied in migraine patients. To the best of our knowledge, only one study compared cortical curvature between migraine patients and healthy controls [18], and no significant differences were reported. It is important to note, nevertheless, that only seven areas were compared between migraine patients and HCs, and cortical curvature was only assessed in one of these regions. In this study by Schwedt et al., the main objective was to compare brain structure between persistent posttraumatic headache and migraine patients. In contrast to our study, in the study by Schwedt et al., an overall cortical curvature comparison between controls and migraine patients was not performed in order to detect curvature alterations in migraine. In our case, increased cortical curvature was observed in both groups of migraineurs compared with HCs. Brain curvature provides a measure of sharper cortical folds [18]. Increased cortical curvature has previously been associated with global or gyral white matter atrophy in multiple sclerosis [31], neurodegenerative diseases [32], and mild traumatic brain injury [33]. King et al. hypothesized that increased cortical curvature could be partly caused by cortical restructuring related to tissue volume loss [33]. In a study of schizophrenia patients, a negative correlation was found between cortical curvature values and fractional

anisotropy values of white matter tracts, suggesting that mean cortical curvature could be related to cortico-cortical connection integrity [34]. The cingulate cortex or precuneus, regions in which we have detected changes in cortical curvature, are included in hippocampal formation and might be involved in first stages of migraine physiopathology. They are also implicated in intrinsic control networks [35]. In the specific case of the left posterior division of the cingulate cortex, we obtained a large effect size in the comparison of EM patients and HCs.

Regarding cortical thickness, decreases were found in EMs and CMs with respect to HCs in several regions. Furthermore, we also found decreased cortical thickness in EMs compared with both CMs and HCs in the right inferior temporal gyrus. In the right inferior temporal gyrus, we obtained a large effect size in the comparison between EMs and HCs. Interestingly, a very similar result for that same region was reported by Maleki et al. [10], where the authors compared high- and low-frequency migraine patients and HCs. Also, cortical thickness in the left superior temporal gyrus was used as a feature to classify between CMs and HCs by Schwedt et al. [9]. Our results also show significant differences between both groups of migraineurs and HCs using that feature. In line with our results, Magon et al. showed generalized thinned cortex in migraine patients compared with healthy controls, particularly in the right middle temporal gyrus [36], as we obtained with EM and CM patients with respect to healthy controls. Chong et al. found decreased cortical thickness in EM patients in the right fusiform gyrus [37], a result that we also obtained (Table 3; Supplementary Data). In contrast to our results, Granziera et al. reported increased cortical thickness in the motion-processing visual areas MTÃ¾ and V3A in migraineurs (with and without aura) compared with healthy controls [23]. Similar results were reported by Gaist et al. in patients with migraine with aura (no patients with migraine without aura were included), finding increased cortical thickness in the V2 and V3A visual areas [38]. DaSilva et al. and Kim et al. reported thickening of the somatosensory cortex in patients with migraine with [24] and without aura [24, 39], but the opposite result (thinner somatosensory cortex) was obtained in patients with migraine with aura (no patients with migraine without aura were included) by Hougaard et al. [40]. Interestingly, Hougaard et al. obtained increased cortical thickness in the hemispheres contralateral to the perceived headache side in the pars opercularis, but no differences were found with regard to aura [41]. Datta et al. identified no significant differences in cortical thickness between migraine patients and healthy controls [42].

Cortical thickness is a marker of gray matter integrity, reflective of the size, density, and arrangement of cells (neurons, neuroglia, and nerve fibers) [43, 44]. Cortical thickness results from previous literature are conflicting. Differences observed between studies could be due to methodological differences (most of the studies employed a priori ROI approaches) or to sample differences. Structural abnormalities in the somatosensory cortex could be related to clinical and demographic factors [36]. One of our results that matches previous literature was thinned cortex in the right fusiform gyrus in migraine patients with respect to healthy controls. Fusiform gyrus has been associated with pain perception and anticipation [45] and with greater pain-induced activation [46]. Another result that matches previous literature is increased cortical thickness in the right inferior temporal gyrus in CM or high-frequency migraine patients compared with low-frequency EM patients. As suggested by Maleki et al., this increased cortical thickness could imply a compensatory adaptive response of the brain to meet the increased demand for sensory processing related to a higher number of migraine attacks [10]. This hypothesis could also explain increased cortical thickness in migraine patients in visual areas from previous literature, although this increase has no clear relationship to aura due to lacking patients with migraine without aura in some studies and no differences

between migraine with and without aura found by Granziera et al. [23]. In EM patients, especially in those with low-frequency headache (as in our sample) and during the initial months, the brain gray matter would not be so well adapted to migraine sensory processing.

Finally, cortical surface area seems to be an excellent biomarker to distinguish CMs from EMs. We identified 27 regions with significant differences between both groups. Among them, the surface area of the left pars triangularis, right insula, bilateral superior temporal gyrus, left postcentral gyrus, and left posterior division of the cingulate cortex were employed to classify CMs from HCs and EMs [9]. These regions are implicated in discrimination of different components of pain and sensorial processing [47]. Messina et al. obtained increased and decreased cortical surface area in patients with migraine (it is not mentioned explicitly, but it seems that no patients with CM were included) with respect to HCs [21]. We only obtained significant decreased surface area in migraine patients (EMs and especially CMs) with respect to HCs, but in EM patients we found no generalized decreased surface area in comparison with controls, as can be seen in the Supplementary Data. Petrusic et al. found no significant differences in cortical surface area between migraine with aura patients and healthy controls [22].

Cortical surface area is determined largely prenatally, in contrast to cortical thickness, which undergoes major changes postnatally [21, 48, 49]. Comparing our cortical surface area results of CM patients to EM patients or to previous literature results, it seems that generalized decreased cortical surface area, especially in regions implicated in discrimination of different components of pain and sensorial processing, is characteristic of CM patients. Decreased cortical surface area in CM patients may reflect enhanced cortical atrophy compared with EM patients and HCs, considering no brain adaptation to pain processes, as suggested before with cortical thickness. Therefore, cortical surface area could be not only a good biomarker to distinguish CM from EM, but also a possible useful feature to predict progression from EM to CM. A possible hypothesis of the surface area state in migraine would be that there might be a genetic predisposition not only to migraine, but also to CM, and area changes would be manifested throughout the migraine course and not so influenced by environmental or external factors, as may happen with cortical thickness. The findings of this study related to cortical surface area must be corroborated in future studies, and possible prediction of CM must be analyzed in longitudinal studies, including genetic data.

With respect to the comparison between both groups of patients with migraine, most of the difference between CM and EM patients was found in the temporal lobe. Previously, Maleki et al. observed diminished connectivity between the hippocampus and temporal lobe, insula, and nucleus accumbens in high-frequency with respect to low-frequency migraine [25]. The authors interpreted this result as a possible diminished interaction with brain regions involved in cognitive or associative processes in high-frequency migraine patients, contributing to the migraine experience [25]. The relevance of the temporal lobe in different types of migraine should be confirmed by connectivity studies.

We performed an additional analysis considering the duration of migraine history as a covariate, due to observed significant differences in this duration between both groups of migraine patients. The addition of the duration of migraine as a covariate in the ANCOVA analysis barely changed the results with respect to the analysis without covariates. In the case of the comparison between EM and CM patients, there was no reduction of the number of significant differences when adding duration of migraine as a covariate. Consequently, observed morphometric differences between EM and CM patients did not seem to be driven by differences in the duration of migraine history.

Our last objective was to examine the possible association between gray matter structural features and clinical characteristics of patients. The significant negative correlations found between duration of migraine and gray matter volume are consistent with previous studies [50, 51]. Furthermore, negative correlations between duration of migraine and gray matter volume in the left insula and in the right superior frontal gyrus have been previously reported [50]. No significant correlations in CM were found for the duration of migraine or the duration of chronic migraine, and no significant differences were found for headache and migraine frequency in either CMs or EMs.

The negative correlation between gray matter volume or cortical surface area and duration of migraine history suggests that gray matter atrophy is related to the cumulative effect of headache or migraine attacks. Considering differences between CM and EM patients, the gray matter atrophy would be related to a mixed effect of Gray Matter Structural Alterations in Migraine 11 duration and frequency of attacks, although no significant correlations were observed within the range of frequencies for CM or EM. In the case of CM patients, the nonsignificant effect of time could be produced because of a kind of steady state related to a possible continuous ictal-like state, as suggested by Neeb et al. [8].

Significant correlations between headache frequency were previously found. Neeb et al. [8] found positive and negative correlation between headache frequency and gray matter volume, but with an uncorrected $P<0.001$ and in all migraineurs, that is, no specific correlations for EM or CM. Valfrè et al. [7] reported that gray matter volume was negatively correlated with headache frequency in migraine patients using unmodulated images, including CM and EM patients in the same sample in the correlation analysis. Kim et al. [50] also found a negative correlation between gray matter volume and headache frequency in some regions, but no correction for multiple comparisons was performed. Kim et al. [33] reported a positive correlation between cortical thickness and lifetime headache frequency, but there was no significant correlation with headache frequency recorded in a threemonth headache diary, and there was no correction for multiple comparisons. In line with our results, no significant correlation between headache frequency and cortical thickness or cortical surface area was reported by DaSilva et al. [24], Messina et al. [21], Petrusic et al. [22], or Hougaard et al. [40]. From our results and previous results, there is no clear association between headache frequency and gray matter changes, considering independently EM or CM. In this study, excluding highfrequency EM patients could have influenced the lack of significant correlations between morphometric parameters and headache frequency.

The observed pairwise significant differences and effect size values (Cohen's d) show interesting patterns in morphometric parameters when comparing both migraine groups with controls and also when comparing EM with CM. These patterns are summarized in Table 8. In general, as could be expected, migraine patients showed higher cortical curvature, lower cortical thickness, lower gray matter volume (except for nucleus accumbens and putamen, both subcortical structures), and lower cortical surface area compared with HCs, corresponding to, at least, medium effect size in statistically significant pairwise comparisons. However, a qualitative interpretation of these results (observing not only P values $<0.05$ in pairwise post hoc comparisons, but also P values $<0.001$ to reach a stricter level of significance) could suggest that the structural brain differences between HCs and EMs might be dominated by a cortical curvature increase, a cortical thickness decrease, and, to a lesser extent, a cortical surface area and gray matter volume decrease. These trends match the results from effect size analysis, where a medium or even large effect size was observed in almost all regions, with significant differences in cortical curvature and thickness with respect to HCs, but only in the few regions with significant differences in gray matter volume and cortical

surface area. Moreover, analyzing cortical surface area, there are no significant differences between EM patients and HCs in most of the regions. Differences between EMs and CMs, on the other hand, seem to indicate that there might be no further increase in cortical curvature and that cortical thickness decreases might be slowed down (no important progression in the decline of thickness). There are even some regions where cortical thickness does not decline, but rises. These regions could be relevant in pain processing or processes related to migraine (e.g., visual areas in migraine with and without aura). Regarding differences between EMs and CMs, decreases in the gray matter volume and, especially, cortical surface area seem to be intensified. Taking all these trends into consideration, the implication could be that not only are there measurable differences in brain structure between EMs and CMs, but also that the nature of EM and CM could be qualitatively different from the differences that appear between HCs and EMs. Caution should be taken regarding this interpretation, which was previously suggested by Neeb et al. [8]. This interpretation would imply that EM and CM may be two different entities instead of one unique entity with different headache frequencies, and naturally an entity different than controls. Further longitudinal studies would be needed in order to corroborate this, especially those focusing on the temporal evolution of patients converting from EM to CM and the possible causal relationships of the diverse differences noted between the three groups.

In this study, high-frequency EM patients (10–14 headache days per month) were excluded. This decision was made in order to avoid potentially misclassified patients, which could mislead the analysis. Compared with Neeb et al. [8], CM patients from our sample had greater headache frequency and similar migraine frequency, while EM patients from our sample had lower headache and migraine frequency. This increased difference in frequency of headache between the EM and CM groups could be a factor explaining the higher number of significant differences found in this study. However, no significant correlations were found between headache or migraine frequency and structural gray matter measures, which could mean that headache or migraine frequency does not have a relevant effect on structural gray matter parameters within the EM or CM groups. In any case, a deeper, specific analysis focusing on high-frequency EM patients would be needed to clarify whether this group of patients is closer to the lowfrequency EM group or the CM group. In the latter case, gray matter changes such as an increase in the cortical thickness of several specific areas, which were observed in our analysis as well as in other previous studies [10, 24, 38], would be expected.

There are several strengths and limitations to this study. About the strengths, this is one of the few studies that has employed different structural parameters to analyze gray matter changes between HCs, EMs, and CMs. In the case of cortical curvature, this is the first study to compare whole-brain cortical curvature differences between migraine patients and healthy controls. Also, this is, to the best of our knowledge, the study with the highest number of participants from those three groups. Even though we defined no a priori regions of interest and consequently corrections for multiple comparisons had to be implemented, the high number of subjects allowed us to observe numerous and very clear differences between the groups. The effects of the lack of these a priori selections, were, however, more evident in the correlation analysis, where only four P values were found to be significant after multiple-comparisons correction analysis, limiting the identification of significant associations. Another limitation is that using ANCOVA for the gray matter volume and surface area analysis implies the assumption of Gaussianity in the values of those parameters, which in some comparisons could be not true. Additionally, we acquired

no T2 or T2-FLAIR MRI sequences to assess white matter hyperintensities (WMHs). Migraine has been associated with an increased risk of WMHs detected on MRI [52]; also, pain in EM patients [53] and an unfavorable prognosis [54] were found to be associated with the occurrence of WMHs. Also, higher WMH load was found to be related to lower cortical thickness in the frontotemporal regions, while this load was related to higher cortical thickness in paracentral regions [55]. Moreover, anxiety and depression were not screened in all patients and not included in the analysis. Anxiety and depression are often comorbid in patients with migraine [56–58]. Gray matter volume reductions in the rostral anterior cingulate cortex in patients with major depressive disorder, and in the parahippocampal gyrus and amygdala in patients with comorbid anxiety disorders, were found [59]. Considering the relationship between depression and anxiety with morphometric parameters, not including these patients in the analysis could be a limitation of our study, but Neeb et al. did not include depression scores in their analysis as a covariate due to the positive association between depression and headache frequency [8]. Finally, important characteristics that could have affected the results, such as aura, were not considered in the analysis.

## 1.5. Conclusions

In this study, several parameters describing the structure of the gray matter were obtained from T1-weighted MR images in a cohort of healthy controls, patients with episodic migraine, and patients with chronic migraine and employed to investigate the differences between them.

A high number of significant differences were found between all groups, generally indicating an increase in cortical curvature and decreases in gray matter volume, cortical thickness, and cortical surface area in migraine patients compared with healthy controls. In the case of cortical curvature, increased values in regions like the cingulate cortex may reflect migraine genesis. Also, gray matter atrophy reflected in generalized cortical thickness loss or decreased gray matter volume could be potential biomarkers for the first stages of the migraine pathophysiology, that is, the first changes that can be seen on MRI.

Furthermore, significant differences were also found in chronic migraine with respect to episodic migraine, suggesting a pattern of structural changes in the brain that could be qualitatively different from those that occur between healthy controls and patients with episodic migraine. Increased cortical thickness in CM compared with EM may involve an adaptive response to meet the increased demand for sensory processing. For gray matter volume, decreased values would show an increased atrophy related to an increased number of headache attacks. Finally, in the case of cortical surface area, decreased values may reflect progression from EM to CM, making this parameter a potentially useful feature of the progression of the disease.

Further work is needed to correlate these findings with different characteristics of migraine patients (aura, allodynia, psychological disturbances) and to elucidate the implications of these findings. Specifically, longitudinal analyses are necessary, especially those focusing on the progression from EM to CM and in the first changes that appear in migraine patients.

**Table 7**. Brain regions where three or more parameters have significant differences.

| Region | Cortical Curvature | Cortical Thickness | Gray Matter Volume | Surface Area |
|---|---|---|---|---|
| Left banks of the superior temporal sulcus | NS | CM < HC | CM < EM | CM < EM |
| Left inferior temporal gyrus | CM > HC<br>EM > HC | CM < HC<br>EM < HC | CM < HC<br>EM < HC | CM < HC<br>EM < HC |
| Left lateral occipital cortex | CM > HC<br>EM > HC | NS | CM < HC | CM < HC<br>EM < HC |
| Left lateral orbital frontal cortex | EM > HC | NS | CM < HC | CM < HC |
| Left precentral gyrus | NS | CM < HC | CM < HC | CM < HC<br>EM < HC |
| Left superior temporal gyrus | NS | CM < HC<br>EM < HC | CM < HC<br>CM < EM | CM < HC<br>EM < HC |
| Right fusiform gyrus | NS | CM < HC<br>EM < HC | CM < HC | CM < HC<br>EM < HC |
| Right middle temporal gyrus | NS | CM < HC<br>EM < HC | CM < HC<br>CM < EM | CM < HC<br>EM < HC |
| Right precentral gyrus | NS | CM < HC<br>EM < HC | CM < HC | CM < HC<br>EM < HC |

The significant results are shown for each case. CM = chronic migraine; EM = episodic migraine; HC = healthy controls; NS = non-significant.

**Table 8**. Summary of the pairwise comparisons between healthy controls (HC), episodic migraine (EM) and chronic migraine (CM) patients.

| Parameter | EM vs. HC | CM vs. HC | CM vs. EM |
|---|---|---|---|
| Cortical Curvature | $\uparrow$ and $\uparrow\uparrow$ | $\uparrow$ | NS |
| Cortical Thickness | $\downarrow\downarrow$ | $\downarrow$ | $\uparrow$ |
| Gray Matter Volume | $\downarrow$ | $\downarrow\downarrow$ | $\downarrow$ |
| Cortical Surface Area | $\downarrow$ and $\downarrow\downarrow$ | $\downarrow\downarrow$ | $\downarrow\downarrow$ |

The showed results are based on the most frequent results, among the significant results, with $p < 0.001$ (ANOVA, Kruskal-Wallis or ANCOVA). NS = non-significant. $\uparrow\uparrow/\downarrow\downarrow$ = increased/decreased measure with $p < 0.001$ in pairwise comparison. $\uparrow/\downarrow$ = increased/decreased measure with $p < 0.05$ in pairwise comparison. If single and double arrow are present in a single cell, this means that both cases are equally frequent.

# 1.6. References

1. Headache Classification Committee of the International Headache Society. The International Classification of Headache Disorders, 3rd edition. Cephalalgia 2018;38(1):1–211.

2. Lipton RB, Fanning KM, Buse DC, et al. Identifying natural subgroups of migraine based on comorbidity and concomitant condition profiles: Results of the Chronic Migraine Epidemiology and Outcomes (CaMEO) study. Headache 2018;58(7):933–47.

3. Bashir A, Lipton RB, Ashina S, Ashina M. Migraine and structural changes in the brain: A systematic review and meta-analysis. Neurology 2013;81(14):1260–8.

4. Kruit MC, Launer LJ, Ferrari MD, van Buchem MA. Infarcts in the posterior circulation territory in migraine. The populationbased MRI CAMERA study. Brain 2005;128(9):2068–77.

5. Jia Z, Yu S. Grey matter alterations in migraine: A systematic review and meta-analysis. Neuroimage Clin 2017;14:130–40.

6. Ashburner J, Friston KJ. Voxel-based morphometry–the methods. Neuroimage 2000;11(6):805–21.

7. Valfrè W, Rainero I, Bergui M, Pinessi L. Voxel-based morphometry reveals gray matter abnormalities in migraine. Headache 2007;48(1):109–17.

8. Neeb L, Bastian K, Villringer K, Israel H, Reuter U, Fiebach JB. Structural gray matter alterations in chronic migraine: Implications for a progressive disease? Headache 2017;57 (3):400–16.

9. Schwedt TJ, Chong CD, Wu T, Gaw N, Fu Y, Li J. Accurate classification of chronic migraine via brain magnetic resonance imaging. Headache 2015;55(6):762–77.

10. Maleki N, Becerra L, Brawn J, Bigal M, Burstein R, Borsook D. Concurrent functional and structural cortical alterations in migraine. Cephalalgia 2012;32(8):607–20.

11. Headache Classification Committee of the International Headache Society. The International Classification of Headache Disorders, 3rd edition (beta version). Cephalalgia 2013;33 (9):629–808.

12. Zigmond AS, Snaith RP. The Hospital Anxiety and Depression Scale. Acta Psychiatr Scand 1983;67(6):361-70.

13. Dale AM, Fischl B, Sereno MI. Cortical surface-based analysis. I. Segmentation and surface reconstruction. Neuroimage 1999;9 (2):179–94.

14. Fischl B, Liu A, Dale AM. Automated manifold surgery: Constructing geometrically accurate and topologically correct models of the human cerebral cortex. IEEE Trans Med Imaging 2001;20(1):70–80.

15. Fischl B, Salat DH, Busa E, et al. Whole brain segmentation: Automated labeling of neuroanatomical structures in the human brain. Neuron 2002;33(3):341–55.

16. Ségonne F, Dale AM, Busa E, et al. A hybrid approach to the skull stripping problem in MRI. Neuroimage 2004;22 (3):1060–75.

17. Desikan RS, Ségonne F, Fischl B, et al. An automated labeling system for subdividing the human cerebral cortex on MRI scans into gyral based regions of interest. Neuroimage 2006;31 (3):968–80.

18. Schwedt TJ, Chong CD, Peplinski J, Ross K, Berisha V. Persistent post-traumatic headache vs. migraine: An MRI study demonstrating differences in brain structure. J Headache Pain 2017;18(1):87.

19. Benjamini Y, Hochberg Y. Controlling the false discovery rate: A practical and powerful approach to multiple testing. J R Stat Soc Ser B 1995;57(1):289–300.

20. Cohen J. Statistical Power Analysis for the Behavioral Sciences. 2nd ed. Hillsdale, NJ: Lawrence Erlbaum Associates, Publishers; 1988.

21. Messina R, Rocca MA, Colombo B, et al. Cortical abnormalities in patients with migraine: A surface-based analysis. Radiology 2013;268(1):170–80.

22. Petrusic I, Dakovic M, Kacar K, Zidverc-Trajkovic J. Migraine with aura: Surface-based analysis of the cerebral cortex with magnetic resonance imaging. Korean J Radiol 2018;19 (4):767–76.

23. Granziera C, DaSilva AFM, Snyder J, Tuch DS, Hadjikhani N. Anatomical alterations of the visual motion processing network in migraine with and without aura. PLoS Med 2006;3(10):e402.

24. DaSilva AFM, Granziera C, Snyder J, Hadjikhani N. Thickening in the somatosensory cortex of patients with migraine. Neurology 2007;69(21):1990–5.

25. Maleki N, Becerra L, Brawn J, McEwen B, Burstein R, Borsook D. Common hippocampal structural and functional changes in migraine. Brain Struct Funct 2013;218(4):903–12.

26. Basar K, Sesia T, Groenewegen H, Steinbusch HW, Visser- Vandewalle V, Temel Y. Nucleus accumbens and impulsivity. Prog Neurobiol 2010;92(4):533–57.

27. Kim SJ, Han KT, Jang SY, Yoo KB, Kim SJ. The association between migraine and types of sleep disorder. Int J Environ Res Public Health 2018;15(12):2648.

28. Yang C-P, Wang S-J. Sleep in patients with chronic migraine. Curr Pain Headache Rep 2017;21(9):39.

29. Sardi NF, Tobaldini G, Morais RN, Fischer L. Nucleus accumbens mediates the pronociceptive effect of sleep deprivation: The role of adenosine A2A and dopamine D2 receptors. Pain 2018; 159(1):75–84.

30. Borsook D, Veggeberg R, Erpelding N, et al. The insula: A hub of activity in migraine. Neuroscientist 2016;22(6):632–52.

31. Deppe M, Marinell J, Krämer J, et al. Increased cortical curvature reflects white matter atrophy in individual patients with early multiple sclerosis. Neuroimage Clin 2014;6:475–87.

32. Im K, Lee JM, Seo SW, Hyung Kim S, Kim SI, Na DL. Sulcal morphology changes and their relationship with cortical thickness and gyral white matter volume in mild cognitive impairment and Alzheimer's disease. Neuroimage 2008;43(1):103–13.

33. King JB, Lopez-Larson MP, Yurgelun-Todd DA. Mean cortical curvature reflects cytoarchitecture restructuring in mild traumatic brain injury. Neuroimage Clin 2016;11:81–9.

34. Lubeiro A, de Luis-García R, Rodríguez M, Álvarez A, de la Red H, Molina V. Biological and cognitive correlates of cortical curvature in schizophrenia. Psychiatry Res 2017;270:68–75.

35. Dodick DW. A phase-by-phase review of migraine pathophysiology. Headache 2018;58(Suppl 1):4–16.

36. Magon S, May A, Stankewitz A, et al. Cortical abnormalities in episodic migraine: A multi-center 3T MRI study. Cephalalgia 2019;39(5):665–73.

37. Chong CD, Dodick DW, Schlaggar BL, Schwedt TJ. Atypical age-related cortical thinning in episodic migraine. Cephalalgia 2014;34(14):1115–24.

38. Gaist D, Hougaard A, Garde E, et al. Migraine with visual aura associated with thicker visual cortex. Brain 2018;141 (3):776–85.

39. Kim JH, Kim JB, Suh SI, Seo WK, Oh K, Koh SB. Thickening of the somatosensory cortex in migraine without aura. Cephalalgia 2014;34(14):1125–33.

40. Hougaard A, Amin FM, Arngrim N, et al. Sensory migraine aura is not associated with structural grey matter abnormalities. Neuroimage Clin 2016;11:322–7.

41. Hougaard A, Amin FM, Hoffmann MB, et al. Structural gray matter abnormalities in migraine relate to headache lateralization, but not aura. Cephalalgia 2015;35(1):3–9.

42. Datta R, Detre JA, Aguirre GK, Cucchiara B. Absence of changes in cortical thickness in patients with migraine. Cephalalgia 2011;31(14):1452–8.

43. Narr KL, Bilder RM, Toga AW, et al. Mapping cortical thickness and gray matter concentration in first episode schizophrenia. Cereb Cortex 2005;15(6):708–19.

44. Schwedt TJ, Berisha V, Chong CD. Temporal lobe cortical thickness correlations differentiate the migraine brain from the healthy brain. PLoS One 2015;10(2):e0116687.

45. Ter Minassian A, Ricalens E, Humbert S, Duc F, Aubé C, Beydon L. Dissociating anticipation from perception: Acute pain activates default mode network. Hum Brain Mapp 2013;34 (9):2228–43.

46. Schwedt TJ, Chong CD, Chiang C-C, Baxter L, Schlaggar BL, Dodick DW. Enhanced pain-induced activity of pain processing regions in a case-control study of episodic migraine. Cephalalgia 2014;34(12):947–58.

47. Noseda R, Burstein R. Migraine pathophysiology: Anatomy of the trigeminovascular pathway and associated neurological symptoms, cortical spreading depression, sensitization, and modulation of pain. Pain 2013;154(Suppl 1):S44–53.

48. Kapellou O, Counsell SJ, Kennea N, et al. Abnormal cortical development after premature birth shown by altered allometric scaling of brain growth. PLoS Med 2006;3(8):e265.

49. Frye RE, Liederman J, Malmberg B, McLean J, Strickland D, Beauchamp MS. Surface area accounts for the relation of gray matter volume to reading-skills and history of dyslexia. Cereb Cortex 2010;20(11):2625–35.

50. Kim JH, Suh SI, Seol HY, et al. Regional grey matter changes in patients with migraine: A voxel-based morphometry study. Cephalalgia 2008;28(6):598–604.

51. Jin C, Yuan K, Zhao L, et al. Structural and functional abnormalities inmigraine patients without aura.NMR Biomed 2013;26(1):58–64.

52. Porter A, Gladstone JP, Dodick DW. Migraine and white matter hyperintensities. Curr Pain Headache Rep 2005;9(4):289–93.

53. Yalcin A, Ceylan M, Bayraktutan OF, Akkurt A. Episodic migraine and white matter hyperintensities: Association of pain lateralization. Pain Med 2018;19(10):2051–7.

54. Xie H, Zhang Q, Huo K, et al. Association of white matter hyperintensities with migraine features and prognosis. BMC Neurol 2018;18(1):93.

55. Tuladhar AM, Reid AT, Shumskaya E, et al. Relationship between white matter hyperintensities, cortical thickness and cognition. Stroke 2015;46(2):425–32.

56. Lantéri-Minet M, Radat F, Chautard MH, Lucas C. Anxiety and depression associated with migraine: Influence on migraine subjects'disability and quality of life, and acute migraine management. Pain 2005;118(3):319–26.

57. Baskin SM, Lipchik GL, Smitherman TA. Mood and anxiety disorders in chronic headache. Headache 2006;46(s3):S76–87.

58. Minen MT, Begasse De Dhaem O, Kroon Van Diest A, et al. Migraine and its psychiatric comorbidities. J Neurol Neurosurg Psychiatry 2016;87(7):741–9.

59. Bora E, Fornito A, Pantelis C, Yücel M. Gray matter abnormalities in major depressive disorder: A meta-analysis of voxel based morphometry studies. J Afffect Disord 2012;138(1–2):9–18.

# 1.7. Supplementary Material

The Supplementary Tables and Figures are included in this section.

**Supplementary Table 1**. Sensitivity analysis of the possible scenarios depending on the alpha and beta variation.

| Option | Confidence level (% ) | Power (% ) | Estimated effect size | Variance | Expected patient loss (% ) | Sample size |
|---|---|---|---|---|---|---|
| a) | 99 | 80 | 0.04 | 0.01 | 10 | 139 |
| b) | 95 | 80 | 0.04 | 0.01 | 10 | 86 |
| c) | 95 | 90 | 0.04 | 0.01 | 10 | 119 |
| d) | 99 | 90 | 0.04 | 0.01 | 10 | 181 |

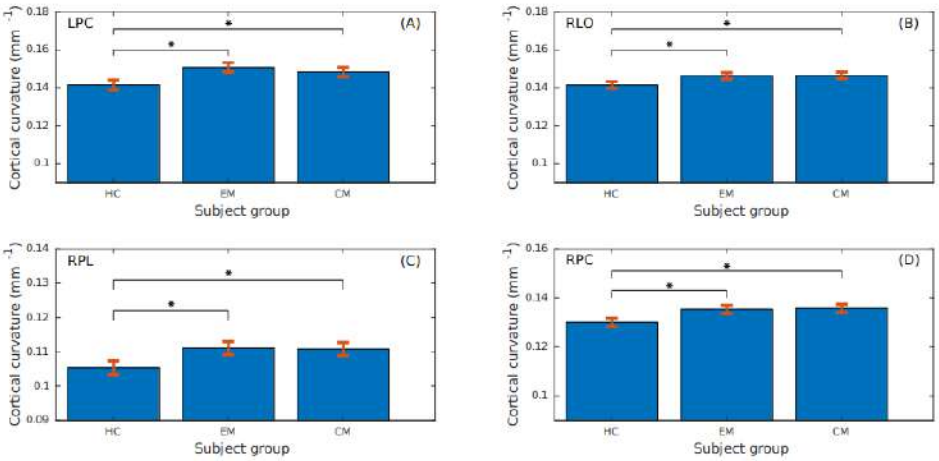


**Supplementary Figure 1**. Cortical curvature bar plots of regions where differences between both groups of migraine patients and healthy controls appeared. P-values of ANOVA or Kruskal-Wallis tests were lower than 0.001 in these regions. (A) LPC = left posterior division of the cingulate cortex; (B) RLO = right lateraloccipital cortex; (C) RPL = right paracentral lobule; (D) RPC = right precuneus cortex.

**Supplementary Table 2**. Cortical curvature comparison between different brain regions in healthy controls (HC), episodic migraine (EM) and chronic migraine (CM) patients.

| Region | HC mean curvature | EM mean curvature | CM mean curvature | EM vs. HC p-value | CM vs. HC p-value | CM vs. EM p-value | p∗ |
|---|---|---|---|---|---|---|---|
| Left cuneus cortex | 151 ± 9 | 155 ± 12 | 157 ± 10 | 0.14 | **0.006** | 0.44 | 0.009 |
| Left inferior temporal gyrus | 136 ± 10 | 141 ± 9 | 142 ± 10 | **0.020** | **0.003** | 0.82 | 0.003 |
| Left lateral occipital cortex | 141 ± 8 | 146 ± 8 | 145 ± 7 | **0.007** | **0.039** | 0.82 | 0.007 |
| Left lateral orbital frontal cortex | 142 ± 8 | 147 ± 10 | 146 ± 9 | **0.008** | 0.062 | 0.73 | 0.009 |
| Left postcentral gyrus | 114 ± 9 | 119 ± 9 | 117 ± 10 | **0.004** | 0.23 | 0.25 | 0.007 |
| Left frontal pole | 181 ± 26 | 196 ± 24 | 191 ± 27 | **0.009** | 0.11 | 0.61 | 0.013 |
| Right Inferior parietal cortex | 131 ± 8 | 135 ± 8 | 135 ± 7 | **0.008** | **0.015** | 0.97 | 0.005 |
| Right Supramarginal gyrus | 129 ± 7 | 134 ± 8 | 131 ± 7 | **0.002** | 0.42 | 0.072 | 0.003 |

Tukey-Kramer post hoc test was used, where p-values from ANOVA or Kruskal-Wallis test were equal or greater than 0.001. Data are expressed as means ± SD ($m^{-1}$).
∗ p-value for ANOVA or Kruskal-Wallis test.

**Supplementary Table 3**. Cohen's d of cortical curvature measures in regions where significant differences between healthy controls (HC), episodic migraine (EM) and chronic migraine (CM) patients were observed.

| Region | EM vs. HC Cohen's d | CM vs. HC Cohen's d | CM vs. EM Cohen's d |
|---|---|---|---|
| Left cuneus (LCu) | 0.36 | **0.65** | 0.21 |
| Left inferior temporal gyrus (LIT) | **0.53** | **0.61** | 0.11 |
| Left lateral occipital cortex (LLO) | **0.55** | 0.47 | -0.12 |
| Left lateral orbital frontal cortex (LLOF) | **0.57** | 0.46 | -0.13 |
| Left postcentral gyrus (LPG) | **0.63** | 0.31 | -0.29 |
| Left posterior division of the cingulate cortex (LPC) | **0.80** | **0.60** | -0.23 |
| Left frontal pole (LFP) | **0.58** | 0.37 | -0.17 |
| Right inferior parietal cortex (RIP) | **0.56** | **0.54** | -0.04 |
| Right lateral occipital cortex (RLO) | **0.62** | **0.68** | -0.03 |
| Right paracentral lobule (RPL) | **0.64** | **0.63** | -0.03 |
| Right precuneus cortex (RPcu) | **0.72** | **0.77** | 0.06 |
| Right supramarginal gyrus (RSG) | **0.65** | 0.25 | -0.40 |

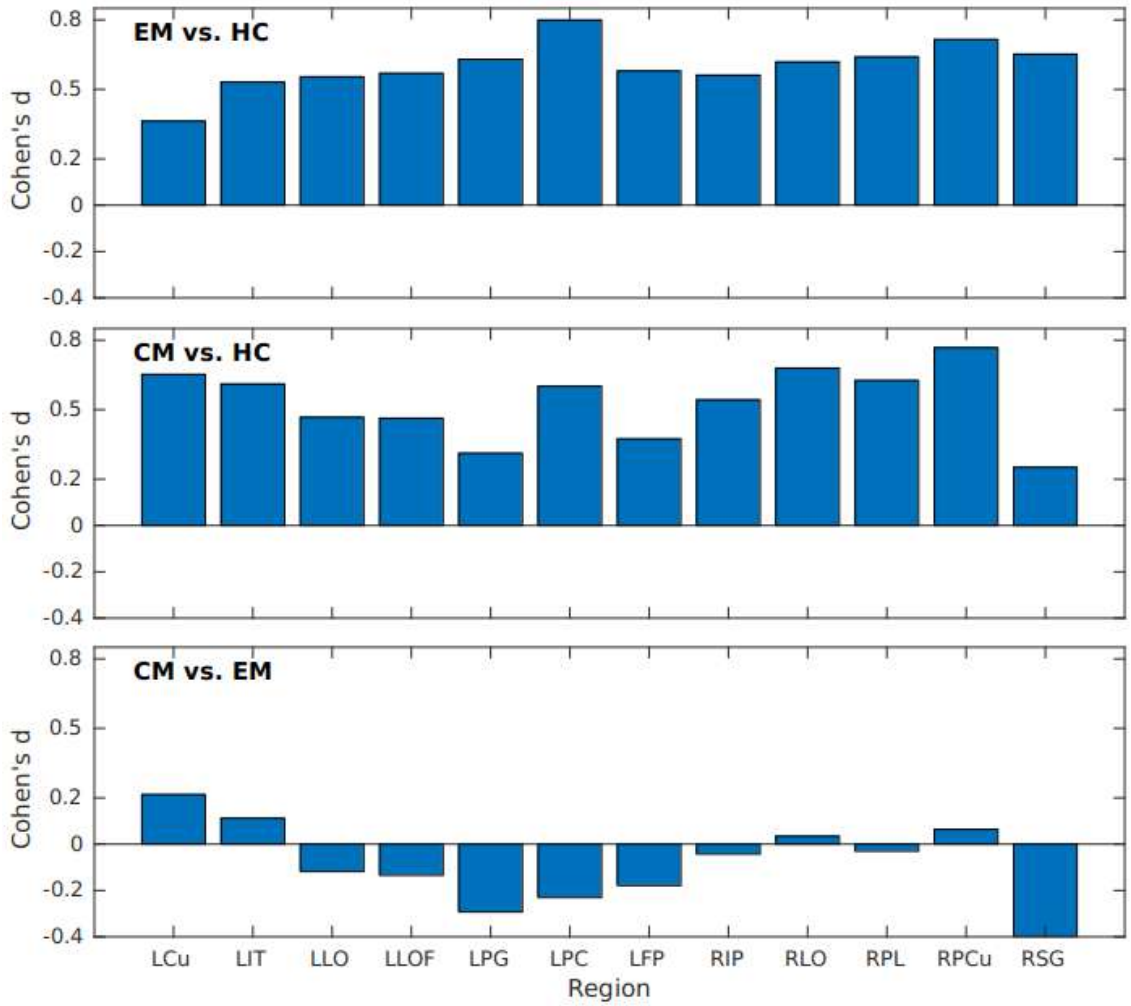


**Supplementary Figure 2**. Cohen's d cortical curvature bar plots of regions where differences between healthy controls, episodic migraine and chronic migraine patients appeared. Region abbreviations can be seen in Supplementary Table 3.

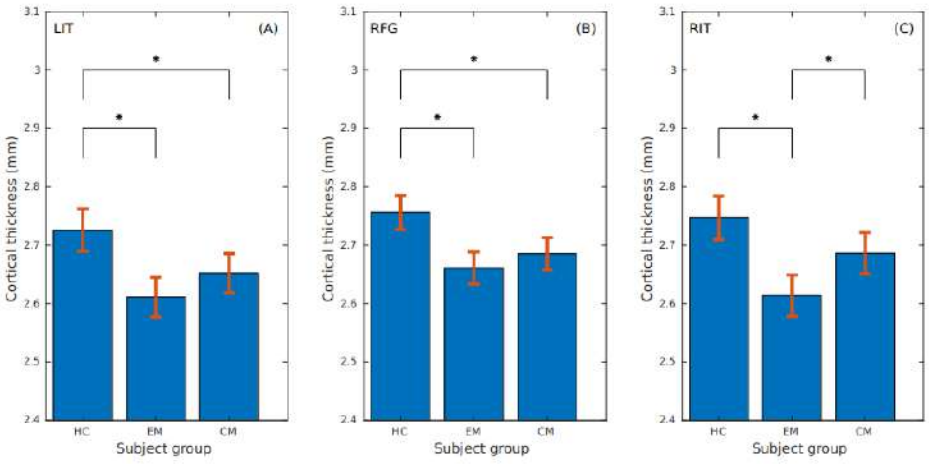


**Supplementary Figure 3**. Cortical thickness bar plots of regions where differences between healthy controls, episodic migraine and chronic migraine patients appeared. P-values of ANOVA or Kruskal-Wallis tests were lower than 0.001 in these regions. (A) LIT = left inferior temporal gyrus; (B) RFG = right fusiform gyrus; (C) RIT = right inferior temporal gyrus.

**Supplementary Table 4**. Cortical thickness comparison between different brain regions in healthy controls (HC), episodic migraine (EM) and chronic migraine (CM) patients.

| Region | HC average thickness | EM average thickness | CM average thickness | EM vs. HC p-value | CM vs. HC p-value | CM vs. EM p-value | p∗ |
|---|---|---|---|---|---|---|---|
| Left banks of the superior temporal sulcus | 2.494 ± 0.167 | 2.426 ± 0.157 | 2.385 ± 0.157 | 0.067 | **0.001** | 0.36 | 0.002 |
| Left caudal middle frontal gyrus | 2.517 ± 0.150 | 2.434 ± 0.133 | 2.464 ± 0.161 | **0.010** | 0.14 | 0.54 | 0.014 |
| Left fusiform gyrus | 2.741 ± 0.133 | 2.654 ± 0.137 | 2.677 ± 0.135 | **0.003** | **0.036** | 0.65 | 0.003 |
| Left middle temporal gyrus | 2.788 ± 0.152 | 2.695 ± 0.177 | 2.692 ± 0.177 | **0.010** | **0.008** | 1 | 0.004 |
| Left paracentral lobule | 2.377 ± 0.151 | 2.308 ± 0.121 | 2.305 ± 0.147 | **0.027** | **0.019** | 0.99 | 0.012 |
| Left precentral gyrus | 2.575 ± 0.127 | 2.500 ± 0.137 | 2.517 ± 0.142 | **0.011** | 0.069 | 0.77 | 0.012 |
| Left superior temporal gyrus | 2.802 ± 0.155 | 2.716 ± 0.173 | 2.722 ± 0.151 | **0.013** | **0.025** | 0.98 | 0.009 |
| Left supramarginal gyrus | 2.542 ± 0.121 | 2.473 ± 0.138 | 2.494 ± 0.114 | **0.012** | 0.11 | 0.64 | 0.015 |
| Right middle temporal gyrus | 2.858 ± 0.163 | 2.771 ± 0.154 | 2.765 ± 0.188 | **0.021** | **0.012** | 0.98 | 0.008 |
| Right precentral gyrus | 2.549 ± 0.139 | 2.476 ± 0.125 | 2.482 ± 0.163 | **0.021** | **0.039** | 0.97 | 0.015 |

Tukey-Kramer post hoc test was used, where p-values from ANOVA or Kruskal-Wallis test were equal or greater than 0.001. Data are expressed as means ± SD (mm).
∗ p-value for ANOVA or Kruskal-Wallis test.

**Supplementary Table 5**. Cohen's d of cortical thickness measures in regions where significant differences between healthy controls (HC), episodic migraine (EM) and chronic migraine (CM) patients were observed.

| Region | EM vs. HC Cohen's d | CM vs. HC Cohen's d | CM vs. EM Cohen's d |
|---|---|---|---|
| Left banks of the superior temporal sulcus (LbSTS) | -0.42 | **-0.68** | -0.26 |
| Left caudal middle frontal gyrus (LCMF) | **-0.59** | -0.34 | 0.20 |
| Left fusiform gyrus (LFG) | **-0.64** | **-0.74** | 0.16 |
| Left inferior temporal gyrus (LIT) | **-0.74** | -0.49 | 0.26 |
| Left middle temporal gyrus (LMT) | **-0.58** | **-0.58** | -0.01 |
| Left paracentral lobule (LPL) | **-0.51** | -0.49 | -0.02 |
| Left precentral gyrus (LPrc) | **-0.57** | -0.42 | 0.13 |
| Left superior temporal gyrus (LST) | **-0.53** | **-0.52** | 0.04 |
| Left supramarginal gyrus (LSG) | **-0.53** | -0.41 | 0.17 |
| Right fusiform gyrus (RFG) | **-0.79** | **-0.55** | 0.18 |
| Right inferior temporal gyrus (RIT) | **-0.88** | -0.36 | 0.44 |
| Right middle temporal gyrus (RMT) | **-0.55** | **-0.52** | -0.03 |
| Right precentral gyrus (RPrc) | **-0.55** | -0.44 | 0.04 |

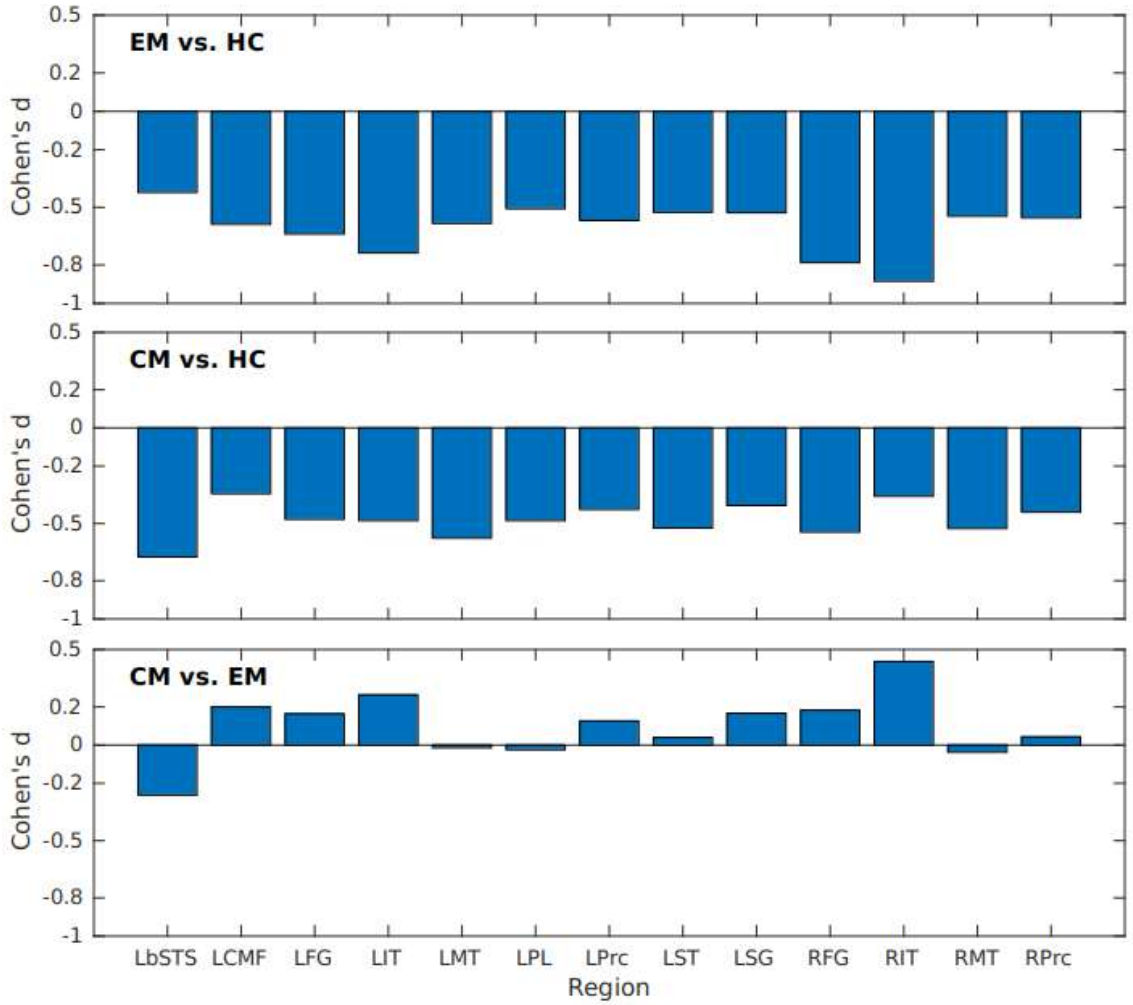


**Supplementary Figure 4**. Cohen's d cortical thickness bar plots of regions where differences between healthy controls, episodic migraine and chronic migraine patients appeared. Region abbreviations can be seen in Supplementary Table 5.

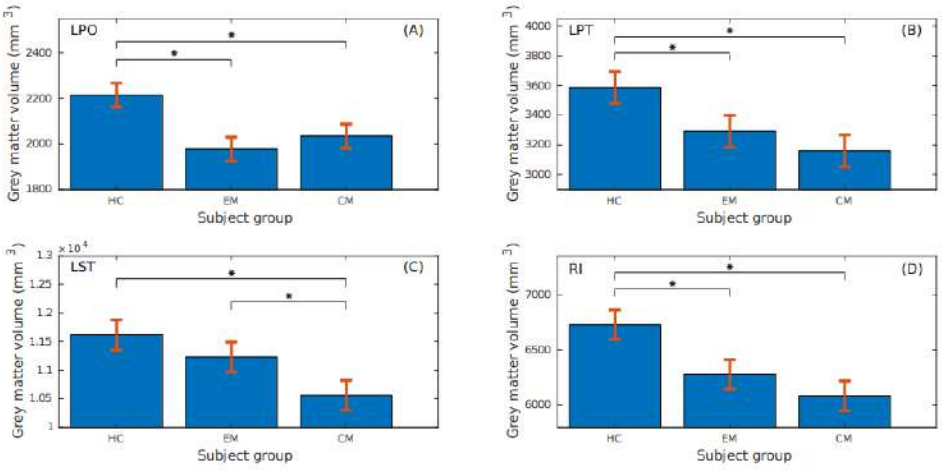


**Supplementary Figure 5**. Grey matter volume bar plots of regions where differences between healthy controls, episodic migraine and chronic migraine patients appeared. P-values of ANCOVA tests were lower than 0.001 in these regions. (A) LPO = left pars orbitalis; (B) LPT = left pars triangularis; (C) LST = left superior temporal gyrus; (D) RI = right insula.

**Supplementary Table 6**. Grey matter volume comparison between different left hemisphere brain regions in healthy controls (HC), episodic migraine (EM) and chronic migraine (CM) patients.

| Region | HC grey matter volume | EM grey matter volume | CM grey matter volume | EM vs. HC p-value | CM vs. HC p-value | CM vs. EM p-value | p∗ |
|---|---|---|---|---|---|---|---|
| Inferior temporal gyrus | 10,054 ± 1,577 | 9,440 ± 1,436 | 9,214 ± 1,270 | **0.041** | **0.003** | 0.63 | 0.003 |
| Lateral occipital cortex | 10,780 ± 1,629 | 10,314 ± 1,437 | 9,980 ± 1,355 | 0.14 | **0.004** | 0.34 | 0.006 |
| Lateral orbitofrontal cortex | 7,167 ± 886 | 6,970 ± 721 | 6,735 ± 777 | 0.30 | **0.004** | 0.17 | 0.006 |
| Middle temporal gyrus | 9,975 ± 1,406 | 9,563 ± 1,450 | 9,141 ± 1,120 | 0.18 | **0.001** | 0.15 | 0.002 |
| Precentral gyrus | 12,700 ± 1,609 | 12,380 ± 1,474 | 11,971 ± 1,124 | 0.38 | **0.008** | 0.20 | 0.012 |
| Precuneus cortex | 9,138 ± 1,351 | 8,889 ± 1,194 | 8,512 ± 1,032 | 0.47 | **0.010** | 0.17 | 0.013 |
| Superior frontal gyrus | 21,088 ± 3,147 | 20,036 ± 2,115 | 19,692 ± 2,116 | **0.029** | **0.002** | 0.67 | 0.002 |
| Supramarginal gyrus | 10,253 ± 1,679 | 9,858 ± 1,374 | 9,373 ± 1,322 | 0.28 | **0.002** | 0.13 | 0.003 |
| Frontal pole | 822 ± 164 | 766 ± 149 | 741 ± 163 | 0.11 | **0.010** | 0.61 | 0.013 |
| Insula | 6,576 ± 795 | 6,466 ± 771 | 6,211 ± 599 | 0.62 | **0.007** | 0.073 | 0.007 |

Tukey-Kramer post hoc test was used, where p-values from ANCOVA test were equal or greater than 0.001. Reported regions in this Table show only significant differences between healthy controls and one or both groups of patients. Data are expressed as means ± SD ($mm^3$) and p-values are adjusted by the effect of total intracranial volume.

∗ p-value for ANCOVA test adjusted by the effect of total intracranial volume.

**Supplementary Table 7**. Grey matter volume comparison between different right hemisphere cortical and subcortical regions in healthy controls (HC), episodic migraine (EM) and chronic migraine (CM) patients.

| Region | HC grey matter volume | EM grey matter volume | CM grey matter volume | EM vs. HC p-value | CM vs. HC p-value | CM vs. EM p-value | p∗ |
|---|---|---|---|---|---|---|---|
| Fusiform gyrus | 9,209 ± 1,254 | 8,881 ± 1,161 | 8,394 ± 1,104 | 0.30 | < **0.001** | 0.065 | 0.001 |
| Lateral occipital cortex | 11,013 ± 1,571 | 10,434 ± 1,384 | 10,286 ± 1,436 | **0.033** | **0.005** | 0.79 | 0.005 |
| Pars orbitalis | 2,537 ± 394 | 2,331 ± 383 | 2,377 ± 330 | **0.004** | **0.034** | 0.74 | 0.004 |
| Precentral gyrus | 12,702 ± 1,745 | 12,293 ± 1,745 | 11,857 ± 1,380 | 0.25 | **0.004** | 0.20 | 0.005 |
| Superior frontal gyrus | 20,234 ± 3,136 | 19,440 ± 2,112 | 19,083 ± 2,049 | 0.12 | **0.012** | 0.63 | 0.015 |
| Frontal pole | 1,016 ± 144 | 923 ± 173 | 950 ± 169 | **0.005** | 0.061 | 0.61 | 0.005 |
| Putamen | 4,921 ± 719 | 5,314 ± 687 | 5,019 ± 683 | **0.010** | 0.74 | 0.064 | 0.010 |
| Pallidum | 1,718 ± 216 | 1,628 ± 244 | 1,628 ± 199 | **0.027** | **0.027** | 1 | 0.013 |
| Nucleus Accumbens | 590 ± 129 | 661 ± 109 | 659 ± 112 | **0.005** | **0.006** | 1 | 0.002 |

Tukey-Kramer post hoc test was used, where p-values from ANCOVA test were equal or greater than 0.001. Reported regions in this Table show only significant differences between healthy controls and one or both groups of patients. Data are expressed as means ± SD ($mm^3$) and p-values are adjusted by the effect of total intracranial volume.

∗ p-value for ANCOVA test adjusted by the effect of total intracranial volume.

**Supplementary Table 8**. Grey matter volume comparison between different brain regions in healthy controls (HC), episodic migraine (EM) and chronic migraine (CM) patients.

| Region | HC grey matter volume | EM grey matter volume | CM grey matter volume | EM vs. HC p-value | CM vs. HC p-value | CM vs. EM p-value | p∗ |
|---|---|---|---|---|---|---|---|
| Left banks of the superior temporal sulcus | 2,297 ± 429 | 2,374 ± 385 | 2,135 ± 0.346 | 0.54 | 0.071 | **0.003** | 0.004 |
| Left transverse temporal cortex | 1,144 ± 236 | 1,154 ± 207 | 1,046 ± 228 | 0.97 | **0.043** | **0.020** | 0.013 |
| Right isthmus-cingulate cortex | 2,366 ± 419 | 2,415 ± 382 | 2,201 ± 299 | 0.73 | **0.034** | **0.003** | 0.003 |
| Right middle temporal gyrus | 11,013 ± 1,691 | 10,833 ± 1,387 | 10,204 ± 1,292 | 0.76 | **0.005** | **0.034** | 0.004 |
| Right superior temporal gyrus | 10,917 ± 1,510 | 10,688 ± 1,328 | 10,182 ± 981 | 0.54 | **0.002** | **0.045** | 0.003 |

Tukey-Kramer post hoc test was used, where p-values from ANCOVA test were equal or greater than 0.001. Reported regions in this Table show significant differences between EM and CM. Data are expressed as means ± SD ($mm^3$) and p-values are adjusted by the effect of total intracranial volume.

∗ p-value for ANCOVA test adjusted by the effect of total intracranial volume.

**Supplementary Table 9**. Cohen's d of left hemisphere grey matter volume measures in regions where significant differences between healthy controls (HC), episodic migraine (EM) and chronic migraine (CM) patients were observed.

| Region | EM vs. HC Cohen's d | CM vs. HC Cohen's d | CM vs. EM Cohen's d |
|---|---|---|---|
| Banks of the superior temporal sulcus (Lb-STS) | 0.19 | -0.42 | **-0.65** |
| Inferior temporal gyrus (LIT) | -0.41 | **-0.59** | -0.17 |
| Lateral occipital cortex (LLO) | -0.30 | **-0.54** | -0.24 |
| Lateral orbital frontal cortex (LLOF) | -0.25 | **-0.52** | -0.31 |
| Middle temporal gyrus (LMT) | -0.29 | **-0.66** | -0.33 |
| Pars orbitalis (LPO) | **-0.77** | **-0.53** | 0.19 |
| Pars triangularis (LPT) | **-0.52** | **-0.75** | -0.25 |
| Precentral gyrus (LPrc) | -0.21 | **-0.53** | -0.31 |
| Precuneus cortex (LPcu) | -0.20 | **-0.52** | -0.34 |
| Superior frontal gyrus (LSF) | -0.40 | **-0.53** | -0.16 |
| Superior temporal gyrus (LST) | -0.25 | **-0.74** | **-0.51** |
| Supramarginal gyrus (LSG) | -0.26 | **-0.59** | -0.36 |
| Frontal pole (LFP) | -0.36 | **-0.50** | -0.16 |
| Transverse temporal cortex (LTT) | 0.04 | -0.43 | **-0.50** |
| Insula (LI) | -0.14 | **-0.52** | -0.37 |
| Cerebellum (LCe) | -0.47 | **-0.77** | -0.23 |

**Supplementary Table 10**. Cohen's d of right hemisphere grey matter volume measures in regions where significant differences between healthy controls (HC), episodic migraine (EM) and chronic migraine (CM) patients were observed.

| Region | EM vs. HC Cohen's d | CM vs. HC Cohen's d | CM vs. EM Cohen's d |
|---|---|---|---|
| Fusiform gyrus (RFG) | -0.27 | **-0.69** | -0.43 |
| Isthmus cingulate gyrus (RIC) | 0.12 | -0.46 | **-0.62** |
| Lateral occipital cortex (RLO) | -0.39 | -0.48 | -0.11 |
| Middle temporal gyrus (RMT) | -0.12 | **-0.54** | -0.47 |
| Pars orbitalis (RPO) | **-0.53** | -0.44 | 0.13 |
| Precentral gyrus (RPrc) | -0.27 | **-0.54** | -0.32 |
| Superior frontal gyrus (RSF) | -0.30 | -0.44 | -0.17 |
| Superior temporal gyrus (RST) | -0.16 | **-0.58** | -0.43 |
| Frontal pole (RFP) | **-0.58** | -0.42 | 0.16 |
| Insula (RI) | **-0.55** | **-0.87** | -0.30 |
| Cerebellum (RCe) | -0.47 | **-0.77** | -0.23 |
| Putamen (RPu) | **0.56** | 0.14 | -0.43 |
| Pallidum (RPa) | -0.39 | -0.43 | 0.00 |
| Nucleus accumbens (RNAc) | **0.59** | **0.57** | -0.01 |

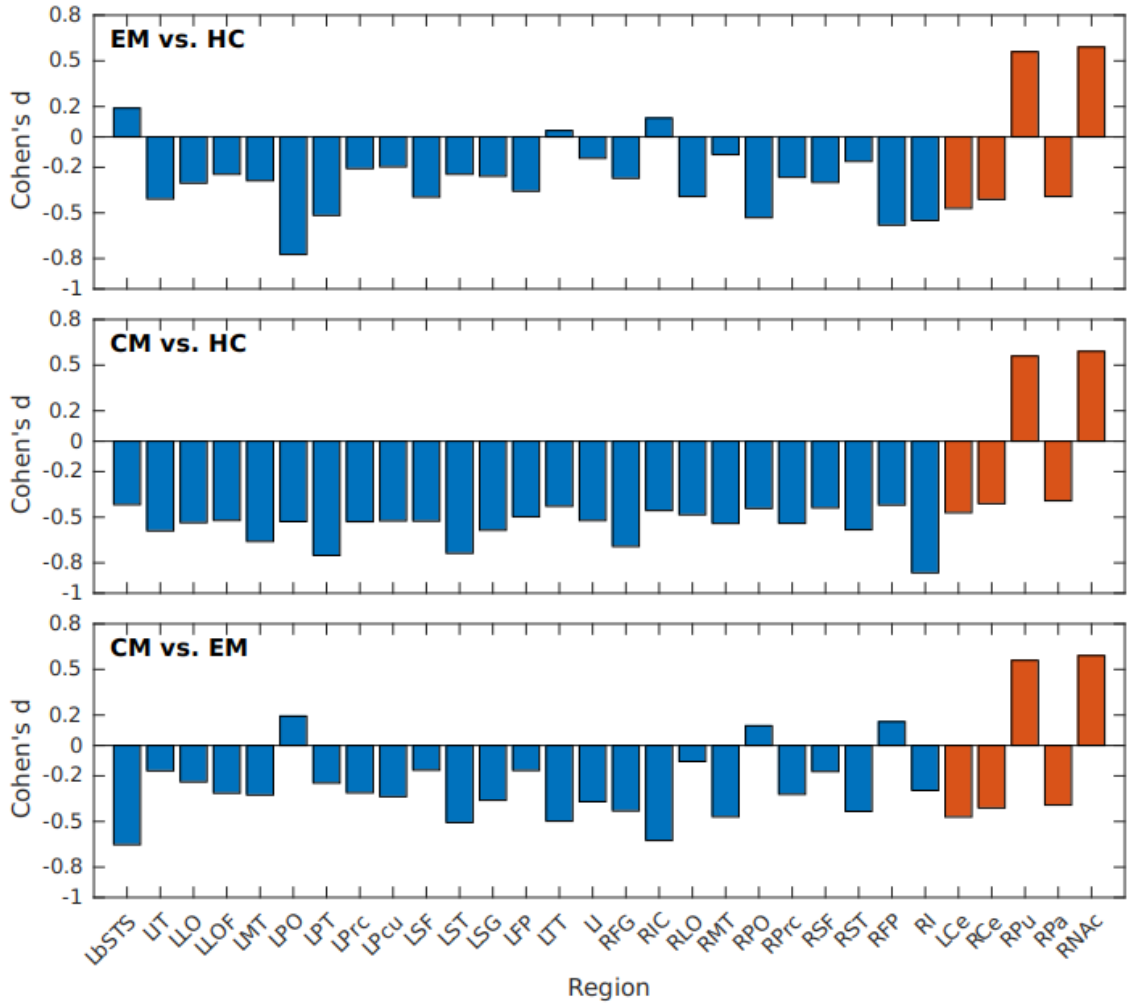


**Supplementary Figure 6**. Cohen's d grey matter volume bar plots of regions where differences between healthy controls, episodic migraine and chronic migraine patients appeared. Blue bars show cortical regions and orange bars subcortical regions. Region abbreviations can be seen in Supplementary Tables 9 and 10.

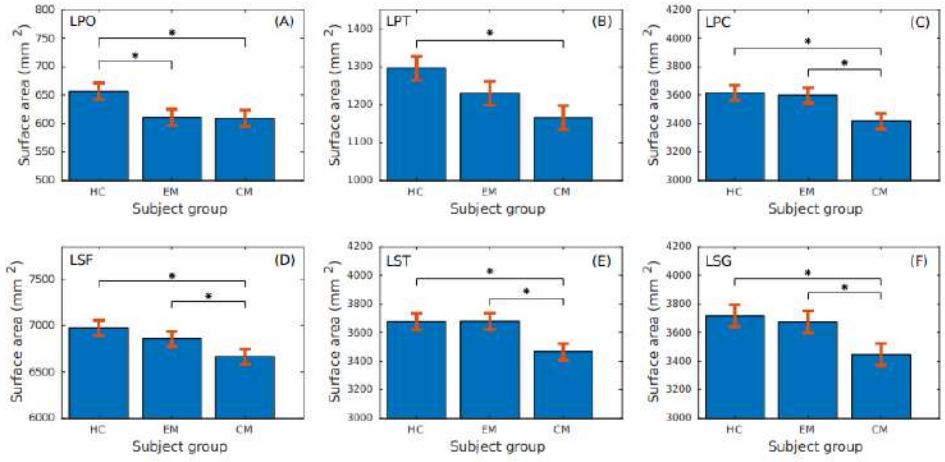


**Supplementary Figure 7**. Surface area bar plots of left hemisphere regions where differences between healthy controls, episodic migraine and chronic migraine patients appeared. P-values of ANCOVA tests were lower than 0.001 in these regions. (A) LPO= left pars orbitalis; (B) LPT = left pars triangularis; (C) LPC = left precuneus cortex; (D) LSF = left superior frontal gyrus; (E) LST = left superior temporal gyrus; (F) LSG = left supramarginal gyrus.

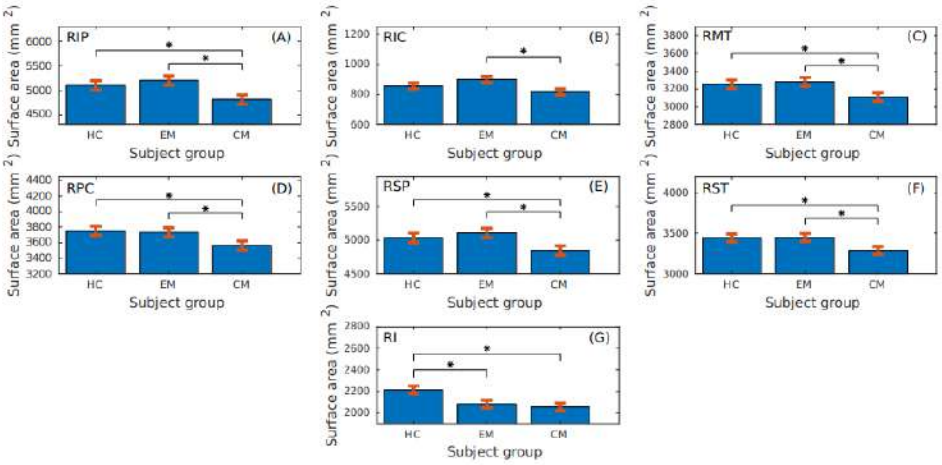


**Supplementary Figure 8**. Surface area bar plots of right hemisphere regions where differences between healthy controls, episodic migraine and chronic migraine patients appeared. P-values of ANCOVA tests were lower than 0.001 in these regions. (A) RIP = right inferior parietal gyrus; (B) RIC = right isthmus cingulate cortex; (C) RMT = right middle temporal gyrus; (D) RPC = right precuneus cortex; (E) RSP = right superior parietal cortex; (F) RST = right superior temporal gyrus; (G) RI = right insula.

**Supplementary Table 11**. Cortical surface area comparison between different brain regions in healthy controls (HC), episodic migraine (EM) and chronic migraine (CM) patients.

| Region | HC surface area | EM surface area | CM surface area | EM vs. HC p-value | CM vs. HC p-value | CM vs. EM p-value | p∗ |
|---|---|---|---|---|---|---|---|
| Left lateral orbital frontal cortex | 2,512 ± 287 | 2,468 ± 244 | 2,402 ± 276 | 0.30 | < **0.001** | 0.059 | 0.001 |
| Right cuneus cortex | 1,513 ± 228 | 1,465 ± 213 | 1,440 ± 181 | 0.10 | **0.013** | 0.69 | 0.015 |
| Right medial orbital frontal cortex | 1,803 ± 179 | 1,731 ± 207 | 1,730 ± 190 | **0.017** | **0.015** | 1 | 0.007 |
| Right frontal pole | 291 ± 37 | 269 ± 42 | 272 ± 40 | **0.004** | **0.014** | 0.92 | 0.003 |

Tukey-Kramer post hoc test was used, where p-values from ANCOVA test were equal or greater than 0.001. Reported regions in this Table show only significant differences between healthy controls and one or both groups of patients. Data are expressed as means ± SD ($mm^2$) and p-values are adjusted by the effect of total surface area.

∗ p-value for ANCOVA test adjusted by the effect of total surface area.

**Supplementary Table 12**. Cortical surface area comparison between different left hemisphere brain regions in healthy controls (HC), episodic migraine (EM) and chronic migraine (CM) patients.

| Region | HC surface area | EM surface area | CM surface area | EM vs. HC p-value | CM vs. HC p-value | CM vs. EM p-value | p∗ |
|---|---|---|---|---|---|---|---|
| Banks of the superior temporal sulcus | 948 ± 162 | 994 ± 134 | 910 ± 118 | 0.11 | 0.24 | < **0.001** | 0.001 |
| Inferior parietal cortex | 4,309 ± 571 | 4,358 ± 559 | 4,133 ± 494 | 0.80 | 0.059 | **0.009** | 0.008 |
| Inferior temporal gyrus | 3,174 ± 419 | 3,136 ± 388 | 3,000 ± 359 | 0.77 | **0.006** | **0.034** | 0.005 |
| Lateral occipital cortex | 4,657 ± 644 | 4,612 ± 560 | 4,397 ± 541 | 0.84 | **0.005** | **0.021** | 0.003 |
| Postcentral gyrus | 3,896 ± 474 | 3,975 ± 418 | 3,806 ± 405 | 0.23 | 0.15 | **0.001** | 0.002 |
| Posterior-cingulate cortex | 1,095 ± 158 | 1,128 ± 165 | 1,059 ± 139 | 0.31 | 0.25 | **0.006** | 0.009 |
| Precentral gyrus | 4,550 ± 568 | 4,572 ± 398 | 4,413 ± 415 | 0.91 | **0.03** | **0.01** | 0.008 |
| Rostral middle frontal gyrus | 5,387 ± 718 | 5,430 ± 662 | 5,197 ± 735 | 0.85 | **0.042** | **0.007** | 0.006 |
| Transverse temporal cortex | 429 ± 67 | 447 ± 63 | 410 ± 64 | 0.19 | 0.20 | **0.001** | 0.002 |

Tukey-Kramer post hoc test was used, where p-values from ANCOVA test were equal or greater than 0.001. Reported regions in this Table show significant differences between EM and CM. Data are expressed as means ± SD ($mm^2$) and p-values are adjusted by the effect of total surface area.
∗ p-value for ANCOVA test adjusted by the effect of total surface area.

**Supplementary Table 13**. Cortical surface area comparison between different right hemisphere brain regions in healthy controls (HC), episodic migraine (EM) and chronic migraine (CM) patients.

| Region | HC surface area | EM surface area | CM surface area | EM vs. HC p-value | CM vs. HC p-value | CM vs. EM p-value | p∗ |
|---|---|---|---|---|---|---|---|
| Banks of the superior temporal sulcus | 873 ± 135 | 910 ± 138 | 850 ± 95 | 0.15 | 0.48 | **0.007** | 0.009 |
| Fusiform gyrus | 2,992 ± 397 | 3,009 ± 383 | 2,841 ± 351 | 0.94 | **0.009** | **0.002** | 0.001 |
| Posterior-cingulate cortex | 1,154 ± 194 | 1,128 ± 172 | 1,071 ± 153 | 0.51 | **0.002** | **0.042** | 0.002 |
| Precentral gyrus | 4,604 ± 571 | 4,593 ± 414 | 4,445 ± 464 | 0.98 | **0.020** | **0.027** | 0.010 |
| Rostral middle frontal gyrus | 5,564 ± 782 | 5,634 ± 752 | 5,348 ± 714 | 0.67 | **0.028** | **0.002** | 0.002 |
| Superior frontal gyrus | 6,685 ± 1,003 | 6,639 ± 648 | 6,453 ± 701 | 0.83 | **0.010** | **0.043** | 0.008 |
| Supramarginal gyrus | 3,411 ± 481 | 3,408 ± 409 | 3,252 ± 433 | 1 | **0.031** | **0.030** | 0.014 |
| Transverse temporal cortex | 315 ± 48 | 326 ± 46 | 305 ± 45 | 0.30 | 0.41 | **0.010** | 0.014 |

Tukey-Kramer post hoc test was used, where p-values from ANCOVA test were equal or greater than 0.001. Reported regions in this Table show significant differences between EM and CM. Data are expressed as means ± SD ($mm^2$) and p-values are adjusted by the effect of total surface area.
∗ p-value for ANCOVA test adjusted by the effect of total surface area.

**Supplementary Table 14**. Cohen's d of left hemisphere cortical surface area measures in regions where significant differences between healthy controls (HC), episodic migraine (EM) and chronic migraine (CM) patients were observed.

| Region | EM vs. HC Cohen's d | CM vs. HC Cohen's d | CM vs. EM Cohen's d |
|---|---|---|---|
| Banks of the superior temporal sulcus (Lb-STS) | 0.31 | -0.26 | **-0.66** |
| Inferior parietal cortex (LIP) | 0.09 | -0.33 | -0.43 |
| Inferior temporal gyrus (LIT) | -0.09 | -0.45 | -0.36 |
| Lateral occipital cortex (LLO) | -0.08 | -0.44 | -0.39 |
| Lateral orbital frontal cortex (LLOF) | -0.16 | -0.39 | -0.25 |
| Pars orbitalis (LPO) | **-0.54** | **-0.51** | -0.02 |
| Pars triangularis (LPT) | -0.34 | **-0.68** | -0.38 |
| Postcentral gyrus (LPG) | 0.18 | -0.20 | -0.41 |
| Posterior division of the cingulate cortex (LPC) | 0.20 | -0.24 | -0.45 |
| Precentral gyrus (LPrc) | 0.05 | -0.28 | -0.39 |
| Precuneus cortex (LPcu) | -0.04 | -0.44 | -0.43 |
| Rostral middle frontal gyrus (LRMF) | 0.06 | -0.26 | -0.33 |
| Superior frontal gyrus (LSF) | -0.13 | -0.35 | -0.29 |
| Superior temporal gyrus (LST) | 0.00 | -0.48 | **-0.52** |
| Supramarginal gyrus (LSG) | -0.07 | -0.49 | -0.46 |
| Transverse temporal cortex (LTT) | 0.29 | -0.28 | **-0.58** |

**Supplementary Table 15**. Cohen's d of right hemisphere cortical surface area measures in regions where significant differences between healthy controls (HC), episodic migraine (EM) and chronic migraine (CM) patients were observed.

| Region | EM vs. HC Cohen's d | CM vs. HC Cohen's d | CM vs. EM Cohen's d |
|---|---|---|---|
| Banks of the superior temporal sulcus (Rb-STS) | 0.27 | -0.20 | **-0.51** |
| Cuneus cortex (RCu) | -0.30 | -0.45 | -0.13 |
| Fusiform gyrus (RFG) | 0.04 | -0.40 | -0.46 |
| Inferior parietal cortex (RIP) | 0.14 | -0.44 | **-0.64** |
| Isthmus cingulate gyrus (RIC) | 0.33 | -0.31 | **-0.65** |
| Medial orbital frontal cortex (RMOF) | -0.37 | -0.39 | 0.00 |
| Middle temporal gyrus (RMT) | 0.06 | -0.36 | -0.47 |
| Posterior division of the cingulate cortex (RPC) | -0.14 | -0.48 | -0.35 |
| Precentral gyrus (RPrc) | -0.02 | -0.31 | -0.34 |
| Precuneus cortex (RPcu) | -0.05 | -0.40 | -0.37 |
| Rostral middle frontal gyrus (RRMF) | 0.09 | -0.29 | -0.39 |
| Superior frontal gyrus (RSF) | -0.06 | -0.27 | -0.28 |
| Superior parietal cortex (RSP) | 0.13 | -0.34 | **-0.53** |
| Superior temporal gyrus (RST) | 0.02 | -0.41 | -0.48 |
| Supramarginal gyrus (RSG) | -0.01 | -0.35 | -0.37 |
| Frontal pole (RFP) | **-0.55** | **-0.50** | 0.06 |
| Transverse temporal cortex (RTT) | 0.25 | -0.20 | -0.46 |
| Insula (RI) | **-0.50** | **-0.62** | -0.13 |

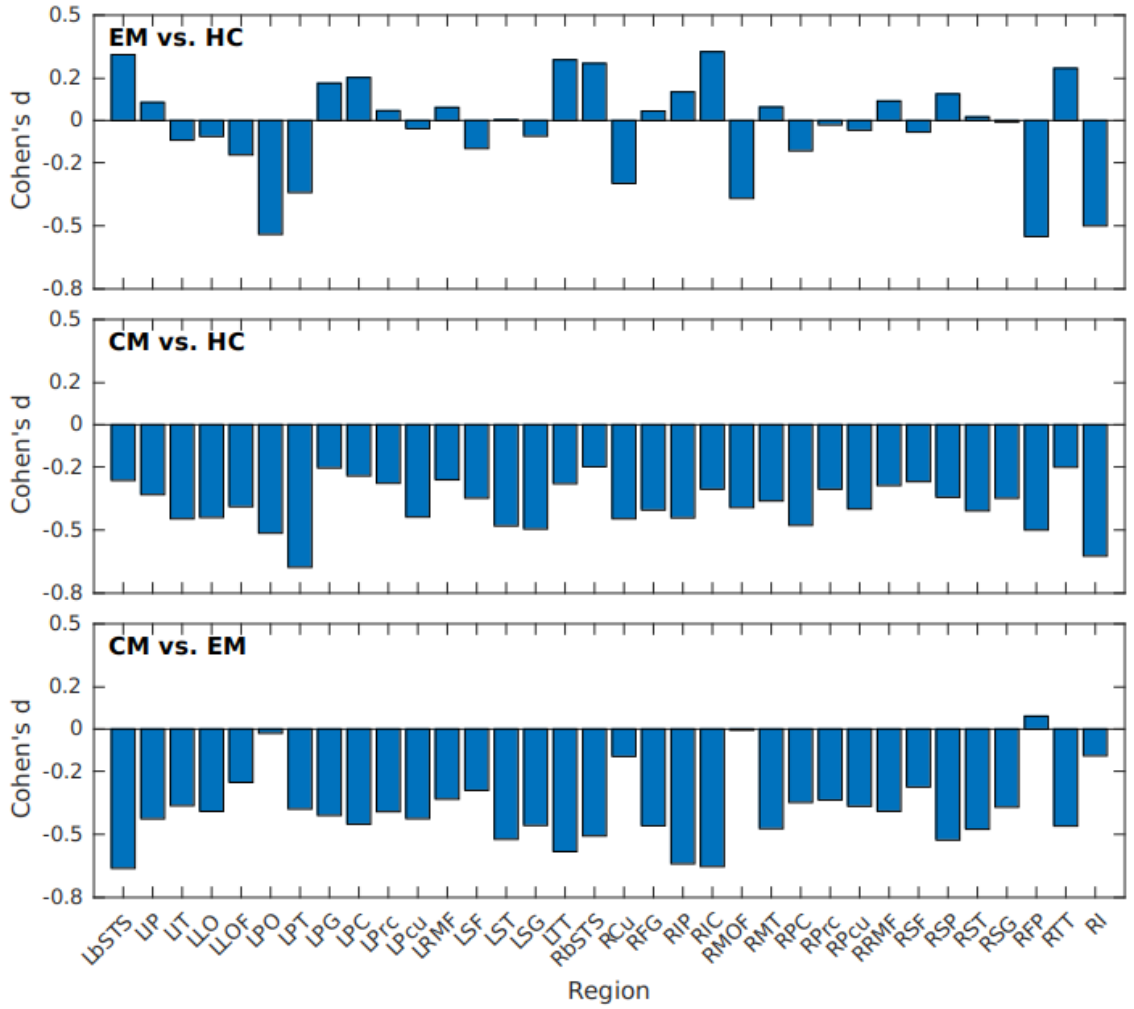


**Supplementary Figure 9**. Cohen's d cortical surface area bar plots of regions where differences between healthy controls, episodic migraine and chronic migraine patients appeared. Region abbreviations can be seen in Supplementary Tables 14 and 15.

# 1.8. Appendix

In this section, ANOVA/Kruskal-Wallis/ANCOVA results that revealed statistically significant differences after FDR correction for multiple comparisons ($p \geq 0.0154$) but did not reach $p < 0.001$ are reported. Comparisons with $p < 0.001$ are reported in the Results section.

Regarding cortical curvature, results with p-values equal or greater than 0.001 (but still statistically significant) showed that both EM and CM had increased cortical curvature compared to HC in the left inferior temporal gyrus ($p = 0.003$), left lateral occipital cortex ($p = 0.007$) and right inferior parietal cortex ($p = 0.005$). No differences between both groups of migraine patients were found.

Differences in cortical thickness with $0.001 \leq p \leq 0.0154$ indicated decreased cortical thickness in both EM and CM with respect to HC in the left fusiform gyrus ($p = 0.003$), bilateral middle temporal gyrus ($p = 0.004$ for left hemisphere, and $p = 0.008$ for right), left paracentral lobule ($p = 0.012$), left superior temporal gyrus ($p = 0.009$) and right precentral gyrus ($p = 0.015$).

Analysing grey matter volume, significant differences with $p \geq 0.001$ were found in decreased volume in both EM and CM compared to HC in the left inferior temporal gyrus ($p = 0.003$), left superior frontal gyrus ($p = 0.006$), right lateral occipital cortex ($p = 0.005$), right pars orbitalis ($p = 0.004$) and right pallidum ($p = 0.013$). Also, decreased grey matter volume in CM compared to EM and HC was observed in the left transverse temporal cortex ($p = 0.013$), right isthmus cingulate cortex ($p = 0.003$), right middle temporal gyrus ($p = 0.004$) and right superior temporal gyrus ($p = 0.003$), and only compared to EM in the left banks of the superior temporal sulcus ($p = 0.004$). Increased grey matter volume in EM compared to HC was observed in the right putamen ($p = 0.010$) and in both groups of migraine patients compared to HC in the right nucleus accumbens ($p = 0.002$).

Regarding cortical surface area, significant differences with $p \geq 0.001$ showed both groups of migraine patients having decreased surface area compared to HC in the right medial orbital frontal cortex ($p = 0.007$) and right frontal pole ($p = 0.003$), and only in CM compared to HC in the left lateral orbital frontal cortex ($p = 0.001$) and right cuneus cortex ($p = 0.015$). Also, decreased surface area in CM compared to EM and HC was observed in 10 regions, and only compared to EM in seven more regions. The 10 regions with significant differences in CM compared to EM and HC were the left inferior temporal gyrus ($p = 0.005$), left lateral occipital cortex ($p = 0.003$), left precentral gyrus ($p = 0.008$), left rostral middle frontal gyrus ($p = 0.006$), right fusiform gyrus ($p = 0.001$), right posterior division of the cingulate cortex ($p = 0.002$), right precentral gyrus ($p = 0.010$), right rostral middle frontal gyrus ($p = 0.002$), right superior frontal gyrus ($p = 0.008$) and right supramarginal gyrus ($p = 0.014$). The seven regions with significant differences in CM compared to EM were the left banks of the superior temporal sulcus ($p = 0.001$), left inferior parietal cortex ($p = 0.008$), left postcentral gyrus ($p = 0.002$), left posterior division of the cingulate cortex ($p = 0.009$), left transverse temporal cortex ($p = 0.002$), right banks of the superior temporal sulcus ($p = 0.009$) and right transverse temporal cortex ($p = 0.014$).

*Chapter 2*

# *Contribution 2: White matter changes in chronic and episodic migraine: a diffusion tensor imaging study*

**Published as**:

*Planchuelo-Gómez, Á.[1], García-Azorín, D.[2], Guerrero, Á.L.[2,3,4], Aja-Fernández, S.[1], Rodríguez, M.[5] and de Luis-García, R[1] (2020). White matter changes in chronic and episodic migraine: a diffusion tensor imaging study. The Journal of Headache and Pain, 21(1):1. doi: 10.1186/s10194-019-1071-3.*

1. Imaging Processing Laboratory, Universidad de Valladolid, Valladolid, Spain
2. Headache Unit, Department of Neurology, Hospital Clínico Universitario de Valladolid, Valladolid, Spain
3. Institute for Biomedical Research of Salamanca (IBSAL), Salamanca, Spain
4. Department of Medicine, Universidad de Valladolid, Valladolid, Spain
5. Department of Radiology, Hospital Clínico Universitario de Valladolid, Valladolid, Spain

The purpose of this study was the analysis of whole-brain white matter regions using DTI-based parameters in patients with CM and EM via TBSS, a method frequently used in the literature. This research supposed the first study to detect statistically significant differences between CM and EM patients assessing diffusion descriptors in white matter regions.

## Abstract

**Background**: White matter alterations have been observed in patients with migraine. However, no microstructural white matter alterations have been found particularly in episodic or chronic migraine patients, and there is limited research focused on the comparison between these two groups of migraine patients.

**Methods**: Fifty-one healthy controls, 55 episodic migraine patients and 57 chronic migraine patients were recruited and underwent brain T1-weighted and diffusion-weighted MRI acquisition. Using Tract-Based Spatial Statistics (TBSS), fractional anisotropy, mean diffusivity, radial diffusivity and axial diffusivity were compared between the different groups. On the one hand, all migraine patients were compared against healthy controls. On the other hand, patients from each migraine group were compared between them and also against healthy controls. Correlation analysis between clinical features (duration of migraine in years, time from onset of chronic migraine in months, where applicable, and headache and migraine frequency, where applicable) and Diffusion Tensor Imaging measures was performed.

**Results**: Fifty healthy controls, 54 episodic migraine and 56 chronic migraine patients were finally included in the analysis. Significant decreased axial diffusivity ($p < .05$ false discovery rate and by number of contrasts corrected) was found in chronic migraine compared to episodic migraine in 38 white matter regions from the Johns Hopkins University ICBM-DTI-81 White-Matter Atlas. Significant positive correlation was found between time from onset of chronic migraine and mean fractional anisotropy in the bilateral external capsule, and negative correlation between time from onset of chronic migraine and mean radial diffusivity in the bilateral external capsule.

**Conclusions**: These findings suggest global white matter structural differences between episodic migraine and chronic migraine. Patients with chronic migraine could present axonal integrity impairment in the first months of chronic migraine with respect to episodic migraine patients. White matter changes after the onset of chronic migraine might reflect a set of maladaptive plastic changes.


**Keywords**: Migraine, Chronic migraine, Diffusion tensor imaging, Magnetic resonance imaging (MRI), Tract-based spatial statistics

# 2.1. Background

According to the IIIrd edition of the International Classification of Headache Disorders (ICHD-3), patients with Chronic Migraine (CM) suffer from headache during 15 or more days per month for more than 3 months, with at least eight of these days with migrainous characteristics [1]. Between 2 and 3% of migraine patients evolve annually from Episodic Migraine (EM) to CM [2]. Some risk factors have been associated with progression from EM to CM, but the pathophysiological mechanisms of this conversion remain to be elucidated. Moreover, EM and CM could represent either two ranges of the same entity, or two subgroups with distinctive characteristics. Previous review studies have exposed that important distinctions exist along the continuum between EM and CM [3, 4], but it is not clear whether CM is a kind of more frequent EM or a distinct entity.

Magnetic Resonance Imaging (MRI) is one of the most powerful technologies available for the study of the migrainous brain. Among its different modalities, diffusion MRI (dMRI) is particularly well suited for the analysis of possible white matter alterations in migraine. dMRI studies have shown changes affecting the white matter in migraineurs with respect to healthy controls; these changes were mainly observed in

the corpus callosum [5–11], thalamus [7, 8, 12, 13], thalamic radiation [7–9, 14, 15] and cingulate gyrus [9, 10, 15–17].

Some studies using dMRI have focused on migraine with and without aura. Even though significant differences have been found [10, 18], using MRI information it remains unclear whether migraine with and without aura area are actually two distinct entities, the manifestations of the same pathophysiological substrate on two different phenotypes [19, 20], or even whether aura can be better defined as a migraine phase, but not a category such as chronic and episodic migraine [21].

Some other studies have employed dMRI to investigate CM. To the best of our knowledge, however, only one study by Neeb et al. searched for possible differences between patients with EM and CM, not finding any significant differences [22]. Other studies compared chronic migraine patients with healthy controls [16] or mixed EM and CM patients in order to compare migraine patients and controls [14]. Previous studies alternatively used T1-weighted MRI images [23, 24] and functional MRI [25], respectively, to compare possible differences between patients with CM and EM. These studies described reduced grey matter volume in CM compared to EM [23] and more activity in CM compared to EM patients with headaches during the scanning in the anterior hypothalamus [25].

The present study performs a detailed comparison of the white matter in EM, CM and healthy controls over a large cohort of subjects, using dMRI data. We hypothesised that there could be white matter structural differences between CM and EM patients, although no significant differences were found in a previous study [22]. In our study, we included a considerably higher number of patients and controls compared to that study. Our goals are to:

1. Investigate whether there are significant differences between CM and EM, and between these groups and healthy controls. To that end, TBSS [26] was employed as dMRI analysis technique.

2. Examine how white matter descriptors based on dMRI relate to clinical features in migraine patients. To that end, a correlation analysis between dMRI parameters and variables such as duration of migraine and time from onset of CM was performed.

# 2.2. Materials and methods

## *2.2.1.* ***Participants***

We conducted an observational analytic study with a case-control design. The target population included patients with migraine. Patients were firstly screened and recruited from the headache outpatient unit at the Hospital ClÃnico Universitario de Valladolid (Valladolid, Spain), a tertiary centre that receives patients both from specialized care and directly from primary care. Inclusion criteria were: a) Diagnosis of episodic or chronic migraine according to the ICHD-3 beta and ICHD-3 criteria [1, 27]; b) no changes in the situation of episodic or chronic migraine in the previous 3 months; c) agreeing to participate and signing the Informed Consent; d) aged between 18 and 60. We excluded patients with a) high frequency Episodic Migraine, suffering between 10 and 14 headache days per month (to avoid any confusion between high frequency EM and CM [28]); b) other noncraniofacial painful conditions occurring 10 or more days per month; c) known major psychiatric diseases (described in anamnesis or presence of Depression or Anxiety according to Hospital Anxiety and Depression Scale [29]); d) other neurological diseases; e) drug or substance abuse; f) pregnancy or childbearing; g) other headache disorders. All the patients scanned

were preventive naÃ¯ve. Patients were asked to keep a headache diary for 3 months (before inclusion) and were classified as EM when they had less than 10 headaches per month, or CM according to ICHD-3 criteria. Participants with EM were not allowed to have headache days with tension-type headache (TTH) phenotype. No healthy controls (HC) were included if they showed a present or past history of migraine, or if any other neurological or psychiatric condition was present, with the sole exception of infrequent TTH. We used a non-probabilistic sampling method by convenience sampling. Healthy controls balanced for age and sex were recruited through hospital and University colleagues and advertisements in these facilities by convenience sampling and snowball sampling.

For all patients, sociodemographic and clinical data were collected, including the duration of migraine disease (years), headache and migraine frequency (days per month) and time from the onset of chronic migraine (months) when applicable. The intake of symptomatic medication, i.e., combination of analgesics and triptan, was considered to verify if patients fulfilled criteria of acute medication overuse (intake at 10 or more days per month). Presence of aura was drawn.

The local Ethics Committee of Hospital Clínico Universitario de Valladolid approved the study (PI: 14–197). All participants read and signed a written consent form prior to their participation.

### *2.2.2.* ***MRI acquisition***

Images were acquired for migraine patients after at least 24 h from the last migraine attack. High-resolution 3D T1-weighted and diffusion-weighted MRI data were acquired using a Philips Achieva 3 T MRI unit (Philips Healthcare, Best, The Netherlands) with a 32-channel head coil in the MRI facility at the Universidad de Valladolid (Valladolid, Spain).

For the anatomical T1-weighted images, the following acquisition parameters were used: Turbo Field Echo (TFE) sequence, repetition time (TR) = 8.1 ms, echo time (TE) = 3.7 ms, flip angle = 8°, 256 x 256 matrix size, 1 x 1 x 1 $mm^3$ of spatial resolution and 160 slices covering the whole brain.

Diffusion-weighted images (DWI) were acquired using the next parameters: TR = 9000 ms, TE = 86 ms, flip angle = 90°, 61 gradient directions, one baseline volume, b-value = 1000 $s/mm^2$, 128 x 128 matrix size, 2 x 2 x 2 $mm^3$ of spatial resolution and 66 axial slices covering the whole brain.

T1 and diffusion-weighted scans were acquired during the same session, starting with the T1 scan followed by the diffusion-weighted scan, between May 2014 and July 2018. Total acquisition time for each subject was around 18 min.

### *2.2.3.* ***Image processing***

MR images were processed before carrying out the statistical analysis using TBSS [26]. For the TBSS analysis, four Diffusion Tensor Imaging (DTI) measures were obtained: Fractional Anisotropy (FA), Mean Diffusivity (MD), Radial Diffusivity (RD) and Axial Diffusivity (AD). In a nutshell, FA reflects the degree of directionality of water diffusivity, MD is a global measure of water diffusion, RD quantifies the diffusion perpendicular to the principal direction and AD is the diffusion in the main direction of the white matter fibres [30].

Prior to the obtention of the four DTI measures, diverse preprocessing procedures were implemented on the DWI data. Diffusion-weighted images were denoised, using dwidenoise tool from MRtrix [31, 32],

eddy currents and motion corrected, using dwipreproc tool from MRtrix [33], and $B_1$ field inhomogeneity corrected, using dwibiascorrect tool with the -fast option from MRtrix [34, 35].

Once the DWI images were preprocessed, a whole brain mask for each image was generated using dwi2-mask tool from MRtrix [36] and, next, diffusion tensors at each voxel were estimated using the dtifit tool from FSL [37], also obtaining FA, MD and AD maps. RD was manually calculated by obtaining the mean of the second and the third eigenvalues, which were also previously computed with dtifit.

For the TBSS method, all participants'FA images were nonlinearly registered using the FNIRT tool from FSL to a template of the averaged FA images (FMRIB-58) in Montreal Neurological Institute (MNI) space; the FNIRT tool uses a b-spline representation of the registration warp field [38]. After registration, a mean FA image was generated and thinned to create a mean FA skeleton of white matter tracts using a FA value of .2 as threshold to distinguish white from grey matter. Then, each subject's aligned FA images were projected onto the mean FA skeleton. In a similar way, the TBSS process was repeated for MD, AD and RD, using the protocol devoted for non-FA images. To identify the white matter tracts, the Johns Hopkins University ICBM-DTI-81 White-Matter Labels Atlas [39, 40] provided in the FSL toolbox was used. However, this atlas does not cover the whole white matter across brain, so we also employed the Johns Hopkins University White-Matter Tractography Atlas [41], which contains a lower number of tracts but covers areas not included in the other atlas. The minimum volume to consider significant results in a region was set to 30 $mm^3$. It must be noted that, because we use an image of 1 $mm^3$ in the MNI space to identify the regions, the volume in $mm^3$ is equal to the number of voxels. Moreover, when we extract the significant results in a region, we consider all the significant voxels from that region, from one or more clusters.

### *2.2.4.* ***Statistical analysis***

We estimated Sample Size according to Chong and Schwedt, 2015 [14]. Based on the FA results from this study in three major tracts, we calculated a worst possible scenario model with an estimated effect size of difference between groups of .02 (greatest difference between groups) and a variance of .003 (greatest single group variance); a type 1-error rate of 1% and 80% power and anticipating a proportion of 10% of lost patients. The expected sample size was 167 participants.

Kolmogorov-Smirnov and Levene's Test for equality of variances tests were used to assess normality and homogeneity of variance in age and duration of migraine in years. To test for significant differences in the age of the three groups, a one-way ANOVA was used if the null hypothesis in Kolmogorov-Smirnov and Levene tests was not rejected; otherwise, Kruskal-Wallis test was employed. To test for significant gender differences, a chi-square test was used. To compare continuous clinical features between migraine patients (i.e., duration of migraine history in years for both groups of patients and time from onset of chronic migraine in months for chronic migraine patients), a two-tailed unpaired t-test was used if the null hypothesis in Kolmogorov-Smirnov and Levene tests was not rejected; otherwise, Mann- Whitney U test was employed. To compare categorical clinical features between migraine patients, Fisher's exact test was employed.

We executed group-wise comparisons of all migraineurs vs. healthy controls, CM vs. EM, EM vs. healthy controls, and CM vs. healthy controls. The voxel-wise TBSS differences in FA, MD, AD and RD values of white matter between the different groups were tested using a permutation-based inference

tool by nonparametric statistics called randomise, implemented in FSL, with the threshold-free cluster enhancement (TFCE) option [42, 43]. Five thousand permutations were set to allow robust statistical inference and the significance threshold for intergroup differences was $p < .05$ after correcting for family wise error (FWE) applying the TFCE option. Additional clinical covariates were added to the comparisons in the cases where significant differences were found. These covariates were analysed individually to evaluate the individual effect of each covariate. In the case of presence of aura, we repeated the original TBSS analysis excluding the patients with migraine with aura. None of the design matrices included duration of migraine and time from onset of CM simultaneously as covariates due to collinearity. Time from onset of CM was also included as a covariate (only in comparisons with CM) because it may correct the results in CM patients in a more meaningful way than the total duration of migraine.

In the cases where significant differences were found, we performed a post-hoc analysis. We applied a false discovery rate (FDR) correction, using the fdr command from FSL, to the TFCE uncorrected p-values. The fdr command provides the uncorrected p-value which sets the level of statistical significance after the FDR correction. To correct for number of contrasts in each case, the final level of statistical significance is equal to the uncorrected p-value from the previous step divided by the number of comparisons (Bonferroni correction).

Effect size was computed using Cohen's d value in regions with significant results from the first analysis (FWE-corrected). For every comparison, the mean value of the most disabled group was subtracted from the mean value of the least disabled or the control group. In the comparisons between both types of migraine, CM is considered the most disabled group, and EM the least disabled group.

To study the relationship between clinical parameters and DTI measures, Spearman's rank correlation coefficient was employed in a ROI-based correlation analysis. Duration of the migraine in both types of migraine patients, time from onset of CM in chronic migraineurs, and headache and migraine frequency for both types of migraine patients were the analysed clinical parameters. It must be clarified that we obtained correlation values in CM and EM patients separately, in order to assess differences or trends within each type of migraine. Our intention was to determine the possible effect of headache or migraine frequency, in the specific range of episodic or chronic migraine, and the possible relationship with time, with special attention to the time from onset of CM. To obtain individual label maps for each subject, the inverse warp fields of the FA images to the MNI image transformation from the TBSS procedure were computed and applied to the Johns Hopkins University ICBM-DTI-81 White Matter Atlas. The ROIs that were selected for the correlation analysis were those for which significant differences were found between at least two groups in any diffusion parameter in the TBSS analysis. All DTI measures (FA, MD, RD and AD) were considered for the correlation analysis. We used all DTI measures to avoid a possible loss of complementary information given by each parameter in the assessment of differences within CM or EM. To correct for multiple comparisons, the Benjamini-Hochberg [44] FDR procedure was applied, and, after this correction, the level of statistical significance was set at $p < .05$.

## 2.3. Results

During the study period, 51 healthy controls, 55 episodic migraine patients and 57 chronic migraine patients were recruited for the study after matching the inclusion and exclusion criteria. No significant structural

abnormality was detected in conventional MRI studies. Due to erroneous results after applying the non-linear registration to the FMRIB-58 image in MNI space, one healthy control, one episodic migraineur and one chronic migraineur were excluded from the study. Demographic and clinical data for the three groups with the remaining participants are summarised in Table 1. Significant differences were found in duration of migraine history in years between the two migraine groups and, as expected, in headache and migraine frequency between the migraine groups.

Considering the significant differences in duration of migraine history between episodic and chronic migraine patients (Table 1), TBSS analysis was repeated including the duration of migraine history as a covariate, as mentioned in the Statistical Analysis section. Presence of aura was added as an additional covariate to duration of migraine history in a posterior analysis. In the case of CM patients, the TBSS analysis was additionally accomplished including the time from onset of CM as a covariate. This covariate was included in a separate analysis from the one with duration of migraine history due to collinearity, as mentioned previously in the Statistical Analysis section.

## *2.3.1.* ***TBSS analysis***

### *A. Results uncorrected for covariates*

No significant differences were found in any of the diffusion indices (FA, MD, RD and AD) between all migraineurs and HC. Dividing all migraineurs into EM and CM, no significant differences were found with respect to HC. With regard to the comparison between CM and EM, no significant differences were found in FA, MD or RD. However, significant lower AD values were found in CM compared to EM in widespread locations across the white matter. These locations correspond to 38 different regions from the ICBM-DTI-81 White Matter Atlas, and six regions from the White Matter Tractography Atlas, and are shown in Tables 2 and 3 and Fig. 1. The FWE-corrected results can be seen in Additional file 1: Figure S1 and Table S1.

In the case of the analysis including only patients with migraine without aura, no new significant results were observed. As in the original sample, significant lower AD values were found in CM compared to EM (FWE-corrected results), but in 10 regions from the ICBM-DTI-81 White Matter Atlas, all of them included in the 38 regions with significant differences. The FWE-corrected results excluding migraine with aura patients can be seen in Additional file 1: Table S2.

### *B. Results corrected for covariates*

After the post-hoc analysis, significant lower AD values were found in CM compared to EM in six regions from the ICBM-DTI-81 White Matter Atlas, and one region (the right corticospinal tract) from the White-Matter Tractography Atlas, when including the time from onset of CM as a covariate. These results are shown in Tables 4 and 5 and Fig. 1. No significant results were observed when correcting for total duration of migraine or for the other DTI measures.

The FWE-corrected results for the diverse covariates are shown.

**Results corrected for duration of migraine history** Including the duration of migraine history as a covariate, no significant differences were found for FA, MD or RD. Significant decreased AD values

in CM with respect to EM were found only in the middle cerebellar peduncle (675 $mm^3$ with $p < .05$ FWE-corrected, minimum p-value = .028), but other 26 regions remained with $p < .1$ FWE-corrected (Additional file 1: Table S3). Also, significant increased AD values in EM with respect to HC were found in seven regions from the left hemisphere (Additional file 1: Table S4). These results can be seen in Additional file 1: Figure S2. No significant differences were found between all migraineurs together and HC, or between CM and HC. Adding the presence of aura as a covariate, significant increased AD values in EM with respect to HC were found in seven regions from the left hemisphere. These seven regions were the same regions that showed significant differences in the analysis including only the duration of migraine history as a covariate. No significant differences were found for FA, MD or RD.

**Results uncorrected for time from onset of CM** In the additional comparisons for CM patients, including time from onset of CM as a covariate, no significant differences were found for MD or RD. Significant decreased AD values in CM with respect to EM were found in 23 regions with $p < .05$ FWE-corrected (Additional file 1: Table S5). Significant decreased FA values in CM compared to HC were found in 15 regions, most of them from the right hemisphere (Additional file 1: Table S6). These results are shown in Additional file 1: Figure S3.

### *C. Effect size*

When comparing between CM and EM Axial Diffusivity values, all Cohen's d values (except for left fornix) were negative, which means that AD values were lower in CM. For the middle cerebellar peduncle, left external capsule and right sagittal stratum, the Cohen's d absolute values were equal or greater than .5, a medium effect size according to [45]. A very similar trend, but with lower Cohen's d absolute values, was found in CM with respect to HC. In the comparison between EM and HC, Cohen's d value was positive in almost all regions, i.e., AD values were higher in EM with respect to HC. In the pontine crossing tract, a medium effect size was obtained (d = .59). These results are depicted in Additional file 1: Table S7 and Figures S4 and S5. Results for the other DTI measures can be seen in Additional file 1: Figures S6, S7, S8, S9, S10 and S11. A summary of these results can be seen in Table 6.

## *2.3.2.* ***Correlation analysis***

After multiple comparisons correction, ROI-based significant positive correlations between time from onset of chronic migraine and mean FA in the right ($\rho = .420$, p = .001) and left ($\rho = .439$, $p < .001$) external capsule were found. Significant negative correlations between time from onset of chronic migraine and mean RD in the right ($\rho = -.427$, p = .001) and left ($\rho = -.439$, $p < .001$) external capsule were found. These results can be seen in Fig. 4.10.

No significant correlations were found neither for mean MD or mean AD, nor duration of the migraine, headache and migraine frequency for both migraine groups in ROI-based correlation analysis.

**Table 1**. Clinical and demographic characteristics of healthy controls (HC), episodic migraine (EM) and chronic migraine (CM).

| | HC (n=50) | EM (n=54) | CM (n=56) | Statistical test |
|---|---|---|---|---|
| Gender, male/female | 11/39 (22/78% ) | 9/45 (17/83% ) | 6/50 (11/89% ) | $\chi^2_{(2,\ N\ =\ 160)} = 2.48$, p = .29† |
| Age (years) | 36.1 ± 13.2 | 37.1 ± 8.2 | 38.1 ± 8.7 | $\chi^2$ (2) = 2.85, p = .24‡ |
| Duration of migraine history (years) | | 14.1 ± 11.1 | 19.6 ± 10.4 | $t_{(108)}$ = -2.7, p = .008§ |
| Time from onset of chronic migraine (months) | | | 24.5 ± 32.9 | |
| Headache frequency (days/month) | | 3.6 ± 1.9 | 23.3 ± 6.3 | U = 44.0, p < .001 |
| Migraine frequency (days/month) | | 3.6 ± 1.9 | 13.9 ± 6.9 | U = 108.5, p < .001 |
| Overusing medication | | 0 (0% ) | 42 (75% ) | p < .001 |
| Aura | | 9 (17% ) | 1 (2% ) | p = .007 |

†Chi-square test. ‡ Kruskal-Wallis test. §Two-tailed, unpaired Student's t-test. Mann-Whitney U test. Fisher's exact test. Data are expressed as means ± SD.

**Table 2**. White matter regions where significant decreased AD values were found in CM compared to EM.

| White Matter tract | Minimum p-value (uncorrected) | Volume ($mm^3$) | MNI peak coordinate (mm), (x,y,z) |
|---|---|---|---|
| Middle cerebellar peduncle | .0002 | 2263 | (-20,-55,-32) |
| Superior cerebellar peduncle R/L | .0002/.0002 | 145/137 | (6,-31,-19) / (-6,-50,-27) |
| Inferior cerebellar peduncle R/L | .0002/.0002 | 81/118 | (9,-42,-38) / (-13,-45,-31) |
| Superior longitudinal fasciculus R/L | .0004/.0004 | 565/821 | (37,-48,14) / (-37,-50,15) |
| Genu of corpus callosum | .0006 | 154 | (-8,27,1) |
| Body of corpus callosum | .0016 | 74 | (-11,-19,30) |
| Splenium of corpus callosum | .0006 | 203 | (21,-48,10) |
| Anterior corona radiata R/L | .0014/.0004 | 105/527 | (19,24,-10) / (-18,25,-8) |
| Superior corona radiata R/L | .0012/.0014 | 253/87 | (21,-9,34) / (-27,-10,25) |
| Posterior corona radiata R/L | .0010/.0010 | 75/140 | (28,-40,21) / (-30,-52,22) |
| External capsule R/L | .0006/.0004 | 400/640 | (33,-3,3) / (-22,16,-12) |
| Posterior limb of internal capsule R/L | .0010/.0008 | 372/400 | (17,-4,8) / (-18,-1,10) |
| Retrolenticular part of internal capsule R/L | .0012/.0012 | 173/161 | (30,-24,2) / (-24,-24,2) |
| Anterior limb of internal capsule R/L | .0006/.0004 | 163/270 | (18,17,-3) / (-14,8,0) |
| Sagittal stratum R/L | .0002/.0006 | 418/316 | (40,-36,-13) / (-40,-15,-14) |
| Posterior thalamic radiation R/L | .0004/.0002 | 333/254 | (34,-56,3) / (-38,-52,3) |
| Cerebral peduncle R/L | .0004/.0002 | 225/257 | (11,-22,-21) / (-10,-13,-12) |
| Corticospinal tract R/L | .0002/.0004 | 107/164 | (10,-22,-23) / (-7,-19,-24) |
| Medial lemniscus R/L | .0002/.0002 | 83/103 | (5,-35,-37) / (-2,-37,-30) |
| Pontine crossing tract | .0002 | 89 | (7,-29,-25) |
| Fornix (cres) R/L | .0004/.0006 | 71/41 | (33,-8,-17) / (-34,-11,-16) |

*continued on next page*

*continued from previous page*

| | | | |
|---|---|---|---|
| Cingulum (hippocampus) L | .0002 | 87 | (-17,-43,-2) |

L = left; R = right.

The column Volume represents the volume from the atlas region with significant differences (FDR-corrected and number of contrasts corrected). The maximum significant uncorrected p-value after corrections was .0032. No regions with volume equal or lower than 30 $mm^3$ were included in this Table. Only regions with FWE-corrected $p < .05$ are included.

**Table 3**. White matter regions where significant decreased AD values were found in CM compared to EM using the Johns Hopkins University White-Matter Tractography Atlas.

| White Matter tract | Minimum p-value (uncorrected) | Volume ($mm^3$) | MNI peak coordinate (mm), (x,y,z) |
|---|---|---|---|
| Anterior thalamic radiation L/R | .0006/.0008 | 36/39 | (-20,17,0) / (9,-30,-15) |
| Corticospinal tract L/R | .0012/.0012 | 152/165 | (-21,-21,2) / (10,-24,-25) |
| Forceps major | .0010 | 126 | (-17,-85,7) |
| Inferior longitudinal fasciculus R | .0004 | 49 | (40,-35,-14) |

L = left; R = right.

The column Volume represents the volume from the atlas region with significant differences (FDR-corrected and number of contrasts corrected). The maximum significant uncorrected p-value after corrections was .0032. No regions with volume equal or lower than 30 $mm^3$ were included in this Table.

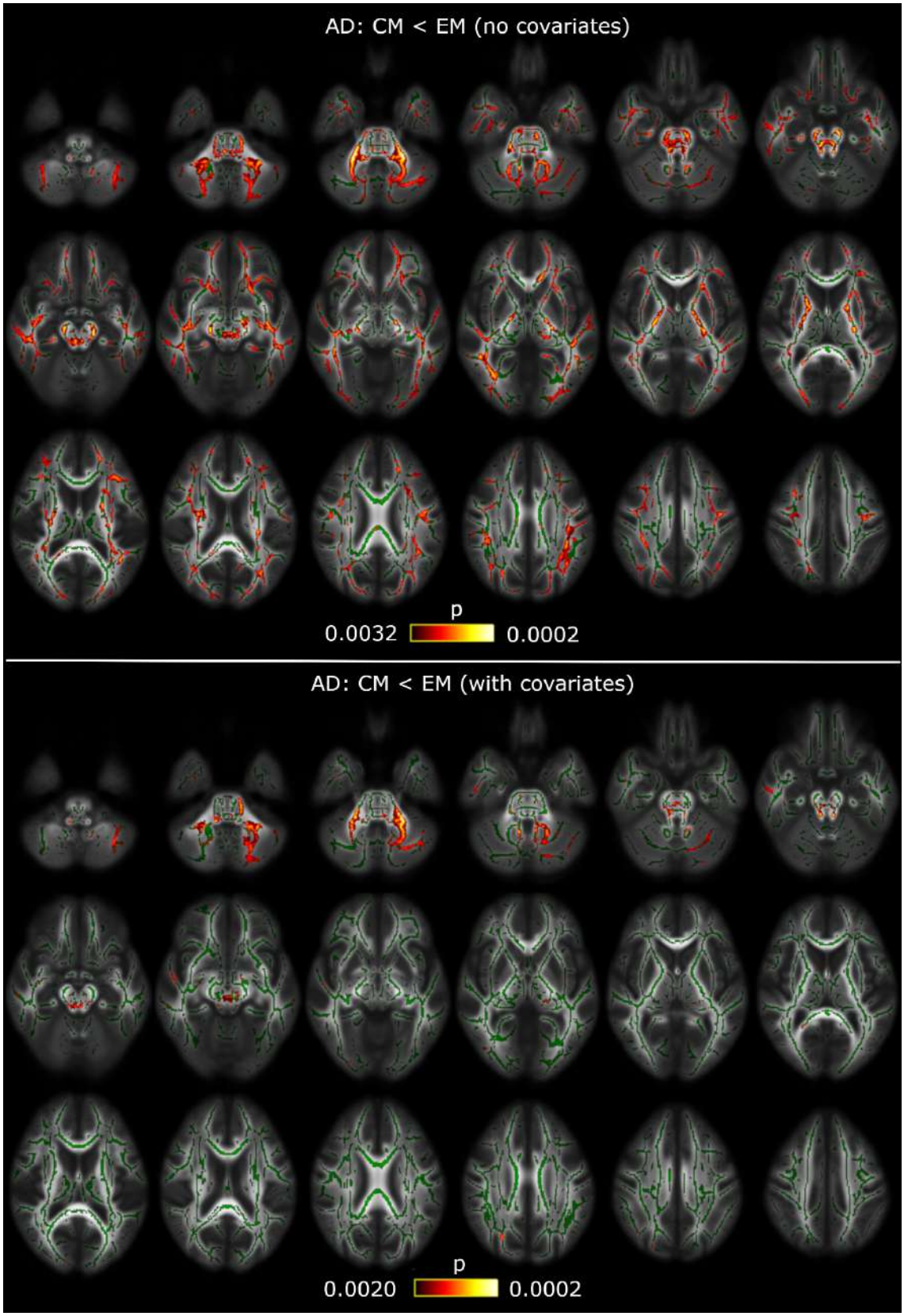


**Fig. 1** White matter alterations in CM compared to EM patients. TBSS shows decreased AD values in CM compared to EM in widespread locations with no covariate corrections (top) and correcting for time from onset of CM (bottom). White matter skeleton is shown in green, and voxels with significant differences in red-yellow. The colour bar shows the p-values (uncorrected). The maximum uncorrected p-value for each case is given by FDR and number of contrasts corrections.

**Table 4**. White matter regions from the ICBM-DTI-81 White Matter Atlas for which significant decreased AD values were found in CM compared to EM considering the effect of time from onset of CM.

| White Matter tract | Minimum p-value (uncorrected) | Volume ($mm^3$) | MNI peak coordinate (mm), (x,y,z) |
|---|---|---|---|
| Middle cerebellar peduncle | .0004 | 1286 | (-16,-52,-30) |
| Superior cerebellar peduncle R/L | .0004/.0002 | 97/109 | (9,-50,-30) / (-6,-42,-26) |
| Inferior cerebellar peduncle L | .0006 | 55 | (-6,-53,-24) |
| External capsule L | .0012 | 34 | (-33,-10,1) |
| Pontine crossing tract | .0006 | 39 | (0,-23,-24) |

L = left; R = right.

The column Volume represents the volume from the atlas region with significant differences (FDR-corrected and number of contrasts corrected). The maximum significant uncorrected p-value after corrections was .0020. No regions with volume equal or lower than 30 $mm^3$ were included in this Table. Only regions with FWE-corrected $p < .05$ are included.

**Table 5**. White matter regions from the Johns Hopkins University White-Matter Tractography Atlas for which significant decreased AD values were found in CM compared to EM considering the effect of time from onset of CM.

| White Matter tract | Minimum p-value (uncorrected) | Volume ($mm^3$) | MNI peak coordinate (mm), (x,y,z) |
|---|---|---|---|
| Corticospinal tract R | .0012 | 31 | (4,-35,-16) |

R = right.

The column Volume represents the volume from the atlas region with significant differences (FDR-corrected and number of contrasts). The maximum significant uncorrected p-value after corrections was .0020. No regions with volume equal or lower than 30 $mm^3$ were included in this Table.

**Table 6**. Summary of white matter regions where significant differences were found in all comparisons.

| White Matter tract | EM > HC∗ | CM < HC∗ | CM < EM |
|---|---|---|---|
| Middle cerebellar peduncle | NS | NS | AD<br>AD + durM∗<br>AD + onsCM |
| Superior cerebellar peduncle R/L | NS | FA + onsCM (R) | AD<br>AD + durM∗ ($p < 0.1$)<br>AD + onsCM |
| Inferior cerebellar peduncle R/L | NS | NS | AD<br>AD + durM∗ ($p < 0.1$)<br>AD + onsCM (L) |
| Superior longitudinal fasciculus R/L | NS | NS | AD<br>AD + durM∗ ($p < 0.1$)<br>AD + onsCM∗ (R) |
| Genu of corpus callosum | NS | NS | AD |
| Body of corpus callosum | NS | FA + onsCM | AD<br>AD + durM∗ ($p < 0.1$) |
| Splenium of corpus callosum | NS | FA + onsCM | AD<br>AD + durM∗ ($p < 0.1$)<br>AD + onsCM∗ |
| Anterior corona radiata R/L | NS | FA + onsCM (R) | AD |
| Superior corona radiata R/L | AD + durM (L) | FA + onsCM (R) | AD<br>AD + durM∗ ($p < 0.1$)<br>AD + onsCM∗ |
| Posterior corona radiata R/L | NS | FA + onsCM (R) | AD<br>AD + durM∗ (L, $p < 0.1$)<br>AD + onsCM∗ (R) |
| External capsule R/L | AD + durM (L) | FA + onsCM (R) | AD<br>AD + durM∗ ($p < 0.1$)<br>AD + onsCM (L; R∗ ) |
| Posterior limb of internal capsule R/L | AD + durM (L) | FA + onsCM (R) | AD<br>AD + durM∗ ($p < 0.1$)<br>AD + onsCM∗ |
| Retrolenticular part of internal capsule R/L | AD + durM (L) | FA + onsCM (R) | AD<br>AD + durM∗ ($p < 0.1$)<br>AD + onsCM∗ |
| Anterior limb of internal capsule R/L | NS | FA + onsCM (R) | AD |
| Sagittal stratum R/L | AD + durM (L) | FA + onsCM (R) | AD<br>AD + durM∗ (R, $p < 0.1$)<br>AD + onsCM∗ (R) |
| Posterior thalamic radiation R/L | AD + durM (L) | NS | AD<br>AD + durM∗ ($p < 0.1$)<br>AD + onsCM∗ (R) |

*continued on next page*

*continued from previous page*

| | | | |
|---|---|---|---|
| Cerebral peduncle R/L | AD + durM (L) | NS | AD<br>AD + durM$*$ ($p < 0.1$)<br>AD + onsCM$*$ |
| Corticospinal tract R/L | NS | NS | AD<br>AD + durM$*$ ($p < 0.1$)<br>AD + onsCM$*$ ($R^+$) |
| Medial lemniscus R/L | NS | NS | AD |
| Pontine crossing tract | NS | NS | AD<br>AD + durM$*$ ($p < 0.1$)<br>AD + onsCM |
| Fornix (cres) R/L | NS | FA + onsCM (R) | AD<br>AD + durM$*$ (R)<br>AD + onsCM$*$ (R) |
| Cingulum (hippocampus) L | NS | NS | AD |
| Anterior thalamic radiation R/L | NS | NS | $AD^+$ |
| Forceps major | NS | NS | $AD^+$ |
| Inferior longitudinal fasciculus R | NS | NS | $AD^+$ |

durM = duration of migraine as covariate; L = left; NS = non-significant; onsCM = time from onset of CM as covariate; R = right; $*$ = only FWE-corrected; $^+$ = significant only in the White-Matter Tractography Atlas.

The column Volume represents the volume from the atlas region with significant results. No regions with volume equal or lower than 30 $mm^3$ were included in this Table.

## 2.4. Discussion

In a TBSS-based dMRI analysis, in relation with the first stated objective of the study, white matter structural changes in Chronic Migraine compared to Episodic Migraine patients were found in 38 regions when AD was considered as DTI measure. These findings suggest global white matter changes in CM compared to EM.

In the analysis excluding patients with migraine with aura, no new results were observed with respect to the analysis with the whole sample, and the regions with significant results were a subset of the regions of the original analysis. Using only patients without aura, higher p-values and lower number of regions with significant differences are obtained. These results suggest that the differences are caused by a loss of statistical power more than the effect of aura itself. Including duration of migraine history as a covariate, differences were found between EM and Healthy Controls in seven regions, but they did not survive the FDR and the number of contrasts corrections. The addition of the presence of aura as a covariate did not change the results with respect to using only the duration of migraine history as a covariate.

Additionally, including time from onset of chronic migraine as a covariate in the comparisons with CM patients, significant decreased values were found in AD between CM and EM. Decreased values were also found in FA in CM with respect to HC, but they did not survive the FDR and the number of contrasts corrections.

In relation with the second objective of the study, correlation analysis was executed between diverse DTI measures and clinical features. Significant correlations between time from onset of chronic migraine and mean FA (positive correlation) and mean RD (negative correlation) in the bilateral external capsule were found.

White matter differences between both groups of migraineurs were not previously found by Neeb et al. in the only study, to the best of our knowledge, which assessed patients with chronic and episodic migraine using DTI [22]. In the present study, however, a considerably bigger cohort was included when compared to that study, and our participants were considerably younger. The influence of age in the white matter diffusion is well-known and has been extensively assessed. The most common pattern is to find decreased FA and increased RD values in older people, while the AD pattern is unclear [30, 46]. Considering the aging-effect, altered DTI measures in healthy people might reduce the diffusion differences between patients and controls in older subjects.

Differences between the two migraine groups were found using AD as a DTI measure. It is known, however, that relationships between DTI-derived parameter changes and specific microstructure alterations are difficult to establish, and therefore results must be interpreted carefully. Winklewski et al. interpreted reduced AD values, as we found in CM compared to EM, as the beginning of demyelination [47]. This reduction, nevertheless, could be ineffective to detect prolonged demyelination [47]. Nonetheless, based on studies in mice, a review study by Alexander et al. linked AD more to axonal damage than demyelination [48]. In a posterior study also in mice, Sun et al. established a relationship between reduced AD values and axonal damage, and between increased RD values and myelin damage, confirmed with immunohistochemistry examinations [49]. In a human study, Pierpaoli et al. found decreased AD in primary lesions and in regions with secondary white matter degeneration [50]. This axonal loss hypothesis has also been exposed for Alzheimer's disease [51] and migraine patients [7].

Previous whole-brain TBSS studies found white matter differences between migraine patients and healthy controls [6–11, 52]. Most of these studies report decreased FA in migraine patients with respect to healthy controls, but one study showed increased FA in migraineurs with respect to healthy controls; in this study, Messina et al. analysed paediatric patients [9], which could explain the difference. Decreased FA can be caused by factors like demyelination, lower packing density or different membrane permeability [53] and is modulated by characteristics such as axon diameter and packing or fibre organization [54].

Results for MD and RD in the literature regarding migraine using TBSS are unclear. On the one hand, increased MD and RD values in migraineurs with respect to healthy controls were obtained in [11, 52], but on the other hand, decreased values were reported in [7–9]. Results obtained with methods different than TBSS, such as ROI-based analysis or tractography, showed increased MD and/or RD values in migraine patients with respect to healthy controls [13, 14, 18, 55]. Increased RD could also be a biomarker of demyelination [47, 48]. There are also studies that found no differences between migraine patients and healthy controls. These studies employed methods whole-brain such as TBSS [22, 56], ROI-based analysis (ictal migraine) [57] and voxel-based whole brain comparison [58].

Interestingly, the trend when comparing AD values between EM and healthy controls is inverted when comparing CM and healthy controls or CM with respect to EM (Additional file 1: Figures S4 and S5). As previously mentioned, AD might be an indicator of axonal loss. This might indicate that the evolution from EM to CM is characterised by a loss of axonal integrity. This result also shows that, in migraine, there could be different processes of axonal behaviour involving different pathophysiological mechanisms.

In contrast to our results, some TBSS studies obtained decreased AD in migraine patients with respect to healthy controls [7–9]. Petrušić et al. also found decreased AD in migraine with aura patients with respect to healthy controls using a tractography approach [15]. We detected the same trend, but only in CM patients. We obtained the opposite result in EM patients, when including duration of migraine as a covariate, but this result was not significant in the post-hoc analysis. In [7, 8], cohort differences (considering only the EM patients in our case), i.e., lower disease duration and higher attack frequency, with possibly high frequency EM patients in the sample of [7, 8], could explain the differences between the studies. In [9], as previously stated, paediatric patients were included in the sample by Messina et al., which could explain the difference.

The analysis of the temporal change in migraine patients adds an interesting insight to the former results.

In the case of EM patients, considering the duration of migraine as a covariate, there was a lower number of regions with significant differences with respect to CM patients. The significant difference in the duration of migraine between both groups of migraine patients could be a confounding factor in the previous results. Furthermore, significant increased AD values in EM compared to HC were observed, possibly due to more precise estimations (less variability) in the case of the values in EM patients.

These results seem to indicate a temporal evolution in CM patients that reflects an adaptation to continuous headache attacks. In the initial months with CM (short-term patients), axonal integrity seems to be damaged, as suggested by decreased FA values in those patients compared to HC when including time from onset of CM as a covariate. Decreased FA values in CM patients with therapy compared to HC, after 6 months follow-up, were reported previously by Gomez-Beldarrain et al. [16]. Considering these results and the decreased AD values in CM with respect to EM, it seems that in progression from EM to CM there might be a process that causes severe white matter alterations.

Later, in CM patients, a set of plastic changes as an adaptation to the frequent headaches may happen. The white matter reorganisation is suggested by positive correlation between FA and time from onset of CM, and by the simultaneous negative correlation between RD and time from onset of CM.

In line with our CM correlation results, Szabó et al., 2017 [10], obtained a trend showing increased FA in migraine with aura patients with respect to healthy controls. In this study, based on increased FA values, the authors hypothesised that repeated painful conditions or increased cortical excitability might cause maladaptive plastic changes in migraine with aura. Moreover, increased FA values were found in people with repeated stimuli in learning processes [59, 60], so something similar could be happening in CM patients, who suffer repeated painful stimuli.

Regarding correlation analysis, we obtained significant correlations between time from onset of chronic migraine and DTI measures (FA and RD) in the bilateral external capsule, but no significant correlations were obtained with the duration of migraine in CM or EM patients.

The external capsule is a part of the central core, a network on top of the brainstem that includes structures like the insular surface, the extreme and internal capsules, the lentiform nucleus or the thalamus [61]. The extreme and external capsules lie in anteroposterior disposition, and they are connected to the anteroinferior part of the insula [61]. The lentiform nucleus is located between the external and internal capsules [61]. The internal, external and extreme capsules connect the insular surface, basal ganglia and thalamus to the cerebral lobes [61]. Russo et al. reported that, in the insula and lentiform nucleus, migraine patients, compared to HC, are characterised by an increased blood oxygenation level dependent response [62]. Furthermore, Borsook et al. exposed that the insula is implicated in processes related to the clinical presentation of migraine and is a hub of activity in migraine [63]. The role of the external capsule in anteroposterior connections and in connections between subcortical regions implied in migraine and cortical regions could be highly relevant in migraine pathogenesis, especially in Chronic Migraine.

In other studies, significant negative correlations between duration of migraine in years (in EM patients) and FA [5, 7], MD [7] or AD [7, 10] were obtained, but also significant positive correlation between duration of migraine and MD [14]. This discrepancy could be explained with methodological and cohort differences. No significant correlation between DTI measures and the external capsule has been previously found in migraine patients, but no correlation between time from onset of chronic migraine and DTI measures has been previously assessed.

In this study, high frequency EM patients (10–14 headache days per month) were excluded. This decision was made in order to avoid misclassified patients, which could mislead the analysis [28]. Compared to Neeb et al. [22], CM patients from our sample had greater headache frequency, while EM patients from our sample had lower headache frequency. This increased difference between the migraine groups, together with the larger cohort size, could be a factor explaining why we obtained significant results in the CM-EM comparison, while no significant results were obtained in [22]. However, no significant correlations were found between headache frequency and DTI measures, which could mean that headache frequency does not have a very relevant effect on diffusion within the EM or CM groups. In any case, a deeper specific analysis, focusing on high frequency EM patients, would be needed to clarify whether this group of patients is closer to the low frequency EM group or to the CM group.

There are several strengths and limitations in this study. About the strengths, this study is, to the best of our knowledge, the white matter study with the highest number of participants simultaneously including Healthy Controls, Episodic Migraine and Chronic Migraine patients. Moreover, the selection

criteria of the patients allowed us to detect significant differences not found previously, especially between EM and CM patients.

About the limitations of this study, due to time constraints in the MRI acquisition process in a clinical setting, we acquired no T2 or T2-FLAIR MRI sequences that would be helpful to assess White Matter Hyperintensities (WMHs). Migraine has been associated with an increased risk for WMHs detected on MRI [64]; also pain in EM patients [65] and an unfavourable prognosis [66] were found to be associated with the occurrence of WMHs. Considering our correlation results in CM patients and the state of the art, the WMHs analysis would have been interesting in this study. Medication overuse was identified in an important percentage of the CM patients in our sample (75%). This might be a confounding factor, due to possible structural differences in the white matter with respect to CM patients without overuse. The exclusion of patients with anxiety or depression implies that there was no chance to assess possible effects of these conditions on brain structure in migraine patients. Anxiety and depression are often comorbid in patients with migraine [67–69]. When MRI were acquired in the patients, they had no attacks in the previous 24 h, but they could be in a prodromal stage, as we did control time from past, but not to the next migraine attack. Altered brain physiology and abnormal functional connectivity have been found in prodromal stages [70, 71], so this is a possible source of bias in the results. Diagnosis of infrequent TTH in controls was done solely by history and not by using a headache diary; however, they were excluded if other headache disorders were present or the frequency of headache in the preceding year was $> 1$ headache day per month or $> 12$ headache days per year. Finally, in the analysis of the presence of aura, the number of patients with migraine with aura was too small to additionally compare the changes in migraine with aura against migraine without aura.

In summary, considering previous studies and our results, a hypothesis about the migraine process could be drafted that distinguishes three states or stages: EM, transition from EM to CM, and CM. In the EM state, there would be some white matter damage, produced mainly by a loss of axonal integrity. Then, in the transition from EM to CM, there would be a loss of axonal integrity, but probably not led by a severe additional damage in myelin. Finally, in the CM state, there would be a series of plastic changes, as an adaptation to a continuous ictal state. Considering this evolution hypothesis, EM might involve a coexistence of loss of white matter integrity and maladaptive plasticity, with more severe integrity damage in the transition to CM, and CM may show predominant maladaptive plasticity, being, in this regard, a different entity with respect to a more frequent EM. An illustration of the hypothesised temporal evolution of the three main DTI measures used here can be seen in Fig. 3.

Anyway, regarding this hypothesis, longitudinal analysis should be performed in order to confirm this possible evolution, and the interpretation of the DTI measures must be carried out cautiously, as mentioned before in this section. Additionally, about the transition from EM to CM, the high frequency EM patients could be especially interesting to investigate. Indeed, it remains to be elucidated whether high frequency EM is actually a transition phase between EM and CM, an intense EM or, considering an extreme case, a low frequency CM.

Although this can be only considered a preliminary hypothesis, it would contribute to explain the high variability in the results in the literature found when comparing migraineurs with healthy controls in terms of white matter diffusion parameters. Indeed, if different trends can be found at different stages of the disease, then the results of global comparisons would depend heavily on the internal composition of the cohort of migraine patients in each study, possibly yielding what seem to be opposite results.

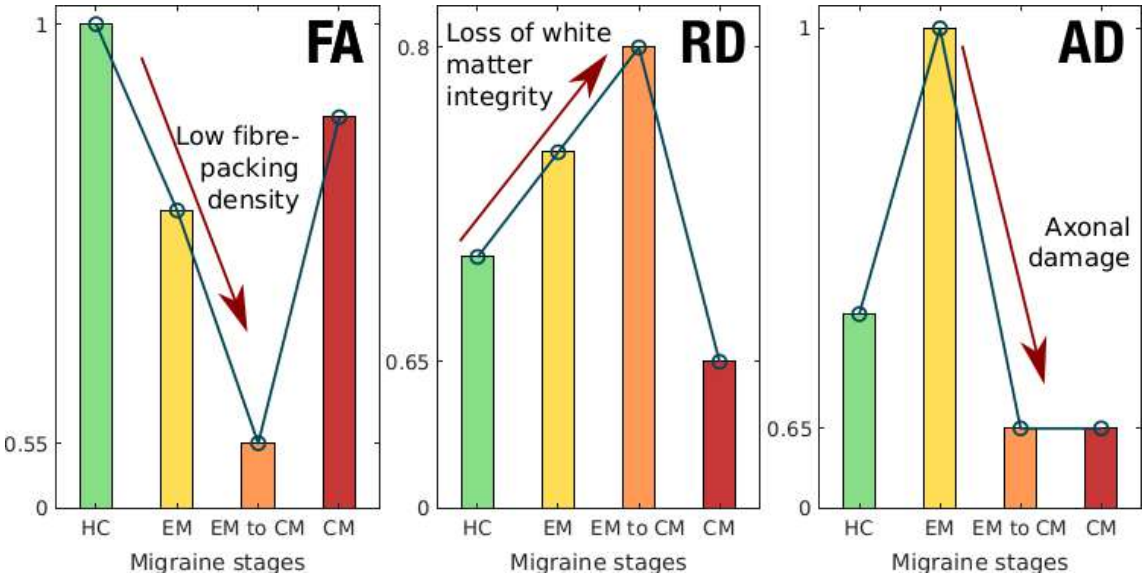


**Fig. 3** DTI measures temporal change hypothesis. Illustrative values are shown for generalized trends in FA, RD and AD (from left to right) in each of the different migraine stages, including a previous healthy control stage. Stages are ordered chronologically from left to right in each subplot. The interpretation of different trends in DTI measures is given in each subplot. The values in the vertical axes should only be used as an orientation to watch the trends and differences between

# 2.5. Conclusions

The current findings suggest global white matter structural differences between Episodic Migraine and Chronic Migraine, with damaged axonal integrity in Chronic Migraine, and between both groups of migraine patients and Healthy Controls. A different temporal pathophysiological evolution with maladaptive plastic changes seems to happen in Chronic Migraine with respect to Episodic Migraine. Further research is needed for these findings to be confirmed. Also, additional clinical features should be considered, longitudinal evaluation should be performed and a possible relationship with functional changes should be assessed.

# 2.6. References

1. Headache Classification Committee of the International Headache Society (2018) The international classification of headache disorders, 3rd edition. Cephalalgia 38(1):1–211

2. Lipton RB, Fanning KM, Buse DC, Martin VT, Reed ML, Manack Adams A et al (2018) Identifying natural subgroups of migraine based on comorbidity and concomitant condition profiles: results of the chronic migraine epidemiology and outcomes (CaMEO) study. Headache 58(7):933–947

3. Katsarava Z, Buse DC, Manack AN, Lipton RB (2012) Defining the differences between episodic migraine and chronic migraine. Curr Pain Headache Rep 16(1):86–92

4. Aurora SK, Brin MF (2017) Chronic migraine: an update on physiology, imaging, and the mechanism of action of two available pharmacologic therapies. Headache 57(1):109–125

5. Li XL, Fang YN, Gao QC, Lin EJ, Hu SH, Ren L et al (2011) A diffusion tensor magnetic resonance image study of Corpus callosum from adult patients with migraine complicated with depressive/anxious disorder. Headache 51(2):237–245

6. Yuan K, Qin W, Liu P, Zhao L, Yu D, Zhao L et al (2012) Reduced fractional anisotropy of Corpus callosum modulates inter-hemispheric resting state functional connectivity in migraine patients without Aura. PLoS One 7(9):e45476

7. Yu D, Yuan K, Qin W, Zhao L, Dong M, Liu P et al (2013) Axonal loss of white matter in migraine without aura: a tract-based spatial statistics study. Cephalalgia. 33(1):34–42

8. Yu D, Yuan K, Zhao L, Dong M, Liu P, Yang X et al (2013) White matter integrity affected by depressive symptoms in migraine without aura: a tractbased spatial statistics study. NMR Biomed 26(9):1103–1112

9. Messina R, Rocca MA, Colombo B, Pagani E, Falini A, Comi G et al (2015) White matter microstructure abnormalities in pediatric migraine patients. Cephalalgia. 35(14):1278–1286

10. Szabó N, Faragó P, Király A, Veréb A, Csete G, Tóth E et al (2017) Evidence for plastic processes in migraine with Aura: a diffusion weighted MRI study. Front Neuroanat 11:138

11. Shibata Y, Ishiyama S, Matsushita A (2018) White matter diffusion abnormalities in migraine and medication overuse headache: A 1.5-T tractbased spatial statistics study. Clin Neurol Neurosurg 174:167–173

12. DaSilva AFM, Granziera C, Tuch DS, Snyder J, Vincent M, Hadjikhani N (2007) Interictal alterations of the trigeminal somatosensory pathway and PAG in migraine. Neuroreport 18(4):301–305

13. Coppola G, Tinelli E, Lepre C, Iacovelli E, Di Lorenzo C, Di Lorenzo G et al (2014) Dynamic changes in thalamic microstructure of migraine without aura patients: a diffusion tensor magnetic resonance imaging study. Eur J Neurol 21(2):287–e13

14. Chong CD, Schwedt TJ (2015) Migraine affects white-matter tract integrity: a diffusion-tensor imaging study. Cephalalgia. 35(13):1162–1171

15. Petrušić I, Daković M, Kačar K, Mićić O, Zidverc-Trajković J (2018) Migraine with aura and white matter tract changes. Acta Neurol Belg 118:485–491

16. Gomez-Beldarrain M, Oroz I, Garcia Zapirain B, Fernandez Ruanova B, Garcia Fernandez Y, Cabrera A et al (2015) Right fronto-insular white matter tracts link cognitive reserve and pain in migraine patients [erratum in J headache pain. 2016;17:22]. J Headache Pain 17:4

17. Liu J, Ma S, Mu J, Chen T, Xu Q, Dun W et al (2017) Integration of white matter network is associated with Interindividual differences in psychologically mediated placebo response in migraine patients. Hum Brain Mapp 38(10):5250–5259

18. Rocca MA, Pagani E, Colombo B, Tortorella P, Falini A, Comi G et al (2008) Selective diffusion changes of the visual pathways in patients with migraine: a 3-T Tractography study. Cephalalgia. 28(10):1061–1068

19. Granziera C, DaSilva AFM, Snyder J, Tuch DS, Hadjikhani N (2006) Anatomical alterations of the visual motion processing network in migraine with and without Aura. PLoS Med 3(10):e402

20. Pietrobon D, Moskowitz MA (2013) Pathophysiology of migraine. Annu Rev Physiol 75:365–391

21. Dodick DW (2018) A phase-by-phase review of migraine pathophysiology. Headache 58(Suppl 1):4–16

22. Neeb L, Bastian K, Villringer K, Gits HC, Israel H, Reuter U et al (2015) No microstructural white matter alterations in chronic and episodic Migraineurs: a case-control diffusion tensor magnetic resonance imaging study. Headache 55(2):241–251

23. Valfrè W, Rainero I, Bergui M, Pinessi L (2008) Voxel-based morphometry reveals gray matter abnormalities in migraine. Headache. 48(1):109–117

24. Neeb L, Bastian K, Villringer K, Israel H, Reuter U, Fiebach JB (2017) Structural gray matter alterations in chronic migraine: implications for a progressive disease? Headache. 57(3):400–416

25. Schulte LH, Allers A, May A (2017) Hypothalamus as a mediator of chronic migraine. Neurology 88(21):2011-2016

26. Smith SM, Jenkinson M, Johansen-Berg H, Rueckert D, Nichols TE, Mackay CE et al (2006) Tract-based spatial statistics: voxelwise analysis of multisubject diffusion data. Neuroimage. 31(4):1487–1505

27. Headache Classification Committee of the International Headache Society (2013) The international classification of headache disorders, 3rd edition (beta version). Cephalalgia 33(9):629–808

28. Serrano D, Lipton RB, Scher AI, Reed ML, Stewart WF, Manack Adams A et al (2017) Fluctuations in episodic and chronic migraine status over the course of 1 year: implications for diagnosis, treatment and clinical trial design. J Headache Pain 18(1):101

29. Zigmond AS, Snaith RP (1983) The hospital anxiety and depression scale. Acta Psychiatr Scand 67(6):361-370

30. Pelletier A, Periot O, Dilharreguy B, Hiba B, Bordessoules M, Chanraud S et al (2015) Age-related modifications of diffusion tensor imaging parameters and white matter Hyperintensities as inter-dependent processes. Front Aging Neurosci 7:255

31. Veraart J, Novikov DS, Christiaens D, Ades-Aron B, Sijbers J, Fieremans E (2016) Denoising of diffusion MRI using random matrix theory. Neuroimage 142:394–406

32. Tournier J-D, Smith R, Raffelt D, Tabbara R, Dhollander T, Pietsch M et al (2019) MRtrix3: A fast, flexible and open software framework for medical image processing and visualisation. bioRxiv

33. Andersson JL, Sotiropoulos SN (2015) An integrated approach to correction for off-resonance effects and subject movement in diffusion MR imaging. Neuroimage. 125:1063–1078

34. Smith SM, Jenkinson M, Woolrich MW, Beckmann CF, Behrens TE, Johansen- Berg H et al (2004) Advances in functional and structural MR image analysis and implementation as FSL. Neuroimage 23:S208–S219

35. Zhang Y, Brady M, Smith S (2001) Segmentation of brain MR images through a hidden Markov random field model and the expectationmaximization algorithm. IEEE Trans Med Imaging 20:45–57

36. Dhollander T, Raffelt D, Connelly A (2016) Unsupervised 3-tissue response function estimation from single-shell or multi-shell diffusion MR data without a co-registered T1 image. ISMRM Work Break Barriers Diffus MRI 5 37. Jenkinson M, Beckmann CF, Behrens TE, Woolrich MW, Smith SM (2012) FSL. Neuroimage 62:782–790

38. Rueckert D, Sonoda LI, Hayes C, Hill DL, Leach MO, Hawkes DJ (1999) Nonrigid registration using free-form deformations: application to breast MR images. IEEE Trans Med Imaging 18(8):712–721

39. Mori S, Wakana S, Nagae-Poetscher LM, van Zijl PC (2005) MRI atlas of human white matter. Elsevier, Amsterdam

40. Oishi K, Zilles K, Amunts K, Faria A, Jiang H, Li X et al (2008) Human brain white matter atlas: identification and assignment of commom anatomical structures in superficial white matter. Neuroimage 43(3):447–457

41. Hua K, Zhang J, Wakana S, Jiang H, Li X, Reich DS et al (2008) Tract probability maps in stereotaxic spaces: analyses of white matter anatomy and tract-specific quantification. Neuroimage 39(1):336–347

42. Nichols TE, Holmes AP (2002) Nonparametric permutation tests for functional neuroimaging: a primer with examples. Hum Brain Mapp 15(1):1–25

43. Smith SM, Nichols TE (2009) Threshold-free cluster enhancement: addressing problems of smoothing, threshold dependence and localisation in cluster inference. Neuroimage. 44(1):83–98

44. Benjamini Y, Hochberg Y (1995) Controlling the false discovery rate: a practical and powerful approach to multiple testing. J R Stat Soc Ser B 57(1):289–300

45. Cohen J (1988) Statistical power analysis for the behavioral sciences, 2nd edn. Lawrence Erlbaum Associates, Publishers, Hillsdale

46. Bennett IJ, Madden DJ, Vaidya CJ, Howard DV, Howard JHJ (2010) Age-related differences in multiple measures of white matter integrity: a diffusion tensor imaging study of healthy aging. Hum Brain Mapp 31(3): 378–390

47. Winklewski PJ, Sabisz A, Naumczyk P, Jodzio K, Szurowska E, Szarmach A (2018) Understanding the physiopathology behind axial and radial diffusivity changes –what do we know? Front Neurol 9:92

48. Alexander AL, Lee JE, Lazar M, Field AS (2007) Diffusion tensor imaging of the brain. Neurotherapeutics 4(3):316–329

49. Sun S-W, Liang H-F, Cross AH, Song S-K (2008) Evolving Wallerian degeneration after transient retinal ischemia in mice characterized by diffusion tensor imaging. Neuroimage. 40(1):1–10

50. Pierpaoli C, Barnett A, Pajevic C, Chen R, Penix LR, Virta A et al (2001) Water diffusion changes in Wallerian degeneration and their dependence on white matter architecture. Neuroimage 13(6 Pt 1):1174–1185

51. Shu N, Wang Z, Qi Z, Li K, He Y (2011) Multiple diffusion indices reveals white matter degeneration in Alzheimer's disease and mild cognitive impairment: a tract-based spatial statistics study. J Alzheimers Dis 26(Suppl 3):275–285

52. Szabó N, Kincses ZT, Párdutz A, Tajti J, Szok D, Tuka A et al (2012) White matter microstructural alterations in migraine: a diffusion-weighted MRI study. Pain 153(3):651–656

53. Kochunov P, Thompson PM, Lancaster JL, Bartzokis G, Smith S, Coyle T et al (2007) Relationship between white matter fractional anisotropy and other indices of cerebral health in normal aging: tract-based spatial statistics study of aging. Neuroimage. 35(2):478–487

54. Beaulieu C (2002) The basis of anisotropic water diffusion in the nervous system - a technical review. NMR Biomed 15(7–8):435–455

55. Ito K, Kudo M, Sasaki M, Saito A, Yamashita F, Harada T et al (2016) Detection of changes in the peri-aqueductal gray matter of patients with episodic migraine using quantitative diffusion kurtosis imaging: preliminary findings. Neuroradiology. 58(2):115–120

56. Tedeschi G, Russo A, Conte F, Corbo D, Caiazzo G, Giordano A et al (2016) Increased interictal visual network connectivity in patients with migraine with aura. Cephalalgia. 36(2):139–147

57. Coppola G, Di Renzo A, Tinelli E, Di Lorenzo C, Di Lorenzo G, Parisi V et al (2016) Thalamo-cortical network activity during spontaneous migraine attacks. Neurology 87(20):2154–2160

58. Zhang J, Wu YL, Su J, Yao Q, Wang M, Li GF et al (2017) Assessment of gray and white matter structural alterations in migraineurs without aura. J Headache Pain 18(1):74

59. Blumenfeld-Katzir T, Pasternak O, Dagan M, Assaf Y (2011) Diffusion MRI of structural brain plasticity induced by a learning and memory task. PLoS One 6(6):e20678

60. Sampaio-Baptista C, Khrapitchev AA, Foxley S, Schlagheck T, Scholz J, Jbabdi S et al (2013) Motor skill learning induces changes in white matter microstructure and myelination. J Neurosci 33(50):19499–19503

61. Ribas EC, YaÄŸmurlu K, de Oliveira E, Ribas GC, Rhoton A (2018) Microsurgical anatomy of the central core of the brain. J Neurosurg 129(3):752–769

62. Russo A, Coppola G, Pierelli F, Parisi V, Silvestro M, Tessitore A et al (2018) Pain perception and migraine. Front Neurol 9:576

63. Borsook D, Veggeberg R, Erpelding N, Borra N, Linnman C, Burstein R et al (2016) The insula: a hub of activity in migraine. Neuroscientist 22(6):632–652

64. Porter A, Gladstone JP, Dodick DW (2005) Migraine and white matter hyperintensities. Curr Pain Headache Rep 9(4):289–293

65. Yalcin A, Ceylan M, Bayraktutan OF, Akkurt A (2018) Episodic migraine and white matter Hyperintensities: Association of Pain Lateralization. Pain Med 19(10):2051–2057

66. Xie H, Zhang Q, Huo K, Liu R, Jian Z-J, Bian Y-T et al (2018) Association of white matter hyperintensities with migraine features and prognosis. BMC Neurol 18:93

67. Lantéri-Minet M, Radat F, Chautard MH, Lucas C (2005) Anxiety and depression associated with migraine: influence on migraine subjects'disability and quality of life, and acute migraine management. Pain 118(3):319–326

68. Baskin SM, Lipchik GL, Smitherman TA (2006) Mood and anxiety disorders in chronic headache. Headache 46(Suppl 3):S76–S87

69. Minen MT, Begasse De Dhaem O, Kroon Van Diest A, Powers S, Schwedt TJ, Lipton R, et al. (2016) Migraine and its psychiatric comorbidities. J Neurol Neurosurg Psychiatry 87(7):741–749

70. May A (2017) Understanding migraine as a cycling brain syndrome: reviewing the evidence from functional imaging. Neurol Sci 38(Suppl 1):125–130

71. Karsan N, Goadsby PJ (2018) Biological insights from the premonitory symptoms of migraine. Nat Rev Neurol 14(12):699–710

## 2.7. Supplementary Material

The Supplementary Tables and Figures are included in this section.

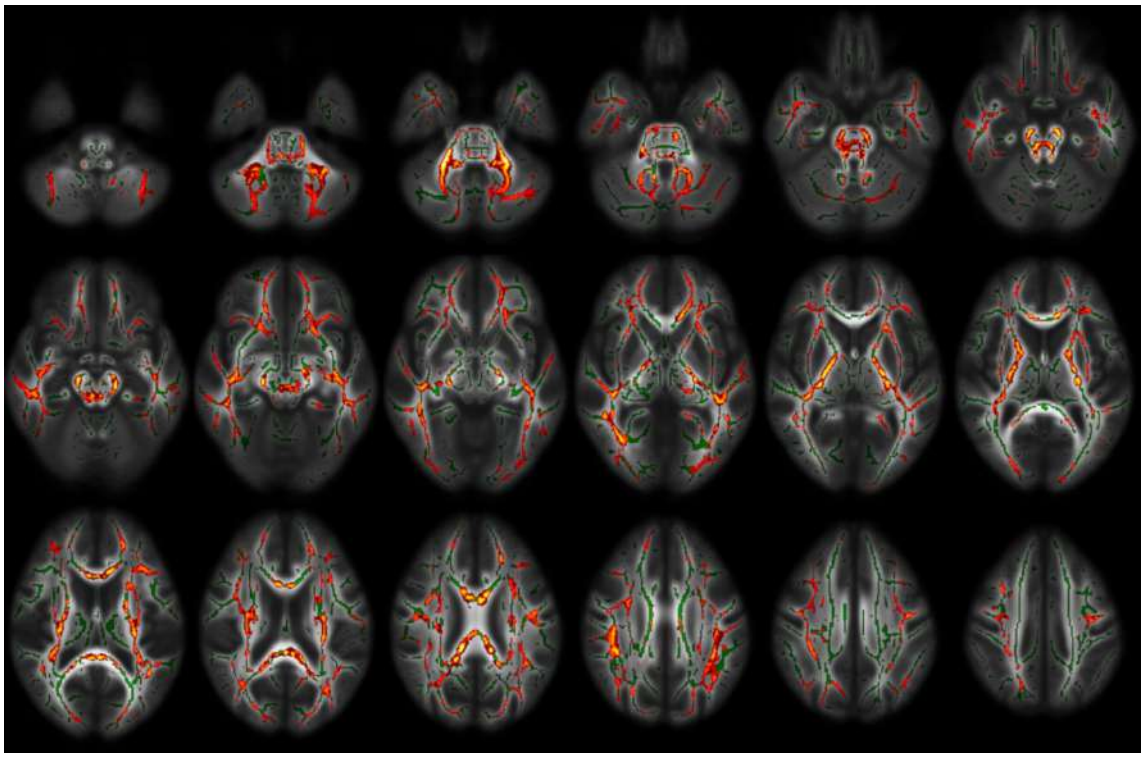

**Supplementary Figure 1. White matter alterations in chronic migraine compared to episodic migraine patients.** TBSS shows decreased AD values in CM compared to EM in widespread locations. White matter skeleton is shown in green, and voxels with significant differences in red-yellow. The color bar shows the p-values (FWE-corrected).

**Supplementary Table 1**. White matter regions where decreased AD values were found in CM compared to EM (FWE-corrected).

| White Matter tract | Minimum p-value (FWE-corrected) | Volume ($mm^3$) | MNI peak coordinate (mm), (x,y,z) |
|---|---|---|---|
| Middle cerebellar peduncle | .007 | 2206 | (-20,-50,-32) |

*continued from previous page*

| | | | |
|---|---|---|---|
| Superior cerebellar peduncle R/L | .020/.020 | 142/126 | (5,-28,-19) / (-4,-28,-19) |
| Inferior cerebellar peduncle R/L | .019/.009 | 75/89 | (12,-43,-35) / (-13,-45,-31) |
| Superior longitudinal fasciculus R/L | .021/.021 | 971/874 | (33,-4,20) / (-36,-49,15) |
| Genu of corpus callosum | .019 | 455 | (-10,28,1) |
| Body of corpus callosum | .032 | 842 | (-4,-30,23) |
| Splenium of corpus callosum | .025 | 873 | (22,-50,25) |
| Anterior corona radiata R/L | .024/.018 | 556/805 | (18,21,-11) / (-18,38,-1) |
| Superior corona radiata R/L | .020/.022 | 666/396 | (28,-16,21) / (-27,-11,20) |
| Posterior corona radiata R/L | .022/.022 | 201/214 | (25,-24,24) / (-30,-52,22) |
| External capsule R/L | .020/.018 | 459/695 | (30,-10,14) / (-22,16,-12) |
| Posterior limb of internal capsule R/L | .020/.022 | 569/536 | (26,-17,13) / (-27,-17,17) |
| Retrolenticular part of internal capsule R/L | .023/.023 | 457/344 | (31,-34,15) / (-25,-22,3) |
| Anterior limb of internal capsule R/L | .022/.020 | 216/290 | (15,-1,7) / (-20,18,3) |
| Sagittal stratum R/L | .022/.022 | 471/359 | (37,-49,-4) / (-41,-18,-13) |
| Posterior thalamic radiation R/L | .022/.022 | 353/279 | (37,-50,-2) / (-35,-52,13) |
| Cerebral peduncle R/L | .020/.022 | 234/265 | (11,-23,-21) / (-9,-19,-20) |
| Corticospinal tract R/L | .019/.023 | 106/165 | (10,-27,-26) / (-7,-18,-22) |
| Medial lemniscus R/L | .020/.015 | 82/103 | (8,-39,-40) / (-7,-37,-40) |
| Pontine crossing tract | .018 | 82 | (8,-31,-27) |
| Fornix (cres) R/L | .024/.024 | 74/45 | (35,-12,-14) / (-34,-15,-13) |
| Cingulum (hippocampus) L | .036 | 56 | (-17,-42,-2) |

FWE = Family-wise error; L = left; R = right.

The column Volume represents the volume from the atlas region with $p < .05$ (FWE-corrected). No regions with volume equal or lower than 30 $mm^3$ were included in this Table.

**Supplementary Table 2**. White matter regions where decreased AD values were found in CM compared to EM considering only patients with migraine without aura (FWE-corrected).

| White Matter tract | Minimum p-value (FWE-corrected) | Volume ($mm^3$) | MNI peak coordinate (mm), (x,y,z) |
|---|---|---|---|
| Middle cerebellar peduncle | .014 | 1382 | (-23,-46,-36) |
| Superior longitudinal fasciculus R | .040 | 388 | (33,-4,20) |
| Superior corona radiata R | .031 | 166 | (28,-17,23) |
| External capsule R | .034 | 103 | (29,-8,18) |
| Posterior limb of internal capsule R | .030 | 428 | (26,-17,13) |
| Retrolenticular part of internal capsule R | .034 | 323 | (31,-30,7) |
| Anterior limb of internal capsule R | .037 | 96 | (15,-1,7) |
| Sagittal stratum R | .034 | 380 | (37,-22,-7) |
| Posterior thalamic radiation R | .037 | 242 | (30,-39,16) |
| Fornix (cres) R | .034 | 52 | (35,-16,-12) |

FWE = Family-wise error; R = right.

The column Volume represents the volume from the atlas region with $p < .05$ (FWE-corrected). No regions with volume equal or lower than 30 $mm^3$ were included in this Table.

**Supplementary Table 3**. White matter regions from the ICBM-DTI-81 White Matter Atlas for which decreased AD values were found in CM compared to EM considering the effect of duration of migraine history (FWE-corrected).

| White Matter tract | Minimum p-value (FWE-corrected) | Volume ($mm^3$) | MNI peak coordinate (mm), (x,y,z) |
|---|---|---|---|
| Middle cerebellar peduncle | .028 | 1816 | (-20,-50,-32) |
| Superior cerebellar peduncle R/L | .066/.067 | 138/124 | (5,-28,-19) / (-4,-28,-19) |
| Inferior cerebellar peduncle R/L | .069/.039 | 44/61 | (13,-42,-36) / (-13,-45,-31) |
| Superior longitudinal fasciculus R/L | .088/.079 | 254/411 | (42,-43,3) / (-36,-50,15) |
| Body of corpus callosum | .094 | 233 | (13,-29,28) |
| Splenium of corpus callosum | .090 | 618 | (-10,-33,25) |
| Superior corona radiata R/L | .091/.095 | 261/71 | (28,-15,21) / (-27,-11,20) |
| Posterior corona radiata L | .080 | 116 | (-28,-51,25) |
| External capsule R/L | .076/.095 | 94/63 | (35,-14,-9) / (-28,-10,17) |
| Posterior limb of internal capsule R/L | .087/.095 | 77/126 | (26,-17,13) / (-23,-20,13) |
| Retrolenticular part of internal capsule R/L | .078/.095 | 323/81 | (38,-29,-1) / (-29,-38,14) |
| Sagittal stratum R | .066 | 407 | (37,-49,-3) |
| Posterior thalamic radiation R/L | .066/.081 | 256/54 | (37,-50,-3) / (-35,-52,13) |
| Cerebral peduncle R/L | .068/.092 | 153/127 | (9,-19,-21) / (-9,-19,-20) |
| Corticospinal tract R/L | .067/.093 | 98/109 | (8,-27,-26) / (-7,-18,-22) |
| Pontine crossing tract | .067 | 51 | (8,-31,-27) |
| Fornix (cres) R | .024 | 37 | (35,-12,-14) |

FWE = Family-wise error; L = left; R = right.

The column Volume represents the volume from the atlas region with p-values $< .1$ (FWE-corrected). No regions with volume equal or lower than 30 $mm^3$ were included in this Table.

**Supplementary Table 4**. White matter regions from the ICBM-DTI-81 White Matter Atlas for which increased AD values were found in EM compared to HC considering the effect of duration of migraine history (FWE-corrected).

| White Matter tract | Minimum p-value (FWE-corrected) | Volume ($mm^3$) | MNI peak coordinate (mm), (x,y,z) |
|---|---|---|---|
| Superior corona radiata L | .026 | 116 | (-26,-11,20) |
| External capsule L | .022 | 303 | (-34,-15,-8) |
| Posterior limb of internal capsule L | .024 | 472 | (-15,-10,0) |
| Retrolenticular part of internal capsule L | .025 | 347 | (-33,-34,6) |
| Sagittal stratum L | .023 | 133 | (-36,-17,-9) |
| Posterior thalamic radiation L | .025 | 38 | (-35,-39,7) |
| Cerebral peduncle L | .024 | 105 | (-15,-13,-5) |

FWE = Family-wise error; L = left.

The column Volume represents the volume from the atlas region with p-values $< .05$ (FWE-corrected). No regions with volume equal or lower than 30 $mm^3$ were included in this Table.

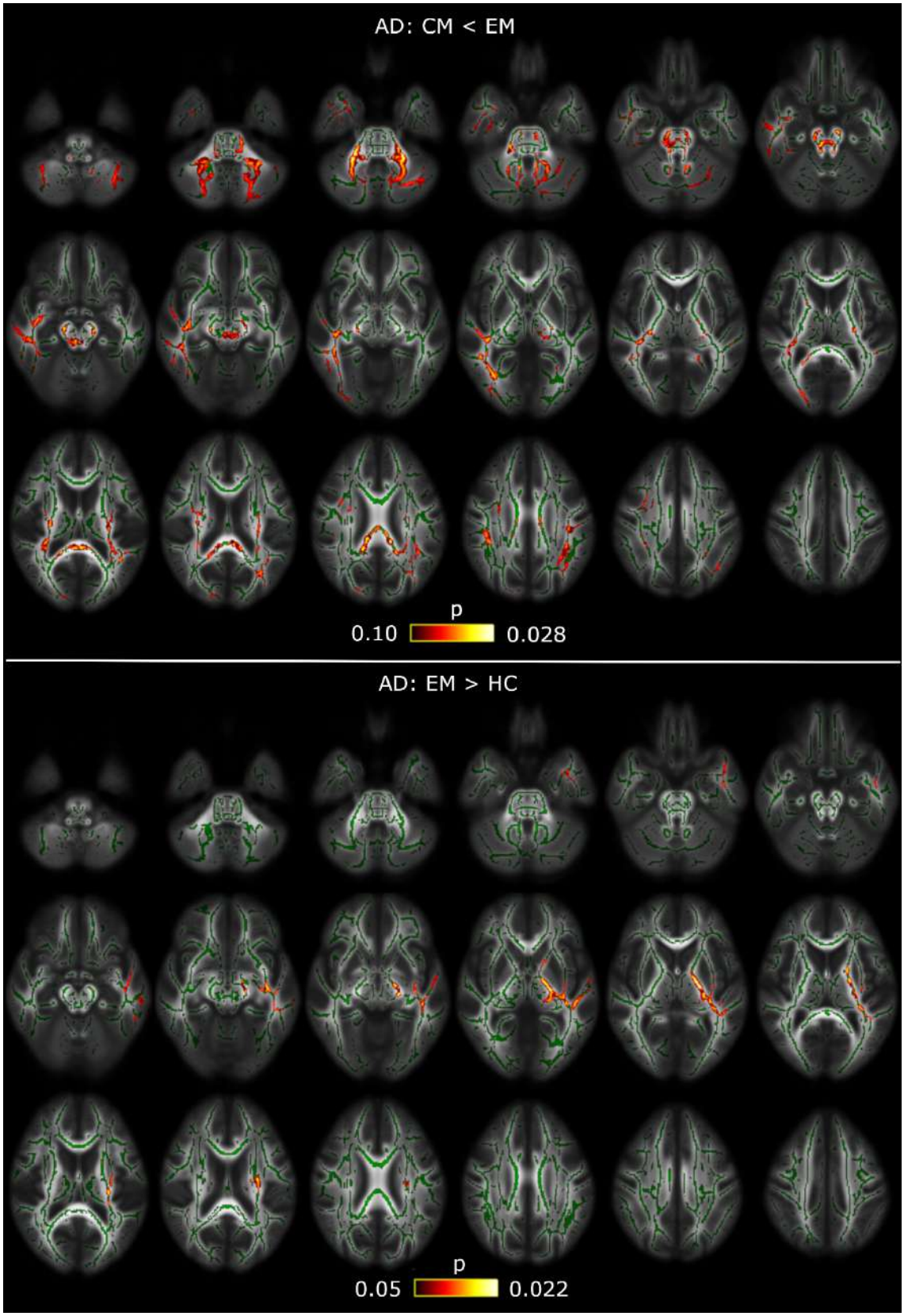


**Supplementary Figure 2. White matter alterations in migraine including duration of migraine history as a covariate**. TBSS showed decreased AD values in CM compared to EM in widespread locations (top) and increased AD values in EM compared to healthy controls (bottom) in left hemisphere locations. White matter skeleton is shown in green, and voxels with the lowest p-values in red-yellow. The colour bar shows the p-values (FWE-corrected).

**Supplementary Table 5**. White matter regions from the ICBM-DTI-81 White Matter Atlas for which significant AD values were found in CM compared to EM considering the effect of time from onset of CM (FWE-corrected).

| White Matter tract | Minimum p-value (FWE-corrected) | Volume ($mm^3$) | MNI peak coordinate (mm), (x,y,z) |
|---|---|---|---|
| Middle cerebellar peduncle | .023 | 1295 | (-20,-50,-32) |
| Superior cerebellar peduncle R/L | .028/.030 | 101/115 | (5,-28,-19) / (-4,-28,-19) |
| Inferior cerebellar peduncle L | .035 | 46 | (-10,-50,-25) |
| Superior longitudinal fasciculus R | .033 | 720 | (32,-4,20) |
| Splenium of corpus callosum | .042 | 32 | (18,-49,27) |
| Superior corona radiata R/L | .030/.032 | 335/136 | (28,-15,19) / (-27,-11,20) |
| Posterior corona radiata R | .035 | 83 | (28,-34,19) |
| External capsule R/L | .033/.031 | 127/171 | (30,-10,14) / (-28,-10,18) |
| Posterior limb of internal capsule R/L | .029/.032 | 301/281 | (26,-17,13) / (-27,-17,17) |
| Retrolenticular part of internal capsule R/L | .031/.032 | 473/59 | (30,-29,7) / (-25,-23,12) |
| Sagittal stratum R | .034 | 150 | (38,-28,-4) |
| Posterior thalamic radiation R | .034 | 51 | (30,-39,16) |
| Cerebral peduncle R/L | .028/.031 | 207/258 | (10,-28,-16) / (-9,-20,-20) |
| Corticospinal tract R/L | .030/.031 | 105/125 | (11,-22,-22) / (-7,-18,-22) |
| Pontine crossing tract | .030 | 56 | (4,-26,-24) |
| Fornix (cres) R | .037 | 46 | (35,-12,-14) |

FWE = Family-wise error; L = left; R = right.

The column Volume represents the volume from the atlas region with p-values $< .05$ (FWE-corrected). No regions with volume equal or lower than 30 $mm^3$ were included in this Table.

**Supplementary Table 6**. White matter regions from the ICBM-DTI-81 White Matter Atlas for which decreased FA values were found in CM compared to HC considering the effect of time from onset of CM (FWE-corrected).

| White Matter tract | Minimum p-value (FWE-corrected) | Volume ($mm^3$) | MNI peak coordinate (mm), (x,y,z) |
|---|---|---|---|
| Superior longitudinal fasciculus R | .033 | 271 | (32,-4,19) |
| Body of corpus callosum | .042 | 47 | (19,-30,31) |
| Splenium of corpus callosum | .042 | 209 | (19,-31,31) |
| Anterior corona radiata R | .033 | 295 | (25,17,12) |
| Superior corona radiata R | .038 | 236 | (32,-6,20) |
| Posterior corona radiata R | .039 | 133 | (25,-23,22) |
| External capsule R | .031 | 661 | (30,1,13) |
| Posterior limb of internal capsule R | .039 | 217 | (24,-19,1) |
| Retrolenticular part of internal capsule R | .036 | 425 | (38,-29,0) |
| Anterior limb of internal capsule R | .035 | 83 | (23,17,11) |
| Sagittal stratum R | .036 | 132 | (33,-23,-4) |
| Fornix (cres) R | .035 | 36 | (33,-22,-6) |

FWE = Family-wise error; L = left; R = right.

The column Volume represents the volume from the atlas region with p-values $< .05$ (FWE-corrected). No regions with volume equal or lower than 30 $mm^3$ were included in this Table.

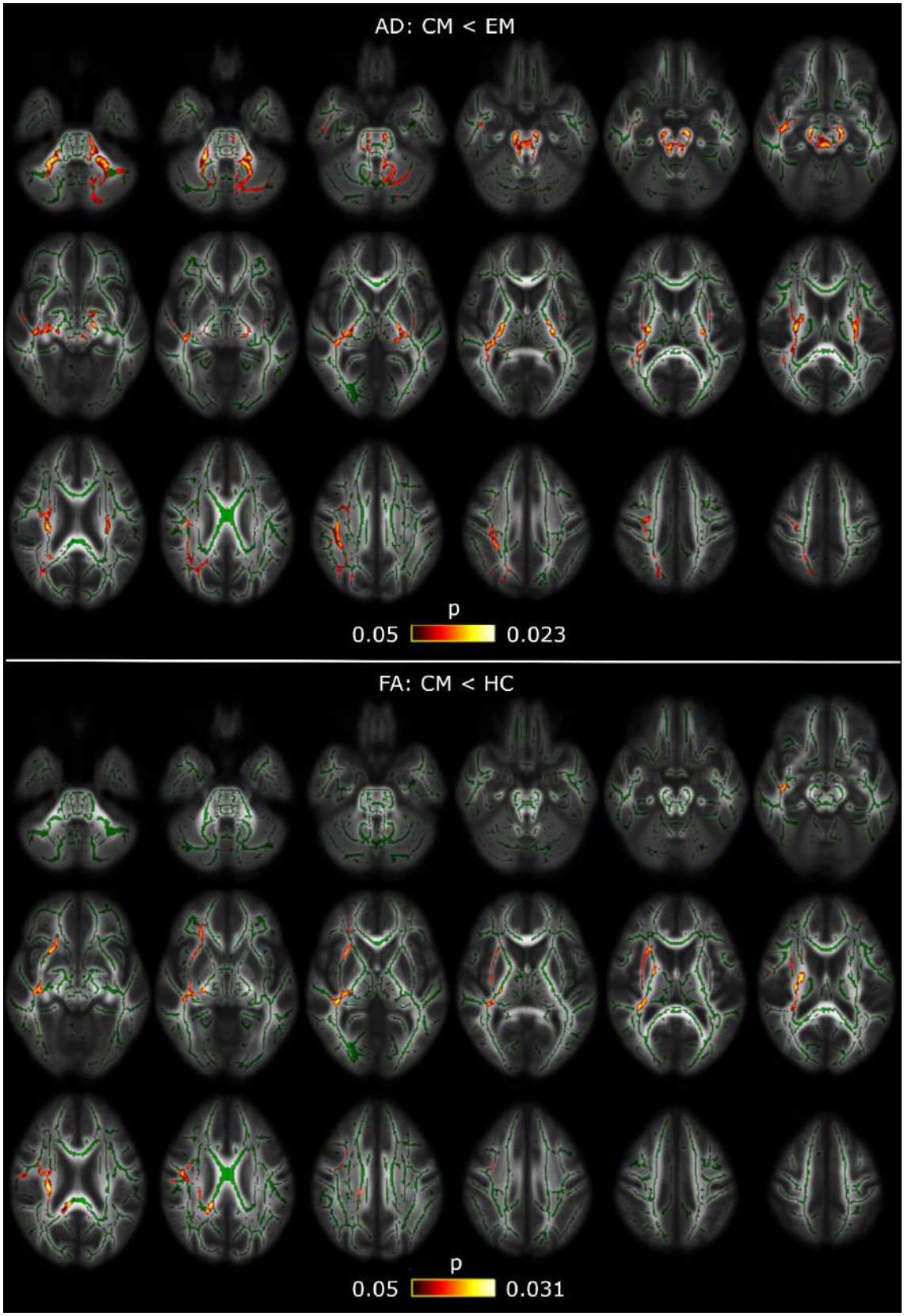


**Supplementary Figure 3. White matter alterations in CM including time from onset of chronic migraine as a covariate**. TBSS showed decreased AD values in CM compared to EM in widespread locations (top) and decreased FA values in CM compared to healthy controls (bottom). Mean white matter skeleton is shown in green, and voxels with the lowest p-values in red-yellow. The color bar shows the p-values (FWE-corrected).

**Supplementary Table 7**. Cohen's d skeleton AD values in regions with significant differences between EM and CM.

| White matter region | EM vs. HC Cohen's d | CM vs. HC Cohen's d | CM vs. EM Cohen's d |
|---|---|---|---|
| Middle cerebellar peduncle (MCP) | .31 | -.29 | **-.60** |
| Superior cerebellar peduncle R (RSCP)/L (LSCP) | .18/.03 | -.23/-.32 | -.40/-.37 |
| Inferior cerebellar peduncle R (RICP)/L (LICP) | .45/.45 | .21/.16 | -.22/-.28 |
| Superior longitudinal fasciculus R (RSLF)/L (LSLF) | .36/.47 | -.05/.01 | -.39/-.46 |
| Genu of corpus callosum (gCC) | -.01 | -.18 | -.17 |
| Body of corpus callosum (bCC) | .01 | -.09 | -.10 |
| Splenium of corpus callosum (sCC) | -.02 | -.30 | -.29 |
| Anterior corona radiata R (RACR)/L (LACR) | .06/.17 | -.14/-.18 | -.21/-.39 |
| Superior corona radiata R (RSCR)/L (LSCR) | .18/-.07 | -.18/-.19 | -.37/-.13 |
| Posterior corona radiata R (RPCR)/L (LPCR) | .15/-.01 | .01/-.16 | -.13/-.15 |
| External capsule R (REC)/L (LEC) | .17/.41 | -.09/-.05 | -.29/**-.50** |
| Posterior limb of internal capsule R (RPIC)/L (LPIC) | .07/.10 | -.29/-.19 | -.41/-.33 |
| Retrolenticular part of internal capsule R (RRIC)/L (LRIC) | .28/.32 | -.09/.05 | -.39/-.34 |
| Anterior limb of internal capsule R (RAIC)/L (LAIC) | -.07/.23 | -.27/-.01 | -.22/-.29 |
| Sagittal stratum R (RSS)/L (LSS) | .26/.31 | -.30/-.04 | **-.57**/-.36 |
| Posterior thalamic radiation R (RPTR)/L (LPTR) | .07/.06 | -.18/-.12 | -.24/-.18 |
| Cerebral peduncle R (RCP)/L (LCP) | .08/.07 | -.15/-.26 | -.27/-.40 |
| Corticospinal tract R (RCT)/L (LCT) | -.11/-.03 | -.18/-.34 | -.08/-.32 |
| Medial lemniscus R (RML)/L (LML) | -.15/-.02 | -.32/-.27 | -.17/-.26 |
| Pontine crossing tract (PCT) | **.59** | .47 | -.03 |
| Fornix (cres) R (RF)/L (LF) | .14/.17 | .02/.20 | -.14/.00 |
| Cingulum (hippocampus) L (LCH) | .07 | -.20 | -.29 |

L = left; R = right.

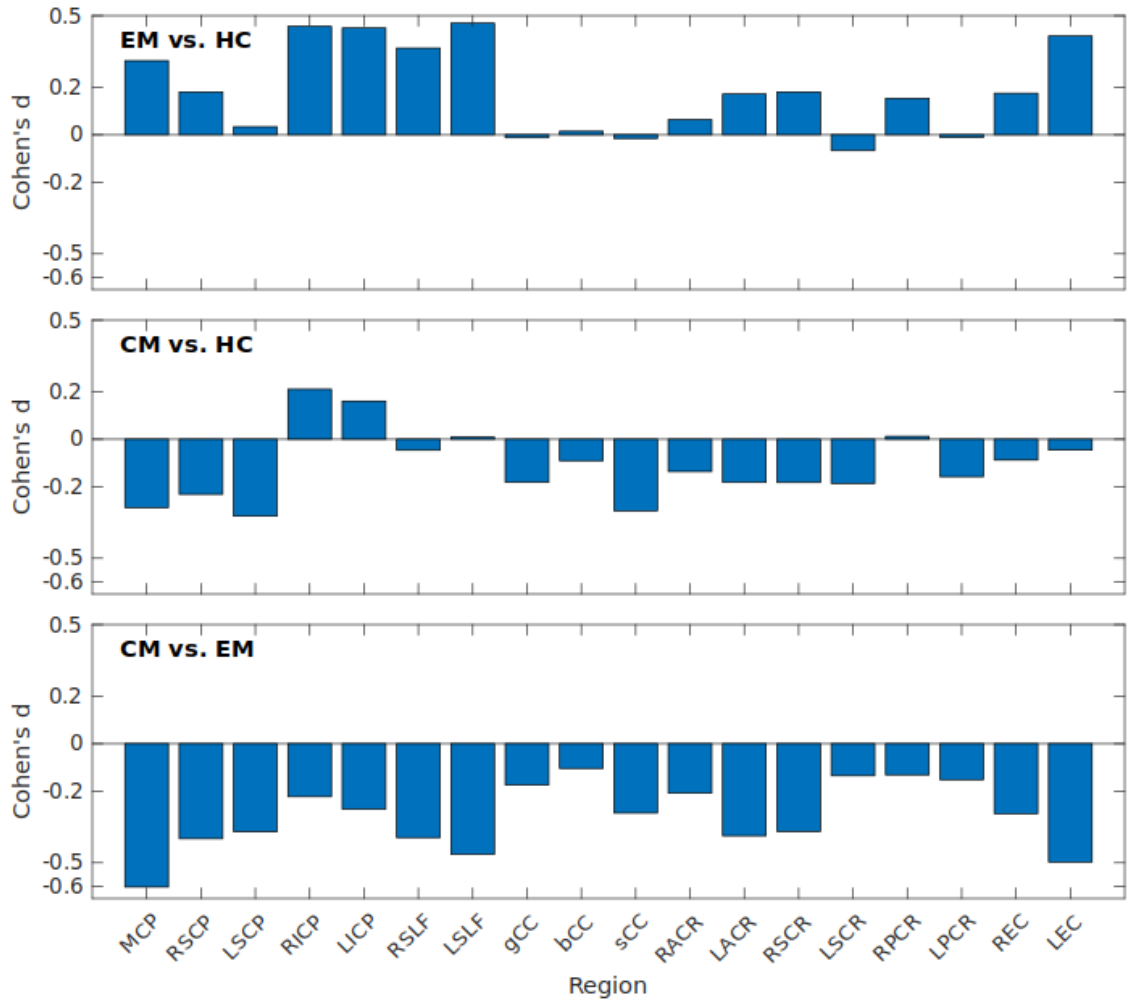


**Supplementary Figure 4 Cohen's AD bar plots of regions with FWE-corrected differences between EM and CM (part 1)**. Values for all possible pairwise comparisons are shown. Region abbreviations can be seen in Supplementary Table 7.

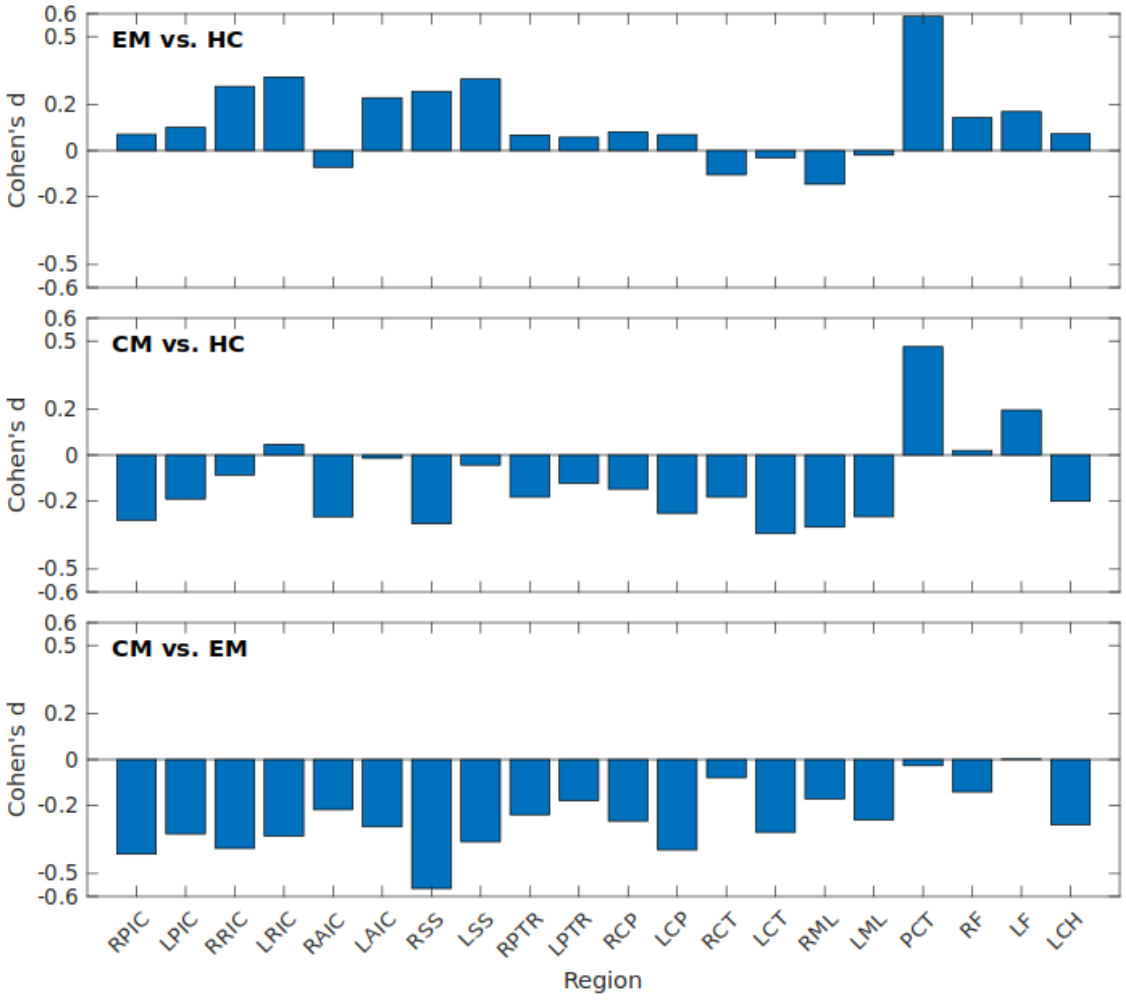


**Supplementary Figure 5 Cohen's AD bar plots of regions with FWE-corrected differences between EM and CM (part 2)**. Values for all possible pairwise comparisons are shown. Region abbreviations can be seen in Supplementary Table 7.

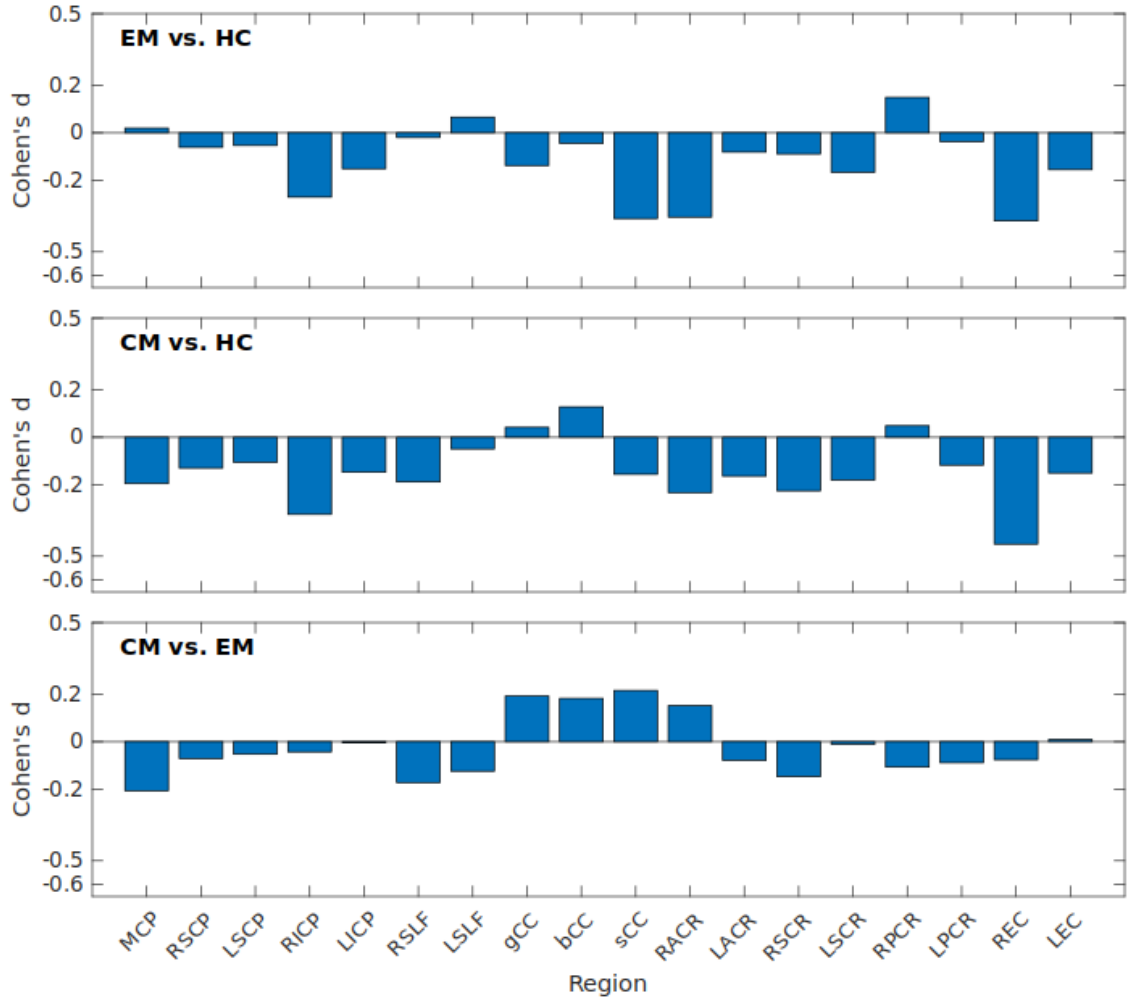


**Supplementary Figure 6 Cohen's d FA bar plots (part 1)**. Values for all possible pairwise comparisons where significant differences in AD between EM and CM patients were found are shown. Region abbreviations can be seen in Supplementary Table 7.

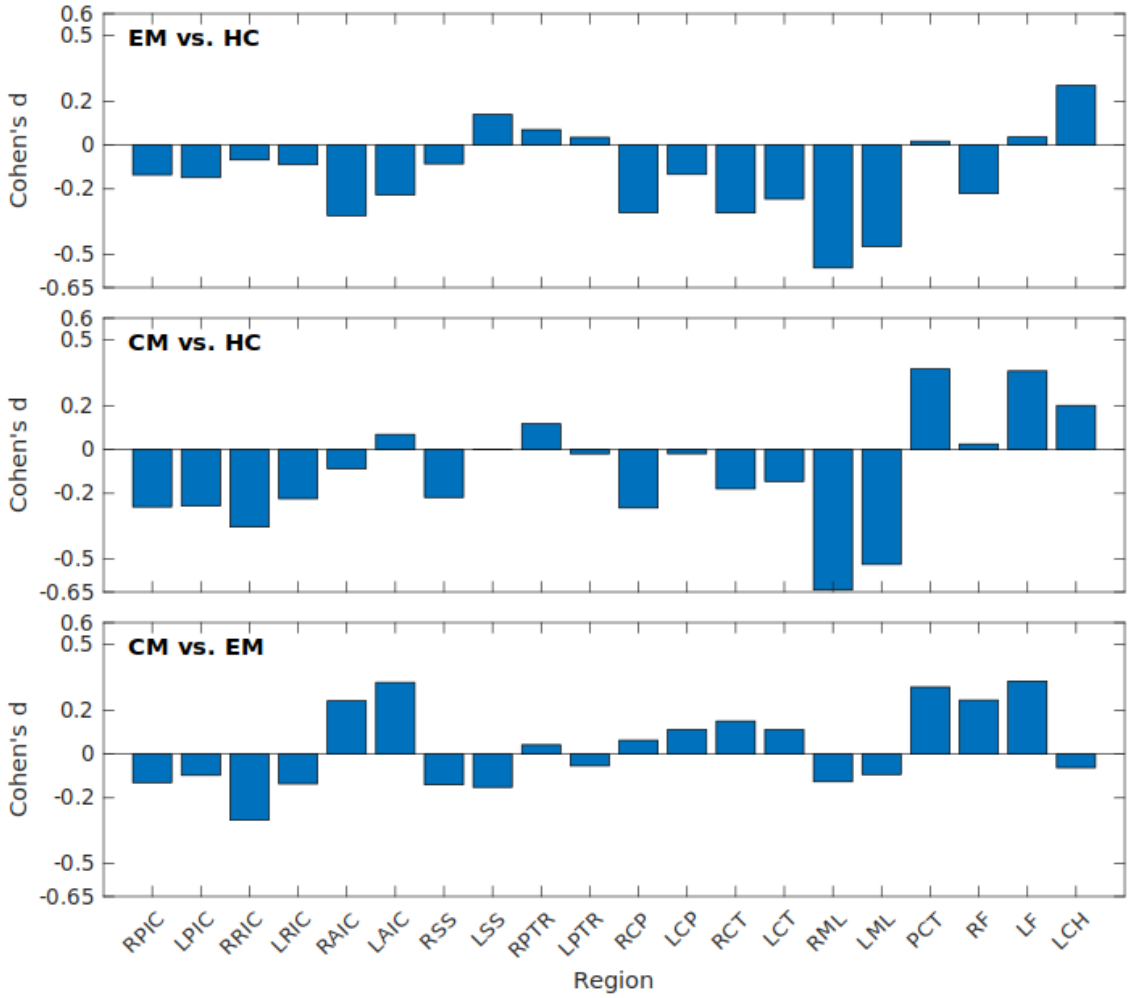


**Supplementary Figure 7 Cohen's d FA bar plots (part 2)**. Values for all possible pairwise comparisons where significant differences in AD between EM and CM patients were found are shown. Region abbreviations can be seen in Supplementary Table 7.

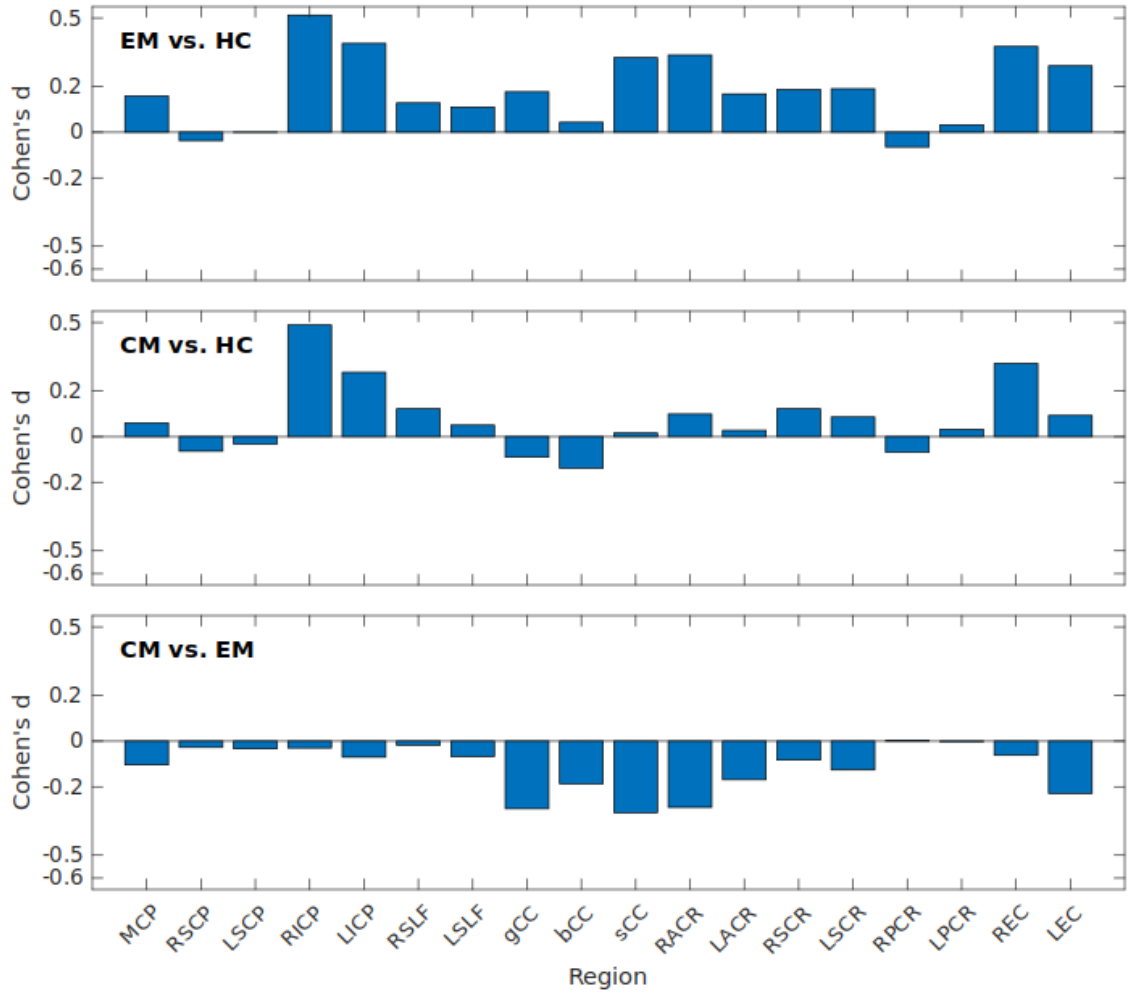


**Supplementary Figure 8 Cohen's d RD bar plots (part 1)**. Values for all possible pairwise comparisons where significant differences in AD between EM and CM patients were found are shown. Region abbreviations can be seen in Supplementary Table 7.

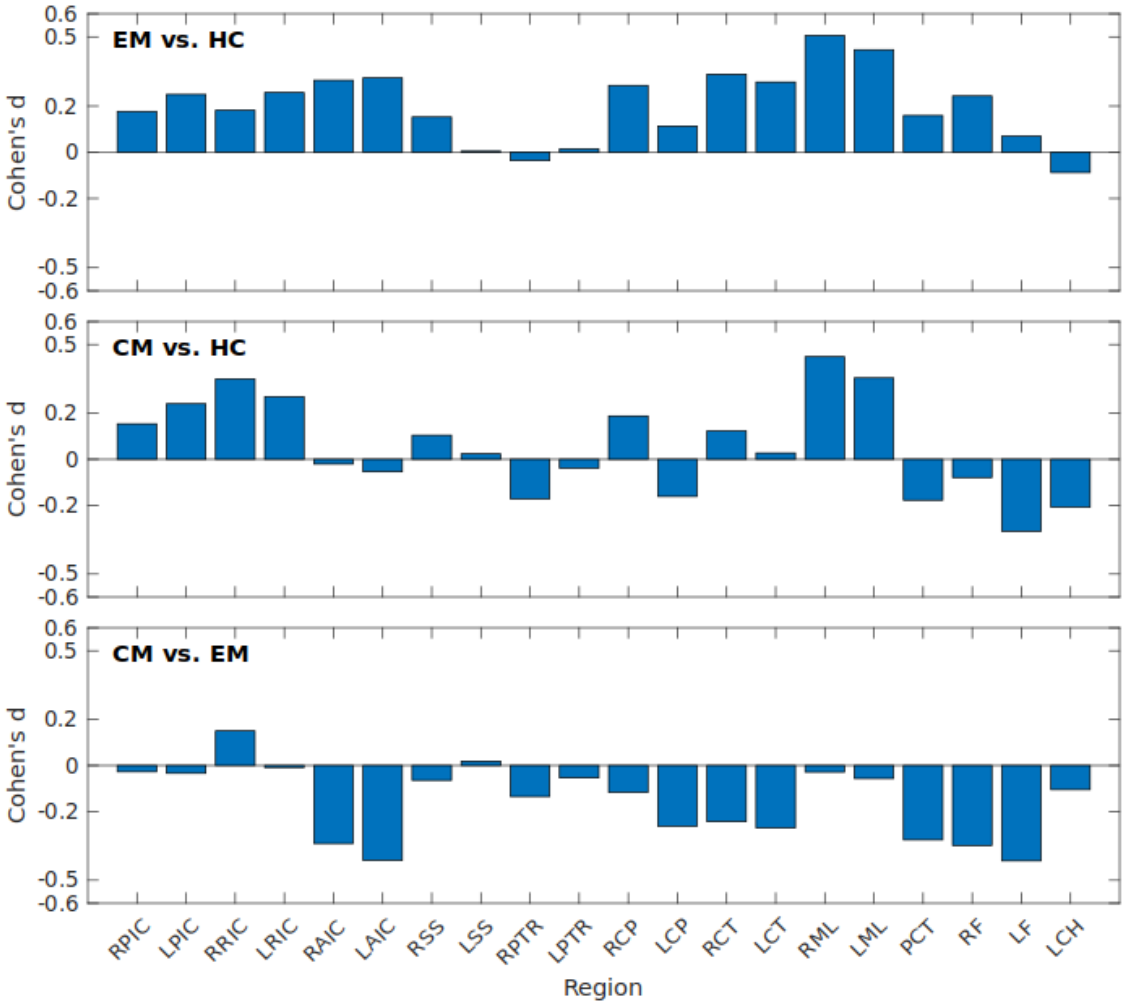


**Supplementary Figure 9 Cohen's d RD bar plots (part 2)**. Values for all possible pairwise comparisons where significant differences in AD between EM and CM patients were found are shown. Region abbreviations can be seen in Supplementary Table 7.

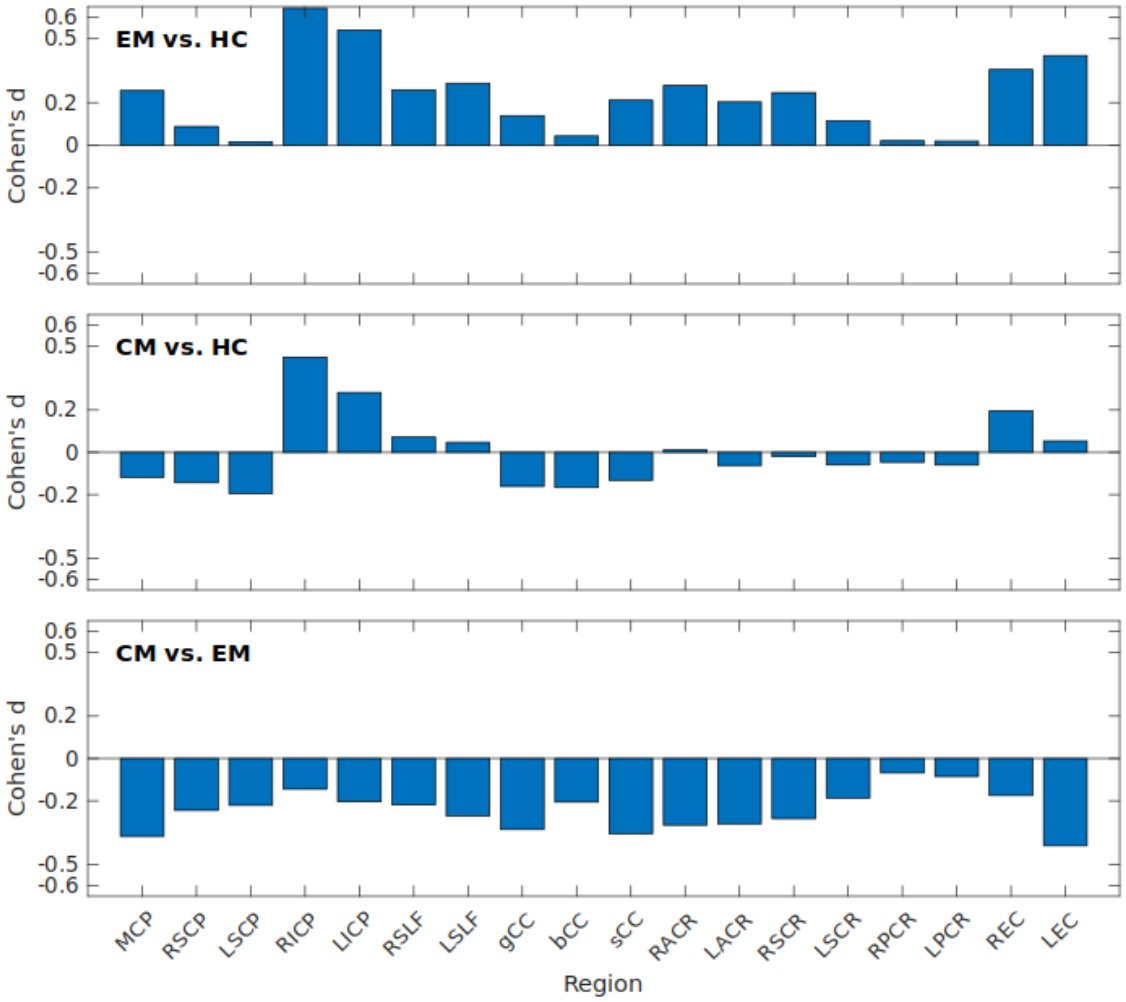


**Supplementary Figure 10 Cohen's d MD bar plots (part 1)**. Values for all possible pairwise comparisons where significant differences in AD between EM and CM patients were found are shown. Region abbreviations can be seen in Supplementary Table 7.

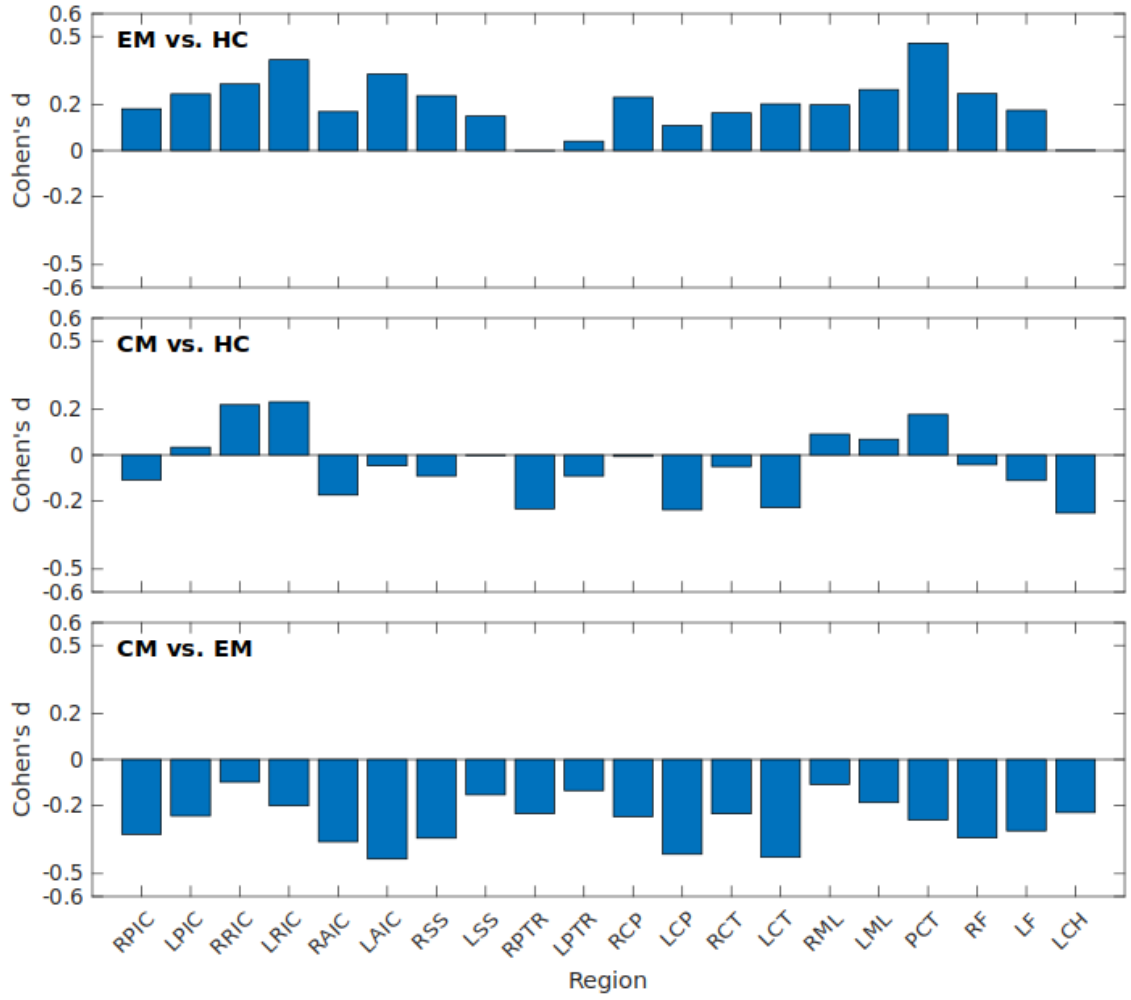


**Supplementary Figure 11 Cohen's d MD bar plots (part 2)**. Values for all possible pairwise comparisons where significant differences in AD between EM and CM patients were found are shown. Region abbreviations can be seen in Supplementary Table 7.

*Chapter 3*

# *Contribution 3: Alternative Microstructural Measures to Complement Diffusion Tensor Imaging in Migraine Studies with Standard MRI Acquisition*

**Published as**:

*Planchuelo-Gómez, Á.[1], García-Azorín, D.[2,3], Guerrero, Á.L.[2,3,4], de Luis-García, R.[1], Rodríguez, M.[5] and Aja-Fernández, S.[1] (2020). Alternative Microstructural Measures to Complement Diffusion Tensor Imaging in Migraine Studies with Standard MRI Acquisition. Brain Sciences, 10 (10),711. doi: 10.3390/brainsci10100711.*

1. Imaging Processing Laboratory, Universidad de Valladolid, Valladolid, Spain
2. Headache Unit, Department of Neurology, Hospital Clínico Universitario de Valladolid, Valladolid, Spain
3. Institute for Biomedical Research of Salamanca (IBSAL), Salamanca, Spain
4. Department of Medicine, Universidad de Valladolid, Valladolid, Spain
5. Department of Radiology, Hospital Clínico Universitario de Valladolid, Valladolid, Spain

The purpose of this study was the evaluation of a new tool, AMURA, to acquire alternative and advanced diffusion measures from diffusion-weighted images obtained with a clinical routine acquisition protocol. The employed measures, RTAP, RTOP and RTPP, were employed for the first time in a migraine study assessing white matter regions. Despite the non-optimal conditions for the extraction of the diffusion measures with AMURA, statistically significant differences between EM patients and controls were identified, a result that could not be found using DTI-based parameters with the same sample and the same TBSS analysis. Therefore, new diffusion measures are presented to complement the results from DTI studies with migraine patients.

### Abstract

The white matter state in migraine has been investigated using diffusion tensor imaging (DTI) measures, but results using this technique are conflicting. To overcome DTI measures, we employed ensemble average diffusion propagator measures obtained with apparent measures using reduced acquisitions (AMURA). The AMURA measures were return-to-axis (RTAP), return-to-origin (RTOP) and return-to-plane probabilities (RTPP). Tract-based spatial statistics was used to compare fractional anisotropy, mean diffusivity, axial diffusivity and radial diffusivity from DTI, and RTAP, RTOP and RTPP, between healthy controls, episodic migraine and chronic migraine patients. Fifty healthy controls, 54 patients with episodic migraine and 56 with chronic migraine were assessed. Significant differences were found between both types of migraine, with lower axial diffusivity values in 38 white matter regions and higher RTOP values in the middle cerebellar peduncle in patients with a chronic migraine ($p < 0.05$ family-wise error corrected). Significantly lower RTPP values were found in episodic migraine patients compared to healthy controls in 24 white matter regions ($p < 0.05$ family-wise error corrected), finding no significant differences using DTI measures. The white matter microstructure is altered in a migraine, and in chronic compared to episodic migraine. AMURA can provide additional results with respect to DTI to uncover white matter alterations in migraine.


**Keywords**: migraine; chronic migraine; diffusion tensor imaging; magnetic resonance imaging (MRI); tract-based spatial statistics; diffusion magnetic resonance imaging

# 3.1. Introduction

Headache attacks in a migraine are characterized by episodes of unilateral pain of moderate to severe intensity, pulsating quality, aggravated by routine physical activity and accompanied by other symptoms, such as nausea and/or vomiting, photophobia and phonophobia, which last between 4 and 72 h [1]. Two main migraine types are currently distinguished: episodic migraine (EM) and chronic migraine (CM). The difference between both types is the frequency of headache days per month, which is 15 or more days in CM, and lower than 15 in EM, during at least three months [1].

To better understand migraine pathophysiology, diverse modalities of magnetic resonance imaging (MRI) have been employed. Among MRI modalities, those based on diffusion MRI (dMRI) give a particular insight on connectivity and white matter structure. Despite the advances of dMRI techniques, most of the migraine studies are based on the analysis of measures derived from diffusion tensor imaging (DTI). However, different DTI studies produce conflicting results. In most studies, the reported values of the fractional anisotropy (FA) were lower in migraine compared to controls in whole brain studies with tract-based spatial statistics (TBSS) [2–5], the most employed technique in dMRI migraine studies. Nonetheless, the opposite result, higher FA values in patients with a migraine, has also been found using the same assessment method [6]. In addition, only three dMRI studies with TBSS as assessment methods compared simultaneously patients with EM and CM, and controls. One study found significantly lower axial diffusivity (AD) values in CM compared to EM [7], another study found lower FA and higher mean diffusivity (MD) values in CM [8], and the other one found no significant differences [9].

To overcome DTI limitations, many different techniques have been proposed in the last decades, implying the acquisition of larger volumes of diffusion data (more gradient directions, more b-values) and, many times, longer processing times. Some examples of these techniques are multi-tensor models [10],

Q-Ball imaging [10,11] or diffusion Kurtosis imaging (DKI) [12]. The trend over the last decade is the direct estimation of the ensemble average diffusion propagator (EAP), the probability density function of the motion of the water molecules inside each voxel [13,14]. The complete characterization of the EAP requires a large number of diffusion-weighted images with relative high b-values in a multishell acquisition. In clinical studies, the whole information provided by the EAP is translated into scalar values that can act as biomarkers. The most common measures are the return-to-origin (RTOP), return-to-plane (RTPP) and return-to-axis probabilities (RTAP) [15]. No dMRI studies with migraine patients have employed EAP-based measures.

Despite the advantages of the EAP-based measures, the calculation of these scalars usually requires long execution and acquisition times, together with very large b-values and a large number of diffusion gradients, not always available in commercial scanners and clinical routine. To solve these problems, a new methodology called Apparent Measures Using Reduced Acquisitions (AMURA) has been developed [16]. This tool allows the estimation of the EAP-related scalars without the explicit calculation of the EAP, using a lower number of samples, even with a single-shell acquisition scheme, assuming that the diffusion signal is independent from the radial direction. This methodology allows shorter MRI acquisition and very fast calculation of scalars. AMURA was initially designed for b-values of at least 2000 s/mm$^2$, compatible with b-values employed in the high angular resolution diffusion imaging technique, which allows better modeling of white matter fiber architecture [11]. However, it could also be used for lower b-values, understanding that the effects measures by the scalars will be weaker.

Our objective was to assess whether EAP-based measures from the AMURA tool, calculated from a DTI compatible diffusion MRI acquisition (single-shell scheme and low b-value) typical in the clinical routine and in migraine diffusion MRI studies, was able to detect additional white matter changes between patients with migraine and controls with respect to DTI scalar measures.

# 3.2. Materials and Methods

## *3.2.1.* ***Participants***

A case-control study was carried out. Patients with a migraine were firstly screened and recruited from the headache outpatient unit at the Hospital ClÃnico Universitario de Valladolid (Valladolid, Spain). The participants from this study have been part of previous studies [7,17]. A total of 50 healthy controls (HCs), 54 patients with EM and 56 with CM were included in the sample. The inclusion criteria included diagnosis of EM or CM following the International Classification of Headache Disorders guidelines (third beta and third version) [1,18], stable situation of EM or CM in the preceding three months, agreement to participate in the study after signing the written informed consent and age from 18 to 60. The exclusion criteria included monthly frequency of a headache from 10 to 14 (exclusion of high frequency EM to avoid confusion with CM [19]), alternative craniofacial pain circumstances with a monthly frequency of 10 or higher, diagnosed major psychiatric disorders (in anamnesis or following the depression threshold from the Hospital Anxiety and Depression Scale [20]), additional neurological diseases or headache disorders, drug or substance abuse and pregnancy or childbearing. Every patient included in the sample was preventive naÃ¯ve and fulfilled a headache diary the three months before inclusion. In some patients, a preventive treatment for migraines was prescribed at the visit. These patients started the prescribed prophylactic treatment after the MRI

acquisition. Patients with EM from the sample suffered no tension-type headache. HC presented neither a present nor past history of migraines, nor major psychiatric or headache disorders, excluding infrequent tension-type headaches. No participants with brain abnormalities detected on T1-weighted MRI data by a radiologist were included in the sample. Patients were sampled following a non-probabilistic method by convenience sampling. Since the first patient (and first visit), all consecutive patients were informed and invited to participate, and enrolled if they agreed and signed the informed consent form. HC were balanced for age and sex by snowball and convenience sampling, following recruitment through advertisements in the University and hospital and colleagues.

Age and gender were gathered from every participant. The following characteristics were collected from every patient: duration of the migraine (years), monthly frequency of headache and migraine attacks (days), number of months from the onset of CM (if pertinent), presence of aura and intake of symptomatic medication for migraine (combination of analgesics and triptan). Acute medication overuse was considered if the intake monthly frequency was equal or higher than 10 according to the headache diary, following the International Classification of Headache Disorders guidelines (third beta and third version) [1,18].

The Hospital Clínico Universitario de Valladolid local Ethics Committee approved this study (PI: 14-197). Participants read and signed a written informed consent form before taking part in the study.

## *3.2.2.* ***MRI Acquisition***

All patients scanned suffered no migraine attacks in the previous 24 h. MRI acquisition was performed with a Philips Achieva 3 T MRI unit (Philips Healthcare, Best, The Netherlands), using a 32-channel head coil in the MRI facility at the University of Valladolid (Valladolid, Spain).

First, high-resolution 3D anatomical T1-weighted images were acquired using the following parameters: Turbo field echo (TFE) sequence, repetition time (TR) = 8.1 ms, echo time (TE) = 3.7 ms, flip angle = 8°, 256 x 256 matrix size, spatial resolution of 1 x 1 x 1 $mm^3$ and 160 slices that cover the whole brain.

Then, diffusion-weighted data were obtained. The parameters employed in the acquisition were TR = 9000 ms, TE = 86 ms, flip angle = 90°, single-shell acquisition with 61 gradient directions and b-value = 1000 $s/mm^2$, one baseline volume, 128 x 128 matrix size, spatial resolution of 2 x 2 x 2 $mm^3$ and 66 slices that cover the whole brain.

Both T1 and diffusion-weighted data were collected between May 2014 and July 2018 in a unique MRI session, starting with the T1 scan. For a single subject, the time for both scans was approximately 18 minutes.

## *3.2.3.* ***MRI Processing***

### *A. Diffusion MRI Preprocessing*

The preprocessing steps were denoising, correction for eddy currents and motion and correction for $B_1$ field inhomogeneity. The MRtrix software [21] was employed to carry out these steps, using the dwidenoise, dwipreproc and dwibiascorrect (-fast option) tools [22–25]. A whole brain mask for each subject was acquired with the dwi2mask tool [26].

## *B. Calculation of the Diffusion Measures*

Two groups of diffusion measures were employed. On the one hand, four measures from DTI were employed: FA, MD, AD and radial diffusivity (RD). On the other hand, three measures were computed with AMURA: RTOP, RTAP and RTPP.

The estimation of the diffusion tensor at each voxel, with the corresponding obtention of FA, AD and MD, was performed with the dtifit tool from the FSL software [27]. RD was manually obtained from the mean value of the second and the third eigenvalues from the diffusion tensor. FA manifests the directionality of water molecules displacement by diffusion, MD the average magnitude of water molecules diffusion, AD the water diffusion in the main direction of white matter fibers and RD the water diffusion in the perpendicular direction with respect to the main direction [28].

AMURA was employed to estimate the RTOP, RTPP and RTAP values. The tool can be downloaded with no restrictions in the following link: https://www.lpi.tel.uva.es/AMURA. We ran AMURA using MATLAB 2019b. The calculation with AMURA saves a great amount of time assuming that the diffusion signal is independent from the radial direction. Details about the mathematical models and the comparison against the whole EAP can be found elsewhere [16]. The RTOP has been pointed out as a better biomarker for cellularity and diffusion restrictions in comparison with the MD [29], the RTPP as a marker of diffusion restriction in the axial direction [14] and the RTAP as a marker of diffusion restriction in the radial direction [14]. A visual comparison of the three measures obtained with the AMURA tool, and the corresponding DTI measures, considering the commented inverse trends with the eigenvalues, is shown in Figure 3.5. It is worth noting that, assuming a simpler Gaussian diffusion propagator, the RTOP, RTPP and RTAP values can be calculated using the diffusion tensor: they are associated with the inverse values of the square root of the three eigenvalues, the first eigenvalue and the second and third eigenvalues, respectively. These equations are shown in Appendix A. Note that RTOP and RTAP depend on the inverse of the smaller eigenvalue. As a consequence, these two measures, when calculated using the diffusion tensor, are very sensitive to noise and outliers. In this study, we discarded this calculation, since it produces very high values in most of the areas of interest (high anisotropy) that makes any further analysis unfeasible. AMURA, on the other hand, produces robust values for the three considered measures.

## *C. Tract-Based Spatial Statistics (TBSS)*

TBSS was employed to compare the diffusion measures in white matter tracts between the three groups of interest [30]. The white matter tracts were identified according to the Johns Hopkins University ICBM-DTI-81 White Matter and the White Matter Tractography Atlas to cover the whole brain [31–33], considering a total of 48 and 20 regions of interest (ROIs), respectively. The first step of TBSS was the nonlinear registration of the participants'FA images to a template of averaged FA images (FMRIB-58) in the Montreal Neurological Institute (MNI) space with the FNIRT tool [34]. After the registration, a mean FA skeleton image was created with an FA threshold value of 0.2 to distinguish white from gray matter. The individual FA images from the subjects were projected onto the mean FA skeleton, and the TBSS projection was repeated for the non-FA images, i.e., MD, AD, RD, RTOP, RTAP and RTPP. The

minimum volume to consider significant results in a single region was 30 $mm^3$, equal to the number of voxels in this study, which could be part of one or more clusters.

### *D. Statistical Analysis*

For the analysis of the quantitative variables, normality and homogeneity of variance were assessed with the Kolmogorov-Smirnov and the Levene's test for equality of variances, respectively. In the comparisons with the three groups, the parametric test employed was a one-way ANOVA, and the Kruskal-Wallis test if normality and homogeneity assumptions were rejected. For the comparisons between both migraine groups, two-tailed unpaired t-test and Mann-Whitney U test were used instead of ANOVA and Kruskal-Wallis tests, respectively. The comparison of gender between the three groups was performed with a chi-squared test, and comparisons of categorical features between both migraine groups were performed with the Fisher's exact test.

Regarding the TBSS analysis, the randomize tool, a permutation-based inference tool by nonparametric statistics, using the threshold-free cluster enhancement (TFCE) option from FSL [35,36], was used to test the voxelwise differences between the three groups. The number of permutations for each comparison was 5000 to perform a robust inference, and $p < 0.05$, family-wise error corrected with the TFCE option, was the statistical threshold to consider significant results.

In a secondary analysis, the TBSS analysis was repeated including the time from onset of CM and the total duration of a migraine as covariates in separate comparisons. Both covariates were not included simultaneously in the analysis because of possible collinearity.

Moreover, the association between the duration of migraine (total duration or time from onset of CM) and DTI and AMURA measures was assessed. To analyze trends within each type of migraine and following the previous study with the same sample [7], we acquired the correlation values in patients with EM and CM independently. The inverse warp fields of the FA images to the MNI space transformation from the TBSS processing steps were obtained and used to obtain individual label maps based on the John Hopkins University ICBM-DTI-81 White Matter atlas. The mean value of each parameter in the diverse regions of the atlas and the Spearman's rank correlation value were employed in the correlation analysis. The results were corrected for multiple comparisons with the Benjamini-Hochberg false discovery rate method [37]. A value of $p < 0.05$, adjusted for multiple comparisons, was considered statistically significant.

## 3.3. Results

Fifty HC, 54 patients with EM and 56 patients with CM were included in the sample. No significant differences in age or gender were found between the three groups. Patients with CM showed significantly higher duration of migraine, frequency of headache and migraine attacks and overuse of medication, and a lower presence of aura. The detailed characteristics from the three groups are shown in Table 1 (also shown in the previous studies with the same sample [7,17]).

### *3.3.1.* ***TBSS***

Using the DTI measures (FA, MD, AD and RD), the only comparison with significant differences was that between both groups of patients with a migraine. Patients with CM showed lower AD values than EM in 38 out of 48 regions from the ICBM-DTI-81 Atlas, and in 15 out of 20 regions from the White Matter Tractography Atlas. These results are depicted in Figure 2, and in Tables 2 and 3.

With respect to the RTOP, RTAP and RTPP values, first, with the assumption of the Gaussian model, the dependence of RTOP and RTAP on the smallest eigenvalue produced a great number of outliers in the areas with high anisotropy that made the TBSS comparisons unfeasible. Hence, we only analyzed the three values using the AMURA tool. As in the DTI comparison mentioned previously, significant differences were found between both groups of migraine patients, with higher RTPP values in patients with CM, but significant results were found only in the middle cerebellar peduncle (significant volume = 370 $mm^3$, minimum corrected p = 0.035, peak at x = -19, y = -45, z = -35 in the MNI space). The RTPP comparison between both migraine groups is depicted in Figure 3. Furthermore, significant differences between patients with EM and HC were found using the RTOP. Patients with EM showed lower RTOP values than HC in 24 of the assessed regions from the ICBM-DTI-81 White Matter Atlas, and in 11 regions from the White Matter Tractography Atlas. The RTOP results are shown in Figure 4.3 and Tables 4 and 5. No significant results with the AMURA tool were found either between patients with CM and HC or using the RTAP measure.

A summary with the previous TBSS results can be found in Figure 5.

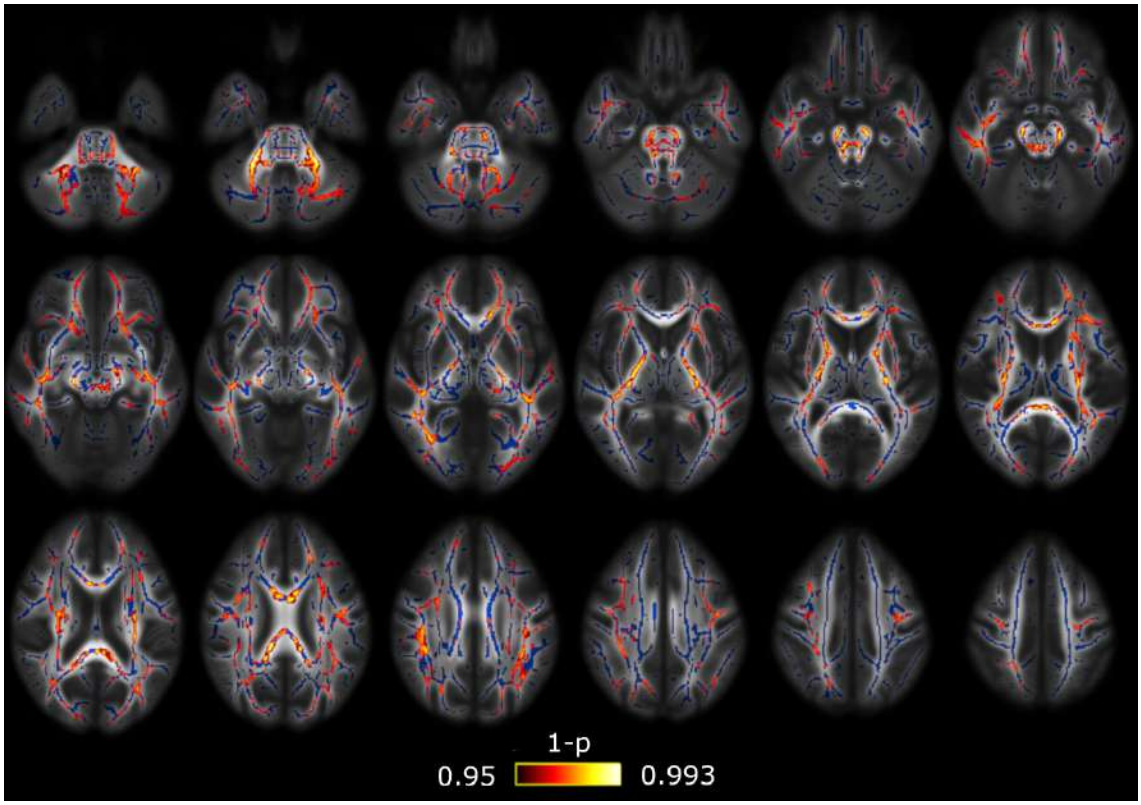


**Figure 2**. Axial diffusivity (AD) alterations in patients with CM in comparison with patients with EM. Widespread significant lower AD values were found in CM. The white matter skeleton is shown in blue and voxels with significant differences in red-yellow. The color bar shows the 1-p values (family-wise error corrected).

**Table 2**. White matter regions from the ICBM-DTI-81 White Matter Atlas for which significant decreased AD values were found in CM compared to EM.

| White Matter tract | Minimum p-value (FWE-corrected) | Volume ($mm^3$) | MNI peak coordinate (mm), (x,y,z) |
|---|---|---|---|
| Middle cerebellar peduncle | .007 | 2206 | (-20,-50,-32) |
| Superior cerebellar peduncle R/L | .020/.020 | 142/126 | (5,-28,-19) / (-4,-28,-19) |
| Inferior cerebellar peduncle R/L | .019/.009 | 75/89 | (12,-43,-35) / (-13,-45,-31) |
| Superior longitudinal fasciculus R/L | .021/.021 | 971/874 | (33,-4,20) / (-36,-49,15) |
| Genu of corpus callosum | .019 | 455 | (-10,28,1) |
| Body of corpus callosum | .032 | 842 | (-4,-30,23) |
| Splenium of corpus callosum | .025 | 873 | (22,-50,25) |
| Anterior corona radiata R/L | .024/.018 | 556/805 | (18,21,-11) / (-18,38,-1) |
| Superior corona radiata R/L | .020/.022 | 666/396 | (28,-16,21) / (-27,-11,20) |
| Posterior corona radiata R/L | .022/.022 | 201/214 | (25,-24,24) / (-30,-52,22) |
| External capsule R/L | .020/.018 | 459/695 | (30,-10,14) / (-22,16,-12) |
| Posterior limb of internal capsule R/L | .020/.022 | 569/536 | (26,-17,13) / (-27,-17,17) |
| Retrolenticular part of internal capsule R/L | .023/.023 | 457/344 | (31,-34,15) / (-25,-22,3) |
| Anterior limb of internal capsule R/L | .022/.020 | 216/290 | (15,-1,7) / (-20,18,3) |
| Sagittal stratum R/L | .022/.022 | 471/359 | (37,-49,-4) / (-41,-18,-13) |
| Posterior thalamic radiation R/L | .022/.022 | 353/279 | (37,-50,-2) / (-35,-52,13) |
| Cerebral peduncle R/L | .020/.022 | 234/265 | (11,-23,-21) / (-9,-19,-20) |
| Corticospinal tract R/L | .019/.023 | 106/165 | (10,-27,-26) / (-7,-18,-22) |
| Medial lemniscus R/L | .020/.015 | 82/103 | (8,-39,-40) / (-7,-37,-40) |
| Pontine crossing tract | .018 | 82 | (8,-31,-27) |
| Fornix (cres) R/L | .024/.024 | 74/45 | (35,-12,-14) / (-34,-15,-13) |

*continued on next page*

*continued from previous page*

| | | | |
|---|---|---|---|
| Cingulum (hippocampus) L | .036 | 56 | (-17,-42,-2) |

FWE = Family-wise error; L = left; R = right.

The column Volume represents the volume from the atlas region with significant results. No regions with volume equal or lower than 30 $mm^3$ were included in this Table.

**Table 3**. White matter regions where significant decreased AD values were found in CM compared to EM using the Johns Hopkins University White-Matter Tractography Atlas.

| White Matter tract | Minimum p-value (FWE-corrected) | Volume ($mm^3$) | MNI peak coordinate (mm), (x,y,z) |
|---|---|---|---|
| Anterior thalamic radiation L/R | .020/.021 | 316/232 | (-21,18,3) / (9,-29,-14) |
| Corticospinal tract L/R | .022/.018 | 627/601 | (-24,-20,9) / (10,-28,-26) |
| Cingulum (hippocampus) L | .036 | 37 | (-17,-43,-2) |
| Forceps major | .024 | 375 | (-18,-85,8) |
| Forceps minor | .018 | 1601 | (-17,39,-2) |
| Inferior fronto-occipital fasciculus L/R | .018/.022 | 994/973 | (-23,27,3)/ (37,-49,-4) |
| Inferior longitudinal fasciculus L/R | .022/.022 | 418/507 | (-35,-52,12)/ (44,-33,-12) |
| Superior longitudinal fasciculus L/R | .021/.021 | 1023/828 | (-36,-50,14)/ (31,-6,17) |
| Superior longitudinal fasciculus (temporal part) R | .022 | 62 | (49,-33,-11) |
| Uncinate fasciculus L | .018 | 83 | (-18,21,-9) |

L = left; R = right.

The column Volume represents the volume from the atlas region with significant differences (FDR-corrected and number of contrasts corrected). The maximum significant uncorrected p-value after corrections was .0032. No regions with volume equal or lower than 30 $mm^3$ were included in this Table.

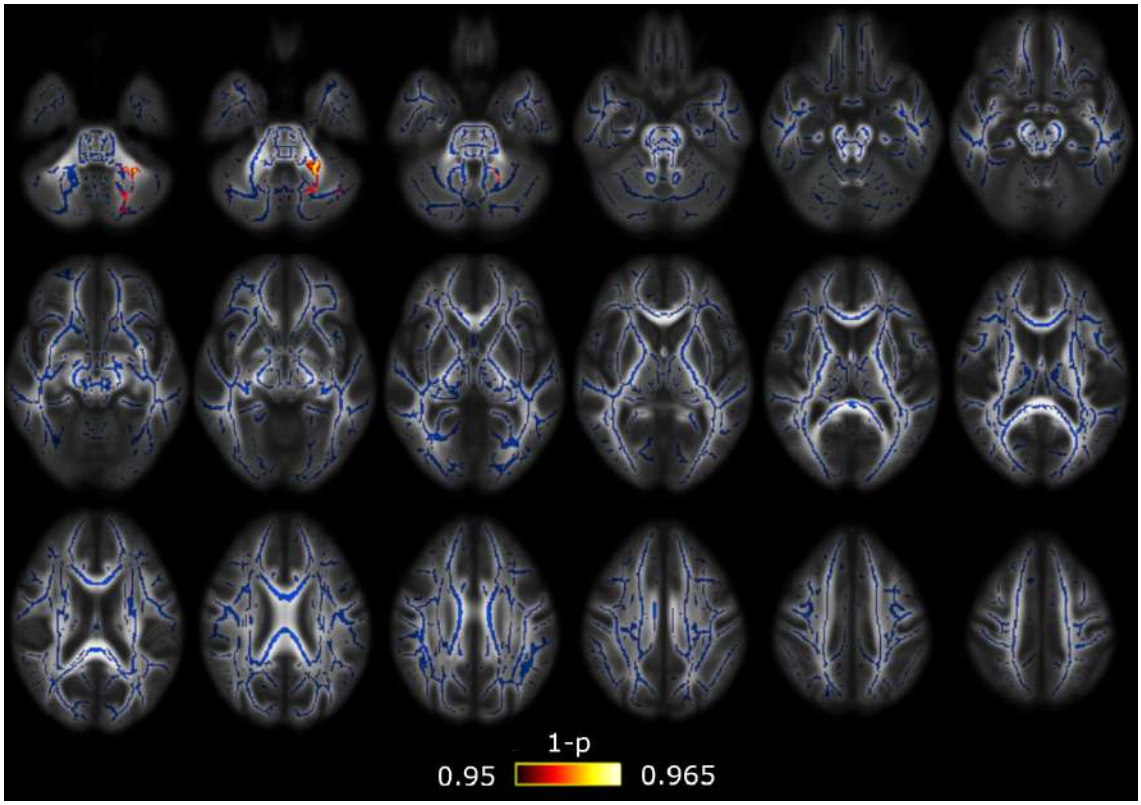


**Figure 3**. Return-to-plane (RTPP) alterations in patients with CM in comparison with patients with EM. Significant higher RTPP values in CM were found only in the middle cerebellar peduncle. The white matter skeleton is shown in blue and voxels with significant differences in red-yellow. The color bar shows the 1-p values (family-wise error corrected).

**Table 3**. White matter regions from the ICBM-DTI-81 White Matter Atlas for which significant decreased RTOP values were found in EM compared to HC.

| White Matter tract | Minimum p-value (FWE-corrected) | Volume ($mm^3$) | MNI peak coordinate (mm), (x,y,z) |
|---|---|---|---|
| Middle cerebellar peduncle | .042 | 908 | (13,-30,-26) |
| Superior cerebellar peduncle R/L | .042/.042 | 65/65 | (7,-32,-19) / (-5,-31,-18) |
| Inferior cerebellar peduncle L | .045 | 96 | (-13,-45,-31) |
| Genu of corpus callosum | .047 | 44 | (18,31,15) |
| Anterior corona radiata R | .044 | 446 | (26,35,-1) |
| Superior corona radiata R | .048 | 84 | (23,-12,19) |
| External capsule R/L | .042/.046 | 415/392 | (33,-19,-2) / (-33,-13,1) |
| Posterior limb of internal capsule R/L | .042/.046 | 285/420 | (20,-20,-4) / (-22,-8,14) |
| Retrolenticular part of internal capsule R/L | .041/.044 | 244/314 | (37,-26,-2) / (-37,-34,2) |
| Anterior limb of internal capsule L | .046 | 43 | (-17,-2,12) |
| Sagittal stratum R/L | .041/.044 | 243/97 | (39,-29,-5) / (-40,-29,-6) |
| Cerebral peduncle R | .042 | 254 | (12,-25,-21) |
| Corticospinal tract R/L | .042/.042 | 156/135 | (11,-25,-22)/ (-7,-25,-26) |
| Medial lemniscus R/L | .045/.046 | 83/87 | (9,-32,-25) / (-4,-37,-30) |
| Pontine crossing tract | .042 | 163 | (-4,-30,-28) |
| Fornix (cres) R | .041 | 148 | (32,-22,-6) |
| Uncinate fasciculus R | .043 | 32 | (35,-4,-14) |

FWE = Family-wise error; L = left; R = right.

The column Volume represents the volume from the atlas region with significant results. No regions with volume equal or lower than 30 $mm^3$ were included in this Table.

**Table 5**. White matter regions where significant decreased RTOP values were found in EM compared to HC using the Johns Hopkins University White-Matter Tractography Atlas.

| White Matter tract | Minimum p-value (FWE-corrected) | Volume ($mm^3$) | MNI peak coordinate (mm), (x,y,z) |
|---|---|---|---|
| Anterior thalamic radiation L/R | .046/.042 | 34/68 | (-7,-36,-27) / (9,-29,-14) |
| Corticospinal tract L/R | .042/.042 | 284/374 | (-7,-25,-26)/ (11,-25,-22) |
| Forceps minor | .046 | 342 | (19,38,16) |
| Inferior fronto-occipital fasciculus L/R | .044/.044 | 240/676 | (-39,-30,-4)/ (37,-27,-3) |
| Inferior longitudinal fasciculus L/R | .043/.042 | 309/167 | (-41,-28,-4)/ (42,-14,-14) |
| Uncinante fasciculus L/R | .048/.044 | 62/71 | (-35,-2,-20)/ (34,1,-16) |

L = left; R = right.

The column Volume represents the volume from the atlas region with significant differences (FDR-corrected and number of contrasts corrected). The maximum significant uncorrected p-value after corrections was .0032. No regions with volume equal or lower than 30 $mm^3$ were included in this Table.

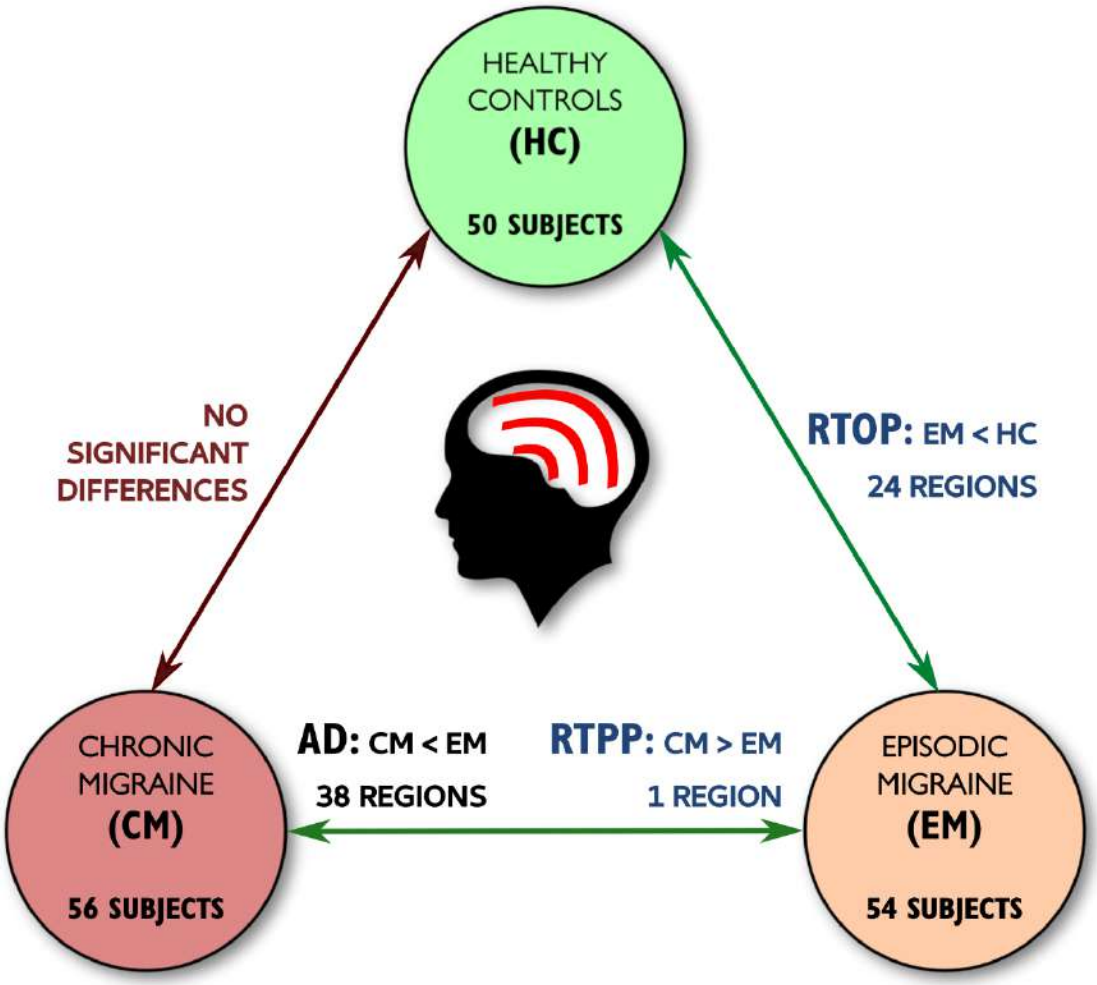


**Figure 5**. Summary of the main tract-based spatial statistics (TBSS) results with DTI and AMURA measures. Significant differences between any migraine group and controls were found only with the RTOP from AMURA, identifying white matter alterations non-measurable with DTI. Differences between CM and EM were found with RTPP from AMURA, and AD from DTI. No differences were found between CM and controls.

**Table 1**. Clinical and demographic characteristics of healthy controls (HC), episodic migraine (EM) and chronic migraine (CM).

| | HC (n=50) | EM (n=54) | CM (n=56) | Statistical test |
|---|---|---|---|---|
| Gender, male/female | 11/39 (22/78% ) | 9/45 (17/83% ) | 6/50 (11/89% ) | $\chi^2_{(2,\ N\ =\ 160)} = 2.48$, p = .29† |
| Age (years) | 36.1 ± 13.2 | 37.1 ± 8.2 | 38.1 ± 8.7 | $\chi^2$ (2) = 2.85, p = .24‡ |
| Duration of migraine history (years) | | 14.1 ± 11.1 | 19.6 ± 10.4 | $t_{(108)}$ = -2.7, p = .008§ |
| Time from onset of chronic migraine (months) | | | 24.5 ± 32.9 | |
| Headache frequency (days/month) | | 3.6 ± 1.9 | 23.3 ± 6.3 | U = 44.0, p < .001 |
| Migraine frequency (days/month) | | 3.6 ± 1.9 | 13.9 ± 6.9 | U = 108.5, p < .001 |
| Overusing medication | | 0 (0% ) | 42 (75% ) | p < .001 |
| Aura | | 9 (17% ) | 1 (2% ) | p = .007 |

†Chi-square test. ‡ Kruskal-Wallis test. §Two-tailed, unpaired Student's t-test. Mann-Whitney U test. Fisher's exact test. Data are expressed as means ± SD.

### *3.3.2.* ***TBSS with Covariates***

After the inclusion of the duration of migraine history as a covariate, lower AD values were found in CM compared to EM in the middle cerebellar peduncle (significant volume = 675 $mm^3$, minimum corrected p = 0.028, peak at x = -20, y = -50, z = -32). The same result was obtained including the time from onset of CM as a covariate in 23 regions. Higher AD values were found in EM in comparison with HC including the duration of migraine history as a covariate in seven regions from the left hemisphere. Lower FA values were identified in CM compared to HC including the time from onset of CM as a covariate in 12 regions located in the right hemisphere and the corpus callosum. These results are shown in Tables A1–A3 (extracted from [7]).

Regarding the EAP-based measures, including the duration of the migraine as a covariate, a very similar result was obtained with the RTPP with respect to the analysis with no additional covariates, finding higher RTPP values in CM compared to EM in the middle cerebellar peduncle (significant volume = 351 $mm^3$, minimum corrected p = 0.039, peak at x = -20, y = -50, z = -32 in the MNI space). Additionally, lower RTPP values were found in patients with EM in comparison with HC in eight regions from the ICBM-DTI-81 White Matter Atlas, with seven regions from the left hemisphere. Including the

time from onset of CM as a covariate, lower RTAP values were found in CM compared to HC in four regions from the right hemisphere included in the ICBM-DTI-81 White Matter Atlas. These results are shown in Tables A4 and A5 and Figures A1 and A2.

Taking into account the significant differences of the presence of an aura and a medication overuse headache between patients with CM and EM, we additionally included both variables in the analysis with multiple covariates, together with the duration of the migraine history.

Including only the presence of an aura as a covariate, with respect to the results with no covariates, AD values were lower in CM than in EM in eight regions, the RTPP was higher in CM than in EM in the middle cerebellar peduncle and no significant RTOP differences between EM and HC were obtained. No additional significant results were identified.

Regarding significant differences between CM and EM in the multivariate model, AD (middle cerebellar peduncle), MD (34 regions) and RD (39 regions) values were lower in CM. The opposite statistically significant trend, i.e., higher values in CM compared to EM, was obtained for RTPP (15 regions), RTOP (42 regions) and RTAP (38 regions). These results are shown in Tables A6–A11 and Figures A3–A5. Similar results, with the same significant statistical comparisons but a different number of regions with significant differences, were obtained including only a medication overuse headache as a covariate. In addition to the previous results, including only medication overuse headache as a covariate, FA values were higher in CM compared to EM in the body (60 voxels, minimum adjusted $p = 0.047$) and splenium (136 voxels, minimum adjusted $p = 0.040$) of the corpus callosum, the left superior corona radiata (68 voxels, minimum adjusted $p = 0.047$) and the left tapetum (35 voxels, minimum adjusted $p = 0.040$).

Statistically significant differences employing the model with the three covariates were obtained between EM and HC. On the one hand, increased AD (eight regions) values were found in EM with respect to HC. On the other hand, reduced RTPP (five regions) values were identified in EM compared to HC. These results are shown in Tables A12 and A13 and Figure A6.

In the comparison between CM and HC, significantly higher FA (10 regions) values were found in CM, and significantly lower RD (14 regions) values were identified in CM. These results are shown in Tables A14 and A15 and Figure A7.

### *3.3.3.* ***Correlation Analysis***

Statistically significant positive correlation was identified between time from onset of CM and mean FA in the left ($\rho = 0.439$, unadjusted $p < 0.001$) and right ($\rho = 0.420$, unadjusted $p = 0.001$) external capsule after the correction for multiple comparisons. Statistically significant negative correlation was found between time from onset of CM and mean RD in the left ($\rho = -0.439$, unadjusted $p < 0.001$) and right ($\rho = -0.427$, unadjusted $p = 0.001$) external capsule. The significant correlation results are shown in Figure 4.10 (extracted from [7]).

No additional statistically significant correlations were found for mean AD or MD, the three EAP-based measures, or the total duration of the migraine in patients with EM or CM.

## 3.4. Discussion

Two main results were obtained with the AMURA tool in comparison with DTI scalar measures, using a dMRI acquisition protocol typical in the clinical routine and migraine studies. On the one hand, with

AMURA, significant differences between patients with CM and EM were obtained with the RTPP, a result provided by AD and DTI. However, the number of regions with significant differences was lower with the RTPP. This lower sensitivity of AMURA was motivated by the fact that RTPP was designed to work with higher b-values. On the other hand, additional significant differences between patients with EM and HC were obtained only with AMURA based on the RTOP results. These results suggest that the AMURA tool may be a great complement to DTI in dMRI studies with migraine patients. We expect that the differences would grow if higher b-values were used.

Regarding the calculation of the EAP-based measures, when using the eigenvalues of the diffusion tensor, we were unable to perform statistical comparisons between the groups with TBSS because the values of RTOP and RTAP in some voxels were extremely high. The very low values of the two smallest eigenvalues in specific voxels explain the inability to work with real values of RTOP and RTAP and DTI. Therefore, the DTI approach is excessively simple to work with EAP-based measures, and tools such as AMURA are needed, especially in those studies with time restrictions and one single b-value.

White matter differences obtained with AMURA are in line with the TBSS results reported with the same sample in a previous study [7]. Lower AD and higher RTPP values in patients with CM compared to EM suggest axonal damage or loss, as previously suggested by Yu et al. [38], or short-term demyelination [39–41]. Anyway, results from DTI scalar measures must be interpreted with caution, considering that the relationship between DTI parameters and microstructural alterations are not completely clear.

The significant differences between patients with CM and EM obtained with the RTPP were a subsample of the results obtained with the AD. It must be considered that the diffusion MRI acquisition protocol was suboptimal for the use of the AMURA tool because of the low b-value and single-shell scheme, and, possibly for that reason, we were unable to identify the same or a similar number of significant differences between the migraine groups. The three measures obtained with the AMURA tool are designed to measure effects related to b-values over 2000 s/mm$^2$ (our b-value was 1000 s/mm$^2$), and RTPP is particularly sensitive to the b-value. Therefore, the RTPP result reflects the potential of AMURA to identify white matter structural changes in migraines using an acquisition protocol more appropriate for the tool.

RTPP differences between patients with CM and EM were found in the middle cerebellar peduncle. The middle cerebellar peduncle connects the cerebellum to the pons. Smaller cerebellar volume has been identified in patients with CM compared to HC [42]. Moreover, it has been suggested that the cerebellum suffers a neuropathological change in a migraine related to spreading depression [43]. The dorsolateral pons has been shown to be activated during a migraine and potentially involved in other mechanisms such as transmission of nociceptive signals to the hypothalamus, amygdala and basal forebrain [44]. Another study by Chong et al. has reported significant deformation of the pons in patients with a migraine [45]. Our results may suggest that the connectivity between the cerebellum and the pons is altered in CM compared to EM, possibly in association with structural changes of these regions linked to the migraine experience.

With respect to the comparison between patients with migraine (EM in this study) and controls, we only obtained significant differences using AMURA. This result reflects that AMURA may be helpful to determine additional microstructural changes between patients with migraine and controls with respect to the single use of DTI.

The lower RTOP values found in patients with EM compared to HC are in line with the most reported result with the MD in previous studies (higher MD in migraines) [2,5,46–51], although the opposite result with the MD (lower MD in migraines) has also been reported [3,6,38,52]. It must be noted that most

patients included in previous migraine studies were patients with EM. In our study, only patients with low frequency EM (less than 10 headache days per month) were included to assure that there were no patients close to the CM frequency threshold.

Some of the white matter regions with higher MD reported previously were identified as regions with significant differences between EM and HC in our study. These regions are the anterior thalamic radiation, the inferior longitudinal fasciculus, the corticospinal tract, the corpus callosum (genu and forceps minor) and the inferior cerebellar peduncle [5,47,49,50]. Higher MD values have been associated with edema andWallerian degeneration [39]. The changes in the anterior thalamic radiation may be associated with structural connections with the thalamus, which has been reported as a key region in migraine pathophysiology. In migraines, the thalamus has been associated with allodynia, photophobia and photoallodynia [53,54] and it has been suggested to have a role in the abnormal functional connectivity in diverse brain networks in the interictal state [55]. The corticospinal tract has been described as an important white matter region in relationship with nociceptive perception [56]. The inferior longitudinal fasciculus connects regions from the temporal and occipital cortex. One of the regions that takes part in the networks connected by the inferior longitudinal fasciculus is the temporal pole, which has shown hyperactivation in functional MRI studies with migraine patients, including connections with the thalamus and the insula [57,58], and loss of gray matter volume and altered cortical thickness [59,60]. Our results and the previous findings suggest that changes in the structural white matter connectivity may be associated with functional connectivity and gray matter alterations in migraine patients.

Regarding previous DTI results in migraines, the reduction of FA in patients with a migraine compared to controls is the most frequent result in diffusion MRI studies [2–5,38,46,49,61–65], but the opposite result has also been reported in pediatric patients by Messina et al. [6] and in the thalamus by Coppola et al. [66]. In this study, we obtained both higher and lower FA values in patients with CM compared to controls, associated with medication overuse headache and duration of the migraine, respectively. Most regions related to both results were different, and the related clusters were not extremely close. A possible reason of these apparently contradictory results would be the coexistence of debilitated and enhanced structural networks in the migraine, as it has been previously suggested [17], which may partially explain the apparently conflicting results in the literature. According to our results, these networks would be related to different pathophysiological mechanisms associated with medication overuse and longitudinal effects. In patients with EM and a medication overuse headache, lower FA values have been reported compared to controls [5]. Additional significant differences were obtained between CM, EM and HC including the duration of the migraine and medication overuse headache, but no changes were specifically related to the presence of an aura, in contrast to previous studies [67]. The lack of significant results associated with an aura in our study may be caused by the relative low number of patients with an aura. Future studies should specifically analyze differences between patients with and without medication overuse headache in patients with CM, and longitudinal studies should be performed to assess the longitudinal effects of CM in white matter.

With respect to the discordance with previous studies, there could be additional reasons. One of the reasons would be methodological. For example, in the study by Rocca et al. (2003), the analyzing method consisted of the study of histogram peaks [52], which is considerably different from methods carried out in the most recent years. Another reason would be associated with different sample characteristics. In the study by Messina et al., the sample was composed of pediatric patients [6], and the changes in the brain

might be different compared to the alterations in adults. The sample by Yu et al. [3] contained patients with depression, which might have influenced the results, considering that our sample included no patients with anxiety or depression.

Regarding the alterations found in this study, it should be elucidated whether the identified changes were migraine-specific. In a previous study including 277 headache free subjects and 246 patients with headaches, including 69 patients with migraines and 76 with tension-type headaches, Kattem Husøy et al. found no significant TBSS differences between migraines and tension-type headaches [49]. In the same study, the authors identified significantly higher AD values in patients with migraines and tension-type headaches compared to headache free subjects, with a higher number of voxels with significant differences in the migraine. Furthermore, patients with any headaches and a new onset headache presented widespread higher AD, MD and RD values compared to controls in the aforementioned study. These results suggest alterations in patients with a headache compared to controls, but with no clear migraine biomarkers in contrast to other headache disorders. The specific migraine microstructural brain changes in comparison with other headache and pain disorders should be analyzed in future studies, in order to uncover the particular pathophysiological characteristics of a migraine. Another aspect that needs to be studied is whether the identified changes are the cause or consequence of the migraine.

There were some limitations worth mentioning in this study. Due to time restrictions related to the MRI acquisition protocol, it was not possible to collect T2 or T2-FLAIR MRI data to assess the presence of white matter hyperintensities. Pain in patients with EM and an adverse prognosis have been related to white matter hyperintensities in migraines [68,69]. Considering the relative high risk of detection of white matter hyperintensities on MRI in migraines and their negative impact, the presence of these lesions might have some influence on the results, although the associated pathophysiology and long-term effects are unclear [70]. The baseline volume from the diffusion MRI acquisition is similar to a T2-weighted image, although its quality is low for the assessment of white matter hyperintensities. In relationship with the relative low acquisition, we performed no multishell acquisition with moderate-to-high b-values, a better scenario for the EAP-based measures, using the AMURA tool or the whole EAP. The absence of diffusion data with higher b-values prevented us from exploiting the full potential of the AMURA tool, although it allowed us to explore its discriminating power in conditions frequent in other migraine clinical MRI studies. The lack of control of the time to the next migraine attack might have influenced our results because some patients were in prodromal instead of interictal state when the MRI data were acquired, and alterations of brain physiology and function have been observed during the prodromal stage [71,72]. Another fact that might have influenced our results is the medication overuse, which was present in most patients with CM (75%), although we corrected the results considering this variable. The presence of anxiety and/or depression, which are frequent in migraines, might influence brain connectivity, as pointed by previous studies. Indeed, a smaller brain volume has been associated with depression in migraine, and migraine with depression may represent a different clinical phenotype with a specific long-term evolution [73]. In our sample, however, there were no patients with anxiety and/or depression. Although this fact prevented us from this possible relationship, the absence of patients with depression or anxiety also avoided the possible bias in the results that could have been caused by the inclusion of this distinct phenotype. The diagnosis of infrequent tension-type headache was not performed using the headache diary, but only the history, which

may be inaccurate to determine more than a unique associated tension-type headache day per month, or annual frequency higher than 12 days.

# 3.5. Conclusions

EAP-based measures obtained with the AMURA tool could detect white matter changes in patients with migraine to complement the results obtained with DTI scalar measures using diffusion MRI protocols with a single-shell acquisition low b-value, which are typical in the clinical routine and migraine clinical studies. Our results support structural connectivity changes between patients with EM and CM, and changes in the brain white matter related to migraine. Future studies should employ diffusion MRI multishell acquisitions with moderate-to-high b-values, when possible, in order to exploit the full potential of AMURA and identify white matter changes in patients with migraine. Other research lines may include the interaction between changes in white matter connectivity, gray matter structure and functional connectivity.

# 3.6. References

1. Headache Classification Committee of the International Headache Society. The International Classification of Headache Disorders, 3rd edition. Cephalalgia 2018, 38, 1–211.

2. Szabó, N.; Kincses, Z.T.; Párdutz, A.; Tajti, J.; Szok, D.; Tuka, A.; Király, A.; Babos, M.; Vörös, E.; Bomboi, G.; et al. White matter microstructural alterations in migraine: A diffusion-weighted MRI study. Pain 2012, 153, 651–656.

3. Yu, D.; Yuan, K.; Zhao, L.; Dong, M.; Liu, P.; Yang, X.; Liu, J.; Sun, J.; Zhou, G.; Xue, T.; et al. White matter integrity affected by depressive symptoms in migraine without aura: A tract-based spatial statistics study. NMR Biomed. 2013, 26, 1103–1112.

4. Gomez-Beldarrain, M.; Oroz, I.; Garcia Zapirain, B.; Fernandez Ruanova, B.; Garcia Fernandez, Y.; Cabrera, A.; Anton-Ladislao, A.; Aguirre-Larracoechea, U.; Garcia-Monco, J.C. Right fronto-insular white matter tracts link cognitive reserve and pain in migraine patients [erratum in J Headache Pain. 2016;17:22]. J. Headache Pain 2015, 17, 4.

5. Shibata, Y.; Ishiyama, S.; Matsushita, A. White matter diffusion abnormalities in migraine and medication overuse headache: A 1.5-T tract-based spatial statistics study. Clin. Neurol. Neurosurg. 2018, 174, 167–173.

6. Messina, R.; Rocca, M.A.; Colombo, B.; Pagani, E.; Falini, A.; Comi, G.; Filippi, M. White matter microstructure abnormalities in pediatric migraine patients. Cephalalgia 2015, 35, 1278–1286.

7. Planchuelo-Gómez,Á.; García-Azorín, D.; Guerrero,Á.L.; Aja-Fernández, S.; Rodríguez, M.; de Luis-García, R. White matter changes in chronic and episodic migraine: A diffusion tensor imaging study. J. Headache Pain 2020, 21, 1.

8. Coppola, G.; Di Renzo, A.; Tinelli, E.; Petolicchio, B.; Di Lorenzo, C.; Parisi, V.; Serrao, M.; Calistri, V.; Tardioli, S.; Cartocci, G.; et al. Patients with chronic migraine without history of medication overuse are characterized by a peculiar white matter fiber bundle profile. J. Headache Pain 2020, 21, 92.

9. Neeb, L.; Bastian, K.; Villringer, K.; Gits, H.C.; Israel, H.; Reuter, U.; Fiebach, J.B. No microstructural White Matter Alterations in Chronic and Episodic Migraineurs: A Case-Control Diffusion Tensor Magnetic Resonance Imaging Study. Headache 2015, 55, 241–251.

10. Tuch, D.S.; Reese, T.G.;Wiegell, M.R.;Wedeen, V.J. Diffusion MRI of Complex Neural Architecture. Neuron 2003, 40, 885–895.

11. Tristán-Vega, A.;Westin, C.-F.; Aja-Fernández, S. Estimation of fiber orientation probability density functions in high angular resolution diffusion imaging. Neuroimage 2009, 47, 638–650.

12. Jensen, J.H.; Helpern, J.A.; Ramani, A.; Lu, H.; Kaczynski, K. Diffusional kurtosis imaging: The quantification of non-gaussian water diffusion by means of magnetic resonance imaging. Magn. Reson. Med. 2005, 53, 1432–1440.

13. Wedeen, V.J.; Hagmann, P.; Tseng, W.-Y.I.; Reese, T.G.; Weisskoff, R.M. Mapping complex tissue architecture with diffusion spectrum magnetic resonance imaging. Magn. Reson. Med. 2005, 54, 1377–1386.

14. Özarslan, E.; Koay, C.G.; Shepherd, T.M.; Komlosh, M.E.; İrfanoğlu, M.O.; Pierpaoli, C.; Basser, P.J. Mean Apparent Propagator (MAP) MRI: A novel diffusion imaging method for mapping tissue microstructure. Neuroimage 2013, 78, 16–32.

15. Ning, L.;Westin, C.-F.; Rathi, Y. Estimating diffusion propagator and its moments using directional radial basis functions. IEEE Trans. Med. Imaging 2015, 34, 2058–2078.

16. Aja-Fernández, S.; de Luis-García, R.; Afzali, M.; Molendowska, M.; Pieciak, T.; Tristán-Vega, A. Microstructure diffusion scalar measures from reduced MRI acquisitions. PLoS ONE 2020, 15, 1–25.

17. Planchuelo-Gómez,Á.; García-Azorín, D.; Guerrero,Á.L.; Aja-Fernández, S.; Rodríguez, M.; de Luis-García, R. Structural connectivity alterations in chronic and episodic migraine: A diffusion magnetic resonance imaging connectomics study. Cephalalgia 2020, 40, 367–383.

18. Headache Classification Committee of the International Headache Society. The International Classification of Headache Disorders, 3rd edition (beta version). Cephalalgia 2013, 33, 629–808.

19. Serrano, D.; Lipton, R.B.; Scher, A.I.; Reed, M.L.; Stewart, W.F.; Manack Adams, A.; Buse, D.C. Fluctuations in episodic and chronic migraine status over the course of 1 year: Implications for diagnosis, treatment and clinical trial design. J. Headache Pain 2017, 18, 101.

20. Zigmond, A.S.; Snaith, R.P. The hospital anxiety and depression scale. Acta Psychiatr. Scand. 1983, 67, 361–370.

21. Tournier, J.-D.; Smith, R.; Raffelt, D.; Tabbara, R.; Dhollander, T.; Pietsch, M.; Christiaens, D.; Jeurissen, B.; Yeh, C.-H.; Connelly, A. MRtrix3: A fast, flexible and open software framework for medical image processing and visualisation. Neuroimage 2019, 202, 116–137.

22. Veraart, J.; Novikov, D.S.; Christiaens, D.; Ades-Aron, B.; Sijbers, J.; Fieremans, E. Denoising of diffusion MRI using random matrix theory. Neuroimage 2016, 142, 394–406.

23. Andersson, J.L.; Sotiropoulos, S.N. An integrated approach to correction for off-resonance effects and subject movement in diffusion MR imaging. Neuroimage 2015, 125, 1063–1078.

24. Smith, S.M.; Jenkinson, M.; Woolrich, M.W.; Beckmann, C.F.; Behrens, T.E.; Johansen-Berg, H.; Bannister, P.R.; De Luca, M.; Drobnjak, I.; Flitney, D.E.; et al. Advances in functional and structural MR image analysis and implementation as FSL. Neuroimage 2004, 23, S208–S219.

25. Zhang, Y.; Brady, M.; Smith, S. Segmentation of brain MR images through a hidden Markov random field model and the expectation-maximization algorithm. IEEE Trans. Med. Imaging 2001, 20, 45–57.

26. Dhollander, T.; Raffelt, D.; Connelly, A. Unsupervised 3-tissue response function estimation from single-shell or multi-shell diffusion MR data without a co-registered T1 image. ISMRM Work. Break. Barriers Diffus. MRI 2016, 5.

27. Jenkinson, M.; Beckmann, C.F.; Behrens, T.E.; Woolrich, M.W.; Smith, S.M. FSL. Neuroimage 2012, 62, 782–790.

28. Pelletier, A.; Periot, O.; Dilharreguy, B.; Hiba, B.; Bordessoules, M.; Chanraud, S.; Pérès, K.; Amieva, H.; Dartigues, J.-F.; Allard, M.; et al. Age-Related Modifications of Diffusion Tensor Imaging Parameters and White Matter Hyperintensities as Inter-Dependent Processes. Front. Aging. Neurosci. 2015, 7, 255.

29. Avram, A.V.; Sarlls, J.E.; Barnett, A.S.; Özarslan, E.; Thomas, C.; Irfanoglu, M.O.; Hutchinson, E.; Pierpaoli, C.; Basser, P.J. Clinical feasibility of using mean apparent propagator (MAP) MRI to characterize brain tissue microstructure. Neuroimage 2016, 127, 422–434.

30. Smith, S.M.; Jenkinson, M.; Johansen-Berg, H.; Rueckert, D.; Nichols, T.E.; Mackay, C.E.; Winkins, K.E.; Ciccarelli, O.; Cader, M.Z.; Matthews, P.M.; et al. Tract-based Spatial Statistics: Voxelwise analysis of multi-subject diffusion data. Neuroimage 2006, 31, 1487–1505.

31. Mori, S.; Wakana, S.; Nagae-Poetscher, L.M.; van Zijl, P.C. MRI Atlas of Human White Matter; Elsevier: Amsterdam, The Netherlands, 2005.

32. Oishi, K.; Zilles, K.; Amunts, K.; Faria, A.; Jiang, H.; Li, X.; Akhter, K.; Hua, K.; Woods, R.; Toga, A.W.; et al. Human brain white matter atlas: Identification and assignment of common anatomical structures in superficial white matter. Neuroimage 2008, 43, 447–457.

33. Hua, K.; Zhang, J.; Wakana, S.; Jiang, H.; Li, X.; Reich, D.S.; Calabresi, P.A.; Pekar, J.J.; van Zijl, P.C.M.; Mori, S. Tract Probability Maps in Stereotaxic Spaces: Analyses of White Matter Anatomy and Tract-Specific Quantification. Neuroimage 2008, 39, 336–347.

34. Rueckert, D.; Sonoda, L.I.; Hayes, C.; Hill, D.L.; Leach, M.O.; Hawkes, D.J. Nonrigid registration using free-form deformations: Application to breast MR images. IEEE Trans. Med. Imaging 1999, 18, 712–721.

35. Nichols, T.E.; Holmes, A.P. Nonparametric permutation tests for functional neuroimaging: A primer with examples. Hum. Brain Mapp 2002, 15, 1–25.

36. Smith, S.M.; Nichols, T.E. Threshold-free cluster enhancement: Addressing problems of smoothing, threshold dependence and localisation in cluster inference. Neuroimage 2009, 44, 83–98.

37. Benjamini, Y.; Hochberg, Y. Controlling the false discovery rate: A practical and powerful approach to multiple testing. J. R. Stat. Soc. Ser. B 1995, 57, 289–300.

38. Yu, D.; Yuan, K.; Qin, W.; Zhao, L.; Dong, M.; Liu, P.; Yang, X.; Liu, J.; Sun, J.; Zhou, G.; et al. Axonal loss of white matter in migraine without aura: A tract-based spatial statistics study. Cephalalgia 2013, 33, 34–42.

39. Alexander, A.L.; Lee, J.E.; Lazar, M.; Field, A.S. Diffusion Tensor Imaging of the Brain. Neurotherapeutics 2007, 4, 316–329.

40. Sun, S.-W.; Liang, H.-F.; Cross, A.H.; Song, S.-K. EvolvingWallerian Degeneration after Transient Retinal Ischemia in Mice Characterized by Diffusion Tensor Imaging. Neuroimage 2008, 40, 1–10.

41. Winklewski, P.J.; Sabisz, A.; Naumczyk, P.; Jodzio, K.; Szurowska, E.; Szarmach, A. Understanding the Physiopathology Behind Axial and Radial Diffusivity Changes –What Do We Know? Front. Neurol 2018, 9, 92.

42. BilgiÃ§, B.; Kocaman, G.; Arslan, A.B.; Noyan, H.; Sherifov, R.; Alkan, A.; Asil, T.; Parman, Y.; Baykan, B. Volumetric differences suggest involvement of cerebellum and brainstem in chronic migraine. Cephalalgia 2016, 36, 301–308.

43. Vincent, M.; Hadjikhani, N. The cerebellum and migraine. Headache 2007, 47, 820–833.

44. Borsook, D.; Burstein, R. The enigma of the dorsolateral pons as a migraine generator. Cephalalgia 2012, 32, 803–812.

45. Chong, C.D.; Plasencia, J.D.; Frakes, D.H.; Schwedt, T.J. Structural alterations of the brainstem in migraine. NeuroImage. Clin. 2016, 13, 223–227.

46. Rocca, M.A.; Pagani, E.; Colombo, B.; Tortorella, P.; Falini, A.; Comi, G.; Filippi, M. Selective Diffusion Changes of The Visual Pathways in Patients with Migraine: A 3-T Tractography Study. Cephalalgia 2008, 28, 1061–1068.

47. Chong, C.D.; Schwedt, T.J. Migraine affects white-matter tract integrity: A diffusion-tensor imaging study. Cephalalgia 2015, 35, 1162–1171.

48. Marciszewski, K.K.; Meylakh, N.; Di Pietro, F.; Macefield, V.G.; Macey, P.M.; Henderson, L.A. Altered brainstem anatomy in migraine. Cephalalgia 2018, 38, 476–486.

49. Kattem Husøy, A.; Eikenes, L.; Håberg, A.K.; Hagen, K.; Stovner, L.J. Diffusion tensor imaging in middle-aged headache sufferers in the general population: A cross-sectional population-based imaging study in the Nord-Trøndelag health study (HUNT-MRI). J. Headache Pain 2019, 20, 78.

50. Qin, Z.; He, X.-W.; Zhang, J.; Xu, S.; Li, G.-F.; Su, J.; Shi, Y.-H.; Ban, S.; Hu, Y.; Liu, Y.-S.; et al. Structural changes of cerebellum and brainstem in migraine without aura. J. Headache Pain 2019, 20, 93.

51. Chong, C.D.; Peplinski, J.; Berisha, V.; Ross, K.; Schwedt, T.J. Differences in fibertract profiles between patients with migraine and those with persistent post-traumatic headache. Cephalalgia 2019, 39, 1121–1133.

52. Rocca, M.A.; Colombo, B.; Inglese, M.; Codella, M.; Comi, G.; Filippi, M. A diffusion tensor magnetic resonance imaging study of brain tissue from patients with migraine. J. Neurol. Neurosurg. Psychiatry 2003, 74, 501–503.

53. Burstein, R.; Jakubowski, M.; Garcia-Nicas, E.; Kainz, V.; Bajwa, Z.; Hargreaves, R.; Becerra, L.; Borsook, D. Thalamic sensitization transforms localized pain into widespread allodynia. Ann. Neurol. 2010, 68, 81–91.

54. Maleki, N.; Becerra, L.; Upadhyay, J.; Burstein, R.; Borsook, D. Direct optic nerve pulvinar connections defined by diffusion MR tractography in humans: Implications for photophobia. Hum. Brain Mapp. 2012, 33, 75–88.

55. Coppola, G.; Di Renzo, A.; Tinelli, E.; Lepre, C.; Di Lorenzo, C.; Di Lorenzo, G.A.; Scapeccia, M.; Parisi, V.; Serrao, M.; Colonnese, C.; et al. Thalamo-cortical network activity between migraine attacks: Insights from MRI-based microstructural and functional resting-state network correlation analysis. J. Headache Pain 2016, 17, 100.

56. Tracey, I.; Mantyh, P.W. The Cerebral Signature for Pain Perception and Its Modulation. Neuron 2007, 55, 377–391.

57. Moulton, E.A.; Becerra, L.; Maleki, N.; Pendse, G.; Tully, S.; Hangreaves, R.; Burstein, R.; Borsook, D. Painful Heat Reveals Hyperexcitability of the Temporal Pole in Interictal and Ictal Migraine States. Cereb. Cortex 2011, 21, 435–448.

58. Hadjikhani, N.; Ward, N.; Boshyan, J.; Napadow, V.; Maeda, Y.; Truini, A.; Caramia, F.; Tinelli, E.; Mainero, C. The missing link: Enhanced functional connectivity between amygdala and visceroceptive cortex in migraine. Cephalalgia 2013, 33, 1264–1268.

59. Coppola, G.; Di Renzo, A.; Tinelli, E.; Iacovelli, E.; Lepre, C.; Di Lorenzo, C.; Di Lorenzo, G.; Di Lenola, D.; Parisi, V.; Serrao, M.; et al. Evidence for brain morphometric changes during the migraine cycle: A magnetic resonance-based morphometry study. Cephalalgia 2015, 35, 783–791.

60. Schwedt, T.J.; Berisha, V.; Chong, C.D. Temporal Lobe Cortical Thickness Correlations Differentiate the Migraine Brain from the Healthy Brain. PLoS ONE 2015, 10, e0116687.

61. Yuan, K.; Qin, W.; Liu, P.; Zhao, L.; Yu, D.; Zhao, L.; Dong, M.; Liu, J.; Yang, X.; von Deneen, K.M.; et al. Reduced Fractional Anisotropy of Corpus Callosum Modulates Inter-Hemispheric Resting State Functional Connectivity in Migraine Patients without Aura. PLoS ONE 2012, 7, e45476.

62. Granziera, C.; DaSilva, A.F.M.; Snyder, J.; Tuch, D.S.; Hadjikhani, N. Anatomical Alterations of the Visual Motion Processing Network in Migraine with and without Aura. PLoS Med. 2006, 3, e402.

63. DaSilva, A.F.M.; Granziera, C.; Tuch, D.S.; Snyder, J.; Vincent, M.; Hadjikhani, N. Interictal alterations of the trigeminal somatosensory pathway and PAG in migraine. Neuroreport 2007, 18, 301–305.

64. Schmitz, N.; Admiraal-Behloul, F.; Arkink, E.B.; Kruit, M.C.; Schoonmann, G.G.; Ferrari, M.D.; Van Buchem, M.A. Attack frequency and disease duration as indicators for brain damage in migraine. Headache 2008, 48, 1044–1055.

65. Li, X.L.; Fang, Y.N.; Gao, Q.C.; Lin, E.J.; Hu, S.H.; Ren, L.; Ding, M.H.; Luo, B.N. A Diffusion Tensor Magnetic Resonance Image Study of Corpus Callosum From Adult Patients With Migraine Complicated With Depressive/Anxious Disorder. Headache 2011, 51, 237–245.

66. Coppola, G.; Tinelli, E.; Lepre, C.; Iacovelli, E.; Di Lorenzo, C.; Di Lorenzo, G.; Serrao, M.; Pauri, F.; Fiermonte, G.; Bianco, F.; et al. Dynamic changes in thalamic microstructure of migraine without aura patients: A diffusion tensor magnetic resonance imaging study. Eur J. Neurol 2014, 21, 287-e13.

67. Szabó, N.; Faragó, P.; Király, A.; Veréb, A.; Csete, G.; Tóth, E.; Kocsis, K.; Kincses, B.; Tuka, B.; Párdutz, A.; et al. Evidence for Plastic Processes in Migraine with Aura: A Diffusion-Weighted MRI Study. Front. Neuroanat 2017, 11, 138.

68. Yalcin, A.; Ceylan, M.; Bayraktutan, O.F.; Akkurt, A. Episodic Migraine and White Matter Hyperintensities: Association of Pain Lateralization. Pain Med. 2018, 19, 2051–2057.

69. Xie, H.; Zhang, Q.; Huo, K.; Liu, R.; Jian, Z.-J.; Bian, Y.-T.; Li, G.-L.; Zhu, D.; Zhang, L.-H.; Yang, J.; et al. Association of white matter hyperintensities with migraine features and prognosis. BMC Neurol 2018, 18, 93.

70. Porter, A.; Gladstone, J.P.; Dodick, D.W. Migraine and white matter hyperintensities. Curr. Pain Headache Rep. 2005, 9, 289–293.

71. May, A. Understanding migraine as a cycling brain syndrome: Reviewing the evidence from functional imaging. Neurol Sci 2017, 38, 125–130.

72. Karsan, N.; Goadsby, P.J. Biological insights from the premonitory symptoms of migraine. Nat. Rev. Neurol. 2018, 14, 699–710.

73. Gudmundsson, L.S.; Scher, A.I.; Sigurdsson, S.; Geerlings, M.I.; Vidal, J.-S.; Eiriksdottir, G.; Garcia, M.I.; Harris, T.B.; Kjartansson, O.; Aspelund, T.; et al. Migraine, depression, and brain volume: The AGES-Reykjavik Study. Neurology 2013, 80, 2138–2144.

## 3.7. Appendix A

The original Appendix A was composed of the RTOP, RTPP and RTAP assuming the diffusion tensor model with a Gaussian probability density functions. These equations have been already presented (Eqs. (3.5), (3.6) and (3.7)). Moreover, the equations for the four DTI-based parameters were presented (Eqs. (2.12), (2.13), (2.14) and (2.15)).

## 3.8. Appendix B

The Supplementary Tables and Figures are included in this section.

**Table A1.** White matter regions from the ICBM-DTI-81 White Matter Atlas for which significant decreased AD values were found in CM compared to EM including the time from onset of CM as a covariate.

| **White Matter Region** | **Minimum p-value (FWE-corrected)** | **Volume ($mm^3$)** | **MNI peak coordinate (mm), (x,y,z)** |
|---|---|---|---|
| Middle cerebellar peduncle | .023 | 1295 | (-20,-50,-32) |
| Superior cerebellar peduncle R/L | .028/.030 | 101/115 | (5,-28,-19) / (-4,-28,-19) |
| Inferior cerebellar peduncle L | .035 | 46 | (-10,-50,-25) |
| Superior longitudinal fasciculus R | .033 | 720 | (32,-4,20) |
| Splenium of corpus callosum | .042 | 32 | (18,-49,27) |
| Superior corona radiata R/L | .030/.032 | 335/136 | (28,-15,19) / (-27,-11,20) |
| Posterior corona radiata R | .035 | 83 | (28,-34,19) |
| External capsule R/L | .033/.031 | 127/171 | (30,-10,14) / (-28,-10,18) |
| Posterior limb of internal capsule R/L | .029/.032 | 301/281 | (26,-17,13) / (-27,-17,17) |
| Retrolenticular part of internal capsule R/L | .031/.032 | 473/59 | (30,-29,7) / (-25,-23,12) |
| Sagittal stratum R | .034 | 150 | (38,-28,-4) |
| Posterior thalamic radiation R | .034 | 51 | (30,-39,16) |
| Cerebral peduncle R/L | .028/.031 | 207/258 | (10,-28,-16) / (-9,-20,-20) |
| Corticospinal tract R/L | .030/.031 | 105/125 | (11,-22,-22) / (-7,-18,-22) |
| Pontine crossing tract | .030 | 56 | (4,-26,-24) |
| Fornix (cres) R | .037 | 46 | (35,-12,-14) |

FWE = Family-wise error; L = left; R = right. The column Volume represents the volume from the atlas region with significant results. No regions with volume equal or lower than 30 $mm^3$ were included in this Table.

**Table A2.** White matter regions from the ICBM-DTI-81 White Matter Atlas for which significant increased AD values were found in EM compared to HC including the duration of migraine as a covariate.

| **White Matter Region** | **Minimum p-value (FWE-corrected)** | **Volume ($mm^3$)** | **MNI peak coordinate (mm), (x,y,z)** |
|---|---|---|---|
| Superior corona radiata L | .026 | 116 | (-26,-11,20) |
| External capsule L | .022 | 303 | (-34,-15,-8) |
| Posterior limb of internal capsule L | .024 | 472 | (-15,10,0) |
| Retrolenticular part of internal capsule L | .025 | 347 | (-33,-34,6) |
| Sagittal stratum L | .023 | 133 | (-36,-17,-9) |
| Posterior thalamic radiation L | .025 | 38 | (-35,-39,7) |
| Cerebral peduncle L | .024 | 105 | (-15,-13,-5) |

FWE = Family-wise error; L = left; R = right. The column Volume represents the volume from the atlas region with significant results. No regions with volume equal or lower than 30 $mm^3$ were included in this Table.

**Table A3.** White matter regions from the ICBM-DTI-81 White Matter Atlas for which significant decreased FA values were found in CM compared to HC including the time from onset of CM as a covariate.

| **White Matter Region** | **Minimum p-value (FWE-corrected)** | **Volume ($mm^3$)** | **MNI peak coordinate (mm), (x,y,z)** |
|---|---|---|---|
| Superior longitudinal fasciculus R | .033 | 271 | (32,-4,19) |
| Body of corpus callosum | .042 | 47 | (19,-30,31) |
| Splenium of corpus callosum | .042 | 209 | (19,-31,31) |
| Anterior corona radiata R | .033 | 295 | (25,17,12) |
| Superior corona radiata R | .038 | 236 | (32,-6,20) |
| Posterior corona radiata R | .039 | 133 | (25,-23,22) |
| External capsule R | .031 | 661 | (30,1,13) |
| Posterior limb of internal capsule R | .039 | 217 | (24,-19,1) |
| Retrolenticular part of internal capsule R | .036 | 425 | (38,-29,0) |
| Anterior limb of internal capsule R | .035 | 83 | (23,17,11) |
| Sagittal stratum R | .036 | 132 | (33,-23,-4) |
| Fornix (cres) R | .035 | 36 | (33,-22,-6) |

FWE = Family-wise error; L = left; R = right. The column Volume represents the volume from the atlas region with significant results. No regions with volume equal or lower than 30 $mm^3$ were included in this Table.

**Table A4.** White matter regions from the ICBM-DTI-81 White Matter Atlas for which significant decreased RTPP values were found in EM compared to HC including the duration of migraine as a covariate.

| **White Matter Region** | **Minimum p-value (FWE-corrected)** | **Volume ($mm^3$)** | **MNI peak coordinate (mm), (x,y,z)** |
|---|---|---|---|
| Superior corona radiata R/L | .046/.040 | 50/87 | (20,-28,40) / (-26,-11,19) |
| External capsule L | .033 | 278 | (-33,-11,1) |
| Anterior limb of internal capsule L | .044 | 31 | (-18,2,12) |
| Posterior limb of internal capsule L | .034 | 377 | (-23,-22,3) |
| Retrolenticular part of internal capsule L | .034 | 315 | (-30,-23,2) |
| Sagittal stratum L | .034 | 114 | (-36,-17,-9) |
| Cerebral peduncle L | .036 | 37 | (-14,-12,-5) |

FWE = Family-wise error; L = left; R = right. The column Volume represents the volume from the atlas region with significant results. No regions with volume equal or lower than 30 $mm^3$ were included in this Table.

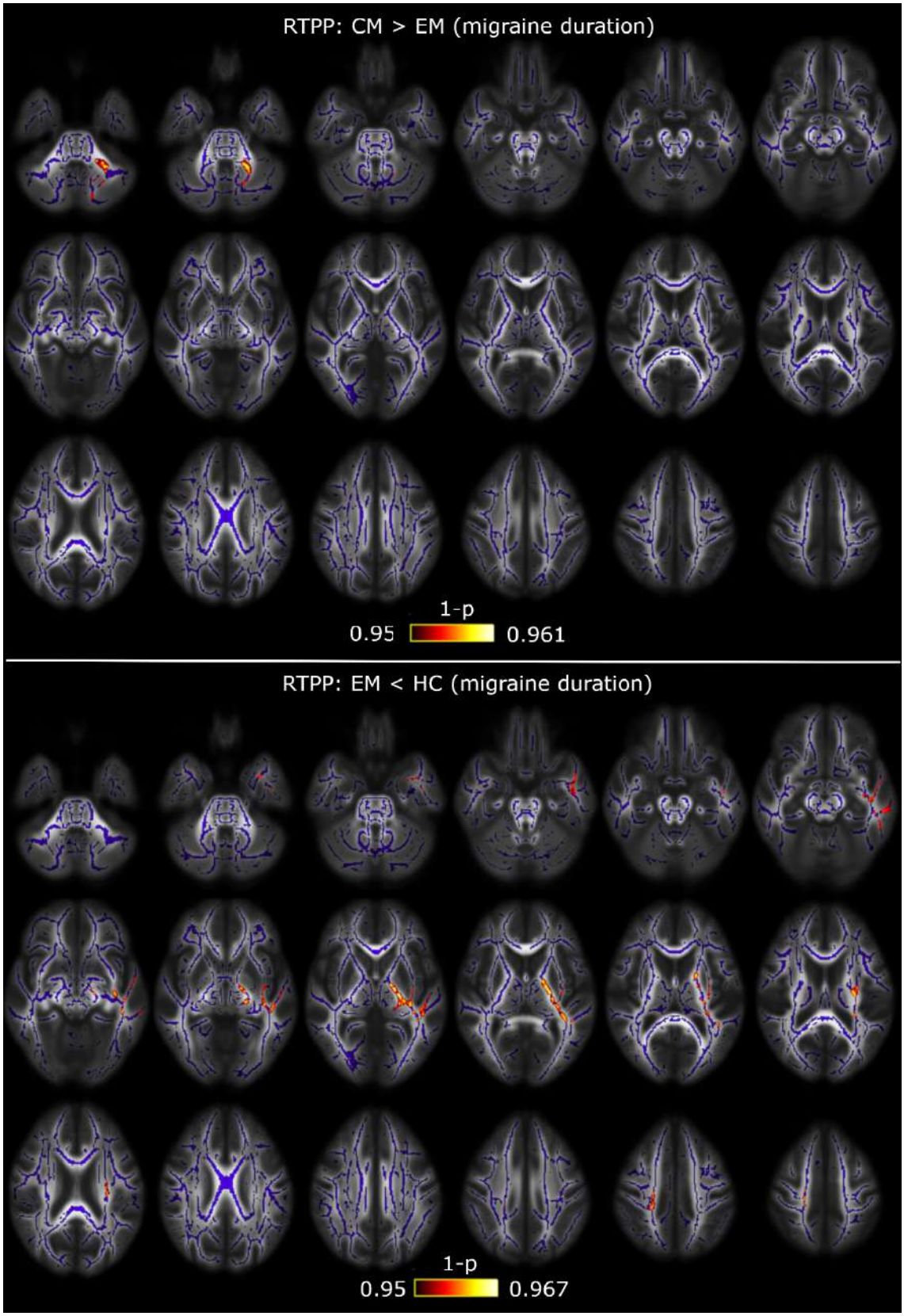


**Figure A1**. RTPP alterations between CM and EM including the duration of the migraine as a covariate. TBSS showed increased RTPP values in CM with respect to EM in the middle cerebellar peduncle (top) and decreased RTPP values in EM compared to HC throughout the left hemisphere and the corona radiata (bottom). The white matter skeleton is shown in blue, and voxels with the lowest p-values in red-yellow. The color bar shows the 1-p-values (FWE-corrected).

**Table A5.** White matter regions from the ICBM-DTI-81 White Matter Atlas for which significant decreased RTAP values were found in CM compared to HC including the time from onset of CM as a covariate.

| **White Matter Region** | **Minimum p-value (FWE-corrected)** | **Volume ($mm^3$)** | **MNI peak coordinate (mm), (x,y,z)** |
|---|---|---|---|
| Superior longitudinal fasciculus R | .046 | 179 | (39,-9,26) |
| External capsule R | .044 | 244 | (33,-14,-3) |
| Retrolenticular part of internal capsule R | .045 | 157 | (34,-21,-2) |
| Sagittal stratum R | .045 | 194 | (39,-18,-12) |

FWE = Family-wise error; L = left; R = right. The column Volume represents the volume from the atlas region with significant results. No regions with volume equal or lower than 30 $mm^3$ were included in this Table.

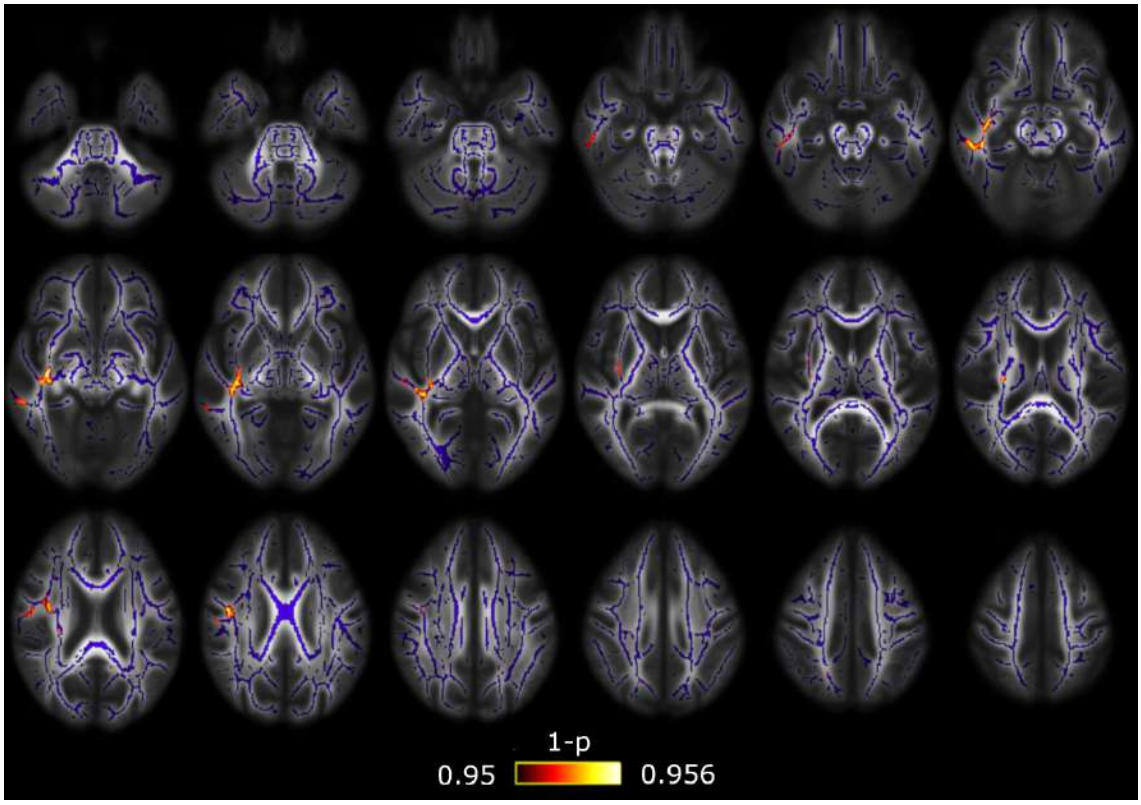


**Figure A2**. RTAP alterations between CM and HC including time from onset of CM as a covariate. TBSS showed decreased RTAP values in CM with respect to HC throughout the right hemisphere. White matter skeleton is shown in blue, and voxels with the lowest p-values in red-yellow. The color bar shows the 1-p-values (FWE-corrected).

**Table A6.** White matter regions from the ICBM-DTI-81 White Matter Atlas for which significant decreased AD values were found in CM compared to EM including the duration of migraine, presence of aura, and medication overuse headache as covariates.

| White Matter Region | Minimum p-value (FWE-corrected) | Volume ($mm^3$) | MNI peak coordinate (mm), (x,y,z) |
|---|---|---|---|
| Middle cerebellar peduncle | .047 | 31 | (-21,-65,-40) |

FWE = Family-wise error; The column Volume represents the volume from the atlas region with significant results. No regions with volume equal or lower than 30 $mm^3$ were included in this Table.

**Table A7.** White matter regions from the ICBM-DTI-81 White Matter Atlas for which significant increased RTPP values were found in CM compared to EM including the duration of migraine, presence of aura, and medication overuse headache as covariates.

| White Matter Region | Minimum p-value (FWE-corrected) | Volume ($mm^3$) | MNI peak coordinate (mm), (x,y,z) |
|---|---|---|---|
| Middle cerebellar peduncle | .026 | 439 | (-23,-55,-42) |
| Superior longitudinal fasciculus R/L | .045/.039 | 52/464 | (33,1,27) / (-36,-4,-18) |
| Anterior corona radiata L | .042 | 66 | (-23,16,27) |
| Superior corona radiata L | .041 | 160 | (-26,4,26) |
| Posterior corona radiata L | .039 | 42 | (-29,-60,21) |
| External capsule R | .018 | 36 | (36,-16,-9) |
| Retrolenticular part of internal capsule R/L | .019/.043 | 239/40 | (39,-38,-3) / (-39,-33,-1) |
| Sagittal stratum R/L | .012/.036 | 387/194 | (44,-29,-14) / (-40,-33,-6) |
| Posterior thalamic radiation R/L | .015/.039 | 188/176 | (39,-41,-2) / (-30,-65,17) |
| Fornix (cres) R | .017 | 75 | (35,-16,-12) |
| Cingulum (hippocampus) R | .017 | 68 | (29,-18,27) |

FWE = Family-wise error; L = left; R = right. The column Volume represents the volume from the atlas region with significant results. No regions with volume equal or lower than 30 $mm^3$ were included in this Table.

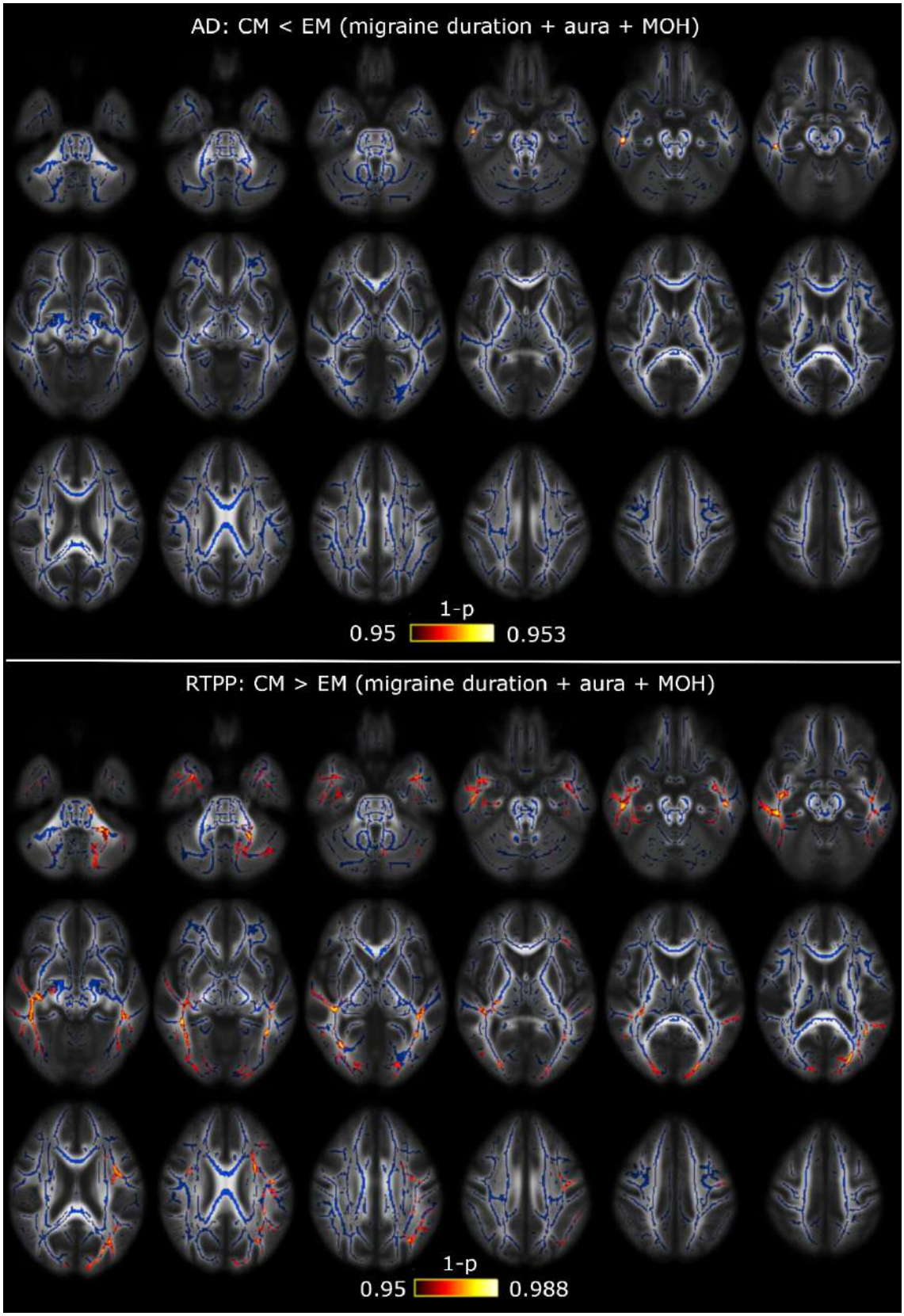


**Figure A3**. AD and RTPP alterations between CM and EM including duration of migraine, presence of aura, and medication overuse headache as covariates. TBSS showed decreased AD and increased RTPP values in CM with respect to EM. White matter skeleton is shown in blue, and voxels with the lowest p-values in red-yellow. The color bar shows the 1-p-values (FWE-corrected). MOH = medication overuse headache.

**Table A8.** White matter regions from the ICBM-DTI-81 White Matter Atlas for which significant decreased MD values were found in CM compared to EM including the duration of migraine, presence of aura, and medication overuse headache as covariates.

| **White Matter Region** | **Minimum p-value (FWE-corrected)** | **Volume ($mm^3$)** | **MNI peak coordinate (mm), (x,y,z)** |
|---|---|---|---|
| Superior longitudinal fasciculus R/L | .012/.012 | 950/1030 | (38,-35,31) / (-35,-35,27) |
| Genu of corpus callosum | .012 | 653 | (18,20,25) |
| Body of corpus callosum | .012 | 1440 | (16,16,29) |
| Splenium of corpus callosum | .009 | 1170 | (26,-58,12) |
| Anterior corona radiata R/L | .011/.012 | 1147/980 | (26,16,25) / (-25,18,21) |
| Superior corona radiata R/L | .011/.012 | 904/820 | (25,12,28) / (-25,6,28) |
| Posterior corona radiata R/L | .009/.012 | 265/246 | (28,-63,19) / (-30,-60,21) |
| External capsule R/L | .012/.012 | 549/576 | (30,11,-1) / (-25,10,14) |
| Posterior limb of internal capsule R/L | .012/.016 | 390/261 | (23,-6,17) / (-22,-10,16) |
| Retrolenticular part of internal capsule R/L | .012/.016 | 390/271 | (30,-38,17) / (-38,-33,0) |
| Anterior limb of internal capsule R/L | .012/.012 | 229/416 | (22,8,13) / (-20,9,13) |
| Sagittal stratum R/L | .014/.016 | 444/309 | (44,-30,-15) / (-40,-28,-7) |
| Posterior thalamic radiation R/L | .008/.012 | 601/470 | (29,-61,13) / (-30,-66,-16) |
| Fornix (cres) R/L | .015/.018 | 171/177 | (33,-7,-19) / (-35,-11,-17) |
| Cingulum R/L | .014/.016 | 53/135 | (10,-46,22) / (-10,-40,28) |
| Cingulum (hippocampus) R/L | .018/.019 | 84/67 | (24,-29,-15) / (-19,-38,-7) |
| Superior fronto-occipital fasciculus R/L | .012/.012 | 59/46 | (22,-1,21) / (-21,1,20) |
| Uncinate fasciculus R | .025 | 35 | (34,0,-15) |
| Tapetum R/L | .009/.016 | 82/75 | (31,-52,14) / (-28,-50,16) |

FWE = Family-wise error; L = left; R = right. The column Volume represents the volume from the atlas region with significant results. No regions with volume equal or lower than 30 $mm^3$ were included in this Table.

**Table A9.** White matter regions from the ICBM-DTI-81 White Matter Atlas for which significant increased RTOP values were found in CM compared to EM including the duration of migraine, presence of aura, and medication overuse headache as covariates.

| **White Matter Region** | **Minimum p-value (FWE-corrected)** | **Volume ($mm^3$)** | **MNI peak coordinate (mm), (x,y,z)** |
|---|---|---|---|
| Middle cerebellar peduncle | .033 | 694 | (-6,-19,-32) |
| Superior cerebellar peduncle R/L | .033/.034 | 66/49 | (6,-29,-19) / (-7,-34,-23) |
| Inferior cerebellar peduncle L | .040 | 113 | (-11,-46,-29) |
| Superior longitudinal fasciculus R/L | .016/.019 | 610/722 | (35,-44,26) / (-32,7,22) |
| Genu of corpus callosum | .018 | 905 | (-13,22,18) |
| Body of corpus callosum | .018 | 1783 | (-13,18,21) |
| Splenium of corpus callosum | .015 | 1680 | (25,-53,19) |
| Anterior corona radiata R/L | .018/.019 | 972/555 | (25,15,28) / (-25,13,23) |
| Superior corona radiata R/L | .018/.019 | 710/793 | (25,12,28) / (-24,5,20) |
| Posterior corona radiata R/L | .014/.019 | 291/287 | (28,-63,19) / (-18,-40,36) |
| External capsule R/L | .019/.019 | 408/250 | (26,17,7) / (-25,10,14) |
| Posterior limb of internal capsule R/L | .020/.019 | 297/390 | (23,-6,17) / (-22,-10,16) |
| Retrolenticular part of internal capsule R/L | .030/.038 | 223/131 | (29,-37,17) / (-38,-33,0) |
| Anterior limb of internal capsule R/L | .019/.019 | 319/436 | (22,18,9) / (-21,14,13) |
| Sagittal stratum R/L | .020/.039 | 252/204 | (38,-15,-12) / (-40,-28,-7) |
| Posterior thalamic radiation R/L | .014/.022 | 529/364 | (28,-64,18) / (-30,-66,16) |
| Cerebral peduncle R/L | .033/.032 | 233/323 | (10,-29,-16) / (-8,-18,-20) |
| Corticospinal tract R/L | .034/.033 | 99/205 | (11,-25,-22) / (-7,-21,-27) |
| Medial lemniscus R/L | .034/.034 | 36/68 | (6,-33,-30) / (-4,-33,-26) |
| Pontine crossing tract | .033 | 217 | (6,-30,-30) |
| Fornix (cres) R | .020 | 164 | (33,7,-19) |
| Cingulum R/L | .029/.019 | 43/160 | (10,-46,22) / (-10,-40,28) |
| Superior fronto-occipital fasciculus R/L | .020/.019 | 61/54 | (22,6,20) / (-21,1,20) |
| Uncinate fasciculus R | .039 | 43 | (34,0,-18) |

*continued on next page*

*continued from previous page*

| | | | |
|---|---|---|---|
| Tapetum R/L | .015/.021 | 78/100 | (31,-52,14) / (-26,-49,19) |

FWE = Family-wise error; L = left; R = right. The column Volume represents the volume from the atlas region with significant results. No regions with volume equal or lower than 30 $mm^3$ were included in this Table.

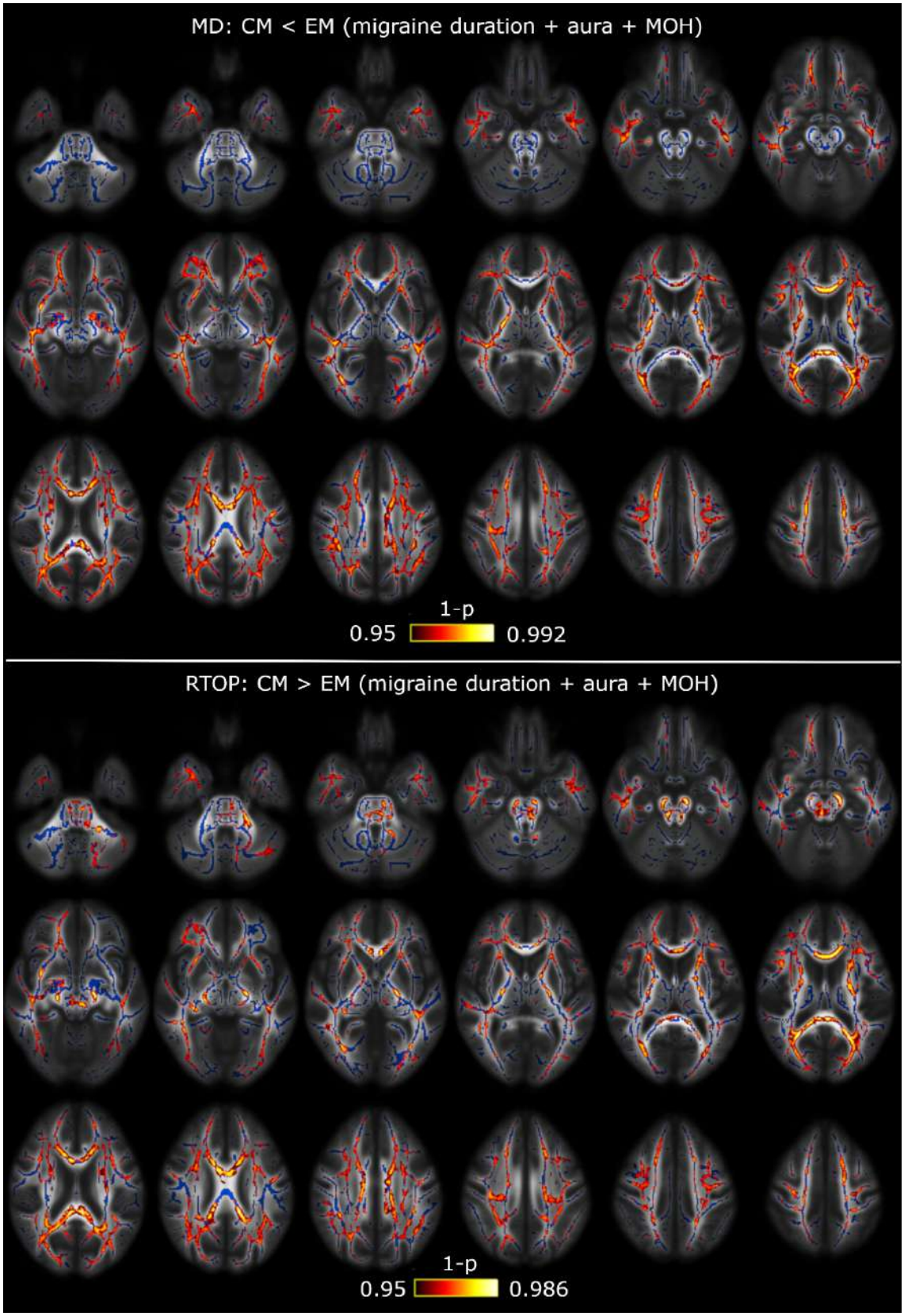


**Figure A4**. MD and RTOP alterations between CM and EM including duration of migraine, presence of aura, and medication overuse headache as covariates. TBSS showed decreased MD and increased RTOP values in CM with respect to EM. White matter skeleton is shown in blue, and voxels with the lowest p-values in red-yellow. The color bar shows the 1-p-values (FWE-corrected). MOH = medication overuse headache.

**Table A10.** White matter regions from the ICBM-DTI-81 White Matter Atlas for which significant decreased RD values were found in CM compared to EM including the duration of migraine, presence of aura, and medication overuse headache as covariates.

| **White Matter Region** | **Minimum p-value (FWE-corrected)** | **Volume ($mm^3$)** | **MNI peak coordinate (mm), (x,y,z)** |
|---|---|---|---|
| Superior cerebellar peduncle R | .043 | 49 | (4,-29,-17) |
| Superior longitudinal fasciculus R/L | .009/.007 | 667/711 | (33,-40,29) / (-28,-44,31) |
| Genu of corpus callosum | .010 | 1005 | (-14,23,19) |
| Body of corpus callosum | .007 | 1749 | (-17,-23,34) |
| Splenium of corpus callosum | .007 | 1192 | (-23,-52,19) |
| Anterior corona radiata R/L | .009/.007 | 1145/728 | (27,12,23) / (-24,13,15) |
| Superior corona radiata R/L | .009/.007 | 966/991 | (26,8,25) / (-26,-18,28) |
| Posterior corona radiata R/L | .007/.007 | 350/392 | (28,-63,16) / (-26,-62,16) |
| External capsule R/L | .009/.007 | 426/362 | (26,16,9) / (-24,15,10) |
| Posterior limb of internal capsule R/L | .011/.008 | 363/277 | (20,-4,12) / (-22,-11,14) |
| Retrolenticular part of internal capsule R/L | .011/.011 | 234/276 | (30,-38,17) / (-37,-34,2) |
| Anterior limb of internal capsule R/L | .009/.007 | 337/440 | (22,7,15) / (-21,14,13) |
| Sagittal stratum R/L | .029/.011 | 267/189 | (40,-14,-16) / (-41,-26,-8) |
| Posterior thalamic radiation R/L | .007/.008 | 512/303 | (28,-63,16) / (-26,-62,16) |
| Pontine crossing tract | .044 | 182 | (-2,-31,-35) |
| Fornix (cres) R/L | .030/.013 | 182/191 | (35,-8,-19) / (-35,-11,-17) |
| Cingulum R/L | .018/.011 | 35/141 | (10,-34,35) / (-9,-39,29) |
| Superior fronto-occipital fasciculus R/L | .009/.007 | 85/61 | (22,6,19) / (-21,1,20) |
| Uncinate fasciculus R | .020 | 43 | (34,1,-15) |
| Tapetum R/L | .008/.008 | 82/75 | (31,-52,14) / (-28,-48,20) |

FWE = Family-wise error; L = left; R = right. The column Volume represents the volume from the atlas region with significant results. No regions with volume equal or lower than 30 $mm^3$ were included in this Table.

**Table A11.** White matter regions from the ICBM-DTI-81 White Matter Atlas for which significant increased RTAP values were found in CM compared to EM including the duration of migraine, presence of aura, and medication overuse headache as covariates.

| **White Matter Region** | **Minimum p-value (FWE-corrected)** | **Volume ($mm^3$)** | **MNI peak coordinate (mm), (x,y,z)** |
|---|---|---|---|
| Middle cerebellar peduncle | .032 | 85 | (9,-21,-39) |
| Superior cerebellar peduncle R/L | .043/.043 | 59/42 | (4,-29,-17) / (-7,-34,-23) |
| Superior longitudinal fasciculus R/L | .032/.021 | 60/54 | (34,-45,28) / (-28,-44,31) |
| Genu of corpus callosum | .033 | 890 | (-13,23,19) |
| Body of corpus callosum | .021 | 1633 | (-17,-24,34) |
| Splenium of corpus callosum | .021 | 1612 | (-23,-52,19) |
| Anterior corona radiata R/L | .031/.021 | 919/498 | (27,12,23) / (-24,13,15) |
| Superior corona radiata R/L | .029/.021 | 672/804 | (19,-23,36) / (-24,3,20) |
| Posterior corona radiata R/L | .021/.021 | 299/327 | (28,-63,19) / (-23,-32,32) |
| External capsule R/L | .032/.021 | 81/157 | (26,16,8) / (-26,10,14) |
| Posterior limb of internal capsule R/L | .011/.008 | 300/420 | (19,-11,2) / (-22,-10,14) |
| Retrolenticular part of internal capsule L | .028 | 127 | (-36,-34,1) |
| Anterior limb of internal capsule R/L | .009/.007 | 364/432 | (23,18,8) / (-22,6,18) |
| Sagittal stratum R/L | .032/.029 | 207/165 | (40,-42,-5) / (-40,-28,-7) |
| Posterior thalamic radiation R/L | .021/.023 | 510/245 | (28,-63,16) / (-27,-63,18) |
| Cerebral peduncle R/L | .032/.031 | 227/319 | (10,-29,-15) / (-17,-16,-6) |
| Corticospinal tract R/L | .032/.032 | 107/141 | (6,-28,-40) / (-7,-20,-24) |
| Medial lemniscus R/L | .032/.032 | 34/61 | (6,-33,-30) / (-4,-33,-26) |
| Pontine crossing tract | .032 | 204 | (-2,-31,-35) |
| Cingulum L | .022 | 162 | (-9,-39,29) |
| Cingulum (hippocampus) R | .042 | 40 | (24,-29,-15) |
| Superior fronto-occipital fasciculus R/L | .032/.021 | 60/54 | (22,5,19) / (-21,1,20) |
| Tapetum R/L | .023/.021 | 82/104 | (31,-52,14) / (-25,-46,20) |

FWE = Family-wise error; L = left; R = right. The column Volume represents the volume from the atlas region with significant results. No regions with volume equal or lower than 30 $mm^3$ were included in this Table.

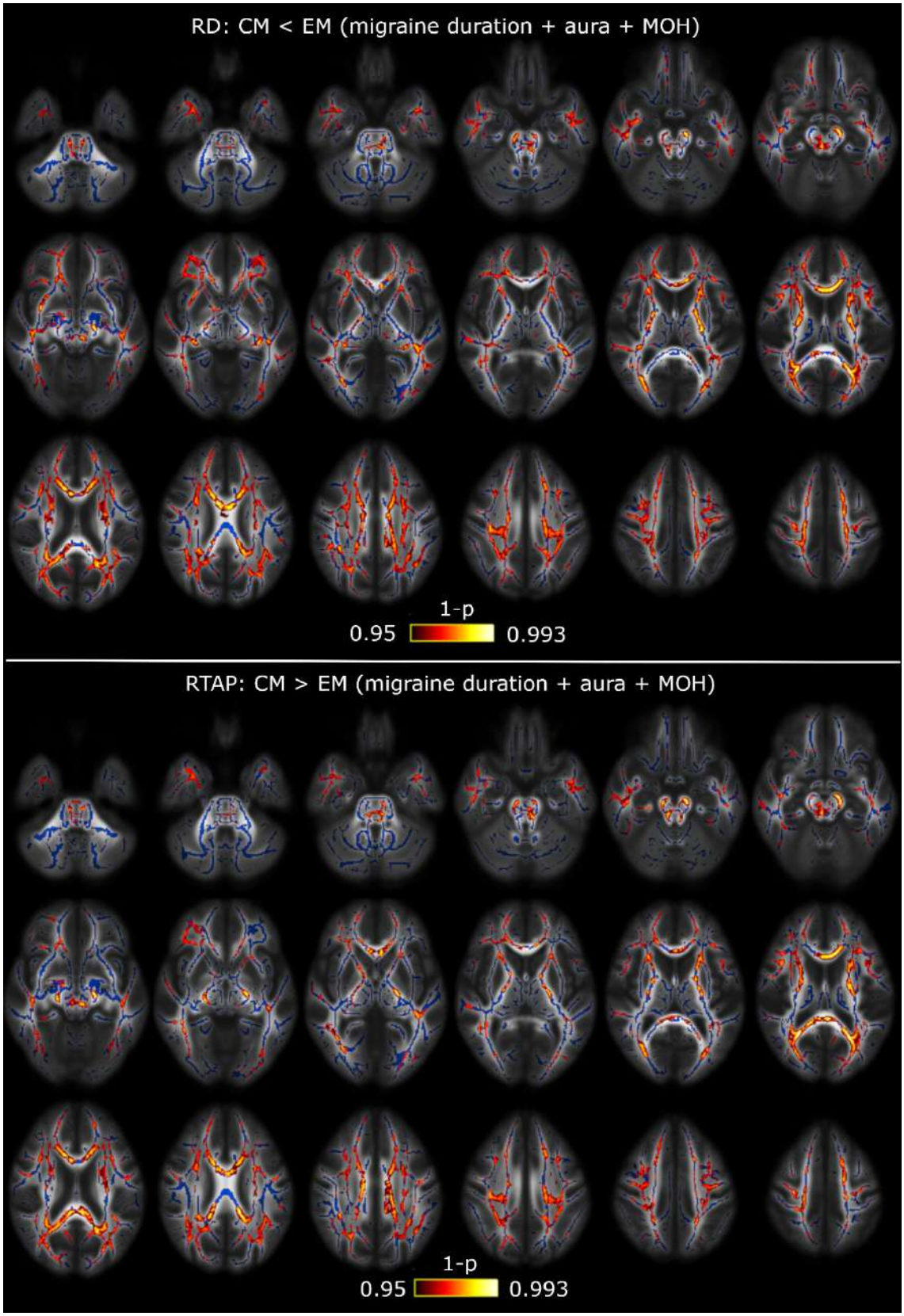


**Figure A5**. RD and RTAP alterations between CM and EM including duration of migraine, presence of aura, and medication overuse headache as covariates. TBSS showed decreased RD and increased RTAP values in CM with respect to EM. White matter skeleton is shown in blue, and voxels with the lowest p-values in red-yellow. The color bar shows the 1-p-values (FWE-corrected). MOH = medication overuse headache.

**Table A12.** White matter regions from the ICBM-DTI-81 White Matter Atlas for which significant increased AD values were found in EM compared to HC including the duration of migraine, presence of aura, and medication overuse headache as covariates.

| **White Matter Region** | **Minimum p-value (FWE-corrected)** | **Volume ($mm^3$)** | **MNI peak coordinate (mm), (x,y,z)** |
|---|---|---|---|
| Superior longitudinal fasciculus L | .042 | 135 | (-29,-25,37) |
| Superior corona radiata L | .040 | 244 | (-22,-23,41) |
| External capsule L | .033 | 281 | (-35,-16,-8) |
| Posterior limb of internal capsule L | .031 | 430 | (-16,-8,4) |
| Retrolenticular part of internal capsule L | .035 | 297 | (-33,-35,6) |
| Anterior limb of internal capsule L | .035 | 37 | (-11,0,2) |
| Sagittal stratum L | .034 | 153 | (-40,-29,-6) |
| Cerebral peduncle L | .033 | 98 | (-15,-13,-5) |

FWE = Family-wise error; L = left; R = right. The column Volume represents the volume from the atlas region with significant results. No regions with volume equal or lower than 30 $mm^3$ were included in this Table.

**Table A13.** White matter regions from the ICBM-DTI-81 White Matter Atlas for which significant decreased RTPP values were found in EM compared to HC including the duration of migraine, presence of aura, and medication overuse headache as covariates.

| **White Matter Region** | **Minimum p-value (FWE-corrected)** | **Volume ($mm^3$)** | **MNI peak coordinate (mm), (x,y,z)** |
|---|---|---|---|
| Superior longitudinal fasciculus L | .046 | 32 | (-41,-38,4) |
| External capsule L | .046 | 127 | (-34,-14,-8) |
| Posterior limb of internal capsule L | .044 | 277 | (-16,-8,4) |
| Retrolenticular part of internal capsule L | .047 | 202 | (-30,-23,2) |
| Sagittal stratum L | .042 | 83 | (-40,-30,-5) |

FWE = Family-wise error; L = left; R = right. The column Volume represents the volume from the atlas region with significant results. No regions with volume equal or lower than 30 $mm^3$ were included in this Table.

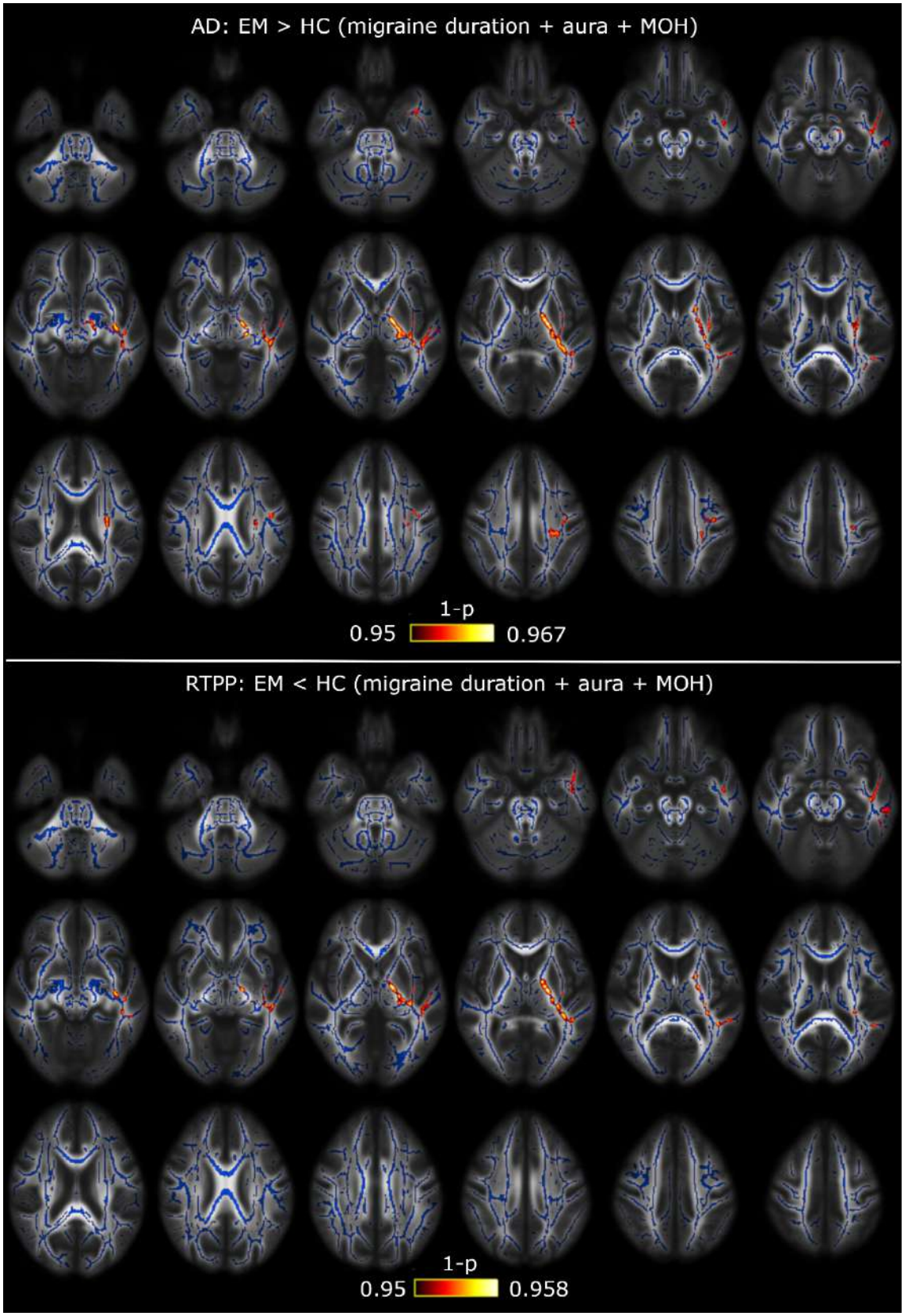


**Figure A6**. AD and RTOP alterations between EM and HC including duration of migraine, presence of aura, and medication overuse headache as covariates. TBSS showed increased AD and decreased RTPP values in EM with respect to HC. White matter skeleton is shown in blue, and voxels with the lowest p-values in red-yellow. The color bar shows the 1-p-values (FWE-corrected). MOH = medication overuse headache.

**Table A14.** White matter regions from the ICBM-DTI-81 White Matter Atlas for which significant increased FA values were found in CM compared to HC including the duration of migraine, presence of aura, and medication overuse headache as covariates.

| **White Matter Region** | **Minimum p-value (FWE-corrected)** | **Volume ($mm^3$)** | **MNI peak coordinate (mm), (x,y,z)** |
|---|---|---|---|
| Superior longitudinal fasciculus R | .037 | 78 | (35,-44,26) |
| Genu of corpus callosum | .037 | 387 | (-14,21,21) |
| Body of corpus callosum | .037 | 463 | (-12,19,21) |
| Splenium of corpus callosum | .034 | 87 | (25,-53,19) |
| Anterior corona radiata R | .042 | 91 | (17,24,24) |
| Superior corona radiata R/L | .049/.046 | 258/48 | (20,-30,41) / (-22,-20,36) |
| Posterior corona radiata R | .020 | 285 | (20,-30,39) |
| Posterior thalamic radiation R | .034 | 100 | (28,-56,17) |
| Tapetum R | .034 | 94 | (30,-46,17) |

FWE = Family-wise error; L = left; R = right. The column Volume represents the volume from the atlas region with significant results. No regions with volume equal or lower than 30 $mm^3$ were included in this Table.

**Table A15.** White matter regions from the ICBM-DTI-81 White Matter Atlas for which significant decreased RD values were found in CM compared to HC including the duration of migraine, presence of aura, and medication overuse headache as covariates.

| **White Matter Region** | **Minimum p-value (FWE-corrected)** | **Volume ($mm^3$)** | **MNI peak coordinate (mm), (x,y,z)** |
|---|---|---|---|
| Superior longitudinal fasciculus R/L | .038/.046 | 218/127 | (35,-48,25) / (-29,-45,31) |
| Genu of corpus callosum | .033 | 566 | (-14,21,21) |
| Body of corpus callosum | .033 | 985 | (-12,19,21) |
| Splenium of corpus callosum | .035 | 314 | (25,-52,22) |
| Anterior corona radiata R/L | .040/.038 | 144/188 | (17,27,21) / (-15,16,30) |
| Superior corona radiata R | .037 | 337 | (20,-29,41) |
| Posterior corona radiata R/L | .035/.046 | 311/120 | (28,-55,20) / (-29,-57,21) |
| Posterior thalamic radiation R/L | .035/.046 | 389/38 | (28,-63,17) / (-31,-52,16) |
| Tapetum R/L | .038/.044 | 95/69 | (30,-47,17) / (-26,-51,18) |

FWE = Family-wise error; L = left; R = right. The column Volume represents the volume from the atlas region with significant results. No regions with volume equal or lower than 30 $mm^3$ were included in this Table.

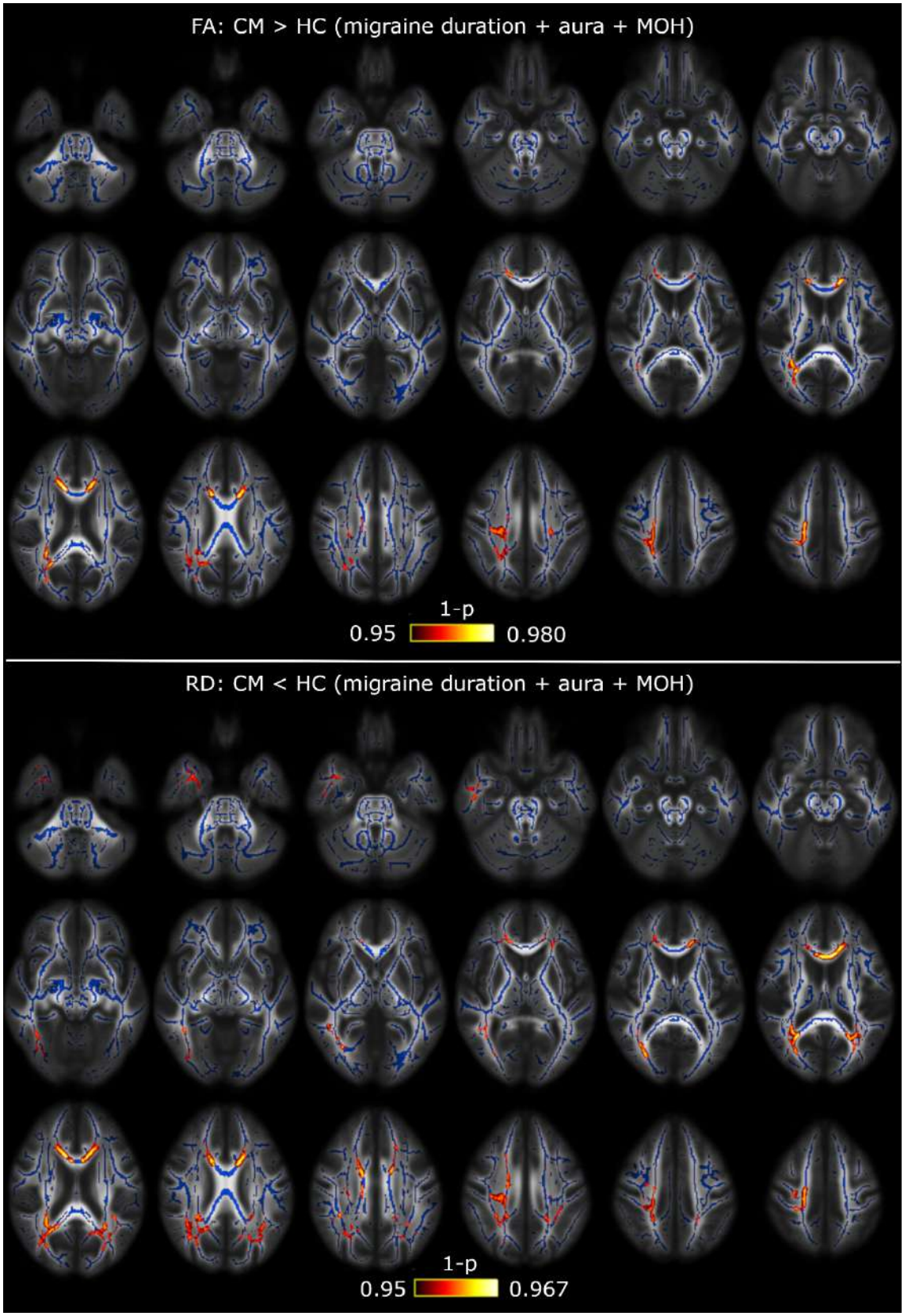


**Figure A7**. FA and RD alterations between CM and HC including duration of migraine, presence of aura, and medication overuse headache as covariates. TBSS showed increased FA and decreased RD values in CM with respect to HC. White matter skeleton is shown in blue, and voxels with the lowest p-values in red-yellow. The color bar shows the 1-p-values (FWE-corrected). MOH = medication overuse headache.

*Chapter 4*

# *Contribution 4: Fewer number of gradient directions in diffusion MRI can be counterbalanced with higher sample size: a migraine clinical study*

**Published as**:

*Planchuelo-Gómez, Á.[1], Aja-Fernández, S.[1], García-Azorín, D.[2], Guerrero, Á.L.[2] and de Luis-García, R.[1] (2020). Fewer number of gradient directions in diffusion MRI can be counterbalanced with higher sample size: a migraine clinical study. In Proceedings of the 28th Annual Meeting of the International Society for Magnetic Resonance in Medicine, 4550.*

1. Imaging Processing Laboratory, Universidad de Valladolid, Valladolid, Spain
2. Headache Unit, Department of Neurology, Hospital Clínico Universitario de Valladolid, Valladolid, Spain

The purpose of this study was the simultaneous assessment of the influence of sample size and number of diffusion gradient orientations in the comparison of DTI-based parameters. The reference comparison was the analysis of the AD in CM and EM patients bearing in mind the identified statistically significant differences in the corresponding TBSS analysis. The main conclusion of this research was that the use of fewer gradient directions in dMRI can be counterbalanced with higher sample size in clinical samples.

## Synopsis

The effect of changes in the acquisition parameters on Diffusion Tensor Imaging (DTI) has been studied, but for very specific situations. A whole-brain comparison of 54 episodic migraine (EM) and 56 chronic migraine (CM) patients, using diffusion schemes of 61, 40 and 21 gradient orientations, was performed. Statistical comparisons were repeated reducing the sample size until no significant differences were found. Higher number of regions with significant lower axial diffusivity in CM compared to EM were found using 61 gradient directions. With a larger sample size, results with 40 and 21 directions were equivalent to results acquired with 61 directions.

# 4.1. Introduction

The effect of changes in the acquisition parameters on Diffusion Tensor Imaging (DTI) scalar measures has been previously studied [1–5]. Particularly, it can be expected that a decrease in the number of gradient directions would affect not only the values, but also the variances of these scalar parameters. Our aim is to study whether this translates into a reduction in the discrimination power of a whole-brain diffusion MRI (dMRI) analysis, and to which extent this can be counterbalanced by means of an increase in the sample size.

# 4.2. Methods

We acquired dMRI data from 54 Episodic Migraine (EM) and 56 Chronic Migraine (CM) patients. Acquisition parameters, including 61 gradient directions, are described elsewhere [6]. The 61 gradient direction scheme was designed so that it can be subsampled to suitable schemes with 40 and 21 directions.

The three groups of diffusion-weighted images (61, 40 and 21 gradient directions) were preprocessed using MRtrix tools [7–10]. Diffusion tensor maps were estimated using the dtifit tool from FSL, and Fractional Anisotropy (FA), Mean (MD), Axial (AD) and Radial Diffusivities (RD) maps were obtained.

FA maps were warped to a common template with the standard tract-based spatial statistics (TBSS) pipeline [11]. The same transformation was applied to MD, AD and RD maps. Voxel-wise pairwise differences were assessed by the nonparametric permutation-based inference randomise tool [12]. One thousand permutations were set and results with $p < 0.05$ (family-wise error corrected) were considered as statistically significant. The minimum volume to consider significant results in a region was set to 30 $mm^3$. Forty-eight regions from the JHU ICBM-DTI-81 White-Matter Labels Atlas were considered in order to find regions with significant differences [13].

To observe the effect of changes in the number of gradient directions, the TBSS inference procedure was repeated in subsamples of the original sample. Starting with 50 subjects in each group, the number of subjects per group was progressively reduced in five subjects for each iteration, until no regions with significant differences were found. For each iteration, 25 repetitions were performed, each of them generating a random subsample of subjects for which the TBSS inference is carried out. This TBSS inference yields significant differences between the two groups (EM vs. CM) in a certain number of white matter regions. The median value of regions with significant differences across the 25 repetitions was considered as the figure of merit for each iteration.

## 4.3. Results

Significant lower AD was found in CM compared to EM in our dataset. The number of regions with significant differences decreases as the number of gradient directions is reduced, obtaining 37 white matter regions for 61 directions, 27 for 40 directions and 20 for 21 directions, when using all subjects for the analysis. Figure 4.13 shows a visual comparison of the detected differences for each configuration of gradient directions. No significant differences were detected for FA, MD or RD.

Figure 4.12 shows the evolution in the number of white matter regions with significant differences when the size of the subject sample is reduced. As can be seen, a decrease in the number of gradients can be compensated by means of an increase in the number of subjects.

## 4.4. Discussion

When designing a white matter study with dMRI, both the acquisition parameters and the expected sample size needed to obtain significant results must be determined a priori. This problem is especially serious when dealing with pathologies where alterations in the white matter are very subtle, as in the case with migraine.

Our results indicate that around 40 subjects per group are needed in order to detect significant differences between EM and CM patients. In fact, a similar study with migraine patients, but a lower sample size, detected no significant differences [14].

As expected, the amount of detected significant differences increases, for a given sample size, when using configurations with a higher number of gradient directions. Nevertheless, the tricky question is the following: how much does fewer gradient directions penalize the discriminant power? In our dataset, reducing the number of gradient directions from 61 to 40 implies the need of around 5-10 additional subjects in each group, and around 10-15 subjects from 61 to 21 directions. This effect is related to the higher variance of the measures when employing fewer gradient directions (fewer samples in the q-space). To obtain similar results using fewer directions, an increase of the sample size is necessary to counterbalance the higher variance.

It is perhaps expected that increasing the sample size can counteract the use of fewer gradient directions. However, these two opposite effects must be quantified in order to make suitable decisions when designing a dMRI study.

In some dMRI studies, the sample size can be hardly increased because of very strict inclusion criteria in order to focus on very specific aspects of certain pathology, among possible reasons. Our results can be useful in those scenarios, in order to design acquisition schemes that are powerful enough to detect significant differences, even for reduced sample sizes.

## 4.5. Conclusion

The use of fewer gradient directions in dMRI can be counteracted with a higher sample size in clinical studies. We have quantified this tradeoff in order to allow better designs of dMRI studies.

# 4.6. References

1. Jones DK. The effect of gradient sampling schemes on measures derived from diffusion tensor MRI: a Monte Carlo study. Magn Reson Med. 2004;51(4):807-815.

2. Landman BA, Farrell JA, Jones CK, Smith SA, Prince JL, Mori S. Effects of diffusion weighting schemes on the reproducibility of DTI-derived fractional anisotropy, mean diffusivity, and principal eigenvector measurements at 1.5T. Neuroimage. 2007;36(4):1123-1138.

3. Lebel C, Benner T, Beaulieu C. Six is enough? Comparison of diffusion parameters measured using six or more diffusion-encoding gradient directions with deterministic tractography. Magn Reson Med. 2012;68(2):474-483.

4. Barrio-Arranz G, de Luis-Garcia R, Tristan-Vega A, Martin-Fernandez M, Aja-Fernandez S. Impact of MR acquisition parameters on DTI scalar indexes: a tractography based approach. PLoS One. 2015;10:e0137905.

5. Aja-Fernández S, Pieciak T, Tristán-Vega A, Vegas-Sánchez-Ferrero G, Molina V, Luis-García R. Scalar diffusion-MRI measures invariant to acquisition parameters: A first step towards imaging biomarkers. Magn Reson Imaging. 2018;54:194-213.

6. Planchuelo-Gómez Á, García-Azorín D, Guerrero ÁL, Aja-Fernández S, Rodríguez M, de Luis-García R. Structural connectivity alterations in chronic and episodic migraine: A diffusion magnetic resonance imaging connectomics study. Cephalalgia. [journal on the Internet]. 2019 [cited 2019 Nov 6]. doi:10.1177/0333102419885392. [Epub ahead of print].

7. Veraart J, Novikov DS, Christiaens D, Ades-Aron B, Sijbers J, Fieremans E. Denoising of diffusion MRI using random matrix theory. Neuroimage. 2016;142:394-406.

8. Andersson JL, Sotiropoulos SN. An integrated approach to correction for off-resonance effects and subject movement in diffusion MR imaging. Neuroimage. 2015;125:1063-1078.

9. Zhang Y, Brady M, Smith S. Segmentation of brain MR images through a hidden Markov random field model and the expectation-maximization algorithm. IEEE Trans Med Imaging. 2001;20:45-57.

10. Smith SM, Jenkinson M, Woolrich MW, et al. Advances in functional and structural MR image analysis and implementation as FSL. Neuroimage. 2004;23:S208-S219.

11. Smith SM, Jenkinson M, Johansen-Berg H, et al. Tract-based Spatial Statistics: voxelwise analysis of multi-subject diffusion data. Neuroimage. 2006;31(4):1487-1505.

12. Nichols TE, Holmes AP. Nonparametric permutation tests for functional neuroimaging: a primer with examples. Hum Brain Mapp. 2002;15(1):1-25.

13. Mori S, Wakana S, Nagae-Poetscher LM, van Zijl PC. MRI Atlas of Human White Matter. Amsterdam: Elsevier; 2005.

14. Neeb L, Bastian K, Villringer K, et al. No microstructural White Matter Alterations in Chronic and Episodic Migraineurs: A Case-Control Diffusion Tensor Magnetic Resonance Imaging Study. Headache. 2015;55(2):241-251.

*Chapter 5*

# *Contribution 5: Structural connectivity alterations in chronic and episodic migraine: A diffusion magnetic resonance imaging connectomics study*

**Published as**:

*Planchuelo-Gómez, Á.[1], García-Azorín, D.[2], Guerrero, Á.L.[2,3], Aja-Fernández, S.[1], Rodríguez, M.[4] and de Luis-García, R[1] (2020). White matter changes in chronic and episodic migraine: a diffusion tensor imaging study. Cephalalgia, 40(4):367-383. doi: 10.1177/0333102419885392.*

1. Imaging Processing Laboratory, Universidad de Valladolid, Valladolid, Spain
2. Headache Unit, Department of Neurology, Hospital Clínico Universitario de Valladolid, Valladolid, Spain
3. Institute for Biomedical Research of Salamanca (IBSAL), Salamanca, Spain
4. Department of Radiology, Hospital Clínico Universitario de Valladolid, Valladolid, Spain

The purpose of this study was the analysis of structural connectivity in patients with CM and EM using a connectomics approach. In this research, the structural connectivity between specific gray matter regions was assessed for the first time in a migraine study using the number of streamlines in the connections between regions as connectivity measure. Higher and lower values of the number of streamlines were found in both migraine groups compared to controls, showing the coexistence of different pathological mechanisms in migraine.

## Abstract

**Objective**: To identify possible structural connectivity alterations in patients with episodic and chronic migraine using magnetic resonance imaging data.

**Methods**: Fifty-four episodic migraine, 56 chronic migraine patients and 50 controls underwent T1-weighted and diffusion-weighted magnetic resonance imaging acquisitions. Number of streamlines (trajectories of estimated fibertracts), mean fractional anisotropy, axial diffusivity and radial diffusivity were the connectome measures. Correlation analysis between connectome measures and duration and frequency of migraine was performed.

**Results**: Higher and lower number of streamlines were found in connections involving regions like the superior frontal gyrus when comparing episodic and chronic migraineurs with controls ($p<.05$ false discovery rate). Between the left caudal anterior cingulate and right superior frontal gyri, more streamlines were found in chronic compared to episodic migraine. Higher and lower fractional anisotropy, axial diffusivity, and radial diffusivity were found between migraine groups and controls in connections involving regions like the hippocampus. Lower radial diffusivity and axial diffusivity were found in chronic compared to episodic migraine in connections involving regions like the putamen. In chronic migraine, duration of migraine was positively correlated with fractional anisotropy and axial diffusivity.

**Conclusions**: Structural strengthening of connections involving subcortical regions associated with pain processing and weakening in connections involving cortical regions associated with hyperexcitability may coexist in migraine.


**Keywords**: Migraine, chronic migraine, diffusion-weighted imaging, tractography, magnetic resonance imaging (MRI), connectomics

# 5.1. Introduction

Chronic migraine (CM) is defined as the presence of headache during 15 or more days per month, with pain of migrainous characteristics at least during eight of those days (1). Although many modifiable and non-modifiable risk factors for evolution from episodic migraine (EM) to CM have been proposed, whether EM and CM are two ranges of the same entity, or two different clinical entities, is still a matter of controversy (2).

White matter alterations in migraine patients have been reported. Rocca et al. described diffusion changes in the optic radiation in migraine patients using diffusion tensor tractography (3). Messina et al. suggested hyperexcitability and early involvement of white matter tracts in migraine, using pediatric patients (4).

Among the various technological tools that can be employed to study the migrainous brain, connectomics is one of the most powerful given the huge amount of data that can be extracted for further analysis. A connectome refers to a description of brain connectivity, a comprehensive map of the full set of elements and interconnections comprising the brain (5). Magnetic resonance imaging (MRI) has been employed to map the human connectome. Diffusion MRI (dMRI) has been used to map the macro-scale axonal structure, while functional MRI has been used to characterize dynamical properties related to brain activity (5).

To analyze structural connectivity differences between migraine patients and healthy controls, dMRI-based tractography offers unique abilities to map whole-brain structural connections (6). In the case of

migraine, previous studies using tractography have found differences between migraine patients and healthy controls in the cingulate gyrus, thalamic radiation, superior longitudinal fasciculus and corticospinal tract (7,8).

More specific structural connectivity studies using diffusion tensor imaging (DTI), comparing migraine patients without aura and healthy controls, were carried out with graph theory as the analyzing method to derive global descriptors of brain connectivity. Graph theory models the brain as a set of nodes (vertices) linked by connections (edges), providing an abstract representation of brain regions (nodes) and their interactions (9). Liu et al. (2013) reported longer global distance connection in patients with migraine, with a lower number of short-distance connections, but a higher number of medium-distance connections, with respect to healthy controls (10). Some studies have reported increased network integration and higher global efficiency in the brain of migraine patients, which could suggest that the brain network in migraine is clustered (10-12). Furthermore, a decoupling between structural and functional connectivity in patients with migraine was reported by Li et al. (2017) (11).

Previous studies have analyzed white matter diffusion alterations in CM patients. Gomez-Beldarrain et al. have reported decreased FA values in CM patients with therapy after six months'follow-up, with respect to healthy controls, in anterior white matter tracts (13). In the same study, however, no EM patients were included in the final analyzed sample because some CM patients reverted to EM during the follow-up. Neeb et al., on the other hand, have compared healthy controls, EM and CM patients, obtaining no significant differences between the groups (14).

However, no specific structural connectivity studies assessing connections between gray matter regions using dMRI or DTI have been performed to study patients with CM, to the best of our knowledge.

The present study performs a detailed comparison of the white matter in EM, CM and healthy controls over a large cohort of subjects, using dMRI data. We hypothesized that there could be structural connectivity changes in migraine patients compared to controls, and that there could be changes also between EM and CM. In contrast to studies that have used graph theory, we analyzed connections between each pair of gray matter regions, using directly the number of streamlines and diffusion descriptors; that is, measures obtained from DTI. Our goals were:

- To investigate whether there are significant structural connectivity differences between CM and EM and compared to healthy controls. To that end, whole-brain structural connectomics was employed as a dMRI analysis technique (5,6).

- To examine possible relationships between structural connectivity measures based on dMRI or DTI and clinical features in migraine patients. Furthermore, possible differences in CM compared to EM in these relationships are especially interesting.

# 5.2. Materials and methods

## *5.2.1.* ***Participants***

We conducted an analytical observational study with a case-control design. Migraine patients were screened and recruited from the headache unit at the Hospital Clínico Universitario de Valladolid (Valladolid, Spain).

We screened patients who had been referred to the above-mentioned unit due to migraine on their first visit. We included patients with a definite diagnosis of EM or CM according to the third edition of the International Classification of Headache Disorders (ICHD-3 and ICHD-3 beta) (1,15), aged between 18 and 60. The patients included in the sample had had a stable clinical situation during the three months before the visit, were preventive treatment naïve, migraine onset had taken place before the age of 50, and they had suffered from migraine for more than a year. In order to avoid confusion between high frequency EM and CM (16), we excluded patients suffering headache on 10–14 days per month. Patients had been asked to keep a migraine diary during three months before inclusion. We also excluded patients if they had other painful conditions apart from headache for more than 9 days per month; had other primary or secondary headaches, except infrequent tension-type headache or medication overuse headache; had other neurological diseases, or were pregnant. We additionally excluded patients with mood disorders (both previously diagnosed or detected by scores from the Hospital Anxiety and Depression Scale (17)). If a preventive treatment was prescribed at the visit, MRI acquisition was performed before starting the prophylactic. Among healthy controls (HC), we excluded those with a present or past history of migraine, other headache disorders other than infrequent tension-type headache, or a prior history of other neurological or psychiatric diseases. We used a non-probabilistic sampling method by convenience sampling. Healthy controls balanced for age and sex were recruited through hospital and University colleagues and advertisements in these facilities by convenience sampling and snowball sampling.

For all patients, sociodemographic and clinical data were collected, including the duration of migraine disease (years), headache and migraine frequency (days per month) and time from the onset of chronic migraine (months) when applicable. We considered the use of symptomatic medication to determine if patients fulfilled the criteria of acute medication overuse (combination of analgesics and triptan intake at 10 or more days per month). The presence of aura was also gathered.

The local Ethics Committee of Hospital Clínico Universitario de Valladolid approved the study (PI: 14-197). All participants read and signed a written consent form prior to their participation.

## *5.2.2.* ***MRI acquisition***

Images were acquired for migraine patients during interictal periods (defined as at least 24 hours from last migraine attack) and between one and two weeks after the clinical visit. High-resolution 3D T1-weighted and diffusion-weighted MRI data were acquired using a Philips Achieva 3T MRI unit (Philips Healthcare, Best, The Netherlands) with a 32-channel head coil in the MRI facility at the Universidad de Valladolid (Valladolid, Spain).

For the anatomical T1-weighted images, the following acquisition parameters were used: Turbo Field Echo sequence, repetition time (TR) = 8.1 ms, echo time (TE) = 3.7 ms, flip angle = 8°, 256 x 256 matrix size, 1 x 1 x 1 $mm^3$ of spatial resolution and 160 slices covering the whole brain.

Diffusion-weighted images (DWI) were obtained using the following parameters: TR = 9000 ms, TE = 86 ms, flip angle = 90°, 61 gradient directions, one baseline volume, b-value = 1000 $s/mm^2$, 128 x 128 matrix size, 2 x 2 x 2 $mm^3$ of spatial resolution and 66 axial slices covering the whole brain.

T1 and diffusion-weighted scans were acquired during the same session, starting with the T1 scan followed by the diffusion-weighted scan, between May 2014 and July 2018. Total acquisition time for each subject was around 18 minutes.

### 5.2.3. Image processing

MRI images were processed to carry out connectomics (5,6).

Firstly, non-brain tissue from the T1-weighted images was removed using the brain extraction tool (BET) from FSL (18,19). Afterwards, automatic gray matter parcellation was computed using FreeSurfer, previously described in detail in (20). The automatic parcellations from FreeSurfer were manually inspected and quality checked.

Separately, diverse preprocessing steps were applied to the DWI data. Diffusion-weighted images were denoised, using the dwidenoise tool from MRtrix (21,22), eddy currents and motion corrected, using the dwipreproc tool from MRtrix (23), and $B_1$ field inhomogeneity corrected, using the dwibiascorrect tool with the -fast option from MRtrix (24,25).

After the DWI preprocessing, a whole brain mask for each diffusion image was generated using the dwi2mask tool from MRtrix (26). With the brain mask and the preprocessed diffusion images, diffusion tensors at each voxel were estimated using the dtifit tool from FSL, obtaining fractional anisotropy (FA) and axial diffusivity (AD) maps among diverse measures. Radial diffusivity (RD) maps were manually obtained calculating the mean of the second and third eigenvalues from the diffusion tensor, values obtained previously with dtifit.

Anatomically-constrained tractography (ACT) was employed as the tractography method (27). Prior to tractography, five-tissue-type (5TT) segmented images for each subject were obtained from the T1-weighted images and the cortical parcellations. The 5ttgen tool from MRtrix was used to have suitable 5TT images for ACT (27). In each subject, the 5TT image and the parcellation from FreeSurfer were linearly registered to the FA image using the FLIRT tool from FSL (28).

Apart from the 5TT images, ACT also needs fiber orientation distributions (FOD) estimations from the DWIs. This, in turn, needs a previous estimation of a response function, which was obtained using the dwi2response tool fromMRtrix (29).Afterwards, FODs were obtained by spherical deconvolution using the dwi2fod tool from MRtrix (30,31). Then, probabilistic tractography was executed using the tckgen tool from MRtrix (32), obtaining 10 million streamlines per subject. A streamline is defined as each of the trajectories that the tractography algorithm computes when employing the diffusion MRI information to obtain a representation of the estimated white matter fiber-tracts. Afterwards, the fiber-tracking data were filtered using the Sphericaldeconvolution Informed Filtering of Tractograms (SIFT2) algorithm (33), which finds an appropriate cross-section multiplier for each streamline.

Finally, structural connectivity matrices were computed from the filtered tractography output and the registered gray matter segmentation volumes. 84 x 84 connectivity matrices, corresponding to the 84 cortical and subcortical regions from the Desikan-Killiany atlas (34), were obtained using mean FA, mean AD, mean RD and the number of streamlines in each connection as connectome metrics. Due to the tractography method that we have employed, the obtained trajectories (streamlines) are non-directional, which means that there is no information about the directionality of the connections. Thus, the connectivity matrices are symmetric by construction, and values on one side of the main diagonal are equal to those on the other side. Therefore, only one half (plus the main diagonal) of the connectivity matrix is relevant and employed for further analysis.

Due to the tractography method employed, it is possible that streamlines start and end in different points belonging to the same gray matter region from the Desikan-Killiany atlas. For this reason, these connections or self-connections; that is, connections with streamlines that start and end in areas from a

unique region, were also included in the analysis. For example, a group of streamlines with its starting point in the anterior insula and finishing point in the posterior insula would be a self-connection insula-insula.

A summary of the whole MRI processing pipeline can be seen in Figure 3.7.

## *5.2.4.* ***Statistical analysis***

We estimated sample size according to Chong and Schwedt (2015) (7). We calculated a worst possible scenario model with an estimated effect size of a difference between groups of .02 and a variance of .003; a type 1-error rate of 1% and 80% power and anticipating a proportion of 10% of lost patients. The expected sample size was 167 participants.

To test for significant sex differences between the three groups, a chi-square test was used. In the case of comparisons of categorical data between only both groups of migraine patients, Fisher's exact test was used.

The Kolmogorov-Smirnov test and Levene's test for equality of variances were used to assess normality and homogeneity of variance in the continuous data, including clinical and demographic data, and values from the connectivity matrices. If continuous data met normality and homogeneity of variance assumptions (when comparing three groups), a one-way ANOVA was used; otherwise, the Kruskal-Wallis test was employed. To compare continuous clinical features between migraine patients, a two-tailed unpaired t-test was used if the clinical variables met normality and homogeneity of variance assumptions; otherwise, the Mann-Whitney U test was employed. To assess differences between two groups in the case of connectome metrics, Tukey-Kramer was the corresponding post-hoc test from the ANOVA test, and the Conover-Iman test was the post-hoc test from the Kruskal-Wallis test.

In order to analyze the structural connectivity matrices, first the mean number of streamlines in each connection (cell from the connectivity matrix) was computed for each group (HC, EM and CM). Next, connections with less than 1000 streamlines (group mean) in all three groups were discarded in order to exclude weak connections from further analysis, due to possible unreliability of the results in these connections. The analysis of the metrics in the remaining connections was previously explained in this section.

Effect size was computed using Cohen's d value in regions with significant results. For every comparison, the mean value of the most disabled group was subtracted from the mean value of the least disabled or the control group. In the comparisons between both types of migraine, CM is considered the most disabled group, and EM the least disabled group.

To study the relationship between clinical parameters and dMRI-DTI descriptors, Spearman's rank correlation coefficient was employed. The analyzed continuous clinical parameters can be seen in the Participants section. Number of streamlines, mean FA, mean AD and mean RD were considered for the correlation analysis. Connections selected for the correlation analysis were those for which significant differences were found between at least two groups in the analysis of connectome metrics.

To correct for multiple comparisons, the Benjamini- Hochberg false discovery rate procedure (35) was applied in the analysis of the connectome metrics and in the correlation analysis.

In all cases, the level of statistical significance was set at $p<.05$.

**Table 1**. Clinical and demographic characteristics of healthy controls (HC), episodic migraine (EM) and chronic migraine (CM).

| | HC (n=50) | EM (n=54) | CM (n=56) | Statistical test |
|---|---|---|---|---|
| Gender, male/female | 11/39 (22/78% ) | 9/45 (17/83% ) | 6/50 (11/89% ) | $\chi^2_{(2,\ N\ =\ 160)} = 2.48$, p = .29† |
| Age (years) | 36.1 ± 13.2 | 37.1 ± 8.2 | 38.1 ± 8.7 | $\chi^2$ (2) = 2.85, p = .24‡ |
| Duration of migraine history (years) | | 14.1 ± 11.1 | 19.6 ± 10.4 | $t_{(108)}$ = -2.7, p = .008§ |
| Time from onset of chronic migraine (months) | | | 24.5 ± 32.9 | |
| Headache frequency (days/month) | | 3.6 ± 1.9 | 23.3 ± 6.3 | U = 44.0, p < .001 |
| Migraine frequency (days/month) | | 3.6 ± 1.9 | 13.9 ± 6.9 | U = 108.5, p < .001 |
| Overusing medication | | 0 (0% ) | 42 (75% ) | p < .001 |
| Aura | | 9 (17% ) | 1 (2% ) | p = .007 |

†Chi-square test. ‡ Kruskal-Wallis test. §Two-tailed, unpaired Student's t-test. Mann-Whitney U test. Fisher's exact test. Data are expressed as means ± SD.

# 5.3. Results

Fifty-one healthy controls, 55 episodic migraine patients and 57 chronic migraine patients were recruited for the study after matching the inclusion and exclusion criteria. Erroneous results in image processing arose in one healthy control, one EM patient and one CM patient, and hence they were finally discarded from the study. Demographic and clinical data for the three groups with the remaining participants are summarized in Table 1. Significant higher headache and migraine frequency (as expected) and duration of migraine (in years) were observed in CM in comparison with EM patients.

Considering the significant differences in duration of migraine history between EM and CM patients (Table 1), an analysis of covariance (ANCOVA) was additionally computed including the duration of the migraine as a covariate firstly, and sex and presence of aura afterwards.

### 5.3.1. Connectomics analysis

Six hundred and twenty (620) connections out of 3570 were finally analyzed after surviving the exclusion criterion; that is, having a mean number of streamlines above 1000 for any of the three groups of subjects. After the multiple comparisons correction, the critical p-value for the results was .00051; that is, only the tests (ANOVA or Kruskal-Wallis) with p-values equal or lower than this critical p-value (for number of streamlines, mean FA, mean AD or mean RD) survived the correction. Significant differences were found in a total of 26 pairs connection-metric. These are 17 connections for the number of streamlines, three connections for the mean FA, four connections for the mean AD and two connections for the mean RD. These results were obtained considering EM and CM patients as different groups; that is, there was not a unique migraine group in the comparisons.

Regarding the number of streamlines, migraineurs showed lower (seven connections) and higher (11 connections) number of streamlines compared to HC (Table 2 and Figure 4.5). In one connection, CM had more streamlines with respect to EM patients (Table 2).

With regard to FA, both groups of migraine patients had decreased mean FA compared to healthy controls in two connections, whereas increased mean FA was found in one connection. Mean FA results are shown in Table 3 and Figure 4.6.

As for AD, both increased and decreased mean AD values were found in migraine patients with respect to healthy controls in four connections. Additionally, significant differences between CM and EM were detected in two of these four cases. Mean AD results are shown in Table 3 and Figure 4.6.

In the case of RD, increased values were found in migraine patients compared to healthy controls in two connections. Moreover, significant differences between CM and EM were detected in one of these two cases. Mean RD results are shown in Table 3 and Figure 4.6.

Including the duration of migraine history as a covariate in an ANCOVA analysis, there were no changes in the connections found to be significant for mean AD, mean RD and mean FA. After the multiple comparisons correction, the critical p-value for this case was .00053. Considering the number of streamlines, 18 connections showed significant differences. Among these 18 connections, four significant connections from the previous analysis showed no significant differences in the ANCOVA analysis, and four non-significant connections in the previous analysis showed significant differences in this case. Lower (eight connections) and higher (10 connections) number of streamlines was detected in migraineurs with respect to HC. In three connections, more streamlines in CM were detected compared to EM. The results for this ANCOVA analysis can be seen in Table 4.

With respect to the ANCOVA analysis adding sex and presence of aura as covariates, there were no changes compared to the analysis that included only the duration of migraine history as a covariate.

When comparing between both groups of migraineurs and HC, many values showed a medium (.5) or even a large effect size (.8 or higher). When comparing CM and EM, connections with medium effect size or close to medium effect size threshold (.5) showed positive Cohen's d values for number of streamlines and negative values for mean AD and RD. These results can be seen in Figures 4 and 5 and in Tables 5 and 6.

### *5.3.2.* ***Correlation analysis***

After multiple comparisons correction, connectome significant positive correlations between time from onset of chronic migraine and mean FA in the right insula self-connection ($\rho$ = .329, p = .013), and between duration of migraine history in CM patients and mean AD in the right hippocampus - right inferior temporal gyrus connection ($\rho$ =.357, p = .007) were found. These results can be seen in Figure 4.11.

No significant negative correlations were found in connectome correlation analysis. No significant correlations were found either for the number of streamlines and mean RD or the duration of migraine history in EM and headache and migraine frequency for both migraine groups in connectome correlation analysis.

**Table 2**. Brain connections number of streamlines comparison between healthy controls (HC), episodic migraine (EM) and chronic migraine (CM) patients.

| ROI1 | ROI2 | HC # of streamlines | EM # of streamlines | CM # of streamlines | EM vs. HC p-value | CM vs. HC p-value | CM vs. EM p-value |
|---|---|---|---|---|---|---|---|
| L pars orbitalis | L pars orbitalis | 12465 ± 5210 | 9267 ± 3152 | 9619 ± 4166 | **.001** | **.001** | 1 |
| L posterior cingulate | L precentral | 4135 ± 2741 | 2694 ± 1769 | 2504 ± 1763 | **.006** | < **.001** | .82 |
| L pars triangularis | L superior frontal | 6543 ± 2488 | 4836 ± 1914 | 5242 ± 2173 | < **.001** | **.007** | .60 |
| L superior frontal | R caudal anterior cingulate | 1400 ± 531 | 1140 ± 631 | 981 ± 434 | **.037** | < **.001** | .27 |
| R pars orbitalis | R pars orbitalis | 14938 ± 5361 | 11432 ± 4336 | 12944 ± 5188 | < **.001** | **.036** | .30 |
| R paracentral | R supramarginal | 2161 ± 1425 | 1081 ± 801 | 1245 ± 1082 | < **.001** | < **.001** | .93 |
| R superior temporal | R temporal pole | 2544 ± 1328 | 1762 ± 1042 | 1732 ± 1072 | **.002** | < **.001** | .99 |
| L banks of STS | L precentral | 734 ± 494 | 1167 ± 850 | 1246 ± 815 | **.008** | < **.001** | .75 |
| L postcentral | L insula | 5822 ± 2027 | 8071 ± 2341 | 7656 ± 2159 | < **.001** | < **.001** | .58 |
| L caudal middle frontal | R caudate | 890 ± 825 | 1409 ± 1038 | 1472 ± 973 | **.002** | < **.001** | .96 |
| L pars opercularis | R caudate | 334 ± 445 | 767 ± 788 | 1011 ± 869 | < **.001** | < **.001** | .41 |
| L superior frontal | R caudate | 1617 ± 1030 | 2554 ± 1388 | 2835 ± 1744 | < **.001** | < **.001** | .95 |
| R thalamus | R caudate | 27047 ± 6478 | 34109 ± 6863 | 31342 ± 5420 | < **.001** | **.001** | .054 |
| L thalamus | R hippocampus | 1755 ± 1952 | 3109 ± 2238 | 3701 ± 2604 | **.007** | < **.001** | .37 |
| L caudal middle frontal | R precentral | 1578 ± 1083 | 1976 ± 999 | 2536 ± 1407 | .066 | < **.001** | .19 |
| L superior frontal | R precentral | 5010 ± 2859 | 7246 ± 2882 | 8049 ± 3669 | < **.001** | < **.001** | .38 |
| L caudal anterior cingulate | R superior frontal | 702 ± 611 | 995 ± 791 | 1307 ± 710 | .051 | < **.001** | **.017** |

L = left; R = right; STS = superior temporal sulcus; # = number.

Tukey-Kramer post hoc test was used for pairwise comparisons. The first seven rows represent connections where one or both groups of migraine patients had lower values compared to healthy controls and differences between both groups of migraine patients were not observed (dashed line drawn after these regions). The next nine rows represent connections where one or both groups of migraine patients had greater values compared to healthy controls and no differences between both groups of migraine patients were observed (dashed line drawn after these regions). The last row represents the connection where significant differences between both groups of migraine patients were observed. When the first two columns contain the same region, they represent a self-connection. Data are expressed as means ± SD. All p-values from ANOVA/Kruskal-Wallis test were equal or lower than .00051.

**Table 3**. Brain connections mean FA and mean AD comparison between healthy controls (HC), episodic migraine (EM) and chronic migraine (CM) patients.

| Metric and ROI1 | ROI2 | HC mean metric | EM mean metric | CM mean metric | EM vs. HC p-value | CM vs. HC p-value | CM vs. EM p-value |
|---|---|---|---|---|---|---|---|
| FA L hippocampus | L entorhinal | .244 ± .028 | .265 ± .035 | .273 ± .033 | **.003** | < **.001** | .39 |
| FA R putamen | R precentral | .421 ± .020 | .407 ± .023 | .404 ± .016 | **.001** | < **.001** | .65 |
| FA R insula | R insula | .300 ± .017 | .288 ± .017 | .286 ± .018 | < **.001** | < **.001** | .94 |
| AD L middle temporal | L putamen | 116 ± 3 | 119 ± 4 | 117 ± 3 | < **.001** | .11 | .075 |
| AD R hippocampus | R fusiform | 123 ± 7 | 119 ± 5 | 117 ± 7 | **.006** | < **.001** | .24 |
| AD R putamen | R inferior temporal | 122 ± 4 | 122 ± 3 | 119 ± 4 | .99 | **.002** | < **.001** |
| AD R hippocampus | R inferior temporal | 126 ± 6 | 124 ± 5 | 121 ± 6 | .13 | < **.001** | **.008** |
| RD L thalamus | L putamen | 506 ± 25 | 525 ± 27 | 520 ± 24 | < **.001** | **.011** | .57 |
| RD L putamen | R caudate | 634 ± 56 | 672 ± 59 | 629 ± 55 | **.002** | .92 | < **.001** |

AD = axial diffusivity; FA = fractional anisotropy; L = left; R = right; RD = radial diffusivity.

Tukey-Kramer post hoc test was used, where significant differences were observed. Data are expressed as means ± SD. AD is expressed in units of $mm^2\ s^{-1} \cdot 10^{-5}$, RD is expressed in units of $mm^2\ s^{-1} \cdot 10^{-6}$ and FA is dimensionless. All p-values from ANOVA/Kruskal-Wallis test were equal or lower than .00051.

**Table 4**. Brain connections number of streamlines comparison between healthy controls (HC), episodic migraine (EM) and chronic migraine (CM) patients including duration of migraine history as a covariate.

| ROI1 | ROI2 | HC # of streamlines | EM # of streamlines | CM # of streamlines | EM vs. HC p-value | CM vs. HC p-value | CM vs. EM p-value |
|---|---|---|---|---|---|---|---|
| L pars orbitalis | L pars orbitalis | 12465 ± 5210 | 9267 ± 3152 | 9619 ± 4166 | < **.001** | **.002** | .90 |
| L posterior cingulate | L precentral | 4135 ± 2741 | 2694 ± 1769 | 2504 ± 1763 | **.002** | < **.001** | .88 |
| L pars triangularis | L superior frontal | 6543 ± 2488 | 4836 ± 1914 | 5242 ± 2173 | < **.001** | **.008** | .60 |
| L superior frontal | R caudal anterior cingulate | 1400 ± 531 | 1140 ± 631 | 981 ± 434 | **.040** | < **.001** | .27 |
| R paracentral | R supramarginal | 2161 ± 1425 | 1081 ± 801 | 1245 ± 1082 | < **.001** | < **.001** | .72 |
| R superior temporal | R temporal pole | 2544 ± 1328 | 1762 ± 1042 | 1732 ± 1072 | **.002** | **.001** | .99 |
| L insula | L thalamus | 6263 ± 2639 | 4798 ± 2273 | 4561 ± 1868 | **.003** | < **.001** | .85 |
| R supra-marginal | R insula | 4974 ± 2606 | 3604 ± 1569 | 3476 ± 1859 | **.002** | < **.001** | .94 |
| L postcentral | L insula | 5822 ± 2027 | 8071 ± 2341 | 7656 ± 2159 | < **.001** | < **.001** | .58 |
| L pars opercularis | R caudate | 334 ± 445 | 767 ± 788 | 1011 ± 869 | **.007** | < **.001** | .18 |
| L superior frontal | R caudate | 1617 ± 1030 | 2554 ± 1388 | 2835 ± 1744 | **.002** | < **.001** | .55 |
| R thalamus | R caudate | 27047 ± 6478 | 34109 ± 6863 | 31342 ± 5420 | **.002** | **.001** | .057 |
| L thalamus | R hippocampus | 1755 ± 1952 | 3109 ± 2238 | 3701 ± 2604 | **.008** | < **.001** | .37 |
| L superior frontal | R precentral | 5010 ± 2859 | 7246 ± 2882 | 8049 ± 3669 | **.001** | < **.001** | .38 |
| L caudal anterior cingulate | R superior frontal | 702 ± 611 | 995 ± 791 | 1307 ± 710 | .088 | < **.001** | .055 |
| L precentral | L superior frontal | 11225 ± 3915 | 12005 ± 3806 | 14132 ± 4433 | .57 | < **.001** | **.013** |
| L middle temporal | L superior parietal | 1435 ± 914 | 1215 ± 830 | 1987 ± 1217 | .51 | **.015** | < **.001** |

*continued on next page*

*continued from previous page*

| | | | | | | | |
|---|---|---|---|---|---|---|---|
| L caudal middle frontal | R precentral | 1578 ± 1083 | 1976 ± 999 | 2536 ± 1407 | .20 | < **.001** | **.038** |

L = left; R = right; # = number.

Tukey-Kramer post hoc test was used for pairwise comparisons. The first eight rows represent connections where one or both groups of migraine patients had lower values compared to healthy controls and differences between both groups of migraine patients were not observed (dashed line drawn after these regions). The next seven rows represent connections where one or both groups of migraine patients had greater values compared to healthy controls and no differences between both groups of migraine patients were observed (dashed line drawn after these regions). The last three rows represent the connections where significant differences between both groups of migraine patients were observed. Underlined regions take part in connections which are exclusive to the analysis considering duration of migraine history as a covariate. When the first two columns contain the same region, they represent a self-connection. Data are expressed as means ± SD. All p-values from ANCOVA test were equal or lower than .00053.

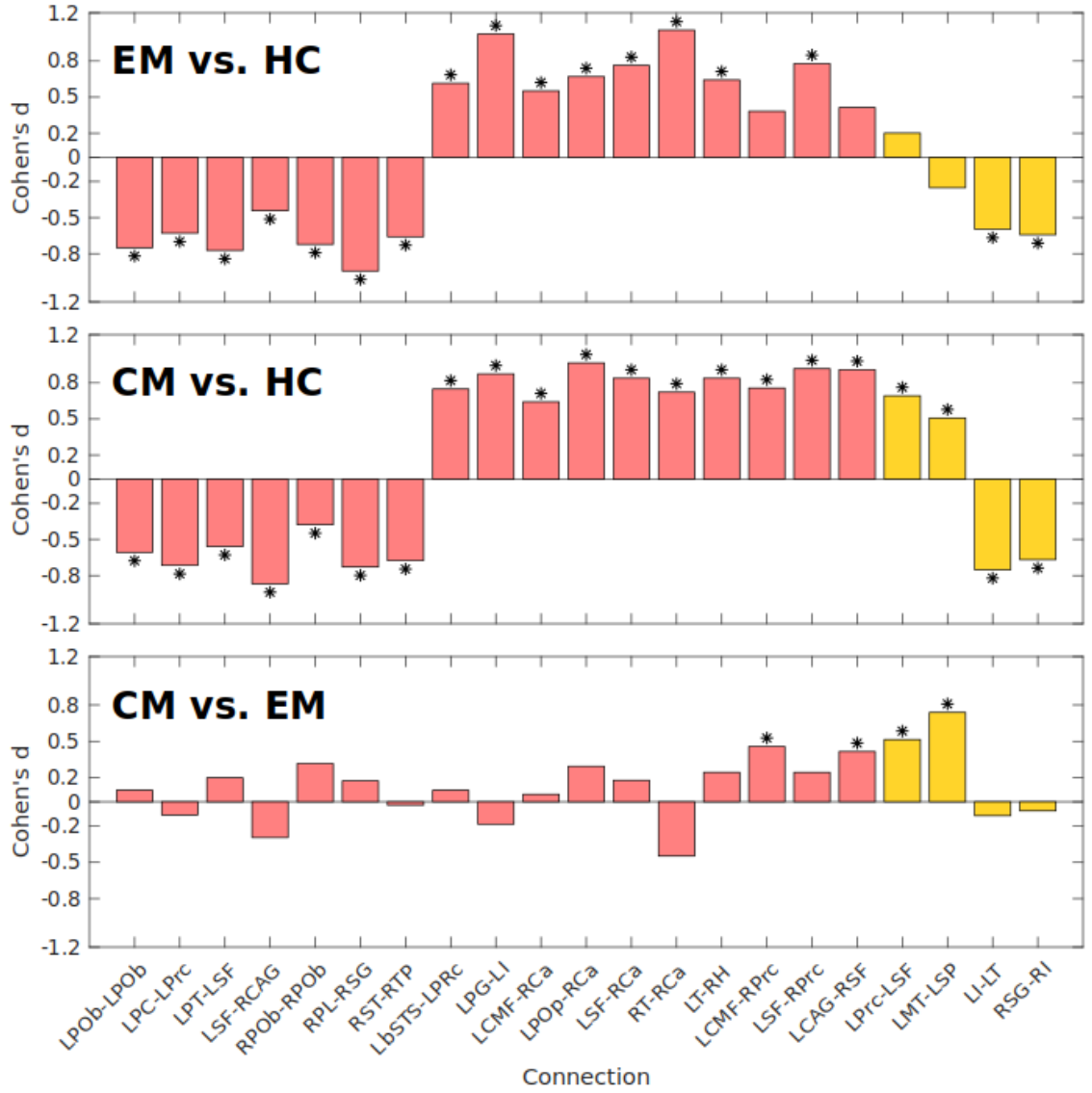


**Figure 4.** Cohen's d number of streamlines bar plots of regions where significant differences between HC, EM and CM were found. Values for all possible pairwise comparisons are shown, including significant results with duration of migraine as a covariate. The last four bars in yellow represent connections with significant results only including duration of migraine history as a covariate. Stars represent pairwise comparisons with significant differences ($p<.05$, including or not including duration of migraine as a covariate). Region abbreviations can be seen in Table 5.

**Table 5**. Cohen's d of number of streamlines in connections where significant differences between healthy controls (HC), episodic migraine (EM) and chronic migraine (CM) patients were observed.

| ROI1 | ROI2 | EM vs. HC Cohen's d | CM vs. HC Cohen's d | CM vs. EM Cohen's d |
|---|---|---|---|---|
| L pars orbitalis (LPOb) | L pars orbitalis (LPOb) | **-.75** | **-.61** | .10 |
| L posterior cingulate (LPC) | L precentral (LPrc) | **-.63** | **-.71** | -.11 |
| L pars triangularis (LPT) | L superior frontal (LSF) | **-.77** | **-.56** | .20 |
| L superior frontal (LSF) | R caudal anterior cingulate (RCAG) | -.44 | **-.87** | -.30 |
| R pars orbitalis (RPOb) | R pars orbitalis (RPOb) | **-.72** | -.38 | .32 |
| R paracentral (RPL) | R supramarginal (RSG) | **-.94** | **-.73** | .17 |
| R superior temporal (RST) | R temporal pole (RTP) | **-.66** | **-.68** | -.03 |
| L banks of STS (LbSTS) | L precentral (LPrc) | **.62** | **.75** | .10 |
| L postcentral (LPG) | L insula (LI) | **1.02** | **.87** | -.18 |
| L caudal middle frontal (LCMF) | R caudate (RCa) | **.55** | **.64** | .06 |
| L pars opercularis (LPOp) | R caudate (RCa) | **.67** | **.97** | .29 |
| L superior frontal (LSF) | R caudate (RCa) | **.76** | **.84** | .18 |
| R thalamus (RT) | R caudate (RCa) | **1.06** | **.72** | -.45 |
| L thalamus (LT) | R hippocampus (RH) | **.64** | **.84** | .24 |
| L caudal middle frontal (LCMF) | R precentral (RPrc) | .38 | **.76** | .46 |
| L superior frontal (LSF) | R precentral (RPrc) | **.78** | **.92** | .24 |
| L caudal anterior cingulate (LCAG) | R superior frontal (RSF) | .41 | **.91** | .41 |
| L precentral (LPrc) | L superior frontal (LSF) | .20 | **.69** | **.51** |

*continued on next page*

*continued from previous page*

| | | | | |
|---|---|---|---|---|
| L middle temporal (LMT) | L superior parietal (LSP) | -.25 | **.51** | **.73** |
| L insula (LI) | L Thalamus (LT) | **-.60** | **-.75** | -.11 |
| R supramarginal (RSG) | R insula (RI) | **-.64** | **-.67** | -.07 |

L = left; R = right; STS = superior temporal sulcus.

When the first two columns contain the same region, they represent a self-connection.

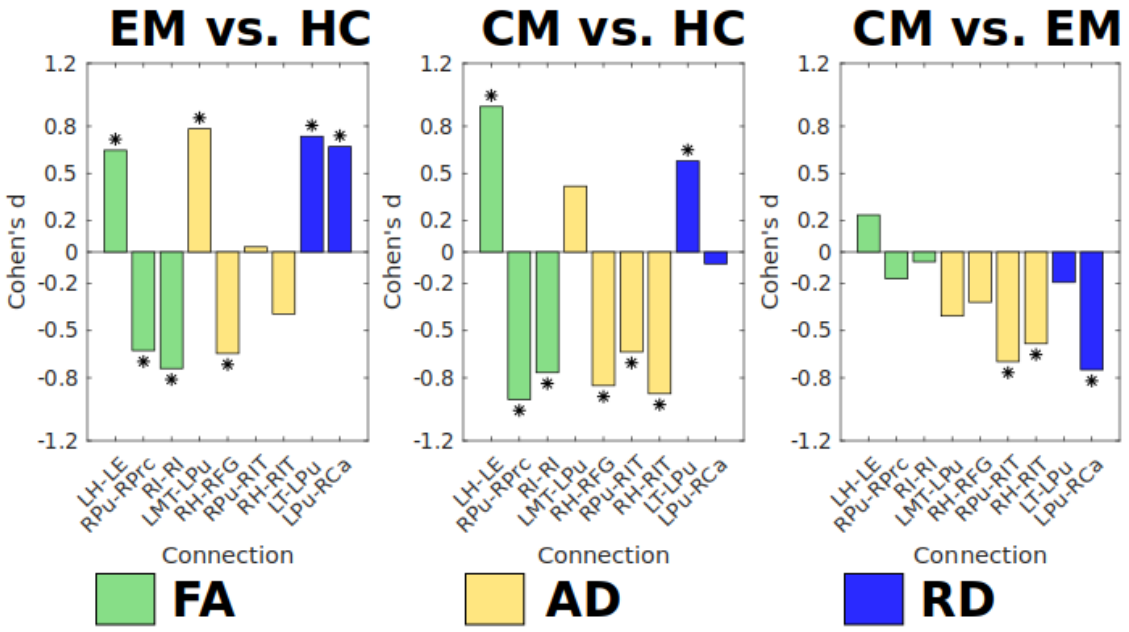


**Figure 5**. Cohen's d mean FA, mean AD and mean RD bar plots of regions where significant differences between HC, EM and CM were found. Values for all possible pairwise comparisons are shown. Stars represent pairwise comparisons with significant differences ($p<.05$). Region abbreviations can be seen in Table 6.

**Table 6**. Cohen's d of mean FA and mean AD values in connections where significant differences between healthy controls (HC), episodic migraine (EM) and chronic migraine (CM) patients were observed.

| Metric and ROI1 | ROI2 | EM vs. HC Cohen's d | CM vs. HC Cohen's d | CM vs. EM Cohen's d |
|---|---|---|---|---|
| FA L hippocampus (LH) | L entorhinal (LE) | **.65** | **.92** | .24 |
| FA R putamen (RPu) | R precentral (RPrc) | **-.63** | **-.94** | -.17 |
| FA R insula (RI) | R insula (RI) | **-.74** | **-.77** | -.06 |
| AD L middle temporal (LMT) | L putamen (LPu) | **.78** | .42 | -.41 |
| AD R hippocampus (RH) | R fusiform (RFG) | **-.65** | **-.85** | -.32 |
| AD R putamen (RPu) | R inferior temporal (RIT) | .03 | **-.64** | **-.70** |
| AD R hippocampus (RH) | R inferior temporal (RIT) | -.39 | **-.90** | **-.58** |
| RD L thalamus (LT) | L putamen (LPu) | **.74** | **.58** | -.19 |
| RD L putamen (LPu) | R caudate (RCa) | **.67** | -.07 | **-.75** |

AD = axial diffusivity; FA = fractional anisotropy; L = left; R = right; RD = radial diffusivity.

# 5.4. Discussion

In this study, we analyzed structural connectivity alterations in migraine patients using dMRI and DTI data and a whole-brain tractography approach. Connectivity measures; that is, the number of streamlines from the tractography and diffusion descriptors (mean FA, mean AD and mean RD), were analyzed in 620 connections between 84 cortical and subcortical gray matter regions.

When comparing migraine patients with healthy controls, we found simultaneously significant higher and lower number of streamlines in migraine patients, suggesting respectively coexistent strengthening and weakening structural connectivity changes in migraine. The same pattern was found for mean FA and AD analysis. In the case of mean RD, increased values were found in migraine patients.

When comparing EM and CM patients, we found more streamlines and decreased mean AD and RD values in CM compared to EM, which suggests two distinct mechanisms of structural connectivity alterations in CM with respect to EM. These two mechanisms might be related to a potential adaptation to painful stimuli and to a possible axonal disturbance, respectively.

In relation with the second objective of the study, correlation analysis was performed between diverse structural connectome measures, including dMRI and DTI descriptors, and clinical features. In the case of CM, time from CM onset was positively correlated with mean FA values. Duration of migraine history in CM patients was also positively correlated with AD values. Since higher FA and/or AD values are in general related to improved connectivity, these correlation results may suggest a possible white matter plastic adaptation to very frequent painful stimuli throughout time in CM patients.

Two patterns could be identified in relation to structural connectivity alterations, based on the analysis of the number of streamlines. The first pattern is a possible weakening (lower number of streamlines) in some connections in migraine patients. An example of this pattern was found in connections within the temporal lobe. Moulton et al. suggested that the temporal lobe is highly affected by migraine and that functional connectivity between the temporal pole and pain processing regions is altered in the interictal state (36). In the other purposed pattern, in migraine patients there might be a strengthening (higher number of streamlines) in other connections involving, in most cases, subcortical regions that is, the caudate nucleus, thalamus and hippocampus, many of these being deeply implicated in migraine pathophysiology, and other regions such as the insula, the superior frontal gyrus and the precentral gyrus. Figure 2 allows a close inspection of the different patterns that are present in the detected differences.

In a review study, Borsook et al. reported that the insula is implicated in processes related to the clinical presentation of migraine and is a hub of activity in migraine (37). In another review, Younis et al. reported the thalamus to be involved in allodynia, central sensitization and photophobia in migraine, and also in the dysfunctional pain modulation and processing (38).

In a meta-analysis study, Jia and Yu reported decreased gray matter volume and increased activation in the precentral gyrus in migraine patients with respect to healthy controls (39). The hippocampus participates in pain processing and is involved in pain-related attention and anxiety (40). The superior frontal gyrus, caudate nucleus, thalamus and hippocampus were classified as rich club regions in migraine patients and healthy controls by Li et al. (2017); that is, regions involved in a great number of connections (11).

Hence, considering the role of the regions involved in connections with higher number of streamlines in migraine, a stronger structural connectivity may indicate a plastic adaptation to painful stimuli in brain regions related to pain processing.

With regard to DTI descriptors, decreased FA values can be caused by several different factors, such as demyelination, lower packing density or different membrane permeability. FA values are also modulated by characteristics such as axon diameter and packing or fiber organization (41). Reduced AD values, on the other hand, may suggest the beginning of demyelination (42), but another hypothesis linked AD more to axonal damage than to demyelination (43). Increased RD values may be associated to white matter neuropathology and myelin damage (43). Nevertheless, biological interpretation of diffusion descriptors is not completely understood, and the results must be interpreted cautiously.

In line with the analysis of the number of streamlines, considering the mean FA values, strengthening in connections with regions implicated in pain processing; for example, the hippocampus, may coexist with weakening in other connections. Taking into account the reduced AD values in connections with the hippocampus, or the increased RD values in connections with the thalamus, there may exist a possible axonal disturbance in the white matter involved in these connections.

Therefore, a higher number of streamlines may suggest not only a potential reinforcement in connections with regions related to pain processing in migraine, but also a possible mechanism to compensate for axonal impairment.

When comparing CM and EM, a similar hypothesis to the comparison between migraineurs and healthy controls can be exposed. In CM, with respect to EM, an apparent reinforcement in some connections with coexistent axonal disturbance may represent that in CM there might be a plastic adaptation to a new state and a procedure to counteract a possible axonal disturbance.

No white matter differences between EM and CM were reported by Neeb et al. using diffusion tensor imaging (14). Therefore, considering our results, we provide a new insight into the differences between episodic and chronic migraine. In the study by Neeb et al., the sample size was considerably smaller than our sample size, which could explain the lack of significant results in that study.

With respect to the analysis of the temporal evolution in migraine, connections with pain processing regions might be evolving throughout the course of migraine, especially in CM patients, due to the high headache frequency. This evolution could counterbalance the initial pathophysiological mechanisms suggested before; that is, connections with pain processing regions would evolve by decreasing number of streamlines. This hypothesis is supported by a reduced number of streamlines in connections with the insula and thalamus when including the duration of migraine as a covariate in the ANCOVA analysis.

Moreover, results indicate that the temporal evolution in CM could be a very different process from that of the temporal evolution of white matter in EM.

Based on our correlation results and the ANCOVA analysis, we hypothesize that CM might evolve in two phases. The first phase would be the progression from EM to CM, and the second phase would be a plastic maladaptation to continuous painful stimuli, especially in pain processing regions.

This plastic maladaptation hypothesis would be supported by significant positive correlations between total duration of migraine and time from onset of chronic migraine in CM patients, and diffusion measures from DTI (FA and AD). Moreover, these correlations were found in connections involving pain processing regions, the insula and the hippocampus.

The modification of the state of white matter in Chronic Migraine would be characterized by a set of maladaptive plastic changes, perhaps caused by repeated painful stimuli or increased cortical excitability, as hypothesized by Szabó et al. (2017) in patients with migraine with aura (44). This CM modification hypothesis may be related to sensitization of CM patients (45). In EM, this modification may be led by loss of white matter integrity.

In other studies, significant negative correlations between duration of migraine in years, in EM patients, and FA was reported in specific white matter pathways (46,47). Significant negative correlations between duration of migraine in years, in EM patients, and AD were also obtained (44,46). These correlation results in EM patients are opposite to the results we obtained in CM patients, showing possible contrary patterns in temporal evolution between EM and CM, as we have hypothesized.

In any case, the influence of duration of migraine in structural connectivity shows the important effect of time in migraine. Therefore, longitudinal studies are very much needed in order to elucidate the nature of these changes and support or discard any hypothesis regarding the evolution of brain connectivity along the disease process.

High frequency EM patients (10-14 headache days per month) were not included in the present study. No significant correlations were found between headache frequency and structural connectivity measures, which could mean that headache frequency does not have a very relevant effect on structural connectivity within the EM or CM groups. We believe that this exclusion criterion was a key factor for the identification of connectivity changes between EM and CM. However, it could also be related to some of the diversity of results found in the literature related to this topic, including the present study.

There are several strengths and limitations in this study. About the strengths, this study is the only one, to the best of our knowledge, which uses brain connectomics based on dMRI tractography to assess connections throughout gray matter regions of the whole brain comparing chronic and episodic migraine patients. Also, this is, to the best of our knowledge, the dMRI tractography study with the highest number of participants simultaneously including healthy controls, EM and CM patients.

About the limitations of this study, we acquired no T2 or T2-FLAIR MRI sequences to evaluate white matter hyperintensities because of the time restrictions of the MRI protocol in a clinical context. Lesions of the white matter related to white matter hyperintensities may have an influence on our results. Patients with anxiety and depression were discarded from the study, as stated in the Participants subsection of the Material and methods section. Most of our patients with CM were overusing medication (42 out of 56). There could be structural differences between CM patients with and without medication overuse, so the medication overuse may be a confounding factor in the identified differences between the analyzed groups. A methodological limitation of our study was that it was not possible to specify the specific white matter tracts where significant differences in the connections between gray matter regions were found. An important limitation in this study was that we could not adjust our results for age, because of the high correlation between age and duration of migraine (collinearity). When MRI were acquired in the patients, they had had no attacks in the previous 24 hours, but they could be in a prodromal stage, as we controlled time from the past attack but not to the next migraine attack. Altered brain physiology and abnormal functional connectivity have been found in prodromal stages (48,49), so this is a possible source of bias in the results. Finally, in the case of the analysis of aura, the number of patients with migraine with aura was too small to perform an analysis comparing migraine with and without aura.

## 5.5. Conclusions

In a dMRI-based connectomics analysis, brain structural connectivity alterations in migraine patients compared to healthy controls, and in chronic migraine compared to episodic migraine, were observed. A higher number of streamlines in connections with subcortical pain processing regions such as the hippocampus or thalamus may reflect a structural strengthening of cerebral pain circuits in migraine patients. Weakening in other connections involving cortical regions associated with hyperexcitability in migraine, like the temporal lobe and particularly the temporal pole, may coexist with that strengthening. To confirm possible plastic maladaptation in the modification of the state of white matter in chronic migraine, especially in connections involving pain processing regions, longitudinal studies are needed.

## 5.6. References

1. Headache Classification Committee of the International Headache Society. The International Classification of Headache Disorders, 3rd edition. Cephalalgia 2018; 38:1–211.

2. Aurora SK and Brin MF. Chronic migraine: An update on physiology, imaging, and the mechanism of action of two available pharmacologic therapies. Headache 2017; 57: 109–125.

3. Rocca MA, Pagani E, Colombo B, et al. Selective diffusion changes of the visual pathways in patients with migraine: A 3-T tractography study. Cephalalgia 2008; 28: 1061–1068.

4. Messina R, Rocca MA, Colombo B, et al. White matter microstructure abnormalities in pediatric migraine patients. Cephalalgia 2015; 35: 1278–1286.

5. Fornito A and Bullmore ET. Connectomics: A new paradigm for understanding brain disease. Eur Neuropsychopharmacol 2015; 25: 733–748.

6. Sinke MRT, Otte WM, Christiaens D, et al. Diffusion MRI-based cortical connectome reconstruction: Dependency on tractography procedures and neuroanatomical characteristics. Brain Struct Funct 2018; 223: 2269–2285.

7. Chong CD and Schwedt TJ. Migraine affects whitematter tract integrity: A diffusion-tensor imaging study. Cephalalgia 2015; 35: 1162–1171.

8. Petrušić I, Daković M, Kačar K, et al. Migraine with aura and white matter tract changes. Acta Neurol Belg 2018; 118: 485–491.

9. Bullmore E and Sporns O. Complex brain networks: Graph theoretical analysis of structural and functional systems. Nat Rev Neurosci 2009; 10: 186–198.

10. Liu J, Zhao L, Nan J, et al. The trade-off between wiring cost and network topology in white matter structural networks in health and migraine. Exp Neurol 2013; 248: 196–204.

11. Li K, Liu L, Yin Q, et al. Abnormal rich club organization and impaired correlation between structural and functional connectivity in migraine sufferers. Brain Imaging Behav 2017; 11: 526–540.

12. Liu J, Ma S, Mu J, et al. Integration of white matter network is associated with interindividual differences in psychologically mediated placebo response in migraine patients. Hum Brain Mapp 2017; 38: 5250–5259.

13. Gomez-Beldarrain M, Oroz I, Garcia Zapirain B, et al. Right fronto-insular white matter tracts link cognitive reserve and pain in migraine patients [erratum in J Headache Pain 2016; 17: 22]. J Headache Pain 2015; 17: 4.

14. Neeb L, Bastian K, Villringer K, et al. No microstructural white matter alterations in chronic and episodic migraineurs: A case-control diffusion tensor magnetic resonance imaging study. Headache 2015; 55: 241–251.

15. Headache Classification Committee of the International Headache Society. The International Classification of Headache Disorders, 3rd edition (beta version). Cephalalgia 2013; 33: 629–808.

16. Serrano D, Lipton RB, Scher AI, et al. Fluctuations in episodic and chronic migraine status over the course of 1 year: Implications for diagnosis, treatment and clinical trial design. J Headache Pain 2017; 18: 101.

17. Zigmond AS and Snaith RP. The hospital anxiety and depression scale. Acta Psychiatr Scand 1983; 67: 361–370.

18. Jenkinson M, Beckmann CF, Behrens TE, et al. FSL. Neuroimage 2012; 62: 782–790.

19. Smith SM. Fast robust automated brain extraction. Hum Brain Mapp 2002; 17: 143–155.

20. Dale AM, Fischl B and Sereno MI. Cortical surfacebased analysis. I. Segmentation and surface reconstruction. Neuroimage 1999; 9: 179–194.

21. Tournier J-D, Smith R, Raffelt D, et al. MRtrix3: A fast, flexible and open software framework for medical image processing and visualisation. Biorxiv 2019.

22. Veraart J, Novikov DS, Christiaens D, et al. Denoising of diffusion MRI using random matrix theory. Neuroimage 2016; 142: 394–406.

23. Andersson JL and Sotiropoulos SN. An integrated approach to correction for off-resonance effects and subject movement in diffusion MR imaging. Neuroimage 2015; 125: 1063–1078.

24. Zhang Y, Brady M and Smith S. Segmentation of brain MR images through a hidden Markov random field model and the expectation-maximization algorithm. IEEE Trans Med Imaging 2001; 20: 45–57.

25. Smith SM, Jenkinson M, Woolrich MW, et al. Advances in functional and structural MR image analysis and implementation as FSL. Neuroimage 2004; 23: S208–S219.

26. Dhollander T, Raffelt D and Connelly A. Unsupervised 3-tissue response function estimation from single-shell or multi-shell diffusion MR data without a co-registered T1 image. ISMRM Workshop on Breaking the Barriers of Diffusion MRI 2016.

27. Smith RE, Tournier J-D, Calamante F, et al. Anatomically- constrained tractography: Improved diffusion MRI streamlines tractography through effective use of anatomical information. Neuroimage 2012; 62: 1924–1938.

28. Jenkinson M, Bannister P, Brady M, et al. Improved optimization for the robust and accurate linear registration and motion correction of brain images. Neuroimage 2002; 17: 825–841.

29. Tournier J-D, Calamante F and Connelly A. Determination of the appropriate b-value and number of gradient directions for high-angular-resolution diffusion-weighted imaging. NMR Biomed 2013; 26: 1775–1786.

30. Tournier J-D, Calamante F, Gadian DG, et al. Direct estimation of the fiber orientation density function from diffusion-weighted MRI data using spherical deconvolution. Neuroimage 2004; 23: 1176–1185.

31. Tournier J-D, Calamante F and Connelly A. Robust determination of the fibre orientation distribution in diffusion MRI: Non-negativity constrained super-resolved spherical deconvolution. Neuroimage 2007; 35: 1459–1472.

32. Tournier J-D, Calamante F and Connelly A. Improved probabilistic streamlines tractography by 2nd order integration over fibre orientation distributions. In: Proceedings of the International Society of Magnetic Resonance in Medicine 2010.

33. Smith RE, Tournier J-D, Calamante F, et al. Enabling dense quantitative assessment of brain white matter connectivity using streamlines tractography. Neuroimage 2015; 119: 338–351.

34. Desikan RS, Ségonne F, Fischl B, et al. An automated labeling system for subdividing the human cerebral cortex on MRI scans into gyral based regions of interest. Neuroimage 2006; 31: 968–980.

35. Benjamini Y and Hochberg Y. Controlling the false discovery rate: A practical and powerful approach to multiple testing. J R Stat Soc Ser B 1995; 57: 289–300.

36. Moulton EA, Becerra L, Maleki N, et al. Painful heat reveals hyperexcitability of the temporal pole in interictal and ictal migraine states. Cereb Cortex 2011; 21: 435–448.

37. Borsook D, Veggeberg R, Erpelding N, et al. The insula: A hub of activity in migraine. Neuroscientist 2016; 22: 632–652.

38. Younis S, Hougaard A, Noseda R, et al. Current understanding of thalamic structure and function in migraine. Cephalalgia 2019; 39: 1675–1682.

39. Jia Z and Yu S. Grey matter alterations in migraine: A systematic review and meta-analysis. Neuroimage Clin 2017; 14: 130–140.

40. Liu HY, Chou KH and Chen WT. Migraine and the hippocampus. Curr Pain Headache Rep 2018; 22: 13.

41. Kochunov P, Thompson PM, Lancaster JL, et al. Relationship between white matter fractional anisotropy and other indices of cerebral health in normal aging: Tractbased spatial statistics study of aging. Neuroimage 2007; 35: 478–487.

42. Winklewski PJ, Sabisz A, Naumczyk P, et al. Understanding the physiopathology behind axial and radial diffusivity changes –what do we know? Front Neurol 2018; 9: 92.

43. Alexander AL, Lee JE, Lazar M, et al. Diffusion tensor imaging of the brain. Neurotherapeutics 2007; 4: 316–329.

44. Szabó N, Faragó P, Kiraály A, et al. Evidence for plastic processes in migraine with aura: A diffusion weighted MRI study. Front Neuroanat 2017; 11: 138.

45. Coppola G, Di Lorenzo C, Schoenen J, et al. Habituation and sensitization in primary headaches. J Headache Pain 2013; 14: 65.

46. Yu D, Yuan K, Qin W, et al. Axonal loss of white matter in migraine without aura: A tract-based spatial statistics study. Cephalalgia 2013; 33: 34–42.

47. Li XL, Fang YN, Gao QC, et al. A diffusion tensor magnetic resonance image study of corpus callosum from adult patients with migraine complicated with depressive/ anxious disorder. Headache 2011; 51: 237–245.

48. May A. Understanding migraine as a cycling brain syndrome: Reviewing the evidence from functional imaging. Neurol Sci 2017; 38: 125–130.

49. Karsan N and Goadsby PJ. Biological insights from the premonitory symptoms of migraine. Nat Rev Neurol 2018; 14: 699–710.

# *Chapter 6*

# *Contribution 6: Multimodal fusion analysis of structural connectivity and gray matter morphology in migraine*

**Published as**:

*Planchuelo-Gómez, Á.[1], García-Azorín, D.[2,3], Guerrero, Á.L.[2,3,4], Aja-Fernández, S.[1], Rodríguez, M.[5] and de Luis-García, R[1] (2021). Multimodal fusion analysis of structural connectivity and gray matter morphology in migraine. Human Brain Mapping, 42(4):908-921. doi: 10.1002/hbm.25267.*

1. Imaging Processing Laboratory, Universidad de Valladolid, Valladolid, Spain
2. Headache Unit, Department of Neurology, Hospital Clínico Universitario de Valladolid, Valladolid, Spain
3. Institute for Biomedical Research of Salamanca (IBSAL), Salamanca, Spain
4. Department of Medicine, Universidad de Valladolid, Valladolid, Spain
5. Department of Radiology, Hospital Clínico Universitario de Valladolid, Valladolid, Spain

The purpose of this study was the simultaneous evaluation of the relationship between gray matter morphometry and structural connectivity parameters in the alterations of migraine patients. To assess the changes from both data modalities, the mCCA-jICA method was employed for first time in a migraine study. Furthermore, as novelty, the technique was adapted to analyze the morphometry and connectivity parameters instead of the modality images (e.g. T1-weighted) or diffusion maps. A clear relationship between the cortical curvature and structural connectivity was established. In migraine patients, strengthened structural networks in migraine were found in connections that involved pain processing regions, while weakened structural connections were found between regions within each lobe. Altered structural connections (mainly strengthened) were identified exclusively in patients with CM.

## Abstract

No specific migraine biomarkers have been found in single-modality MRI studies. We aimed at establishing biomarkers for episodic and chronic migraine using diverse MRI modalities. We employed canonical correlation analysis and joint independent component analysis to find structural connectivity abnormalities that are related to gray matter morphometric alterations. The number of streamlines (trajectories of estimated fiber-tracts from tractography) was employed as structural connectivity measure, while cortical curvature, thickness, surface area, and volume were used as gray matter parameters. These parameters were compared between 56 chronic and 54 episodic migraine patients, and 50 healthy controls. Cortical curvature alterations were associated with abnormalities in the streamline count in episodic migraine patients compared to controls, with higher curvature values in the frontal and temporal poles being related to a higher streamline count. Lower streamline count was found in migraine compared to controls in connections between cortical regions within each of the four lobes. Higher streamline count was found in migraine in connections between subcortical regions, the insula, and the cingulate and orbitofrontal cortex, and between the insula and the temporal region. The connections between the caudate nucleus and the orbitofrontal cortex presented worse connectivity in chronic compared to episodic migraine. The hippocampus was involved in connections with higher and lower number of streamlines in chronic migraine. Strengthening of structural networks involving pain processing and subcortical regions coexists in migraine with weakening of cortical networks within each lobe. The multimodal analysis offers a new insight about the association between brain structure and connectivity.


**Keywords**: brain, connectome, diffusion magnetic resonance imaging, magnetic resonance imaging, migraine disorders

# 6.1. Introduction

Migraine is a primary headache disorder characterized by recurrent attacks with unilateral, pulsatile and moderate or severe intensity, lasting from four to 72 hr (Headache Classification Committee of the International Headache Society, 2018). Migraine can be divided into two types: episodic migraine (EM) and chronic migraine (CM). CM is characterized by headache occurring on 15 or more days per month for more than 3 months during which, on at least eight of these days, the headache has migrainous characteristics (Headache Classification Committee of the International Headache Society, 2018), while EM patients suffer from headache during less than 15 days per month. The number of headache days per month is the unique criterion to distinguish between both types and, currently, there is no specific CM biomarker.

The migrainous brain has been studied in vivo, using different imaging techniques, in several neuroimaging studies. The vast majority of these studies are based on the separated analysis of individual MRI modalities. In the interictal phase of migraine, structural and functional changes in EM and CM have been observed in regions involved in pain such as the hippocampus and the cingulate cortex, with connectivity alterations which might influence multisensory integration, pain experience, and chronification (Messina, Filippi, & Goadsby, 2018). A meta-analysis reported decreased gray matter volume in migraine compared to controls in several regions (Jia & Yu, 2017), although the results may be controversial (Burke et al., 2020). Functional and diffusion MRI have also been employed separately to characterize migraine, but no migraine biomarkers could be identified (Skorobogatykh et al., 2019) or the results between studies are conflicting. CM patients have shown higher functional connectivity in the pain matrix compared to

EM (Lee et al., 2019), and alterations in structural connectivity involving regions like the putamen or the temporal cortex have been found (Planchuelo-Gómez et al., 2020a). With respect to separate gray and white matter alterations, on the one hand, decreased axial diffusivity in diverse white matter tracts (Planchuelo- Gómez et al., 2020b) and reduced cortical thickness, gray matter volume and area have been found in CM (Planchuelo-Gómez, García- Azorín, Guerrero, Rodríguez, et al., 2020). On the other hand, no significant differences between CM and EM have been found using diffusion tensor imaging (DTI) and voxel-based morphometry independently (Neeb et al., 2015, 2017).

Although differences between patients and controls in diverse individual MRI modalities have been reported, it is essential to assess simultaneously data from different sources to understand migraine pathophysiology. Changes observed using different modalities are likely different aspects of a more complex brain alteration pattern that cannot be completely understood using a single modality. It is therefore of paramount importance to assess the existing relationships between these independently found alterations to create a more global picture of the pathophysiology of migraine.

Some authors have previously studied change patterns combining different imaging techniques. The simplest method is a direct correlation analysis between different modalities. In migraine with aura patients, resting state activity has been found to be correlated with fractional anisotropy and radial diffusivity in the corpus callosum (Faragó et al., 2019). However, note that the whole relationship is not totally resolved, since the correlation method does not analyze covariance patterns between the assessed modalities.

More sophisticated approaches have been used to assess other neurological disorders from this perspective. The most employed techniques are those based on canonical correlation analysis (CCA) and independent component analysis (ICA). Multimodal CCA (mCCA) followed by joint ICA (jICA) has allowed to perform a simultaneous analysis of images or maps from different modalities (Sui et al., 2011), including tissue types such as gray and white matter. It has been used to characterize patients with schizophrenia (Lottman et al., 2018; Sui et al., 2011, 2013), Alzheimer's disease (Ouyang et al., 2015) and obsessive-compulsive disorder (Kim, Jung, Kim, Jang, & Kwon, 2015). Furthermore, other techniques have been employed to assess healthy controls (HCs), such as hybrid connICA (Amico & Goñi, 2018) and linked ICA (Llera, Wolfers, Mulders, & Beckmann, 2019). Nevertheless, none of these methods has been used to analyze migraine.

The aim of this study is to investigate alteration patterns that may arise from the joint analysis of gray matter morphology and structural connectivity. From the identification of diverse morphological and structural connectivity patterns, our objective was the obtention of biomarkers for EM and CM compared to controls, and of specific CM biomarkers. To that end, mCCA-jICA was employed. To the best of our knowledge, this is the first study to combine neuroimaging data from these two sources using this kind of approach, as well as the first study to focus on migraine using a modality fusion methodology. We hypothesize that the joint analysis of gray matter morphology and structural connectivity will allow the discovery of new alteration patterns that cannot be found using a single modality.

# 6.2. Materials and methods

## 6.2.1. Participants

We included 160 subjects, divided in 50 HC, 54 EM patients, and 56 CM patients. The same subjects were included in previous studies (Planchuelo-Gómez, et al., 2020a, 2020b). The inclusion and exclusion criteria for patients and controls were the same that were described in both studies and can be found in Supplementary File 1.

The patients kept a headache diary in the 3 months prior to the MRI acquisition and were in stable situation when they were included in the study. This diary was used to evaluate headache and migraine frequency. The frequency values of the month of the scan were taken as reference for quantitative analysis. Patients with high frequency EM (10–14 headache days per month) were discarded to avoid confusion with EM or CM. More details can be found in Supplementary File 1.

To ensure that the controls suffered neither migraine nor headache with migrainous features, a questionnaire was provided to the HC. The questionnaire included questions related to previous diagnosis of migraine, made by a neurologist or a primary care physician, and migraine features according to the criteria C and D of Migraine without aura from the third edition of the International Classification of Headache Disorders (Headache Classification Committee of the International Headache Society, 2018). Together with questions related to the Criterion C, we also included a specific question related to the frequency of headache in more than 15 days per month. To evaluate the intensity of pain (Criterion C), the subject was asked whether an activity should be stopped, or needed to lay in bed, at least for 2 hr because of headache. In case of unclear situation with a control, a neurologist specialized in headache disorders was asked to clarify the inclusion of the subject in the study.

## 6.2.2. MRI acquisition

In the same session, high-resolution 3D T1- and diffusion-weighted images (DWI) were acquired using a Philips Achieva 3 T MRI unit (Philips Healthcare, Best, The Netherlands) with a 32-channel head coil.

For the anatomical T1-weighted images, the following acquisition parameters were used: Turbo Field Echo sequence, repetition time (TR) = 8.1 ms, echo time (TE) = 3.7 ms, flip angle = 8°, 256 x 256 matrix size, 1 x 1 x 1 $mm^3$ of spatial resolution and 160 slices covering the whole brain.

DWI were acquired using the next parameters: TR = 9,000 ms, TE = 86 ms, flip angle = 90°, 61 gradient directions, one baseline volume, b-value = 1,000 $s/mm^2$, 128 x 128 matrix size, 2 x 2 x 2 $mm^3$ of spatial resolution and 66 axial slices covering the whole brain.

The acquisition protocol was the same that was used in Planchuelo-Gómez, et al. (2020a, 2020b). Further details can be found in Supplementary File 1.

## 6.2.3. Features estimation

Two groups of variables were used as features to describe gray matter structure and the connections between the gray matter regions. The first group was composed of four gray matter morphometric characteristics: cortical curvature, cortical thickness, surface area, and gray matter volume. The cortical curvature is related to the folding of the cortex, while the cortical thickness and the surface area are strongly related

to the gray matter volume. On the other hand, the number of streamlines was used as a parameter to represent structural connectivity. The streamlines are the trajectories of white matter fiber tracts that are estimated with a tractography algorithm.

The analysis of this study was based on the comparison of these five measures between patients with EM and CM, and HC, after the application of a multimodal fusion procedure. The obtention of the features is briefly explained on the following two subsections.

### *A. Morphometric gray matter features*

From the T1-weighted images, cortical curvature, cortical thickness and surface area were obtained for 68 cortical regions from the Desikan-Killiany atlas (Desikan et al., 2006), and gray matter volume was also calculated for the previous 68 regions plus 16 subcortical regions from the same atlas. The full image processing is described in (Planchuelo-Gómez, García-Azorín, Guerrero, Rodríguez, et al., 2020) and Supplementary File 1. The FreeSurfer automatic cortical parcellation pipeline was used to extract the gray matter features.

For each subject, the output of this analysis was composed of three 1x68 vectors, referring to curvature, thickness and area in the 68 cortical, and one 1x84 vector with the gray matter volume values in the 68 cortical plus 16 subcortical regions.

### *B. Structural connectivity*

The T1-weighted images and the DWI data were employed to get structural connectivity matrices. The full processing pipeline, including DWI preprocessing, is described in (Planchuelo-Gómez, et al., 2020a) and Supplementary File 1.

Briefly, using MRtrix tools (Tournier et al., 2019), anatomically-constrained tractography (10 million streamlines per subject) was performed after estimating the fiber orientation distributions from the DWIs and the five-tissue-type segmented images from the T1-weighted images (Smith, Tournier, Calamante, & Connelly, 2012).

As a result of this analysis, a symmetric 84x84 matrix was obtained for each subject. Connections with less than 1,000 streamlines (group mean) in the three groups of study were discarded. After the removal of these weak connections, the result was a 1x620 feature vector per subject.

### *C. mCCA and jICA*

The main assumption of this method is that the multimodal dataset is a linear mixture of mixing profiles and independent sources. The fusion of mCCA and jICA allows to overcome the limitations of both methods when they are used independently. mCCA provides an initial estimation for jICA, and the components from each modality are linked due to the maximum correlation across the datasets assumed by the canonical variates from CCA (Correa, Li, Adali, & Calhoun, 2008).

The mCCA-jICA method was first developed in (Sui et al., 2011) for the joint analysis of gray and white matter in schizophrenia. The Fusion ICA Toolbox (FIT), version 2.0d, was employed to implement the method. Using this tool, images, image-like data (e.g., DTI maps) or other type or data such as EEG or genetic data can be used as an input. In our case, the feature vectors described before for gray matter morphology and structural connectivity were employed.

Before the description of the mCCA-jICA method, it is important to explain two concepts: The principal components and the canonical variants.

The principal components are the result of a decomposition technique, the principal component analysis (PCA). The objective of this method is to summarize the information from a large dataset into a set of uncorrelated variables that at the same time keep a maximized variance. In other words, PCA aims at explaining the variability of a dataset using few variables. These variables are the principal components, which are ordered from highest to lowest explained variance.

ICA, which is the technique actually employed in this study, is somehow similar to PCA. However, in ICA the independent components that are obtained are not only uncorrelated as the principal components from PCA, but also do not hold any higher order dependence. Finally, in contrast to PCA, the independent components from ICA are equally important.

On the other hand, CCA is a method employed to identify and quantify relationships between two datasets using few variables. For each dataset, there is a group of canonical variants (the result of CCA) that explain the variability within a dataset and between the two datasets. Each pair of canonical variants is independent from other pairs, and the pairs are ordered from highest to lowest correlation. The procedure we have employed is as follows:

1. *Determination of number of components*: Before starting mCCA, the number of principal components for each modality and the number of independent components should be elucidated. In the original method (Sui et al., 2011), the number of components was obtained using the minimum description length criteria (Li, Adali, & Calhoun, 2007). This method is suitable for images, with thousands or millions of elements (pixels or voxels), but our data dimensionality is relatively small (in the order of hundreds), so we decided to use alternative criteria.

   To determine the number of components from each modality, we followed the Horn's test (Horn, 1965). We computed the eigenvalues from the original data and randomly generated data of the same dimensionality. The eigenvalues from the random data were obtained for 500 generated datasets. Each eigenvalue from the original data was then compared to the corresponding eigenvalue from the random data, taking the 95th percentile value from the 500 random datasets as the eigenvalue to be compared. The number of components to retain in each feature was equal to the number of eigenvalues from the original dataset greater than the 95th percentile corresponding eigenvalue from the random data.

2. *Determination of number of canonical variants*: Once the number of components for each feature was obtained, the number of canonical variants is equal to the minimum number of components of the features that were analyzed.

3. *Dimension reduction on the data using singular value decomposition*: We follow the same procedure implemented in Sui et al. (2011), with the necessary adaptations to our data (more details in Supplementary File 2).

4. mCCA followed by jICA: Similar to Sui et al. (2011), described in detail in Supplementary File 2.

A summary of the whole procedure is shown in Figure 3.8.

The results from this procedure were:

1. A matrix of mixing coefficients, with values for each subject and component. This result determines the weight of a modality in each group.

2. The source components represented as Z-scores for each study group (HC, EM, and CM) and modality (gray matter morphology or structural connectivity), with one value per region or connection. This result represents the regions or connections which are more strengthened or weakened in each group. The components were sorted from highest to lowest correlation between the mixing coefficients from each modality, that is, IC1 has the highest correlation between the mixing coefficients from each modality, and the last IC has the lowest correlation.

### *6.2.4.* ***Statistical analysis***

There are obvious relations between the different gray matter morphology features. For instance, the gray matter volume of a cortical region is correlated to its thickness and area. Because of this, considering all gray matter morphology features together in the mCCA-jICA pipeline would yield mixing coefficients that are not independent.

Because of this, a separate mCCA-jICA full procedure was performed for each gray matter morphometric feature, in order to assess the relationship of structural connectivity with each feature. Therefore, there were four main sets of results:

1. Curvature and connectivity.
2. Thickness and connectivity.
3. Surface and connectivity.
4. Gray matter volume and connectivity.

Due to the absence of subcortical values of curvature, thickness, and area, in these situations we discarded the connections where only subcortical regions were involved. Hence, the input corresponding to the structural connectivity was a 1x570 vector instead of a 1x620 vector in these cases.

As secondary analysis, we repeated the same procedure with all the gray matter morphometric parameters, except gray matter volume, to assess possible relationships between them (because of evident reasons, volume is related to thickness and area).

#### *A. Mixing coefficients*

The ICA loadings or mixing coefficients quantify the weight of the pattern represented by the independent component of each modality in each subject. Comparing these coefficients between the groups, it can be checked whether a specific pattern from an independent source or component is reinforced in patients with respect to controls and vice versa.

If mixing coefficients from a specific component were significantly different between groups in both modalities, this would be a joint component. This kind of components shows a joint variance across modalities (Stephen et al., 2013) and changes between groups in one modality would be linked to changes in another modality.

The alternative situation occurs when significant differences between groups are found only in one modality. In this case, the corresponding components would be modal-specific. These components can

differentiate the groups using the data from one modality (Lottman et al., 2018) and modifications from the modality where significant differences were found would not be linked a priori to changes in other assessed modalities.

Normality and homogeneity of variance of the mixing coefficients were analyzed with the Kolmogorov-Smirnov test and Levene's test for equality of variances, respectively. If the normality and homogeneity assumptions were met, a one-way analysis of variance (ANOVA) was used, and the Kruskal-Wallis test otherwise. Two-by-two comparisons were performed with the post hoc Tukey-Kramer test for ANOVA results, or the Conover-Iman test for the Kruskal-Wallis results. As a secondary analysis, the presence of aura was included as an additional covariate considering that previous studies have reported differences between patients with migraine with and without aura (Messina et al., 2013; Szabó et al., 2017).

For each couple of gray matter and structural connectivity features, results were corrected for multiple comparisons using the Benjamini–Hochberg false discovery rate method (Benjamini & Hochberg, 1995). The total number of comparisons, excluding the post hoc tests, was equal to the number of independent components multiplied by the number of modalities (two).

The level of statistical significance was set at $p < .05$.

### *B. Source components*

To identify the regions and connections which were altered in a specific component, the Z-scores distributions were analyzed. The regions or connections that contained positive and negative outliers of the distribution, that is, absolute values larger than three scaled median absolute deviations from the median, were considered respectively as strengthened and weakened regions or connections.

In the analysis of source components from structural connectivity, diverse pairs of connected regions should be identified. Some of these pairs could share one of the connected regions. In this situation, the identified connections would represent a strengthened or weakened network, that is, a group of interconnected regions with altered structural connectivity.

### *C. Correlation analysis*

Correlations of mixing coefficients from components and modalities with significant differences between groups and clinical parameters were obtained to study the potential impact of the discovered patterns in migraine symptoms. These clinical parameters were the duration of disease, time from onset of CM in these patients, and headache and migraine frequency. The Spearman's rank correlation coefficient was the employed measure.

## 6.3. Results

### *6.3.1.* ***Subject characteristics***

Table 1 shows the clinical and demographic characteristics of the subjects. There were no significant differences in age and gender between the subjects from different groups. With respect to EM, CM patients had a longer duration of disease, higher headache and migraine frequency, higher proportion of patients

**Table 1**. Clinical and demographic characteristics of healthy controls (HC), episodic migraine (EM) and chronic migraine (CM).

| | HC (n=50) | EM (n=54) | CM (n=56) | Statistical test |
|---|---|---|---|---|
| Gender, male/female | 11/39 (22/78% ) | 9/45 (17/83% ) | 6/50 (11/89% ) | $\chi^2_{(2,\ N\ =\ 160)} = 2.48$, p = .29† |
| Age (years) | 36.1 ± 13.2 | 37.1 ± 8.2 | 38.1 ± 8.7 | $\chi^2$ (2) = 2.85, p = .24‡ |
| Duration of migraine history (years) | | 14.1 ± 11.1 | 19.6 ± 10.4 | $t_{(108)}$ = -2.7, p = .008§ |
| Time from onset of chronic migraine (months) | | | 24.5 ± 32.9 | |
| Headache frequency (days/month) | | 3.6 ± 1.9 | 23.3 ± 6.3 | U = 44.0, p < .001 |
| Migraine frequency (days/month) | | 3.6 ± 1.9 | 13.9 ± 6.9 | U = 108.5, p < .001 |
| Overusing medication | | 0 (0% ) | 42 (75% ) | p < .001 |
| Aura | | 9 (17% ) | 1 (2% ) | p = .007 |

†Chi-square test. ‡ Kruskal-Wallis test. §Two-tailed, unpaired Student's t-test. Mann-Whitney U test. Fisher's exact test. Data are expressed as means ± SD.

overusing medication, and lower proportion of aura. Further details can be found in Planchuelo-Gómez, et al. (2020a, 2020b).

### *6.3.2.* ***Components with significant differences***

Three componentes with significant differences were found:

1. One multimodal component (IC1) was identified in the analysis of gray matter cortical curvature and structural connectivity.
2. One modal-specific component was identified in the analysis of cortical thickness and structural connectivity (IC5, structural connectivity specific component).
3. One modal-specific component was identified in the analysis of gray matter volume and structural connectivity (IC3, structural connectivity specific component).

No significant differences were found in the analysis of surface area and connectivity after correction for multiple comparisons (four independent components were obtained). The comparisons of each component with significant differences between CM, EM, and HC are presented in three sections.

## *A. Cortical curvature and structural connectivity*

Two independent components were obtained. The number of retained components was two in the case of the cortical curvature, and 22 for the structural connectivity. A joint component was identified (IC1), indicating association between the changes in curvature and in structural connectivity.

According to the values of the mixing coefficients and IC1 Zscores, EM patients presented higher curvature values in the bilateral frontal pole in comparison to HC (mixing coefficients; $F_{2,157} = 5.26$, corrected $p = .012$; Tukey-Kramer test $p = .004$). Also, CM patients showed higher gray matter curvature in the left rostral anterior cingulate cortex with respect to controls, but statistical significance was not reached in this comparison (Tukey-Kramer test $p = .064$).

Based on the connectivity mixing coefficients and IC1 Z-scores, significant higher connectivity was observed in EM compared to HC (mixing coefficients; $F_{2,157} = 6.53$, corrected $p = .008$; Tukey-Kramer test $p = .001$), and in CM compared to HC (Tukey-Kramer test $p = .044$). In EM compared to HC, connections between regions from the parietal cortex, especially in the superior area, were reinforced in patients. In CM compared to HC, connections between the cingulate cortex and frontal regions, and connections between the hippocampus and regions from the temporal cortex, were strengthened. In both patient groups, strengthened connections between orbitofrontal regions, the putamen and the insula were observed. Connections between orbitofrontal regions and the caudate nucleus were decayed in CM with respect to EM. Reinforced connections between the hippocampus, the putamen and the insula were found exclusively in CM. Following IC1 sources from the three groups, connections of the pars orbitalis and triangularis with the rostral middle frontal gyrus were only detected in controls. Detailed strengthened and decayed networks are shown in Supplementary Tables 1–4, indicated as connections with positive and negative outliers (from IC1 sources), respectively.

Mixing coefficients of IC1 of both modalities were significantly correlated (Pearson's $r = .579$, $p < .001$). IC1 mixing coefficients violin plots from both modalities can be seen in Figure 2a,b.

A summary of these networks can be found in Figure 3 and Supplementary Figure 1. The previous significant results suffered no variations when adjusting them by the effect of the presence of aura.

## *B. Cortical thickness and structural connectivity*

Six independent components were obtained. The number of components was six in the case of the cortical thickness, and 22 for the structural connectivity. A structural connectivity modal-specific component was identified (IC5). No significant differences were detected in any thickness component.

Following mixing coefficients values and IC5 Z-scores, lower structural connectivity values were found in EM compared to HC (mixing coefficients; $F_{2,157} = 9.41$, corrected $p = .002$; Tukey-Kramer test $p = .007$), and in CM compared to HC (Tukey-Kramer test $p < .001$).

In both EM and CM patient groups, connections between diverse gyri within the temporal cortex and fusiform gyrus were weakened with respect to controls. Connections between regions from the parietal lobule, precuneus, cuneus, pericalcarine cortex, and supramarginal gyrus were also debilitated in patients

compared to controls. Weakening in EM with respect to controls was also observed in connections between frontal regions, connections which were not found in the IC5 specific CM source, reflecting a possible weakening in CM compared to EM.

Observing IC5 sources from the three groups, exclusive debilitated connections were found in CM between the superior temporal gyrus, isthmus cingulate cortex, thalamus, and hippocampus. Following IC5 sources from the three groups, strengthened connections of the pars orbitalis and triangularis with frontal regions were only found in controls.

Reinforced connections in the patient groups with respect to the controls were found between the insula and the temporal cortex.

IC5 structural connectivity mixing coefficients can be found in Figure 2c. Detailed strengthened and decayed networks are shown in Supplementary Tables 5–9, indicated as connections with positive and negative outliers (from IC5 sources) respectively. A summary of the networks from this section can be found in Figure 4 and Supplementary Figure 2. The previous significant results suffered no variations when adjusting them by the effect of the presence of aura.

## *C. Gray matter volume and structural connectivity*

Five independent components were obtained. The number of retained components was five in the case of the gray matter volume, and 21 for the structural connectivity. A structural connectivity, modal-specific component was identified (IC3). No significant differences were detected in any volume component.

In this analysis, differences between groups were more related to differences between IC3 sources from the three groups, that is, different sign of Z-scores in the patients compared to HC, than to higher or lower weight (mixing coefficients) of the connections.

Structural connectivity was strengthened in patients with respect to controls in the network composed of the thalamus, caudate nucleus, lateral orbitofrontal cortex, precentral gyrus, putamen, rostral anterior cingulate cortex, insula (only in EM), and hippocampus (only in CM). In EM with respect to controls, connectivity was also reinforced in the connection of the superior parietal cortex with the postcentral gyrus and paracentral lobule.

Migraine patients presented weakened structural connectivity in comparison to controls in networks mentioned in the previous cases, for example, the connections within the temporal and the frontal cortex.

EM patients mixing coefficients were significantly higher in comparison to controls ($F_{2,157} = 6.01$, corrected $p = .031$; Tukey-Kramer test $p = .002$). No significant differences were found in comparisons with CM patients mixing coefficients.

IC3 structural connectivity mixing coefficients can be found in Figure 2d. Detailed strengthened and decayed networks are shown in Supplementary Tables 10–15, indicated as connections with positive and negative outliers (from IC3 sources), respectively. A summary of the networks from this section can be found in Figure 5 and Supplementary Figures 3 and 4. The previous significant results suffered no variations when adjusting them by the effect of the presence of aura.

### 6.3.3. Relation between gray matter morphometric features

From the simultaneous analysis of curvature and thickness ($F_{2,157} = 5.36$, corrected $p = .022$; Tukey-Kramer test EM vs. HC $p = .004$), and also that of curvature and area ($F_{2,157} = 4.41$, corrected $p = .046$; Tukey-Kramer test EM vs. HC $p = .010$), a significant curvature modal-specific component was obtained. Results were similar to those from the analysis of curvature and structural connectivity. Patients with EM showed higher curvature compared to HC in regions such as the frontal and temporal poles. Higher curvature (Z-score positive outlier) was found in the left rostral anterior cingulate cortex in patients with CM, but no significant results related to mixing coefficients were identified in CM.

A significant area modal-specific component in the analysis of curvature and area was found. This component showed that surface was higher in EM compared to CM ($F_{2,157} = 3.86$, corrected $p = .046$; Tukey-Kramer test $p = .027$). No specific region (outlier) was identified in the EM source, but the associated Z-scores from the bilateral superior frontal gyrus, where specific regions were found in EM, the right inferior parietal cortex, and the right middle frontal gyrus were higher than two.

No significant results were identified for the cortical thickness.

### 6.3.4. Correlation analysis

No significant correlation between mixing coefficients and clinical parameters was found.

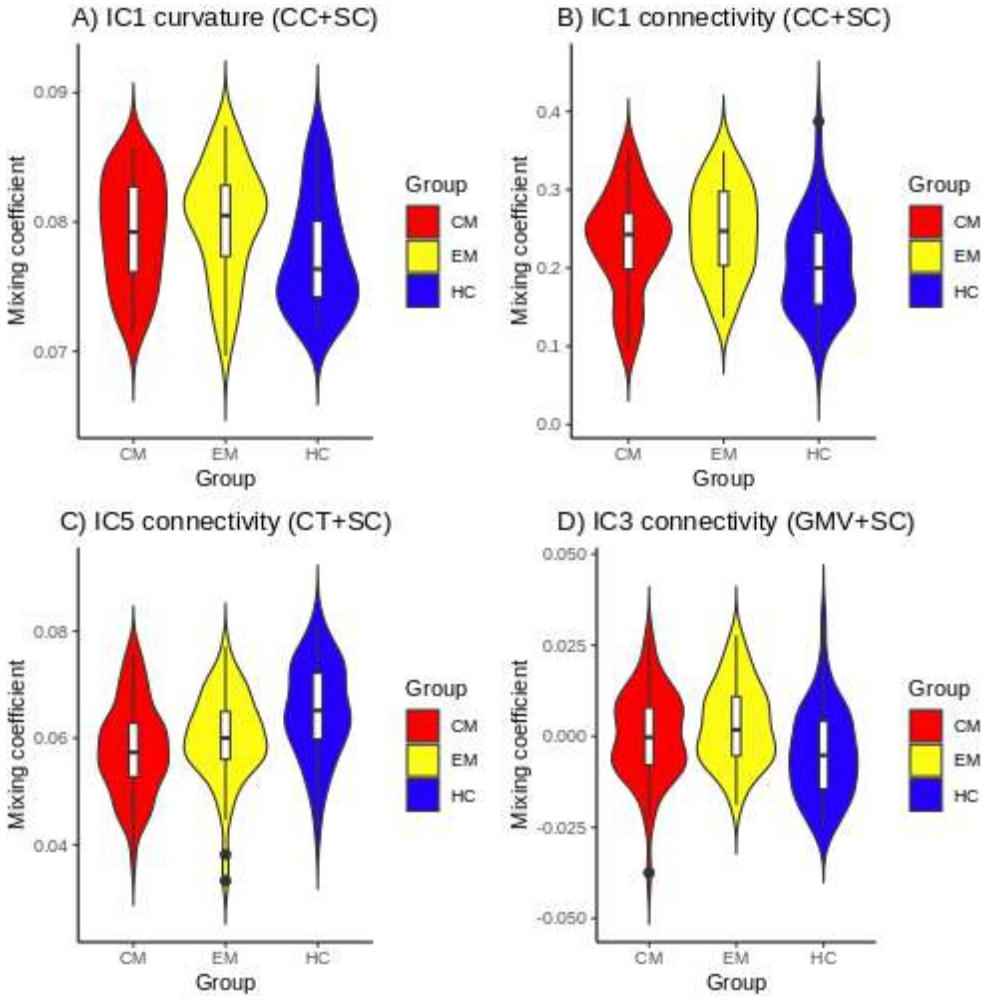


**Figure 2**. Violin and box plots illustrating the distribution of the mixing coefficient values on each group in the comparisons with significant differences. Significant higher mixing coefficients in both patient groups compared to controls in (a) mean cortical curvature (CC) is higher in the patients in the regions with positive Z-scores. The same significant trend is shown in (b), and the interpretation is the same but with structural connectivity (SC). Significant lower coefficients in both patient groups with respect to controls are shown in (c), which means that SC is debilitated in patients than in controls in the connections with positive Z-scores. (d) Significant higher coefficients in episodic migraine (EM) in comparison to healthy control (HC), with the same interpretation as (b) for positive Z-scores and mixing coefficients, and the opposite trend for negative coefficients and positive Z-scores (or positive coefficients and negative Z-scores). CT, cortical thickness; GMV, gray matter volume.

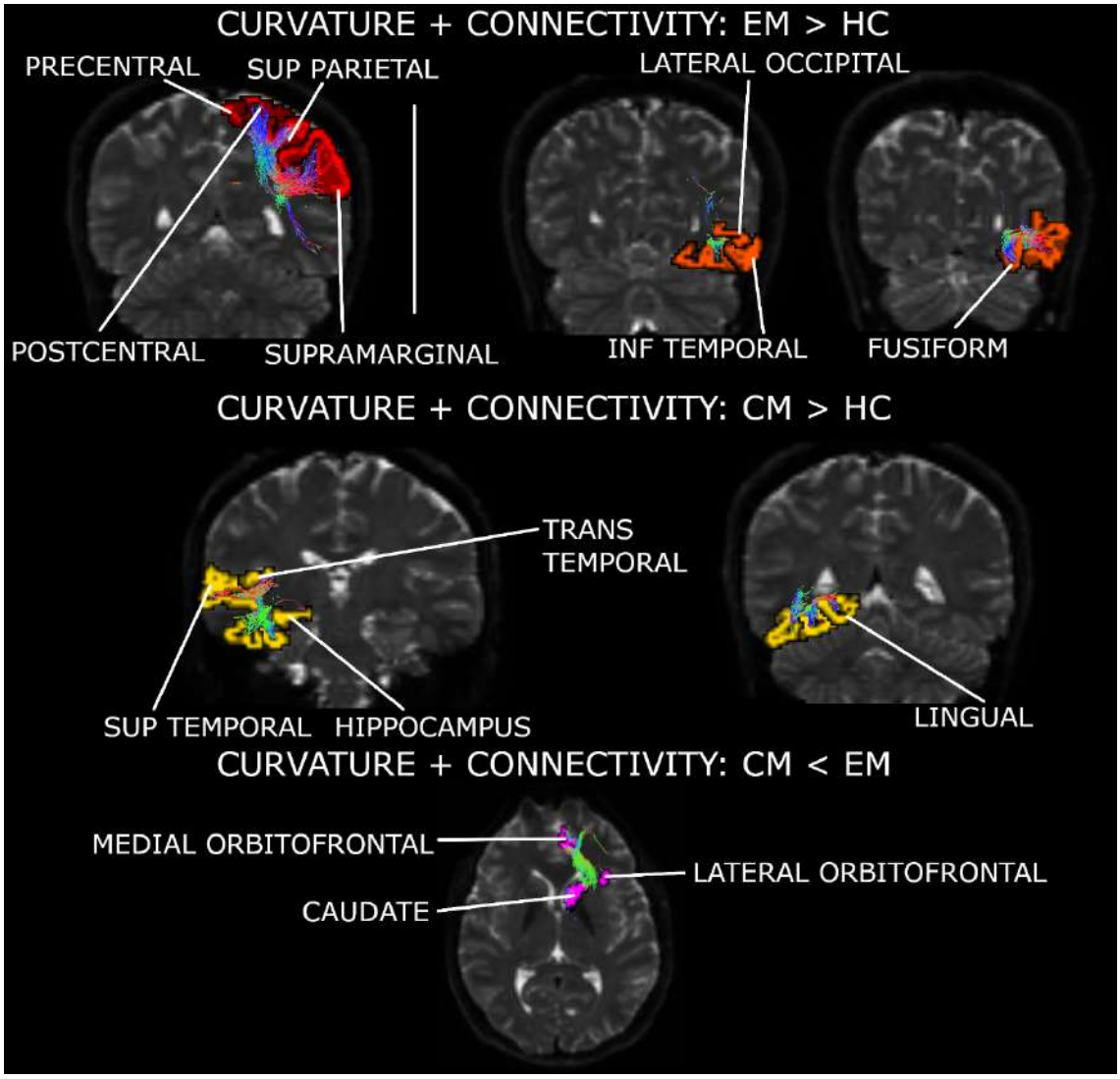


**Figure 3**. Major networks found for the first independent component (fusion of curvature and connectivity). Two networks were strengthened in episodic migraine (EM) compared to healthy control (HC), with involved regions from central, parietal, temporal and occipital areas. One network was reinforced in chronic migraine (CM) compared to HC, with involved regions from the temporal cortex and the hippocampus. The network involving regions from the orbitofrontal cortex and the caudate nucleus was debilitated in CM with respect to EM. Regions represented in a hemisphere may be associated with a specific or both hemispheres (more details can be found in Supplementary File 3). INF, inferior; SUP, superior.

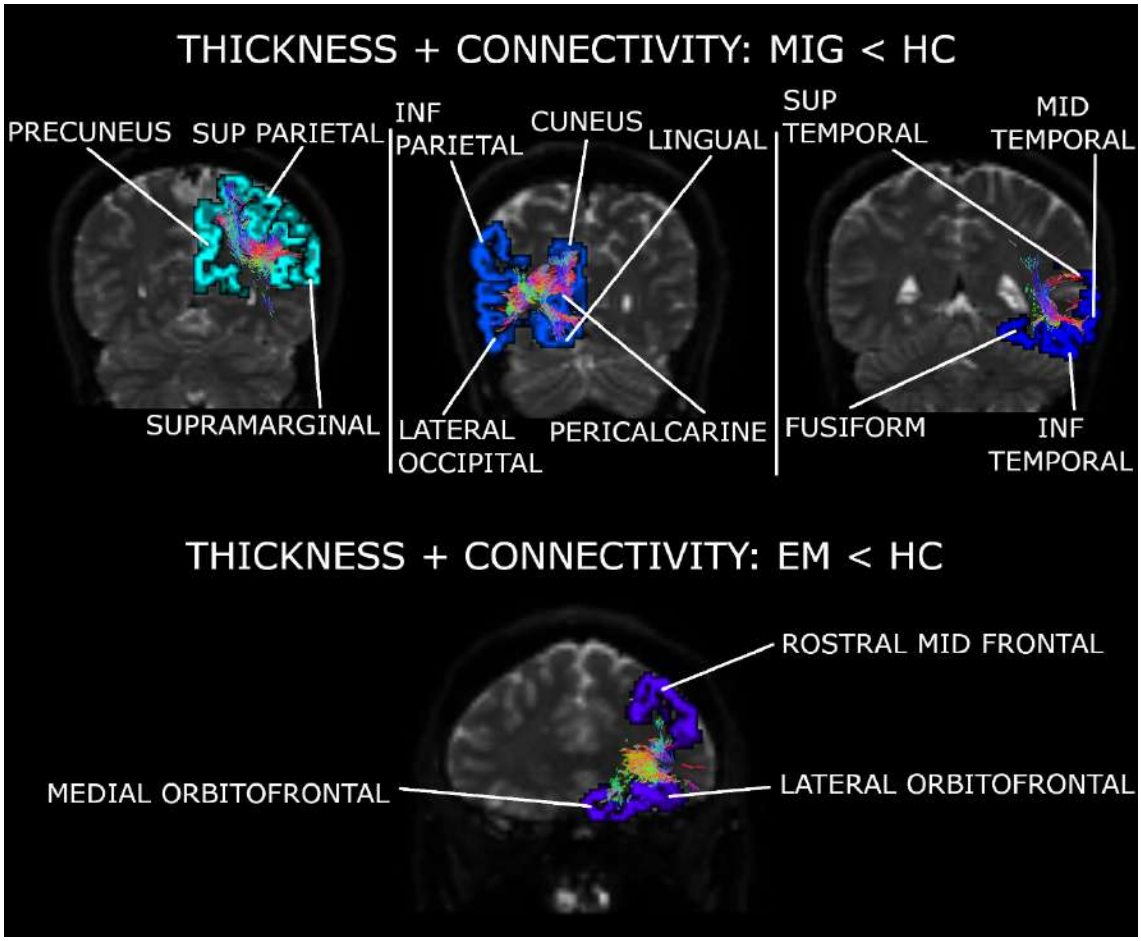


**Figure 4**. Major networks found for the fifth independent component (fusion of thickness and connectivity). Three networks were debilitated in both migraine groups in comparison to controls. These networks included regions from the parietal, occipital, and temporal lobes. One network including regions from the frontal cortex was damaged in chronic migraine (CM) compared to healthy control (HC). Regions represented in a hemisphere may be associated with a specific or both hemispheres (more details can be found in Supplementary File 3). INF, inferior; MID, middle; MIG, migraine (results from episodic migraine [EM] and CM); SUP, superior.

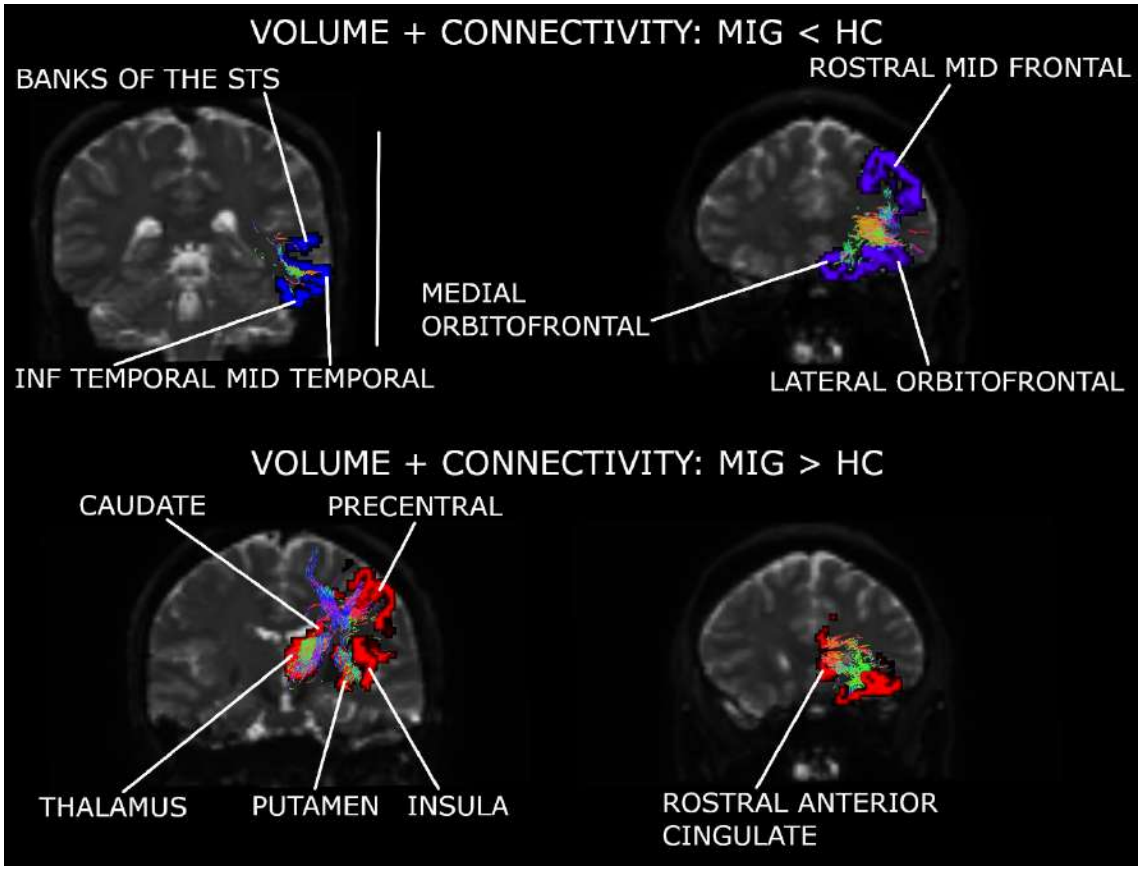


**Figure 5**. Major networks found for the third independent component (fusion of gray matter volume and connectivity). Two networks were debilitated in both migraine groups compared to controls. These regions included areas from the temporal and frontal lobes. One network was strengthened in both migraine groups with respect to controls. This network included subcortical regions, the insula, one region from the frontal cortex and the cingulate gyrus and the precentral gyrus. Regions represented in a hemisphere may be associated with a specific or both hemispheres (more details can be found in Supplementary File 3). INF, inferior; MID, middle; MIG, migraine (results from episodic migraine [EM] and chronic migraine [CM]); STS, superior temporal sulcus.

# 6.4. Discussion

This study introduces two main novel elements. On the one hand, it is the first study to compare migraine patients and controls with an integrated multimodal approach, mCCA-jICA. On the other hand, mCCA-jICA was employed for the first time to analyze simultaneously features from structural connectivity (connectomics) and gray matter morphometry, instead of directly using maps from MRI (e.g., DTI) or segmented images (e.g., gray matter). This new approach allowed us to identify structural network differences in EM and CM with respect to controls, and in CM compared with EM. More importantly, cortical curvature differences between EM and HC were detected and found to be related to the structural connectivity.

## *6.4.1.* ***Gray matter morphometry***

We found significant higher curvature in EM compared to HC, and increased expression in the rostral anterior cingulate gyrus in CM. The increased curvature in both groups of migraine patients is in line with our previous results with the same sample (Planchuelo-Gómez, García-Azorín, Guerrero, Rodríguez, et al., 2020) but, interestingly, the regions found with higher or reinforced curvature in migraine in this study were different from our previous study analyzing gray matter morphometry. While multimodal analysis may be able to uncover new patterns, this does not exclude the need for single-modality conventional analyses.

Although both studies follow the same general trends (increased curvature in migraine), the differences between them may reflect that cortical curvature changes could be related to two different but related mechanisms. The first process, suggested by the results of this study, would be influenced by increased structural connectivity between gray matter regions. The second would be related to white matter atrophy, as suggested previously in multiple sclerosis and schizophrenia studies analyzing curvature and DTI measures (Deppe et al., 2014; Lubeiro et al., 2017).

The differences between the two studies with the same sample may come from the mathematical model employed in this study. On the one hand, the curvature values assessed in the direct comparison (Planchuelo-Gómez, García-Azorín, Guerrero, Rodríguez, et al., 2020) reflect the effect of all the biological processes or external factors which might influence the brain structure. On the other hand, the results from this study indicate the specific enhanced features which are related to another specific mechanism, in this case, the association between cortical curvature and structural connectivity. Thus, the methodology employed in this study is able to detect the relationships between individual biological processes or factors.

No joint components were found using cortical thickness, surface area and gray matter volume as morphometric features. In contrast, functional connectivity alterations have been found in regions where gray matter volume loss was identified in migraine (Burke et al., 2020). In that study, positive and negative functional connections between these regions, extracted from (Jia & Yu, 2017), and other regions were found. Considering also the results from (Burke et al., 2020), it may be hypothesized that, at least in migraine, cortical curvature changes would be related to changes in structural connectivity, and even white matter structure, while changes in gray matter volume would be more related to changes in functional connectivity. The possible association of gray matter morphometry and structural connectivity

**Table 2**. Identified structural networks with differences between healthy controls, episodic migraine and chronic migraine patients.

| | |
|---|---|
| CM, EM < HC | 1. Lateral orbitofrontal – Medial orbitofrontal – Rostral middle frontal |
| | 2. **Rostral middle frontal** – Pars orbitalis – Pars triangularis |
| | 3. Banks of the superior temporal sulcus – Inferior temporal – Middle temporal – Fusiform – Superior temporal |
| | 4. Cuneus – Lingual – Lateral occipital – **Inferior parietal** |
| | 5. **Inferior parietal** – Precuneus – Supramarginal – Superior parietal |
| CM, EM > HC | 1. Rostral anterior cingulate – Thalamus – Caudate – Putamen – Lateral orbitofrontal – Medial orbitofrontal – **Insula** |
| | 2. **Insula** – Fusiform – Inferior temporal |
| | |
| Worsened in EM | 1. Postcentral – Supramarginal – Inferior parietal |
| Enhanced in EM | 1. Superior parietal – Supramarginal – Precentral – Postcentral – Paracentral |
| | 2. Fusiform – Inferior temporal – Lateral occipital |
| | |
| Worsened in CM | 1. Insula – Pallidum - Fusiform |
| | 2. Thalamus – Hippocampus – Superior temporal – Isthmus cingulate |
| CM < EM | 1. Lateral orbitofrontal – Medial orbitofrontal – Caudate |
| Enhanced in CM | 1. Insula – Putamen – Parahippocampal - **Hippocampus** |
| | 2. **Hippocampus** – Fusiform – Inferior temporal – Superior temporal – Lingual – Transverse temporal |

Regions in bold are implied in two different networks with the same trend. Underlined regions are implied in diverse networks with reinforced and debilitated connectivity in migraine, EM or CM.

with functional connectivity should be studied in the future, especially considering that no clear relationship between curvature, thickness and area was found according to our results.

### *6.4.2.* ***Structural connectivity***

Three main structural connectivity patterns were obtained with the joint modal analysis, which are summarized in Table 2 and Figure 4.7. The first and second identified patterns were weakened and strengthened connectivity in migraine patients compared to controls, and the third pattern was related to specific networks expressed in EM and CM.

## *A. Weakened connectivity in migraine*

Several networks were weakened in migraine (both EM and CM) in comparison to HC. These networks contained in most of the cases regions within each of the four lobes. The same trend in connections within the temporal and the frontal lobes has been detected in a connectomics study (Planchuelo-Gómez, et al., 2020a), but, in the present study, the detection of these networks was better defined thanks to the multimodal analysis.

One of the regions involved in debilitated networks was the inferior parietal cortex. Increased blood oxygen level-dependent (BOLD) signal using functional MRI (fMRI) has been found in the inferior parietal cortex in migraine with aura (Hougaard et al., 2014). Thickening has also been found in the inferior parietal cortex in migraine with aura compared to HC and migraine without aura (Messina et al., 2013). The inferior parietal lobe is involved in visuotemporal attention (Shapiro, Hillstrom, & Husain, 2002). We did not detect simultaneous thinning or thickening related to structural connectivity alterations. Therefore, taking into account the fMRI results, weakened structural connectivity could be related to strengthened functional connectivity in migraine. This result is unusual, although coexistence of high functional connectivity and low structural connectivity has been found in healthy subjects (Koch, Norris, & Hund-Georgiadis, 2002), and inverse correlation between both types of connectivity has been identified in multiple sclerosis (Lowe et al., 2008). Further studies are needed to assess the relationship between structural and functional connectivity.

Higher cortical thickness has been reported in migraine in comparison to HC in the middle frontal gyrus (Messina et al., 2013). Increased BOLD signal has been found in the inferior frontal cortex in migraine (Hougaard et al., 2014), an area connected with the rostral middle frontal gyrus in our results (debilitated connectivity in migraine). The anterior part of the frontal lobe takes part in executive functions (Koechlin & Hyafil, 2007). The frontal region results from the literature were similar to those mentioned for the inferior parietal cortex. The concordance of these results is in line with the previous hypothesis about opposite trends between structural and functional connectivity.

## *B. Strengthened connectivity in migraine*

Subcortical regions and the insula were involved in networks found to be strengthened in both EM and CM with respect to controls. The same trend has been reported previously (Planchuelo-Gómez, et al., 2020a), but with some differences in the connections with significant differences. The insula was involved in the two identified networks reinforced in EM and CM. Thinning and gray matter volume loss have been found in migraine compared to HC (Messina et al., 2013; Planchuelo-Gómez, García-Azorín, Guerrero, Rodríguez, et al., 2020). Positive functional connections between regions with gray matter volume loss and the insula have been identified (Burke et al., 2020), but involved regions were different with respect to those included in Table 2. The insula has been reported to be involved in many functional alterations in migraine, processing afferent and efferent information (Borsook et al., 2016). Hence, our results would reinforce the idea of the key role of the insula in migraine not only in functional connectivity, but also in strengthened structural connectivity.

One of the identified strengthened networks in migraine included the thalamus, the caudate nucleus and the putamen. Lower volume in thalamic nuclei has been found in migraine compared to HC (Magon et al., 2015). In a review, the thalamus has been reported to be involved in dysfunctional pain modulation

and processing, allodynia, central sensitization, and photophobia in migraine (Younis, Hougaard, Noseda, & Ashina, 2019). Reduced volume in the caudate (Yuan et al., 2013) and in the putamen (Petrusic, Dakovic, & Zidverc- Trajkovic, 2019) has been reported in migraine compared to HC, and also dysfunctional connectivity in the putamen, suggesting that the putamen is a key region in the integration of information in migraine (Zhao et al., 2014). In the case of CM, higher gray matter volume compared to controls has been identified in the putamen (Neeb et al., 2017), a result possibly related to one of the enhanced networks in CM from our results, which was composed of the insula, putamen, parahippocampal gyrus, and hippocampus. The caudate nucleus may play an important role in the modulation of the pain experience (Wunderlich et al., 2011). Following the possible opposite trends between the functional and the structural connectivity mentioned before in the connections between cortical regions, the results with the subcortical regions were consistent, but with higher structural and lower functional connectivity instead. Some connected regions with increased structural connectivity in our study have shown increased functional connectivity during migraine attacks (Amin et al., 2018). Thus, the structural connectivity in migraine may reflect the networks which are hyper- and hypoactive in ictal state. In interictal state, the functional connectivity could be counterbalanced compared to the ictal state, while the brain may suffer structural changes as an adaptation to attacks.

An interesting situation with opposite trends for the structural connectivity was observed in the orbitofrontal cortex. The orbitofrontal cortex was involved in a weakened network in migraine, within the frontal lobe, and a strengthened network, in connections with the insula and the putamen. Reduced gray matter volume and increased functional connectivity with the dorsal anterior cingulate cortex have been found in the orbitofrontal cortex in migraine patients (Jin et al., 2013; Kim et al., 2008). Lower gray matter volume in the orbitofrontal cortex has been related to poor response to treatment in migraine (Jia & Yu, 2017).

## *C. Structural networks in EM and CM*

The connections with the orbitofrontal cortex played a role not only in the identification of differences between migraine patients and HC, but also between CM and EM. The only network with clear differences from the sources between CM and EM was composed of lateral and medial orbitofrontal regions from the Desikan-Killiany atlas and the caudate nucleus. A neuropsychological evaluation study has reported worse orbitofrontal task performance in CM with respect to EM and HC and associated this baseline performance with negative outcome after one year follow-up (Gómez-Beldarrain, Carrasco, Bilbao, & García-Moncó, 2011). In an fMRI study, the caudate nucleus presented lower response to noxious stimulation in high-frequency EM in comparison to low-frequency EM, and also lower functional connectivity with the insula and higher gray matter volume (Maleki et al., 2011). These previous results and our findings suggest that the structural and functional connectivity of the orbitofrontal cortex with pain processing regions such as the caudate nucleus and the insula may play a key role in the effect of the treatment and progression of migraine.

About the exclusive networks found for EM, the weakened network was composed of regions from the parietal lobe, a result in line with the comparison between migraine patients and HC. The strengthened networks in EM were composed of regions from two lobes. One of these networks included regions from the parietal and frontal lobes, and the other one from the temporal and occipital lobes. This finding suggests

that connections between regions from different lobes, possibly integrating diverse aspects related to the functions affected by the pain experience, may be reinforced in EM compared to controls.

The hippocampus was the region which was highlighted only in the CM exclusive networks. In the two CM reinforced networks, the hippocampus was one of the regions involved. In a review, the hippocampus has been reported as a key region related to migraine prognosis, associating a smaller volume and higher values of graph theory measures from DTI with a worse prognosis (Liu, Chou, & Chen, 2018). Thus, the hippocampus structural connectivity with regions from the inferior temporal lobe or the insula and putamen seems to be a possible CM biomarker.

The hippocampus was also involved in a weakened network in CM that presented connections with the thalamus and the superior temporal gyrus. Another debilitated network in migraine contained the insula, the pallidum and the fusiform gyrus. In high-frequency EM, higher functional connectivity in the connection between the insula and the pallidum has been observed in comparison to low-frequency EM (Maleki et al., 2011). These results may imply that the hippocampus may not only participate as an active structural connection center in CM, but also may be involved in damaged structural connections with the thalamus, an important pain processing region.

### *6.4.3.* ***Novel perspective of the multimodal fusion analysis***

Throughout the discussion section, we have hypothesized a possible inverse relationship between structural and functional connectivity. These possible opposite trends may show a maladaptation process to counterbalance strengthened or weakened structural connectivity. Thus, multimodal fusion analysis may be helpful to uncover new relationships between brain structure and function and raise new hypotheses.

Sophisticated fusion methods can be useful for purposes beyond simply obtaining replicated results from direct comparison of MRI features. Methods such as mCCA-jICA allow to capture complex covariance and relationships between specific modalities and to find joint alteration patterns between diverse groups of interest. Therefore, the mCCA-jICA method can identify additional alterations which are complementary to the single-modality analysis and find alteration patterns related to simultaneous changes in brain structure and activity. The fusion methods may help to better understand and integrate findings from diverse modalities.

### *6.4.4.* ***Limitations***

This study has some limitations. Concerning the dataset, and as mentioned in our previous studies with the same sample (Planchuelo- Gómez, et al., 2020a, 2020b), white matter hyperintensities could not be assessed due to the lack of T2 or T2-FLAIR MRI sequences, and there could be a certain bias in the CM patients due to the great percentage (75%) of medication overuse patients. Additionally, we controlled that the patients suffered no migraine attacks during the 24 hr prior to the MRI acquisition, but there was no control for the next 24 hr (or more). Therefore, some patients could possibly have been scanned in the prodromal phase of migraine, instead of the interictal phase, which might have influenced the results. With regard to the streamline count as a connectivity measure, although its use has been sometimes

controversial, current trends consider it to be an acceptable metric for connectivity as long as it is based on appropriate tractography methods, such as the anatomically-constrained tracking algorithm that we employed (Yeh, Jones, Liang, Descoteaux, & Connelly, 2020). About limitations regarding specifically this study, no fMRI data were available to confirm the hypothesis of the inverse relationship between structural and functional connectivity, and thus we could only associate our structural connectivity findings to results from the literature. With respect to the sources used to identify the networks or specific regions on the independent components, the criterion to highlight them was not based on statistical inference, but only on Z-score outliers from independent components with significant differences between groups.

## 6.5. Conclusion

Our findings suggest that, in migraine patients, structural networks composed of cortical regions within each lobe are weakened, while networks with subcortical or pain processing regions such as the insula are strengthened. In migraine, cortical curvature changes are related to structural connectivity alterations, which may be also affected by functional connectivity, while cortical thickness, surface area, and gray matter volume changes may be associated with the functional activity variations. The strengthened and/or weakened connections with the hippocampus and damaged structural connectivity between the orbitofrontal cortex and the caudate nucleus may be biomarkers for CM. Reinforced connections between the central sulcus and regions from the superior parietal cortex were found in EM. Fusion methods such as mCCA-jICA allow to assess relationships between multiple modalities, providing additional insights and results. Future multimodal studies analyzing the possible inverse relationship between structural and functional connectivity, and the relationship between gray and white matter structure and activity in migraine patients, need to be performed.

## 6.6. References

Amico, E., & Goñi, J. (2018). Mapping hybrid functional-structural connectivity traits in the human connectome. Network Neuroscience, 2(3), 306–322.

Amin, F. M., Hougaard, A., Magon, S., Sprenger, T., Wolfram, F., Rostrup, E., & Ashina, M. (2018). Altered thalamic connectivity during spontaneous attacks of migraine without aura: A resting-state fMRI study. Cephalalgia, 38(7), 1237–1244.

Benjamini, Y., & Hochberg, Y. (1995). Controlling the false discovery rate: A practical and powerful approach to multiple testing. Journal of the Royal Statistical Society. Series B (Methodological), 57(1), 289–300.

Borsook, D.,Veggeberg, R., Erpelding,N., Borra, N., Linnman,C., Burstein, R., & Becerra, L. (2016). The insula: A hub of activity in migraine. Neuroscientist, 22(6), 632–652.

Burke, M. J., Joutsa, J., Cohen, A. L., Soussand, L., Cooke, D., Burstein, R., & Fox, M. D. (2020). Mapping migraine to a common brain network. Brain, 143(2), 541–553.

Correa, N. M., Li, Y. O., Adali, T., & Calhoun, V. D. (2008). Canonical correlation analysis for feature-based fusion of biomedical imaging modalities and its application to detection of associative networks in schizophrenia. IEEE Journal of Selected Topics in Signal Processing, 2(6), 998–1007.

Deppe, M., Marinell, J., Krämer, J., Duning, T., Ruck, T., Simon, O. J., ... Meuth, S. G. (2014). Increased cortical curvature reflects white matter atrophy in individual patients with early multiple sclerosis. NeuroImage: Clinical, 6, 475–487.

Desikan, R. S., Ségonne, F., Fischl, B., Quinn, B. T., Dickerson, B. C., Blacker, D., ... Killiany, R. J. (2006). An automated labeling system for subdividing the human cerebral cortex on MRI scans into gyral based regions of interest. NeuroImage, 31(3), 968–980.

Faragó, P., Tóth, E., Kocsis, K., Kincses, B., Veréb, D., Király, A., ... Kincses, Z. T. (2019). Altered resting state functional activity and microstructure of the white matter in migraine with Aura. Frontiers in Neurology, 10, 1039.

Gómez-Beldarrain, M., Carrasco, M., Bilbao, A., & García-Moncó, J. C. (2011). Orbitofrontal dysfunction predicts poor prognosis in chronic migraine with medication overuse. The Journal of Headache and Pain, 12(4), 459–466.

Headache Classification Committee of the International Headache Society. (2018). The international classification of headache disorders, 3rd edition. Cephalalgia, 38(1), 1–211.

Horn, J. L. (1965). A rationale and test for the number of factors in factor analysis. Psychometrika, 30(2), 179–185.

Hougaard, A., Amin, F. M., Hoffmann, M. B., Rostrup, E., Larsson, H. B., Asghar, M. S., ... Ashina, M. (2014). Interhemispheric differences of fMRI responses to visual stimuli in patients with side-fixed migraine aura. Human Brain Mapping, 35(6), 2714–2723.

Jia, Z., & Yu, S. (2017). Grey matter alterations in migraine: A systematic review and meta-analysis. NeuroImage: Clinical, 14, 130–140.

Jin, C., Yuan, K., Zhao, L., Zhao, L., Yu, D., von Deneen, K. M., ... Tian, J. (2013). Structural and functional abnormalities in migraine patients without aura. NMR in Biomedicine, 26(1), 58–64.

Kim, J. H., Suh, S. I., Seol, H. Y., Oh, K., Seo, W. K., Yu, S. W., ... Koh, S. B. (2008). Regional grey matter changes in patients with migraine: A voxel-based morphometry study. Cephalalgia, 28(6), 598–604.

Kim, S. G., Jung, W. H., Kim, S. N., Jang, J. H., & Kwon, J. S. (2015). Alterations of gray and White matter networks in patients with obsessive-compulsive disorder: A multimodal fusion analysis of structural MRI and DTI using mCCA+jICA. PLoS One, 10(6), e0127118.

Koch, M. A., Norris, D. G., & Hund-Georgiadis, M. (2002). An investigation of functional and anatomical connectivity using magnetic resonance imaging. NeuroImage, 16(1), 241–250.

Koechlin, E., & Hyafil, A. (2007). Anterior prefrontal function and the limits of human decision-making. Science, 318(5850), 594–598.

Lee, M. J., Park, B.-Y., Cho, S., Kim, S. T., Park, H., & Chung, C.-S. (2019). Increased connectivity of pain matrix in chronic migraine: A restingstate functional MRI study. The Journal of Headache and Pain, 20(1), 29.

Li, Y. O., Adali, T., & Calhoun, V. D. (2007). Estimating the number of independent components for functional magnetic resonance imaging data. Human Brain Mapping, 28(11), 1251–1266.

Liu, H. Y., Chou, K. H., & Chen, W. T. (2018). Migraine and the hippocampus. Current Pain and Headache Reports, 22(2), 13.

Llera, A., Wolfers, T., Mulders, P., & Beckmann, C. F. (2019). Interindividual differences in human brain structure and morphology link to variation in demographics and behavior. Elife, 8, e44443.

Lottman, K. K., White, D. M., Kraguljac, N. V., Reid, M. A., Calhoun, V. D., Catao, F., & Lahti, A. C. (2018). Four-way multimodal fusion of 7 T imaging data using an mCCA+jICA model in first-episode schizophrenia. Human Brain Mapping, 39(4), 1475–1488.

Lowe, M. J., Beall, E. B., Sakaie, K. E., Koenig, K. A., Stone, L., Marrie, R. A., & Phillips, M. D. (2008). Resting state sensorimotor functional connectivity in multiple sclerosis inversely correlates with transcallosal motor pathway transverse diffusivity. Human Brain Mapping, 29(7), 818–827.

Lubeiro, A., de Luis-García, R., Rodríguez, M., Álvarez, A., de la Red, H., & Molina, V. (2017). Biological and cognitive correlates of cortical curvature in schizophrenia. Psychiatry Research: Neuroimaging, 270, 68–75.

Magon, S., May, A., Stankewitz, A., Goadsby, P. J., Tso, A. R., Ashina, M., ... Sprenger, T. (2015). Morphological abnormalities of thalamic subnuclei in migraine: A multicenter MRI study at 3 tesla. Journal of Neuroscience, 35 (40), 13800–13806.

Maleki, N., Becerra, L., Nutile, L., Pendse, G., Brawn, J., Bigal, M., ... Borsook, D. (2011). Migraine attacks the basal ganglia. Molecular Pain, 7, 71.

Messina, R., Filippi, M., & Goadsby, P. J. (2018). Recent advances in headache neuroimaging. Current Opinion in Neurology, 31(4), 379–385.

Messina, R., Rocca, M. A., Colombo, B., Valsasina, P., Horsfield, M. A., Copetti, M., ... Filippi, M. (2013). Cortical abnormalities in patients with migraine: A surface-based analysis. Radiology, 268(1), 170–180.

Neeb, L., Bastian, K., Villringer, K., Gits, H. C., Israel, H., Reuter, U., & Fiebach, J. B. (2015). No microstructural white matter alterations in chronic and episodic migraineurs: A case-control diffusion tensor magnetic resonance imaging study. Journal of Headache, 55(2), 241–251.

Neeb, L., Bastian, K., Villringer, K., Israel, H., Reuter, U., & Fiebach, J. B. (2017). Structural gray matter alterations in chronic migraine: Implications for a progressive disease? Journal of Headache, 57(3), 400–416.

Ouyang, X., Chen, K., Yao, L., Hu, B., Wu, X., Ye, Q., & Guo, X. (2015). Simultaneous changes in gray matter volume and white matter fractional anisotropy in Alzheimer's disease revealed by multimodal CCA and joint ICA. Alzheimer's Disease Neuroimaging Initiative, 301, 553–562.

Petrusic, I., Dakovic, M., & Zidverc-Trajkovic, J. (2019). Subcortical volume changes in migraine with aura. Journal of Clinical Neurology, 15(4), 448–453.

Planchuelo-Gómez, Á., García-Azorín, D., Guerrero, Á. L., Aja-Fernández, S., Rodríguez, M., & de Luis-García, R. (2020a). Structural connectivity alterations in chronic and episodic migraine: A diffusion magnetic resonance imaging connectomics study. Cephalalgia, 40(4), 367–383.

Planchuelo-Gómez, Á., García-Azorín, D., Guerrero, Á. L., Aja-Fernández, S., Rodríguez, M., & de Luis-García, R. (2020b). White matter changes in chronic and episodic migraine: A diffusion tensor imaging study. Journal of Headache and Pain, 21(1), 1.

Planchuelo-Gómez, Á., García-Azorín, D., Guerrero, Á. L., Rodríguez, M., Aja-Fernández, S., & de Luis-García, R. (2020). Gray matter structural alterations in chronic and episodic migraine: A morphometric magnetic resonance imaging study. Pain Medicine.

Shapiro, K., Hillstrom, A. P., & Husain, M. (2002). Control of visuotemporal attention by inferior parietal and superior temporal cortex. Current Biology, 12(15), 1320–1325.

Skorobogatykh, K., van Hoogstraten, W. S., Degan, D., Prischepa, A., Savitskaya, A., Ileen, B. M., ... Amin, F. M. (2019). Functional connectivity studies in migraine: What have we learned? The Journal of Headache and Pain, 20(1), 108.

Smith, R. E., Tournier, J.-D., Calamante, F., & Connelly, A. (2012). Anatomically-constrained tractography: Improved diffusion MRI streamlines tractography through effective use of anatomical information. NeuroImage, 62, 1924–1938.

Stephen, J. M., Coffman, B. A., Jung, R. E., Bustillo, J. R., Aine, C. J., & Calhoun, V. D. (2013). Using joint ICA to link function and structure using MEG and DTI in schizophrenia. NeuroImage, 83, 418–430.

Sui, J., He, H., Pearlson, G. D., Adali, T., Kiehl, K. A., Yu, Q., ... Calhoun, V. D. (2013). Three-way (N-way) fusion of brain imaging data based on mCCA+jICA and its application to discriminating schizophrenia. NeuroImage, 66, 119–132.

Sui, J., Pearlson, G., Adali, T., Kiehl, K. A., Caprihan, A., Liu, J., ... Calhoun, V. D. (2011). Discriminating schizophrenia and bipolar disorder by fusing FMRI and DTI in a multimodal CCA+ joint ICA model. NeuroImage, 57(3), 839–855.

Szabó, N., Faragó, P., Király, A., Veréb, A., Csete, G., Tóth, E., ... Kincses, Z. T. (2017). Evidence for plastic processes in migraine with aura: A diffusion weighted MRI study. Frontiers in Neuroanatomy, 11, 138.

Tournier, J.-D., Smith, R., Raffelt, D., Tabbara, R., Dhollander, T., Pietsch, M., ... Connelly, A. (2019). MRtrix3: A fast, flexible and open software framework for medical image processing and visualisation. NeuroImage, 202, 116137.

Wunderlich, A. P., Klug, R., Stuber, G., Landwehrmeyer, B., Weber, F., & Freund, W. (2011). Caudate nucleus and insular activation during a pain suppression paradigm comparing thermal and electrical stimulation. Open Neuroimaging, 5, 1–8.

Yeh, C.-H., Jones, D. K., Liang, X., Descoteaux, M., & Connelly, A. (2020). Mapping structural connectivity using diffusion MRI: Challenges and opportunities. Journal of Magnetic Resonance Imaging.

Younis, S., Hougaard, A., Noseda, R., & Ashina, M. (2019). Current understanding of thalamic structure and function in migraine. Cephalalgia, 39(13), 1675–1682.

Yuan, K., Zhao, L., Cheng, P., Yu, D., Zhao, L., Dong, T., ... Tian, J. (2013). Altered structure and resting-state functional connectivity of the basal ganglia in migraine patients without aura. Journal of Pain, 14(8), 836–844.

Zhao, L., Liu, J., Yan, X., Dun, W., Yang, J., Huang, L., ... Liang, F. (2014). Abnormal brain activity changes in patients with migraine: A short-term longitudinal study. Journal of Clinical Neurology, 10(3), 229–235.

# 6.7. Supplementary File 1

In this file, diverse aspects from previous studies not developed in the main manuscript are explained.

## *6.7.1.* ***Participants***

The inclusion and exclusion criteria for patients and controls are described here from (Planchuelo-Gómez, García-Azorín, Guerrero, Aja-Fernández, et al., 2020a, 2020b).

Migraine patients were screened and recruited at the headache unit at the Hospital Clínico Universitario de Valladolid (Valladolid, Spain), being classified as Episodic Migraine (EM) or Chronic Migraine (CM) following the third edition of the International Classification of Headache Disorders (ICHD and ICHD-3 beta) aged between 18 and 60 (Headache Classification Committee of the International Headache Society, 2013, 2018). Patients were clinically stable the three months before the visit, preventive treatment naïve and with migraine onset before the age of 50. All patients agreed to participate in the study and signed an Informed Consent.

Patients were excluded if they suffered headache on 10-14 days per month (to avoid confusion between high frequency EM and CM), non-craniofacial painful conditions occurring 10 or more days per month apart from migraine, known major psychiatric diseases and other neurological diseases or headache disorders. Drug and substance abuse, pregnancy and childbearing were other exclusion criteria.

## *6.7.2.* ***MRI acquisition details***

Migraine patients were scanned between one and two weeks after the clinical visit if the last migraine attack happened at least 24 hours before the acquisition. The first acquisition was the T1-weighted, being followed by the diffusion-weighted scan. The images were obtained between May 2014 and July 2018. Total acquisition time for a single subject was around 18 minutes.

## *6.7.3.* ***Morphometry processing pipeline***

A detailed summary of the processing pipeline explained in (Planchuelo-Gómez, García-Azorín, Guerrero, Rodríguez, et al., 2020) is shown.

The first step was to extract the non-brain tissue from the T1-weighted images. The FreeSurfer gray matter parcellation was performed afterwards. FreeSurfer parcellation includes skull stripping, automated Talairach transformation, segmentation of subcortical grey and white matter, intensity normalization, grey-white matter boundary tessellation and surface deformation. The results from the parcellation were

examined individually. Cortical curvature, cortical thickness, surface area and gray matter volume were extracted for the 68 cortical regions from the Desikan-Killiany atlas (Desikan et al., 2006). The gray matter volume was also extracted for the 16 subcortical regions from the same atlas. These 84 cortical and subcortical regions were used as regions in the structural connectivity matrices analyzed in this study.

### *6.7.4.* ***Structural connectivity processing pipeline***

A detailed summary of the processing pipeline explained in (Planchuelo-Gómez, García-Azorín, Guerrero, Aja-Fernández, et al., 2020a) is shown.

Apart from the FreeSurfer parcellation, diffusion-weighted images were preprocessed. The first step was to denoise the images. The next steps were corrections for eddy currents, motion and $B_1$ field inhomogeneity. From the preprocessed images, a whole brain mask was obtained. Separately, five-tissue-type segmented images were obtained from the T1-weighted images and the cortical parcellation in each subject. The fiber orientation distributions (FOD) were estimated using the diffusion images to perform tractography, after the estimation of the response function. Spherical deconvolution was employed in the estimation of the FOD. The diffusion mask, the five-tissue-type image, registered previously to the diffusion space for each subject, and the FOD were used to perform anatomically-constrained tractography on each subject, computing 10 million streamlines.

From the tractography, structural connectivity matrices were acquired. The gray matter cortical parcellation regions were included in the structural connectivity matrix from each subject.

### *6.7.5.* ***References***

Desikan, R. S., Ségonne, F., Fischl, B., Quinn, B. T., Dickerson, B. C., Blacker, D., Buckner, R. L., Dale, A. M., Maguire, R. P., Hyman, B. T., Albert, M. S., & Killiany, R. J. (2006). An automated labeling system for subdividing the human cerebral cortex on MRI scans into gyral based regions of interest. NeuroImage, 31(3), 968–980.

Headache Classification Committee of the International Headache Society. (2013). The International Classification of Headache Disorders, 3rd edition (beta version). Cephalalgia, 33(9), 629–808.

Headache Classification Committee of the International Headache Society. (2018). The International Classification of Headache Disorders, 3rd edition. Cephalalgia, 38(1), 1–211.

Planchuelo-Gómez, Á., García-Azorín, D., Guerrero, Á. L., Aja-Fernández, S., Rodríguez, M., & de Luis-García, R. (2020a). Structural connectivity alterations in chronic and episodic migraine: A diffusion magnetic resonance imaging connectomics study. Cephalalgia, 40(4), 367–383.

Planchuelo-Gómez, Á., García-Azorín, D., Guerrero, Á. L., Aja-Fernández, S., Rodríguez, M., & de Luis-García, R. (2020b). White matter changes in chronic and episodic migraine: a diffusion tensor imaging study. J Headache Pain, 21(1), 1.

Planchuelo-Gómez, Á., García-Azorín, D., Guerrero, Á. L., Rodríguez, M., Aja-Fernández, S., & de Luis-García, R. (2020). Grey matter structural alterations in chronic and episodic migraine: a morphometric magnetic resonance imaging study. Pain Medicine.

## 6.8. Supplementary File 2

In this file, the diverse mCCA-jICA steps are explained in more detail.

**A. Input Data**

The morphometric data, i.e., cortical curvature, cortical thickness, surface area and gray matter volume were considered as the first modality. From the Freesurfer pipeline, explained in detail in (Planchuelo-Gómez, García-Azorín, Guerrero, Rodríguez, et al., 2020), an 84-length vector for the gray matter volume, and a 68-length for the other features, were obtained for each subject. Each value from the vector corresponded to a specific region from the Desikan-Killiany atlas (Desikan et al., 2006). For each feature, the vectors from each group (HC, EM and CM) were arranged together and sorted following the group order. The input matrix for the next step, $X_1$, contained the values of the features in each subject, corresponding the first 50 rows to the HC values, the next 54 rows to EM, and the last 56 to CM. Each column from X1 represented a specific region from the atlas.

The structural connectivity data, i.e., the number of streamlines between the reconstructed trajectories using tractography, were considered as the second modality. The full procedure to obtain a structural connectivity square matrix with the 84 regions from the Desikan-Killiany atlas is explained in (Planchuelo-Gómez, García-Azorín, Guerrero, Aja-Fernández, et al., 2020). We decided not to consider possible spurious connections. To that end, we discarded the connections with less than 1000 streamlines (the total number of streamlines per tractography was 10 million) in the three groups (group mean). Six hundred and twenty (620) connections survived the previous exclusion criterion. Furthermore, considering that cortical curvature, thickness and surface area only have values for cortical regions, connections where only subcortical regions were involved were also discarded for the analysis were $X_1$ represented the data from one of the previous features. Therefore, for each subject, a 620-length vector or a 570-length vector were used depending on the gray matter morphometric parameter. The vectors from the subjects of each group were organized as explained in the previous paragraph to obtain $X_2$. Each column from $X_2$ represented a connection between two regions expressed as the number of streamlines. A graphical representation is shown:

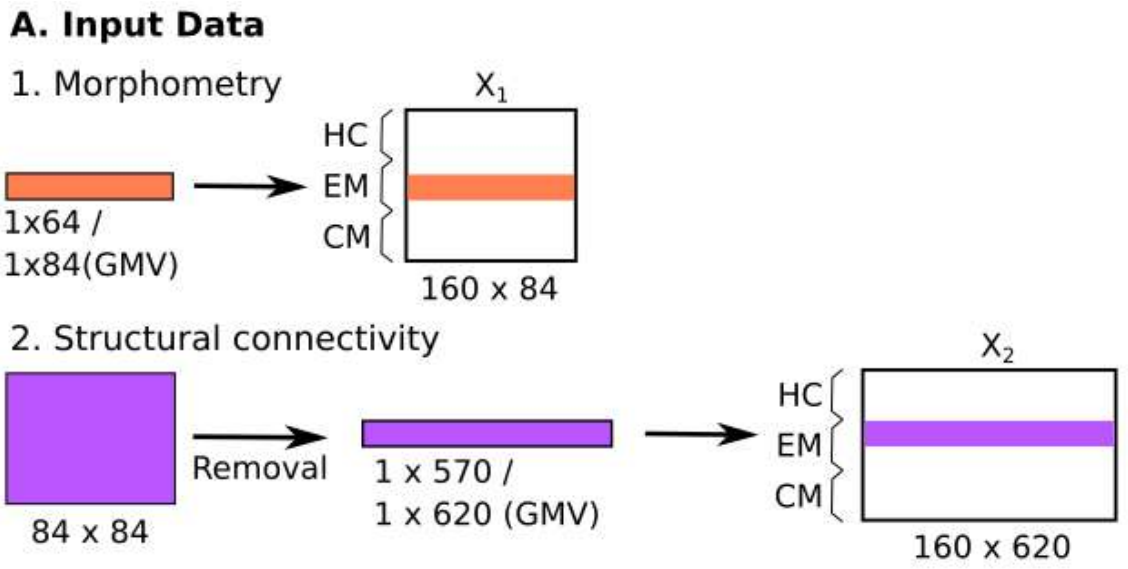


GMV = Gray Matter Volume. GMV is the gray matter feature taken as example. The number under each matrix represent its dimensions (rows $X$ columns).

### Overview of mCCA-jICA

Before explaining the full method, it is important to explain the main assumption from the whole process. As explained in (Kim et al., 2015; Sui et al., 2011), the multimodal dataset $\mathbf{X_k}$ is a linear mixture of sources $S_k$ and the nonsingular matrix or mixing profile $\mathbf{A_k}(k = \{1, 2\})$:

$$\mathbf{X_k} = \mathbf{A_k}\mathbf{S_k} \tag{6.1}$$

where $\mathbf{A_k}$ has dimension of subjects by number of components (N), and $\mathbf{S_k}$ has dimension of number of components by number of regions (k = 1) or connections (k = 2). $\mathbf{A_k}$ represents the contribution of each source to the corresponding feature set and its two columns are assumed to be highly correlated. The fusion of mCCA and jICA allows to overcome restrictions from both methods. On the one hand, with respect to mCCA, complete source separation is not normally reached for a small number of datasets (Sui et al., 2011), as in this case. On the other hand, the ICA model only allows one mixing profile instead of one mixing profile per modality. Thus, mCCA allows to have correlated components between diverse modalities and its results are the initialization of jICA, which allows to obtain independent components that alleviate the limitations of mCCA to reach a better source separation. The concept of the mixing profile is explained with more detail in step D.

### B. mCCA

The objective of this step was to maximize the correlation between the analyzed modalities. Following the methods described by (Sui et al., 2011), Singular Value Decomposition (SVD) was performed on $X_k$ to reduce the dimension and discard noise or redundancy values. For the morphometric parameters, 99.7% of non-zero eigenvalues were retained for the gray matter volume (98.9% for the structural connectivity), 99.6% for the cortical curvature, 99.8% for the cortical thickness and 99.5% for the surface area (98.8% for the structural connectivity when combined with the last three parameters). After SVD, the linear mixture model of mCCA was applied to compute the associated components:

$$\mathbf{X_k} = \mathbf{D_k}\mathbf{C_k} \tag{6.2}$$

where $\mathbf{D_k}$ are the canonical variants and $\mathbf{C_k}$ the associated components ($k = \{1, 2\}$). The canonical variants represent the contribution of the associated components to the individual features (Kim et al., 2015). The variants from each modality represent the mixing profile and have maximum correlation. The number of columns of $\mathbf{D_k}$ (and the number of rows of $\mathbf{C_k}$) is equal to the minimum number of independent components between the modalities obtained with the Horn's test (Horn, 1965), explained in the main manuscript. The associated components represent the sources from each modality, but not a set of complete independent components or total source separation. A graphical representation is shown:

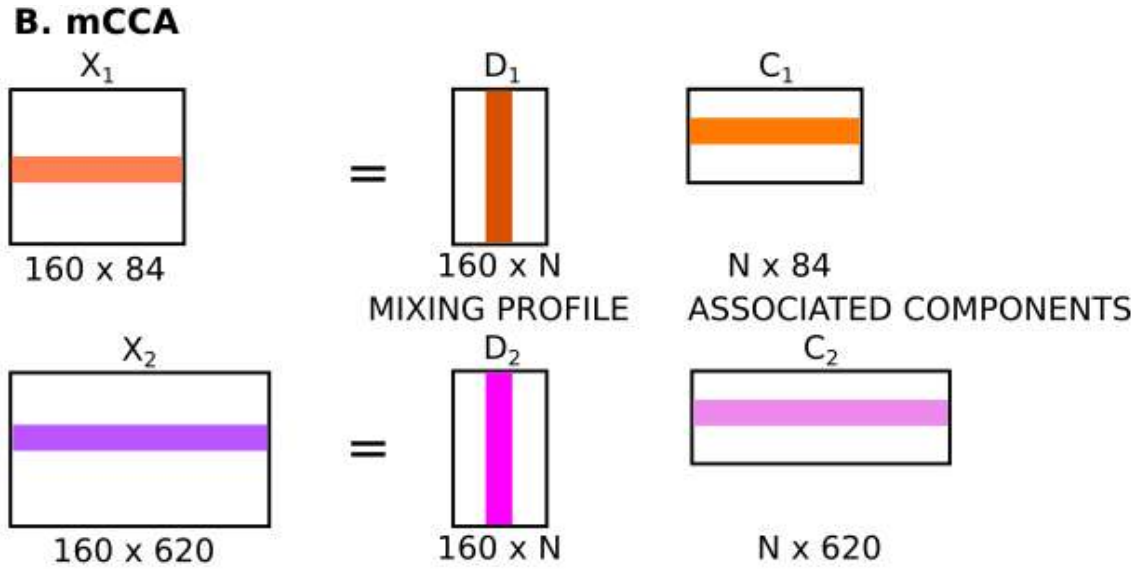


N = number of joint independent components. The mCCA step models the input data ($X_{1,2}$) from each modality as the product of the mixing profile ($D_{1,2}$) and the associated component ($C_{1,2}$).

### C. jICA

The objective of this step was to maximize the independence of the associated components from mCCA and obtain independent sources for each modality.

In this step, the associated components from mCCA were concatenated and introduced as the input for jICA. The model of jICA was applied to calculate the independent sources or joint independent components in the following way:

$$\mathbf{C} = \mathbf{W^{-1}S} \tag{6.3}$$

where $\mathbf{C}$ is the concatenation of $\mathbf{C_1}$ and $\mathbf{C_2}$, [$\mathbf{C_1}$,$\mathbf{C_2}$], $\mathbf{W^{-1}}$ the pseudoinverse of the demixing matrix and $\mathbf{S}$ the concatenation of $\mathbf{S_1}$ and $\mathbf{S_2}$, [$\mathbf{S_1}$,$\mathbf{S_2}$], the independent sources for each modality. $\mathbf{W^{-1}}$ represents the contribution of each independent source to its corresponding associated component. $\mathbf{S}$ has the same dimensions with respect to $\mathbf{C}$, and $\mathbf{W^{-1}}$ is a square matrix with number of rows and columns equal to the number of rows of $\mathbf{C}$ and $\mathbf{S}$, the number of independent components. A graphical representation is shown:

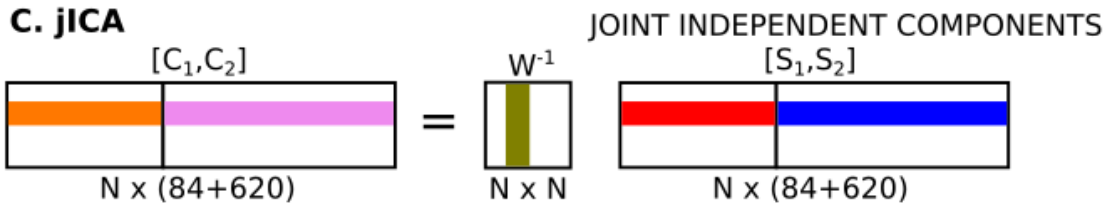


The jICA step models the concatenation of both associated components as the product of the demixing matrix ($W^{-1}$) and the joint independent components ($S_{1,2}$).

### D. Mixing coefficients per modality

The objective of this step was to obtain a mixing profile per modality for all the subjects. The mixing matrix/profile per modality represents the contribution of the sources to the individual features of each modality. Considering similar sources between the groups of study (controls and patients with episodic and chronic migraine in our case), i.e., regions or connections which are highly represented in a source, the mixing matrix shows which subjects contribute more to the expression of the source. Grouping the mixing coefficients according to the groups of study, and assuming positive values of the Z-scores from the sources and the mixing coefficients, higher values of the mixing coefficients are directly related to higher values of the assessed feature. Therefore, for similar sources, the statistical comparison of the mixing coefficients is similar to the comparison of the features between the groups of interest in the regions or connections represented by the source. The interpretation of the results of the analysis is explained at the end of this file (before the references).

We show together equations (6.2) and (6.3), considering the results per modality in equation (6.3):

$$\left\{\begin{array}{c}\mathbf{X_k = D_k C_k}\\ \mathbf{C = W^{-1} S}\end{array}\right\} \rightarrow \mathbf{X_k = D_k W^{-1} S_k}. \tag{6.4}$$

To compute the mixing matrix per modality, we show together equation (6.4) and the equation from the whole mCCA-jICA method, equation (6.1):

$$\left\{\begin{array}{c}\mathbf{X_k = D_k W^{-1} S_k}\\ \mathbf{X_k = A_k S_k}\end{array}\right\} \rightarrow \mathbf{A_k = D_k W^{-1}} \tag{6.5}$$

where $\mathbf{A_k}$ is the mixing matrix per modality, i.e., the matrix with the mixing coefficients. The number of rows of $\mathbf{A_k}$ is equal to the number of subjects, and the number of columns to the number of independent components (same dimensions with respect to $\mathbf{D_k}$). A graphical representation is shown:

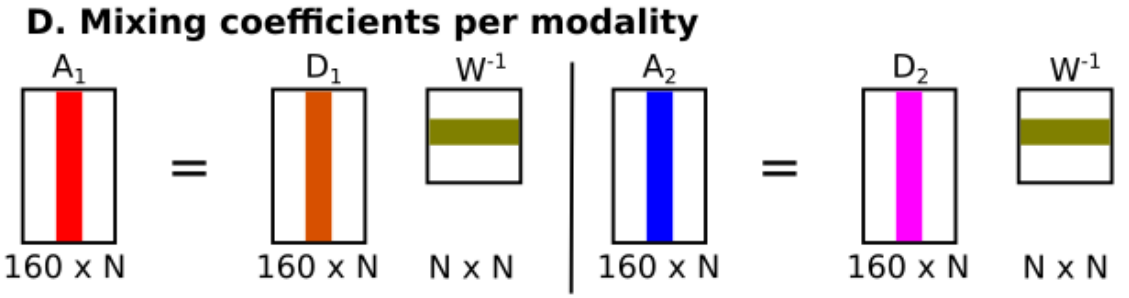


The mixing coefficients for each modality ($A_{1,2}$) are obtained by the product of the mixing profile and the demixing matrix.

The graphical representations from each step are displayed together:

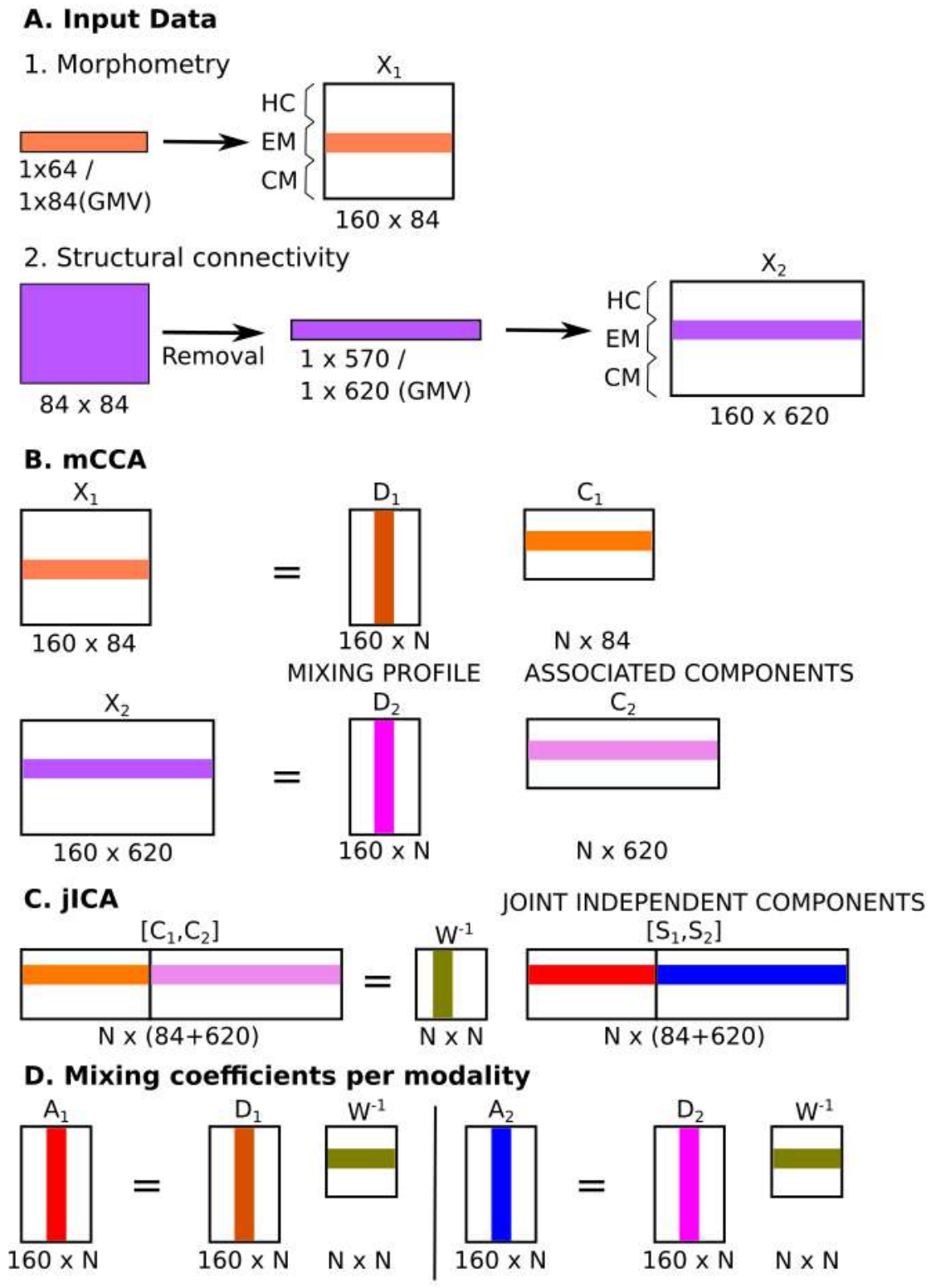


The mixing coefficients are compared between the three groups (HC, EM and CM) to identify differences in a morphometric parameter and/or structural connectivity. The Z-scores from sources $S_{1,2}$ represent the weight of each region or connection to the joint independent component. Red and blue are used to indicate the values which are analyzed (statistics or outliers and Z-scores).

### Analysis of mCCA-jICA

The results of this method were analyzed using the independent sources ($\mathbf{S_k}$) and the mixing coefficients ($\mathbf{A_k}$).

Each column of $S_1$ represented the value of a morphometric feature for a specific region, and each column of $\mathbf{S_2}$ represented the value of the number of streamlines for a specific connection between two gray matter regions. The values of $\mathbf{S_k}$ were expressed as Z-scores. To collect the independent sources from each assessed group, we show equation (6.1) using the pseudoinverse matrix of the mixing matrix:

$$\mathbf{S_{Group,k}} = \mathbf{A^{-1}_{Group,k}} \mathbf{X_{Group,k}} \tag{6.6}$$

where *Group* is equal to HC (first 50 rows of $\mathbf{X_k}$ and first 50 columns of $\mathbf{A_k^{-1}}$), EM (next 54 positions) or CM (last 56 positions). The independent sources from each group were compared to analyze whether the same regions and connections were expressed in all the groups. If different regions or connections were expressed from one group to another, or if they were equal but expressed with opposite signs, i.e., negative Z-scores in one group and positive Z-scores in the other group, differences between groups would be found. If the regions or connections were equal, then the differences between groups would be analyzed using the mixing coefficients.

For the analysis of the mixing coefficients, each column of $\mathbf{A_k}$ (an independent component) was taken and the values were compared using statistical tests. Each independent component contained the values of the three groups, corresponding the first 50 rows to HC, the next 54 to EM, and the last 56 to CM.

As explained in (Lottman et al., 2018) and the main manuscript, if the Z-scores from a source and the mixing coefficients were positive and significantly higher in one group with respect to another, the corresponding feature would be more expressed (higher values) in the group with higher coefficient values in the regions or connections represented by the source. If the Z-scores were negative and the mixing coefficients were positive and significantly higher in one group with respect to another, the feature would be less expressed (lower values) in the group with higher coefficient values in the regions/connections represented by the source. The opposite interpretation would be followed for negative mixing coefficients. Moreover, when significant differences were found in a specific component for both modalities, this component would be called joint component. A modal-specific component would show significant differences in only one of the modalities.

### References

Desikan, R. S., Ségonne, F., Fischl, B., Quinn, B. T., Dickerson, B. C., Blacker, D., Buckner, R. L., Dale, A. M., Maguire, R. P., Hyman, B. T., Albert, M. S., & Killiany, R. J. (2006). An automated labeling system for subdividing the human cerebral cortex on MRI scans into gyral based regions of interest. NeuroImage, 31(3), 968–980.

Horn, J. L. (1965). A rationale and test for the number of factors in factor analysis. Psychometrika, 30(2), 179–185.

Kim, S. G., Jung, W. H., Kim, S. N., Jang, J. H., & Kwon, J. S. (2015). Alterations of Gray and White Matter Networks in Patients with Obsessive-Compulsive Disorder: A Multimodal Fusion Analysis of Structural MRI and DTI Using mCCA+jICA. PLoS ONE, 10(6), e0127118.

Lottman, K. K., White, D. M., Kraguljac, N. V, Reid, M. A., Calhoun, V. D., Catao, F., & Lahti, A. C. (2018). Four-way multimodal fusion of 7 T imaging data using an mCCA+jICA model in first-episode schizophrenia. Hum Brain Mapp, 39(4), 1475–1488.

Planchuelo-Gómez, Á., García-Azorín, D., Guerrero, Á. L., Aja-Fernández, S., Rodríguez, M., & de Luis-García, R. (2020). Structural connectivity alterations in chronic and episodic migraine: A diffusion magnetic resonance imaging connectomics study. Cephalalgia, 40(4), 367–383.

Planchuelo-Gómez, Á., García-Azorín, D., Guerrero, Á. L., Rodríguez, M., Aja-Fernández, S., & de Luis-García, R. (2020). Grey matter structural alterations in chronic and episodic migraine: a morphometric magnetic resonance imaging study. Pain Medicine.

Sui, J., Pearlson, G., Adali, T., Kiehl, K. A., Caprihan, A., Liu, J., Yamamoto, J., & Calhoun, V. D. (2011). Discriminating Schizophrenia and Bipolar Disorder by Fusing FMRI and DTI in A Multimodal CCA+ Joint ICA Model. NeuroImage, 57(3), 839–855.

# 6.9. Supplementary File 3

The Supplementary Tables and Figures are included in this section.

**Supplementary Table 1.** Networks with positive jICA outlier values (Z > 0) in controls from the fusion of cortical curvature and structural connectivity**.**

| Hemisphere | Network regions |
|---|---|
| Left | Precentral – Superior parietal – Postcentral – Supramarginal |
| Right | Supramarginal – Inferior parietal – Precuneus – Superior parietal – Postcentral – Paracentral – Precentral |
| | |
| Left | Pericalcarine – Lateral occipital – Fusiform – Superior temporal |
| | |
| Right | Caudal middle frontal – Rostral middle frontal – Superior frontal |
| | |
| Right | Transverse temporal – Postcentral – Hippocampus – Fusiform – Superior temporal – Transverse temporal |
| | |
| Right | Pars orbitalis – Rostral middle frontal – Pars triangularis |
| | |
| Right | Inferior temporal – Fusiform – Lingual |

No inter hemispheric connections were detected as outliers.

**Supplementary Table 2**. Networks with positive jICA outlier values (Z > 0) in EM patients from the fusion of cortical curvature and structural connectivity.

| Hemisphere | Network regions |
|---|---|
| Left | Precuneus – Superior parietal – Postcentral – Precentral – Supramarginal |
| Right | Caudal middle frontal – Precentral – Paracentral – Superior parietal – Inferior parietal – Supramarginal – Postcentral |
| | |
| Left | Lateral occipital – Fusiform – Inferior temporal |
| | |
| Left/Right | Medial orbito frontal – Lateral orbito frontal – Caudate |
| Left/Right | Medial orbito frontal – Lateral orbito frontal – Putamen – Insula |

No inter hemispheric connections were detected as outliers. The three underlined regions mean that all possible pairs of regions are connected between them.

**Supplementary Table 3**. Networks with negative jICA outlier values (Z < 0) in CM patients from the fusion of cortical curvature and structural connectivity.

| Hemisphere | Network regions |
|---|---|
| Left | Cuneus – Lateral occipital – Lingual |
| Right | Cuneus – Lateral occipital – Precuneus |
| | |
| Left | Banks of the superior temporal sulcus – Superior temporal – Middle temporal |
| | |
| Left | Medial orbito frontal – Lateral orbito frontal – Caudate |

No inter hemispheric connections were detected as outliers.

**Supplementary Table 4**. Networks with positive jICA outlier values (Z > 0) in CM patients from the fusion of cortical curvature and structural connectivity.

| Hemisphere | Network regions |
|---|---|
| Left | Parahippocampal – Hippocampus – Fusiform – Superior temporal – Transverse temporal |
| Right | Parahippocampal – Hippocampus – Insula – Putamen |
| | |
| Left | Insula – Putamen – Lateral orbito frontal – Rostral middle frontal – Superior frontal |
| Left | Medial orbito frontal – Putamen – Lateral orbito frontal – Rostral middle frontal – Superior frontal |
| Left | Rostral anterior cingulate – Putamen – Lateral orbito frontal – Rostral middle frontal – Superior frontal |
| | |
| Right | Caudal anterior cingulate – Superior frontal – Rostral middle frontal |
| | |
| Right | Inferior parietal – Superior parietal – Pericalcarine |
| | |
| Right | Inferior temporal – Superior temporal – Fusiform – Lateral occipital |
| Right | Inferior temporal – Superior temporal – Fusiform – Lingual |
| Right | Inferior temporal – Superior temporal – Transverse temporal |

No inter hemispheric connections were detected as outliers.

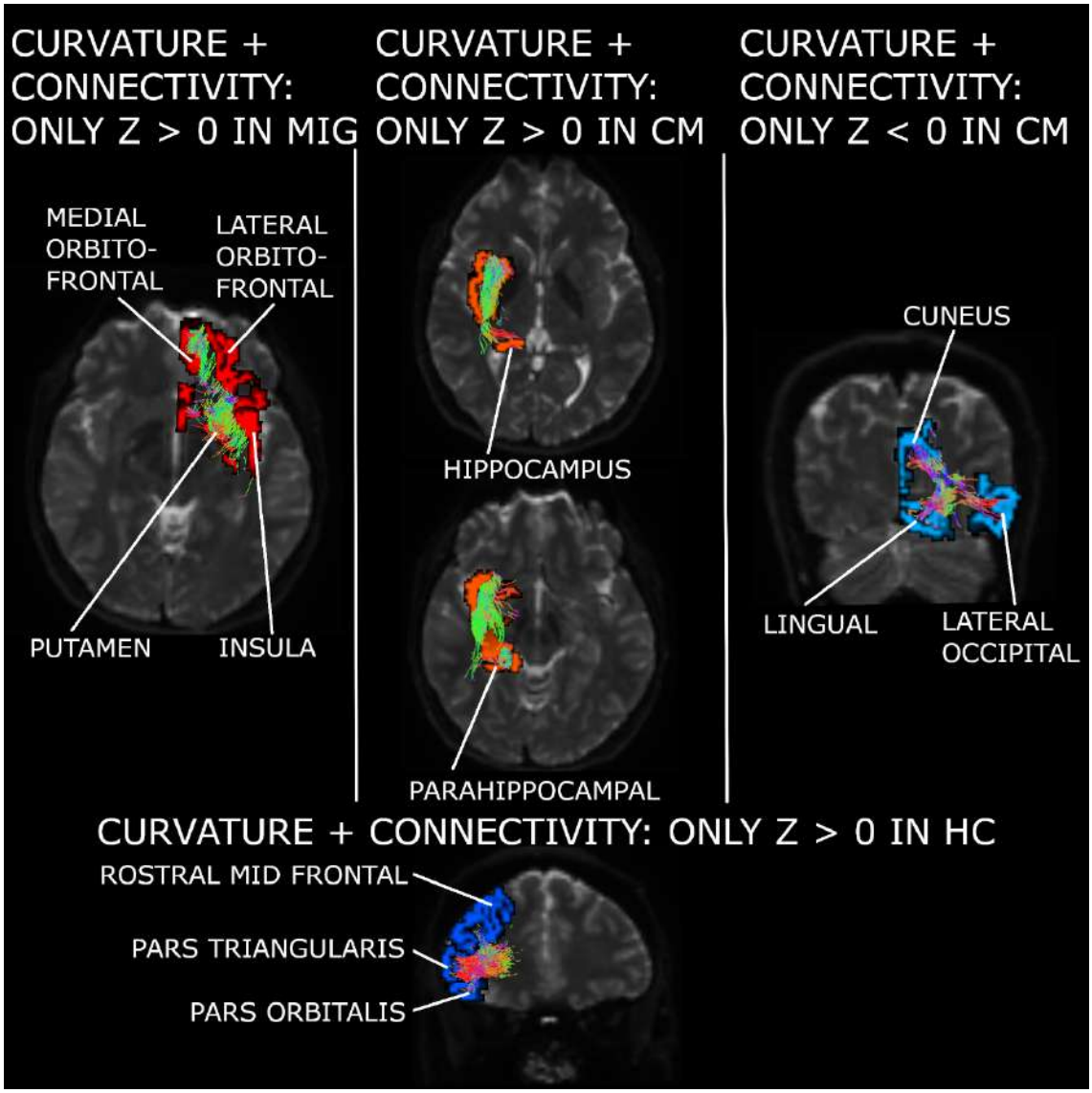


**Supplementary Figure 1 Additional networks found for the first independent component (fusion of curvature and connectivity)**. Networks enhanced or worsened only in migraine, CM or HC are shown. MID = middle; MIG = migraine.

**Supplementary Table 5**. Networks with positive jICA outlier values (Z > 0) in controls from the fusion of cortical thickness and structural connectivity.

| Hemisphere | Network regions |
|---|---|
| Left | Precuneus – Superior parietal – Supramarginal |
| Left | Inferior parietal – Superior parietal – Supramarginal |
| Right | Precuneus – Superior parietal – Inferior parietal – Lateral occipital – Fusiform – Inferior temporal |
| Right | Lingual – Lateral occipital – Fusiform – Inferior temporal |
| | |
| Left | Medial orbito frontal – Lateral orbito frontal – Rostral middle frontal – Pars orbitalis |
| Left | Medial orbito frontal – Lateral orbito frontal – Rostral middle frontal – Pars triangularis |
| | |
| Left | Middle temporal – Inferior temporal – Superior temporal |
| Left | Fusiform – Inferior temporal – Superior temporal |
| | |
| Right | Superior parietal – Cuneus – Pericalcarine |
| | |

No inter hemispheric connections were detected as outliers. Three underlined regions mean that all possible pairs of regions are connected between them.

**Supplementary Table 6**. Networks with negative jICA outlier values (Z < 0) in EM patients from the fusion of cortical thickness and structural connectivity.

| Hemisphere | Network regions |
|---|---|
| Right | Paracentral – Precentral – Superior parietal – Postcentral |
| Right | Paracentral – Precentral – Superior parietal – Pericalcarine |

No inter hemispheric connections were detected as outliers.

**Supplementary Table 7**. Networks with positive jICA outlier values (Z > 0) in EM patients from the fusion of cortical thickness and structural connectivity.

| Hemisphere | Network regions |
|---|---|
| Left | Precuneus – Superior parietal – Inferior parietal – Supramarginal |
| | |
| Left | Banks of the superior temporal sulcus – Middle temporal – Inferior temporal – Superior temporal – Fusiform |
| Right | Banks of the superior temporal sulcus – Middle temporal – Inferior temporal – Superior temporal – Transverse temporal |
| Right | Fusiform – Insula – Inferior temporal – Middle temporal |
| | |
| Left | Cuneus – Lateral occipital – Lingual |
| Left/Right | Cuneus – Lateral occipital – Pericalcarine |
| | |
| Right | Inferior Parietal – Pericalcarine – Lingual |
| | |
| Right | Medial orbito frontal – Lateral orbito frontal – Rostral middle frontal |

No inter hemispheric connections were detected as outliers. Three underlined regions mean that all possible pairs of regions are connected between them.

**Supplementary Table 8**. Networks with negative jICA outlier values (Z $<$ 0) in CM patients from the fusion of cortical thickness and structural connectivity.

| Hemisphere | Network regions |
|---|---|
| Left | Caudal middle frontal – Precentral – Superior parietal |
| | |
| Left | Superior temporal – Isthmus cingulate – Thalamus |
| Left | Superior temporal – Isthmus cingulate – Hippocampus |

No inter hemispheric connections were detected as outliers.

**Supplementary Table 9**. Networks with positive jICA outlier values (Z $>$ 0) in CM patients from the fusion of cortical thickness and structural connectivity.

| Hemisphere | Network regions |
|---|---|
| Left | Inferior parietal – Precuneus – Superior parietal – Cuneus |
| Left | Lateral occipital – Superior parietal - Supramarginal |
| Right | Precuneus – Superior parietal – Cuneus – Lateral occipital – Inferior parietal |
| | |
| Left | Insula – Fusiform – Inferior temporal – Middle temporal – Superior temporal – Banks of the superior temporal sulcus |
| Right | Superior temporal – Inferior temporal – Middle temporal |
| Right | Insula – Inferior temporal – Fusiform |

No inter hemispheric connections were detected as outliers. Three underlined regions mean that all possible pairs of regions are connected between them.

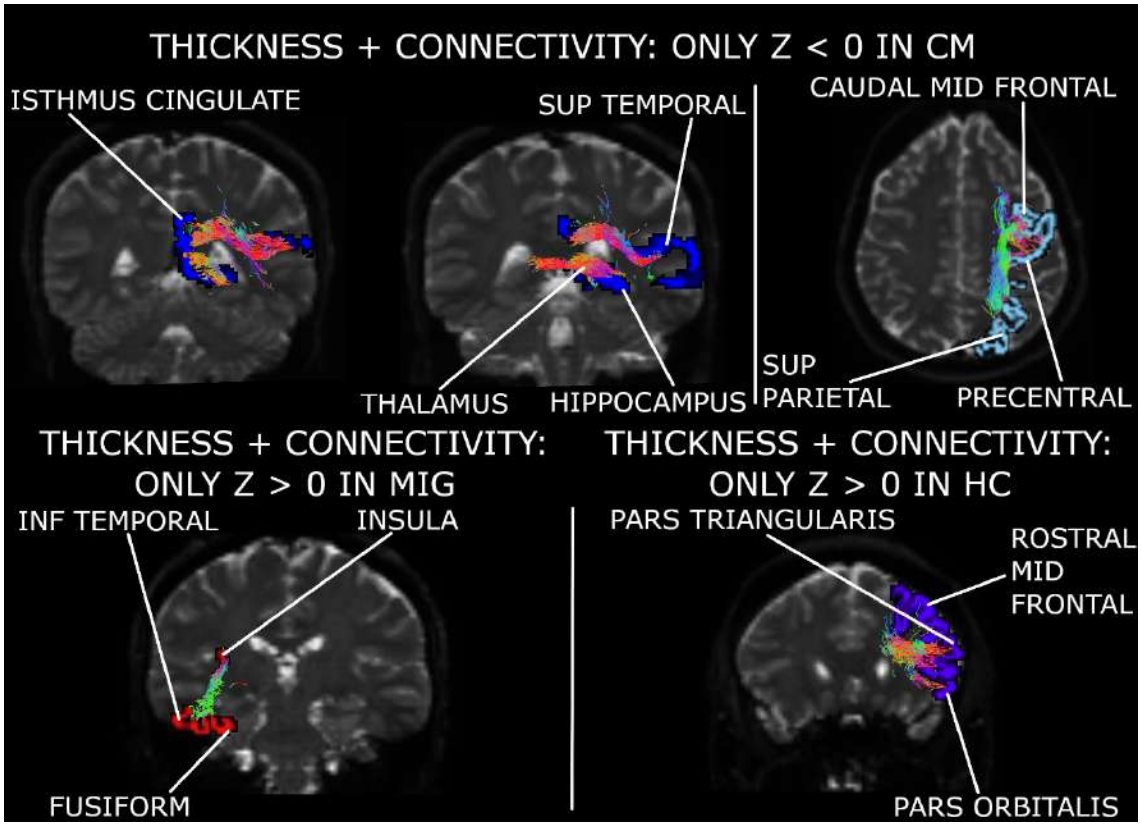


**Supplementary Figure 2 Additional networks found for the fifth independent component (fusion of thickness and connectivity)**. Networks enhanced or worsened only in migraine, CM or HC are shown. INF = inferior; MID = middle; MIG = migraine (results from EM and CM); SUP = superior.

**Supplementary Table 10**. Networks with negative jICA outlier values (Z < 0) in controls from the fusion of gray matter volume and structural connectivity.

| Hemisphere | Network regions |
|---|---|
| Left | Paracentral – Precentral – Caudate – Thalamus – Putamen – Hippocampus |
| Left | Putamen – Lateral orbito frontal – Caudate |
| | |
| Left | Cuneus – Superior parietal – Postcentral |
| | |
| Right | Postcentral – Paracentral – Precentral |

No inter hemispheric connections were detected as outliers.

**Supplementary Table 11**. Networks with positive jICA outlier values (Z > 0) in controls from the fusion of gray matter volume and structural connectivity.

| Hemisphere | Network regions |
|---|---|
| Left | Banks of the superior temporal sulcus – Middle temporal – Inferior temporal |
| | |
| Left | Medial orbito frontal – Lateral orbito frontal – Rostral middle frontal |

No inter hemispheric connections were detected as outliers.

**Supplementary Table 12**. Networks with negative jICA outlier values (Z < 0) in EM patients from the fusion of gray matter volume and structural connectivity.

| Hemisphere | Network regions |
|---|---|
| Left | Banks of the superior temporal sulcus – Middle temporal – Inferior temporal – Superior temporal – Fusiform |
| Right | Banks of the superior temporal sulcus – Middle temporal – Inferior temporal – Insula – Fusiform |
| | |
| Left | Lateral orbito frontal – Rostral middle frontal – Pars triangularis |
| Left | Pars orbitalis – Rostral middle frontal – Pars triangularis |
| Right | Lateral orbito frontal – Rostral middle frontal – Pars orbitalis |
| | |
| Left | Inferior parietal – Supramarginal – Postcentral |
| | |
| Right | Cuneus – Pericalcarine – Lateral occipital - Precuneus |
| | |

No inter hemispheric connections were detected as outliers. The three underlined regions mean that all possible pairs of regions are connected between them.

**Supplementary Table 13**. Networks with positive jICA outlier values (Z > 0) in EM patients from the fusion of gray matter volume and structural connectivity.

| Hemisphere | Network regions |
|---|---|
| Left | Thalamus – Caudate – Lateral orbito frontal – Putamen – Insula |
| Right | Precentral – Thalamus – Caudate – Lateral orbito frontal |
| Right | Precentral – Thalamus – Caudate – Rostral anterior cingulate |
| | |
| Right | Pericalcarine – Superior parietal – Postcentral |
| Right | Paracentral – Superior parietal – Postcentral |

No inter hemispheric connections were detected as outliers. The three underlined regions mean that all possible pairs of regions are connected between them.

**Supplementary Table 14**. Networks with negative jICA outlier values (Z < 0) in CM patients from the fusion of gray matter volume and structural connectivity.

| Hemisphere | Network regions |
|---|---|
| Left | Cuneus – Lateral occipital – Inferior parietal |
| Left | Cuneus – Lateral occipital – Lingual |
| Right | Cuneus – Pericalcarine – Lateral occipital – Precuneus |
| | |
| Left | Banks of the superior temporal sulcus – Superior temporal – Inferior temporal – Middle temporal |
| Right | Superior temporal – Inferior temporal – Middle temporal |
| | |
| Right | Lateral orbito frontal – Rostral middle frontal – Pars orbitalis |
| | |
| Right | Caudal middle frontal – Superior frontal – Paracentral |
| | |
| Right | Pallidum – Insula – Fusiform |

No inter hemispheric connections were detected as outliers. Three underlined regions mean that all possible pairs of regions are connected between them.

**Table S15**. Networks with positive jICA outlier values (Z > 0) in CM patients from the fusion of gray matter volume and structural connectivity.

| Hemisphere | Network regions |
|---|---|
| Left | Thalamus – Caudate – Precentral |
| Right | Thalamus – Caudate – Putamen |
| | |
| Left | Lateral orbito frontal – Putamen – Medial orbito frontal |
| | |
| Right | Rostral anterior cingulate – Putamen – Insula |

No inter hemispheric connections were detected as outliers.

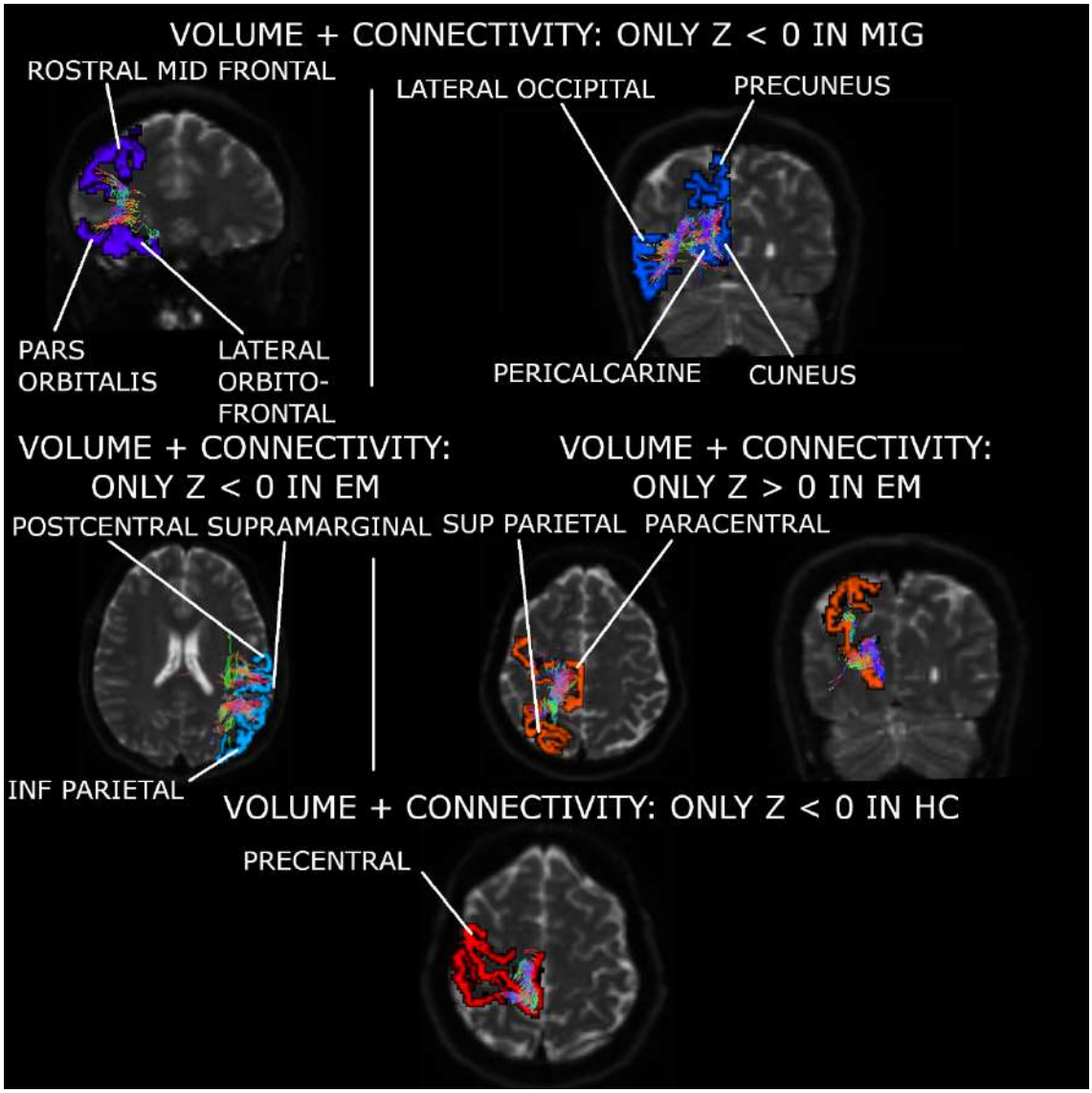


**Supplementary Figure 3 Additional networks found for the third independent component (fusion of gray matter volume and connectivity), part 1**. Networks enhanced or worsened only in migraine, EM or HC are shown. INF = inferior; MID = middle; MIG = migraine (results from EM and CM); SUP = superior.

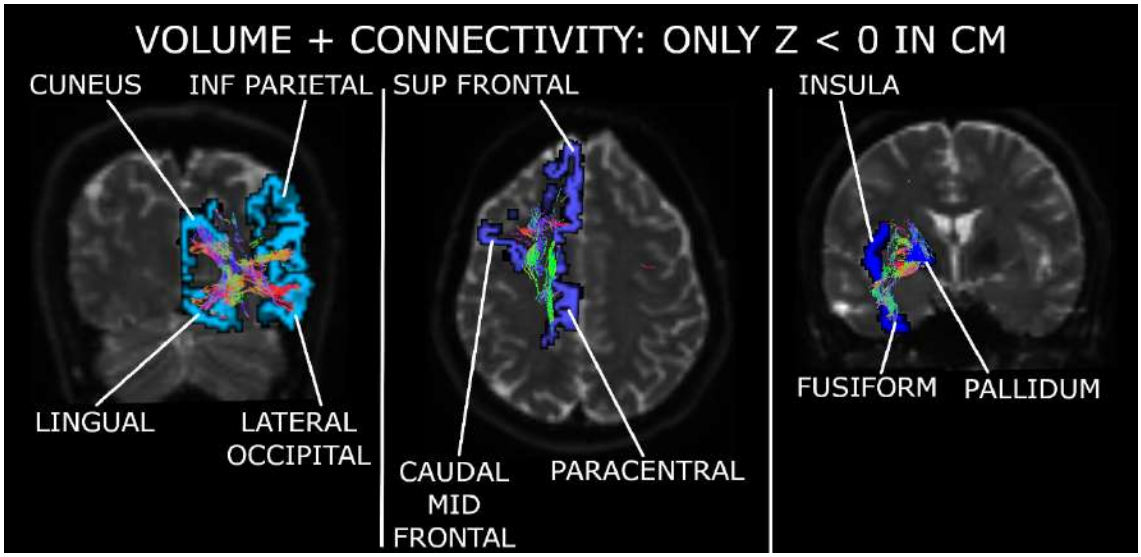


**Supplementary Figure 4 Additional networks found for the third independent component (fusion of gray matter volume and connectivity), part 2**. Networks worsened only in CM are shown. INF = inferior; MID = middle; SUP = superior.

# Appendices

# *Chapter A*

# *Questionnaire provided to the controls*

The original questionnaire provided to the controls before their inclusion in the study was in Spanish. Therefore, the translated questions into English are shown in this part of the appendix. The possible answer to all questions were *No* and *Yes*. From the fourth to the last question, the complete answer was *Yes, at least occasionally*.

**Group 0**:

1. Do you have a positive diagnosis of migraine by a primary care physician or a neurologist?
2. Have you suffered from headache in any moment of your life?

**Group 1**:

3. Do you suffer from headache more than half of the days?
4. Are your headache attacks pulsating, i.e., accompanied by the heartbeat?
5. When suffering from headache, do you need to stop working or another activity, bed rest or lying down during at least two hours?
6. Is the pain located on one side of the head?
7. Is your headache aggravated by normal physical exercise (e.g. climbing stairs or bending over)? Or does your headache encourage you to avoid any physical activity?

**Group 2**:

8. When suffering from headache, does the light bother you?
9. When suffering from headache, does noise bother you?
10. When suffering from headache, do you have nausea or vomiting?

# *Chapter B*

# ***Regions of the Desikan-Killiany Atlas***

The 34 cortical regions, including the cerebellum, from the Desikan-Killiany atlas that were assessed in this analysis are shown below in the same order that are labeled in the FreeSurfer pipeline:

1. Banks of the superior temporal sulcus.
2. Caudal anterior cingulate gyrus.
3. Caudal middle frontal gyrus.
4. Cuneus cortex.
5. Entorhinal cortex.
6. Fusiform gyrus.
7. Inferior parietal cortex.
8. Inferior temporal gyrus.
9. Isthmus-cingulate cortex.
10. Lateral occipital cortex.
11. Lateral orbital frontal cortex.
12. Lingual gyrus.
13. Medial orbital frontal cortex.
14. Middle temporal gyrus.
15. Parahippocampal gyrus.
16. Paracentral lobule.
17. Pars opercularis.
18. Pars orbitalis.
19. Pars triangularis.
20. Pericalcarine cortex.
21. Postcentral gyrus.
22. Posterior-cingulate cortex.
23. Precentral gyrus.

24. Precuneus cortex.
25. Rostral anterior cingulate cortex.
26. Rostral middle frontal gyrus.
27. Superior frontal gyrus.
28. Superior parietal cortex.
29. Superior temporal gyrus.
30. Supramarginal gyrus.
31. Frontal pole.
32. Temporal pole.
33. Transverse temporal cortex.
34. Insula.

The region 35 is the cerebellum. The remaining seven subcortical regions are shown below, starting with number 36, following the labeling from FreeSurfer:

36. Thalamus.
37. Caudate nucleus.
38. Putamen.
39. Pallidum (globus pallidus).
40. Hippocampus.
41. Amygdala.
42. Nucleus accumbens.

# *Chapter C*

# *Regions of the JHU-ICBM-DTI-81 Atlas*

In this appendix, the white matter regions from the JHU-ICBM-DTI-81 Atlas are shown. The regions are listed following the order of the labels included in FSL, but are not numbered here to avoid unnecessary repetitions (for a bilateral region, the right area has a specific number and the left area the immediate following number). The atlas is composed of 48 regions, including the bilateral cases. The white matter regions assessed in this project were:

- Middle cerebellar peduncle.
- Pontine crossing tract.
- Genu of corpus callosum.
- Body of corpus callosum.
- Splenium of corpus callosum.
- Fornix (column and body).
- Corticospinal tract.
- Medial lemniscus.
- Inferior cerebellar peduncle.
- Superior cerebellar peduncle.
- Cerebral peduncle.
- Anterior limb of internal capsule.
- Posterior limb of internal capsule.
- Retrolenticular part of internal capsule.
- Anterior corona radiata.
- Superior corona radiata.
- Posterior corona radiata.
- Posterior thalamic radiation (includes optic radiation).
- Sagittal stratum (includes inferior longitudinal fasciculus and inferior fronto-occipital fasciculus).

- External capsule.
- Cingulum (cingulate gyrus).
- Cingulum (hippocampus).
- Fornix (cres)/Stria terminalis.
- Superior longitudinal fasciculus.
- Superior fronto-occipital fasciculus.
- Uncinate fasciculus.
- Tapetum.

# *Chapter D*

# *White Matter Tractography Atlas*

The regions that compose the White Matter Tractography Atlas are strongly related to the JHU-ICBM-DTI-81 Atlas, but cover areas that are not included in the JHU-ICBM-DTI-81 Atlas. The atlas is composed of 20 regions, including the bilateral cases. The regions included in the White Matter Tractography Atlas are:

- Anterior thalamic radiation.
- Corticospinal tract.
- Cingulum (cingulate gyrus)
- Cingulum (hippocampus)
- Forceps major
- Forceps minor
- Inferior fronto-occipital fasciculus
- Inferior longitudinal fasciculus
- Superior longitudinal fasciculus
- Uncinate fasciculus
- Superior longitudinal fasciculus (temporal part)